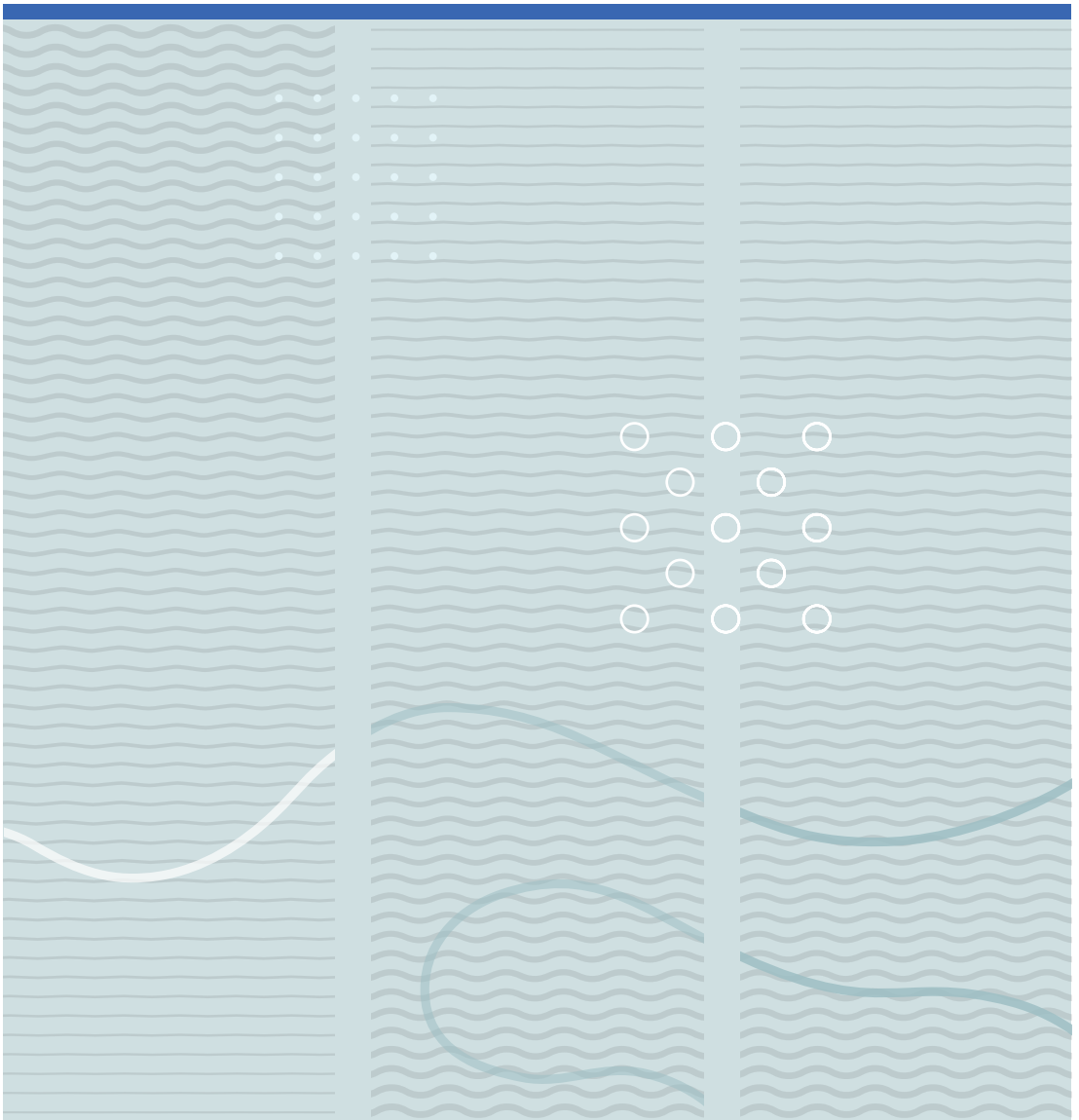Sumudu S. Karunarathne

Physicochemical data for amine based CO$_2$ capture process

USN

Sumudu S. Karunarathne

Physicochemical data for amine based CO_2 capture process

A PhD dissertation in
Process, Energy and Automation Engineering

Dedicated to my parents, family and friends

Preface

This thesis is submitted as partial fulfilment of the requirement for the degree of Philosophiae Doctor (PhD) at the University of South-Eastern Norway (USN). The research project was funded by the Ministry of Education and Research of the Norwegian Government, for three years starting from October 2016. This research project was conducted under the supervision of Professor Lars Erik Øi and with the guidance from co-supervisor Professor II Dag Arne Eimer from the Faculty of Technology, Natural sciences and Maritime studies, USN.

The study is mainly focused on evaluating the physical properties of density and viscosity of different amines and their blends that can be used in amine-based post-combustion CO_2 capture process. Different empirical correlations with theoretical background were suggested for the density and viscosity of liquid amine mixtures. The uncertainty of density and viscosity measurements were evaluated for both pure liquids and mixtures with CO_2. The laboratory experiments were performed at the CO_2 laboratories at Porsgrunn campus, USN.

A pilot plant study of post-combustion was done using a laboratory CO_2-rig located at Porsgrunn campus, USN. The density and viscosity variations of the solvent were analysed through a series of lab experiments under different process conditions. Process simulations were performed to investigate and compare modelling in Aspen HYSYS and Aspen Plus environments.

The thesis is presented in two parts. The first part describes the literature of post-combustion CO_2 capture including CO_2 capture methods, measured physical properties of density and viscosity with reported correlations, the approach of Artificial Neural Networks (ANNs) to represent density and viscosity data and process simulation based on equilibrium-based and rate-based models. Further, it includes experimental methods for density, viscosity and CO_2 loading analysis, a brief overview of results with a discussion and uncertainty analysis of density and viscosity measurements.

The second part lists the collection of research articles published and submitted under this project.

Acknowledgement

VI

Abstract

Amine based post-combustion carbon capture is a highly discussed CO_2 removal method from flue gas. Large-scale CO_2 capture facilities with effective solvents are required to make a significant impact on reducing CO_2 emissions from power plants and existing facilities. Physical properties of solvents play a major role in designing process equipment. Measured properties like density, viscosity and surface tension are used in mathematical models developed for mass transfer and interfacial area that are used in designing absorption columns. Further, developed correlations to represent measured physical properties are useful in process simulations.

This work presents measured density and viscosity data of both CO_2 loaded and non-loaded aqueous amine mixtures at different amine concentrations, temperatures and CO_2 loadings. Density and viscosity increase with the increase of CO_2 loading and decrease with the increase of temperature. The excess volume of binary and ternary aqueous amine mixtures was calculated from measured density data and correlated using a Redlich-Kister type polynomial. A density correlation proposed by Aronu was adopted to correlate densities of $MEA + H_2O$ mixtures. A correlations based on density deviation ρ_γ were proposed for $MDEA + H_2O$, $DMEA + H_2O$ and $DEEA + H_2O$ mixtures. Aronu's density correlation was modified to fit densities of $MEA + H_2O + CO_2$ mixtures. For $AMP + MEA + H_2O + CO_2$ mixtures, density was correlated using a modified Weiland's correlation and a Setschenow type correlation. The accuracies of density data fits were satisfactory as the average absolute relative deviation (AARD) was typically less than 1% and correlations are suitable to perform engineering calculations.

Eyring's viscosity model based on Eyring's absolute rate theory was adopted to calculate the free energy of activation for viscous flow ΔG_0^+ of CO_2 loaded and non-loaded aqueous amine mixtures. Further, the excess free energy of activation for viscous flow ΔG_0^{E+} was calculated and a Redlich-Kister type polynomial was proposed to fit the measured viscosities of aqueous amine mixtures. For the mixtures of $MEA + H_2O + CO_2$ and $AMP + MEA + H_2O + CO_2$, empirical correlations were proposed to fit calculated ΔG_0^+ from Eyring's viscosity model and then the correlation was used to represent the measured viscosities. The viscosity deviation η^E was determined for aqueous amine mixtures to investigate types of intermolecular interactions in the mixtures. Further, a modified Weiland's correlation and a Setschenow type correlation were proposed to correlate viscosities of $AMP + MEA + H_2O + CO_2$ mixtures. The accuracies of the viscosity data fits were typically less than 2% AARD and the proposed correlations can be recommended to use in engineering calculations.

The approach of using feedforward backpropagation artificial neural networks (ANNs) to represent densities and viscosities of CO_2 loaded and non-loaded aqueous amine solutions gained high accuracies in data fit compared to the conventional empirical correlations. The ANNs are with multiple inputs of mole fractions of amines, CO_2 and temperature of the mixtures, one hidden layer and one output that is either density or viscosity of the mixtures. The optimum number of neurons in the hidden layer was found by calculating Mean Squared Error (MSE) over thirty neurons.

The experiments performed in a CO_2-rig located at USN Porsgrunn illustrates the variations of density and viscosity at the top and the bottom of the absorber column at different liquid flow rates. The density of the solvent increased although the temperature increased due to the exothermal reaction between CO_2 and MEA. The influence of temperature increase caused to decrease the viscosity at the bottom of the column even the CO_2 loading is higher than at the top of the column. Process simulations were performed to predict the variations of density and viscosity of the column.

List of papers

Article A - Karunarathne, S.S.; Eimer, D.A.; Øi, L.E. Density, viscosity and free energy of activation for viscous flow of monoethanol amine (1) + H_2O (2) + CO_2 (3) mixtures. Fluids 2020, 5, 13.

Article B - Karunarathne, S.S.; Eimer, D.A.; Øi, L.E. Density, viscosity and free energy of activation for viscous flow of CO_2 loaded 2-amino-2-methyl-1-propanol (AMP), monoethanol amine (MEA) and H_2O mixtures. Journal of Molecular Liquids 2019, accepted.

Article C - Karunarathne, S.S.; Eimer, D.A.; Jens, K.J.; Øi, L.E. Density, viscosity and excess properties of ternary aqueous mixtures of MDEA + MEA, DMEA + MEA and DEEA + MEA. Fluids 2020, 5, 27.

Article D - Karunarathne, S.S.; Eimer, D.A.; Øi, L.E. Density, viscosity and excess properties of binary aqueous mixtures of MDEA + H_2O, DMEA + H_2O and DEEA + H_2O. Applied Sciences 2020, 10, 3196.

Article E - Karunarathne, S.S.; Chhantyal, K.; Eimer, D.A.; Øi, L.E. Artificial neural networks (ANNs) for density and viscosity predictions of CO_2 loaded alkanolamine + H_2O mixtures. Chemengineering 2020, 4, 29.

Article F - Karunarathne, S.S.; Eimer, D.A.; Øi, L.E. Physical properties of MEA + Water + CO_2 mixtures in post-combustion CO_2 capture: A review of correlations and experimental studies. Journal of Engineering 2020, Article ID 7051368.

Article G - Karunarathne, S.S.; Eimer, D.A.; Øi, L.E. The effect of CO_2 loading on the flow behaviour of amine and water mixtures. Annual transactions of the Nordic rheology society, vol. 27, 2019.

Article H - Karunarathne, S.S.; Eimer, D.A.; Øi, L.E. Free energies of activation for viscous flow of different amine mixtures in post combustion CO_2 capture. TCCS -10, Trondheim, Norway, pp. 77-82, 2019.

Article I - Karunarathne, S.S.; Øi, L.E. Applicability of NRTL model for prediction of the viscosity of alkanolamine + water mixtures. In Proceedings of the 60th SIMS Västeräs, Sweden, pp. 73-77, 2019.

Article J - Karunarathne, S.S.; Øi, L.E. Density and viscosity correlations for aqueous 3-amino-1-propanol and monoethanol amine mixtures. In Proceedings of the 60th SIMS Västeräs, Sweden, pp. 67-72, 2019.

Article K - Karunarathne, S.S.; Øi, L.E. Aspen HYSYS and Aspen Plus simulations for amine based absorption process compared to results from experiments in CO_2-rig. TCCS -10, Trondheim, Norway, pp. 83-89, 2019.

Article L - Karunarathne, S.S.; Eimer, D.A.; Øi, L.E. Density and viscosity variations in an amine based absorption column. In Proceedings of 14th Greenhouse Gas Control Technologies Conference (GHGT-14), Melbourne.

Article M - Karunarathne, S.S.; Eimer, D.A.; Øi, L.E. Model Uncertainty of interfacial area and mass transfer coefficients in absorption column packings. In Proceedings of the 58th SIMS Reykjavik, Iceland; pp. 144-150.

Article N - Karunarathne, S.S.; Eimer, D.A.; Øi, L.E. Evaluation of systematic error and uncertainty of viscosity measurements of mixtures of monoethanol amine and water in coaxial cylinder rheometers. International Journal of Modeling and Optimization 2018, 8, 260-265.

Article O - Karunarathne, S.S.; Eimer, D.A.; Øi, L.E. Uncertainty comparison of viscosity measurements of CO_2 loaded MEA and water mixtures in a coaxial rheometer using Monte Carlo simulation and GUM method. IJEE 2019, 10, 77-86.

Papers summary

Article A presents measured density and viscosity of MEA + H_2O + CO_2 mixtures at different MEA concentrations, temperatures and CO_2 loadings. The density of aqueous MEA and CO_2 loaded aqueous MEA mixtures were fitted to empirical correlations. For the viscosity measurements, Eyring's viscosity model based on absolute rate theory was adopted to calculate free energy and excess free energy of activation for viscous flow. Empirical correlations were proposed to correlate viscosities of aqueous MEA and CO_2 loaded aqueous MEA mixtures using Eyring's viscosity model.

Article B discusses measured density and viscosity of AMP + MEA + H_2O + CO_2 mixtures at different MEA concentrations, temperatures and CO_2 loadings. Empirical correlations were fitted to the measured properties. Eyring's viscosity model based on absolute rate theory was used to calculate free energy, enthalpy and entropy of activation for viscous flow. The excess molar volume and viscosity deviation of AMP + MEA + H_2O mixtures were analysed to understand the intermolecular interactions among molecules.

Article C presents measured density and viscosity of ternary mixtures of MDEA + MEA + H_2O, DMEA + MEA + H_2O and DEEA + MEA + H_2O at different amine concentrations and temperatures. The excess molar volume was determined using density data and a Redlich – Kister type polynomial was proposed to fit measured densities. The excess free energy of activation for viscous flow was calculated from Eyring's viscosity model and a Redlich – Kister type polynomial was proposed to fit measured viscosities. The excess molar volumes, viscosity deviations and excess free energy of activation for viscous flow were analysed to describe the intermolecular interactions among the molecules. The excess entropy of activation for viscous flow was calculated and compared with the variation against amine concentration and temperature.

Article D presents measured density and viscosity of binary mixtures of MDEA + H_2O, DMEA + H_2O and DEEA + H_2O at different amine concentrations and temperatures. The excess molar volume was found and compared using density data of different mixtures and Redlich – Kister type polynomials were proposed to fit measured densities. Correlations for the partial molar volume of different mixtures were developed using the proposed Redlich – Kister type polynomials for excess molar volume. For the viscosities, empirical correlations were proposed to fit the measured viscosities. The McAllister's three-body model was adopted to fit the kinematic viscosities found through dynamic viscosity and density data. The excess free energy, enthalpy and entropy of activation for viscous flow were determined using Eyring's viscosity model and compared with the properties among each mixture.

Article E illustrates the applicability of Artificial Neural Networks (ANNs) to represent densities and viscosities of CO_2 loaded and non-loaded aqueous amine mixtures. Feedforward backpropagation ANNs with a single hidden layer were trained using measured densities and viscosities at different amine concentrations, temperatures and CO_2 loadings. The accuracies of the data fit using ANNs were compared with conventional empirical correlations proposed in the literature.

Article F discusses a review of experimental data and correlations of density, viscosity and surface tension for the solutions of pure MEA, aqueous MEA and CO_2 loaded aqueous MEA. The data sources for the solutions are tabulated with measured concentration, pressure and temperature range. Different density and viscosity correlations were examined for their accuracies by comparing them with different data sources existing in the literature.

Article G illustrates the effect of CO_2 loading on the flow behaviour of amine and water mixtures. The shear stress was measured by a rheometer at different shear rates of MEA + H_2O + CO_2 and AMP + MEA + H_2O + CO_2 mixtures. The objective of this study was to observe the variation of flow behaviour from Newtonian to non-Newtonian due to the presence of CO_2 in the mixtures.

Article H is a study of free energy of activation for viscous flow of aqueous ternary amine mixtures of MDEA + MEA + H_2O, MDEA + DEA + H_2O and AMP + DEA + H_2O. The excess molar volume, viscosity deviation and excess free energy of activation for viscous flow were studied to analyse the intermolecular interaction among the molecules. Redlich – Kister type polynomials were proposed to correlate calculated excess free energy of activation for viscous flow and the correlations used to represent the viscosities of the mixtures.

Article I shows the applicability of the NRTL model with Eyring's viscosity model based on absolute rate theory to predict viscosities of MEA + H_2O and AMP + MEA + H_2O. Here, correlations were proposed to use with excess Gibbs free energy of mixing to replace excess free energy of activation for viscous flow that is derived from Eyring's viscosity model.

Article J reports a study of density and viscosity correlations for MEA + H_2O and 3A1P + H_2O. Kinematic viscosity of mixtures was correlated using a McAllister's three-body model with temperature dependency. The viscosity deviation and excess free energy of activation for viscous flow were determined to analyse intermolecular interactions among the molecules.

Article K illustrates simulations of the post-combustion CO_2 capture process using equilibrium-based and rate-based approaches. For the equilibrium-based approach, the Murphree efficiency was adjusted to achieve the CO_2 removal efficiency measured from the CO_2 pilot plant at USN. In the rate-based approach, the interfacial area factor (IAF) was adjusted to achieve measured CO_2 removal efficiency. Then the CO_2 removal efficiency obtained at different liquid flow rates was compared under different simulation approaches. The measured physical properties of density and viscosity of the solvent at the absorber top and the bottom were compared with simulations in the rate-based approach.

Article L presents a study of post-combustion CO_2 capture in a CO_2 pilot plant at USN. The CO_2 removal efficiency of the absorber was calculated by measuring the CO_2 concentration of the inlet and outlet gas streams. The physical properties of density and viscosity of the solvent were measured at the absorber top and bottom of the absorber. The empirical correlations proposed for density and viscosity of MEA + H_2O + CO_2

mixtures in literature were compared with measured properties to examine their accuracies in data prediction.

Article M reports the propagation of uncertainty of input parameters in a mathematical model to make model output uncertain. The mathematical models involved in absorber column design comprise physical properties especially density, viscosity and surface tension. Monte Carlo Simulation (MCS) method was used to evaluate the uncertainty propagation of mass transfer and interfacial area models suggested for random and structured packings.

Article N discusses the random error, systematic error and uncertainty involved in viscosity measurements in a coaxial cylinder rheometer. The uncertainty of viscosity measurements was evaluated using the Guide to the Expression of Uncertainty in Measurement (GUM) method through identified uncertainty sources involved in the measuring technique. Viscosities of aqueous MEA at higher temperatures and different concentrations were presented with estimated parameters of an empirical correlation.

Article O compares two different approaches to evaluate the uncertainty of viscosity measurement in a coaxial cylinder rheometer. MCS method is an alternative approach to the GUM methods that discusses the propagation of distribution while the GUM method discusses the uncertainty through a mathematical model. Here, MCS was used to validate the uncertainty calculated by the GUM method for viscosity measurement in CO_2 loaded and non-loaded aqueous MEA solutions.

List of tables

List of figures

Nomenclature

Latin letters	Description	Units
a	Length of molecular jump	$[m]$
E	Activation energy of viscous flow	$[J \cdot mol^{-1}]$
$g(r)$	Radial distribution function	
ΔG_o^+	Free energy of activation for viscous flow	$[J \cdot mol^{-1}]$
ΔG_o^{E+}	Excess free energy of activation for viscous flow	$[J \cdot mol^{-1}]$
ΔG^{E*}	Excess Gibbs free energy of mixing	$[J \cdot mol^{-1}]$
ΔG_{mix}^*	Gibbs free energy of a mixing	$[J \cdot mol^{-1}]$
G_{ij}	Interaction parameter	
h	Planck constant	$[m^2 \cdot kg \cdot s^{-1}]$
ΔH_o^+	Enthalpy of activation for viscous flow	$[J \cdot mol^{-1}]$
k	Boltzmann's constant	$[J \cdot K^{-1}]$
k_1	Slope of the straight line	
K	Regression parameter	
m	Mass of one molecule	$[kg]$
M_i	Molecular weight of ith component	$[g \cdot mol^{-1}]$
N	Avogadro number	$[mol^{-1}]$
N_i, N_j	Number of carbon atoms of components i and j	
n	Number of data	
n_i	Mole numbers	
P	Pressure	$[Pa]$
P_c	Critical pressure	$[Pa]$
r	Molecular radial distance	$[m]$
r_{net}	Net rate of molecular jump	per molecule
R	Universal gas constant,	$[J \cdot mol^{-1} \cdot K^{-1}]$
ΔS_o^+	Entropy of activation for viscous flow	$[J \cdot mol^{-1} K^{-1}]$
t	Temperature,	$[°C]$
T	Temperature,	K
T_c	Critical temperature,	K
T_0	Reference temperature 308 K	K
u	Uncertainty	
u	Weight fraction of water and amines in Eq (13)	
U	Expanded uncertainty	
v	Frequency of molecular jumps	per molecule
v_x	Velocity of fluid in x direction	$[m \cdot s^{-1}]$
$\overline{V_i}$	Partial molar volume of a component	$[m^3 \cdot mol^{-1}]$
V_i^0	Molar volume of ith pure component	$[m^3 \cdot mol^{-1}]$
V^E	Excess molar volume	$[m^3 \cdot mol^{-1}]$
V	Molar volume of the mixture	$[m^3 \cdot mol^{-1}]$
V_c	Critical volume	$[m^3]$
w	mass fractions	$[------]$

$wt\%$	Weight percentage	[------]
W_{CO_2}	Loaded basis weight fraction CO_2	
$W_{CO2added}$	CO_2 added to the solution on a mass basis	[------]
W_{vis}	Interaction parameter	
x_i	Mole fraction of ith component	[------]
x_1	Mole fraction of MEA	[------]
x_2	Mole fraction of water	[------]
x_3	Mole fraction of CO_2 in Eq (141)	[------]
x_4	Mole fraction of CO_2 in Eq (142), Eq (143) and Eq (144)	[------]
Y_i^E	Measured property	
Y_i^C	Calculated property	
Z	Compressibility factor	[------]

Greek letters	Description	Units
ρ	Density of a mixture	$[kg \cdot m^{-3}]$
ρ_i	Density of ith component	$[kg \cdot m^{-3}]$
ρ_γ	Density deviation	$[kg \cdot m^{-3}]$
$\rho_{unloaded}$	Density of an aqueous mixture	$[kg \cdot m^{-3}]$
ρ_{loaded}	Density of a CO_2 loaded aqueous mixture	$[kg \cdot m^{-3}]$
η	Viscosity	$[Pa \cdot s]$
$\Delta\eta$	Viscosity deviation	$[Pa \cdot s]$
η^E	Excess viscosity	$[Pa \cdot s]$
η_{ideal}	Viscosity of an ideal mixture	$[Pa \cdot s]$
η_{H_2O}	Viscosity of water	$[Pa \cdot s]$
η_γ^*	Viscosity deviation	$[Pa \cdot s]$
$\eta_{unloaded}$	Viscosity of an aqueous mixture	$[Pa \cdot s]$
η_{loaded}	Viscosity of a CO_2 loaded aqueous mixture	$[Pa \cdot s]$
σ	Surface tension	$[N \cdot m^{-1}]$
σ_{mix}	Surface tension of a mixture	$[N \cdot m^{-1}]$
β	Bulk thermal expansively, Eq(13)	$[K^{-1}]$
β	Thermal expansion coefficient	$[K^{-1}]$
α	CO_2 loading	[mol CO_2/mol amine]
Φ	Volume expansion due to CO_2	$[m^3]$
τ_{yx}	Shear stress	$[Pa]$
v_{ideal}	Kinematic viscosity of an ideal mixture	$[m^2 \cdot s^{-1}]$
v	Kinematic viscosity	$[m^2 \cdot s^{-1}]$
ζ	Friction coefficient related to the intermolecular force field	$[kg \cdot s^{-1}]$
$\Psi_2(r)$	Square well model parameters	
$\varphi(r)$	Intermolecular potential function	
δ	Distance between two fluid layers	$[m]$
ξ	Reduced, inverse viscosity	$[(Pa \cdot s)^{-1}]$
ω	Acentric factor	[------]

Abbreviations

AARD	Average absolute relative deviation
AMP	2-amino-2-methyl-1-propanol
ANN	Artificial Neural Network
BR	Bayesian Regularization
CCS	Carbon capture and storage
DEA	Diethanol amine
DMEA	Dimethylethanolamine
DEEA	Diethylethanolamine
EOR	Enhanced oil recovery
GUM	Guide to the Expression of Uncertainty in Measurements
IAF	Interfacial area factor
MCS	Monte Carlo Simulation
MDEA	N-Methyldiethanolamine
MEA	Monoethanol amine
MSE	Mean Squared Error
NRTL	Non-random two liquid
PCC	Post-combustion CO_2 capture
3A1P	3-Amino-1-propanol

Table of contents

1 Introduction

This chapter provides an overview of carbon capture and storage including post-combustion, pre-combustion and oxyfuel combustion. A brief discussion is made on post-combustion CO_2 capture, the importance of the physical properties of solvents in amine-based capture technology and the future of carbon capture and storage. The chapter comprises the research problems, research objectives and the outline of the research.

1.1 Background

Climate changes and the global temperature increase are some of the most critical issues that scientists are struggling to answer today. The excessive emissions of gases that have the capability to trap the radiation emitted from the earth's surface can contribute to increase the global temperature. Major greenhouse gases like water vapour (H_2O), Carbon dioxide (CO_2), Methane (CH_4), Ozone (O_3) and Nitrous oxide (N_2O) can be found in all layers of the atmosphere [1]. During the last century, the consumption of fossil fuels has increased immensely because of the increase of global energy demand in the electricity, transport and production sectors. Accordingly, the CO_2 level in the atmosphere has risen unprecedentedly and it has become the major reason for the climate changes that the world is facing today. Scientists believe that the CO_2 level has elevated approximately from 300 ppm to 400 ppm in the atmosphere due to human activities over the last 100 years and will continue to increase unless necessary precautions are not taken [2-4]. According to the Intergovernmental Panel on Climate Change (IPCC), there were 7887 sources with CO_2 emissions of 13466 $MtCO_2yr^{-1}$ reported in the year 2000 and it continues to increase [5]. Figure 1.1 shows the variation of atmospheric CO_2 concentration and global temperature for the last century.
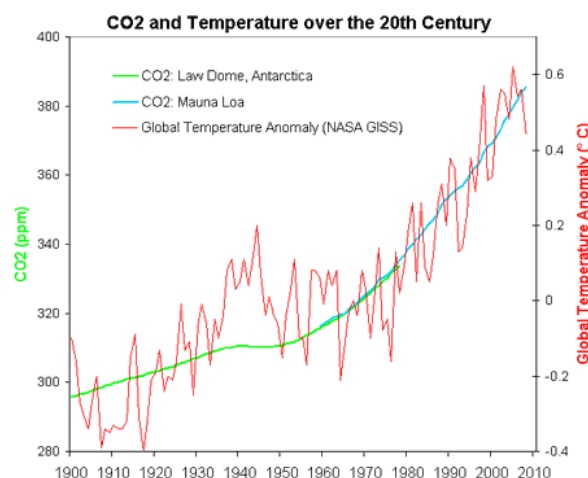
Figure 1.1: CO_2 green line derived from ice cores obtained at Law Dome, East Antarctica (CDIAC). CO_2 blue line measured at Mauna Loa (NOAA). Global temperature anomaly (GISS) [6]

Several agreements have been made to control the CO_2 emissions and the United Nations Framework on Climate Change (UNFCCC) is the main international agreement on climate change. Currently, the European council handles two issues related to UNFCCC that are the second period of the Kyoto protocol (2013 -2020) and newly signed Paris agreement to cover the period from 2020 onwards [7].

Carbon capture and storage (CCS) provides feasible solutions to use fossil fuels by not increasing the atmospheric CO_2 level. CCS has mainly three branches consisting of different CO_2 removal techniques; Post-combustion, Pre-combustion and Oxyfuel combustion [5]. Figure 1.2 presents an overview of possible methodologies in CCS.
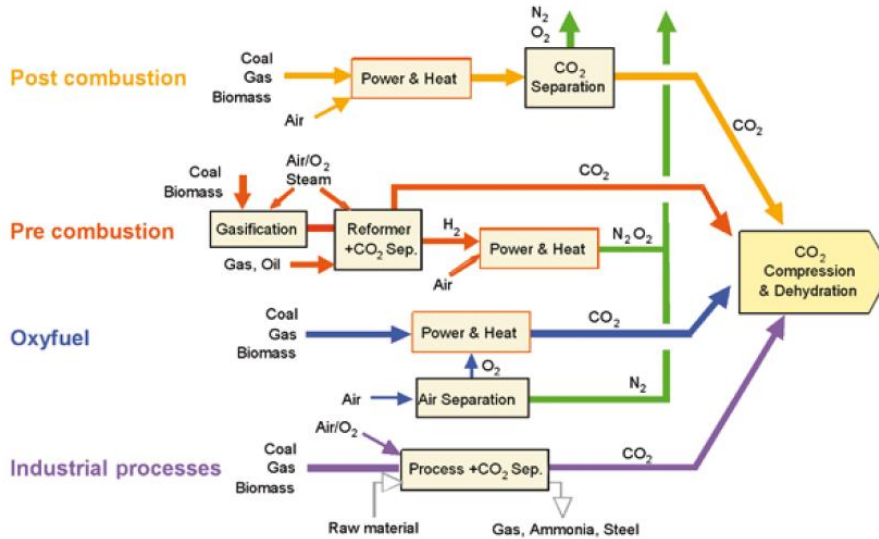
Figure 1.2: Overview of CO_2 capture processes and systems [5]

The advancement in research activities in all branches is vital to select an optimum process that meets the requirements of the stakeholders. Post-combustion CO_2 capture consists of several treatment techniques in which the driving force for the mass transfer is the partial pressure of the CO_2 in the flue gas. Different methods have been studied extensively in post-combustion capture to bring the cost of operation into a reasonable level.
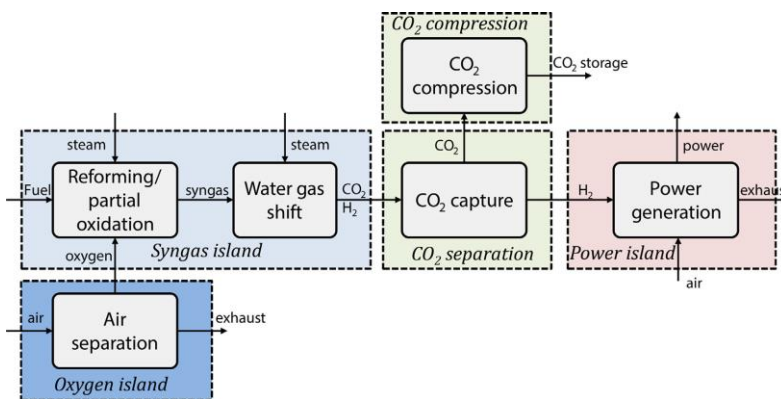
Figure 1.3: Schematic of pre-combustion capture for power generation: Jansen, et al. [8]

In pre-combustion, synthesis gas (syngas) composed mainly of carbon monoxide and hydrogen is produced via reacting a fuel with a controlled amount of oxygen, air or steam. Figure 1.3 gives the schematic of pre-combustion capture for power generation.

The water-gas shift converts CO (carbon monoxide) in the syngas into CO_2. This CO_2 is removed by using conventional washing steps around ambient temperature [8].

Oxyfuel combustion involves oxygen that is separated from cryogenic air separation to react with fuel in the power plant. The gas emission is rich in CO_2 and water vapour. Then the separation of CO_2 from the flue gas can be done through condensation of water and low temperature purification processes [9]. As a result of recent developments to reduce the cost of oxygen production in the air separation unit, the applicability of oxyfuel combustion may be increased in the industry [10].

1.2 Post Combustion CO_2 Capture (PCC)

Post-combustion CO_2 capture (PCC) is the methodology of capturing CO_2 from the flue gas after the combustion of fossil fuels. The capturing of CO_2 can be performed by using different mass transfer operations such as absorption and desorption, adsorption and membrane separation. Each technique has its own advantages and disadvantages. The process optimization has to be done considering both energy demand, capital and operation cost of the process. A conceptual diagram of the PCC is shown in Figure 1.4.
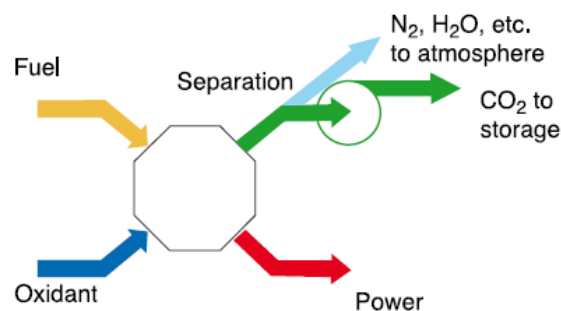
Figure 1.4: Schematic of post-combustion capture [5]

Post-combustion CO_2 capture using a solvent process is regarded as one of the most mature carbon capture technologies [2]. Figure 1.5 illustrates an overview of PCC including other aspects like adsorption and membrane technologies.
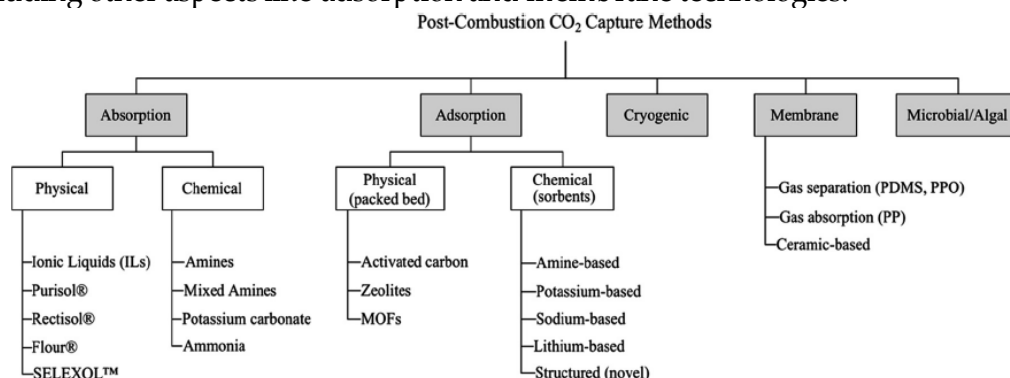
Figure 1.5: Main carbon separation/capture methods in the post-combustion CO_2 capture: Aghaie, et al. [11]

1.2.1 Absorption and Desorption Process

The technology is included with both chemical and physical absorption of CO_2. Alkanolamines, amino acid salts, aqueous chilled ammonia and ionic liquids react and capture CO_2 from the flue gas stream. The amine-based technology is already in use for CO_2 capture from natural gas. Probably, it will be the dominant technology for removing CO_2 from flue gas of coal-fired power plants in 2030 [12]. Aqueous alkanolamines are widely used and investigated for the CO_2 removal from flue gas streams.

Amino acid salts contain an amino group (-NH_2) as in the amine to absorb CO_2. The volatility of the solution is reduced by converting the carboxylic group into a salt [13]. The high CO_2 absorption rate, high thermal stability, high biodegradability, low ecological toxicity, low volatility and resistance to O_2 degradation have made amino acid salts favourable for PCC [14, 15].

Aqueous ammonia shows several advantages over conventional amines such as low cost, less corrosiveness and it does not degrade due to the presence of O_2 and other species in the flue gas [16]. The escape of ammonia with the CO_2 product stream at the stripper gas outlet is a loss and requires ammonia makeup, which is a disadvantage of using aqueous ammonia in PCC.

Ionic liquids can capture CO_2 through either chemical absorption or physical absorption [17]. They are organic salts, which form a stable liquid at room temperature [18]. Generally, the CO_2 solubility is more influenced by the anion than cation in physical absorption. Other factors that affect the CO_2 solubility are free volume and size of the ionic liquid. For chemical absorption, ionic liquids with an amino-functional group that can react with CO_2 can be used [17]. A systematic review of the use of ionic liquids in PCC is presented by Aghaie, et al. [11].

1.2.2 Adsorption Process

Cyclical removal of CO_2 from flue gas using adsorption is an alternative to challenge disadvantages engaged with aqueous amine processes like low contact area between gas and liquid, low CO_2 loading and corrosion effects [17]. The rate-limiting factor for the process is the diffusion of CO_2 from flue gas to the pores of the adsorbent. The review performed by Choi, et al. [19] listed details of potential physisorbents and chemisorbents for CO_2 removal. The use of zeolites and activated carbon as physisorbents have been reported through isotherm and kinetic studies. Due to the acid nature of CO_2, alkaline metal oxides, especially with low charge/radius ratio like (Na_2O/K_2O) and (CaO/MgO) are applicable as chemisorbents to capture CO_2. There are possibilities to improve adsorption and selectivity via chemical modifications on the surface of the solid materials to acquire high surface area. This is achieved by using amine-impregnated and amine-grafted materials. A critical analysis of adsorbents in the literature is performed by Sayari, et al. [20] who describe the different characteristics of different materials.

1.2.3 Membrane Separation Process

The potential of membrane separation has been recognized as an energy efficient process for the CO_2 capture from flue gas [21, 22]. Brinkmann, et al. [23] reported studies using different polymer and ceramic membranes for the coal-fired power plants. Possible types of membrane modules for the gas separation applications are envelope-type, spiral wound and hollow fiber modules. Merkel, et al. [24] outlined some general design issues, which affect the selection of the optimum membrane and module for PCC. The performance of the membrane system is restricted by the pressure ratio of the membrane and cannot achieve 90% capture of CO_2 from a single-stage membrane process. Thus, a multi-stage treatment process is required to enhance the CO_2 recovery and purity. Figure 1.6 illustrates the flow diagram of a two-step vacuum membrane process for CO_2 capture from flue gas.
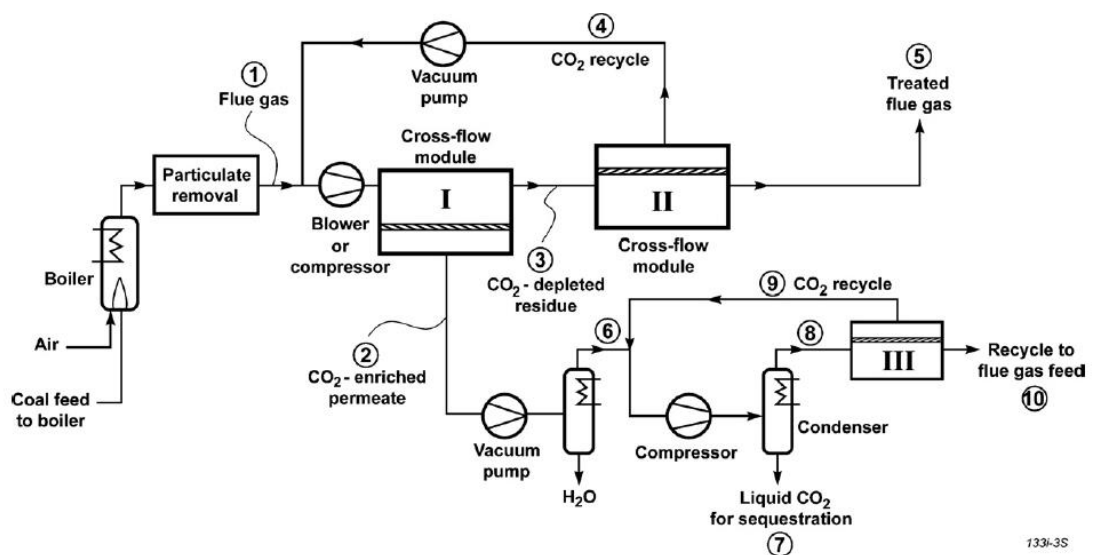
Figure 1.6: Simplified flow diagram of a two-step vacuum membrane process to capture and sequester CO_2 in flue gas: Merkel, et al. [24]

Leung, et al. [25] provide a comparison of different separation technologies. The advantages of the absorption process are it is the most matured process for CO_2 separation, which gives a high absorption efficiency (> 90%)[5]. The high energy requirement (with MEA: 3 MJ/kg CO_2) for the CO_2 desorption and inadequate understanding of environmental impacts related to solvent degradation are considered as disadvantages [25-27]. For the adsorption process, advantages are the high absorption efficiency and availability of low cost physical adsorbents. High energy demand for regeneration is a drawback for this technology [2, 20, 27]. The advantage of using membranes is low energy requirement (0.5-6 MJ/kg CO_2) compared to other available technologies. The associated disadvantages are the low purity of CO_2 removal and low removal efficiencies[28].

1.3 Physical Properties of Solvents in Amine Based CO_2 Capture

Physical properties like density, viscosity, surface tension, thermal conductivity and diffusivity are important in different aspects of amine-based post-combustion such as equipment design, mathematical modelling and simulations. The properties of density, viscosity and surface tension appear in mass transfer correlations of both random and structured packing for absorption and desorption columns. The properties of thermal conductivity and diffusivity are highlighted in the correlations for heat transfer in both absorber and heat exchanger units. The solvent involved in the CO_2 capture method is mainly amine + H_2O + CO_2 mixtures and CO_2 loading vary during the different operations in the process. Accordingly, measurement of physical properties is important to make the process more efficient and to optimize.

1.4 Future of CCS

The future of CCS depends on the efficiency of the CO_2 capture technologies and the reliable storage facilities to capture CO_2. The cost is a crucial factor in CCS to use the existing fossil fuels to extract the economic value of it while preserving the environment. CCS has to compete with the use of other reliable energy sources like renewable and nuclear energy. Idem, et al. [13] assessed progress that has been gained by CO_2 capture processes with reactive solvents. A significant improvement has been observed in the reduction of heat duty especially in smaller pilot plants from 5.0 to 1.8 GJ/ton CO_2 via the development of energy efficient solvents and process optimization. There is a new trend for catalysts in amine-based post-combustion CO_2 capture in the future. This could reduce the size of process equipment and heat duties in the reactive solvent based PCC.

For CO_2 storage, Figure 1.7 demonstrates the geological storage options for CO_2. Metz, et al. [5] tabulated existing and planned geological storage project all over the world. The increased interest in enhanced oil recovery (EOR) has opened opportunities for new CO_2 storage facilities.
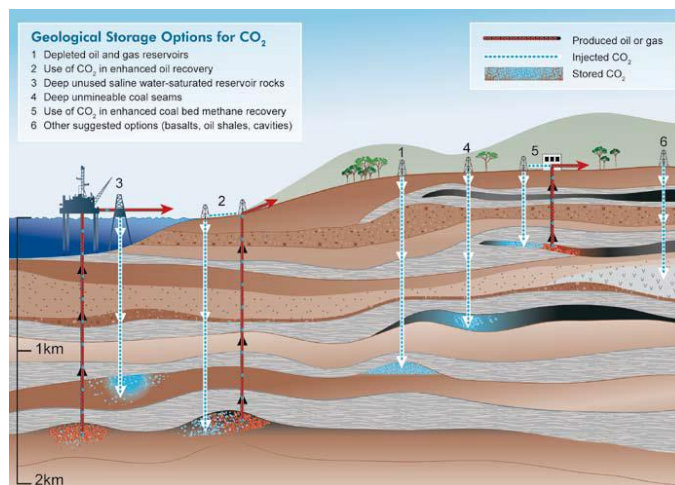
Figure 1.7: Methods for storing CO_2 in deep underground geological formations [5]

1.5 Research Problems

Physical property data are very important in designing process equipment like absorption and desorption columns, heat exchangers, reboilers and selection of pumps and blowers to the CO_2 capture process. The measured physical properties like density and viscosity of different amine mixtures are available in the literature with developed correlations to represent data. Nevertheless, there is a lack of available measured data especially for CO_2 loaded solutions for potential solvents that can be used in PCC. In addition, available empirical correlations to represent measured data need to be improved and new correlations have to be suggested with better accuracies. The availability of density and viscosity data of CO_2 loaded solutions helps to enhance the accuracy of mass transfer, heat transfer and interfacial area calculations that are essential in both equipment design and process simulations. The uncertainty associated with measured data helps to calculate the safety factors for the designs. In process modelling and simulations, the accuracy of physical properties helps to improve the simulation results.

1.6 Research Objectives

The objective of the PhD project was to measure physical properties such as density and viscosity of solvents that are used in post-combustion CO_2 capture. The main idea was to quantify those physical properties by performing laboratory experiments under different conditions like temperatures, amine and CO_2 concentrations. Additionally, compare the uncertainty evaluation related to measured viscosity data with different approaches as the Guide to the Expression of Uncertainty in Measurement (GUM) and Monte Carlo Simulation (MCS) methods. The second objective was to build correlations to predict those physical properties for unmeasured conditions. Further, perform experiments in the laboratory CO_2-rig located at the University of South-Eastern Norway (USN) to investigate the density and viscosity variations in the absorber and model the system using both equilibrium-based and rate-based approaches in Aspen HYSYS and Aspen Plus environments. Finally, evaluation of the effect of uncertainties in physical property data on process parameters should be performed via a statistical and probabilistic study of the post-combustion CO_2 capture process.

1.7 Outline of the Research

This research focuses on measuring density and viscosity of MEA (Monoethanol amine) + H_2O + CO_2, AMP (2-Amino-2-methyl-1-propanol) + MEA + H_2O + CO_2, MDEA (N-methyldiethanolamine) + H_2O, DEEA (2-(diethylamino)ethanol) + H_2O, DMEA (2-(dimethylamino)ethanol) + H_2O, MDEA + MEA + H_2O, DMEA + MEA + H_2O and DEEA + MEA + H_2O mixtures at different temperatures, amine and CO_2 concentrations. Empirical correlations were developed for both density and viscosity data and Eyring's viscosity model was adopted to evaluate free energy of activation for viscous flow. The uncertainty of density and viscosity measurements was evaluated using the GUM

approach and uncertainty of viscosity measurement was compared with the MCS method. The propagation of uncertainty of physical properties in mass transfer coefficient and interfacial area correlations was investigated using the MCS method. Finally, equilibrium-based and rate-based approaches were adopted to simulate absorber column operated with aqueous MEA and the removal efficiencies and physical property predictions with experiments were done in the laboratory CO_2-rig.

2 Literature Review

This chapter presents literature of amine technology, physical properties of different amine solutions such as density and viscosity with reported correlations, applicability to use Artificial Neural Networks to represent physical properties and process simulations of post-combustion capture.

2.1 Amine Technology

2.1.1 Process Description of Amine Based CO_2 Capture from Flue Gas

The process of amine-based PCC is consisting of several mass and heat transfer operations. Primarily there is a process of chemical absorption of CO_2 into the aqueous amine solution. Figure 2.1 illustrates the process flow of a general CO_2 capture process, which is used for the CO_2 removal from flue gas.

The flue gas coming from the power plant with the pressure close to atmospheric pressure [29] is sent to the absorber column bottom. The CO_2-lean aqueous amine solution comes to the top of the absorber and they meet countercurrently. There is a mass transfer across the gas/liquid interface in that CO_2 in the flue gas migrate into the CO_2-lean amine solution. The concentration difference of CO_2 between the flue gas stream and the solution is the main driving force for the mass transfer. CO_2 reacts with amine and forms several species of carbamate, carbonate and bicarbonate. The carbamate formation varies depending on the type of amine used as the solvent. Then the CO_2-rich amine solution goes through the lean/rich heat exchanger to increase the stream temperature before it goes to the desorber. It is an advantage to save some energy through this heat exchanger to reduce the overall energy demand of the process. The captured CO_2 is released in the desorber/stripper column. Heat is given through the reboiler to reverse the carbamate formation reaction to release CO_2. The typical operating conditions for aqueous MEA solvent is 115-120 °C at the stripper bottom. Desorption is an energy-intensive process, which represent up to 70-80% of the plant operational cost [26, 30].

The liquid stream coming out from the desorber contains CO_2-lean amine solution at a high temperature. The stream is sent through the lean/rich heat exchanger to recover some of the heat before it is recycled back into the absorber. The CO_2 taken out from the desorber needs to be compressed and transported to the storage facility. In commercial scale, tanks, pipelines and ships are used for gaseous and liquid CO_2. For pipelines, the operating pressures are between 10 to 80 MPa [5]. CO_2 has to be compressed up to 150-250 bars prior to export [31]. CO_2 has been used in various sectors including chemical and oil, food, mineralization, power and pharmaceutical [32]. In the oil industry, EOR application has a high demand for CO_2. The purity of CO_2 is crucial in the industries of food and pharmaceutical.
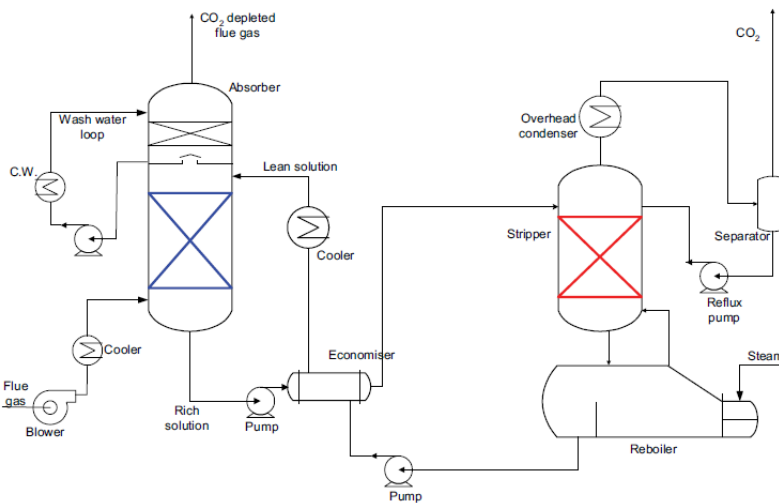
Figure 2.1: Post-combustion CO_2 capture process with absorption and desorption: Svendsen and Eimer [33]

2.1.2 Amine as an Absorbent

The use of amine in the removal of acid gas of CO_2, H_2S and other sulphur species from natural gas is a well-established chemical absorption technology [34, 35]. The general formula of the amine is $NR_1R_2R_3$ where R_1, R_2 and R_3 can be either hydrogen or hydrocarbon groups. Primary amines with general formula NH_2R are considered as the most reactive amines, followed by secondary (NHR_1R_2) and tertiary amines ($NR_1R_2R_3$) [35]. Alkanolamines are commonly used in acid gas treating due to the enhanced water solubility and reduced volatility from the hydroxyl group [36]. MEA (monoethanol amine, $H_2NC_2H_4OH$) is a primary amine with a high absorption rate, it is relatively cheap and relatively low hazardous to the environment compared to other amines [29]. The chemical absorption with MEA has been highly studied through laboratory experiments and process simulations for CO_2 removal from flue gas. MEA is regarded as the benchmark solvent of PCC to evaluate other potential absorbents by considering the different characteristics of the absorption rate of CO_2, absorption capacity, degradation and corrosion. The main drawbacks of MEA are its high regeneration energy due to the stable carbamate formation during the reaction with CO_2, oxidative and thermal degradation and a high corrosion tendency. Typical process parameters of MEA in acid gas treating are shown in Table 2.1.

DEA (diethanol amine) is a secondary amine with a high CO_2 absorption rate [37]. The regeneration energy of DEA is less compared to MEA but DEA has a lower absorption rate than that of MEA [35]. Aqueous DEA solvent is not considered as the best choice for CO_2 capture due to the irreversible side reactions and formation of corrosive products.

Table 2.1: Operating parameters for MEA system [35].

Operating parameter	
wt% (weight percentage)	15 to 25
Rich amine acid gas loading (mol acid gas $\cdot$ mol MEA^{-1})	0.45 to 0.52
Acid gas pickup (mol acid gas $\cdot$ mol MEA^{-1})	0.33 to 0.4
Lean solution residual acid gas (mol acid gas $\cdot$ mol MEA^{-1})	0.12 $\pm$

Tertiary amines have gained higher attention as they show several characteristics that are in favour of optimizing the CO_2 capture process. Tertiary amines have a low energy demand for the regeneration and higher absorption capacity compared to other amines [38]. The reaction between CO_2 and aqueous tertiary amines reveal a high CO_2 loading value of up to 1 mol CO_2 / mol amine as it does not form carbamate as primary and secondary amines [39]. Since there is no hydrogen atom attached to the nitrogen atom, the carbamation reaction cannot take place. This leads to the formation of bicarbonate that releases lower heat than that of carbamate formation [40]. The rate of CO_2 absorption is low in tertiary amines compared to primary and sterically hindered amines [41]. MDEA (N-methyldiethanolamine) is the most used tertiary amine in acid gas removal [29].

The use of one amine with H_2O as a solvent cannot fulfil all requirements that are favourable in PCC. The aqueous blends of primary, secondary with tertiary amine are studied to achieve an acceptable level of CO_2 absorption rate, absorption capacity and low energy demand to make this technology more economically feasible for PCC [38, 42-44].

2.1.3 CO_2 Absorber

The chemical absorption of CO_2 into amine takes place in the absorber. The absorber can either consist of plates or packing materials. In acid gas treating, a column with structured packing is preferred owing to high efficiency, high capacity and low pressure drop [29]. The exothermic reaction between the amine and CO_2 results in high temperature at the bottom compared to the top. These temperature variations affect the physicochemical properties of amine + H_2O + CO_2 system. Svendsen and Eimer [33] demonstrate the variations of gas and liquid temperature, CO_2 loading, mole fraction and partial pressure in an absorber through simulations as shown in Figure 2.2. The effect of CO_2 loading on physical properties of density, viscosity and surface tension has been widely studied for various amine, water mixtures for years. This results in variations of overall mass transfer between gas and liquid interface along the absorber column. It is common practice to use an average overall mass transfer coefficient in the absorber design, but this can lead to high uncertainty in the characteristics of the column such as packing height, column diameter and pressure drop. This issue has been addressed by Nookuea, et al. [45] who suggested an optimized design procedure for absorbers in PCC to reduce the uncertainty. A detailed analysis of uncertainties related

to absorber design, cost estimation and physical properties has been discussed by Øi [29]. Karunarathne, et al. [46] studied the propagation of uncertainty of physical properties through the mass transfer and interfacial area correlations. Still, there is a research gap to fill by analysing the propagation of uncertainty of physical properties through the mass transfer and interfacial area correlations in the design calculations of packed bed height and column diameter calculations.
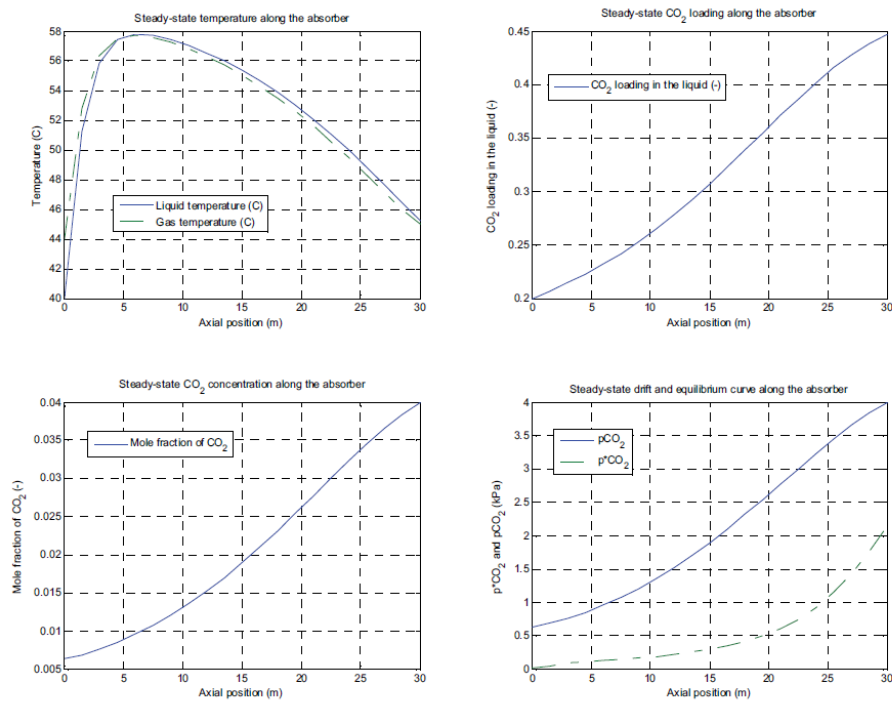
Figure 2.2: Variation of the gas and liquid temperature, CO_2 loading, mole fraction and partial pressure in an absorber: Svendsen and Eimer [33]

2.1.4 CO_2 Desorber

The reboiler applies heat to reverse the carbamate formation reaction to release CO_2 into the gas phase. The operating temperature and pressure of the desorber depend on the type of amine that is used in the absorption desorption cycle. For an aqueous MEA system, it is rather high as 120 °C [47] due to the high heat of reaction between MEA and CO_2. The theoretical background of chemical desorption and the required conditions of chemical absorption theory to apply on chemical desorption were discussed by Astarita and Savage [48]. The experimental study performed by Jamal, et al. [49], [50] revealed the possibility to use desorption experimental data to determine forward and backward rate constants. An Aspen Plus simulation model for 30 mass% MEA was built and validated using experimental data by Garcia, et al. [51] to predict stripped CO_2 and loading of the CO_2-lean solution.

2.2 Amine Reaction with CO2 and Its Mechanisms

The chemistry of CO2 with primary, secondary and tertiary amines in aqueous solutions has been discussed in the literature and several reaction mechanisms were also proposed to understand the reaction between CO2 and aqueous amines. Primary and secondary amines are separately discussed from tertiary amines since the reaction mechanisms are different [31].

The reaction between CO2 with water forms carbonic acid and it is involved in two protonation equilibria [52]. The reaction has two reversible pathways of formation of bicarbonate and Brønstedt acid-base interaction between the carbonic acid and amine.

$$H_2CO_3 \leftrightarrow HCO_3^- + H^+ \tag{R1}$$

$$RNH_2 + H^+ \leftrightarrow RNH_3^+ \tag{R2}$$

In carbamate formation, there are at least two different reaction paths of amine reaction with carbonic acid and with dissolved CO2.

$$2RNH_2 + H_2CO_3 \rightleftharpoons RNHCO_2^- + RNH_3^+ + H_2O \tag{R3}$$

$$2RNH_2 + CO_{2(aq)} \rightleftharpoons RNHCO_2^- + RNH_3^+ \tag{R4}$$
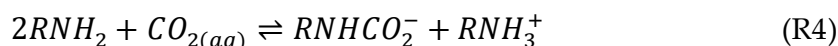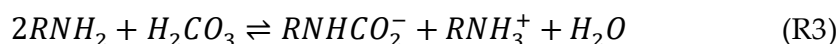
The formation of carbamate is the most important in CO2 with amine reaction. The Zwitterion mechanism is considered as the most prominent mechanism in which a zwitterion forms through the reaction of amine and CO2. This zwitterion further reacts with a base (B) by exchanging a proton to form the carbamate.

$$CO_2 + R_1R_2NH \leftrightarrow R_1R_2N^+HCOO^- \tag{R5}$$

$$R_1R_2N^+HCOO^- + B \leftrightarrow BH^+ + R_1R_2NCOO^- \tag{R6}$$
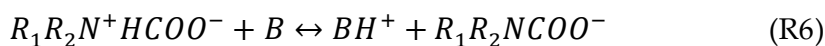
Termolecular mechanism of Crooks and Donnellan (1989) [53] and Australian approach [31, 54] are other suggested mechanisms to explain reaction between CO2 and amine.

2.3 Physical Properties

2.3.1 Density

Density is a characteristic property of a substance defined by mass per volume. It is important to understand the pressure and temperature dependence of the density of both pure and liquid mixtures. Typically, density increases with increasing pressure and it decreases with increasing temperature.

The density of a real liquid mixture deviates from an ideal liquid mixture due to the intermolecular attraction between component molecules. This deviation is discussed in the term of excess molar volume V^E of the liquid mixture. Then the mixture density is described by using excess molar volumes and molar volumes of the pure substances as given in Eq (1).

$$\rho = \frac{\sum_1^2 x_i \cdot M_i}{V^E + \sum_1^2 \frac{x_i \cdot M_i}{\rho_i}} \tag{1}$$

The mathematical relationship based on thermodynamics for the excess molar volumes enables to analyse measured density under different solution compositions. The excess molar volume V^E is defined as

$$V^E = V - x_1 V_1^0 - x_2 V_2^0 \tag{2}$$

$$V^E = \frac{[x_1 M_1 + x_2 M_2]}{\rho} - \frac{x_1 M_1}{\rho_1} - \frac{x_2 M_2}{\rho_2} \tag{3}$$

Several reasons can be discussed for the rise of V^E in a liquid mixture. Generally, three types of interactions between components are considered in a liquid mixture [55]: (1) physical interactions due to the dispersion forces or weak dipole-dipole interaction. This makes a positive (+ Ve) contribution signifying an expansion the mixture, (2) specific or chemical interactions including charge transfer, forming of H-bonds and other complex-forming interactions with a negative (–Ve) contribution, and (3) differences in size and shape of the component molecules in the mixture provide a structural contribution by arranging within the vacant spaces in each other's structure by giving a negative (–Ve) contraction.

The theory of Prigogine-Flory-Patterson attempts to illustrate molecular interactions that result in V^E of molecules which differ in size and shape. There, V^E is divided into interactional contribution, a free volume contribution and a pressure contribution [56, 57].

Algebraic representation of the thermodynamic properties of nonelectrolyte solutions is discussed by Redlich and Kister [58]. It is easily understandable and has been applied on many occasions for various liquid mixtures. There, the excess molar volume is presented in a power series for a binary mixture as follows

$$V^E = x_2(1 - x_2) \sum_{i=0}^{i=n} A_i (1 - 2x_2)^i \tag{4}$$

The partial molar volume describes the contribution made by a substance in a mixture to the overall volume of the solution.

$$\overline{V_i} = \left(\frac{\partial V}{\partial n_i}\right)_{T,p,n_j} \qquad (5)$$

A relation between partial molar volumes and excess molar volumes of MEA solution can be developed using Eq (2) and Eq (5) via differentiation and algebra.

$$\overline{V_1} = V^E + V_1^0 - x_2\left(\frac{\partial V^E}{\partial x_2}\right)_{T,p} \qquad (6)$$

$$\overline{V_2} = V^E + V_2^0 - (1-x_2)\left(\frac{\partial V^E}{\partial x_2}\right)_{T,p} \qquad (7)$$

Eq (6) and (7) can be further simplified by substituting the differential form of Eq (4) on the derivative term of excess volume with respect to the mole fraction of Eq (6) and (7). The details of this calculation can be found in Maham, et al. [59].

2.3.2 Density Meters

Different methods are available to measure the density of liquids. The accuracy of the measurement varies with the adopted method. Hydrometers are low in cost and simple to use. They are easily broken, requires a high volume of sample to perform the measurement, a high volume of solvent to clean the instrument and has low accuracy. Pycnometers are highly used in both research and industry. It has advantages and disadvantages similar to hydrometers. Oscillation-type density meters provide high accuracy. Additionally, it has a range of advantages like easy to operate, low sample required, a low solvent volume required for the cleaning and they are easy to clean.

2.3.3 Density of Amine + H_2O + CO_2 Mixtures

In this section, the focus is given to amines of pure MEA, AMP (2-amino-2-methyl-1-propanol), MDEA, DEEA (2-(diethylamino)ethanol) and DMEA (2-(dimethylamino)ethanol) and their mixtures. The literature of measured density is tabulated with relevant references and conditions. The relevant correlations for the pure amines, aqueous amine and CO_2 loaded aqueous amines are tabulated and the limitations are discussed as stated by the authors.

2.3.3.1 Density Measurements

The density of pure primary, secondary and tertiary amines are discussed for many occasions in various studies. Even though the applicability of aqueous anime mixtures is considered in PCC, pure liquid data can be beneficial in building density correlations. The aim is to tabulate the available sources of density measurement of pure, aqueous

and CO_2 loaded aqueous amine solutions that are relevant for this project. Table 2.2 lists the source for the measured density of pure MEA with relevant temperature ranges and instrument used. Abundant resources available for pure MEA with different measuring techniques, but existing sources are inadequate for the density of aqueous and CO_2 loaded aqueous MEA solutions.

Table 2.2: Density measurements: Pure MEA.

Source	Temperature (K)		No of points	Method
	Low	High		
Touhara, et al. [60]	298.15		1	-
Yang, et al. [61]	293.15	343.15	6	Anton Paar (DMA 5000M)
Li and Shen [62]	303.15	353.15	8	Gay-Lusac pycnometer
Wang, et al. [63]	293.45	360.65	5	Pycnometer
DiGuilio, et al. [64]	294.4	431.3	8	Pycnometer
Page, et al. [65]	283.15	313.15	3	Flow densimeter (picker)
Maham, et al. [59]	298.15	353.15	5	Anton Paar (DMA 45)
Guevara and Rodriguez [66]	298.15	333.15	8	Sodev 03D vibrating densimeter
Lee and Lin [67]	303.15	323.15	3	Pycnometer
Song, et al. [68]	303.15	343.15	5	Pycnometer
Kapadi, et al. [69]	303.15	318.15	4	Anton Paar (DMA 5000)
Islam, et al. [70]	293.15		1	Pycnometer
Valtz, et al. [71]	281.15	353.15	37	Anton Paar (DMA 5000)
Geng, et al. [72]	288.15	323.15	8	Pycnometer
Pouryousefi and Idem [73]	295.15	333.15	4	Anton Paar (DMA 4500/DMA 5000)
Amundsen, et al. [74]	298.15	353.15	5	Anton Paar (DMA 4500)
Taib and Murugesan [75]	303.15	353.15	6	Anton Paar (DMA 5000)
Taib and Murugesan [76]	293.15	353.15	16	Anton Paar (DMA 5000M)
Han, et al. [77]	298.15	423.15	20	Anton Paar (DMA 4500/DMA HP)
Abuin, et al. [78]	298.15		1	Anton Paar (DSA 5000)
Yang, et al. [61]	293.15	343.15	6	Anton Paar (DMA 5000M)
Xu, et al. [79]	293.15	333.15	5	Anton Paar (DMA 5000)

Table 2.3 lists sources for the measured density of aqueous MEA with relevant temperature ranges and concentrations. Literature report the concentration as a mole fraction of the MEA and water or mass percentage of the mixture.

Table 2.3: Density measurements: MEA + H_2O mixtures.

Source	Concentration: mass% MEA		Temperature (K)		No of points
	Low	High	Low	High	
Weiland, et al. [80]	10	40	298.15		4
Amundsen, et al. [74]	20	90	298.15	353.15	30
Han, et al. [77]	30	90	298.15	423.15	140
Hartono, et al. [81]	6.2	30	293.15	353.15	15
Mandal, et al. [82]	30		293.15	323.15	7
Li and Lie [83]	20		303.15	353.15	6
Zhang, et al. [84]	30		298.15	353.15	9
	Concentration: x_1[a] MEA		Temperature (K)		No of points
Page, et al. [65]	0.00118	0.99695	283.15	313.15	62
Maham, et al. [59]	0.0054	0.9660	298.15	353.15	100
Lee and Lin [67]	0.1000	0.9000	303.15	323.15	27
Kapadi, et al. [69]	0.1122	0.8486	303.15	383.15	32
Pouryousefi and Idem [73]	0.0155	0.9192	295.15	333.15	80

x_1[a] = mole fraction of amine

Table 2.4: Density measurements: MEA + H_2O + CO_2 mixtures.

Source	Concentration: mass% MEA in (MEA + H_2O) solutions		CO_2 loading α (mol CO_2/mol MEA)		Temperature (K)	No of points
	Low	High	Low	High		
Weiland, et al. [80]	10	40	0.05	0.5	298.15	40
Amundsen, et al. [74]	20	40	0.1	0.5	298.15-353.15	68
Han, et al. [77]	30	60	0.1	0.56	298.15-423.15	240
Jayarathna, et al. [36]	20	70	0.1	0.5	303.15-333.15	144
Jayarathna, et al. [85]	80		0.07	0.51	313.15-343.15	64
Hartono, et al. [81]	6.2	30	0.1	0.5	293.15-353.15	68
Zhang, et al. [84]	30		0.14	0.49	298.15-353.15	33

The density of CO_2 loaded solutions is important especially in the design of process equipment and mathematical modelling and simulations. Variations of density with CO_2 loading affect the physical and chemical properties of the solvent. The literature available for CO_2 loaded aqueous MEA is given in Table 2.4.

Similar to the MEA, measured density for pure, aqueous and CO_2 loaded aqueous mixtures of MDEA, AMP, DEEA and DMEA were gathered. Accordingly, Table 2.5, 2.8, 2.10 and 2.13 show the literature found for the density of pure MDEA, AMP, DEEA and DMEA respectively. Table 2.6, 2.9, 2.11 and 2.14 show the literature found for the density of MDEA + H_2O, AMP + H_2O, DEEA + H_2O and DMEA + H_2O mixtures respectively. Further, Table 2.7, 2.12 and 2.15 show the literature found for the density of MDEA + H_2O + CO_2, DEEA + H_2O + CO_2 and DMEA + H_2O + CO_2 mixtures respectively.

Table 2.5: Density measurements: Pure MDEA.

Source	Temperature (K)	No of points	Method
DiGuilio, et al. [64]	293.1 – 424.1	10	Pycnometer
Han, et al. [86]	298.15 – 423.15	20	DMA 4500 / DMA HP
Maham, et al. [87]	298.15 – 353.15	7	DMA 45
Hawrylak, et al. [88]	298.15 – 318.15	3	SODEV Model-02D / DMA 45 Anton Paar
Chowdhury, et al. [89]	303.15 – 323.15	5	Pycnometer
Pouryousefi and Idem [73]	295.15-333.15	4	Anton Paar (DMA 4500/DMA 5000)
Li and Shen [62]	303.15-353.15	8	Gay-Lusac pycnometer
Al-Ghawas, et al. [90]	288.15-333.15	10	Gay-Lusac pycnometer
Wang, et al. [63]	292.85-361.35	5	Pycnometer
Henni, et al. [91]	298.15-343.15	5	DMA 45
Aguila-Hernández, et al. [92]	313.15-333.15	3	DMA 45
Paul and Mandal [93]	288-333	3	Gay-Lusac pycnometer
Rebolledo-Libreros and Trejo [94]	313.15-333.15	3	Sodev 03D vibrating tube densimeter
Bernal-García, et al. [95]	283.15-363.15	17	DMA 5000
Pinto, et al. [96]	293.15-353.15	6	DMA 4500M

Table 2.6: Density measurements: MDEA + H₂O mixtures.

Source	Concentration: mass% MDEA		Temperature (K)		No of points
	Low	High	Low	High	
Li and Lie [97]	20	30	303.15	333.15	8
Han, et al. [86]	30	90	298.15	423.15	140
Al-Ghawas, et al. [90]	10	50	288.15	333.15	50
Rinker, et al. [98]	10	50	333.15	373.15	15
Muhammad, et al. [99]	32.28	48.80	298.15	338.15	9
Welsh and Davis [100]	50		283.15	353.15	5
Mandal, et al. [82]	30		293.15	323.15	7
	Concentration: x_1[a] MDEA		Temperature (K)		No of points
Bernal-García, et al. [95]	0.0604	0.7430	313.15	363.15	28
Pinto, et al. [96]	0.04466	0.90136	293.15	353.15	55
Maham, et al. [87]	0.0079	0.9475	298.15	353.15	112
Hawrylak, et al. [88]	0.0050	0.9800	298.15	318.15	72

x_1[a] = mole fraction of amine

Table 2.7: Density measurements: MDEA + H₂O + CO₂ mixtures.

Source	Concentration: mass% MDEA in (MDEA + H₂O) solutions		CO₂ loading: α (mol CO₂/mol MDEA)		Temperature (K)	No of points
	Low	High	Low	High		
Weiland, et al. [80]	30	60	0.05	0.64	298.15	44
Han, et al. [86]	30	40	0.1	0.5	298.15-423.15	57
Pinto, et al. [96]	23.8	50	0.04	0.4	293.15-3533.15	45

Table 2.8: Density measurements: Pure AMP.

Source	Temperature (K)	No of points	Method
Li and Lie [83]	303.15-353.15	6	Pycnometer
Xu, et al. [101]	305.05-363.85	6	Pycnometer
Aguila-Hernández, et al. [92]	313.15-333.15	3	DMA 45
Zhang, et al. [102]	303.155-353.147	11	DMA 5000

Table 2.9: Density measurements: AMP + H_2O mixtures.

Source	Concentration: mass% AMP		Temperature (K)		No of points
	Low	High	Low	High	
Xu, et al. [101]	9.05	88.32	293.15	363.85	35
Welsh and Davis [100]	50		283.15	333.15	6

Zúñiga-Moreno, et al. [103], [104] measured the density of AMP + H_2O mixtures for the temperature range from 313.06 K to 362.65 K at higher pressures from 1 MPa to 24 MPa using a VTD, Anton Paar DMA 60/512P density meter.

Table 2.10: Density measurements: Pure DEEA.

Source	Temperature (K)	No of Points	Method
Hawrylak, et al. [88]	298.15-318.15	3	SODEV Model-02D / DMA 45 Anton Paar
Lebrette, et al. [105]	278.15-353.15	7	DMA 45 Anton Paar
Zhang, et al. [106]	293.15-313.15	4	DMA 602 Anton Paar
Pinto, et al. [96]	293.15-353.15	6	DMA 4500M Anton Paar

Table 2.11: Density measurements: DEEA + H_2O mixtures.

Source	Concentration: x_1[a] DEEA		Temperature (K)		No of points
	Low	High	Low	High	
Hawrylak, et al. [88]	0.0053	0.9835	298.15	318.15	75
Lebrette, et al. [105]	0.0039	0.9544	278.15	353.15	133
Zhang, et al. [106]	0.0281	0.9949	293.15	313.15	92
Pinto, et al. [96]	0.05580	0.98365	293.15	353.15	106
	Concentration: mass% DEEA		Temperature (K)		No of points
Zhang, et al. [84]	15	45	298.15	353.15	21

x_1[a] = mole fraction of amine

Table 2.12: Density measurements: DEEA + H₂O + CO₂ mixtures.

Source	Concentration: mass% DEEA in (DEEA + H₂O) solutions		CO₂ loading α (mol CO₂/mol DEEA)		Temperature (K)	No of points
	Low	High	Low	High		
Pinto, et al. [96]	24	61	0.14	0.79	293.15-343.15	56
Zhang, et al. [84]	15	45	0.26	0.83	298.15-353.15	69

Table 2.13: Density measurements: Pure DMEA.

Source	Temperature (K)	No of points	Method
Zhang, et al. [106]	293.15-313.15	4	DMA 602 Anton Paar
Maham, et al. [107]	278.15-353.15	7	DMA 45 Anton Paar
Chowdhury, et al. [108]	303.15-323.15	5	Pycnometer (MBL)
Bernal-García, et al. [109]	293.15-363.15	15	DMA 500 Anton Paar
Hawrylak, et al. [88]	298.15-318.15	3	SODEV Model-02D / DMA 45 Anton Paar
Zhang, et al. [84]	298.15-353.15	7	DMA 5000M
Idris, et al. [110]	293.15-343.15	11	DMA 4500 Anton Paar
Pinto, et al. [96]	293.15	6	DMA 4500M Anton Paar

Table 2.14: Density measurements: DMEA + H₂O mixtures.

Source	Concentration: x_1 [a] DMEA		Temperature (K)		No of points
	Low	High	Low	High	
Zhang, et al. [106]	0.0041	0.9705	293.15	313.15	84
Maham, et al. [107]	0.0059	0.9545	278.15	353.15	126
Chowdhury, et al. [108]	0.0135	0.9046	303.15	323.15	75
Bernal-García, et al. [109]	0.0121	0.8950	293.15	363.15	159
Hawrylak, et al. [88]	0.0247	0.9846	298.15	318.15	60
Pinto, et al. [96]	0.18168	0.97986	293.15	353.15	66
	Concentration :mass% DMEA		Temperature (K)		No of points
Zhang, et al. [84]	15	45	303.15	353.15	18
Idris, et al. [110]	10	90	293.15	343.15	88

x_1 [a] = mole fraction of amine

Concepción, et al. [111] measured the density of DMEA + H_2O mixtures at elevated pressures from 0.1 MPa to 140 MPa using a density meter DMAHPM from Anton Paar.

Table 2.15: Density measurements: DMEA + H_2O + CO_2 mixtures.

Source	Concentration: mass% DMEA in (DMEA + H_2O) solutions		CO_2 loading α (mol CO_2/mol DMEA)		Temperature (K)	No of points
	Low	High	Low	High		
Zhang, et al. [84]	15	45	0.08	0.83	303.15-353.15	45
Idris, et al. [110]	30		0.1	0.54	293.15-343.15	55

2.3.3.2   Density Correlations

Table 2.16 gives an overview of the correlations developed and used to fit density of pure amine, aqueous amine and CO_2 loaded aqueous amine solutions. A polynomial relation as shown in Eq (8) is the easiest way to correlate density data with respect to temperature. This correlation is more suitable to fit densities of pure substances rather than mixtures. This approach has been adopted in many occasions to correlate density of pure MEA [36], AMP [101], DEEA [84], MDEA [90] and DMEA [84, 110]. An empirical correlation that is based on critical temperature of pure MEA ($T_c = 678.2\,K$) was suggested by Valtz, et al. [71] as given in Reid, et al. [112]. The correlation that was used to fit measured density data is shown in Eq (9).

For aqueous amine mixtures, the correlations based on the excess volume of mixtures are commonly used. The expressions that are given earlier in Eq (2) and Eq (3) were adopted to calculate the excess volume of binary mixtures and fit a Redlich – Kister polynomial as given in Eq (4) with parameters having temperature dependency. Then the density of the mixture is calculated by the expression shown in Eq (1). For MEA + H_2O mixtures Amundsen, et al. [74] and Lee and Lin [67] fitted density data according to the Redlich – Kister polynomial. The study performed by Han, et al. [77] extended the range of measured density data up to 423.15 K and fitted a correlation as given in Eq (4). Hartono, et al. [81] adopted the same approach of fitting density data by using a correlation that is based on excess volumes. This correlation is similar to the Redlich – Kister type polynomial but has less number of parameters as given in Eq (10) with acceptable accuracy. Yang, et al. [61] suggested a similar correlation for the excess volume of MEA + H_2O mixtures as shown in Eq (11). Maham, et al. [59], [105, 107] used measured densities of MEA + H_2O, DEEA + H_2O and MDEA + H_2O mixtures to determine excess volumes and correlated using the Redlich – Kister polynomial. This study also evaluated the partial molar volumes of the binary mixtures. The correlation developed for excess molar volume can be used to evaluate the density of the mixtures.

The pressure and temperatures effect on the density of MEA + H_2O mixtures were studied by Sobrino, et al. [113]. A modified Tammann-Tait equation as given in Eq (12) was suggested to correlate measured densities at different pressures, temperatures and compositions.

For the density of CO_2 loaded aqueous MEA and CO_2 loaded aqueous MDEA mixtures, Licht and Weiland proposed a model in 1989 to predict the density of aqueous amines including MEA Eq (13). Weiland, et al. [114] proposed a correlation to fit the measured data as shown from Eq (14) to Eq (17). There, the dissolved CO_2 is presented as unreacted and mole fractions of amine, H_2O and CO_2 were calculated accordingly. Hartono, et al. [81] developed a correlation as given from Eq (18) to Eq (20), which required the density of MEA + H_2O mixtures to calculate the density of CO_2 loaded aqueous MEA solutions. Shokouhi, et al. [115] suggested a Setschenow type correlation as shown in Eq (21) and Eq (22) to fit measured densities of CO_2 loaded aqueous MDEA. The Setschenow type correlation has been adopted for correlating density, viscosity, surface tension, heat capacity, thermal diffusivity and thermal conductivity [115, 116]. Zhang, et al. [84] correlate measured densities of CO_2 loaded DMEA + H_2O as given in Eq (23) and Eq (24). Idris, et al. [110] correlate densities of CO_2 loaded DMEA + H_2O using the correlation proposed by Weiland, et al. [114]. For the CO_2 loaded DEEA + H_2O, Zhang, et al. [84] used the same correlations mentioned in Eq (23) and Eq (24).

Table 2.16: Overview of the density correlations.

Correlation	
$\rho = a_1 + a_2 T + a_3 T^2$	(8)
$\rho = \dfrac{A}{B^{\left[1+\left(1-\frac{T}{T_C}\right)^C\right]}} \times \dfrac{M_i}{1000}$	(9)
$V^E = x_1 x_2 \cdot 10^{-6} \cdot (A_0 + A_1 t + A_2 x_1 + A_3 x_1^2)$	(10)
$V^E = x_1 x_2.(A_0 + A_1 T + A_2 x_1)$	(11)
$\rho(T,p) = \dfrac{A_0 + A_1 T + A_2 T^2}{1 - C\, ln\left(\dfrac{B_0 + B_1 T + B_2 T^2 + p}{B_0 + B_1 T + B_2 T^2 + 0.1 MPa}\right)}$	(12)
$\dfrac{1}{\rho} = u_w V_w^0 e^{[\beta_w (T-T_0)]} + u_{A_1} V_{A_1}^0 e^{[\beta_{A_1}(T-T_0)]} + u_{A_2} V_{A_2}^0 e^{[\beta_{A_2}(T-T_0)]}$ $+ w_{CO_2} V_{CO_2}^0 e^{[\beta_{CO_2}(T-T_0)]}$	(13)
$\rho = \dfrac{x_1 M_1 + x_2 M_2 + x_3 M_3}{V}$	(14)
$V = x_1 V_1 + x_2 V_2 + x_3 V_3 + x_1 x_2 V^* + x_1 x_3 V^{**}$	(15)
$V_1 = \dfrac{M_1}{aT^2 + bT + c}$	(16)
$V^{**} = d + e x_1$	(17)
$\rho_{loaded} = \dfrac{\rho_{unloaded}}{1 - w_{co2added}(1 - \Phi^3)}$	(18)
$w_{co2added} = \dfrac{\alpha x_1 M_3}{x_1 M_1 + (1 - x_1 - \alpha x_1) M_2 + \alpha x_1 M_3}$	(19)
$\Phi = \dfrac{a_1 x_1 \alpha + a_2 x_1}{a_3 + x_1}$	(20)
$ln\left(\dfrac{\rho_{loaded}}{\rho_{unloaded}}\right) = \sum_{i=1}^{2} A_i \alpha^i$	(21)
$A_i = a_{i,0} + a_{i,1} T$	(22)
$\rho(T, w_2, \alpha) = \rho_0(T, w_2)(1 + d\alpha w_2)$	(23)

$$x_2 = w_2[w_2 + (1 - w_2)(M_2/M_1)]^{-1} \tag{24}$$

2.3.4 Viscosity

Viscosity is referred to as the internal fluid friction or the resistance to deformation by applied stress [117]. The collision and interaction among fluid molecules signify the viscosity that makes it difficult to form a generalized theoretical approach that suits all scenarios. Poling, et al. [117] stated about the absence of a comparable theoretical basis for the estimation of liquid viscosity and it is recommended to determine liquid viscosities through experimental data.

Isaac Newton (1643-1727) initially proposes the concept of viscosity by relating the shear stress and velocity gradient of fluid flow [118]. It is the ratio of shear stress per unit area to velocity gradient as shown in Eq (25).

$$\tau_{yx} = -\eta \frac{dv_x}{dy} \tag{25}$$

Viscosity is a transport property in a fluid that is used to characterise the behaviour of the fluid. Several factors such as shear rate, temperature, pressure, moisture and concentration have effects on liquid viscosity [119]. In chemical engineering applications, viscosity data of pure and liquid mixtures are important in the design and optimization of industrial processes. The viscosity coefficient appears in heat and mass transfer correlations of packing materials that are used in the design of absorption columns and heat transfer correlations involved in heat exchanger design. Theoretical derivations for viscosity are limited for certain special scenarios. This literature study discusses such theoretical models, semi-theoretical and empirical models or correlations for pure and liquid mixtures.

Monnery, et al. [120] critically reviewed the predictive and correlative methods of viscosity for pure component and mixtures of dilute gases, dense gases and liquids.

2.3.4.1 Theoretical models

The foundation for most of the theoretical models for dense gas or liquid phase transport properties is statistical mechanics in which thermodynamics and transport properties are described in terms of distribution functions [120]. Kirkwood, et al. [121] derived an expression for viscosity by relating the momentum flux through velocity averages to the distribution function as given in Eq (26)

$$\eta = \frac{\rho mkT}{2\zeta} + \frac{\pi\zeta}{15kT}\rho^2 \int_0^\infty \frac{d\varphi(r)}{dr} g(r)\Psi_2(r) r^3 dr \tag{26}$$

As described by Monnery, et al. [120], the complexities and uncertainties involved in this method with obtained results make it inefficient in engineering applications. Semi-theoretical and empirical models are attractive in engineering applications as they are easy to understand and can be easily implemented in a computer program for process simulations.

2.3.4.2 Semi-theoretical models

2.3.4.2.1 Reaction rate theory

Eyring [122] explained the mechanism of fluid friction or the viscosity between adjacent fluid layers according to the theory of absolute rate. Individual molecules are constantly in motion in a pure liquid that is at rest. These motions are confined to vibrations of each molecule within a cage that is created by its nearest neighbours due to the closed packing of molecules [118]. The cage is represented as an energy barrier and the activation energy is discussed as the energy necessary to slip over this potential barrier to the next equilibrium position by an individual molecule in the same plane [118, 122]. Figure 2.3 illustrates the change of energy in the molecule while moving in the x direction by overcoming the potential barrier.
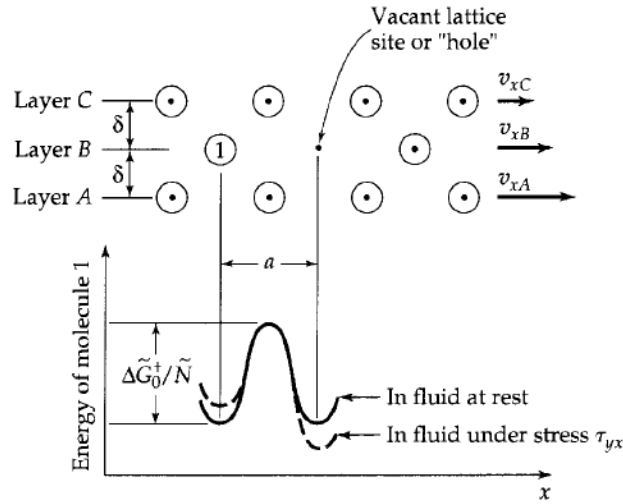
Figure 2.3: Demonstration of an escape process in the flow of a liquid. Molecule '1' has to pass through the energy barrier to reach the vacant place: Bird, et al. [118]

Eyring reveals that a liquid at rest undergoes rearrangement in which one molecule at a time escape from the cage into a vacant place known as a hole [118]. These molecular motions occur in both forward and backward directions and the frequency of molecular jumps is given by the rate equation.

$$\text{v} = \frac{kT}{h} \, exp\left(\frac{-\Delta G_o^+}{RT}\right) \tag{27}$$

When the liquid flows in x direction, the frequency of molecular rearrangements is increased. Accordingly, the potential energy barrier get effected under the applied shear stress τ_{yx} in such a way that

$$-\Delta G^+ = -\Delta G_o^+ \pm \left(\frac{a}{\delta}\right)\left(\frac{\tau_{yx}V}{2}\right) \tag{28}$$

Here the term $\pm(a/\delta)\left(\tau_{yx}V/2\right)$ represents an approximation to the work done on the molecules as they move to the top of the potential energy barrier in which positive sign is for moving with the applied shear stress and a negative sign is for moving against the applied shear stress.

The velocity gradient and the net rate r_{net} of molecular jumps are related as follows

$$-\frac{dv_x}{dy} = \frac{a}{\delta} r_{net} \tag{29}$$

The net rate r_{net} of molecular jumps can be given as

$$r_{net} = \frac{kT}{h} exp\left(\frac{-\Delta G_o^+}{RT}\right)\left(exp\left(\frac{+a\tau_{yx}V}{2\delta RT}\right) - exp\left(\frac{-a\tau_{yx}V}{2\delta RT}\right)\right) \tag{30}$$

$$r_{net} = \frac{kT}{h} exp\left(\frac{-\Delta G_o^+}{RT}\right)\left(2sinh\left(\frac{a\tau_{yx}V}{2\delta RT}\right)\right) \tag{31}$$

It is considered that $a\tau_{yx}V/2\delta RT << 1$. Then by using Taylor series, Eq (31) can be simplified as

$$r_{net} = \frac{kT}{h} exp\left(\frac{-\Delta G_o^+}{RT}\right)\left(\frac{a\tau_{yx}V}{\delta RT}\right) \tag{32}$$

Finally, the dynamic viscosity can be expressed as

$$\eta = \left(\frac{\delta}{a}\right)^2 \frac{hN}{V} exp\left(\frac{\Delta G_o^+}{RT}\right) \tag{33}$$

The term δ/a can be set equal to 1 without losing accuracy since the ΔG_o^+ is usually determined empirically by fitting Eq (33) to measured viscosity data.

The application of this model is vast and used for both pure and liquid mixture analysis. Salinas, et al. [123] adopted Eyring's theory to build a viscosity model using cubic equations of state for pure liquids. Weirong and Lempe [124] used the theory combining the cubic equation of state for the viscosities of liquid mixtures. Atashrouz, et al. [125] analysed the viscosity of ionic liquids using Eyring's theory and a modified Gibbs energy model.

McAllister developed a model to correlate kinematic viscosities based on Eyring's theory[126]. The intermolecular interactions were considered as three-body and four-body interactions and the rate of each individual interaction regarded as proportional to the energy of activation in the same way as the reaction rate of a chemical reaction. His approach is explained below.
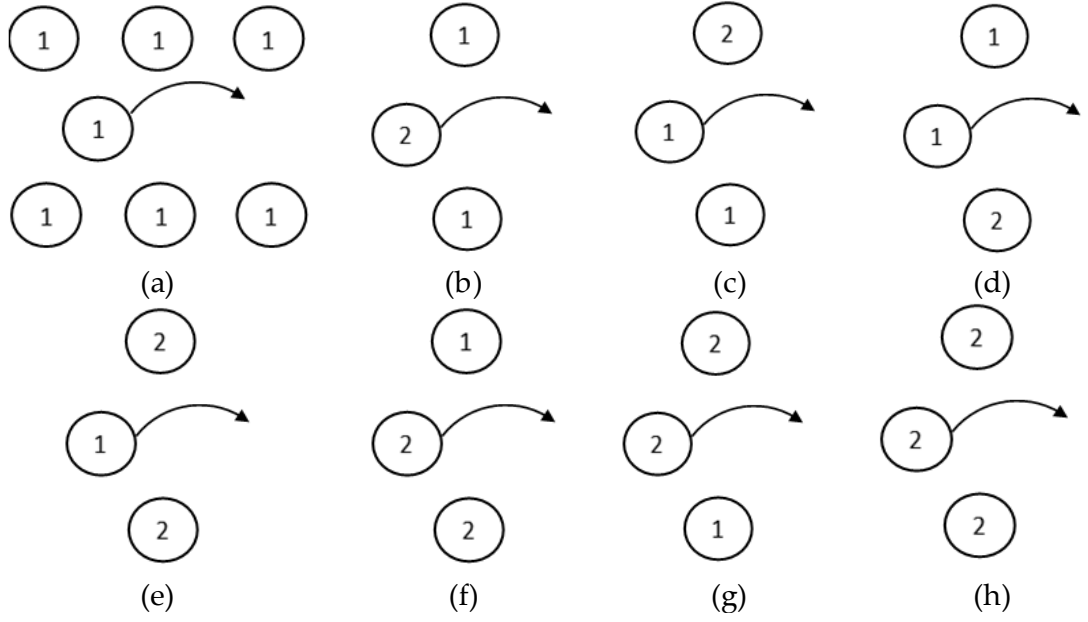
Figure 2.4: Types of interactions in a binary mixture three-body model: McAllister [126]

In a binary mixture, Figure 2.4 illustrates the viscosity interactions of the three-body model. The main assumption of the model development is that the free energy of activation for viscous flow is additive and the probability for the interactions is dependent only on the concentration and it is independent of free energy of activation. Accordingly, the free energy of activation for viscous flow is given as

$$\Delta G_o^+ = x_1^3 \Delta G_1^+ + x_1^2 x_2 \Delta G_{121}^+ + 2x_1^2 x_2 \Delta G_{112}^+ + x_1 x_2^2 \Delta G_{212}^+ + 2x_1 x_2^2 \Delta G_{122}^+ + x_2^3 \Delta G_2^+ \quad (34)$$

$$\Delta G_o^+ = x_1^3 \Delta G_1^+ + x_1^2 x_2 (\Delta G_{121}^+ + 2\Delta G_{112}^+) + x_1 x_2^2 (\Delta G_{212}^+ + 2\Delta G_{122}^+) + x_2^3 \Delta G_2^+ \quad (35)$$

Where

$$\Delta G_{12}^+ = \frac{\Delta G_{121}^+ + 2\Delta G_{112}^+}{3} \quad (36)$$

$$\Delta G_{21}^+ = \frac{\Delta G_{212}^+ + 2\Delta G_{122}^+}{3} \quad (37)$$

Corresponding kinematic viscosity can be assigned for each type of free activation energy for viscous flow.

Here, the following relation was regarded to relate free activation energy with free activation enthalpy and entropy.

$$\Delta G_o^+ = \Delta H_o^+ - T\Delta S_o^+ \quad (38)$$

Based on Eqs (33)-(38) the kinematic viscosities can be written as:

For the binary liquid mixture:

$$v = \frac{hN}{M_{avg}} e^{-\Delta s_o^+/R} e^{\Delta H_o^+/RT} \tag{39}$$

For the pure component 1: (40)

$$v_1 = \frac{hN}{M_1} e^{-\Delta s_1^+/R} e^{\Delta H_1^+/RT} \tag{41}$$

For b, c and d type interactions in Figure 2.4

$$v_{12} = \frac{hN}{M_{12}} e^{-\Delta s_{12}^+/R} e^{\Delta H_{12}^+/RT} \tag{42}$$

For e, f and g type interactions in Figure 2.4

$$v_{21} = \frac{hN}{M_{21}} e^{-\Delta s_{21}^+/R} e^{\Delta H_{21}^+/RT} \tag{43}$$

For the pure component 2:

$$v_2 = \frac{hN}{M_2} e^{-\Delta s_2^+/R} e^{\Delta H_2^+/RT} \tag{44}$$

Finally, the McAllister three-body model is derived as

$$ln(v) = x_1^3 \cdot ln(v_1) + 3x_1^2 x_2 \cdot ln(v_{12}) + 3x_1 x_2^2 \cdot ln(v_{21}) + x_2^3 \cdot ln(v_2) - ln(x_1 + x_2 \cdot [M_2/M_1]) + 3x_1^2 x_2 \cdot ln([2 + M_2/M_1]/3) + 3x_1 x_2^2 \cdot ln([1 + 2M_2/M_1]/3) + x_2^3 \cdot ln(M_2/M_1) \tag{45}$$

For molecules with different size having ratio of radius more than 1.5, three bodied interactions may not be adequate. In such cases other interactions involving more than three molecules in a three dimensional space have to be considered for better viscosity predictions.

Due to the many adjustable parameters, the McAllister's three-body and four-body interaction models become more empirical. The determination of those parameters demands experimental studies. To make McAllister's models more theoretically based, Asfour, et al. [127] suggested a method to predict model parameters from pure component properties. Accordingly, the correlation for parameters is given as

$$\frac{v_{ij}}{(v_i^2 v_j)^{1/3}} = 1 + k_1 \frac{(N_i - N_j)^2}{(N_i^2 N_j)^{1/3}} \tag{46}$$

The relation between McAllister parameters and pure component kinematic viscosities are shown as

$$v_{ji} = v_{ij} \left(\frac{v_j}{v_i}\right)^{1/3} \tag{47}$$

This method allows using the McAllister model without fitting to experimental data, the model was tested for four n-alkanes, and kinematic viscosity predictions were with AARD within 1.0%.

2.3.4.2.2 Corresponding states

The Dutch theoretical physicist van der Waals established the theory of corresponding states based on the equation of state [128]. In theory, it was shown that at the critical point

$$\left(\frac{\partial P}{\partial V}\right)_T = \left(\frac{\partial^2 P}{\partial V^2}\right)_T = 0 \tag{48}$$

Accordingly, a universal function for variables V, T and P exists as given in Eq (49) for all substances.

$$f\left(\frac{V}{V_c}, \frac{T}{T_c}, \frac{P}{P_c}\right) = 0 \tag{49}$$

Here, the subscription c refers to the critical point. The reduced properties for temperature (T_r), pressure (P_r) and volume (V_r) are stated as $T_r = \frac{T}{T_c}$, $P_r = \frac{P}{P_c}$ and $V_r = \frac{V}{V_c}$ [129].

In another way, it says that the equations of state for any fluid in the form of reduced properties, the same equation is valid for any other fluid. A derivation of the theory of corresponding state by using classical statistics with certain assumptions concerning the property of the molecules was done by Pitzer [130]. Helfand and Rice [131] discussed the application of the theory for transport properties like viscosity, thermal conductivity and self-diffusivity. As the principle stated, under the same reduced conditions, a dimension-less property of one matter is equal to that of another matter [132]. The reduced property X of two pure fluids

$$X'(T_r, V_r) = X^o(T_r, V_r) \tag{50}$$

$$X'(T_r, P_r) = X^o(T_r, P_r) \tag{51}$$

Preston, et al. [129] used the theory of corresponding state to develop correlations for the viscosity of cryogenic liquids and their mixtures. The study performed by Tham and Gubbins [133] applied the theory to correlate viscosities of dense fluids and extended the work for nonpolar polymeric fluids [134].

From the generalized corresponding state principle, if compressibility Z and reduced viscosity ($\eta\xi$) of the pure fluid and the reference fluid 'o' are at the same reduced temperature T_r and reduced pressure P_r, the pure liquid is defined to be in the corresponding state with a reference fluid. Then the Z and ($\eta\xi$) are given by

$$Z = Z^o \tag{52}$$

$$(\eta\xi) = (\eta\xi)^o \tag{53}$$

$$\xi = V_c^{2/3} T_c^{-1/2} M_c^{-1/2} \tag{54}$$

The expanded compressibility factor as a power series in the acentric factor [135]

$$Z = Z^o + \omega Z^1 \tag{55}$$

The Z^o and Z^1 in Eq (55) are functions of T_r and P_r. Z^o is the compressibility of a simple fluid with zero acentric factor, which is a spherical reference substance. The study performed by Letsou and Stiel [136] extended this approach for viscosities of liquids and rewrite Eq (53) as shown in Eq (56).

$$ln(\eta\xi) = ln(\eta\xi)^{(o)} + \omega ln(\eta\xi)^{(1)} \tag{56}$$

Teja and Rice [137] proposed a generalized corresponding state principle for thermodynamic properties using two nonspherical reference fluids that do not require spherical fluid as one of the references. Eq (57) and Eq (58) refer to the models for compressibility factor and viscosity and (r1) and (r2) refer to the nonspherical reference fluids.

$$Z = Z^{(r1)} + \frac{\omega - \omega^{(r1)}}{\omega^{(r2)} - \omega^{(r1)}} \left[Z^{(r2)} - Z^{(r1)} \right] \tag{57}$$

$$ln(\eta\xi) = ln(\eta\xi)^{(r1)} + \frac{\omega - \omega^{(r1)}}{\omega^{(r2)} - \omega^{(r1)}} \left[ln(\eta\xi)^{(r2)} - ln(\eta\xi)^{(r1)} \right] \tag{58}$$

Teja and Rice [137] describe the calculation procedure to calculate the viscosity of the liquid mixtures with relevant steps.

2.3.4.3 Empirical correlations for viscosity of pure and liquid mixtures

Various empirical correlations have been proposed to relate viscosity variation with temperature. The correlation shown in Eq (59) is initially proposed by de Guzman (1913) to describe the viscosity and temperature relationship. Currently, it is known as the Andrade (1934) equation [138].

$$ln(\eta) = A + \frac{B}{T} \tag{59}$$

Even though Andrade developed the model semi-theoretically, the parameters A and B needed to be found empirically via fitting the model to the measured viscosity data. Vogel [139] modified the correlation by adding a third parameter C as shown in Eq (60).

$$ln(\eta) = A + \frac{B}{T+C} \tag{60}$$

Other suggested correlations are

$$ln(\eta) = A + \frac{B}{T^3} \tag{61}$$

$$ln(\eta) = A + \frac{B}{T} + \frac{C}{T^2} \tag{62}$$

$$ln(\eta) = A + \frac{B}{T^C} \tag{63}$$

$$ln(\eta) = A + ln(T) + \frac{B}{T} \tag{64}$$

The Orrick and Erbar method provide a group contribution technique to estimate A and B in Eq (65) [117].

$$ln\left(\frac{\eta}{\rho M}\right) = A + \frac{B}{T} \tag{65}$$

The correlation is given in Eq (66) proposed by van Velzen, et al. [140]. The parameters B and T_o are related to the molecular structure.

$$ln(\eta) = B\left(\frac{1}{T} - \frac{1}{T_o}\right) \tag{66}$$

For liquid mixtures, Grunberg and Nissan [141] correlate viscosity of a mixture with viscosities of pure components [117].

$$ln(\eta) = \sum x_i ln(\eta_i) + \frac{1}{2}\sum\sum x_i x_j\, G_{ij} \tag{67}$$

The G_{ij} is an adjustable interaction parameter in which $G_{ii} = 0$. The correlation for binary mixtures is

$$ln(\eta) = x_1 ln(\eta_1) + x_2 ln(\eta_2) + x_1 x_2 G_{12} \tag{68}$$

This correlation is extensively used for binary liquid mixtures. The interaction parameter can be either regressed using measured data or found by a group contribution technique. Based on the studies for various mixtures, Poling, et al. [117] reported that Grunberg and Nissan's correlation is not recommended for aqueous mixtures.

2.3.4.4 Viscometers and rheometers

Rheology is considered as the analysis of material deformation and flow behaviour when the fluid is subjected to an external force. Elastic behaviour and viscous (or plastic) behaviour are two extremes of rheological behaviours. In elastic behaviour, when the applied force is removed the deformation reverses spontaneously and for the viscous (or plastic) behaviour deformation ceases after the applied force is removed. Most of the alkanolamines suggested for PCC are Newtonian fluids that fall into the viscous (or plastic) behaviour. Newtonian fluids exhibit a characteristic in a way that shear stress is proportional to the strain rate and viscosity does not change with shear conditions. This

is illustrated in Figure 2.5 (a) and 2.5 (b). A quantitative analysis of such fluids can be carried out by using viscometers and rheometers.

(a)   (b)
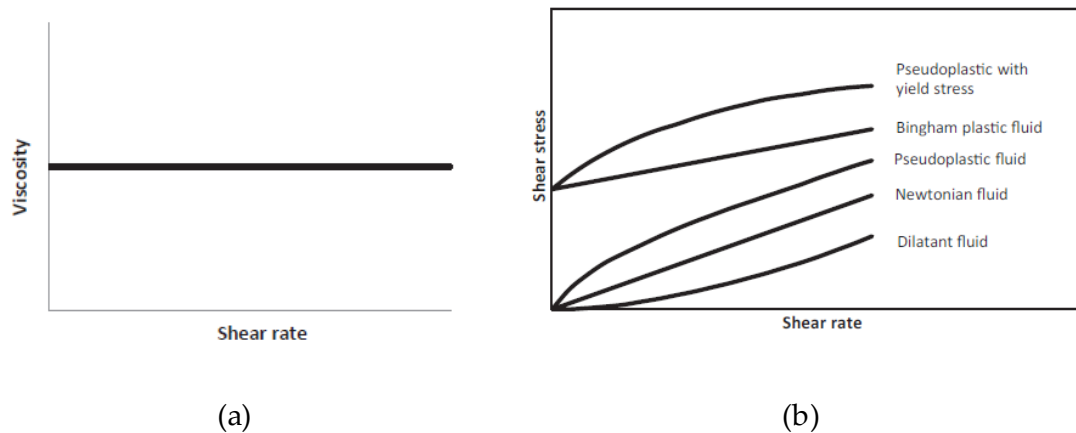
Figure 2. 5: (a): Newtonian fluid, (b): Flow curves for Newtonian and non-Newtonian fluid: Kulkarni and Shaw [142]

Viscometer or rheometer refers to the instrument that is used to measure the way that the fluid flows as a response to applied forces. The main difference between these two instruments is the quality of component and control capabilities [143]. A rheometer provides a wide range of applications to analyse essential properties to describe fluids that cannot be characterized by a single value of viscosity. Two different types of rheometers, shear rheometers and extensional rheometers are used to characterise viscosity depending on the applied stress that is either shear stress or extensional stress respectively. Shear rheometers either controls the shear strain and measure the resulting shear stress or controls the shear stress and measure the resulting shear strain. Extension viscometers measure the viscosity coefficient of a substance when the applied stress is extension stress. The materials that show tensile deformation over applied stress are commonly analysed by extension rheometry. Table 2.17 tabulates several types of rheometers that are commonly used.

Table 2.17: Commercially available viscometers and rheometers for viscosity measurements.

Rheometer	Description
Falling ball	-Simple and precise
	-Work according to the Hopper principle
	-Measure the viscosity of liquids by analysing the falling time of a ball with known density and diameter through a tube [144]
	-Suitable for both Newtonian and non-Newtonian fluids [145]
Falling cylinder	-Viscometric information is obtained by falling a cylindrical slug into a long cylindrical container filled with fluid.

	- Suitable for both Newtonian and non-Newtonian fluids [146]
Rotational	-Measure the required torque to rotate immersed geometry.
	-Several geometries are available: spindle type, concentric cylinder, cone and plate and parallel plate
	-Spindle type geometry can be used to measure a wide range of viscosities by using a multiple speed transmission and interchangeable spindles [147].
	-Concentric cylinder geometry is suitable for pourable liquids. Disadvantages: require a large sample volume and difficult to load polymer melt with high viscosity.

2.3.5 Viscosity of Amine + H_2O + CO_2 Mixtures

This section discusses the measured viscosities and relevant correlations for the amines of pure MEA, AMP, MDEA, DEEA and DMEA and their mixtures. The correlation for the pure amines, aqueous amine and CO_2 loaded aqueous amines are tabulated and the limitations are discussed as stated by the authors.

2.3.5.1 Viscosity Measurements

In this section, the viscosity data of amines with their aqueous and CO_2 loaded aqueous mixtures is discussed. The considered amines are MEA, AMP, MDEA, DEEA and DMEA and their mixtures. The literature of measured viscosities is tabulated with relevant references and conditions. The viscosity of pure MEA, MDEA, AMP, DEEA and DMEA are listed in Table 2.18, 2.21, 2.24, 2.26 and 2.29 respectively. For aqueous solutions, the viscosity of MEA + H_2O, MDEA + H_2O, AMP + H_2O, DEEA + H_2O and DMEA + H_2O are listed in Table 2.19, 2.22, 2.25, 2.27 and 2.30 respectively. Further, viscosity of CO_2 loaded aqueous solutions of MEA + H_2O + CO_2, MDEA + H_2O + CO_2, DEEA + H_2O + CO_2 and DMEA + H_2O + CO_2 are listed in Table 2.20, 2.25, 2.28 and 2.31 respectively.

Table 2.18: Viscosity measurement: Pure MEA.

Source	Temperature (K)		No of points	Method
	Low	High		
DiGuilio, et al. [64]	303.6	423.7	8	Cannon-Ubbelohde capillary viscometer
Li and Lie [83]	303.15	353.15	6	Cannon-Fenske routine viscometer
Lee and Lin [67]	303.15	323.15	3	Haake falling-ball viscometer
Song, et al. [68]	303.15	343.15	5	Ubbelohde viscometer

Kapadi, et al. [69]	303.15	318.15	4	Ubbelohde viscometer
Mandal, et al. [82]	293.15	353.15	10	Ostwald viscometer
Islam, et al. [70]	293.15	323.15	6	U-tube Ostwald viscometer
Geng, et al. [72]	288.15	323.15	8	Ubbelohde viscometer
Amundsen, et al. [74]	298.15	353.15	5	ZIDIN viscometer
Abuin, et al. [78]	298.15		1	Ubbelohde viscometer
Arachchige, et al. [148]	293.15	423.15	15	Anton Paar MCR 101 (Double-gap rheometer)
Xu, et al. [79]	293.15	333.15	5	Anton Paar AMVn

Table 2.19: Viscosity measurement: MEA + H_2O mixtures.

Source	Concentration: mass% MEA		Temperature (K)		No of points
	Low	High	Low	High	
Weiland, et al. [80]	10	40	298.15		4
Amundsen, et al. [74]	20	90	298.15	353.15	30
Arachchige, et al. [148]	10	90	293.15	353.15	72
Hartono, et al. [81]	6.2	30	293.15	353.15	26
Arachchige, et al. [149]	10	90	363.15	423.15	63
Idris, et al. [150]	50	90	298.15	373.15	128
Li and Lie [83]	30		303.15	353.15	6
Zhang, et al. [84]	30		298.15	353.15	7
Mandal, et al. [82]	30		298.15	323.15	7
	Concentration: x_1 [a] MEA		Temperature (K)		No of points
Lee and Lin [67]	0.1	0.9	303.15	323.15	27
Kapadi, et al. [69]	0.1122	0.8486	303.15	318.15	32
Islam, et al. [70]	0.03219	0.72956	303.15	323.15	45

x_1 [a] = mole fraction of amine

Table 2.20: Viscosity measurement: MEA + H_2O + CO_2 mixtures.

Source	Concentration: mass% MEA in (MEA + H_2O) solutions		CO_2 loading α (mol CO_2/mol MEA)		Temperature (K)	No of points
	Low	High	Low	High		
Weiland, et al. [80]	10	40	0.05	0.5	298.15	20
Amundsen, et al. [74]	20	40	0.1	0.5	298.15-353.15	75
Fu, et al. [151]	20	40	0.1	0.5	298.15	15
Hartono, et al. [81]	6.2	30	0.11	0.5	293.15-353.15	100
Idris, et al. [150]	50	80	0.08	0.52	298.15-373.15	320

Source						
Arachchige, et al. [152]	10	50	0.1	0.5	293.15-423.15	375
Zhang, et al. [84]		30	0.14	0.49	298.15-353.15	23

Table 2.21: Viscosity measurements: Pure MDEA.

Source	Temperature (K)	No of points	Method
Li and Lie [83]	303.15-353.15	6	Cannon-Fenske routine viscometer
Henni, et al. [91]	298.15-343.15	5	Ubbelohde suspended level , Cannon-Ubbelohde
Paul and Mandal [93]	288-333	3	Ostwald viscometer
Bernal-García, et al. [153]	313.15-363.15	4	Cannon-Fenske routine viscometer
Teng, et al. [154]	298.15-353.15	5	Ubbelohde-type viscometers (Schott Gerate Type 24 501 Capillary viscometers)
Arachchige, et al. [148]	293.15-423.15	15	Anton Paar Physica MCR 101 (Double-gap rheometer)
Kummamuru, et al. [155]	298.15-373.15	16	Anton Paar Physica MCR 101 (Double-gap rheometer)
Pinto, et al. [156]	293.15-353.15	5	Anton Paar Physica MCR 100 (Double gap rheometer)

Table 2.22: Viscosity measurement: MDEA + H_2O mixtures.

Source	Concentration: x_1 [a] MDEA		Temperature (K)		No of points
	Low	High	Low	High	
Teng, et al. [154]	0.0079	0.8989	298.15	353.15	70
Bernal-García, et al. [153]	0.0604	0.7430	313.15	363.15	28
Pinto, et al. [156]	0.0447	0.9014	293.15	353.15	40
	Concentration: mass% MDEA		Temperature (K)		No of points
Welsh and Davis [100]	50		283.15	333.15	6
Arachchige, et al. [148]	10	90	293.15	353.15	72
Arachchige, et al. [149]	10	90	363.15	423.15	63
Kummamuru, et al. [155]	10	95	298.15	373.15	128
Weiland, et al. [80]	30	60	298.15		4

x_1 [a] = mole fraction of amine

Table 2.23: Viscosity measurement: MDEA + H_2O + CO_2 mixtures.

Source	Concentration: mass% MDEA in (MDEA + H_2O) solutions		CO_2 loading α (mol CO_2/mol MDEA)		Temperature (K)	No of points
	Low	High	Low	High		
Weiland, et al. [80]	10	40	0.05	0.5	298.15	40
Pinto, et al. [156]	50		0.0452	0.1863	293.15-353.15	24

Table 2.24: Viscosity measurements: Pure AMP.

Source	Temperature (K)	No of points	Method
Li and Lie [83]	303.15-353.15	6	Cannon-Fenske routine viscometer
Henni, et al. [157]	298.15-343.15	4	Cannon-Ubbelohde viscometers

Table 2.25: Viscosity measurement: AMP + H_2O mixtures.

Source	Concentration: x_1[a] AMP		Temperature (K)		No of points
	Low	High	Low	High	
Henni, et al. [157]	0.0503	0.9001	298.15	343.15	66
	Concentration: (mol/m^3) AMP		Temperature (K)		No of points
Xu, et al. [101]	2	3	296.75	349.85	12
	Concentration: mass% AMP		Temperature (K)		No of points
Welsh and Davis [100]	50		283.15	333.15	6

x_1[a] = mole fraction of amine

Table 2.26: Viscosity measurement: Pure DEEA.

Source	Temperature (K)	No of points	Method
Maham, et al. [158]	298.15-353.15	5	Ubbelohde-type viscometers (Schott Gerate Type 24 501 Capillary viscometers)
Pinto, et al. [156]	293.15-353.15	8	Anton Paar Physica MCR 100 (double gap rheometer)

Table 2.27: Viscosity measurement: DEEA + H_2O mixtures.

Source	Concentration: x_1[a] DEEA		Temperature (K)		No of points
	Low	High	Low	High	
Maham, et al. [158]	0.0039	0.9544	298.15	353.15	95
Pinto, et al. [156]	0.0082	0.8993	293.15	353.15	112

x_1[a] = mole fraction of amine

Table 2.28: Viscosity measurement: DEEA + H_2O + CO_2 mixtures.

Source	Concentration: mass% DMEA in (DEEA + H_2O) solutions		CO_2 loading α (mol CO_2/mol DEEA)		Temperature (K)	No of points
	Low	High	Low	High		
Zhang, et al. [84]	15	45	0.08	0.83	303.15-353.15	45
Pinto, et al. [156]	23.5	60.8	0.0905	0.6752	293.15-353.15	75

Table 2.29: Viscosity measurement: Pure DMEA.

Source	Temperature (K)	No of points	Method
Bernal-García, et al. [109]	313.15-353.15	5	Cannon-Fenske viscometers
Pinto, et al. [156]	293.15-353.15	5	Anton Paar Physica MCR 100 (double gap rheometer)

Table 2.30: Viscosity measurement: DMEA + H_2O mixtures.

Source	Concentration: x_1[a] DMEA		Temperature (K)		No of points
	Low	High	Low	High	
Bernal-García, et al. [109]	0.1009	0.8950	313.15	353.15	40
Pinto, et al. [156]	0.0425	0.9083	293.15	353.15	30

x_1[a] = mole fraction of amine

Concepción, et al. [111] measured viscosity of DMEA + H_2O mixtures at elevated pressures from 0.1 MPa to 140 MPa using a falling body viscometer.

Table 2.31: Viscosity measurement: DMEA + H$_2$O + CO$_2$ mixtures.

Source	Concentration: mass% DMEA in (DMEA + H$_2$O) solutions		CO$_2$ loading α (mol CO$_2$/mol DMEA)		Temperature (K)	No of points
	Low	High	Low	High		
Zhang, et al. [84]	15	45	0.08	0.83	303.15-353.15	45

2.3.5.2 Viscosity Correlations

The viscosity of amine solutions shows typical liquid dependence on temperature and pressure in which viscosity decreases with the increase of temperature and viscosity increase with the increase of pressure. Table 2.32 summarizes the correlations that were found for the different types of amines especially MEA, MDEA, AMP, DEEA, DMEA and their aqueous and CO$_2$ loaded aqueous mixtures.

The relation of viscosity of pure amines with temperature can be represented by the Arrhenius equation shown in Eq (69) and Teng, et al. [154] listed activation energies together with values calculated from the data presented in DiGuilio, et al. [64] and Al-Ghawas, et al. [90] for viscous flows for pure amines of MEA, MDEA, DEEA and DMEA. DiGuilio, et al. [64] used a modified Andrade (1934) viscosity model [138] by Vogel [139] as shown in Eq (70).

The viscosity of binary amine mixtures is correlated in different ways. The common approach is by calculating the viscosity deviation η^E based on the pure components of the mixture. A Redlich-Kister type polynomial as shown in Eq (71) was proposed by Islam, et al. [70] for aqueous MEA, Bernal-García, et al. [153] for aqueous MDEA, Bernal-García, et al. [109] for aqueous DMEA mixtures. Teng, et al. [154] proposed a polynomial correlation as given in Eq (72) for aqueous MDEA and it has also been used by Arachchige, et al. [149] for aqueous MEA and aqueous MDEA mixtures. Maham, et al. [159] used the correlation given in Eq (73) to fit the viscosity deviation of aqueous MEA and aqueous DEEA mixtures [158] presented by Grunberg and Nissan [141] in Eq (68) for binary mixtures. Hartono, et al. [81] used the same approaches but instead of using a Redlich-Kister polynomial to fit the viscosity deviations a simplified correlation was proposed as given in Eq (74) for aqueous MEA mixtures. The applicability of the McAllister three-Body model as shown in Eq (45) was tested by Lee and Lin [67] and Amundsen, et al. [74] for aqueous MEA mixtures. The parameters were calculated through a fit of kinematic viscosity data at different temperatures. Idris, et al. [150] discussed four approaches based on Heric and Brewer [160], Jouyban, et al. [161], Herráez, et al. [162] as given by Eq (75), Eq (76) and Eq (77) respectively. Further, a Redlich-Kister type polynomial was also fitted for the viscosity deviation as given in Eq (71).

The pressure and temperature effect on viscosity of MEA + H$_2$O mixtures and MDEA + H$_2$O mixtures were studied by Sobrino, et al. [113]. A viscosity function of temperature and pressure as given in Eq (78) was suggested by Comuñas, et al. [163] to correlate

measured densities of aqueous MEA + H2O and MDEA + H2O at different pressure, temperature and compositions.

For viscosity of CO_2 loaded aqueous solutions, Weiland, et al. [114] suggested a correlation for CO_2 loaded aqueous MEA and CO_2 loaded aqueous MDEA solutions as illustrated in Eq (79). Hartono, et al. [81] presented a correlation for viscosity of CO_2 loaded aqueous MEA as given in Eq (80) and (81). Idris, et al. [150] used a Setschenow type correlation to fit CO_2 loaded aqueous MEA at higher MEA concentrations. This correlation has been adopted by Shokouhi, et al. [115] to correlate CO_2 loaded aqueous MDEA mixtures as shown in Eq (82) and Eq (83). Zhang, et al. [84] proposed two correlations for CO_2 loaded aqueous DMEA and CO_2 loaded aqueous DEEA solutions as given in Eq (84) and Eq (85) respectively. A different approach was taken by Matin, et al. [164] to correlate viscosity of CO_2 loaded aqueous MEA. There, different terms were tested to replace excess free energy of activation for viscous flow ΔG_0^{E+} of Eyring's viscosity representation as given in Eq (89) based on absolute rate theory [122]. The approach is based on combining different equations as shown in Eq (86) to Eq (89). Having tested Gibbs free energy of mixing ΔG_{mix}^* and excess Gibbs free energy of mixing ΔG^{E*} of MEA and H2O, Matin, et al. [164] concluded that inversed sign of Gibbs free energy of mixing as the most appropriate term to replace the ΔG_0^{E+} to get more accurate predictions.

Table 2.32: Overview of the viscosity correlations.

Correlation	
$\eta = Ae^{E/RT}$	(69)
$ln(\eta) = A + \frac{B}{T+C}$	(70)
$\Delta\eta = x_1 x_2 \sum_{i=0}^{n} B_i (2x_1 - 1)^i$	(71)
$ln(\eta) = ln(\eta_0) + \sum_{i=1}^{n} a_i x_1^i$	(72)
$\Delta ln(\eta) = x_1 x_2 \sum_{i=0}^{n} B_i (2x_1 - 1)^i$	(73)
$\Delta ln(\eta) = x_1 x_2 (b_1 + b_2 t + b_3 t^2 + b_4 x_1)$	(74)
$ln(\eta) = x_1 ln(\eta_1) + x_2 ln(\eta_2) + x_1 ln(M_1) + x_2 ln(M_2) - ln(x_1 M_1 + x_2 M_2)$ $+ x_1 x_2 \sum_{i=0}^{n} [A_i (x_1 - x_2)^i]$	(75)
$ln(\eta) = x_1 ln(\eta_1) + x_2 ln(\eta_2) + x_1 x_2 \sum_{i=0}^{n} \left[\frac{A_i(x_1-x_2)^i}{T}\right]$	(76)
$\eta = \eta_1 + (\eta_2 - \eta_1)x_2^{\sum_{i=0}^{n}(A_i x_2^i)}$	(77)
$\eta(T,P) = Aexp\left[\frac{B}{T-C}\right]exp\left[Dln\left(\frac{P+E(T)}{0.1+E(T)}\right)\right]$	(78)
$\frac{\eta}{\eta_{H_2O}} = exp\left(\frac{[(a \cdot w_{MEA} + b)T + (c \cdot w_{MEA} + d)][\alpha(e \cdot w_{MEA} + f \cdot T + g) + 1]w_{MEA}}{T^2}\right)$	(79)
$ln(\eta_{loaded}) = x_3 ln(\eta_\gamma^*) + (1 - x_3)ln(\eta_{unloaded})$	(80)
$ln(\eta_\gamma^*) = \frac{a_1 x_1 + a_2 \alpha x_1}{a_3 + x_1}$	(81)

$$ln\left(\frac{\eta_{loaded}}{\eta_{unloaded}}\right) = \sum_{i=1}^{2} A_i \alpha^i \tag{82}$$

$$A_i = a_{i,0} + a_{i,1} T \tag{83}$$

$$ln\left[\frac{\eta}{\eta_{H_2O}}\right] = a_1 w_2^2 + a_2 w_2^3 + a_3 \alpha w_2^3 + \frac{b_1}{(T/T_0)+C} \tag{84}$$

$$ln\left[\frac{\eta}{\eta_{H_2O}}\right] = a_1 \sqrt{w_2} + a_2 \alpha w_2^2 + a_3 \alpha^2 w_2 + \frac{b_1 w_2}{(T/T_0)+C} \tag{85}$$

$$\eta = \frac{hN}{V} exp\left(\frac{\Delta G_0^+}{RT}\right) \tag{86}$$

$$\frac{\eta}{\eta_{ideal}} = \frac{V_{ideal}}{V} exp\left(\frac{\Delta G_0^{E+}}{RT}\right) \tag{87}$$

$$ln(\eta V) = ln(\eta V)_{ideal} + \frac{\Delta G_0^{E+}}{RT} \tag{88}$$

$$ln(\eta V) = \sum_i x_i \cdot ln\left(\eta_i V_i^0\right) + \frac{\Delta G_0^{E+}}{RT} \tag{89}$$

For the viscosities of aqueous binary mixtures, the approaches given in Eq (71) and Eq (73) are recommended to correlate viscosity data. For the CO_2 loaded aqueous amine mixtures, the correlations proposed from Eq (79) to Eq (81) are recommended to fit measured viscosities. Those correlations are easy to implement and reported accuracies in literature for data fits are acceptable. If the mixture contains more than one amine for CO_2 loaded solutions, above mentioned correlations from Eq (79) to Eq (81) need to be modified before regression.

2.3.6 Liquid Mixture Analysis

As described by Kauzmann and Eyring [165], the viscosity of a mixture strongly depends on the entropy of the mixture that has relations with liquid structure and intermolecular interactions between the components of the mixture [166]. Using the Grunberg and Nissan [141] correlation for the viscosity of binary mixtures Vogel and Weiss [167] pointed out that for a liquid mixture, a positive deviation as $G_{12} > 0$ is connected with a negative deviation from Raoult's law, which gives negative enthalpy of mixing indicating weak to strong interactions between mixed species. A negative deviation as $G_{12} < 0$ is connected with a positive deviation from Raoult's law, which gives positive enthalpy of mixing indicating no specific interactions between mixed species. Vogel and Weiss [167] also commented that in addition to the excess energy and viscosity the entropy of mixing and the volume of mixing should be equally important for the viscosity.

The excess properties of molar volume V^E, dynamic viscosity η^E and free energy of activation for viscous flow ΔG_0^{E+} are useful properties to analyse liquid mixtures including binary and tertiary amine + H_2O. Section 2.3.1 emphasizes the use of V^E to analyse mixture characteristics. Fort and Moore [168] discussed the significance of the sign of η^E as evaluated by Eq (90) in which η^E is slightly negative for a system involving weak dipole interaction and positive for a system may involve stronger dipole interaction and hydrogen bonding.

$$\eta^E = \eta - \sum x_i \eta_i \tag{90}$$

Meyer, et al. [169] reported that ΔG_0^{E+} can be used like viscosity deviation η^E to identify molecular interactions. This was supported by the authors [170-174] suggesting that for the binary mixtures ΔG_0^{E+} is positive for the mixtures that exhibit strong specific interactions between unlike molecules presence over all other kinds of interactions. Besides, ΔG_0^{E+} is negative for mixtures with weak interactions like dispersion forces in the mixture.

The interaction parameter G_{12} in Grunberg and Nissan [141] as given in Eq (68) has been adopted to analyze intermolecular interactions in the binary mixtures. Fort and Moore [168] suggested that G_{12} is a better measure of strength of the interactions. Katti and Chaudhri [175] have introduced an interaction parameter W_{vis}/RT that shows the same trend as G_{12}.

$$ln(\eta V) = \sum_i x_i \cdot ln(\eta_i V_i^0) + \frac{x_1 x_2 W_{vis}}{RT} \tag{91}$$

From the study of binary mixtures, Nigam and Mahl [176] reported a criterion to analyse binary mixtures based on both η^E and G_{12} as follows.

In which,

   a) For binary mixtures with strong specific interactions, $\eta^E > 0$ and $G_{12} > 0$ with large magnitude
   b) For binary mixtures with weak specific interactions, $\eta^E < 0$ and $G_{12} > 0$
   c) For binary mixtures with dispersion forces, $\eta^E < 0$ and $G_{12} < 0$ with large magnitude

2.4 Artificial Neural Networks for the Estimation of Physical Properties

The applications of Artificial Neural Networks (ANN) in data science to build non-linear models to understand complex patterns in the data is vast [177]. ANNs are computational algorithms that are inspired by the function of neurons in the animal's central nervous system. ANNs are capable of performing machine learning and pattern recondition. A schematic of an ANN is shown in Figure 2.6.

The structure of an ANN is consisting of an input layer, hidden layer and output layer. The circles in Figure 2.6 are known as nodes (neurons) that are interconnected as biological neurons. A layer is a collection of nodes in which a node can take multiple weighted inputs. Then the activation function is applied to the sum of these inputs in order to generate the output.
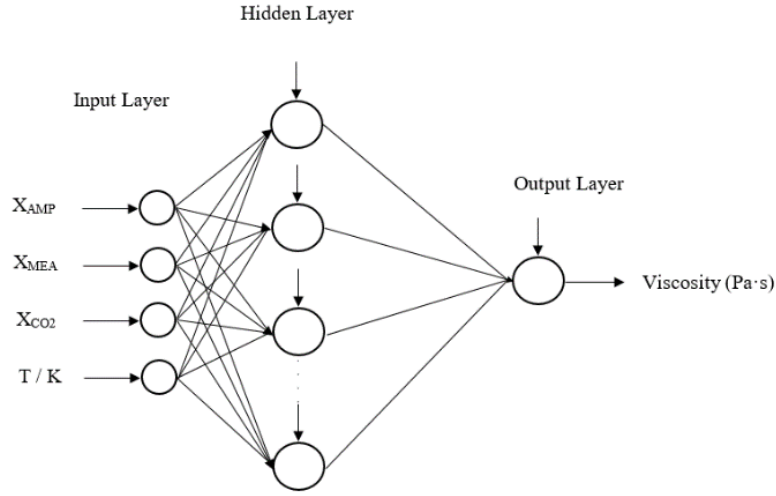
Figure 2.6: A schematic of feed forward artificial neural network with one hidden layer

Input layer: The place where the input data are fed into the network.

Hidden layer: The hidden layer is a part of the network and does not belong to the input layer or output layer. There can be multiple hidden layers in an ANN depending on the nature of the input data.

Output layer: The functioning of an output layer depends on the actions of the hidden units and the weights between the hidden and the output units.

2.4.1 Activation Function

Several activation functions are available to use in the hidden layer as sigmoid, inverse tangent, hyperbolic tangent and saturated linear function. For the ANN developed in this study, the transfer or the activation function in the hidden layer is a hyperbolic tangent (τ) and a linear relation (ψ) is used for the output layer. The output of the network can be described as follows [178]:

$$\theta_s = IW_{(s,1)} In_1 + IW_{(s,2)} In_2 + \cdots + IW_{(s,k)} In_k + b_s^{(1)} \tag{92}$$

Where, IW, In and $b^{(1)}$ are the output results of the neurons in the hidden layer, the input weights, the inputs and bias of neuron in the hidden layer.

The hyperbolic tangent (τ) and liner relation (ψ) are given in Eq (93) and (94).

$$f = \tau(\theta_s) = \frac{2}{1 + exp(-2\theta_s)} - 1 \tag{93}$$

$$g = \psi(LW \cdot f + b^{(2)}) \tag{94}$$

Where LW, and $b^{(2)}$ are the weights and bias in the output layer.

2.5 Process Simulations in PCC

Process simulations of amine-based PCC are performed based on two approaches of equilibrium-based and rate-based models for the absorption of CO_2 into aqueous alkanolamine mixtures. In the equilibrium-based approach, the relation between vapour and liquid is considered to be at thermodynamical equilibrium with each other. In the rate-based approach, mass and heat transfer phenomena are adopted to treat the separation process.

2.5.1 Murphree Efficiency Based Simulations

The ideal scenario of complete thermodynamic equilibrium between vapour and liquid streams is not feasible in a real separation process. Accordingly, stage or tray efficiency is introduced to deal with the non-ideality of the process. Tray efficiency is described in several ways [179]. The point efficiency is defined as the ratio of change of composition at a point to the change of composition that would occur on a theoretical stage. Instead of a single point, Murphree efficiency is defined for the entire tray as given in Eq (95).

$$E_M = \frac{(y_n - y_{n-1})}{(y_n^* - y_{n-1})} \tag{95}$$

The overall column efficiency E_o is given as

$$E_o = \frac{number\ of\ ideal\ stages}{number\ of\ real\ stages} \tag{96}$$

And these two efficiencies can be related as

$$E_o = \frac{ln\left[1 + E_M\left(\frac{mV}{L} - 1\right)\right]}{ln\left(\frac{mV}{L}\right)} \tag{97}$$

For a packed column, Murphree efficiency of a tray is applicable for a packing section with a certain height.

2.5.2 Rate-Based Simulations

Rate-based modelling of an absorption process is a non-equilibrium approach in which a continuous mass and heat transfer is considered through the vapour-liquid interface. The methodology for the rate-based approach is to perform material balance, energy balance with appropriate equilibrium models and mass and energy transfer models. The equilibrium models can be used to calculate the concentration of the species in the reaction system.

2.5.3 Equilibrium Models for Amine + H₂O + CO₂ Systems

Vapour–liquid equilibria of CO_2 in aqueous amine solution undergoes both phase and chemical equilibria [180]. Kent and Eisenberg [181] proposed an equilibrium model based on the Henry's law constant (H_{CO_2}) and equilibrium constants for reactions involving amine, water and CO_2. The Kent-Eisenberg model is simple as it assumes the activity coefficients and fugacity coefficients to be unity (ideal liquid and gas phase). Li and Mather [182] correlated solubility of CO_2 in a mixed alkanolamine mixture using the Clegg-Pitzer equation that comprises an extended Debye-Huckel term [183].

Debye-Huckel theory [184] describes the deviation of electrolyte solution from an ideal solution by introducing a method to calculate the activity coefficient γ_i of an ion in a dilute solution [128]. Chen, et al. [185] developed an electrolyte local composition model by combining the extended form of the Debye-Huckel equation proposed by Pitzer [186] and the non-random two liquid (NRTL) model [128, 187]. The extended Debye-Huckel equation was adopted to represent the contribution of long-range ion-ion interactions, while all kinds of contributions from the short-range interactions are represented by the local composition concept. Accordingly, the Pitzer-Debye-Huckel expression and the local composition expression are added to define an excess Gibbs energy expression for electrolyte solutions.

$$\frac{G^{ex^*,El-NRTL}}{RT} = \frac{G^{ex^*,pdh}}{RT} + \frac{G^{ex^*,lc}}{RT} \qquad (98)$$

Similarly,

$$ln\gamma_i = ln\gamma_i^{pdh} + ln\gamma_i^{lc} \qquad (99)$$

A model of vapour-liquid equilibria (VLE) for an acid gas-alkanolamine was proposed by Austgen, et al. [188] based on the Electrolyte-NRTL model of Chen, et al. [185]. In this model, parameters were fitted for MEA + H₂O + CO₂ system VLE data to obtain adjustable parameters and binary energy interaction parameters of the model.

2.5.4 Aspen HYSYS and Aspen Plus Simulation Environments

Aspen Plus and Aspen HYSYS are process simulators equipped with many methods to calculate material and energy balance of the process. It also facilitates the environment for different approaches e.g. equilibrium-based and rate-based approaches for absorption column simulations. For the calculation of VLE, Aspen HYSYS is available with Kent-Eisenberg [181] and Li-Mather [189] models, while in Aspen Plus, Chen-Austgen model [188] can be used. In the latest version of Aspen HYSYS, an amine package is recommended to replace the Kent-Eisenberg or Li-Mather models.

2.5.5 Physical Property Methods

For the physical properties, the measured density and viscosity of MEA + H₂O + CO₂ by Weiland, et al. [80] or Hartono, et al. [81] can be regressed to estimate relevant model

parameters. In Aspen Plus, the Clarke model called VAQCLK for liquid molar volume is available with regressed model parameters. This model determines the liquid molar volume of aqueous electrolyte solutions using Amagat's law as shown in Eq (100) and the relationship between partial molar volume of an electrolyte and its mole fraction in the solvent as illustrated in Eq (101) [190].

$$V_m^l = \sum_i x_i V_i \tag{100}$$

Where V_m^l, x_i and V_i are molar volume of the mixture, mole fraction and the molar volume of the components respectively.

$$V_{ca} = V_{ca}^\infty + A_{ca}\frac{\sqrt{x_{ca}}}{1+\sqrt{x_{ca}}} \tag{101}$$

Where V_{ca} is the partial molar volume of electrolytes, x_{ca} is the apparent electrolyte mole fraction and V_{ca}^∞, A_{ca} are regression parameters.

In Aspen Plus, the option code 1 signifies the quadratic mixing rule for solvent in which the interaction parameter VLQKIJ for MEA and H2O can be regressed against density data of MEA + H2O from Kapadi, et al. [69] and Han, et al. [77]. For the main electrolyte (MEAH+, HCO3-), (MEAH+, MEACOO-) and (MEAH+, CO3^2-), the Clarke model parameters V_{ca}^∞ named as VLCLK/1 can also be regressed against experimental MEA + H2O + CO2 density data. Aspen Plus provides the Jones-Dole electrolyte correction model, referred as MUL2JONS to model the liquid viscosities in a MEA + H2O + CO2 mixture. There, the model calculates the correction to the liquid mixture viscosity of a solvent mixture due to the presence of electrolytes. The Jones-Dole electrolyte correction model is described as follows [190],

$$\eta = \eta_{solv}(1 + \sum_{ca} \Delta\eta_{ca}) \tag{102}$$

Where η, η_{solv} and $\Delta\eta_{ca}$ are the viscosity of the liquid mixture, viscosity of the liquid mixture calculated by the Andrade/DIPPR model and contribution to the viscosity correction due to apparent electrolyte ca from cation c and anion a respectively.

The measured viscosity data of MEA + H2O mixtures can be adopted to determine the interaction parameters MUKIJ and MULIJ between MEA and H2O in the Aspen liquid mixture model. And, the Jones-Dole model parameters in $\Delta\eta_{ca}$, IONMUB, for MEAH+ and MEACOO- are possible to regress against MEA + H2O + CO2 viscosity data [191].

In principle, it is possible to integrate specific correlations in simulation programs like Aspen HYSYS and Aspen Plus. However, this requires use of complex tools to obtain. In the future, integration of new correlations including specific parameters may be more convenient.

3 Materials and Sample Preparation

This chapter describes the materials that has been used in the research and explains the methods that were adopted to prepare samples and calculation procedures of CO_2 loading in an amine + H_2O + CO_2 mixture.

3.1 Materials

Different types of amines were used in the project. They fall into primary amines, sterically hindered primary amines and tertiary amines. Table 3.1 provides information about the molecular structure and IUPAC name of each amine. The purity of the material used and relevant sources are listed in Table 3.2.

Monoethanol amine:
Monoethanol amine is a primary amine and it is considered as the benchmark solvent in PCC. It has a high absorption rate of CO_2 but the absorption capacity is relatively low compared to the secondary and tertiary amines. As a result of stable carbamate formation during the reaction with CO_2 the regeneration energy is high in MEA. It is a drawback of using MEA alone as an aqueous solvent to capture CO_2 in PCC. The formation of stable carbamates limits the theoretical CO_2 loading to 0.5 mol CO_2 / mol amine.

2-Amino-2-methyl-1-propanol:
AMP is a sterically hindered primary amine. It has a high absorption capacity, absorption rate, selectivity and degradation resistance which are advantages over conventional amines for CO_2 removal from acid gases. AMP forms a rather unstable carbamate reacting with CO_2. Low stability constant results in carbamate hydrolysis forming bicarbonate and free amine. This free amine again reacts with CO_2 by leading to an overall stoichiometric loading capacity of 1 mol of CO_2/mol of amine [192]. Further, AMP has low regeneration energy compared to MEA and it is an added advantage in terms of energy utilization in the process.
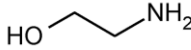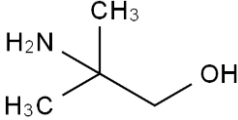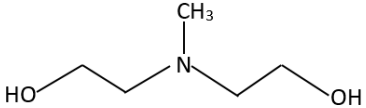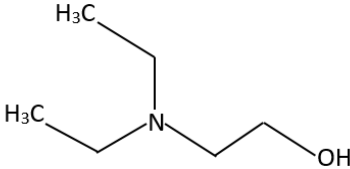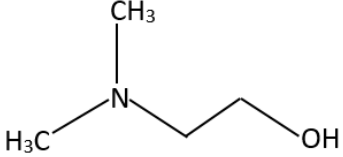
N-methyldiethanolamine:
MDEA is a tertiary amine that is formed by replacing the hydrogen atom, which is attached to DEA by a methyl group. MDEA has a high CO_2 absorption capacity as it forms unstable carbamate during the reaction with CO_2. This leads to a theoretical CO_2 loading of 1 mol CO_2 / mol amine. MDEA shows a relatively slow reaction rate and low heat of absorption compared to MEA. Further, MDEA is capable of removing H_2S selectively from H_2S and CO_2 gas mixtures [35].

Dimethylethanolamine:
DMEA is a tertiary amine with one hydroxyl group and two methyl groups attached to the nitrogen atom. It is a novel amine with good degradation resistance, high CO_2 absorption capacity and low regeneration energy [193, 194]. A comprehensive study

performed by Ling, et al. [195] discusses the solubility and mass transfer studies of DMEA as a solvent in PCC.

Table 3.1: Molecular structures and IUPAC names of amines.

Material	Structure
Monoethanolamine (MEA)	2-aminoethanol
2-Amino-2-methyl-1-propanol (AMP)	2-amino-2-methyl-1-propanol
N-methyldiethanolamine (MDEA)	2-(2-Hydroxyethyl-methyl-amino)ethanol
Diethylethanolamine (DEEA)	2-(diethylamino)ethanol
Dimethylethanolamine (DMEA)	2-(dimethylamino)ethanol

Diethylethanolamine:
DEEA is a tertiary amine having a similar molecular structure to DMEA in which instead of two methyl groups as in DMEA, DEEA has two ethyl groups attached to the nitrogen atom. A study performed by Liebenthal, et al. [196] showed that the use of DEEA can reduce energy consumption compared to 30 mass % aqueous MEA solvent.

Table 3.2: Provenance and purity of the materials

Chemical Name	Source	Mole fraction Purity[a]	Purification
AMP	Sigma-Aldrich	BioUltra, ≥0.99 (GC)	no
MEA	Sigma-Aldrich	≥0.995	no
MDEA	Merck KGaA	≥0.98	no
DEEA	Sigma-Aldrich	≥0.995	no
DMEA	Alfa Aesar	≥0.99	no
CO_2	AGA Norge AS	≥0.9999	no
N_2 (Nitrogen)	AGA Norge AS	-	no
NaOH (Sodium Hydroxide)	Merck KGaA	-	no
HCl (Hydrochloric acid)	Merck KGaA	-	no
$BaCl_2 \cdot 2H_2O$ (Barium Chloride dihydrate)	Merck KGaA	≥0.99	no

[a]As given by the supplier

3.2 Sample Preparation

Two types of samples as aqueous amine and CO_2 loaded amine mixtures were used in density and viscosity measurements. For all sample preparations, deionized water (Milli Q, resistivity 18.2 MΩ·cm) was degassed to remove any dissolved gases using a rotavapour connected to a vacuum pump. All the materials are weighed using an electronic balance from METTLER TOLEDO (XS403S). Aqueous amine mixtures were prepared by weighing pure amine and water in different mass ratios. They were mixed to form a sample with 100 g and stirred until it became a homogeneous mixture. For the CO_2 loaded aqueous amine mixtures, a series of samples were prepared with different CO_2 loadings by mixing aqueous amine and different volumes of CO_2 loaded aqueous amine. After mixing the sample was stirred firmly and stored until they are used in the density and viscosity measurements.

3.3 CO_2 Loading of Amine Solutions

Two CO_2 loading apparatuses were available in the laboratory to perform CO_2 loading as shown in Figure 3.1. The reaction between amine and CO_2 is exothermal. Thus, heat is generated during the CO_2 bubbling and solution temperature increases. This will lead to evaporate some amount of amine in the solution. Therefore final amine concentration was analysed after the CO_2 loading. Figure 3.1 shows the CO_2 loading apparatus available in the laboratory. This study adopted the apparatus shown in Figure 3.1 b. There, CO_2 was bubbled through 100 g of aqueous amine sample. The pH of the solution was continuously monitored using a pH electrode of InLab Expert pt 1000 from METTLER TOLEDO until it becomes steady over time. At a steady pH value, it was concluded that all amines in the solution have participated in the reaction with CO_2. This procedure was done three times and all solutions were mixed together and stirred for approximately 2 hours. Then the solution was stored for 24 hours allowing to complete

all the reactions and get the sample matured. Pinto, et al. [96] discussed about possible amine loss during CO_2 bubbling in non-loaded solutions. It was reported that 1.3% solvent loss during the loading procedure.
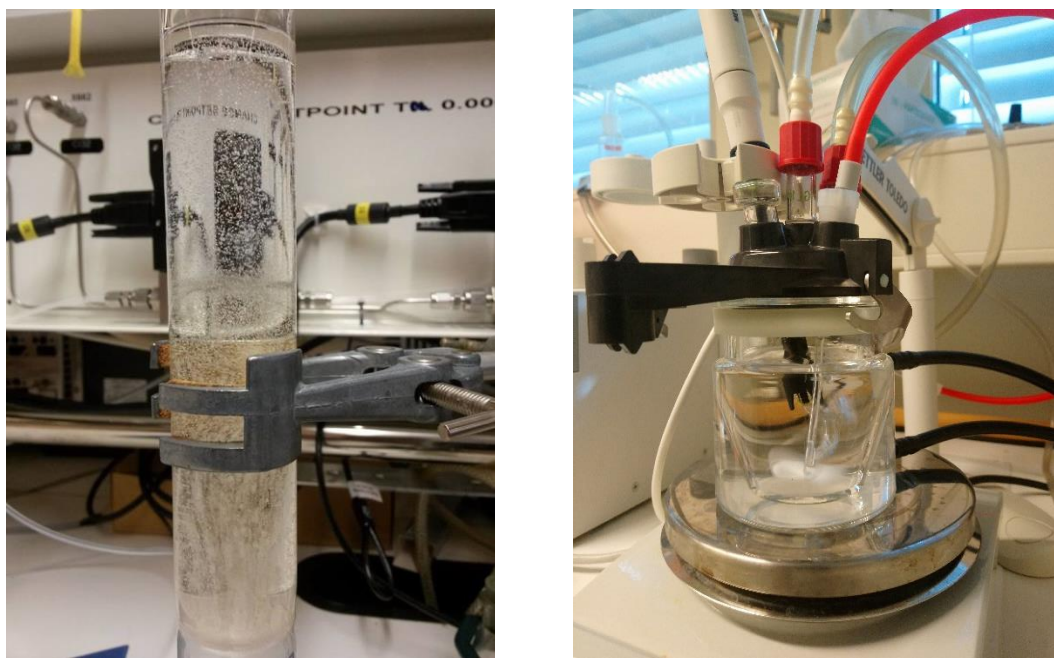
(a)   (b)

Figure 3.1: CO_2 loading apparatus

3.4 CO_2 Loading Analysis

The CO_2 concentration in amine + H_2O + CO_2 solutions is determined by a method based on precipitation of $BaCO_3$ and titration as stated by [36, 77]. There, a sample of amine + H_2O + CO_2 with a weight (0.25-0.3) g was mixed with 50 mL of 0.1 mol·L^{-1} NaOH and 50 mL of 0.3 mol·L^{-1} $BaCl_2$. In order to ensure the completion of the precipitation reaction, the mixture was boiled for 10 minutes (approximately) and was cooled in a water bath. Then the precipitate was filtered through a hydrophilic polypropylene membrane filter (45 μm). The filter cake was transferred into 100 mL of deionized water before titration with 0.1 mol·L^{-1} HCl. Then the titration was performed until the solution pH reached a value 2. The solution should be stirred during the titration to dissolve all the precipitate before pH reaches the desired value. In order to determine the excess HCl, the mixture was titrated back with a 0.1 mol·L^{-1} NaOH solution. Then, the amine concentration was found through a separate titration. There a sample with 1 g of amine solution is transferred into 100 mL of deionized water and titrated with a 1 mol·L^{-1} HCl solution. This method was followed to analyse the CO_2 loading of all CO_2 loaded amine mixtures and all the titrations were carried out using a METTLER TOLEDO-T50 titrator.

3.4.1 Reaction Equations

3.4.1.1 Titrations for CO₂ Loading Analysis

The following chemical reactions (R7) take place during the boiling of sample containing CO₂ loaded amine, 0.3 mol·L⁻¹ BaCl₂ and 0.1 mol·L⁻¹ NaOH.

$$Ba^{2+} + CO_2 + 2OH^- \rightarrow BaCO_3 + H_2O \tag{R7}$$

The reaction between $BaCO_3$ precipitate and 0.1 mol·L⁻¹ HCl is shown in (R8)

$$BaCO_3 + 2HCl \rightarrow BaCl_2 + CO_2 + H_2O \tag{R8}$$

The reaction between excess HCl with 0.1 mol·L⁻¹ NaOH

$$HCl + NaOH \rightarrow NaCl + H_2O \tag{R9}$$

3.4.1.2 Titration for Amine Concentration

The reaction (R10) and (R11) that are written based on MEA are taking place with the presence of 1 mol·L⁻¹ HCl.

$$NH_2(CH_2)_2OH + H_2O \rightarrow NH_3^+(CH_2)_2OH + OH^- \tag{R10}$$

$$OH^- + HCl \rightarrow H_2O + Cl^- \tag{R11}$$
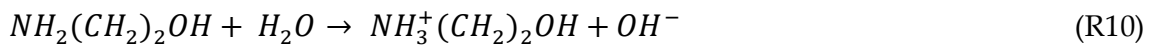
3.4.2 CO₂ Loading Calculation

The amount of CO₂ (moles) per mass of MEA and water in the amine sample is calculated by the following equations:

As described in reaction (R8), two moles of HCl are equivalent to one mole of CO₂. The amount of CO₂ moles ($n_{CO2\,sample}$) in the sample can be found using the HCl concentration (C_{HCl}), NaOH concentration (C_{NaOH}), HCl volume (V_{HCl}), and NaOH volume (V_{NaOH}) as given in Eq (103).

$$n_{CO2\,sample} = \frac{C_{HCl}.V_{HCl} - C_{NaOH}.V_{NaOH}}{2} \tag{103}$$

The amount of CO₂ (moles) in the blank sample ($n_{CO2(BS)}$) is found as shown in Eq (104).

$$n_{CO2(BS)} = \frac{C_{HCl}.V_{HCl(BS)} - C_{NaOH}.V_{NaOH(BS)}}{2} \tag{104}$$

Then the mass of the CO_2 in the blank sample ($m_{CO2(BS)}$) is calculated as

$$m_{CO2(BS)} = n_{CO2(BS)} \cdot M_{CO2} \tag{105}$$

M_{CO2} is the molecular weight of CO_2

Then the mass of CO_2 loaded ($m_{CO2\ sample}$) is calculated by

$$m_{CO2\ sample} = n_{CO2\ sample} \cdot M_{CO2} - m_{CO2(BS)} \tag{106}$$

The mass of MEA and water ($m_{MEA+water}$) in the sample

$$m_{MEA+water} = m_{sample(CO2\ loaded)} - m_{CO2\ sample} \tag{107}$$

and

$$\frac{n_{CO2}}{m_{MEA+water}} = \frac{n_{CO2\ sample} - n_{CO2(BS)}}{m_{MEA+water}} \cdot 1000 \frac{g}{kg} \tag{108}$$

Then the factor f is calculated as follows

$$f = \frac{m_{CO2\ sample}}{m_{sample(CO2\ loaded)}} \tag{109}$$

The concentration of MEA is calculated the following way

From the reaction (R10) and (R11), one mole of HCl is equivalent to one mole of MEA

$$m_{MEA} = C_{HCl} \cdot V_{HCl} \cdot M_{MEA} \tag{110}$$

M_{MEA} is the molecular weight g·mol⁻¹ of MEA

The mass of MEA and water in the sample

$$m_{MEA+water} = m_{sample(CO2\ loaded)} - m_{CO2\ sample} \tag{111}$$

$$m_{MEA+water} = m_{sample(CO2\ loaded)} - f\, m_{sample(CO2\ loaded)} \tag{112}$$

Then the weight percentage of MEA is given as

$$wt\%\ MEA = \frac{m_{MEA}}{m_{MEA+water}} \cdot 100\% \tag{113}$$

The CO_2 loading is calculated as follows

$$\frac{n_{MEA}}{m_{MEA+water}} = \frac{\left(\frac{wt\%MEA}{100\%}\right)}{M_{MEA}} \cdot 1000 \frac{g}{kg} \tag{114}$$

$$\alpha_{CO2} = \frac{n_{CO2}}{n_{MEA}} = \frac{\frac{n_{CO2}}{m_{MEA+water}}}{\frac{n_{MEA}}{m_{MEA+water}}} \tag{115}$$

For the mixtures with more than one amine, Eq (110) cannot be adopted to calculate the amine percentage in the mixture as the molecular weight of amine mixtures is unknown. Nevertheless, CO_2 loading can be determined according to Eq (115) in which n_{MEA} is replaced by n_{Amine} that can be found from the reactions (R10) and (R11).

4 Measuring Instruments

This section describes the instruments that were used to perform the density and viscosity measurements of different amine mixtures. It explains the procedures and calibration methods of the instruments.

4.1 Density Measurements

4.1.1 Density Meter

The density of all solutions were measured using a density meter (DMA 4500) from Anton Paar, which is operated at atmospheric pressure. DMA 4500 is a high accuracy density meter consisting of a U-tube that is oscillated at its fundamental frequency [197, 198]. The U-tube is made of borosilicate glass and it is the main unit in the instrument. A special care needs to be given to make sure that all wetted parts made of PTFE (Polytetrafluoroethylene) adopters and sensor (U-tube) are resistant to the sample. The effect from ambient influence is minimized by placing the sensor in a glass housing (measuring cell) and the space is filled with a special gas to establish a good thermal contact with the temperature regulator [199]. The temperature regulation in the density meter is performed by Peltier elements. This technology replaces the use of water bath for the temperature regulation that is inefficient. Peltier elements produce a heat flux using the electric current flow depending on the direction of the current; one side of a Peltier element gets heated up while other side cools down.

The oscillation frequency vary with the density of the filled sample. An accurate measurement of the oscillation frequency leads to determine the true density of the sample. This oscillation frequency (characteristic frequency) is a function of sample density and it is given as follows

$$\tau = 2\pi \sqrt{\frac{\rho v + m}{c}} \tag{116}$$

Where τ is the oscillation period, ρ is sample density, v is cell volume, m is cell mass and c is spring constant.

$$\rho = \frac{(\tau^2 - H)}{G} \tag{117}$$

$$G = \frac{4\pi^2 v}{c} \tag{118}$$

$$H = \frac{4\pi^2 m}{c} \tag{119}$$

The schematic shown in Figure 4.1 illustrates the configuration of the U-tube and other accessories in the density meter.

Piezo elements provide a more precise method to excite the sensor than using a system of magnets that put additional weights on the oscillating sensor. A piezo element is a crystal or ceramic material where dimensions can be changed by applying an electrical voltage. The measuring of oscillation is determined by the optical pick-ups, which detect a light beam that is interrupted by an oscillating glass sensor.
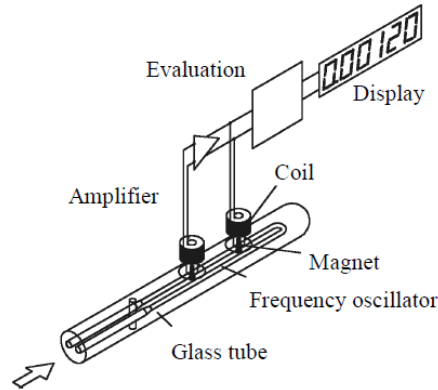
Figure 4.1: Schematic of the U-tube in the density meter [200]

The viscosity of the sample has an effect on the oscillation frequency. The shear forces generated between the fluid and the tube due to oscillation result in damping. This damping of U-tube oscillation can be given in a form of mathematical relation as in Eq (120)[198]. The density can be overestimated due to the damping, which is promoted by viscosity of the sample. This effect is compensated in modern density meters by using a special technique of applying two different oscillation modes and viscosity correction is performed automatically.

$$k \approx C'\sqrt{\eta} \tag{120}$$

Where k is the error in (kg·m⁻³), C' is a constant ((kg·s·m⁻⁵)⁰·⁵) and η is viscosity (Pa·s)

Where k is the error in (kg·m^{-3}), C' is a constant ((kg·s·m^{-5})$^{0.5}$) and η is viscosity (Pa·s)

Table 4.1: lists several technical information related to the DMA 4500 density meter.

Table 4. 1: DMA 4500 technical information.

Measuring range	0-3 g·cm^{-3}
Repeatability, s.d[a]	
Density	1x10^{-5} g·cm^{-3}
Temperature	0.01 °C
Measuring temperature	0 °C to +90 °C (32 to 194 °F)

[a] Standard deviation

4.1.2 Density Measurements in DMA 4500

The borosilicate glass U-tube enables to see the filling of sample to identify the formation or trapping of bubbles in the cell. During the density measurements, a sample with 3-5 mL volume (typically holds about 0.7 mL of sample) is introduced into the oscillating U-tube. At elevated temperatures (> 40 °C), a new sample is introduced to the density meter at each temperature for the density measurement to minimize the error due to the amine evaporation and CO_2 escape from the U-tube. There is a challenge especially for CO_2 loaded solutions that the concentration may vary during the measurements.

4.2 Viscosity Measurement

4.2.1 Rheometer

A rheometer from Anton Paar (Physica MCR 101) was used to perform viscosity measurements of all amine + H_2O + CO_2 mixtures. The dynamic viscosity was measured via a double-gap pressure cell XL measuring system that is recommended for the low viscous solutions since the probe provides a high surface area between the fluid and the probe [201]. The rheometer is built with an internal temperature controller that has a standard temperature uncertainty of 0.03 K. In order to measure viscosities at temperatures below 303.15 K, an external cooling system (Anton Paar Viscotherm VT2) has been employed with standard temperature uncertainty 0.02 K [150]. A sample of 7mL is fed into the gap between the fixed outer and inner wall of the rotating cylinder. The rotating cylinder is rotated at fixed rpm in order to give a constant shear rate. The instrument measures the applied torque, shear stress and calculates the dynamic viscosity accordingly. A schematic of the double-gap pressure cell XL is given in Figure 4.2.
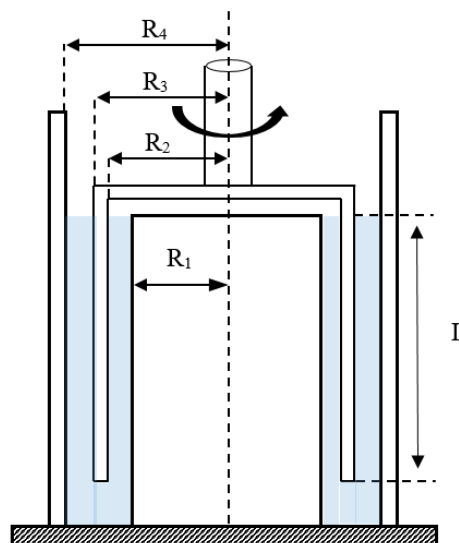
Figure 4.2: Schematic of double-gap geometry of the rheometer [202]

Table 4.2 gives technical information about the double-gap pressure cell XL of the Physica MCR 101 rheometer.

The viscosity of liquid is determined according to the model as described below.

$$\tau = \frac{1+\delta^2}{(\delta^2 R_3^2 + R_2^2)} \cdot \frac{T}{4000\pi L\, C_L} \tag{121}$$

$$\dot{\gamma} = \frac{\pi n}{30} \cdot \frac{1+\delta^2}{\delta^2 - 1} \tag{122}$$

$$\omega = \frac{2\pi}{60} n \tag{123}$$

Where τ, $\dot{\gamma}$, T, δ, R_i/R_e, ω and n are shear stress, shear rate, torque, radius ratio, internal/external cylinder radius, angular velocity and speed respectively.

Table 4.2: Technical information of the double-gap pressure cell XL.

Maximum Pressure	150 bar
Maximum Temperature	180 °C
Concentricity of measuring systems	±0.01 mm
Parallelism of measuring systems	±0.01 mm

It is important to select the proper shear rate in the rheometer to get an accurate viscosity of the amine solution. Figure 4.3 illustrates the relationship of viscosity vs shear rate that is provided by the manufacturer in which double-gap pressure cell XL denoted as DG35.12/XL/Pr (green box) is the valid measuring system for this work.
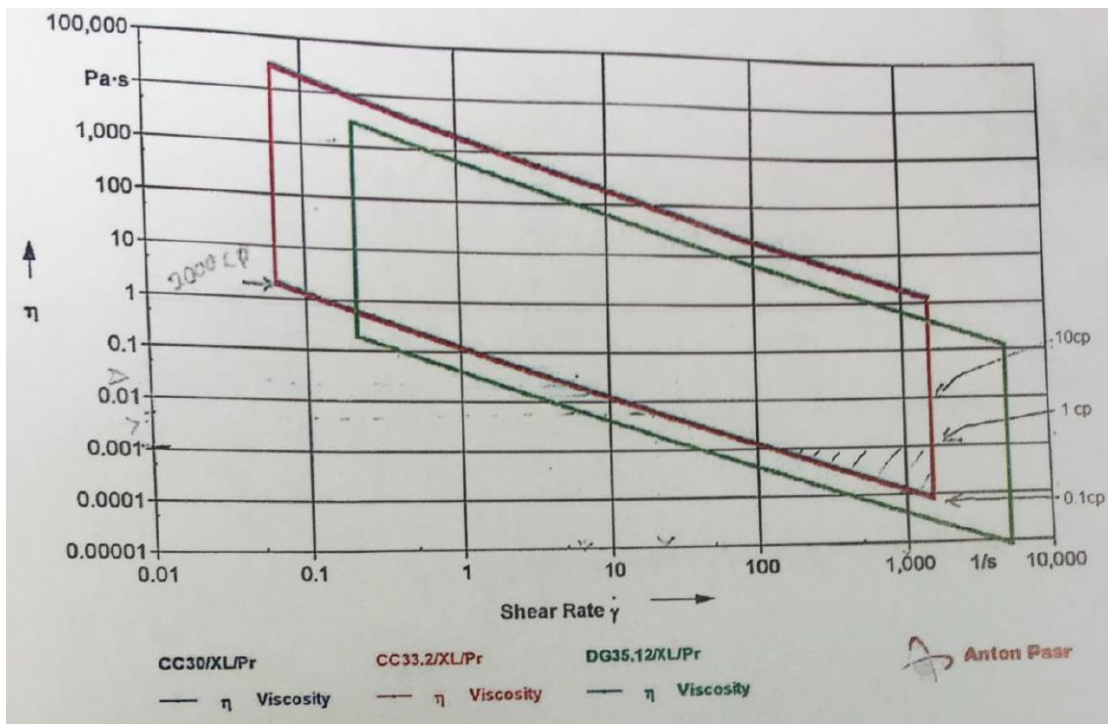
Figure 4.3: Viscosity and shear rate relation for different measuring methods [203]

4.2.2 Shear Rate

The selection of shear rate was done by performing viscosity measurements at different shear rates of 200, 400, 600, 800, 1000 and 1200 s^{-1}. The considered shear rates are within the range as shown in Figure 4.3. The viscosity was measured 10 times with 10 s time intervals at 303.15 K. The standard deviations of the measured viscosities at each shear stress were calculated. As given in Table 4.3, the standard deviation decreases with the increase of shear rate. A shear rate, which gives a low standard deviation, has to be selected for the viscosity measurements. At the CO_2-laboratory in USN, 1000 s^{-1} of shear rate has been used for the viscosity measurement of amine + H_2O and amine + H_2O + CO_2 mixtures and it has a low standard deviation compared to lower shear rates. Accordingly, 1000 s^{-1} was selected to carry out viscosity measurements in this study.

Table 4.3: Variation of the standard deviation of viscosity measurements with shear rate.

Shear rate (s^{-1})	Standard deviation (mPa·s)		
	30% MEA	40% MEA	50% MEA
200	0.0421	0.0345	0.0460
400	0.0243	0.0189	0.0235
600	0.0137	0.0088	0.0113
800	0.0061	0.0039	0.0059
1000	0.0029	0.0020	0.0059
1200	0.0010	0.0005	0.0055

4.2.3 Air check, Motor Adjustment and Calibration

The checking of the rheometer includes air check and viscosity measurement of a certified viscosity standard that is also known as standard oil. Air check and motor adjustment were performed prior to viscosity measurements to examine the quality of the motor adjustment and the conditions of the bearings. The residual friction in the bearing is measured during the motor adjustment. The measured values are saved and will be used in the viscosity measurements. Figure 4.4 shows the measured torque with deflection angle of air check before and after the motor adjustment.

Calibration of the rheometer is performed using a standard calibration fluid (S3S) provided by the Paragon Scientific Ltd. The standard oil is tested in accordance with ASTM D445. The uncertainties related with standard oil is given in Table 4.4 as provided by the supplier. The viscosity of standard oil was measured to identify the measurement error in the instrument and final viscosity measurements of all the amine solutions are corrected accordingly. Table 4.5 gives viscosities of the standard oil (S3S) as given by the supplier.
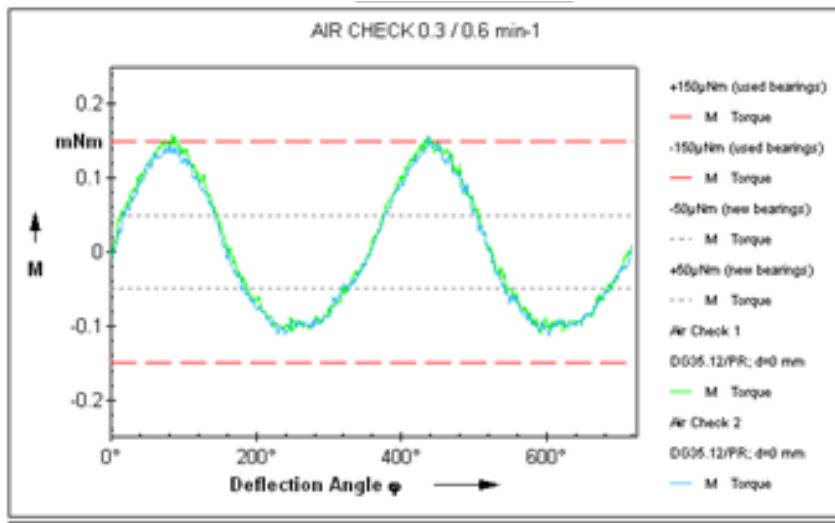
Figure 4.4: First air check (green line) before the motor adjustment and second air check (blue line) after the motor adjustment.

Table 4.4: Uncertainties related with viscosity standard.

Viscosity range	Expanded Uncertainty	
	Kinematic viscosity mm²s⁻¹ (cSt)	Dynamic viscosity mPa·s (cP)
0.3 to 7.4	± 0.07%	± 0.07%
7.4 to 10	± 0.09%	± 0.09%
10 to 30	± 0.12%	± 0.12%
30 to 72	± 0.14%	± 0.14%

Table 4.5: Viscosities of the standard oil (S3S) as given by the supplier.

Temperature (°C)	Viscosities of the standard oil / mPa·s
20.00	3.709
25.00	3.264
37.78	2.434
40.00	2.323
50.00	1.910
60.00	1.600
80.00	1.175
98.89	0.9161
100.00	0.9036
150.00	0.5339

4.2.4 Setting up Viscosity Experiments

The viscosity experiments in the rheometer were performed using the Rheoplus software (version 3.0x), which comes with the Physica MCR 101 rheometer. Figure 4.5 and 4.6 illustrate the details of the setup for viscosity measurements under constant

shear rate at different temperatures. Figure 4.5 shows how the software was used to arrange viscosity measurements below 303.15 K.

The external cooling system was activated while the viscosity was measured as shown in a red circle in Figure 4.5. The temperature of the cooling system was set two degrees below the desired temperature as shown in the green circle. For the viscosity measurements at and above 303.15 K, only the existing temperature controller was employed as illustrated in Figure 4.6.
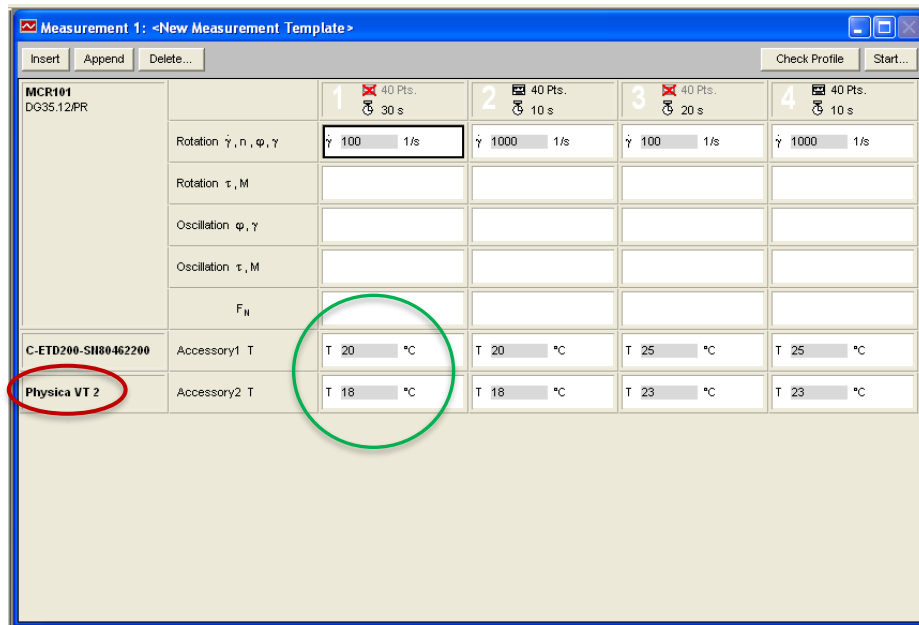
Figure 4.5: Setup for the viscosity measurements below 303.15 K.
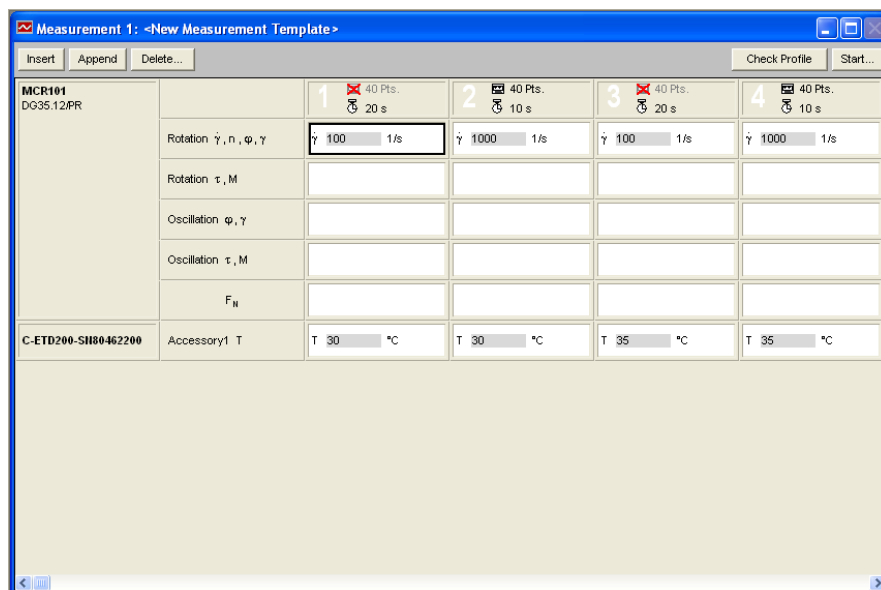
Figure 4.6: Setup for the viscosity measurements above 303.15 K.

4.2.5 Effect of Applied Pressure on Viscosity Measurements
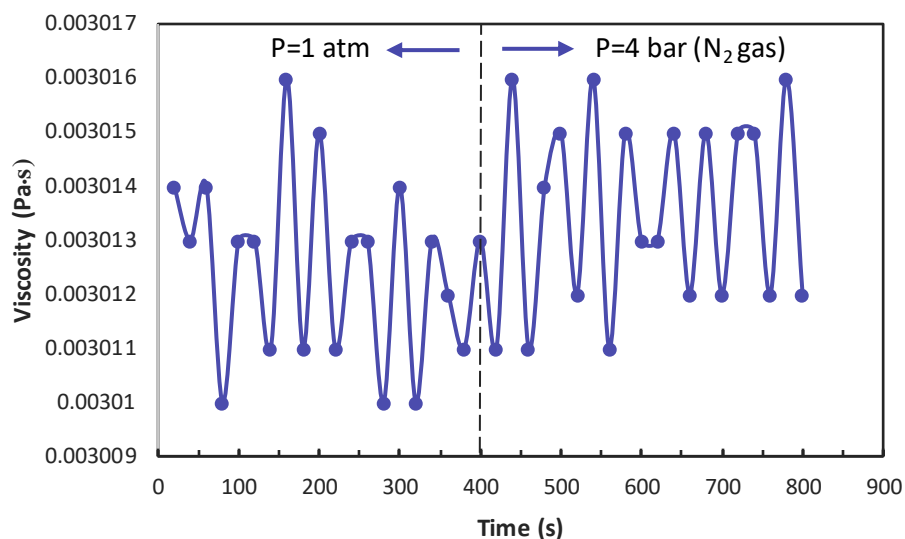
Figure 4.7: Viscosity at 40% MEA 60% H_2O mixtures at 303.15 K and P= 1 atm and P = 4 bar (N_2 gas).
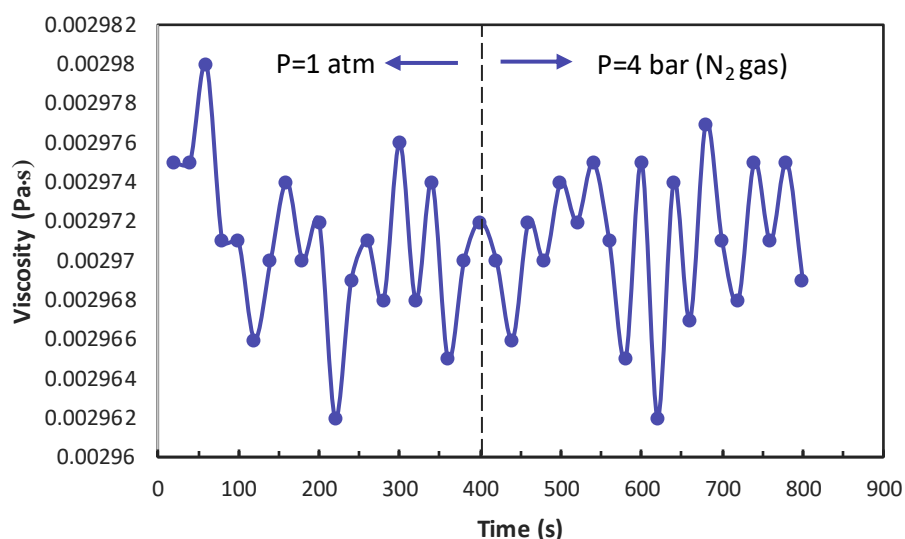
Figure 4.8: Viscosity at 27% AMP 3% MEA 70% H_2O mixtures at 303.15 K and P= 1 atm and P= 4 bar (N_2 gas).

For the viscosity measurements of CO_2 loaded aqueous amine solutions, a pressure of 4 bar using N_2 gas was applied to avoid possible CO_2 and amine escape from the solution. A test was performed to see the effect of applied pressure on the viscosity of the solution. There, the viscosity of the sample was measured under atmospheric pressure and applied 4 bar pressure with N_2 gas. The study shows the variation of viscosity due to the increase of pressure is less than 0.1% for the considered MEA + H_2O and AMP + MEA + H_2O mixtures. Figure 4.7 and 4.8 illustrate the effect of pressure on dynamic viscosity. This indicates that in most cases the effect of pressure can be neglected.

5 Results and Discussion

This chapter presents a brief overview of the results of density and viscosity measurements for CO_2 loaded and unloaded aqueous amine mixtures, pilot plant study, correlations for the physical properties and process simulations.

5.1 Density and Viscosity Measurements

Table 5.1-5.6 provide an overview of measured conditions of amine concentrations, temperatures and CO_2 loadings for the density and viscosity of amine mixtures. Each data point was obtained from an average of three measurements.

Table 5.1: Amine concentrations and temperatures of density measurements in binary mixtures.

Mixtures	Concentration: x_1[a]		Temperature (K)		No of points
	Low	High	Low	High	
MEA + H_2O	0.1122	1	293.15	363.15	64
MDEA + H_2O	0.0609	1	293.15	353.15	130
DMEA + H_2O	0.0797	1	293.15	353.15	130
DEEA + H_2O	0.0618	1	293.15	353.15	130

[a] mole fraction of the amine

Table 5.2: Amine concentrations and temperatures of viscosity measurements in binary mixtures.

Mixtures	Concentration: x_1[a]		Temperature (K)		No of points
	Low	High	Low	High	
MEA + H_2O	0.1122	1	293.15	363.15	64
MDEA + H_2O	0.0609	1	293.15	363.15	150
DMEA + H_2O	0.0797	1	293.15	363.15	150
DEEA + H_2O	0.0618	1	293.15	363.15	150

[a] mole fraction of the amine

Table 5.3: Amine concentrations and temperatures of density measurements in ternary mixtures.

Mixture	Temperature (K)		No of points
	Low	High	
15 mass% MDEA + 15 mass% MEA + 70 mass% H_2O	293.15	343.15	11
20 mass% MDEA + 10 mass% MEA + 70 mass% H_2O	293.15	343.15	11
25 mass% MDEA + 5 mass% MEA + 70 mass% H_2O	293.15	343.15	11
30 mass% MDEA + 0 mass% MEA + 70 mass% H_2O	293.15	343.15	11
15 mass% DMEA + 15 mass% MEA + 70 mass% H_2O	293.15	343.15	11
20 mass% DMEA + 10 mass% MEA + 70 mass% H_2O	293.15	343.15	11
25 mass% DMEA + 5 mass% MEA + 70 mass% H_2O	293.15	343.15	11

Mixture	Low	High	points
30 mass% DMEA + 0 mass% MEA + 70 mass% H_2O	293.15	343.15	11
15 mass% DEEA + 15 mass% MEA + 70 mass% H_2O	293.15	343.15	11
20 mass% DEEA + 10 mass% MEA + 70 mass% H_2O	293.15	343.15	11
25 mass% DEEA + 5 mass% MEA + 70 mass% H_2O	293.15	343.15	11
30 mass% DEEA + 0 mass% MEA + 70 mass% H_2O	293.15	343.15	11

Table 5.4: Amine concentrations and temperatures of viscosity measurements in ternary mixtures.

Mixture	Temperature (K)		No of
	Low	High	points
15 mass% MDEA + 15 mass% MEA + 70 mass% H_2O	293.15	363.15	15
20 mass% MDEA + 10 mass% MEA + 70 mass% H_2O	293.15	363.15	15
25 mass% MDEA + 5 mass% MEA + 70 mass% H_2O	293.15	363.15	15
30 mass% MDEA + 0 mass% MEA + 70 mass% H_2O	293.15	363.15	15
15 mass% DMEA + 15 mass% MEA + 70 mass% H_2O	293.15	363.15	15
20 mass% DMEA + 10 mass% MEA + 70 mass% H_2O	293.15	363.15	15
25 mass% DMEA + 5 mass% MEA + 70 mass% H_2O	293.15	363.15	15
30 mass% DMEA + 0 mass% MEA + 70 mass% H_2O	293.15	363.15	15
15 mass% DEEA + 15 mass% MEA + 70 mass% H_2O	293.15	363.15	15
20 mass% DEEA + 10 mass% MEA + 70 mass% H_2O	293.15	363.15	15
25 mass% DEEA + 5 mass% MEA + 70 mass% H_2O	293.15	363.15	15
30 mass% DEEA + 0 mass% MEA + 70 mass% H_2O	293.15	363.15	15

Table 5.5: Amine concentrations, CO_2 loadings and temperatures of density measurements in mixtures.

Mixture	CO_2 loading (mol CO_2/mol amine)	Temperature (K)	No of points
30 mass% MEA + 70 mass% H_2O	0, 0.095, 0.175, 0.328, 0.445, 0.543	293.15-353.15	39
40 mass% MEA + 60 mass% H_2O	0, 0.105, 0.215, 0.325, 0.436, 0.548	293.15-353.15	39
50 mass% MEA + 50 mass% H_2O	0, 0.092, 0.186, 0.290, 0.395, 0.495	293.15-353.15	41
21 mass% AMP + 9 mass% MEA + 70 mass% H_2O	0, 0.107, 0.210, 0.308, 0.400, 0.518	293.15-343.15	66
24 mass% AMP + 6 mass% MEA + 70 mass% H_2O	0, 0.083, 0.165, 0.314, 0.418, 0.508	293.15-343.15	66
27 mass% AMP + 3 mass% MEA + 70 mass% H_2O	0, 0.072, 0,152, 0.246, 0.461, 0.511	293.15-343.15	66

Table 5.6: Amine concentrations, CO_2 loadings and temperatures of viscosity measurements in mixtures.

Mixture	CO_2 loading (mol CO_2/mol amine)	Temperature (K)	No of points
30 mass% MEA + 70 mass% H_2O	0, 0.095, 0.175, 0.328, 0.445, 0.543	293.15-353.15	42
40 mass% MEA + 60 mass% H_2O	0, 0.105, 0.215, 0.325, 0.436, 0.548	293.15-353.15	42
50 mass% MEA + 50 mass% H_2O	0, 0.092, 0.186, 0.290, 0.395, 0.495	293.15-353.15	42
21 mass% AMP + 9 mass% MEA + 70 mass% H_2O	0, 0.107, 0.210, 0.308, 0.400, 0.518	293.15-363.15	48
24 mass% AMP + 6 mass% MEA + 70 mass% H_2O	0, 0.083, 0.165, 0.314, 0.418, 0.508	293.15-363.15	48
27 mass% AMP + 3 mass% MEA + 70 mass% H_2O	0, 0.072, 0,152, 0.246, 0.461, 0.511	293.15-363.15	48

5.2 Density of Non-Loaded Aqueous Mixtures

The density of different aqueous amine mixtures was measured at different concentrations and temperatures. Measured densities of MEA + H_2O mixtures are listed in Article **A**. Figure 5.1 illustrates the variation of density with MEA concentration and temperature. A correlation used by Aronu, et al. [204] as given in Eq (126) was adopted to fit the density data and accuracy of the data fit was examined by Average Absolute Relative Deviation AARD (%) and Absolute Maximum Deviation AMD as given in Eq (124) and Eq (125).

$$AARD\,(\%) = \frac{100\%}{N} \sum_{i=1}^{N} \left| \frac{Y_i^E - Y_i^C}{Y_i^E} \right| \tag{124}$$

$$AMD = MAX \left| Y_i^E - Y_i^C \right| \tag{125}$$

$$\rho = \left(k_1 + \frac{k_2 x_2}{T} \right) exp \left(\frac{k_3}{T^2} + \frac{k_4 x_1}{T} + k_5 \left(\frac{x_1}{T} \right)^2 \right) \tag{126}$$

A review reported in Article **F** examined the accuracies in terms of AARD and AMD of presented density correlations for aqueous MEA solutions. Article **F** presents the accuracies obtained from different correlations with different data sources found in literature. The studied correlations were able to represent density data with less than 0.2 % AARD.
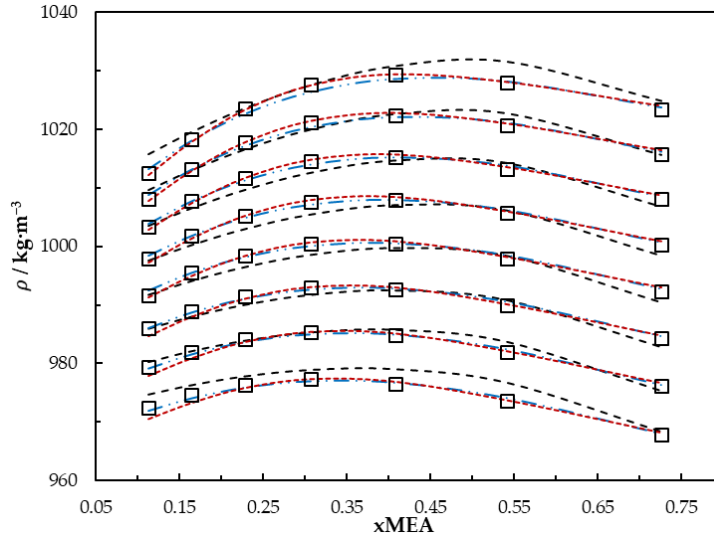
Figure 5.1: Density of aqueous MEA mixtures at different concentrations and temperatures (293.15, 303.15, 313.15, 323.15, 333.15, 343.15, 353.15 and 363.15) K. Data: from this work, '□'. Correlation representations: from this work, '- - -'; Hartono, et al. [81], '- ·· -'; Han, et al. [77], '···'.

The correlation shown in Eq (126) was used to fit the density data published by Idris and Eimer [205] for 3A1P + H₂O mixtures. The accuracy of the data fit was reported as 1.9 kg·m⁻³ average absolute deviation (AAD) and a comparison of accuracies from different correlations is given in Article **J.**

The densities of MDEA + H₂O, DMEA + H₂O and DEEA + H₂O mixtures at different concentrations and temperatures were measured and are reported in Article **D.** Densities of pure amines of MDEA, DMEA and DEEA were measured and were compared with data reported in literature. The excess molar volume V^E of the mixtures showed a negative deviation indicating the presence of strong intermolecular interactions like H-bonds among unlike molecules. A Redlich-Kister [58] type polynomial for excess molar volume V^E as given in Eq (4) and for density deviation $ln(\rho_\gamma)$ as defined by Eq (128) were proposed to fit density data and calculated parameters are listed in Article **D.** Both correlations were in good agreement with measured data and were able to fit densities with less than 0.5% AARD.

$$\rho = \frac{\sum_{i=1}^{2} x_i M_i}{V^E + \sum_{i=1}^{2} \frac{x_i M_i}{\rho_i}} \tag{127}$$

$$ln(\rho) = ln(\rho_\gamma) + \sum_{i=1}^{i=2} x_i \rho_i \tag{128}$$

$$ln(\rho_\gamma) = x_1 x_2 \sum_{i=0}^{i=n} A_i (1 - 2x_2)^i \tag{129}$$

The Redlich-Kister coefficients (A_i) of excess molar volume V^E were adopted to calculate the partial molar volume of aqueous mixtures at different concentrations and temperatures.

Figure 5.2 illustrates the variation of partial molar volumes of MDEA + H₂O, DMEA + H₂O and DEEA + H₂O mixtures. A detailed description of the correlation development and calculations are provided in Article **D**.
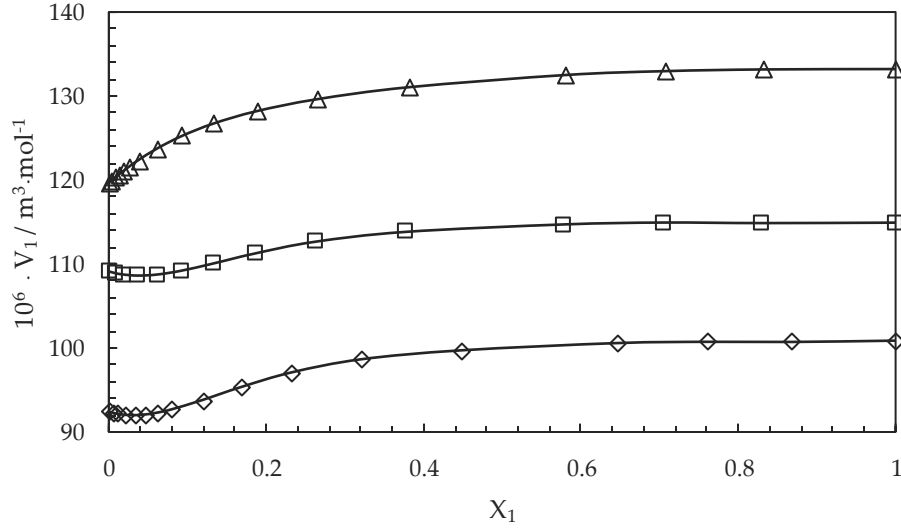
Figure 5.2: Partial molar volumes of MDEA in (MDEA + H₂O), '□'; DMEA in (DMEA + H₂O), '◊'; DEEA in (DEEA + H₂O), '△'at 298.15 K.

Article **B** and Article **C** present the measured densities of AMP + MEA + H₂O and MDEA + MEA + H₂O, DMEA + MEA + H₂O and DEEA + MEA + H₂O mixtures respectively. The density was measured at different amine concentrations and temperatures and excess molar volume V^E was found to examine the intermolecular interactions and molecular packing in the mixtures. All aqueous ternary mixtures showed a negative deviation of excess molar volume V^E indicating the existence of strong intermolecular interactions like H-bonds among unlike molecules. Densities were correlated using Redlich-Kister type polynomials for the correlation proposed in Eqs (130)-(133).

$$V^E = V_{12}^E + V_{23}^E + V_{13}^E \tag{130}$$

$$V_{jk}^E = x_j x_k \sum_{i=0}^n A_i \left(x_j - x_k\right)^i \tag{131}$$

$$A_i = a + b(T) + c(T)^2 \tag{132}$$

$$\rho = \frac{\sum_{i=1}^3 x_i M_i}{V^E + \sum_{i=1}^3 \frac{x_i M_i}{\rho_i}} \tag{133}$$

Figure 5.3 shows a comparison of correlations with the measured data for AMP + MEA + H₂O mixtures. The calculated parameters are given in Article **B** and Article **C**. The proposed correlation for densities of aqueous ternary mixtures was able to fit data with less than 0.1% AARD.
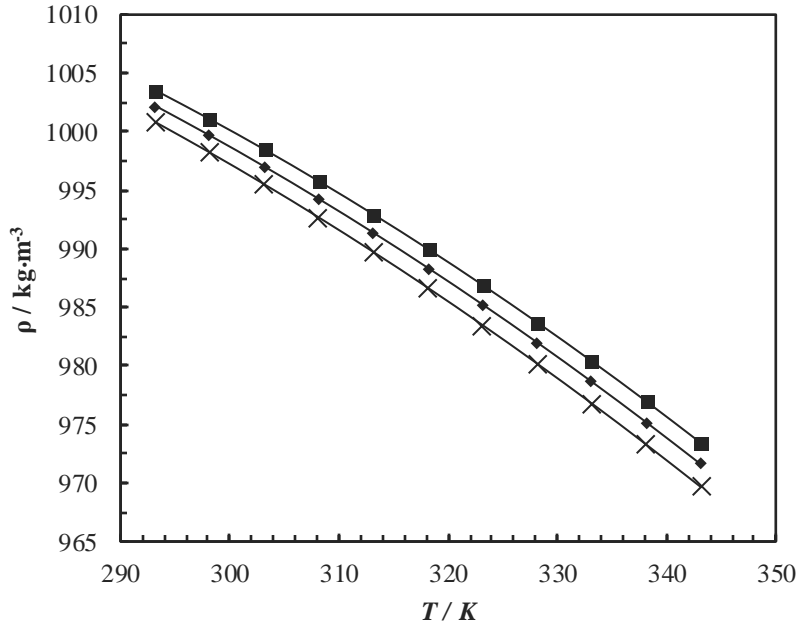
Figure 5.3: Density of AMP + MEA + H₂O mixtures: measured data; 21 mass % AMP + 9 mass % MEA + 70 mass % H₂O, '■', 24 mass % AMP + 6 mass % MEA + 70 mass % H₂O, '◆', 27 mass % AMP + 3 mass % MEA + 70 mass % H₂O, 'x', correlation; '—'.

5.3 Density of CO₂ Loaded Aqueous Mixtures

The density of CO_2 loaded aqueous MEA increases with the increase of CO_2 loading in the solution. Figure 5.4 illustrates density variation observed for CO_2 loaded aqueous MEA solution with 30 mass % MEA concentration. The correlation given in Eq (126) was modified as shown in Eq (134) to fit the measured densities at different CO_2 loadings and temperatures.

$$\rho = \left(a_1 + a_2(T) + a_3(T)^2 + a_4 x_3\right)\left(k_1 + \frac{k_2 x_2}{T}\right) exp\left(\frac{k_3}{T^2} + \frac{k_4 x_1}{T} + k_5 \left(\frac{x_1}{T}\right)^2\right) \qquad (134)$$

The measured densities of CO_2 loaded aqueous MEA solutions with 40 mass % and 50 mass % MEA concentration are presented in Article **A.** The proposed correlation for CO_2 loaded MEA solutions was able to fit the density data with 0.15% AARD. This study also compared the reported densities and correlation in literature with our work as shown in Figure 5.4. Article **F** revealed that the proposed density correlations in literature for CO_2 loaded aqueous MEA were able to represent published density data in different sources with an accuracy less than 1% AARD.
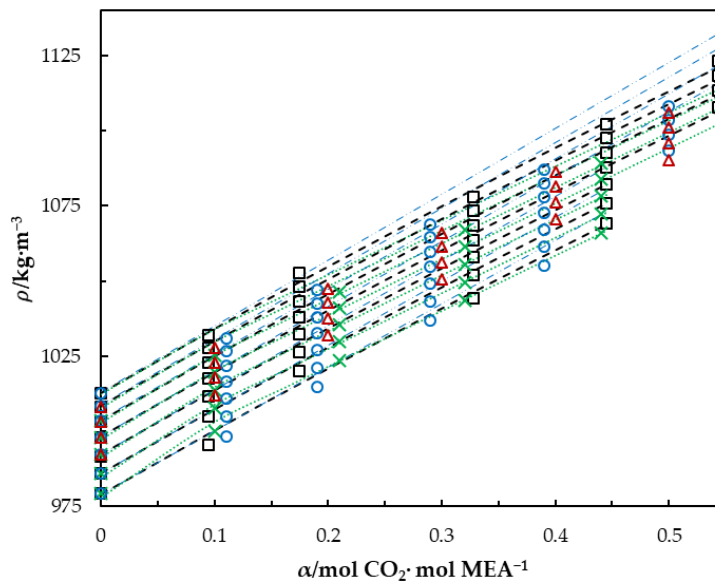
Figure 5. 4: Density of CO_2 loaded MEA ($w_1 = 0.3$) solution at different CO_2 loadings and temperatures (293.15, 303.15, 313.15, 323.15, 333.15, 343.15 and 353.15) K. Data: from this work, '□'; Hartono, et al. [81], 'O'; Han, et al. [77], 'x'; Jayarathna, et al. [36], '△'. Correlation: from this work, '- - -'; Hartono, et al. [81], '- ·· -'; Han, et al. [77], '···'.
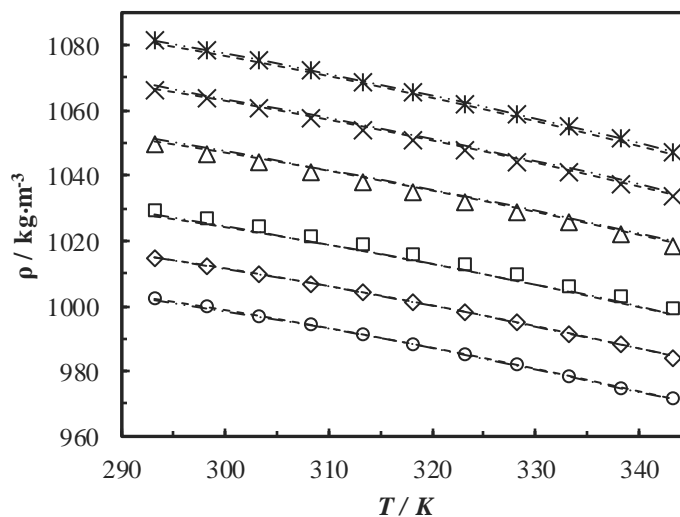
Figure 5.5: Density of CO_2 loaded 24 mass % AMP + 6 mass % MEA + 70 mass % H_2O at different temperatures and CO_2 loadings (α / mol $CO_2 \cdot$ mol amine^{-1}): 0.000, '○'; 0.083, '◇'; 0.165, '□'; 0.314, '△'; 0.418, 'x'; 0.508, '҂'. Correlations: Setschenow-type, '- - -'; Modified Weiland's, '- ·· -'.

The measured densities of CO_2 loaded aqueous AMP + MEA mixtures at different amine concentrations, temperatures and CO_2 loadings are reported in Article **B**. The results revealed that density increases with the increase of CO_2 loading. Density decreases with

the increase of temperature. Correlations based on Weiland's density and Setschenow-type correlations were adopted to fit the measured densities as shown in Figure 5.5.

Here, the modified Weiland's correlation was used to fit density data with the whole range of AMP and MEA concentrations, CO_2 loadings and temperatures. The accuracies of regression were found as 0.42 % AARD and 13.7 $kg \cdot m^{-3}$ AMD.

5.4 Viscosity of Non-Loaded Aqueous Mixtures

The measured viscosity of MEA + H_2O mixtures at different concentrations and temperatures are given in Article **A** with the viscosity data found at the same concentrations and temperatures from literature. The Eyring's viscosity model [122] based on absolute rate theory was adopted to calculate the excess free energy ΔG_0^{E+} of activation for viscous flow. A Redlich-Kister type polynomial was proposed to correlate ΔG_0^{E+}. The proposed correlation was able to represent measured viscosity data at 1.4% AARD. The applicability of the NRTL model to calculate excess free energy ΔG_0^{E+} of activation for viscous in Eyring's viscosity model for MEA + H_2O mixtures was discussed in Article **I**. A correlation was proposed to use the excess Gibbs free energy of mixing ΔG^{E*} from the NRTL model to replace ΔG_0^{E+} from Eyring's viscosity model as given in Eq (135) and Eq (136). Figure 5.6 compares the correlation with measured viscosities for MEA + H_2O mixtures. It was observed that the correlation was able to fit the viscosity data with 1.3% AARD and 1 $mPa \cdot s$ AMD.

$$-\Delta G^{E*}/\Delta G_0^{E+} = f(x_1, T) \tag{135}$$

$$f(x_1, T) = a + bx_1T + cT^2 \tag{136}$$
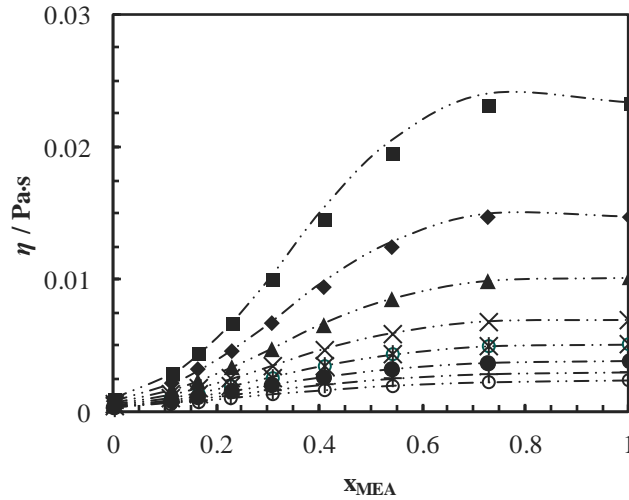
Figure 5.6: Comparison of measured viscosity of MEA + H_2O mixtures with correlation at temperatures: 293.15 K, '■'; 303.15 K, '◆'; 313.15 K, '▲'; 323.15 K, 'x'; 333.15 K, 'ж'; 343.15 K, '●'; 353.15 K, '+'; 363.15 K, '○'. The dash—dotted lines represent the correlation.

The viscosity of MDEA + H_2O, DMEA + H_2O and DEEA + H_2O was measured at different concentrations and temperatures. The viscosity deviation η^E was calculated from measured viscosities as given in Eq (137).

$$\eta^E = \eta - \sum_{i=1}^{i=2} x_i \eta_i \tag{137}$$

$$\eta^E = x_1 x_2 \sum_{i=0}^{i=n} A_i (1 - 2x_2)^i \tag{138}$$

The viscosity deviation η^E is negative for the H_2O-rich region for MDEA + H_2O mixtures indicating the presence of weak intermolecular interactions. It gradually becomes positive with the increase of MDEA concentration in the mixture. Both DMEA + H_2O and DEEA + H_2O mixtures show a positive viscosity deviation for the whole range of amine concentration indicating the existence of strong intermolecular interactions among the unlike molecules. The Redlich-Kister type polynomials were used to correlate η^E calculated from measured viscosities as shown in Eq (139).

$$ln(\eta) = \sum_{i=1}^{I=2} x_i ln(\eta_i) + x_1 x_2 G_{12} \tag{139}$$

The correlation proposed by Grunberg and Nissan [141] as shown in Eq (139) was adopted to interpret the strength of the intermolecular interactions between components in a binary mixture [168]. The calculated parameters of the proposed model for G_{12} are presented in Article **D.** The correlations were able to represent measured viscosities with the accuracy of 4.7% AARD.

The kinematic viscosity was calculated via measured dynamic viscosity and density of the aqueous mixtures. The McAllister's [126] three-body model was used to correlate kinematic viscosity MEA + H_2O mixtures. The temperature dependence of the model was considered as described from Eq (41) to Eq (44).
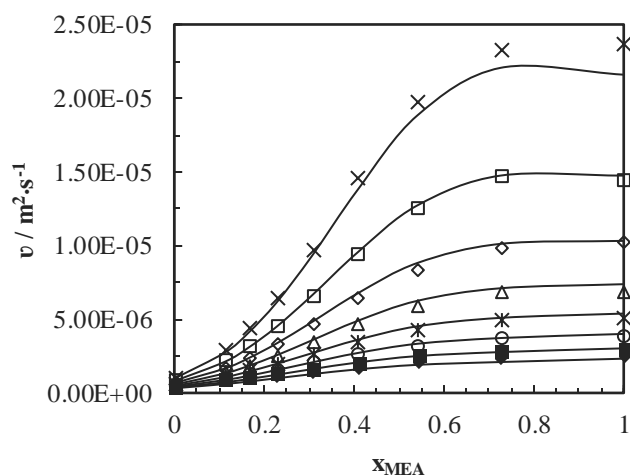
Figure 5.7: Kinematic viscosity of MEA + H₂O mixtures at temperatures: 293.15 K, 'x'; 303.15 K, '□'; 313.15 K, '◇'; 323.15 K, '△'; 333.15 K, '✳'; 343.15 K, '○'; 353.15 K, '■'; 363.15 K, '◆'. The solid lines represent the McAllister model.
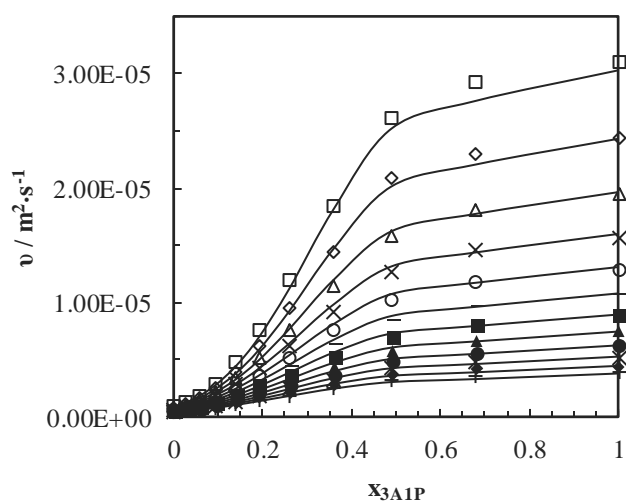
Figure 5.8: Kinematic viscosity of 3A1P + H₂O mixtures at temperatures: : 298.15 K, '□'; 303.15 K, '◇'; 308.15 K, '△'; 313.15 K, 'x'; 318.15 K, '○'; 323.15 K, '-'; 328.15 K, '■'; 333.15 K, '▲'; 338.15 K, '●'; 343.15 K, '✳'; 348.15 K, '◆'; 353.15 K, '+'. The solid lines represent the McAllister model.

The viscosity of ternary amine mixtures MDEA + MEA + H₂O, DMEA + MEA + H₂O and DEEA + MEA + H₂O were measured at different amine concentrations and temperatures. Viscosity increase with the increase of tertiary amine concentration and viscosity decreased with the increase of temperature. A correlation was proposed to fit the calculated excess free activation energy ΔG_0^{E+} for viscous flow. The suggested correlations were able to represent measured viscosities with less than 0.15% AARD. Further details regarding the correlation and calculated parameters are presented in Article **C**.

5.5 Viscosity of CO₂ Loaded Aqueous Mixtures

The viscosity of CO_2 loaded aqueous MEA mixtures was measured at different MEA concentrations, CO_2 loadings and temperatures. The viscosity increases with the increase of CO_2 loading and viscosity decreases with the increase of temperature. Figure 5.9 describes the viscosity variation of CO_2 loaded aqueous MEA solution with 30 mass % MEA concentration. Eyring's viscosity model was adopted to correlate measured viscosities for the free energy of activation ΔG_0^+ for viscous flow. The correlations reported in literature for MEA + H_2O + CO_2 mixtures were examined and were compared as shown in Figure 5.9 with the proposed correlation in this work. The proposed correlation is given in Eq (141). The calculated parameters and accuracies of the correlations are presented in Article **A.**
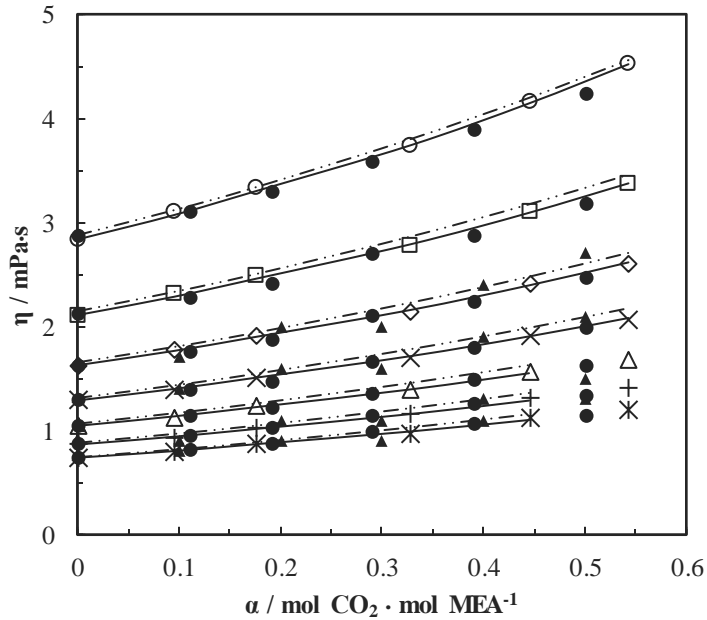
Figure 5.9:Viscosity of CO_2 loaded aqueous MEA (w_1=0.3) solutions at different CO_2 loadings and temperatures. Data: from this work, 293.15 K, 'o'; 303.15 K, '□'; 313.15 K, '◇'; 323.15 K, 'x'; 333.15 K, '△'; 343.14 K, '+'; 353.15 K, 'ж'; Hartono, et al. [81], '●'; Amundsen, et al. [74], '▲'. Correlation: from this work, '—'; Hartono, et al. [81], '-··-'.

$$ln(V\eta)_{CO2\,loaded} = ln(V\eta)_{unloaded} + f(x_3, T) \tag{140}$$

$$f(x_3, T) = x_3(d_1 + d_2 T + d_3 x_3) \tag{141}$$

The Eyring's viscosity model was used to correlate the measured viscosities of AMP + MEA + H_2O + CO_2 mixtures. A modified Weiland's viscosity correlation and Setschenow-type correlation as given in Eq (142) and Eq (143) respectively were

proposed to fit the viscosity data. Further, a correlation was developed to fit the calculated free energy of activation ΔG_0^+ from viscosity and density data as given in Eq (145). Then, the correlation was examined to represent the viscosities. A comparison of the proposed correlation was performed in Article **B** and calculated parameters were listed with corresponding accuracies of the data fit. Figure 5.10 and Figure 5.11 illustrate the viscosity variation with different CO loadings and temperatures as given in Article **B**.

$$\frac{\eta}{\eta_{H_2O}} = exp\left[\frac{[(ax_1+bx_2+c)T+(dx_1+ex_2+f)][x_4(gx_1+hx_2+iT+j)+10^3](x_1+x_2)}{T^2}\right] \tag{142}$$

$$ln\left(\frac{\eta}{\eta_0}\right) = \left(a_{0,0} + a_{0,1}T\right)x_4 + \left(a_{1,0} + a_{1,1}T\right)x_4^2 + \left(a_{2,0} + a_{2,2}T\right)x_4^3 \tag{143}$$

$$ln(\eta V)_{CO_2 loaded} = ln(\eta V)_{unloaded} + f(x_1,x_2,x_4,T) \tag{144}$$

$$f(x_1,x_2,x_4,T) = x_4(k_1 + k_2T + k_3x_4)(k_4x_1 + k_5x_2 + k_6) \tag{145}$$
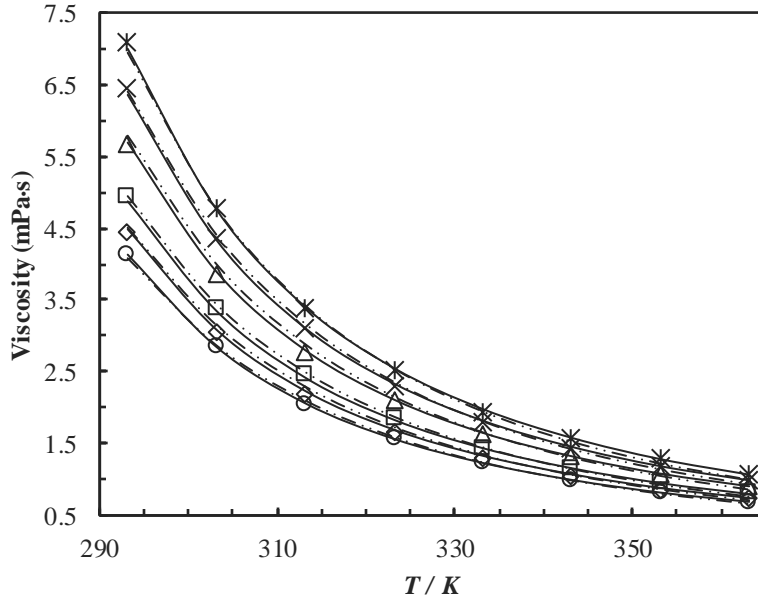
Figure 5.10: Viscosity of CO₂ loaded 24 mass % AMP + 6 mass % MEA + 70 mass % H₂O at different temperatures and CO₂ loadings (α / mol CO₂ · mol amine⁻¹): 0.000, '○'; 0.083, '◇'; 0.165, '□'; 0.314, '△'; 0.418, 'x'; 0.508, 'ж'. Correlations: Setschenow-type, '——'; Modified Weiland's, '- ·· -'.
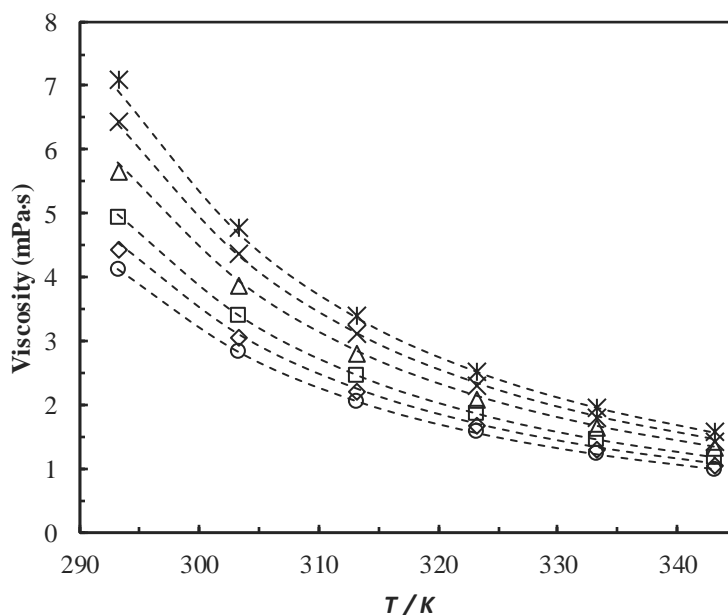
Figure 5.11: Viscosity of CO_2 loaded 24 mass % AMP + 6 mass % MEA + 70 mass % H_2O at different temperatures and CO_2 loadings (α / mol $CO_2 \cdot$ mol amine^{-1}): 0.000, '○'; 0.083, '◇'; 0.165, '□'; 0.314, '△'; 0.418, 'x'; 0.508, 'ж'. Correlation: '- - -'.

5.6 Artificial Neural Networks for Physical Properties

The applicability of Artificial Neural Network (ANN) based models to represent the density and viscosity of both CO_2 loaded and unloaded mixtures was examined. For the physical property models, mole fractions of components and the temperature are considered as inputs for the network. One hidden layer with multiple neurons is adopted for the training with the learning algorithm of Bayesian Regularization (BR). The optimum number of neurons for the hidden layer was found by analyzing the cost function of Mean Squared Error (MSE) for BR as given in Eq (146) over thirty neurons [206]. All the networks are with a single output for density and viscosity in each amine mixture. The input data sets were divided into 70%, 15% and 15% randomly for the training, validation and test. Data were scaled in the range of (-1,+1) before they were used for the training of the ANN. The ANNs consisting of one hidden layer with a single output similar to the architecture as shown in Figure 2.6 were adopted in this study.

$$Cost\ function = \frac{1}{2N} \sum_{i=1}^{N} \left\{ \left(Y_i^E - Y_i^C \right)^2 + \lambda W^2 \right\} \tag{146}$$

The main advantage of the BR learning algorithm is that it minimizes the mean squared error and weight parameters of the network.
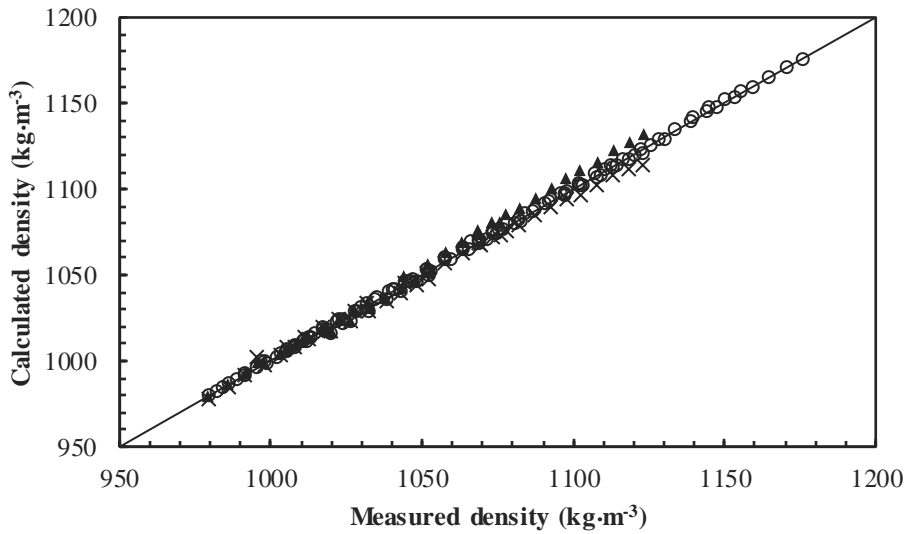
Figure 5.12: Comparison of correlated density with measured density for MEA + H₂O + CO₂ mixtures. ANN, '○'; Hartono, et al. [81], '▲'; Han, et al. [77], 'x'.
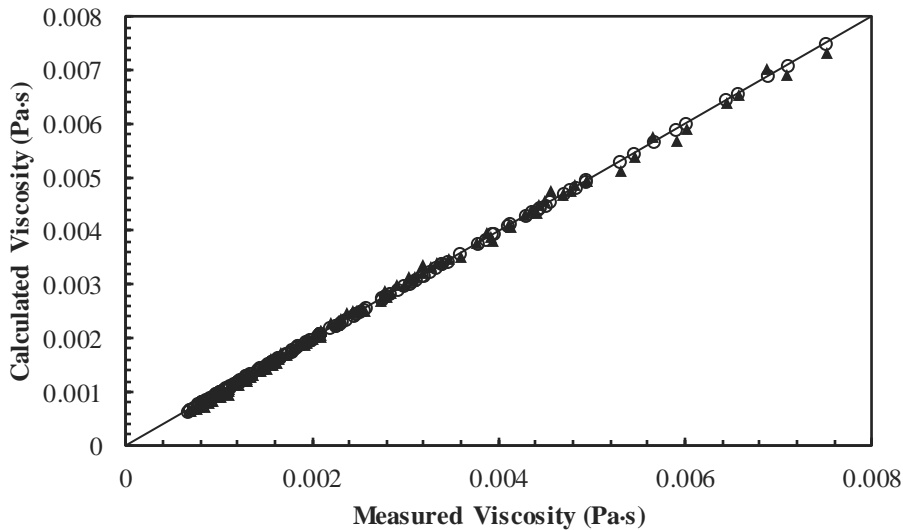
Figure 5.13: Comparison of correlated density with measured density for AMP + MEA + H₂O + CO₂ mixtures. ANN, '○'; Modified Weiland's correlation, '▲'.

The calculated weights and bias of the ANNs are reported in the supporting document attached with Article **E**. The results showed that the proposed ANNs for all types of mixtures represent measured density and viscosity data with higher accuracies. Article **E** presents a comparison of accuracies for data representation between correlations available in literature and ANNs proposed in this study.

5.7 Process Simulation for Physical Properties

The performed rate-based simulation on the absorption column was compared with the reported density and viscosity variations reported in Article **L**. A series of laboratory experiments were conducted using the CO_2 pilot plant located at USN Porsgrunn.

The simulations were performed in Aspen Plus using default parameter values described in section 2.5.5.
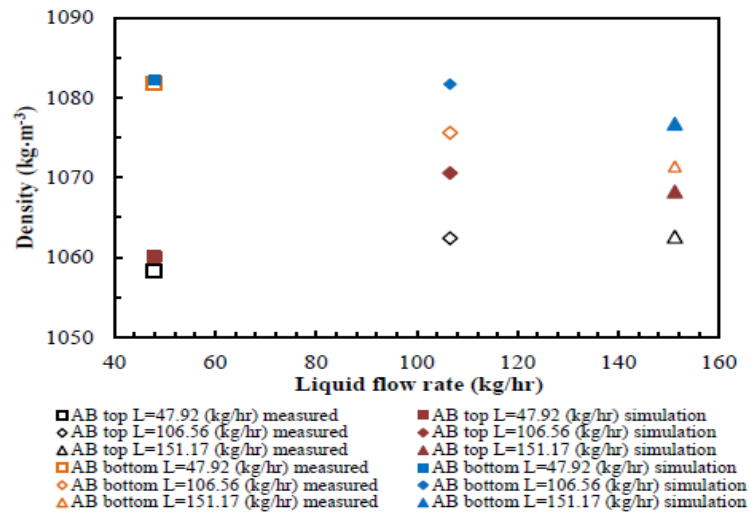
Figure 5.14: Comparison of the measured densities with the simulation.
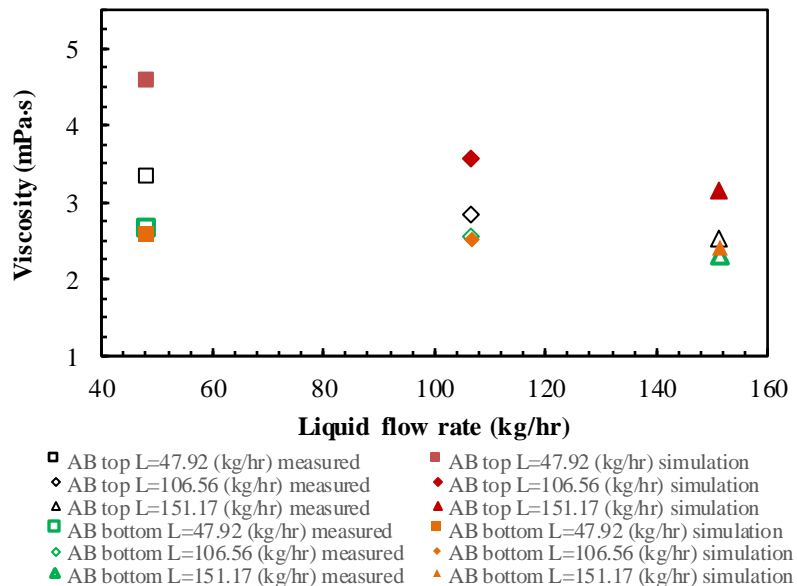
Figure 5.15: Comparison of the measured viscosities with the simulation.

Article **K** discussed a comparison of equilibrium-based and rate-based model for aqueous MEA based CO_2 capture. Aspen HYSYS and Aspen Plus were used to simulate a CO_2 capture pilot plant using equilibrium-based and rate-based models respectively. There the density and viscosity predictions were obtained using default parameter values in Aspen Plus. The results showed a relatively high deviation for the measured viscosity compared to the simulation especially at absorber top under low flow rates. There can be uncertainty in the simulation due to the use of default values for the parameters and uncertainty involved in experiments during the sampling from the CO_2 pilot plant and measurement of density and viscosity of solvents.

5.8 Discussion

This study mainly focused on measuring physical properties of density and viscosity of different CO_2 loaded and non-loaded aqueous amine mixtures at different amine concentrations, CO_2 loadings and temperatures. Further, it focused on developing correlations to fit measured properties used in engineering calculations. The measured data helped to cover the unmeasured states especially temperature. The proposed correlations for density and viscosity were able to fit the data with acceptable accuracies indicating that correlations can be used in engineering calculations.

The excess molar volume, viscosity deviation and excess free energy of activation for viscous flow gave understanding on types of intermolecular interactions present in the aqueous amine mixtures. The calculated excess properties were also useful in developing correlations. The number of parameters used in the Redlich-Kister type polynomial affects the accuracy of data fitting in the correlation. Less number of parameters lead to a decrease in accuracy of the fit while a high number parameters cause data overfitting. The accuracies that were obtained in this study for density and viscosity correlations were in a similar order of magnitude as the accuracies reported in literature. The proposed Aronu's correlation deviates from a Redlich-Kister type polynomial based correlations, but observed deviations are acceptable.

Eyring's viscosity model based on absolute rate theory is based on a mechanism to liquid viscous flow. This lays a theoretical foundation to develop viscosity correlations rather than fitting a curve to match measured data. Further development of theoretical insight to explain free energy of activation for viscous flow for CO_2 loaded amine mixtures is an area for a future research work

For the ANN models, the proposed networks are with a single hidden layer with multiple inputs. This study can be extended to investigate the applicability of ANN with multiple hidden layers to reduce the number of neurons in the network. Further, it would be interesting to use a different set of data to compare the calculated and the measured properties.

The comparison made between measured densities and viscosities of pure amines with literature data indicates that the density meter and the rheometer were calibrated properly prior to the experiments. Discussions about such comparisons are made in

Article **A**, **B**, **C** and **D**. The formation of air bubbles was observed at higher temperatures (> 323.15 K) for CO_2 loaded solutions with high loading values. Such conditions were identified through visual observations of the U-tube and those measured data were omitted. The performance of bearings in the measuring system of the rheometer was examined by the tests known as the air check and the motor adjustment. The bearings were replaced several times due to the poor performance identified during those tests.

During the CO_2 loading, there can be an amine loss due to evaporation. The amine concentration in CO_2 loaded solutions was determined using the titration performed with 1 mol·L^{-1} HCl. This amine loss was neglected in the calculation of mole fractions of the amine, H_2O and CO_2 during the regression.

In the CO_2 laboratory rig experiments, there can be uncertainty in density and viscosity measurements due to the presence of impurities and degradation products of the solvent. The uncertainty in temperature measurements and sample collection also has an influence on the result.

The uncertainty analysis of density and viscosity measurements was discussed in Article **A**, **B**, **C** and **D**. In this analysis, the amine loss during the CO_2 loading was not considered as an uncertainty source, but it is recommended to take that into account as well to make the analysis more precise.

6   Uncertainty Analysis of Physical Properties

This chapter provides an overview of the uncertainty analysis performed on density and viscosity measurements.

6.1 Measurement Uncertainty

The outcome of a measured property depends on the measuring system, the measurement procedure, the skill of the operator, the environment and other effects [207]. As a result, no measurement is exact and measurement uncertainty is stated as a statistical parameter that discusses the possible fluctuations of a measured property [208]. An average value of the dispersion of a number of indication values carries the information of an estimation of the true quantity value and that would not generally be adequate to consider as a final value for a measured property.

Measurement error refers to the deviation of measured quantity from its true value or reference. There are two types of errors involved in measurements known as systematic and random errors. Systematic error is a quantifiable measurement error (offset), which remains constant in replicate measurements. The random error varies in an unpredictable manner in replicate measurements.

The corrections that are made for the measurement errors are often performed prior to the uncertainty analysis as described according to the Guide to the Expression of Uncertainty in Measurements (GUM)[209, 210]. The GUM method provides a different approach rather than express the results of measurement by giving the best estimate of the measurand along with the information about random and systematic errors. The GUM approach enables us to express the results of measurement as the best estimate of measurand together with associated measurement uncertainty.

6.1.1 Uncertainty of Viscosity Measurements

The uncertainty of viscosity measurements is raised due to the uncertainty sources involved in the measuring method. Several uncertainty sources were identified for both aqueous and CO_2 loaded solutions. Figure 6.1 illustrates the considered uncertainty sources for the viscosity measurement of aqueous amine solutions.

The mathematical model for a double-gap viscometer as shown in Eq (147) provides the relevant uncertainty sources for the uncertainty of viscosity measurements. There are additional uncertainty sources involved in viscosity measurement that are not shown in the model. Such sources are added to the model equation as shown in Eq (148). The uncertainty analysis was done by following the guidelines provided by GUM and QUAM (Quantifying Uncertainty in Analytical Measurement)[210].
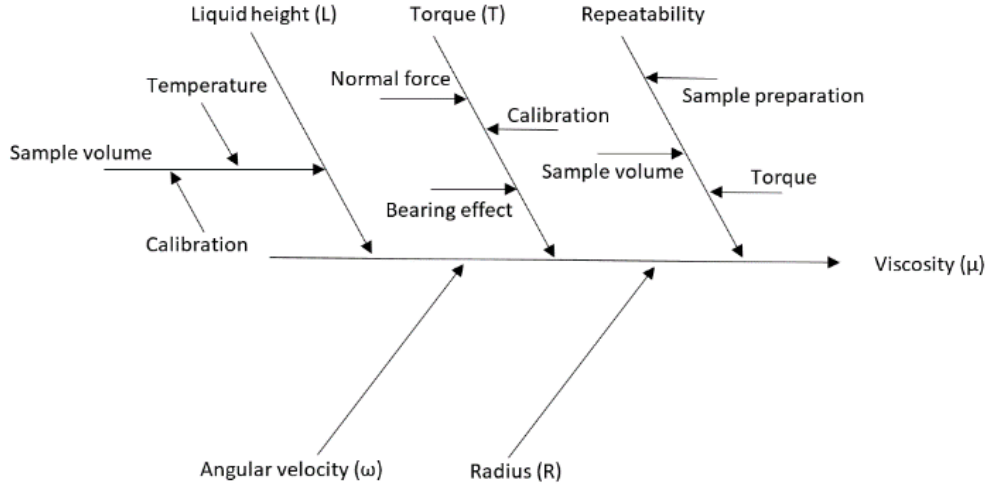
Figure 6.1: Cause and effect diagram for uncertainty analysis of viscosity measurement [211].

$$\eta = \frac{T}{4\pi L\omega R^2 \left(\frac{k_1^2}{k_1^2 - 1} + \frac{k_2^2 k_3^2}{k_3^2 - k_2^2} \right)} \tag{147}$$

Here, T is torque, η is dynamic viscosity, L is the liquid height, R is the radius of the inner fixed cylinder, ω is angular velocity, $R_1 = K_1 R$, $R_2 = K_2 R$ and $R_3 = K_3 R$.

$$\eta = \frac{T}{4\pi L\omega R^2 \left(\frac{k_1^2}{k_1^2 - 1} + \frac{k_2^2 k_3^2}{k_3^2 - k_2^2} \right)} f_p f_t f_w f_{rep} \tag{148}$$

Where f_p is purity of MEA, f_t is temperature, f_w is weight measurement and f_{rep} is repeatability. Those factors are added to the original viscosity expression to consider uncertainty sources, which are not shown in Eq (147).

In the GUM method, the propagation of uncertainty based on the first-order Taylor series approximation is considered in the uncertainty evaluation. A Gaussian distribution is assumed as the probability distribution and that is also used to define confidence intervals.

Consider a measuring system as described in Eq (149).

$$y = f(x_1, x_2, \dots, x_N) \tag{149}$$

Where y is the measurand and $x_1, x_2, \dots x_N$ are the input quantities. The propagation of uncertainty according to the Taylor series expansion of y,

$$u^2(y) = \sum_{i=1}^{N} \left(\frac{\partial f}{\partial x_i} \right)^2 u^2(x_i) + 2 \sum_{i=1}^{N-1} \sum_{j=i+1}^{N} \frac{\partial f}{\partial x_i} \frac{\partial f}{\partial x_j} u(x_i, x_j) \tag{150}$$

In Eq (150), $(\partial f / \partial x_i)$ gives the partial derivatives (sensitivity coefficients) [212, 213], $u^2(y)$ is the variance of the measuring result, the variance of the input quantity x_i is given by $u^2(x_i)$ and the covariance between x_i and x_j is given by $u(x_i, x_j)$ [213].

$$U(y) = ku(y) \tag{151}$$

In general, calculated combined uncertainty from Eq (151) is defined as the standard uncertainty with the coverage factor k=1 which covers 68% of the interval. It is common to represent uncertainty as an expanded uncertainty with k =1.96 or 2, which covers approximately 95% of the interval.

Table 6.1 lists the considered uncertainty sources with corresponding distributions and values. The calculated uncertainties for the viscosity of different MEA solutions are given in Table 6.2. The attached Article **N** and Article **O** provide more information about the analysis.

Table 6.1: Uncertainty sources with corresponding distributions and values[202].

Input quantity X_i	Probability Distribution	Uncertainty $U(x_i)$
Torque (τ)	Triangular	$0.082 \ \mu Nm$
Level (L)	Gaussian	$0.45 \ mm$
Angular velocity (ω)	Triangular	$0.01 \ rad \cdot s^{-1}$
Radius (R)	Triangular	$4.1 \ \mu m$
Purity	Rectangular	2.886×10^{-3}
Temperature	Triangular	2.45×10^{-4}
Weight measurement	Rectangular	8×10^{-6}
CO_2 loading	Gaussian	0.013
Repeatability	Gaussian	0.00348

The uncertainty sources in the viscosity measurement was calculated as follows.

Torque (τ):

The Anton Paar user manual [214] provide the accuracy of torque measurement as,

Torque accuracy: max. (0.2 μNm; 0.05%)

Then a triangular distribution was considered to calculate the uncertainty of torque.

Standard uncertainty of torque (τ) measurement

$$u(\tau) = \frac{0.2}{\sqrt{6}} = 0.082 \ \mu Nm$$

Angular Velocity (ω):

All the viscosity measurements were performed under a shear rate of 1000 1/s. for this analysis $\pm$ 1 1/s of accuracy was assumed to determine the uncertainty of angular velocity. Using Eq (152), Eq (153) and triangular distribution, the standard uncertainty of angular velocity (ω) was determined as,

$$\dot{\gamma} = \frac{\pi n}{30} \cdot \frac{1+\delta^2}{\delta^2 -1} \tag{152}$$

$$\omega = \frac{2\pi}{60} n \tag{153}$$

$$u(\omega) = 0.01 \text{rad·s}^{-1}$$

Level (L):

The liquid was transferred using a 10 mL syringe with an accuracy of ± 0.1 mL. Using a triangular distribution, the uncertainty of volume measurement was determined as ± 0.4 mL. Then using the geometry of the double-gap rheometer, the standard uncertainty of level was calculated as 0.45 mm.

Radius (R):

For the analysis, ± 0.01 mm of accuracy was assumed to determine the uncertainty of the radius of the cylindrical geometries. Assuming a triangular distribution for the uncertainty, ± 4.1 µm was obtained for the standard uncertainty of radius.

Purity (P):

The purity of the monoethnaol amine is 99.5%. Considering a rectangular distribution for the standard uncertainty $u(f_p)$ was calculated as,

$$u(p) = \frac{0.005}{\sqrt{3}} = 0.0029 = u(f_p)$$

The $u(f_p)$ vary with the material; here considered only monoethano amine for the aqueous monoethanol amine mixtures.

Temperature (T):

The temperature accuracy of the instrument is ± 0.03 K. A triangular distribution and an average temperature of the measuring range (293.15 K – 393.15 K) were assumed to calculate the uncertainty of temperature $u(f_T)$.

Standard uncertainty of temperature,

$$u(T) = \frac{0.03}{\sqrt{6}} = 0.012 \ K$$

$$u(f_T) = \frac{0.01225}{50} = 0.000245$$

Weight measurement (*w*):

The linearity of the balance is considered as ± 0.2 mg. A rectangular distribution was assumed for the uncertainty of weight measurement. Accordingly, for two weight measurements for a binary mixture:

The standard uncertainty of weight measurement,

$$u(w) = 2. \left(\frac{0.2}{\sqrt{3}}\right)^2 = 0.16\text{mg}$$

Considering a sample volume of 20g

$$u(f_w) = \frac{0.16 \times 10^{-3}}{20} = 0.000008$$

Repeatability

Standard deviation of 0.0076 mPa·s was observed for the measured viscosity of 2.179 mPa·s. Accordingly,

$$u(f_{rep}) = \frac{0.0076}{2.179} = 0.0035$$

Table 6.2: Measurement uncertainty of viscosity for different solutions

Property	Solution	Uncertainty (95% confidence at k=2)
Viscosity	Pure	± 0.0162 mPa·s
	Aqueous MEA	± 0.0162 mPa·s
	CO$_2$ loaded aqueous MEA	± 0.0353 mPa·s

6.1.2 Uncertainty of Density Measurements

A similar approach was adopted as explained in section 6.1.1 to evaluate uncertainty in density measurement. The uncertainty sources of material purity, weight measurement, temperature, CO$_2$ loading and repeatability were considered during the uncertainty analysis. The influence of uncertainty in temperature on density measurement was determined by calculating the gradient $\partial\rho/\partial T$ of density against temperature. A similar approach was used to calculate the influence of uncertainty in CO$_2$ loading on density measurement in which gradient of density against CO$_2$ loading, $\partial\rho/\partial\alpha$, was found from measured densities at different CO$_2$ loadings. Finally, $(\partial\rho/\partial T)\cdot u(T)$ and $(\partial\rho/\partial\alpha)\cdot u(\alpha)$ were determined to find standard uncertainties of density measurement due to the temperature and CO$_2$ loading. For CO$_2$ loaded aqueous monoethanol amine mixtures,

the gradient $\partial\rho/\partial T$ of density against temperature was found as 0.73 kg·m^{-3}·K^{-1} and the corresponding uncertainty in ρ that is $(\partial\rho/\partial T)\cdot u(T)$ was calculated as ± 0.009 kg·m^{-3}. The gradient of density against CO_2 loading, $\partial\rho/\partial\alpha$, was found as 334 kg·m^{-3} and the corresponding uncertainty in ρ, $(\partial\rho/\partial\alpha)\cdot u(\alpha)$ was calculated as ± 1.67 kg·m^{-3}. The standard combined uncertainties for density measurement $u(\rho)$ for different monoethanol amine mixtures are listed in Table 6.3.

Table 6.3: Measurement uncertainty of density for different solutions

Property	Solution	Uncertainty (95% confidence at k=2)
Density	Pure	± 7.1 kg·m^{-3}
	Aqueous MEA	± 7.1 kg·m^{-3}
	CO_2 loaded aqueous MEA	± 7.8 kg·m^{-3}

6.2 Model Uncertainty

A mathematical model is an abstract version of reality. Various assumptions are made during the model derivations to develop relations between parameters through mathematical equations [215]. The input quantities of the model may not be very precise due to the various reasons like errors made during the measurements. Thus, uncertainty in model output is caused by uncertain model structure and parameter values [216]. The errors in the model structure compared to the real system, numerical approximations in simulations and assumptions can cause model output uncertainty. The uncertain estimation of model input parameters also leads to model output uncertain. The evaluation of uncertainty caused by the model structure is more difficult than the uncertainty evaluation due to the parameter value. Article **M** discussed the propagation of uncertainties of input parameters through the correlations proposed for mass transfer coefficient and interfacial area in a packed bed absorber column.

7 Conclusions and Recommendations

7.1 Aim

This research study was mainly focused on measuring physical properties of density and viscosity of CO_2 loaded and non-loaded aqueous amine mixtures and develop empirical correlations to fit measured data. The uncertainties of the density and viscosity measurements were evaluated and were reported with measured data. Experiments were performed in a CO_2 pilot plant to evaluate CO_2 removal efficiencies and density and viscosity variations of the solvent at the absorber top and bottom and were compared with the simulations.

7.2 Conclusions

Density and viscosity were measured in aqueous binary mixtures of $MEA + H_2O$, $MDEA + H_2O$, $DMEA + H_2O$ and $DEEA + H_2O$ and in aqueous ternary mixtures of $AMP + MEA + H_2O$, $MDEA + MEA + H_2O$, $DMEA + MEA + H_2O$, and $DEEA + MEA + H_2O$. Density correlations based on Redlich – Kister type polynomial for excess molar volume and Aronu's density correlation were used to fit measured densities. The proposed correlations were able to fit the data with less than 1% AARD. Viscosity correlations based on Redlich – Kister type polynomials for viscosity deviation and excess free energy of activation for viscous flow from Eyring's viscosity model were adopted to fit measured viscosities normally with AARD less than 2%.

Density and viscosity increase with the increase of CO_2 loading and decrease with the increase of temperature. The modified Aronu's density correlation for $MEA + H_2O + CO_2$ mixtures was proposed. For the densities of $AMP + MEA + H_2O + CO_2$ mixtures, the proposed modified Weiland's density correlation and a Setschenow type correlation gave acceptable deviations from the measured data. The viscosities of $MEA + H_2O + CO_2$ were correlated by using Eyring's viscosity model that is based on the absolute rate theory. The free energy of activation for viscous flow for the $MEA + H_2O + CO_2$ was calculated and was reported at different CO_2 loadings and temperatures. For the viscosities of $AMP + MEA + H_2O + CO_2$ mixtures, a modified Weiland's viscosity correlation and a Setschenow type correlation were proposed. Further, a correlation based on Eyring's viscosity model also proposed with the calculated free energy of activation for viscous flow. The developed viscosity correlations are recommended to perform engineering calculations.

In the simulations, both equilibrium-based and rate-based approaches were able to reveal CO_2 removal from the gas stream as shown in the CO_2 pilot plant. Two adjustable parameters of Murphree efficiency and interfacial area factor were adjusted to get simulated CO_2 removal efficiency close to the experiments.

7.3 Recommendations for Future Work

This PhD work was able to provide new measured density and viscosity data of both CO_2 loaded and non-loaded aqueous amine solutions. New correlations were proposed to fit the density and viscosity data with acceptable accuracies. This work can be further extended in the following directions.

7.3.1 Experimental Study for New Data

The mixtures of DMEA + MEA + H_2O and DEEA + MEA + H_2O have been studied to investigate CO_2 absorption performance. There is a lack of data for density and viscosity of CO_2 loaded and non-loaded solution. It is also recommended to perform experiments to measure density and viscosity of the CO_2 loaded AMP + MEA + H_2O mixtures to expand the data region. There is a lack of viscosity data for the CO_2 loaded MEA + H_2O at higher temperatures (>373.15 K).

7.3.2 Development of New Correlations

It is suggested to develop a theoretical background of density and viscosity correlations. It is possible to develop a theoretical insight into the free energy of activation for viscous flow parameter in Eyring's viscosity model. The NRTL, UNIQUAC (universal quasichemical) or UNIFAC (UNIQUAC-functional group activity coefficients) – type models for activation energy term in Eyring's viscosity model for CO_2 loaded and non-loaded amine mixtures would be interesting.

7.3.3 Uncertainty Propagation

One of the major uses for density and viscosity data is in process simulation tools for design and dimensioning purposes. It would be interesting to evaluate uncertainty propagation methods to determine the uncertainty in design using uncertainty in measurements.

8 References

[1] N. Borduas and N. M. Donahue, "The Natural Atmosphere: Greenhouse Gases " in *Green Chemistry*, B. Torok and T. Dransfield Eds.: Elsevier, 2018, pp. 131-150.

[2] M. Wang, A. S. Joel, C. Ramshaw, D. Eimer, and N. M. Musa, "Process intensification for post-combustion CO_2 capture with chemical absorption: A critical review," *Appl. Energy*, vol. 158, pp. 275–291, 2015.

[3] T. H. Oh, "Carbon capture and storage potential in coal-fired plant in Malaysia- A review," *Renewable Sustainable Energy Rev.,* vol. 14, pp. 2697-2709, 2010, doi: 10.1016/j.rser.2010.06.003.

[4] "Scripps CO_2 program: CO_2 concentration at Mauna Loa Observatory, Hawaii." http://scrippsco2.ucsd.edu/ (accessed 25 Dec, 2019).

[5] B. Metz, O. Davidson, H. D. Coninck, M. Loos, and L. Meyer, "IPCC Special Report on Carbon Dioxide Capture and Storage," United States of America, New York, 2005.

[6] "skepticalscience:The CO_2/Temperature correlation over the 20th century " Skeptical Science. https://skepticalscience.com/The-CO2-Temperature-correlation-over-the-20th-Century.html (accessed Jan 25, 2019).

[7] "European Council Council of the European Union." (accessed 25 June, 2019).

[8] D. Jansen, M. Gazzani, G. Manzolini, E. v. Dijk, and M. Carbo, "Pre-combustion CO_2 capture," *Int. J. Greenhouse Gas Control*, vol. 40, pp. 167-187, 2015, doi: 10.1016/j.ijggc.2015.05.028.

[9] R. Stanger *et al.*, "Oxyfuel combustion for CO_2 capture in power plants," *Int. J. Greenhouse Gas Control,* vol. 40, pp. 55-125, 2015, doi: 10.1016/j.ijggc.2015.06.010.

[10] Y. Hu, "CO_2 capture from oxy-fuel combustion power plants," PhD, Department of Chemical Engineering and Technology KTH Royal Institute of Technology, Stockholm, Sweden, 2011.

[11] M. Aghaie, N. Rezaei, and S. Zendehboudi, "A systematic review on CO_2 capture with ionic liquids: Current status and future prospects," *Renewable Sustainable Energy Rev.,* vol. 96, pp. 502-525, 2018, doi: 10.1016/j.rser.2018.07.004.

[12] G. T. Rochelle, "Amine Scrubbing for CO_2 Capture," *Science* vol. 325, no. 5948, pp. 1652-1654, 2009.

[13] R. Idem *et al.*, "Practical experience in post-combustion CO_2 capture using reactive solvents in large pilot and demonstration plants," *Int. J. Greenhouse Gas Control*, vol. 40, pp. 6-25, 2015, doi: 10.1016/j.ijggc.2015.06.005.

[14] Z. Zhang, Y. Li, W. Zhang, J. Wang, M. R. Soltanian, and A. G. Olabi, "Effectiveness of amino acid salt solutions in capturing CO2: A review," *Renewable Sustainable Energy Rev.,* vol. 98, pp. 179-188, 2018, doi: 10.1016/j.rser.2018.09.019.

[15] H. Chen, T.-C. Tsai, and C.-S. Tan, "CO_2 capture using amino acid sodium salt mixed with alkanolamines," *Int. J. Greenhouse Gas Control,* vol. 79, pp. 127-133, 2018, doi: 10.1016/j.ijggc.2018.10.002.

[16] H. Yu *et al.*, "Results from trialling aqueous ammonia-based post-combustion capture in a pilot plant at Munmorah Power Station: Gas purity and solid

precipitation in the stripper," *Int. J. Greenhouse Gas Control,* vol. 10, pp. 15-25, 2012, doi: 10.1016/j.ijggc.2012.04.014.

[17]   C. H. Yu, C. H. Huang, and C. S. Tan, "A Review of CO_2 Capture by Absorption and Adsorption " *Aerosol Air Qual. Res.,* vol. 12, pp. 745-769, 2012.

[18]   S. Babamohammadi, A. Shamiri, and M. K. Aroua, "A review of CO_2 capture by absorption in ionic liquid-based solvents," *Rev chem Eng,* vol. 31 no. 4, pp. 383-412, 2015.

[19]   S. Choi, J. H. Drese, and C. W. Jones, "Adsorbent materials for carbon dioxide capture from large anthropogenic point sources," *ChemSusChem* vol. 2, pp. 796 – 854, 2009.

[20]   A. Sayari, Y. Belmabkhout, and R. Serna-Guerrero, "Flue gas treatment via CO_2 adsorption," *Chem Eng J,* vol. 171, no. 3, pp. 760-774, 2011, doi: 10.1016/j.cej.2011.02.007.

[21]   A. Skorek-Osikowska, J. Kotowicz, and K. Janusz-Szymańska, "Comparison of the Energy Intensity of the Selected CO_2-Capture Methods Applied in the Ultra-supercritical Coal Power Plants," *Energy Fuels,* vol. 26, no. 11, pp. 6509-6517, 2012, doi: 10.1021/ef201687d.

[22]   J. Xu *et al.*, "Post-combustion CO_2 capture with membrane process: Practical membrane performance and appropriate pressure," *J. Membr. Sci.,* vol. 581, pp. 195-213, 2019, doi: 10.1016/j.memsci.2019.03.052.

[23]   T. Brinkmann *et al.*, "Investigating the influence of the pressure distribution in a membrane module on the cascaded membrane system for post-combustion capture," *Int. J. Greenhouse Gas Control,* vol. 39, pp. 194-204, 2015, doi: 10.1016/j.ijggc.2015.03.010.

[24]   T. C. Merkel, H. Lin, X. Wei, and R. Baker, "Power plant post-combustion carbon dioxide capture: An opportunity for membranes," *J. Membr. Sci.,* vol. 359, no. 1, pp. 126-139, 2010, doi: 10.1016/j.memsci.2009.10.041.

[25]   D. Y. C. Leung, G. Caramanna, and M. M. Maroto-Valer, "An overview of current status of carbon dioxide capture and storage technologies," *Renewable Sustainable Energy Rev.,* vol. 39, pp. 426-443, 2014, doi: 10.1016/j.rser.2014.07.093.

[26]   D. Aaron and C. Tsouris, "Separation of CO_2 from flue gas: A review," *Sep. Sci. Technol.,* vol. 40, pp. 321-348, 2005, doi: 10.1081/ss-200042244.

[27]   M. Clausse, J. Merel, and F. Meunier, "Numerical parametric study on CO_2 capture by indirect thermal swing adsorption," *Int. J. Greenhouse Gas Control,* vol. 5, no. 5, pp. 1206-1213, 2011, doi: 10.1016/j.ijggc.2011.05.036.

[28]   A. Brunetti, F. Scura, G. Barbieri, and E. Drioli, "Membrane technologies for CO2 separation," *J. Membr. Sci.,* vol. 359, no. 1, pp. 115-125, 2010, doi: 10.1016/j.memsci.2009.11.040.

[29]   L. E. Øi, "Removal of CO_2 from exhaust gas," PhD, Faculty of Technology, Telemark University College, Porsgrunn, Norway, 2012.

[30]   R. Idem *et al.*, "Pilot plant studies of the CO_2 capture performance of aqueous MEA and Mixed MEA/MDEA solvents at the University of Regina CO_2 capture technology development plant and the Boundary Dam CO_2 capture demonstration plant," *Ind. Eng. Chem. Res* vol. 45, pp. 2414-2420, 2005, doi: 10.1021/ie050569e.

[31]   D. A. Eimer, *Gas Treating: Absorption Theory and Practice*. John Wiley & Sons. Ltd 2014.

[32]   E. I. Koytsoumpa, C. Bergins, and E. Kakaras, "The CO_2 economy: Review of CO_2 capture and reuse technologies," *J Supercrit Fluids*, vol. 132, pp. 3-16, 2018, doi: 10.1016/j.supflu.2017.07.029.

[33]   J. A. Svendsen and D. Eimer, "Case Studies of CO_2 Capture Columns based on Fundamental Modeling," *Energy Procedia*, vol. 4, pp. 1419-1426, 2011, doi: 10.1016/j.egypro.2011.02.007.

[34]   A. Hartono and H. F. Svendsen, "Density, viscosity, and excess properties of aqueous solution of diethylenetriamine (DETA)," *J. Chem. Thermodynamics*, vol. 41, pp. 973-979, 2009, doi: 10.1016/j.jct.2008.11.012.

[35]   A. J. Kidnay and W. R. Parrish, *Fundamentals of Natural Gas Processing*. Boca Raton,: Taylor & Francis Group, 2006.

[36]   S. Jayarathna, A. Weerasooriya, S. Dayarathna, D. A. Eimer, and M. C. Melaaen, "Densities and surface tensions of CO_2 loaded aqueous monoethanolamine solution with r=(0.2 to 0.7) at T=(303.15 to 333.15)K," *J. Chem. Eng. Data*, vol. 58, pp. 986-992, 2013.

[37]   O. F. Dawodu and A. Meisen, "Solubility of carbon dioxide in aqueous mixtures of alkanolamines," *J. Chem. Eng. Data*, vol. 39, pp. 548-552, 1994, doi: 10.1021/je00015a034.

[38]   W. Jiang *et al.*, "A comparative kinetics study of CO_2 absorption into aqueous DEEA/MEA and DMEA/MEA blended solutions " *AlChE J.*, vol. 64, no. 4, pp. 1350-1358, 2017, doi: 10.1002/aic.16024.

[39]   G. Sartori and D. W. Savage, "Sterically hindered amines for CO_2 removal from gases," *Ind. Eng. Chem. Fundamen.*, vol. 22, no. 2, pp. 239-249, 1983.

[40]   P. D. Vaidya and E. Y. Kenig, "CO_2-alkanolamine reaction kinetics: A review of recent studies," *Chem. Eng. Technol*, vol. 30, no. 11, pp. 1467-1474, 2007, doi: 10.1002/ceat.200700268.

[41]   C. Nwaoha *et al.*, "Carbon dioxide (CO_2) capture performance of aqueoustri-solvent blends containing 2-amino-2-methyl-1-propanol (AMP) and methyldiethanolamine (MDEA) promoted by diethylenetriamine (DETA)," *Int. J. Greenhouse Gas Control*, vol. 53, pp. 292-304, 2016, doi: 10.1016/j.ijggc.2016.08.012.

[42]   A. Naami, T. Sema, M. Edali, Z. Liang, R. Idem, and P. Tontiwachwuthikul, "Analysis and predictive correlation of mass transfer coefficient KGav of blended MDEA-MEA for use in post-combustion CO_2 capture," *Int. J. Greenhouse Gas Control*, vol. 19, pp. 3-12, 2013, doi: 10.1016/j.ijggc.2013.08.008.

[43]   M. W. Arshad, H. F. Svendsen, P. L. Fosbøl, N. von Solms, and K. Thomsen, "Equilibrium Total Pressure and CO_2 Solubility in Binary and Ternary Aqueous Solutions of 2-(Diethylamino)ethanol (DEEA) and 3-(Methylamino)propylamine (MAPA)," *J. Chem. Eng. Data*, vol. 59, no. 3, pp. 764-774, 2014, doi: 10.1021/je400886w.

[44]   W. Conway *et al.*, "CO_2 absorption into aqueous amine blended solutions containing monoethanolamine (MEA), N,N-dimethylethanolamine (DMEA), N,N-diethylethanolamine (DEEA) and 2-amino-2-methyl-1-propanol (AMP) for

post-combustion capture processes," *Chem. Eng. Sci.,* vol. 126, pp. 446-454, 2015, doi: 10.1016/j.ces.2014.12.053.

[45]   W. Nookuea, Y. Tan, H. Li, E. Thorin, and J. Yan, "Impacts of thermo-physical properties of gas and liquid phases on design of absorber for CO_2 capture using monoethanolamine," *Int. J. Greenhouse Gas Control,* vol. 52, pp. 190-200, 2016, doi: 10.1016/j.ijggc.2016.07.012.

[46]   S. S. Karunarathne, D. A. Eimer, and L. E. Øi, "Model Uncertainty of Interfacial Area and Mass Transfer Coefficients in Absorption Column Packings," in *Proceedings of the 58th SIMS* Reykjavik, Iceland, 2017, pp. 144-150.

[47]   L. E. Øi, J. Lundberg, M. Pedersen, P. M. Hansen, and M. C. Melaaen, "Measurements of CO_2 Absorption and Heat Consumption in Laboratory Rig," *Energy Procedia,* vol. 63, pp. 1569-1577, 2014, doi: 10.1016/j.egypro.2014.11.166.

[48]   G. Astarita and D. W. Savage, "Theory of chemical desorption," *Chem. Eng. Sci.,* vol. 35, no. 3, pp. 649-656, 1980, doi: 10.1016/0009-2509(80)80015-7.

[49]   A. Jamal, A. Meisen, and C. Jim Lim, "Kinetics of carbon dioxide absorption and desorption in aqueous alkanolamine solutions using a novel hemispherical contactor—I. Experimental apparatus and mathematical modeling," *Chem. Eng. Sci.,* vol. 61, no. 19, pp. 6571-6589, 2006, doi: 10.1016/j.ces.2006.04.046.

[50]   A. Jamal, A. Meisen, and C. Jim Lim, "Kinetics of carbon dioxide absorption and desorption in aqueous alkanolamine solutions using a novel hemispherical contactor—II: Experimental results and parameter estimation," *Chem. Eng. Sci.,* vol. 61, no. 19, pp. 6590-6603, 2006, doi: 10.1016/j.ces.2006.04.047.

[51]   M. Garcia, H. K. Knuutila, and S. Gu, "Aspen Plus simulation model for CO_2 removal with MEA: Validation of desorption model with experimental data," *J. Environ. Chem. Eng.,* vol. 5, no. 5, pp. 4693-4701, 2017, doi: 10.1016/j.jece.2017.08.024.

[52]   N. McCann *et al.,* "Kinetics and mechanism of carbamate formation from CO_2(aq), carbonate species, and monoethanolamine in aqueous solution," *J. Phys. Chem,* vol. 113, pp. 5022-5029, 2009.

[53]   J. E. Crooks and J. P. Donnellan, "Kinetics of the reaction between carbon dioxide and tertiary amines," *J. Org. Chem.,* vol. 55, no. 4, pp. 1372-1374, 1990/02/01 1990, doi: 10.1021/jo00291a056.

[54]   W. Conway *et al.,* "Toward the understanding of chemical absorption processes for post-combustion capture of carbon dioxide: Electronic and steric considerations from the kinetics of reactions of CO_2(aq) with sterically hindered amines," *Environ. Sci. Technol.,* vol. 47, no. 2, pp. 1163-1169, 2013, doi: 10.1021/es3025885.

[55]   A. R. Mahajan and S. R. Mirgane, "Excess molar volumes and viscosities for the binary mixtures of n-Octane, n-Decane, n-Dodecane, and n-Tetradecane with Octan-2-ol at 298.15 K," *Journal of Thermodynamics,* vol. 2013, pp. 1-11, 2013, doi: 10.1155/2013/571918.

[56]   F. Qi and H. Wang, "Application of Prigogine–Flory–Patterson theory to excess molar volume of mixtures of 1-butyl-3-methylimidazolium ionic liquids with N-methyl-2-pyrrolidinone," *J. Chem. Thermodyn.,* vol. 41, no. 2, pp. 265-272, 2009, doi: 10.1016/j.jct.2008.09.003.

[57] T. M. Letcher and R. C. Baxter, "Application of the Prigogine-Flory-Patterson theory part I. Mixtures ofn-alkanes with bicyclic compounds, benzene, cyclohexane andn-hexane," *J. Solution Chem.*, vol. 18, no. 1, pp. 65-80, 1989, doi: 10.1007/BF00646083.

[58] O. Redlich and A. T. Kister, "Algebraic representation of thermodynamic properties and the classification of solutions," *Ind. Eng. Chem.*, vol. 40, no. 2, pp. 345-348, 1948.

[59] Y. Maham, T. T. Teng, L. G. Hepler, and A. E. Mather, "Densities, excess molar volumes, and partial molar volumes for binary mixtures of Water with Monoethanolamine, Diethnolamine, and Triethanolamine from 25 to 80 ^{o}C," *J. Solution Chem.*, vol. 23, no. 2, pp. 195-205, 1994.

[60] H. Touhara, S. Okazaki, F. Okino, H. Tanaka, K. Ikari, and K. Nakanishi, "Thermodynamic properties of aqueous mixtures of hydrophilic compounds 2. Aminoethanol and its methyl derivatives," *J. Chem. Thermodynamics*, vol. 14, pp. 145-156, 1982.

[61] F. Yang, X. Wang, W. Wang, and Z. Liu, "Densities and excess properties of primary amines in alcoholic solutions," *2013,* vol. 58, pp. 785-791, 2013.

[62] M. H. Li and K. P. Shen, "Densities and solubilities of solutions of Carbon Dioxide in water+Monoethanolamine+N-Methyldiethanolamine," *J. Chem. Eng. Data,* vol. 37, pp. 288-290, 1992.

[63] Y. W. Wang, S. Xu, F. D. Otto, and A. E. Mather, "Solubility of N_2O in alkanolamines and in mixed solvents " *The Chemical Engineering Journal,* vol. 48, pp. 31-40, 1992.

[64] R. M. DiGuilio, R. J. Lee, S. T. Schaeffer, L. L. Brasher, and A. S. Teja, "Densities and viscosity of the ethanolamines " *J. Chem. Eng,* vol. 37, pp. 239-242, 1992.

[65] M. Page, J. Y. Huot, and C. Jolicoeur, "A comprehensive thermodynamics investigation of water-ethanolamine mixtures at 10, 25, and 40 ^{o}C," *Can. J. Chem,* vol. 71, pp. 1064-1072, 1993.

[66] F. M. Guevara and A. T. Rodriguez, "Liquid density as a function of temperature of five organic solvents " *J. Chem. Eng. Data,* vol. 29, pp. 204-206, 1984.

[67] M. J. Lee and T. K. Lin, "Density and viscosity for Monoethanolamine+Water,+Ethanol, and+2-Propanol," *J. Chem. Eng. Data,* vol. 40, pp. 336-339, 1995.

[68] J. H. Song, S. B. Park, J. H. Yoon, and H. Lee, "Densities and viscosities of Monoethanolamine + Ethylene Glycol + Water," *J. Chem. Eng. Data,* vol. 41, pp. 1152-1154, 1996.

[69] U. R. Kapadi, D. G. Hundiwale, N. B. Patil, and M. K. Lande, "Viscosity, excess molar volume of binary mixtures of ethanolamine with water at 303.15, 303.15, 313.15 and 318.15K," *Fluid Phase Equilib.,* vol. 201, pp. 335-341, 2002.

[70] M. N. Islam, M. M. Islam, and M. N. Yeasmin, "Viscosity of aqueous solution of 2-methoxyethanol, 2-ethoxyethanol, and ethanolamine," *J. Chem. Thermodynamics,* vol. 36, pp. 889-893, 2004.

[71] A. Valtz, C. Coquelet, and D. Richon, "Volumetric properties of the monoethanolamine-methanol mixture at atmospheric pressure from 283.15 to 353.15 K," *Thermochim. Acta,* vol. 428, pp. 185-191, 2005.

[72] Y. Geng *et al.*, "Density, viscosity and electrical conductivity of 1-butyl-3-methylimidazolium hexafluorophosphate+monoethanolamine and + N, N-dimethylethanolamine," *J. Mol. Liq.*, vol. 2008, pp. 100-108, 2008.

[73] F. Pouryousefi and R. O. Idem, "New analytical technique for carbon dioxide absorption solvents " *Ind. Eng. Chem. Res*, vol. 47, pp. 1268-1276, 2008.

[74] T. G. Amundsen, L. E. Øi, and D. A. Eimer, "Density and viscosity of monoethanolamine + water + carbon dioxide from (25 to 80) ^{o}C," *J. Chem. Eng. Data*, vol. 54, pp. 3096-3100, 2009.

[75] M. M. Taib and T. Murugesan, "Densities and Excess molar volumes of binary mixtures of Bis(2-hydroxyethyl)ammonium acetate + water and monoethanolamine + Bis(2-hydroxyethyl)ammonium acetate at temperature from (303.15 to 353.15) K," *J. Chem. Eng. Data*, vol. 55, pp. 5910-5913, 2010.

[76] M. M. Taib and T. Murugesan, "Density, refractive index, and excess properties of 1-Butyl-3-methylimidazolium Tetrafluoroborate with water and Monoethanolamine," *J. Chem. Eng. Data*, vol. 57, pp. 120-126, 2012.

[77] J. Han, J. Jin, D. A. Eimer, and M. C. Melaaen, "Density of water (1) + Monoethanolamine (2) + CO_2 (3) from (298.15 to 413.15) K and surface tension of water (1) + Monoethanolamine (2) from (303.15 to 333.15) K," *J. Chem. Eng. Data*, vol. 57, pp. 1095-1103, 2012.

[78] A. G. Abuin, D. G. Diaz, and J. M. Navaza, "Density, speed of sound, and viscosity of Monoethanolamine + Water + N-Ethyl-2-pyrrolidone from T=(293.15 to 323.15) K," *J. Chem. Eng. Data*, vol. 58, pp. 3387-3391, 2013.

[79] F. Xu *et al.*, "Solubility of CO_2 in aqueous mixtures of monoethanolamine and dicyanamide-based ionic liquids " *Fluid Phase Equilib.*, vol. 365, pp. 80-87, 2014.

[80] R. H. Weiland, J. C. Dingman, D. Benjamin, and G. J. Browning, "Density and viscosity of some partially carbonated aqueous alkanolamine solutions and their blends," *J. Chem. Eng. Data*, vol. 43, pp. 378-382, 1998.

[81] A. Hartono, E. O. Mba, and H. F. Svendsen, "Physical properties of partially CO_2 loaded aqueous monoethanolamine (MEA)," *J. Chem. Eng. Data* vol. 59, pp. 1808-1816, 2014.

[82] B. P. Mandal, M. Kundu, and S. S. Bandyopadhyay, "Density and viscosity of aqueous solution of (N-Methyldiethanolamine + Monoethanolamine), (N-Methyldiethanolamine + Diethanolamine), (2-Amino-2-methyl-1-propanol + Monoethanolamine), and (2-Amino-2-methyl-1-propanol + Diethanolamine)," *J. Chem. Eng. Data*, vol. 48, pp. 703-707, 2003.

[83] M. H. Li and Y. C. Lie, "Densities and viscosity of solutions of Monoethanolamine + N-Methyldiethanolamine + Water and Monoethanolamine + 2-Amino-2-methyl-1-propanol + Water," *J. Chem. Eng. Data*, vol. 39, pp. 444-447, 1994.

[84] J. Zhang, P. S. Fennell, and J. P. M. Trusler, "Density and viscosity of partially carbonated aqueous tertiary alkonolamine solution at temperature between (298.15 and 353.15)K," *J. Chem. Eng. Data*, vol. 60, pp. 2392-2399, 2015.

[85] S. A. Jayarathna, C. K. Jayarathna, D. A. Kottage, S. Dayarathna, D. A. Eimer, and M. C. Melaaen, "Density and surface tension measurement of partially carbonated aqueous monoethanolamine solutions " *J. Chem. Eng. Data*, vol. 58, pp. 343-348, 2013.

[86]   J. Han, J. Jin, D. A. Eimer, and M. C. Melaaen, "Density of Water (1) + Diethanolamine (2) + CO$_2$ (3) and Water (1) + N-Methyldiethanolamine (2) + CO$_2$ (3) from (298.15 to 423.15) K," *J. Chem. Eng. Data,* vol. 57, no. 6, pp. 1843-1850, 2012, doi: 10.1021/je300345m.

[87]   Y. Maham, T. T. Teng, A. E. Mather, and L. G. Hepler, "Volumetric properties of (water + diethanolamine) systems," *Can. J. Chem,* vol. 73, pp. 1514-1519, 1995.

[88]   B. Hawrylak, S. E. Bruke, and R. Palepu, "Partial molar and excess volumes and adiabatic compressibilities of binary mixtures of ethanolamines with water," *J. Solution Chem.,* vol. 29, no. 6, pp. 575-593, 2000.

[89]   F. I. Chowdhury, S. Akhtar, and M. A. Saleh, "Densities and excess molar volumes of aqueous solutions of some diethanolamines " *Phys. Chem. Liq.,* vol. 47, no. 6, pp. 638-652, 2009.

[90]   H. A. Al-Ghawas, D. P. Hagewiesche, G. Ruiz-Ibanez, and O. C. Sandall, "Physicochemical properties important for carbon dioxide absorption in aqueous methyldiethanolamine," *J. Chem. Eng. Data,* vol. 34, no. 4, pp. 385-391, 1989, doi: 10.1021/je00058a004.

[91]   A. Henni, Y. Maham, P. Tontiwachwuthikul, A. Chakma, and A. E. Mather, "Densities and Viscosities for Binary Mixtures of N-Methyldiethanolamine + Triethylene Glycol Monomethyl Ether from 25 °C to 70 °C and N-Methyldiethanolamine + Ethanol Mixtures at 40 °C," *J. Chem. Eng. Data,* vol. 45, no. 2, pp. 247-253, 2000, doi: 10.1021/je9902140.

[92]   J. Aguila-Hernández, R. Gómez-Quintana, F. Murrieta-Guevara, A. Romero-Martínez, and A. Trejo, "Liquid Density of Aqueous Blended Alkanolamines and N-Methylpyrrolidone as a Function of Concentration and Temperature," *J. Chem. Eng. Data,* vol. 46, no. 4, pp. 861-867, 2001, doi: 10.1021/je0002944.

[93]   S. Paul and B. Mandal, "Density and Viscosity of Aqueous Solutions of (N-Methyldiethanolamine + Piperazine) and (2-Amino-2-methyl-1-propanol + Piperazine) from (288 to 333) K," *J. Chem. Eng. Data,* vol. 51, no. 5, pp. 1808-1810, 2006, doi: 10.1021/je060195b.

[94]   M. E. Rebolledo-Libreros and A. Trejo, "Density and Viscosity of Aqueous Blends of Three Alkanolamines: N-Methyldiethanolamine, Diethanolamine, and 2-Amino-2-methyl-1-propanol in the Range of (303 to 343) K," *J. Chem. Eng. Data,* vol. 51, no. 2, pp. 702-707, 2006, doi: 10.1021/je050462y.

[95]   J. M. Bernal-García, M. Ramos-Estrada, G. A. Iglesias-Silva, and K. R. Hall, "Densities and Excess Molar Volumes of Aqueous Solutions of n-Methyldiethanolamine (MDEA) at Temperatures from (283.15 to 363.15) K," *J. Chem. Eng. Data,* vol. 48, no. 6, pp. 1442-1445, 2003, doi: 10.1021/je030120x.

[96]   D. D. D. Pinto, J. G. M. S. Monteiro, B. Johnsen, H. F. Svendsen, and H. Knuutila, "Density measurements and modelling of loaded and unloaded aqueous solutions of MDEA (N-methyldiethanolamine), DMEA (N,N-dimethylethanolamine), DEEA (diethylethanolamine) and MAPA (N-methyl-1,3-diaminopropane)," *Int. J. Greenhouse Gas Control,* vol. 25, pp. 173-185, 2014, doi: 10.1016/j.ijggc.2014.04.017.

[97]   M.-H. Li and Y.-C. Lie, "Densities and viscosities of solutions of Monoethanolamine + N-Methyldiethanolamine + water and Monoethanolamine

+ 2-Amino-2-methyl-1-propanol + water," *J. Chem. Eng. Data*, vol. 39, pp. 444-447, 1994.

[98] E. B. Rinker, D. W. Oelschlager, A. T. Colussi, K. R. Henry, and O. C. Sandall, "Viscosity, density, and surface tension of binary mixtures of water and N-methyldiethanolamine and water and diethanolamine and tertiary mixtures of these amines with water over the temperature range 20-100.ºC," *J. Chem. Eng. Data*, vol. 39, no. 2, pp. 392-395, 1994, doi: 10.1021/je00014a046.

[99] A. Muhammad, M. I. A. Mutalib, T. Murugesan, and A. Shafeeq, "Density and excess properties of aqueous N-methyldiethanolamine solutions from (298.15 to 338.15) K," *J. Chem. Eng. Data*, vol. 53, no. 9, pp. 2217-2221, 2008, doi: 10.1021/je800416y.

[100] L. M. Welsh and R. A. Davis, "Density and viscosity of aqueous blends of N-methyldiethanolamine and 2-amino-2-methyl-1-propanol," *J. Chem. Eng. Data*, vol. 40, no. 1, pp. 257-259, 1995, doi: 10.1021/je00017a055.

[101] S. Xu, F. D. Otto, and A. E. Mather, "Physical properties of aqueous AMP solutions," *J. Chem. Eng. Data*, vol. 36, no. 1, pp. 71-75, 1991, doi: 10.1021/je00001a021.

[102] K. Zhang, B. Hawrylak, R. Palepu, and P. R. Tremaine, "Thermodynamics of aqueous amines: excess molar heat capacities, volumes, and expansibilities of {water+ methyldiethanolamine (MDEA)} and {water + 2-amino-2-methyl-1-propanol (AMP)}," *J. Chem. Thermodyn.*, vol. 34, no. 5, pp. 679-710, 2002, doi: 10.1006/jcht.2002.0937.

[103] A. Zúñiga-Moreno, L. A. Galicia-Luna, J. M. Bernal-García, and G. A. Iglesias-Silva, "Densities and Derived Thermodynamic Properties of 2-Amino-2-methyl-1-propanol + Water Mixtures at Temperatures from (313 to 363) K and Pressures up to 24 MPa," *J. Chem. Eng. Data*, vol. 53, no. 1, pp. 100-107, 2008/01/01 2008, doi: 10.1021/je700406p.

[104] A. Zúñiga-Moreno, L. A. Galicia-Luna, J. M. Bernal-García, and G. A. Iglesias-Silva, "Densities and derived thermodynamic properties of 2-amino-2-methyl-1-propanol + water mixtures at temperatures from (313 to 363) K and pressures up to 24 MPa," *J. Chem. Eng. Data*, vol. 53, no. 4, pp. 1047-1047, 2008, doi: 10.1021/je800129g.

[105] L. Lebrette, Y. Maham, T. T. Teng, L. G. Hepler, and A. E. Mather, "Volumetric properties of aqueous solutions of mono, and diethylethanolamines at temperatures from 5 to 80 °C II," *Thermochim. Acta*, vol. 386, no. 2, pp. 119-126, 2002, doi: 10.1016/S0040-6031(01)00813-9.

[106] F.-Q. Zhang, H.-P. Li, M. Dai, J.-P. Zhao, and J. P. Chao, "Volumetric properties of binary mixtures of water with ethanolamine alkyl derivatives," *Thermochim. Acta*, vol. 254, pp. 347-357, 1995, doi: 10.1016/0040-6031(94)02127-A.

[107] Y. Maham, T. T. Teng, L. G. Hepler, and A. E. Mather, "Volumetric properties of aqueous solutions of monoethanolamine, mono- and dimethylethanolamines at temperatures from 5 to 80 °C I," *Thermochim. Acta*, vol. 386, no. 2, pp. 111-118, 2002, doi: 10.1016/S0040-6031(01)00812-7.

[108] F. I. Chowdhury, S. Akhtar, M. A. Saleh, M. U. Khandaker, Y. M. Amin, and A. K. Arof, "Volumetric and viscometric properties of aqueous solutions of some

monoalkanolamines," *J. Mol. Liq.,* vol. 223, pp. 299-314, 2016, doi: 10.1016/j.molliq.2016.08.033.

[109] J. M. Bernal-García, K. R. Hall, A. Estrada-Baltazar, and G. A. Iglesias-Silva, "Density and viscosity of aqueous solutions of N,N-dimethylethanolamine at p=0.1 MPa from T=(293.15 to 363.15) K," *J. Chem. Thermodyn.,* vol. 37, no. 8, pp. 762-767, 2005, doi: 10.1016/j.jct.2004.11.016.

[110] Z. Idris, J. Chen, and D. A. Eimer, "Densities of aqueous 2-Dimethylaminoethanol solutions at temperatures of (293.15 to 343.15) K," *J. Chem. Eng. Data,* vol. 62, no. 3, pp. 1076-1082, 2017, doi: 10.1021/acs.jced.6b00888.

[111] E. I. Concepción, Á. Gómez-Hernández, M. C. Martín, and J. J. Segovia, "Density and viscosity measurements of aqueous amines at high pressures: DEA-water, DMAE-water and TEA-water mixtures," *J. Chem. Thermodyn.,* vol. 112, pp. 227-239, 2017, doi: 10.1016/j.jct.2017.05.001.

[112] R. C. Reid, J. M. Prausnitz, and B. E. Poling, *The properties of gas and liquids.* New York: McGraw-Hill, 1987.

[113] M. Sobrino, E. I. Concepcion, A. G. Hernandez, M. C. Martin, and J. J. Segovia, "Viscosity and density measurements of aqueous at high pressure: MDEA-water and MEA-water mixtures for CO_2 capture," *J. Chem. Thermodynamics,* vol. 98, pp. 231-241, 2016.

[114] R. H. Weiland, J. C. Dingman, D. B. Cronin, and G. J. Browning, "Density and viscosity of some partially carbonated aqueous alkanolamine solutions and their blends," *J. Chem. Eng. Data,* vol. 43, pp. 378-382, 1998.

[115] M. Shokouhi, A. H. Jalili, F. Samani, and M. Hosseini-Jenab, "Experimental investigation of the density and viscosity of CO_2-loaded aqueous alkanolamine solutions," *Fluid Phase Equilib.,* vol. 404, pp. 96-108, 2015, doi: 10.1016/j.fluid.2015.06.034.

[116] M. Shokouhi, A. H. Jalili, M. Hosseini-Jenab, and M. Vahidi, "Thermo-physical properties of aqueous solutions of N,N-dimethylformamide," *J. Mol. Liq.,* vol. 186, pp. 142-146, 2013, doi: 10.1016/j.molliq.2013.07.005.

[117] B. E. Poling, J. M. Prausnitz, and J. P. O'connell, *The properties of gases and liquids* New York, US: The Mc Graw-Hill Companies, Inc., 2001.

[118] R. B. Bird, W. E. Stewart, and E. N. Lightfoot, *Transport Phenomena*, second edition ed. USA: John Wiley & Sons, Inc., 2002.

[119] S. G. E. Giap, "The hidden property of Arrhenius-type relationship: Viscosity as a function of temperature," *J. Phys. Sci.,* vol. 21, no. 1, pp. 29-39, 2010.

[120] W. D. Monnery, W. Y. Svrcek, and A. K. Mehrotra, "Viscosity: A critical review of practical predictive and correlative methods," *Can J Chem Eng,* vol. 73, pp. 3-40, 1995.

[121] J. G. Kirkwood, F. P. Buff, and M. S. Green, "The statistical mechanical theory of transport processes. III. The coefficients of shear and bulk viscosity of liquids," *J. Chem. Phys,* vol. 17, no. 10, pp. 988-994, 1949.

[122] H. Eyring, "Viscosity, Plasticity, and Diffusion as example of absolute reaction rates," *J. Chem. Phys.,* vol. 4, pp. 283-291, 1936.

[123] R. M. Salinas, F. G. Sanchez, and O. H. Garduza, "Viscosity model for pure liquids based on Eyring theory and cubic EOS," *AIChE J.,* vol. 49, no. 3, pp. 799-804, 2003.

[124] J. Weirong and D. A. Lempe, "Calculation of viscosities of liquid mixtures using Eyring's theory in combination with cubic equation of state," *Chinese J. Chem. Eng,* vol. 14, no. 6, pp. 770-779, 2006.

[125] S. Atashrouz, M. Zarghampour, S. Abdolrahimi, G. Pazuki, and B. Nasernejad, "Estimation of the viscosity of ionic liquids containing binary mixtures based on the Eyring's theory and a modified Gibbs energy model," *J. Chem. Eng. Data,* vol. 59, no. 11, pp. 3691-3704, 2014, doi: 10.1021/je500572t.

[126] R. A. McAllister, "The viscosity of liquid mixtures.," *AlChE J.,* vol. 6, pp. 427-431, 1960.

[127] A. F. A. Asfour, E. F. Copper, J. Wu, and R. R. Zahran, "Prediction of the McAllister model parameters from pure component properties for liquid binary n-alkane systems," *Ind. Eng. Chem. Res.,* vol. 30, no. 7, pp. 1666-1669, 1991, doi: 10.1021/ie00055a040.

[128] J. M. Prausnitz, R. N. Lichtenthaler, and E. G. d. Azevedo, *Molecular thermodynamics of fluid-phase equilibria*. Prentice Hall PTR, 1999.

[129] G. T. Preston, T. W. Chapman, and J. M. Prausnitz, "Transport properties of cryogenic liquid and their mixtures " *Cryogenics,* vol. 7, pp. 274-279, 1967.

[130] K. S. Pitzer, "Corresponding states for perfect liquids," *J. Chem. Phys,* vol. 7, , pp. 583-590 1939, doi: 10.1063/1.1750496.

[131] E. Helfand and S. A. Rice, "Principle of corresponding state for transport properties " *J. Chem. Phys,* vol. 32, no. 6, p. 16421644, 1959.

[132] A. H. Nhaesi, "A study of the predictive models for the viscosity of multi-component liquid regular solutions.," PhD, University of Windsor, 1998.

[133] M. J. Tham and K. E. Gubbins, "Corresponding principle for transport properties of dense fluids," *I&EC fundamentals,* vol. 8, no. 4, pp. 791-795, 1969.

[134] M. J. Tham and K. E. Gubbins, "Correspondence principle for transport properties of dense fluids. Nonpolar polyatomic fluids," *I&EC fundamentals,* vol. 9, no. 1, pp. 63-70, 1970.

[135] K. S. Pitzer, D. Z. Lippmann, R. F. Curl, C. M. Huggins, and D. E. Petersen, "The volumetric and thermodynamic properties of fluids. II. Compressibility factor, vapor pressure and entropy of vaporization1," *J. Am. Chem. Soc.,* vol. 77, no. 13, pp. 3433-3440, 1955, doi: 10.1021/ja01618a002.

[136] A. Letsou and L. I. Stiel, "Viscosity of saturated nonpolar liquids at elevated pressures " *AlChE J.,* vol. 19, no. 2, pp. 409-411, 1973.

[137] A. S. Teja and P. Rice, "Generalized corresponding state method for the viscosities of liquid mixtures " *Ind. Eng. Chem. Fundam,* vol. 20, pp. 77-81, 1981.

[138] E. N. d. C. Andrade, "LVIII. A theory of the viscosity of liquids. Part II, Philosophical Magazine Series 7," vol. 17, no. 113, pp. 698-732, 1934.

[139] D. H. Vogel, "Das Temperaturabhaengigkeitsgesetz der Viskositaet von Fluessigkeiten," *Physikalische Zeitschrift,* vol. 22, pp. 645-646, 1921.

[140] D. van Velzen, R. L. Cardozo, and H. Langenkamp, "A liquid viscosity-temperature-chemical constitution relation for organic compounds," *Industrial & Engineering Chemistry Fundamentals,* vol. 11, no. 1, pp. 20-25, 1972, doi: 10.1021/i160041a004.

[141] L. Grunberg and A. H. Nissan, "Mixture law for viscosity," *Nature,* vol. 164, no. 4175, pp. 799-800, 1949, doi: 10.1038/164799b0.

[142] V. S. Kulkarni and C. Shaw, *Essential Chemistry for Formulators of Semisolid and Liquid Dosages*. Elsevier Inc., 2016.

[143] "An introduction to viscosity and rheology." ATA scientific instruments. (accessed 18 Jun, 2018).

[144] D. o. E. T. (KTH) and N. E. n.-f. h. exchange. *SOP for falling ball viscometer (Hopper)*.

[145] S. G. Etemad, R. Bagheri, and S. Z. Heris, "Theoretical and experimental study of falling - cylinder rheometer," *Iranian Journal of Chemical Engineering* vol. 1, no. 1, pp. 19-27, 2004.

[146] E. Ashare, R. B. Bird, and J. A. Lescarboura, "Falling cylinder viscometer for non-newtonian fluids," *AlChE J.,* vol. 11, no. 5, pp. 910-916, 1965.

[147] M. Kutz, *Handbook of materials selection*. Canada: John Wiley & Sons, Inc 2001.

[148] U. S. P. R. Arachchige, N. Aryal, D. A. Eimer, and M. C. Melaaen, "Viscosities of pure and aqueous solutions of Monoethanolamine (MEA), Diethanolamine (DEA), and N-Methyldiethanolamine (MDEA)," in *Annual transactions of the nordic rheology society*, 2013, vol. 21.

[149] U. S. P. R. Arachchige, B. Singh, K. Prajapati, and M. C. Melaaen, "Viscosities of aqueous solutions of Monoethanolamine (MEA), Diethanolamine (DEA) and N-Methyldiethanolamine (MDEA) at T=(90-150) $^{\circ}$C," in *Annual transactions of the nordic rheology society*, 2014, vol. 22.

[150] Z. Idris, N. B. Kummamuru, and D. A. Eimer, "Viscosity measurement of unloaded and CO_2-loaded aqueous monoethanolamine at higher concentrations," *J. Mol. Liq.,* vol. 243, pp. 638-645, 2017.

[151] D. Fu, L. Chen, and L. Qin, "Experiment and model for the viscosity of carbonated MDEA-MEA aqueous solutions," *Fluid Phase Equilib.,* vol. 319, pp. 42-47, 2012.

[152] U. S. P. R. Arachchige, B. Singh, K. Prajapati, and M. C. Melaaen, "Dynamic viscosity of partially carbonated aqueous monoethanolamine (MEA) from (20 to 150) $^{\circ}$C," *Applied Chemical Engineering* vol. 1, pp. 1-10, 2018.

[153] J. M. Bernal-García, L. A. Galicia-Luna, K. R. Hall, M. Ramos-Estrada, and G. A. Iglesias-Silva, "Viscosities for Aqueous Solutions of N-Methyldiethanolamine from 313.15 to 363.15 K," *J. Chem. Eng. Data,* vol. 49, no. 4, pp. 864-866, 2004, doi: 10.1021/je0302250.

[154] T. T. Teng, Y. Maham, L. G. Hepler, and A. E. Mather, "Viscosity of aqueous solutions of N-Methyldiethanolamine and of Diethanolamine," *J. Chem. Eng. Data,* vol. 39, pp. 290-293, 1994.

[155] N. B. Kummamuru, Z. Idris, and D. A. Eimer, "Viscosity measurement and correlation of unloaded and CO_2-loaded aqueous solutions of N-methyldiethanolamine-piperazine," *J. Chem. Eng. Data,* vol. 64, no. 11, pp. 4692-4700, 2019, doi: 10.1021/acs.jced.9b00021.

[156] D. D. D. Pinto, B. Johnsen, M. Awais, H. F. Svendsen, and H. K. Knuutila, "Viscosity measurements and modeling of loaded and unloaded aqueous solutions of MDEA, DMEA, DEEA and MAPA," *Chem. Eng. Sci.,* vol. 171, pp. 340-350, 2017, doi: 10.1016/j.ces.2017.05.044.

[157] A. Henni, J. J. Hromek, P. Tontiwachwuthikul, and A. Chakma, "Volumetric properties and viscosities for aqueous AMP solutions from 25 °C to 70 °C," *J. Chem. Eng. Data*, vol. 48, no. 3, pp. 551-556, 2003, doi: 10.1021/je0201119.

[158] Y. Maham, L. Lebrette, and A. E. Mather, "Viscosities and excess properties of aqueous solutions of Mono- and Diethylethanolamines at temperatures between 298.15 and 353.15 K," *J. Chem. Eng. Data*, vol. 47, no. 3, pp. 550-553, 2002, doi: 10.1021/je015528d.

[159] Y. Maham, C. N. Liew, and A. E. Mather, "Viscosities and excess properties of aqueous solutions of ethanolamines from 25 to 80°C," *J. Solution Chem.*, vol. 31, no. 9, pp. 743-756, 2002, doi: 10.1023/A:1021133008053.

[160] E. L. Heric and J. G. Brewer, "Viscosity of some binary liquid nonelectrolyte mixtures," *J. Chem. Eng. Data*, vol. 12, no. 04, pp. 574-583, 1967.

[161] A. Jouyban, M. Khoubnasabjafari, Z. Vaez-Gharamaleki, Z. Fekari, and W. E. Acree, Jr., "Calculation of the viscosity of binary liquids at various temperatures using Jouyban-Acree model," (in eng), *Chemical & pharmaceutical bulletin*, vol. 53, no. 5, pp. 519-23, May 2005.

[162] J. V. Herráez, R. Belda, O. Díez, and M. Herráez, "An equation for the correlation of viscosities of binary mixtures," *J. Solution Chem.*, vol. 37, no. 2, pp. 233-248, 2008, doi: 10.1007/s10953-007-9226-2.

[163] M. J. P. Comuñas, A. Baylaucq, C. Boned, and J. Fernández, "High-pressure measurements of the viscosity and density of two Polyethers and two Dialkyl Carbonates," *Int. J. Thermophys.*, vol. 22, no. 3, pp. 749-768, 2001/05/01 2001, doi: 10.1023/A:1010770831215.

[164] N. S. Matin, J. E. Remias, and K. Liu, "Application of electrolyte-NRTL model for prediction of the viscosity of carbon dioxide loaded aqueous amine solutions " *Ind. Eng. Chem. Res*, vol. 52, pp. 16979-16984, 2013.

[165] W. Kauzmann and H. Eyring, "The viscous flow of large molecules," *J. Am. Chem. Soc.*, vol. 62, no. 11, pp. 3113-3125, 1940, doi: 10.1021/ja01868a059.

[166] H. R. Rafiee, S. Ranjbar, and F. Poursalman, "Densities and viscosities of binary and ternary mixtures of cyclohexanone, 1,4-dioxane and isooctane from T=(288.15 to 313.15)K," *J. Chem. Thermodyn.*, vol. 54, pp. 266-271, 2012, doi: 10.1016/j.jct.2012.05.005.

[167] H. Vogel and A. Weiss, "Transport properties of liquids, 111. viscosity of Athermal liquid mixtures," *Ber. Bunsenges. Phys. Chem*, vol. 86, pp. 193-198, 1982.

[168] R. J. Fort and W. R. Moore, "Viscosities of binary liquid mixtures," *Transactions of the faraday society*, vol. 62, pp. 1112-1119, 1966.

[169] R. Meyer, M. Meyer, J. Metzger, and A. Peneloux, "Thermodynamic and physicochemical properties of binary solvent " *Journal de Chimie Physique et de Physico-Chimie Biologique*, vol. 68, pp. 406-412, 1971.

[170] C. M. Kinart, W. J. Kinart, and A. Ćwiklińska, "2-Methoxyethanol–Tetrahydrofuran–binary liquid system. Viscosities, densities, excess molar volumes and excess Gibbs activation energies of viscous flow at various temperatures," *J. Therm. Anal. Calorim.*, vol. 68, no. 1, pp. 307-317, 2002, doi: 10.1023/A:1014981921097.

[171] A. Ćwiklińska and C. M. Kinart, "Thermodynamic and physicochemical properties of binary mixtures of nitromethane with {2-methoxyethanol+2-

[157] A. Henni, J. J. Hromek, P. Tontiwachwuthikul, and A. Chakma, "Volumetric properties and viscosities for aqueous AMP solutions from 25 °C to 70 °C," *J. Chem. Eng. Data*, vol. 48, no. 3, pp. 551-556, 2003, doi: 10.1021/je0201119.

[158] Y. Maham, L. Lebrette, and A. E. Mather, "Viscosities and excess properties of aqueous solutions of Mono- and Diethylethanolamines at temperatures between 298.15 and 353.15 K," *J. Chem. Eng. Data*, vol. 47, no. 3, pp. 550-553, 2002, doi: 10.1021/je015528d.

[159] Y. Maham, C. N. Liew, and A. E. Mather, "Viscosities and excess properties of aqueous solutions of ethanolamines from 25 to 80°C," *J. Solution Chem.*, vol. 31, no. 9, pp. 743-756, 2002, doi: 10.1023/A:1021133008053.

[160] E. L. Heric and J. G. Brewer, "Viscosity of some binary liquid nonelectrolyte mixtures," *J. Chem. Eng. Data*, vol. 12, no. 04, pp. 574-583, 1967.

[161] A. Jouyban, M. Khoubnasabjafari, Z. Vaez-Gharamaleki, Z. Fekari, and W. E. Acree, Jr., "Calculation of the viscosity of binary liquids at various temperatures using Jouyban-Acree model," (in eng), *Chemical & pharmaceutical bulletin*, vol. 53, no. 5, pp. 519-23, May 2005.

[162] J. V. Herráez, R. Belda, O. Díez, and M. Herráez, "An equation for the correlation of viscosities of binary mixtures," *J. Solution Chem.*, vol. 37, no. 2, pp. 233-248, 2008, doi: 10.1007/s10953-007-9226-2.

[163] M. J. P. Comuñas, A. Baylaucq, C. Boned, and J. Fernández, "High-pressure measurements of the viscosity and density of two Polyethers and two Dialkyl Carbonates," *Int. J. Thermophys.*, vol. 22, no. 3, pp. 749-768, 2001/05/01 2001, doi: 10.1023/A:1010770831215.

[164] N. S. Matin, J. E. Remias, and K. Liu, "Application of electrolyte-NRTL model for prediction of the viscosity of carbon dioxide loaded aqueous amine solutions " *Ind. Eng. Chem. Res*, vol. 52, pp. 16979-16984, 2013.

[165] W. Kauzmann and H. Eyring, "The viscous flow of large molecules," *J. Am. Chem. Soc.*, vol. 62, no. 11, pp. 3113-3125, 1940, doi: 10.1021/ja01868a059.

[166] H. R. Rafiee, S. Ranjbar, and F. Poursalman, "Densities and viscosities of binary and ternary mixtures of cyclohexanone, 1,4-dioxane and isooctane from T=(288.15 to 313.15)K," *J. Chem. Thermodyn.*, vol. 54, pp. 266-271, 2012, doi: 10.1016/j.jct.2012.05.005.

[167] H. Vogel and A. Weiss, "Transport properties of liquids, 111. viscosity of Athermal liquid mixtures," *Ber. Bunsenges. Phys. Chem*, vol. 86, pp. 193-198, 1982.

[168] R. J. Fort and W. R. Moore, "Viscosities of binary liquid mixtures," *Transactions of the faraday society*, vol. 62, pp. 1112-1119, 1966.

[169] R. Meyer, M. Meyer, J. Metzger, and A. Peneloux, "Thermodynamic and physicochemical properties of binary solvent " *Journal de Chimie Physique et de Physico-Chimie Biologique*, vol. 68, pp. 406-412, 1971.

[170] C. M. Kinart, W. J. Kinart, and A. Ćwiklińska, "2-Methoxyethanol–Tetrahydrofuran–binary liquid system. Viscosities, densities, excess molar volumes and excess Gibbs activation energies of viscous flow at various temperatures," *J. Therm. Anal. Calorim.*, vol. 68, no. 1, pp. 307-317, 2002, doi: 10.1023/A:1014981921097.

[171] A. Ćwiklińska and C. M. Kinart, "Thermodynamic and physicochemical properties of binary mixtures of nitromethane with {2-methoxyethanol+2-

butoxyethanol} systems at T=(293.15, 298.15, 303.15, 308.15, and 313.15)K," *J. Chem. Thermodyn.,* vol. 43, no. 3, pp. 420-429, 2011, doi: 10.1016/j.jct.2010.10.016.

[172] T. M. Aminabhavi, M. I. Aralaguppi, G. Bindu, and R. S. Khinnavar, "Densities, shear viscosities, refractive indices, and speeds of sound of Bis(2-methoxyethyl) Ether with Hexane, Heptane, Octane, and 2,2,4-Trimethylpentane in the temperature interval 298.15-318.15 K," *J. Chem. Eng. Data,* vol. 39, no. 3, pp. 522-528, 1994, doi: 10.1021/je00015a028.

[173] K. Ohnishi, I. Fujihara, and S. Murakami, "Thermodynamic properties of decalins mixed with hexane isomers at 298.15 K. II. Excess volumes and isentropic compressibilities," *Fluid Phase Equilib.,* vol. 46, no. 1, pp. 73-84, 1989, doi: 10.1016/0378-3812(89)80276-6.

[174] M. Domínguez, A. Camacho, M. C. López, F. M. Royo, and J. S. Urieta, "Excess molar volumes and excess viscosities of ternary mixtures (2-butanol + 1-chlorobutane + 1-butylamine) and (2-methyl-2-propanol + 1-chlorobutane + 1-butylamine) at 298. 15 K," *Can. J. Chem.,* vol. 73, no. 6, pp. 896-901, 1995, doi: 10.1139/v95-112.

[175] P. K. Katti and M. M. Chaudhri, "Viscosities of binary mixtures of Benzyl Acetate with Dioxane, Aniline, and m-Cresol," *J. Chem. Eng. Data,* vol. 9, no. 3, pp. 442-443, 1964, doi: 10.1021/je60022a047.

[176] R. K. Nigam and B. S. Mahl, "Molecular interaction in binary liquid mixtures of dimethylsulfoxide with chlroethanes & chlroethenes," *Indian Journal of Chemistry* vol. 9, pp. 1255-1258, 1971.

[177] A. R. Khataee and M. B. Kasiri, "Artificial neural networks modeling of contaminated water treatment processes by homogeneous and heterogeneous nanocatalysis," *Journal of Molecular Catalysis A: Chemical,* vol. 331, no. 1, pp. 86-100, 2010, doi: 10.1016/j.molcata.2010.07.016.

[178] C. I. Rocabruno-Valdés, L. F. Ramírez-Verduzco, and J. A. Hernández, "Artificial neural network models to predict density, dynamic viscosity, and cetane number of biodiesel," *Fuel,* vol. 147, pp. 9-17, 2015, doi: 10.1016/j.fuel.2015.01.024.

[179] H. Z. Kister, *Distillation Design* USA: McGraw-Hill, Inc, 1992.

[180] B. K. Mondal, S. S. Bandyopadhyay, and A. N. Samanta, "Equilibrium solubility measurement and Kent-Eisenberg modeling of CO_2 absorption in aqueous mixture of N-methyldiethanolamine and hexamethylenediamine," *Greenhouse Gas Sci Technol,* vol. 7, pp. 202-214, 2017.

[181] R. L. Kent and B. Eisenberg, "Better data for amine treating " *Hydrocarbon Processing,* vol. 55, no. 2, pp. 87-90, 1976.

[182] Y.-G. Li and A. E. Mather, "Correlation and prediction of the solubility of Carbon Dioxide in a mixed Alkanolamine solution," *Ind. Eng. Chem. Res.,* vol. 33, no. 8, pp. 2006-2015, 1994, doi: 10.1021/ie00032a017.

[183] S. L. Clegg and K. S. Pitzer, "Thermodynamics of multicomponent, miscible, ionic solutions: generalized equations for symmetrical electrolytes," *J. Phys. Chem.,* vol. 96, no. 8, pp. 3513-3520, 1992, doi: 10.1021/j100187a061.

[184] P. Debye and E. Huckel, "Zur Theorie der Elektrolute," *Phys Z,* vol. 24, no. 9, pp. 185-206, 1923.

[185] C.-C. Chen, H. I. Britt, J. F. Boston, and L. B. Evans, "Local composition model for excess Gibbs energy of electrolyte systems " *AlChE J.,* vol. 28, no. 4, pp. 588-596, 1982.

[186] K. S. Pitzer, "Electrolytes. From dilute solutions to fused salts," *J. Am. Chem. Soc.,* vol. 102, no. 9, pp. 2902-2906, 1980, doi: 10.1021/ja00529a006.

[187] H. Renon and J. M. Prausnitz, "Local composition in thermodynamic excess functions for liquid mixtures " *AlChE J.,* vol. 14, no. 1, pp. 135-144, 1968.

[188] D. M. Austgen, G. T. Rochelle, X. Peng, and C. C. Chen, "Model of vapor-liquid equilibria for aqueous acid gas-alkanolamine systems using the electrolyte-NRTL equation," *Ind. Eng. Chem. Res.,* vol. 28, no. 7, pp. 1060-1073, 1989, doi: 10.1021/ie00091a028.

[189] Y. Li and A. E. Mather, "Correlation and prediction of the solubility of carbon dioxide in a mixed alkanol solution " *Ind. Eng. Chem. Res,* vol. 33, pp. 2006-2015, 1994.

[190] *Aspen physical property system: Physical property methods and models 11.1*, USA: Aspen Technology, Inc., 2001.

[191] "Rate-Based model of the CO_2 capture process by MEA using Aspen Plus ".

[192] B. P. Mandal, A. K. Biswas, and S. S. Bandyopadhyay, "Absorption of carbon dioxide into aqueous blends of 2-amino-2-methyl-1-propanol and diethanolamine," *Chem. Eng. Sci.,* vol. 58, pp. 4137-4144, 2003.

[193] D. Fernandes *et al.*, "Protonation constants and thermodynamic properties of amines for post combustion capture of CO_2," *J. Chem. Thermodyn.,* vol. 51, pp. 97-102, 2012, doi: 10.1016/j.jct.2012.02.031.

[194] I. Kim and H. F. Svendsen, "Comparative study of the heats of absorption of post-combustion CO_2 absorbents," *Int. J. Greenhouse Gas Control,* vol. 5, no. 3, pp. 390-395, 2011, doi: 10.1016/j.ijggc.2010.05.003.

[195] H. Ling, H. Gao, and Z. Liang, "Comprehensive solubility of N_2O and mass transfer studies on an effective reactive N,N-dimethylethanolamine (DMEA) solvent for post-combustion CO_2 capture," *Chem Eng J,* vol. 355, pp. 369-379, 2019, doi: 10.1016/j.cej.2018.08.147.

[196] U. Liebenthal, D. D. D. Pinto, J. G. M. S. Monteiro, H. F. Svendsen, and A. Kather, "Overall process analysis and optimisation for CO_2 capture from coal fired power plants based on phase change solvents forming two liquid phases," *Energy Procedia*, vol. 37, pp. 1844-1854, 2013, doi: 10.1016/j.egypro.2013.06.064.

[197] "Instruction Manual: DMA 4500/5000, Density/Specific Gravity/Concentration Meter."

[198] D. Fitzgerald, "Technical assessment of the anton paar DMA 5000 density meter."

[199] "U-tube technology in digital laboratory density meters." Anton Paar GmbH. https://wiki.anton-paar.com/en/u-tube-technology-in-digital-laboratory-density-meters/#c19162 (accessed 05/08, 2019).

[200] A. Furtado, E. Batista, I. Spohr, and E. Filipe, "Measurement of density using oscillation type density meters calibration, traceability and uncertainties " presented at the 14eme Congrès International de Métrologie, 2009.

[201] "Food Network Solution Complete Food Network Information Center." Food Network Solution Co., Ltd. .

http://www.foodnetworksolution.com/wiki/word/6044/concentric-cylinder-viscometer (accessed 2017).

[202] S. S. Karunarathne, D. A. Eimer, and L. E. Øi, "Uncertainty comparison of viscosity measurements of CO_2 loaded MEA and water mixtures in a coaxial rheometer using Monte Carlo simulation and GUM method," *IJEE*, vol. 10, no. 2, pp. 77-86, 2019.

[203] Z. Idris, "Operating manual for rheometer," 2015.

[204] U. E. Aronu, A. Hartono, and H. F. Svendsen, "Density, viscosity, and N_2O solubility of aqueous amino acid salt and amine amino acid salt solutions " *J. Chem. Thermodynamics,* vol. 45, pp. 90-99, 2012.

[205] Z. Idris and D. A. Eimer, "Density measurements of unloaded and CO_2 loaded 3 - Amino-1-propanol solutions at temperatures (293.15 to 353.15) K," *J. Chem. Eng. Data,* vol. 61, no. 1, pp. 173-181, 2016.

[206] K. Chhantyal, "Sensor data fusion based modelling of drilling fluid return flow through open channels," PhD, Faculty of Technology, Natural Science and Maritime Studies, University of South-Eastern Norway, 2018.

[207] S. Bell, *A Beginner's Guide to Uncertainty of Measurement*. United Kingdom: Centre for Basic, Thermal and Length Metrology, National Physical Laboratory, 1999.

[208] V. R. Meyer, "Measurement uncertainty," *Journal of Chromatography,* vol. 1158, pp. 15-24, 2007.

[209] JCGM, *Evaluation of measurement data — Supplement 1 to the "Guide to the expression of uncertainty in measurement" — Propagation of distributions using a Monte Carlo method*, 2008.

[210] S. L. R. Ellison and A. Williams, *Quantifying uncertainty in analytical measurement* 2012.

[211] S. S. Karunarathne, D. A. Eimer, and L. E. Øi, "Evaluation of systematic error and uncertainty of viscosity measurements of mixtures of monoethanol amine and water in coaxial cylinder rheometers," *International Journal of Modeling and Optimization,* vol. 8, no. 5, pp. 260-265, 2018.

[212] C. E. Papadopoulos and H. Yeung, "Uncertainty estimation and Monte Carlo simulation method," *Flow Meas. Instrum.,* vol. 12, pp. 291-298, 2001.

[213] M. Desenfant and M. Priel, "Road map for measurement uncertainty evaluation " *Measurement,* vol. 39, pp. 841-848, 2006.

[214] "Instruction Manual: Physica MCR Series, Physica MCR 51 / 101 / 301 / 501, Physica Smartpave."

[215] S. S. Karunarathne, D. A. Eimer, and L. E. Øi, "Model uncertainty of interfacial area and mass transfer coefficients in absorption column packings," in *Proceedings of the 58th SIMS*, Reykjavik, Iceland, 2017.

[216] D. P. Loucks, E. v. Beek, J. R. Stedinger, J. P. M. Dijkman, and M. T. Villars, *Water resources systems planning and management: An introduction to methods, models and applications*. UNESCO, 2005.

Published and submitted research articles

Article A

Density, viscosity and free energy of activation for viscous flow of monoethanolamine (1) + H_2O (2) + CO_2 (3) mixtures.

Density, Viscosity and Free Energy of Activation for Viscous Flow of Monoethanol Amine (1) + H₂O (2) + CO₂ (3) Mixtures

Sumudu S. Karunarathne, Dag A. Eimer and Lars E. Øi *

Faculty of Technology, Natural Sciences and Maritime Studies, University of South-Eastern Norway, Kjølnes Ring 56, 3901 Porsgrunn, Norway; sumuduunimrt@gmail.com (S.S.K.); dag.a.eimer@usn.no (D.A.E.)
* Correspondence: lars.oi@usn.no; Tel.: +47-35575141

Abstract: Densities and viscosities of aqueous monoethanol amine (MEA) and CO_2-loaded aqueous MEA are highly relevant in engineering calculations to perform process design and simulations. Density and viscosity of the aqueous MEA were measured in the temperature range of 293.15 K to 363.15 K with MEA mass fractions ranging from 0.3 to 1.0. Densities of the aqueous MEA were fitted for a density correlation. Eyring's viscosity model based on absolute rate theory was adopted to determine the excess free energy of activation for viscous flow of aqueous MEA mixtures and was correlated by a Redlich–Kister polynomial. Densities and viscosities of CO_2-loaded MEA solutions were measured in the temperature range of 293.15 K to 353.15 K with MEA mass fractions of 0.3, 0.4 and 0.5. The density correlation used to correlate aqueous MEA was modified to fit CO_2-loaded density data. The free energy of activation for viscous flow for CO_2-loaded aqueous MEA solutions was determined by Eyring's viscosity model and a correlation was proposed to represent free energy of activation for viscous flow and viscosity. This can be used to evaluate quantitative and qualitative properties in the MEA + H₂O + CO_2 mixture.

Keywords: density; viscosity; Eyring's viscosity model; MEA

1. Introduction

Post-combustion CO_2 capture (PCC) using absorption and desorption has gained great attention in the last decades and several amines have been investigated for their absorption efficiency. In acid gas treatment, monoethanol amine (MEA, IUPAC name: 2-aminoethanol) has been used since 1930 [1]. It is the benchmark amine for the evaluation of other amines in CO_2 capture performance considering absorption efficiency, reaction rates, energy demand and corrosion resistance. A blend of 30% MEA with 70% H₂O by mass is a standard in PCC. Higher reaction rates of MEA with CO_2 compared to secondary and tertiary amines enables optimization of the dimensions and operational parameters of the absorber column. MEA's low-absorption capacity and high-energy demand for desorption and poor corrosion resistance are arguments against the use of MEA at the commercial scale [2,3].

Density and viscosity of pure, aqueous and CO_2-loaded aqueous MEA have been studied and reported in the literature under different temperatures, MEA concentrations and CO_2 loadings [1,4–12]. These data are vital for development of empirical correlations that are useful in various aspects of process equipment design and process simulations. Density is important to determine the physical solubility of CO_2 in solvent, the solvent kinetics and mass transfer. Viscosity is frequently used in the modified Stoke–Einstein equation to estimate diffusivity that is necessary for calculating mass transfer and kinetic properties [13,14]. Many references are available for data of aqueous MEA solutions under different MEA concentrations and temperatures. There is a lack of measured data for physical properties

of CO_2-loaded solutions at different CO_2 loadings under different MEA concentrations. In order to reduce the unmeasured regions and to check the validity of measured data, further experimental studies are necessary.

Amundsen, Øi and Eimer [6] have used the McAllister three-body model [15] to represent the kinematic viscosity. Weiland, Dingman, Cronin and Browning [9] and Hartono, Mba and Svendsen [10] measured both density and viscosity of CO_2-loaded aqueous MEA solutions and proposed correlations to fit the data. The approach of using a Redlich-Kister [16] type polynomial to predict excess volume for the aqueous MEA solutions in the density correlations is widely used. A similar approach to correlate excess viscosity is adopted by Islam, et al. [17] for aqueous MEA.

In this work, density and viscosity of aqueous MEA and CO_2-loaded aqueous MEA were measured. The density correlation proposed by Aronu, Hartono and Svendsen [14] for the aqueous amino acid salt and amine amino acid salt solutions was used to correlate the density data of aqueous MEA. The same correlation was modified to predict the density of CO_2-loaded aqueous MEA solutions. The parameters of the correlations were found through a regression analysis. Eyring's viscosity model [18] was used to calculate the free energy of activation for viscous flow of the aqueous MEA solutions and parameters of the Redlich-Kister type polynomial were estimated by regression. For the viscosity of CO_2-loaded solutions, the difference of activation energy between CO_2-loaded aqueous MEA and aqueous MEA solutions were calculated, and a correlation was proposed.

2. Materials and Methods

2.1. Sample Preparation and CO_2 Loading Analysis

Descriptions of materials used in this study are given in Table 1. The Milli-Q water (resistivity 18.2 MΩ·cm) was degassed using a rotary evaporator connected to a vacuum pump to remove any dissolved gasses. The weights of liquids were measured through an electronic balance from Mettler Toledo (XS403S, Mettler Toledo, Greifensee, Switzerland) with a resolution of 1 mg. Aqueous MEA solutions with MEA to H_2O mass ratio w_1 = 0.3, 0.4, and 0.5 were prepared and fully loaded by bubbling CO_2 through the solution until the pH become steady over time. Then different CO_2-loaded solutions were prepared by diluting them with corresponding aqueous MEA. The amount of CO_2 loaded to the aqueous MEA was determined by a titration method in which CO_2 was fixed as $BaCO_3$ via adding 50 mL of each 0.1 M NaOH and 0.3 M $BaCl_2$ to 0.1–0.2 g of CO_2 loaded solution. All the samples were boiled for approximately 10 min to ensure the completion of chemical reactions and were cooled until the temperature reaches the room conditions. Eventually, $BaCO_3$ was separated by filtering using a hydrophilic polypropylene membrane filter (47 mm, 0.45 μm). The filtered $BaCO_3$ was put into 100 mL of distilled water and titrated with 0.1 M HCl until the solution reached pH of 2. Meanwhile, care needed to be taken to make sure all the $BaCO_3$ was dissolved during the titration. Then, the sample was boiled and cooled again before it was titrated with 0.1 M NaOH. Finally, the MEA concentration of mixtures was determined by titrating 1 g of CO_2-loaded solution with 1 M HCl.

Table 1. Materials used in this study [a,b].

Chemical Name	CAS Reg. No.	Mole Fraction Purity [a]	Source	Purification
monoethanol amine (MEA)	141-43-5	≥0.995 (GC [b])	Sigma–Aldrich	no
carbon dioxide (CO_2)	124-38-9	0.99999	AGA Norge AS	no
nitrogen (N_2)	7727-37-9	0.99999	AGA Norge AS	no
sodium hydroxide (NaOH)	1310-73-2	-	Merck KGaA	no
hydrochloric acid (HCl)	7647-01-0	-	Merck KGaA	no
barium chloride dihydrate ($BaCl_2 \cdot 2H_2O$)	10326-27-9	≥0.99	Merck KGaA	no

[a] As mentioned by the supplier. [b] Gas-liquid chromatography.

2.2. Density Measurements

The density of aqueous MEA and CO_2-loaded aqueous MEA was measured by a DMA 4500 density meter from Anton Paar (Graz, Austria). The standard calibration procedure for DMA 4500 was performed using degassed water and air at 293.15 K occasionally, while density checks were performed frequently to check the validity of the previous calibration at 293.15 K. Samples were inserted into the U-tube with care to prevent the presence of air bubbles in the tube. Measurements were performed using a separate sample at each temperature and composition. A cleaning and drying process of the U-tube was performed every time before a new sample was introduced. Density measurements were performed for the aqueous MEA of w_1 from 0.3 to 1 for the temperature range from 293.15 K to 363.15 K and CO_2-loaded aqueous MEA of w_1 = 0.3, 0.4 and 0.5 under different CO_2 loading for the temperature range from 293.15 K to 353.15 K. Final density data are presented as an average of three density measurements at each temperature and composition.

2.3. Viscosity Measurements

The dynamic viscosity was measured using a double-gap concentric rheometer Physica MCR 101 from Anton Paar (pressure cell XL DG35.12/PR; measuring cell serial number 80462200) (Graz, Austria). The standard viscosity solution S3S from Paragon Scientific Ltd. was used to calibrate the rheometer at different temperatures. The calibration and the measurement were done by using 7 mL of liquid volume under the shear rate (γ) of 1000 s^{-1}. Having compared with the reference viscosity data, measured viscosities of standard viscosity solution were used to determine the viscosity deviations at different temperatures. For temperatures where the supplier did not specify any reference viscosities, expected viscosity deviations were obtained via interpolation. A temperature controlling system with standard temperature uncertainty of ±0.03 K is equipped with the rheometer. An external cooling system of Anton Paar Viscotherm VT2 (Graz, Austria) with standard temperature uncertainty of ±0.02 K is employed for better temperature control in the range from 293.15 K to 303.15 K. The solution in the rheometer was pressured by N_2 gas (p = 4 bar) to minimize the possible release of MEA and CO_2 into the gas phase. Viscosity measurements were performed for the aqueous MEA of w_1 from 0.3 to 1 in the temperature range from 293.15–363.15 K and CO_2-loaded aqueous MEA with w_1 = 0.3, 0.4 and 0.5 under different CO_2 loadings for the temperature range from 293.15 K to 353.15 K. The viscosity data presented in this study are the averaged measurements for minimum of three different measurements.

3. Experimental Uncertainty

The Guide to the expression of Uncertainty in Measurement (GUM) [19,20] approach was adopted for the uncertainty evaluations using the mathematical models defined for the instruments for density and viscosity measurements. Several uncertainty sources including purity of MEA, weight measurements, repeatability, CO_2 loading and temperature were considered in addition to the uncertainty sources in the model equations during the uncertainty evaluation. The temperature accuracy of DMA 4500 and Physica MCR 101 Anton Paar are both specified as ±0.03 K. Considered standard uncertainties u for the density measurements are $u(\alpha)$ = ±0.005 (CO_2 loading mol CO_2/mol MEA), $u(w)$ = ±2 × 10^{-4} kg (weight measurement), $u(p)$ = ±0.003 (MEA purity), $u(T)$ = ±0.012 K (temperature) and $u(rep)$ = ±0.13 kg·m^{-3} (repeatability). The gradient $\partial\rho/\partial T$ of density against temperature was found as 0.73 kg·m^{-3}·K^{-1} and the corresponding uncertainty in ρ that is $(\partial\rho/\partial T) u(T)$ was calculated as ±0.009 kg·m^{-3}. The gradient of density against CO_2 loading, $\partial\rho/\partial\alpha$, was found as 334 kg m^{-3} and the corresponding uncertainty in ρ, $(\partial\rho/\partial\alpha) u(\alpha)$ was found as ±1.67 kg·m^{-3}. The standard combined uncertainty for density measurement $u(\rho)$ was found as $u(\rho)$ = ±3.90 kg·m^{-3}. Accordingly the combined expanded uncertainty $U_c(\rho)$ for density of CO_2-loaded aqueous MEA is $U_c(\rho)$ = ±7.80 kg·m^{-3} (level of confidence = 0.95, where k = 2).

The considered standard uncertainties u for the viscosity measurements are $u(\alpha)$ = ±0.005 (CO_2 loading mol CO_2/mol MEA), $u(w)$ = ±2 × 10^{-4} kg (weight measurement), $u(p)$ = ±0.003 (MEA purity),

$u(T) = \pm0.012$ K (temperature) and $u(rep) = \pm0.008$ mPa·s (repeatability). The standard combined uncertainty for viscosity measurement $u(\eta)$ was found as $u(\eta) = \pm0.018$ mPa·s. Accordingly the combined expanded uncertainty U_c is $U_c(\eta) = \pm0.036$ mPa·s (level of confidence = 0.95, where $k = 2$).

4. Results and Discussion

This section discusses the density, viscosity and free energy of activation for viscous flow in aqueous and CO_2-loaded aqueous MEA solutions. The correlations to represent density and viscosity data were evaluated using average absolute relative deviation and absolute maximum deviation (AARD and AMD) as given in Equations (1) and (2).

$$AARD(\%) = \frac{100\%}{N} \sum_{i=1}^{N} \left| \frac{Y_i^E - Y_i^C}{Y_i^E} \right| \tag{1}$$

$$AMD = MAX \left| Y_i^E - Y_i^C \right| \tag{2}$$

where N, Y_i^E and Y_i^C refer the number of data points, the measured property and calculated property respectively.

4.1. Density of MEA (1) + H_2O (2) + CO_2 (3) Mixtures

Many approaches in density correlations are based on suggesting a Redlich–Kister polynomial to fit the excess volume properties of the mixture. One of the drawbacks of the excess volume approach using a Redlich–Kister polynomial to calculate density is the complexity of the correlation due to a high number of parameters. The density correlation proposed by Aronu, Hartono and Svendsen [14] as given by Equation (3) was used to fit the measured aqueous density data. The estimated parameters are presented in Table 2. The correlation was in good agreement with measured data with AARD = 0.12% for the w_1 range from 0.3 to 0.9. The same parameters were used to fit the density of CO_2-loaded solutions by introducing a function with new parameters for the temperature and CO_2 mole fraction as illustrated in Equation (4).

Table 2. Correlation parameters for density of aqueous MEA.

MEA/w_1	T/K	No. Points	Parameters
0.3–0.9	293.15–363.15	56	$k_1 = 683.5$ $k_2 = 1.344 \times 10^5$ $k_3 = -1.089 \times 10^4$ $k_4 = 145.2$ $k_5 = 567.9$
	AARD (%)		0.12
	AMD (kg·m^{-3})		3.45

Correlation for the density of aqueous MEA:

$$\rho = \left(k_1 + \frac{k_2 x_2}{T}\right) exp\left(\frac{k_3}{T^2} + \frac{k_4 x_1}{T} + k_5 \left(\frac{x_1}{T}\right)^2\right) \tag{3}$$

where ρ, T, x_1, x_2 and k_i are density, temperature, mole fractions of MEA, H_2O of the aqueous mixture and estimated parameter vector.

The measured densities of aqueous MEA solutions are listed in Table 3. A comparison between correlations that are based on excess volume presented by Hartono, Mba and Svendsen [10] and Han, Jin, Eimer and Melaaen [1] with this work is shown in Figure 1. The accuracy of the correlation fit is acceptable compared to the literature [1,10]. The correlation deviates from measured density

with AMD of 3.45 kg·m^{-3} at $w_1 = 0.8$ and $T = 293.15$ K. This deviation is less than the measurement uncertainty reported in this study for aqueous MEA.

Table 3. Measured density ρ/kg·m^{-3} of aqueous MEA [a,b,c,d,e].

w_1	x_1	Measured Density ρ/kg·m^{-3}							
		293.15 K	303.15 K	313.15 K	323.15 K	333.15 K	343.15 K	353.15 K	363.15 K
0.3	0.1122	1012.6 1012.68 [d]	1008.2 1008.4 [b] 1008.31 [d] 1008.2 [e]	1003.3 1003.3 [b] 1003.4 [c] 1003.45 [d] 1003.3 [e]	997.9 998.1 [b] 998.1 [c] 998.07 [d] 998.1 [e]	991.6 992.3 [b] 992.23 [d] 992.3 [e]	986.0 986.1 [b] 985.8 [c] 985.96 [d]	979.4 979.4 [b] 979.4 [c] 979.27 [d]	972.3 972.5 [b]
0.4	0.1643	1018.4	1013.3 1013.8 [b] 1013.3 [e]	1007.8 1008.3 [b] 1007.7 [c] 1007.8 [e]	1001.8 1002.3 [b] 1001.8 [c] 1002.1 [e]	995.5 996.1 [b] 995.7 [e]	988.9 989.4 [b] 988.9 [c]	981.9 982.4 [b] 981.9 [c]	974.6 975.0 [b]
0.5	0.2278	1023.6	1017.8 1018.2 [b] 1017.8 [e]	1011.6 1012.1 [b] 1011.7 [c] 1011.8 [e]	1005.2 1005.6 [b] 1005.3 [c] 1005.4 [e]	998.4 999.0 [b] 998.7 [e]	991.4 991.9 [b] 991.5 [c]	984.1 984.5 [b] 984.2 [c]	976.4 976.9 [b]
0.6	0.3067	1027.7	1021.2 1021.4 [b] 1021.3 [e]	1014.5 1014.7 [b] 1014.6 [e]	1007.6 1007.8 [b] 1007.8 [e]	1000.4 1000.7 [b] 1000.6 [e]	993.0 993.2 [b]	985.4 985.6 [b]	977.4 977.7 [b]
0.7	0.4077	1029.3	1022.4 1022.8 [b] 1022.6 [e]	1015.2 1015.7 [b] 1015.5 [c] 1015.5 [e]	1007.9 1008.3 [b] 1008.2 [c] 1008.2 [e]	1000.4 1000.8 [b] 1000.6 [e]	992.7 993.1 [b] 993.0 [c]	984.8 985.2 [b] 985.0 [c]	976.4 977.1 [b]
0.8	0.5412	1028.1	1020.8 1021.0 [b]	1013.3 1013.5 [b]	1005.7 1005.9 [b]	997.9 998.2 [b]	990.0 990.2 [b]	981.9 982.1 [b]	973.6 973.9 [b]
0.9	0.7264	1023.5	1015.8 1016.2 [b]	1008.1 1008.5 [b] 1008.4 [c]	1000.3 1000.6 [b] 1000.6 [c]	992.4 992.7 [b]	984.3 984.6 [b] 984.6 [c]	976.1 976.5 [b] 976.4 [c]	967.8 968.1 [b]
1	1.0000	1015.9	1008.1 1008.0 [b]	1000.1 1000.0 [b] 1000.3 [c]	992.1 992.0 [b] 992.3 [c]	984.0 983.9 [b]	975.9 975.8 [b] 976.0 [c]	967.6 967.5 [b] 967.8 [c]	959.3 959.2 [b]

[a] Standard uncertainties u are $u(w) = \pm 2 \times 10^{-4}$ kg, $u(p) = \pm 0.003$, $u(T) = \pm 0.012$ K, $u(rep) = \pm 0.13$ kg·m^{-3}. The combined expanded uncertainty U_c is $U_c(\rho) = \pm 7.10$ kg·m^{-3} (level of confidence = 0.95, where $k = 2$). [b] Han, Jin, Eimer and Melaaen [1], [c] Amundsen, Øi and Eimer [6], [d] Hartono, Mba and Svendsen [10], [e] Jayarathna, Weerasooriya, Dayarathna, Eimer and Melaaen [8].
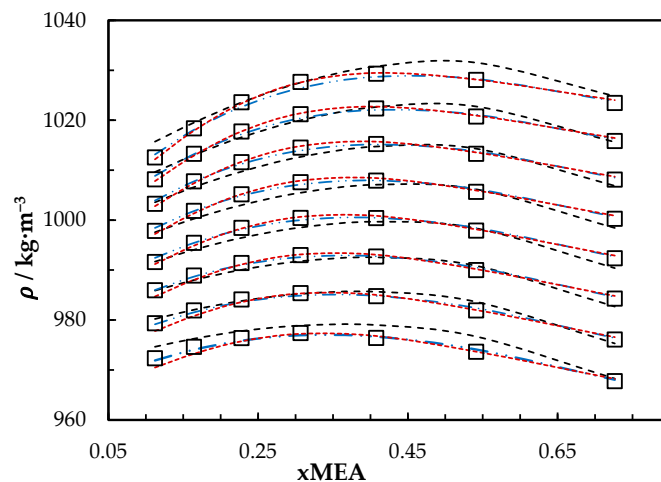
Figure 1. Density of aqueous MEA mixtures at different concentrations and temperatures (293.15, 303.15, 313.15, 323.15, 333.15, 343.15, 353.15 and 363.15) K. Data: from this work, '□'. Correlation predictions: from this work, '- - -'; Hartono, Mba and Svendsen [10], '----'; Han, Jin, Eimer and Melaaen [1], '· · ·'.

Correlation for the density of CO_2-loaded aqueous MEA:

$$\rho = (a_1 + a_2(T) + a_3(T)^2 + a_4 x_3)\left(k_1 + \frac{k_2 x_2}{T}\right)exp\left(\frac{k_3}{T^2} + \frac{k_4 x_1}{T} + k_5\left(\frac{x_1}{T}\right)^2\right)$$ (4)

The measured density of CO_2-loaded aqueous MEA of $w_1 = 0.3$, 0.4 and 0.5 solutions are shown in Table 4 and the correlation described in Equation (4) used to fit the data. At higher CO_2 loadings ($\alpha > 0.5$), formation of air bubbles was noticed in the U-tube beyond temperatures of 323.15 K in DMA 4500. This increases the uncertainty of the density measurements. Accordingly, densities at temperatures up to 323.15 K are shown for the solutions with $w_1 = 0.3$ and 0.4. The same was observed for the solution of $w_1 = 0.5$ with $\alpha = 0.495$ at above $T = 343.15$ K. Figure 2 shows the comparison of correlations proposed by Hartono, Mba and Svendsen [10], Han, Jin, Eimer and Melaaen [1] with this work for MEA solution of $w_1 = 0.3$. Measured densities at $w_1 = 0.4$ and 0.5 are given in Figures 3 and 4 with data from the literature. The correlation by Hartono, Mba and Svendsen [10] deviates positively from the measured data with AMD of 8.9 kg·m^{-3} while Han, Jin, Eimer and Melaaen [1] deviates negatively with AMD of 9.5 kg·m^{-3} at higher CO_2 loadings. The required parameters of Equation (4) for the CO_2-loaded solutions are listed in Table 5. The AMD from Equation (4) is lower than that from the other correlations.

Table 4. Measured density ρ/kg·m^{-3} of CO_2-loaded (α/mol CO_2·mol MEA^{-1}) aqueous MEA [a].

x_3	α	Measured Density ρ/kg·m^{-3}						
		293.15 K	303.15 K	313.15 K	323.15 K	333.15 K	343.15 K	353.15 K
$w_1 = 0.3$								
0.0000	0.000	1012.6	1008.2	1003.3	997.9	991.6	986.0	979.4
0.0105	0.095	1032.0	1027.6	1022.8	1017.4	1011.6	1005.1	995.5
0.0193	0.175	1052.5	1048.1	1043.3	1038.1	1032.4	1026.4	1020.1
0.0355	0.328	1077.8	1073.4	1068.6	1063.4	1057.9	1052.0	1044.1
0.0476	0.445	1103.3	1097.7	1092.8	1087.6	1082.1	1075.7	1069.3
0.0574	0.543	1123.1	1118.4	1113.4	1107.9			
$w_1 = 0.4$								
0.0000	0.000	1018.4	1013.3	1007.8	1001.9	995.5	988.9	981.9
0.0170	0.105	1045.6	1040.7	1035.3	1029.6	1023.6	1017.3	1010.6
0.0341	0.215	1073.4	1068.5	1063.3	1057.8	1051.9	1045.8	1039.4
0.0507	0.325	1102.0	1097.2	1092.0	1086.5	1080.8	1074.9	1068.6
0.0669	0.436	1130.3	1125.4	1120.2	1114.7	1109.2	1103.2	1097.0
0.0826	0.548	1155.5	1150.4	1145.1	1139.5			
$w_1 = 0.5$								
0.0000	0.000	1023.6	1017.8	1011.6	1005.2	998.4	991.4	984.1
0.0205	0.092	1052.3	1046.7	1040.9	1034.7	1028.3	1021.7	1014.8
0.0406	0.186	1082.4	1077.0	1071.4	1065.5	1059.4	1053.0	1046.4
0.0620	0.290	1112.7	1107.4	1101.9	1096.2	1090.3	1084.2	1077.9
0.0825	0.395	1144.5	1139.2	1133.8	1128.3	1122.5	1116.6	1110.5
0.1013	0.495	1175.7	1170.4	1165.0	1159.4	1153.6	1147.5	

[a] Standard uncertainties u are $u(\alpha) = \pm 0.005$, $u(w) = \pm 2 \times 10^{-4}$ kg, $u(p) = \pm 0.003$, $u(T) = \pm 0.012$ K, $u(rep) = \pm 0.13$ kg·m^{-3}. The combined expanded uncertainty U_c is $U_c(\rho) = \pm 7.80$ kg·m^{-3} (level of confidence = 0.95, where $k = 2$).

Table 5. Density correlation parameters for CO_2-loaded aqueous MEA.

Parameters	$w_1 = 0.3$	$w_1 = 0.4$	$w_1 = 0.5$
a_1	0.6802	0.7731	0.7506
a_2	0.001951	0.001354	0.001494
a_3	-2.97×10^{-6}	-2.015×10^{-6}	-2.237×10^{-6}
a_4	2.346	2.164	2.015
AARD (%)	0.15	0.08	0.15
AMD (kg·m^{-3})	4.2	2	3.8
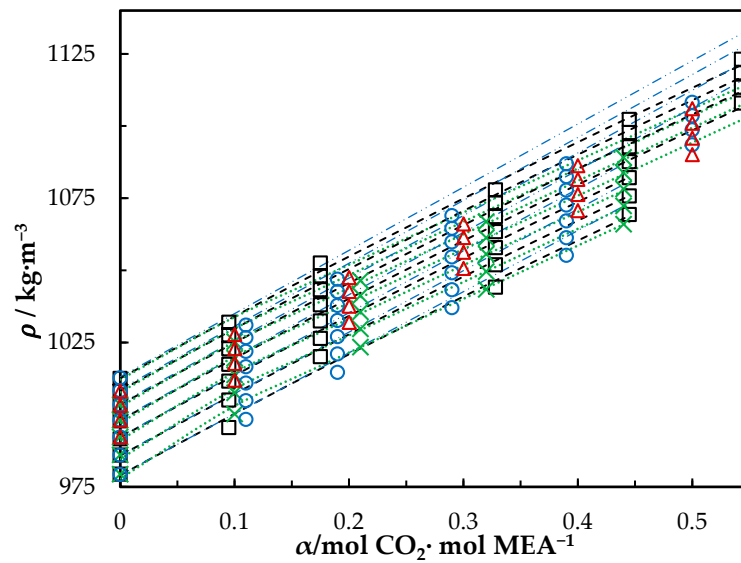
Figure 2. Density of CO_2-loaded MEA ($w_1 = 0.3$) solution at different CO_2 loadings and temperatures (293.15, 303.15, 313.15, 323.15, 333.15, 343.15 and 353.15) K. Data: from this work, '□'; Hartono, Mba and Svendsen [10], 'O'; Han, Jin, Eimer and Melaaen [1], '×'; Jayarathna, Weerasooriya, Dayarathna, Eimer and Melaaen [8], '△'. Correlation: from this work, '- - -'; Hartono, Mba and Svendsen [10], '-⋅⋅-'; Han, Jin, Eimer and Melaaen [1], '⋅⋅⋅'.

Figure 3. Density of CO_2-loaded MEA ($w_1 = 0.4$) solution at different CO_2 loadings and temperatures (293.15, 303.15, 313.15, 323.15, 333.15, 343.15 and 353.15) K. Data: from this work, '□'; Han, Jin, Eimer and Melaaen [1], '×'; Jayarathna, Weerasooriya, Dayarathna, Eimer and Melaaen [8], '△'. Correlation: from this work, '- - -'.

Figure 4. Density of CO_2-loaded MEA ($w_1 = 0.5$) solution at different CO_2 loadings and temperatures (293.15, 303.15, 313.15, 323.15, 333.15, 343.15 and 353.15) K. Data: from this work, '□'; Han, Jin, Eimer and Melaaen [1], 'x'; Jayarathna, Weerasooriya, Dayarathna, Eimer and Melaaen [8], '△'. Correlation: from this work, '- - -'.

4.2. Viscosity of MEA (1) + H$_2$O (2) + CO$_2$ (3) Mixtures

The Eyring's viscosity model based on absolute rate theory is shown in Equation (5). Here, viscous flow is treated as a chemical reaction considering the elementary process as the motion of a single molecule from one equilibrium position to another over a potential energy barrier [21,22].

$$\eta = \frac{hN_A}{V} exp\left(\frac{\Delta G^*}{RT}\right) \tag{5}$$

where η, V, h, N_A, ΔG^*, R and T are dynamic viscosity, molar volume, Planck's constant, Avogadro's number, free energy of activation for viscous flow, universal gas constant and temperature respectively. For binary liquid mixtures, Equations (5) and (6) were adopted to derive Equation (7) to calculate excess free energy of activation for viscous flow ΔG^{E*}.

$$\frac{\eta}{\eta_{ideal}} = \frac{V_{ideal}}{V} exp\left(\frac{\Delta G^{E*}}{RT}\right) \tag{6}$$

$$\frac{\Delta G^{E*}}{RT} = ln(\eta V) - \sum_{i=1}^{i=2} x_i ln\left(\eta_i V_i^0\right) \tag{7}$$

where x_i, η_i and V_i^0 ($i = 1$ for MEA and $i = 2$ for H$_2$O) are the mole fraction of components in the mixture, dynamic viscosity and molar volume of pure liquids.

The ΔG^{E*} was evaluated via measured viscosity and density data of aqueous MEA for w_1 from 0.3 to 1 and MEA temperatures from 293.15 K to 363.15 K. Viscosity and density of pure water for this study were taken from Korson, et al. [23] and Kestin, et al. [24]. A Redlich–Kister type correlation was used to fit the derived term $\Delta G^{E*}/RT$ and estimated parameters are given in Table 6. The measured viscosities of aqueous MEA are tabulated with literature data in Table 7. Our previous work has reported viscosities of aqueous MEA from $w_1 = 0.3$ to $w_1 = 0.5$ in Karunarathne, et al. [25]. Figure 5

shows the calculated and fitted ΔG^{E*} and Figure 6 compares the measured with calculated viscosities using the proposed correlation in this work and correlations suggested in the literature.

$$\frac{\Delta G^{E*}}{RT} = x_1 x_2 \sum_{i=0}^{i=2} C_i (1 - 2x_2)^i \tag{8}$$

$$C_i = a_i + b_i(T) \tag{9}$$

Table 6. Parameters of the excess free energy of activation for viscous flow correlation.

w_1	T/K	Parameters
0–1	298.15–363.15	$a_0 = 16.2$ $b_0 = -0.03473$ $a_1 = -4.853$ $b_1 = 0.008315$ $a_2 = -6.433$
		$b_2 = 0.02065$
	$R^2 = 0.998$	

Table 7. Measured viscosity η of aqueous MEA [a,b,c,d].

w_1	x_1	Measured Viscosity η/mPa·s							
		293.15 K	303.15 K	313.15 K	323.15 K	333.15 K	343.15 K	353.15 K	363.15 K
0.3	0.1122	2.836 2.874 [b] 2.879 [b]	2.109 2.133 [b] 2.130 [b]	1.628 1.628 [b] 1.638 [b] 1.67 [c]	1.290 1.305 [b] 1.318 [b] 1.33 [c]	1.046 1.055 [b] 1.067 [b]	0.866 0.878 [b] 0.874 [b] 0.92 [c]	0.740 0.742 [b] 0.740 [b] 0.77 [c]	0.687
0.4	0.1643	4.285	3.080	2.305 2.28 [c]	1.782 1.75 [c]	1.417	1.154 1.14 [c]	0.960 0.95 [c]	0.808
0.5	0.2278	6.610	4.580 4.69 [d]	3.310 3.39 [c] 3.37 [d]	2.454 2.54 [c] 2.53 [d]	1.915 1.94 [d]	1.528 1.57 [c] 1.54 [d]	1.243 1.28 [c] 1.26 [d]	1.029 1.05 [d]
0.6	0.3067	10.217	6.769 6.92 [d]	4.736 4.77 [d]	3.444 3.45 [d]	2.602 2.62 [d]	2.031 2.04 [d]	1.620 1.62 [d]	1.319 1.34 [d]
0.7	0.4077	15.348	9.823 9.89 [d]	6.664 6.96 [c] 6.69 [d]	4.720 4.94 [c] 4.76 [d]	3.461 3.49 [d]	2.615 2.79 [c] 2.63 [d]	2.029 2.18 [c] 2.04 [d]	1.616 1.63 [d]
0.8	0.5412	20.521	12.840 13.38 [d]	8.534 8.82 [d]	5.937 6.11 [d]	4.295 4.41 [d]	3.217 3.26 [d]	2.483 2.49 [d]	1.962 1.97 [d]
0.9	0.7264	24.027	14.963 15.12 [d]	9.879 10.20 [c] 9.95 [d]	6.829 7.06 [c] 6.88 [d]	4.936 4.94 [d]	3.683 3.81 [c] 3.67 [d]	2.832 2.93 [c] 2.82 [d]	2.222 2.23 [d]
1	1.0000	23.376	14.748 14.77 [d]	10.108 9.61 [c] 9.84 [d]	6.935 6.72 [c] 6.87 [d]	5.067 4.98 [d]	3.834 3.69 [c] 3.72 [d]	2.974 2.85 [c] 2.85 [d]	2.364 2.26 [d]

[a] The pressure was maintained by N_2 gas ($p = 4$ bar) during the experiments. Standard uncertainties u are $u(w) = \pm 2 \times 10^{-4}$ kg, $u(p) = \pm 0.003$, $u(T) = \pm 0.012$ K, $u(rep) = \pm 0.008$ mPa·s. The combined expanded uncertainty U_c is $U_c(\eta) = \pm 0.016$ mPa·s (level of confidence = 0.95, where $k = 2$). [b] Hartono, Mba and Svendsen [10], [c] Amundsen, Øi and Eimer [6], [d] Idris, et al. [26].

The viscosities from the correlation were in good agreement with measured data as shown in Figure 6. The proposed correlation was able to calculate viscosities with AARD 1.4% and with AMD 0.79 mPa·s. Table 8 summarizes the AARD and AMD of different suggested correlations.

Figure 5 illustrates the variation of ΔG^{E*} over the whole range of concentrations at different temperatures. At a specific temperature, ΔG^{E*} increases with the increase of MEA concentration until it reaches a maximum at x_{MEA} about 0.41 and then gradually decreases. The ΔG^{E*} decreases with the

increase of temperature while composition for maximum ΔG^{E*} is almost constant. A similar effect was observed for other aqueous amine mixtures [27,28].
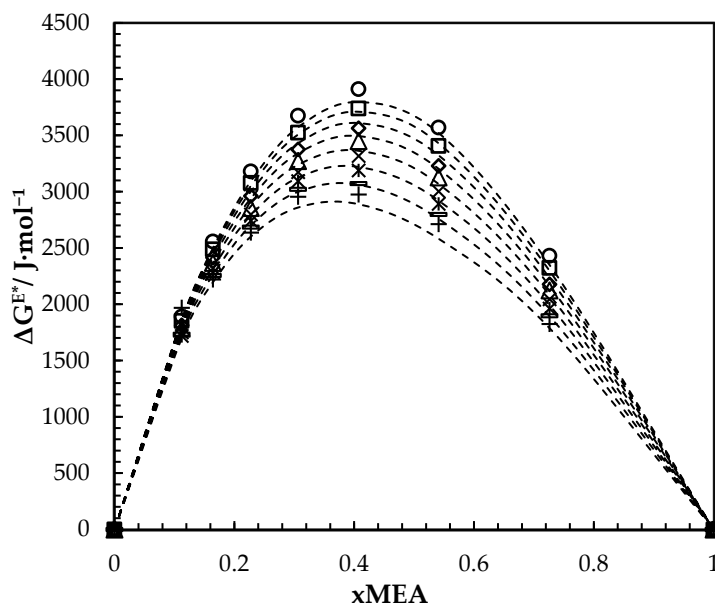
Figure 5. Calculated and fitted ΔG^{E*} for aqueous MEA solutions at different concentrations and temperatures. Calculated: 293.15 K, '○'; 303.15 K, '□'; 313.15 K, '◇'; 323.15 K, '△'; 333.15 K, 'x'; 343.15 K, 'ж'; 353.15 K, '-'; 363.15 K, '+'. Correlation: '- - -'.
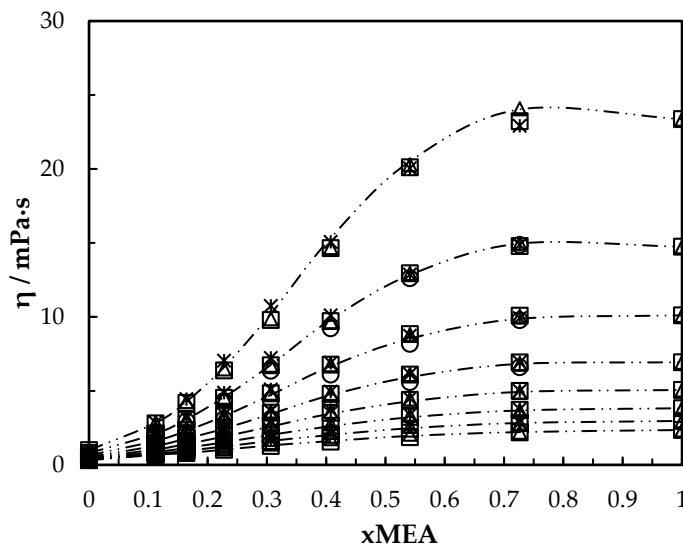
Figure 6. Viscosity of aqueous MEA solutions at different concentrations and temperatures (293.15, 303.15, 313.15, 323.15, 333.15, 343.15, 353.15, 363.15 K). Data: from this work, '-·-'. Correlation: from this work, '□'; Hartono, Mba and Svendsen [10], '△'; Arachchige, Aryal, Eimer and Melaaen [11], 'ж'; Islam, Islam and Yeasmin [17], '○'.

Table 8. Average absolute relative deviations and absolute maximum deviation of different suggested correlations for viscosity of aqueous MEA solutions from $w_1 = 0$ to $w_1 = 1$ and 293.15–363.15 K.

Source (s)	No. Parameters	AARD (%)	AMD (mPa·s)
This work	6	1.4	0.79
Hartono, et al. [10]	4	2.4	0.66
Arachchige, et al. [11]	7	3.5	1.1
Islam, et al. [17]	4	5.1	0.59

The excess volume V^E and excess viscosity η^E of aqueous MEA was determined by Equations (10) and (11) to analyze the molecular interaction between MEA and H_2O.

$$V^E = V - (x_1 V_1^0 + x_2 V_2^0) \tag{10}$$

$$\eta^E = \eta - (x_1 \eta_1 + x_2 \eta_2) \tag{11}$$

The $\Delta G^{E*} > 0$ and $V^E < 0$ for the considered MEA concentrations while η^E is negative (< 0) for the water-rich region and gradually become positive (> 0) with the increase of MEA concentration. The $\Delta G^{E*} > 0$ indicates that the viscosity of aqueous MEA solutions has greater viscosities than that of ideal mixtures [29]. The V^E can be negative as a result of the chemical or specific interaction and the structural contribution due to the difference in shape and size [30]. According to Eyring's viscosity model, it can be argued that more energy is required to make necessary holes for molecules to jump in when they are closely packed. The sign of η^E emphasizes strong specific interactions such as hydrogen bonding, which causes complex formations in the amine-rich region and weak interactions in the water-rich region [31].

The viscosity of CO_2-loaded aqueous MEA solutions is given by Table 9 for $w_1 = 0.3, 0,4$ and 0.5 under different CO_2 loading in the temperature range from 293.15–353.15 K. The measured viscosities at $w_1 = 0.3$, $w_1 = 0.4$ and 0.5 are shown in Figures 7–9 respectively with data from the literature. It was observed that the viscosity of solution increases with the increase of CO_2 dissolved in the mixture for all three different MEA concentrations and it decreases with the increase of temperature. The ΔG^* was calculated for both CO_2-loaded and CO_2-unloaded solutions and the difference was considered to develop a correlation as shown in Equations (12) and (13) to predict the viscosity of CO_2-loaded solutions.

Table 9. Measured viscosity of CO_2-loaded (α/mol CO_2 mol·MEA^{-1}) aqueous MEA [a].

x_3	α	Measured Viscosity (η/mPa·s)						
		293.15 K	303.15 K	313.15 K	323.15 K	333.15 K	343.15 K	353.15 K
$w_1 = 0.3$								
0.0000	0.000	2.836	2.109	1.628	1.290	1.046	0.866	0.740
0.0105	0.095	3.103	2.305	1.768	1.397	1.128	0.937	0.788
0.0193	0.175	3.338	2.476	1.910	1.511	1.228	1.021	0.865
0.0355	0.328	3.730	2.764	2.138	1.699	1.384	1.152	0.977
0.0476	0.445	4.164	3.105	2.403	1.913	1.562	1.308	1.118
0.0574	0.543	4.515	3.360	2.602	2.064	1.680	1.403	1.191
$w_1 = 0.4$								
0.0000	0.000	4.285	3.080	2.305	1.782	1.417	1.154	0.960
0.0170	0.105	4.793	3.423	2.567	1.985	1.590	1.302	1.090
0.0341	0.215	5.524	3.944	2.968	2.308	1.851	1.526	1.286
0.0507	0.325	6.496	4.655	3.502	2.726	2.198	1.813	1.524
0.0669	0.436	7.639	5.442	4.084	3.177	2.556	2.111	1.781
0.0826	0.548	8.820	6.203	4.614	3.544	2.821	2.302	1.917
$w_1 = 0.5$								
0.0000	0.000	6.610	4.580	3.310	2.454	1.915	1.528	1.243
0.0205	0.092	7.859	5.378	3.926	2.955	2.303	1.838	1.493
0.0406	0.186	9.518	6.529	4.756	3.594	2.813	2.269	1.866
0.0620	0.290	11.611	7.904	5.710	4.291	3.328	2.667	2.190
0.0825	0.395	14.854	10.073	7.247	5.422	4.227	3.409	2.809
0.1013	0.495	19.348	12.841	9.068	6.678	5.169	4.118	3.365

[a] The pressure was maintained by N_2 gas ($p = 4$ bar) during the experiments. Standard uncertainties u are $u(\alpha) = \pm 0.005$, $u(w) = \pm 2 \times 10^{-4}$ kg, $u(p) = \pm 0.003$, $u(T) = \pm 0.012$ K, $u(rep) = \pm 0.008$ mPa·s.
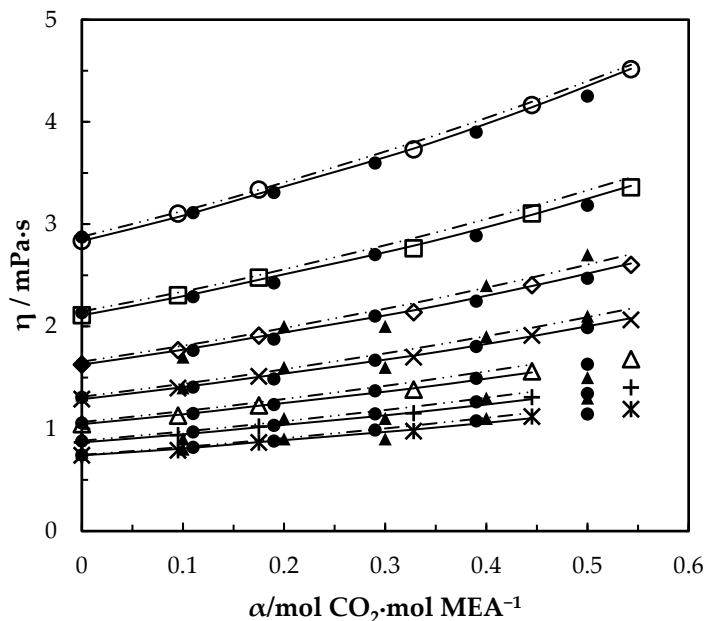
Figure 7. Viscosity of CO_2-loaded aqueous MEA ($w_1 = 0.3$) solutions at different CO_2 loadings and temperatures. Data: from this work, 293.15 K, '○'; 303.15 K, '□'; 313.15 K, '◇'; 323.15 K, '×'; 333.15 K, '△'; 343.14 K, '+'; 353.15 K, 'ж'; Hartono, Mba and Svendsen [10], '●'; Amundsen, Øi and Eimer [6], '▲'. Correlation: from this work, '- - -'; Hartono, Mba and Svendsen [10], '-⋯-'.
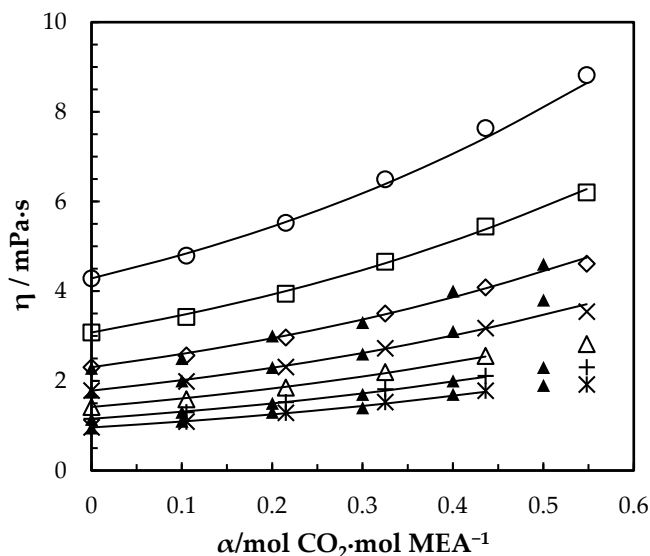
Figure 8. Viscosity of CO_2-loaded aqueous MEA ($w_1 = 0.4$) solutions at different CO_2 loadings and temperatures. Data: from this work, 293.15 K, '○'; 303.15 K, '□'; 313.15 K, '◇'; 323.15 K, '×'; 333.15 K, '△'; 343.14 K, '+'; 353.15 K, 'ж'; Amundsen, Øi and Eimer [6], '▲'. Correlation: from this work, '—'.

The combined expanded uncertainty U_c is $U_c(\eta) = \pm 0.036$ mPa·s (level of confidence = 0.95, where $k = 2$).

$$ln(V\eta)_{CO2\ loaded} = ln(V\eta)_{unloaded} + f(x_3, T) \qquad (12)$$

$$f(x_3, T) = x_3(d_1 + d_2T + d_3x_3) \qquad (13)$$
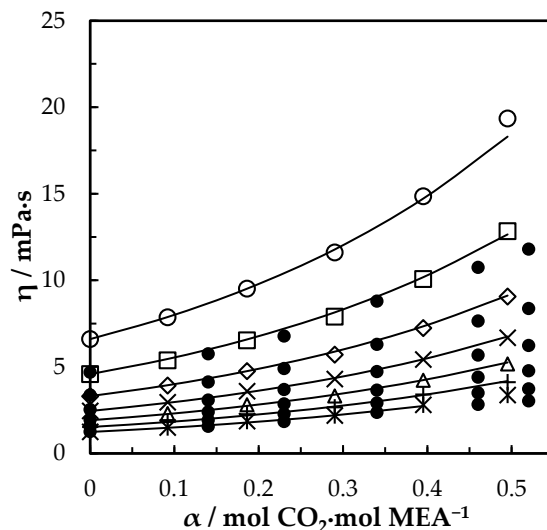
Figure 9. Viscosity of CO_2-loaded aqueous MEA ($w_1 = 0.5$) solutions at different CO_2 loadings and temperatures 293.15 K, '○'; 303.15 K, '□'; 313.15 K, '◇'; 323.15 K, 'x'; 333.15 K, '△'; 343.14 K, '+'; 353.15 K, 'ж'; Idris, Kummamuru and Eimer [26], '●'. Correlation: from this work, '—'.

The calculated AARD shows that the predicted and measured viscosities are in good agreement and parameters for the correlation are given in Table 10. The molar volume of CO_2-loaded aqueous MEA solutions was calculated using the mole fraction of dissolved CO_2 that was determined via CO_2 loading analysis. In a real solution, CO_2 reacts with MEA to form carbamate and bicarbonate ions and the solution becomes an electrolyte. Here it is assumed as unreacted and molar volumes were calculated using Equation (14) [32]. This approach was taken to represent dissolved CO_2 in aqueous MEA [7,10,26] and used in the viscosity correlation by Hartono, Mba and Svendsen [10].

$$V_{loaded} = \frac{\sum_1^3 x_i M_i}{\rho_{loaded}}$$

(14)

Table 10. Parameters of viscosity correlation for CO_2-loaded solutions.

T/K	Parameters	$w_1 = 0.3$	$w_1 = 0.4$	$w_1 = 0.5$
	d_1	4.536	2.554	8.533
298.15–343.15	d_2	0.006765	0.01205	−0.0037
	d_3	12.08	19.46	17.79
AARD (%)		0.58	1.13	1.25
AMD (mPa·s)		0.03	0.22	1.04

The variations of ΔG^* with CO_2 loading and temperature are shown in Figure 10a–c. For CO_2 loaded solutions, ΔG^* increases with the increase of dissolved CO_2 while it decreases with temperature. The amount of ions present in the solution due to the formation of carbamate and bicarbonate increases with the CO_2 loading, which results in higher ionic strength as discussed by Matin, et al. [33]. At higher ionic strengths, ions can create an ionic field that attract water molecules to form clusters, which leads to higher viscosity. The increase of ΔG^* implies the increase of potential barrier for the molecule transfer. The molecular interactions among the molecules in CO_2-loaded solutions may enhance the strength of energy barrier more than that of unloaded solutions. The correlation given in Equation (15) was proposed to fit ΔG^* for the CO_2-loaded aqueous MEA of $w_1 = 0.3$, 0,4 and 0.5. On the other hand, since the Eyring's viscosity model is based on the motion of individual molecules from one equilibrium position to another; it does not explain the effect of hydrogen bond network on the bulk viscosity of the various CO_2-loaded aqueous [34] MEA solutions. Further, the model has molar volume as a parameter

that needs to be known to calculate the viscosity. This can be done by using calculated molar volume from density data measured under the same conditions or from a correlation.

$$\Delta G^*_{CO2\ loaded} = \Delta G^*_{unloaded} + x_3 RT(d_1 + d_2 T + d_3 x_3) \tag{15}$$
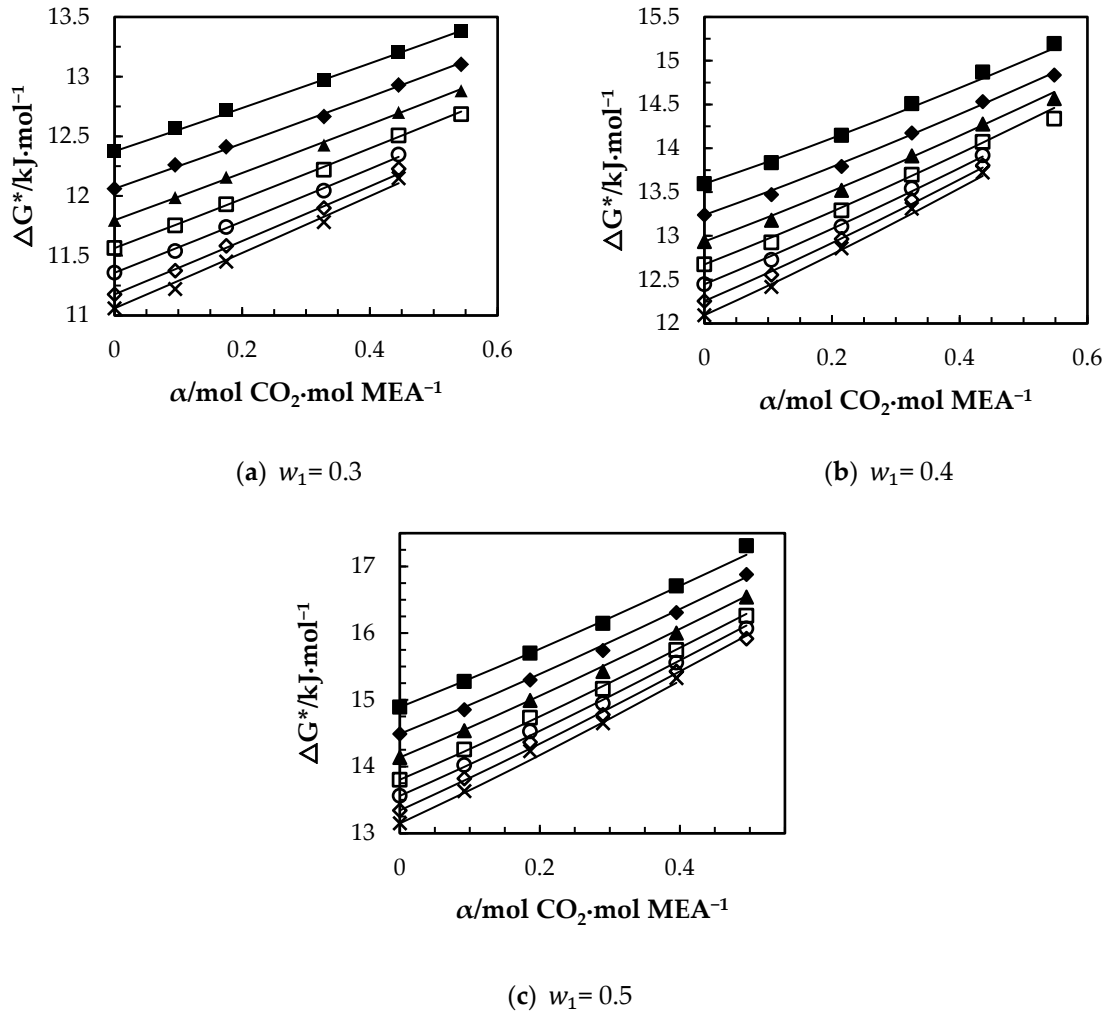
(**a**) $w_1 = 0.3$

(**b**) $w_1 = 0.4$

(**c**) $w_1 = 0.5$

Figure 10. Variation of free energy of activation for viscous flow of CO_2-loaded aqueous MEA: (**a**) $w_1 = 0.3$, (**b**) $w_1 = 0.4$, (**c**) $w_1 = 0.5$ solutions at different CO_2 loadings and temperatures of $T = 293.15$ K, '■'; 303.15 K, '♦'; 313.15 K, '▲'; 323.15 K, '□'; 333.15 K, '○'; 343.15 K, '◇'; 353.15 K, '✕' from Eyring's viscosity model. '—' from correlation in Equation (15).

The relationship between $Rln(\eta V/(hN_A))$ vs. $1/T$ gives information about activation parameters in which enthalpy of activation for viscous flow ΔH^* is given by the gradient and entropy of activation for viscous flow ΔS^* is given by the intercept of the curve under different mole fractions of the components. The ΔG^*, ΔH^* and ΔS^* are connected through the equation $\Delta G^* = \Delta H^* - T\Delta S^*$. Accordingly, Eyring's viscosity model is given as follows.

$$\eta = \frac{hN_A}{V} exp\left(\frac{\Delta H^*}{RT} - \frac{\Delta S^*}{R}\right) \tag{16}$$

Tables 11 and 12 list the calculated ΔG^* directly from Eyring's viscosity model, and ΔH^* and ΔS^* from the relation shown in Equation (16). It is observed that ΔG^*, ΔH^* and ΔS^* are positive for all considered mixtures while ΔH^* is greater than $T\Delta S^*$. This reveals that the influence of enthalpy of activation to the free energy of activation is greater than entropy of activation for viscous flow. Further,

this work shows how ΔG^* can be regarded as a parameter to regress and also can be regarded as a parameter with a physical meaning.

Table 11. Free energy of activation for viscous flow $\Delta G^*/kJ \cdot mol^{-1}$ for CO_2-loaded aqueous MEA.

T/K		293.15	303.15	313.15	323.15	333.15	343.15	353.15
w_1	x_3	Free Energy $\Delta G^*/kJ \cdot mol^{-1}$						
0.3	0.0000	12.375	12.062	11.798	11.564	11.358	11.177	11.060
	0.0105	12.571	12.262	11.988	11.753	11.539	11.376	11.222
	0.0193	12.721	12.413	12.159	11.931	11.740	11.583	11.451
	0.0355	12.970	12.667	12.428	12.220	12.044	11.900	11.783
	0.0476	13.210	12.931	12.702	12.507	12.347	12.228	12.150
	0.0574	13.382	13.105	12.883	12.685			
0.4	0.0000	13.595	13.240	12.936	12.674	12.448	12.255	12.094
	0.0170	13.835	13.471	13.179	12.924	12.726	12.556	12.419
	0.0341	14.148	13.793	13.521	13.291	13.105	12.965	12.860
	0.0507	14.509	14.175	13.914	13.698	13.540	13.413	13.312
	0.0669	14.870	14.534	14.278	14.072	13.919	13.807	13.725
	0.0826	15.194	14.837	14.568	14.337			
0.5	0.0000	14.891	14.489	14.137	13.802	13.560	13.344	13.148
	0.0205	15.275	14.853	14.538	14.255	14.022	13.819	13.631
	0.0406	15.701	15.299	14.992	14.733	14.526	14.366	14.230
	0.0620	16.147	15.741	15.426	15.165	14.945	14.779	14.648
	0.0825	16.707	16.309	16.002	15.747	15.559	15.427	15.325
	0.1013	17.311	16.879	16.543	16.262	16.069	15.918	

Table 12. Free energy of activation for viscous flow $\Delta G^*/kJ \cdot mol^{-1}$ for CO_2-loaded aqueous MEA.

w_1	x_3	$\Delta H^*/kJ \cdot mol^{-1}$	$\Delta S^*/J \cdot (mol \cdot K)^{-1}$
0.3	0.0000	18.834	22.301
	0.0105	19.150	22.696
	0.0193	18.902	21.360
	0.0355	18.716	19.895
	0.0476	18.400	18.003
	0.0574	20.173	23.234
0.4	0.0000	20.897	25.215
	0.0170	20.688	23.742
	0.0341	20.377	21.642
	0.0507	20.266	20.026
	0.0669	20.379	19.209
	0.0826	23.540	28.578
0.5	0.0000	23391	29.339
	0.0205	23147	27.247
	0.0406	22773	24.566
	0.0620	23389	25.142
	0.0825	23381	23.248
	0.1013	25441	28.114

5. Conclusions

Densities and viscosities of MEA (1) + H_2O (2) mixtures have been measured for the mass fraction w_1 from 0.3 to 1 and temperatures in the range 273.15 K to 363.15 K. The density data were correlated using the correlation proposed by Aronu, Hartono and Svendsen for w_1 from 0.3 to 0.9. The accuracy of the measured density with correlation predictions are acceptable as the AARD is 0.12% and AMD is 3.45 kg·m^{-3}. The viscosity data were correlated using a Redlich–Kister type polynomial fitted to the excess free energy of activation for viscous flow ΔG^{E*} obtained via the Eyring's viscosity model for

the w_1 from 0 to 1 and temperatures in a range from 273.15 K to 363.15 K. The developed correlation was able to represent the measured viscosities with AARD = 1.4% and AMD = 0.79 mPa·s, which is acceptable in engineering calculations.

The densities of CO_2-loaded aqueous MEA solutions were measured at temperatures ranging from 293.15 K to 353.15 K for w_1 of 0.3, 0.4 and 0.5. Density of CO_2-loaded solutions increases with the CO_2 loading and decreases with temperature. The density correlation proposed by Aronu, Hartono and Svendsen was modified to correlate the density data. The AMD between correlated and experimental densities are 4.2 kg·m^{-3}, 2 kg·m^{-3} and 4.5 kg·m^{-3} for CO_2-loaded solutions with w_1 of 0.3, 0.4 and 0.5 respectively.

The viscosities of CO_2-loaded aqueous MEA solutions were measured at temperatures ranging from 293.15 K to 353.15 K for w_1 of 0.3, 0.4 and 0.5. As CO_2 loading increased, the viscosity increased and the viscosity decreased with the increase of temperature. A correlation was proposed for the free energy of activation for viscous flow using CO_2 mole fraction and temperature to correlate viscosity data. The AMD between correlated and experimental viscosities are 0.03 mPa·s, 0.22 mPa·s and 1.04 mPa·s for CO_2-loaded solutions with w_1 of 0.3, 0.4 and 0.5 respectively. The proposed correlation is recommended to use in engineering calculations.

Author Contributions: Supervision, L.E.Ø. and D.A.E.; Writing-original draft, S.S.K. All authors have read and agreed to the published version of the manuscript.

Conflicts of Interest: The authors declare no conflict of interest.

References

1. Han, J.; Jin, J.; Eimer, D.A.; Melaaen, M.C. Density of water (1) + Monoethanolamine (2) + CO2 (3) from (298.15 to 413.15) K and surface tension of water (1) + Monoethanolamine (2) from (303.15 to 333.15) K. *J. Chem. Eng. Data* **2012**, *57*, 1095–1103. [CrossRef]

2. Nwaoha, C.; Saiwan, C.; Supap, T.; Idem, R.; Tontiwachwuthikul, P.; Rongwong, W.; Al-Marri, M.J.; Benamor, A. Carbon dioxide (CO2) capture performance of aqueoustri-solvent blends containing 2-amino-2-methyl-1-propanol (AMP) and methyldiethanolamine (MDEA) promoted by diethylenetriamine (DETA). *Int. J. Greenh. Gas Control* **2016**, *53*, 292–304. [CrossRef]

3. Kidnay, A.J.; Parrish, W.R. *Fundamentals of Natural Gas Processing*; Taylor & Francis Group: Boca Raton, FL, USA, 2006.

4. Maham, Y.; Teng, T.T.; Hepler, L.G.; Mather, A.E. Densities, excess molar volumes, and partial molar volumes for binary mixtures of Water with Monoethanolamine, Diethnolamine, and Triethanolamine from 25 to 80 °C. *J. Solut. Chem.* **1994**, *23*, 195–205. [CrossRef]

5. Yang, F.; Wang, X.; Wang, W.; Liu, Z. Densities and excess properties of primary amines in alcoholic solutions. *J. Chem. Eng. Data* **2013**, *58*, 785–791. [CrossRef]

6. Amundsen, T.G.; Øi, L.E.; Eimer, D.A. Density and viscosity of monoethanolamine + water + carbon dioxide from (25 to 80) °C. *J. Chem. Eng. Data* **2009**, *54*, 3096–3100. [CrossRef]

7. Jayarathna, S.A.; Jayarathna, C.K.; Kottage, D.A.; Dayarathna, S.; Eimer, D.A.; Melaaen, M.C. Density and surface tension measurement of partially carbonated aqueous monoethanolamine solutions. *J. Chem. Eng. Data* **2013**, *58*, 343–348. [CrossRef]

8. Jayarathna, S.; Weerasooriya, A.; Dayarathna, S.; Eimer, D.A.; Melaaen, M.C. Densities and surface tensions of CO2 loaded aqueous monoethanolamine solution with r = (0.2 to 0.7) at T = (303.15 to 333.15) K. *J. Chem. Eng. Data* **2013**, *58*, 986–992. [CrossRef]

9. Weiland, R.H.; Dingman, J.C.; Cronin, D.B.; Browning, G.J. Density and viscosity of some partially carbonated aqueous alkanolamine solutions and their blends. *J. Chem. Eng. Data* **1998**, *43*, 378–382. [CrossRef]

10. Hartono, A.; Mba, E.O.; Svendsen, H.F. Physical properties of partially CO2 loaded aqueous monoethanolamine (MEA). *J. Chem. Eng. Data* **2014**, *59*, 1808–1816. [CrossRef]

11. Arachchige, U.S.P.R.; Aryal, N.; Eimer, D.A.; Melaaen, M.C. Viscosities of pure and aqueous solutions of Monoethanolamine (MEA), Diethanolamine (DEA), and N-Methyldiethanolamine (MDEA). In Proceedings of the Annual Transactions of the Nordic Rheology Society, Copenhagen, Demark, 12–14 June 2013.

12. Hsu, C.-H.; Li, M.-H. Viscosities of Aqueous Blended Amines. *J. Chem. Eng. Data* **1997**, *42*, 714–720. [CrossRef]

13. Versteeg, G.F.; Van Swaaij, W.P.M. Solubility and diffusivity of acid gases (carbon dioxide, nitrous oxide) in aqueous alkanolamine solutions. *J. Chem. Eng. Data* **1988**, *33*, 29–34. [CrossRef]

14. Aronu, U.E.; Hartono, A.; Svendsen, H.F. Density, viscosity, and N2O solubility of aqueous amino acid salt and amine amino acid salt solutions. *J. Chem. Thermodyn.* **2012**, *45*, 90–99. [CrossRef]

15. McAllister, R.A. The viscosity of liquid mixtures. *AIChE. J.* **1960**, *6*, 427–431. [CrossRef]

16. Redlich, O.; Kister, A.T. Algebraic representation of thermodynamic properties and the classification of solutions. *Ind. Eng. Chem.* **1948**, *40*, 345–348. [CrossRef]

17. Islam, M.N.; Islam, M.M.; Yeasmin, M.N. Viscosity of aqueous solution of 2-methoxyethanol, 2-ethoxyethanol, and ethanolamine. *J. Chem. Thermodyn.* **2004**, *36*, 889–893. [CrossRef]

18. Eyring, H. Viscosity, Plasticity, and Diffusion as example of absolute reaction rates. *J. Chem. Phys.* **1936**, *4*, 283–291. [CrossRef]

19. JCGM. Evaluation of measurement data—Supplement 1 to the Guide to the Expression of Uncertainty In Measurement—Propagation of Distributions Using a Monte Carlo Method. In *JCGM 101: 2008*; JCGM: Sevres, France, 2008.

20. Ellison, S.L.R.; Williams, A. *Eurachem/CITAC Guide: Quantifying Uncertainty in Analytical Measurement*, 3rd ed.; 2012; Available online: http://www.eurachem.org (accessed on 15 November 2019).

21. Nhaesi, A.H. A Study of the Predictive Models for the Viscosity of Multi-Component Liquid Regular Solutions. Ph.D. Thesis, University of Windsor, Windsor, UK, 1998. Available online: https://core.ac.uk/download/pdf/72774384.pdf (accessed on 15 November 2019).

22. Macías-Salinas, R.; Aquino-Olivos, M.A.; García-Sánchez, F. Viscosity modelling of reservoir fluids over wide temperature and pressure ranges. *Chem. Eng. Trans.* **2013**, *32*, 1573–1578. [CrossRef]

23. Korson, L.; Hansen, W.D.; Millero, F.J. Viscosity of water at various temperatures. *J. Phys. Chem.* **1969**, *73*, 34–39. [CrossRef]

24. Kestin, J.; Sokolov, M.; Wakeham, W.A. Viscosity of liquid water in the range −8 °C to 150 °C. *J. Phys. Chem. Ref. Data* **1978**, *7*, 941–948. [CrossRef]

25. Karunarathne, S.S.; Eimer, D.A.; Øi, L.E. Evaluation of systematic error and uncertainty of viscosity measurements of mixtures of monoethanol amine and water in coaxial cylinder rheometers. *Int. J. Model. Optim.* **2018**, *8*, 260–265. [CrossRef]

26. Idris, Z.; Kummamuru, N.B.; Eimer, D.A. Viscosity measurement of unloaded and CO2-loaded aqueous monoethanolamine at higher concentrations. *J. Mol. Liq.* **2017**, *243*, 638–645. [CrossRef]

27. Hartono, A.; Svendsen, H.F. Density, viscosity, and excess properties of aqueous solution of diethylenetriamine (DETA). *J. Chem. Thermodyn.* **2009**, *41*, 973–979. [CrossRef]

28. Maham, Y.; Liew, C.N.; Mather, A.E. Viscosities and Excess Properties of Aqueous Solutions of Ethanolamines from 25 to 80 °C. *J. Solut. Chem.* **2002**, *31*, 743–756. [CrossRef]

29. Heric, E.L.; Brewer, J.G. Viscosity of some binary liquid nonelectrolyte mixtures. *J. Chem. Eng. Data* **1967**, *12*, 574–583. [CrossRef]

30. Mahajan, A.R.; Mirgane, S.R. Excess molar volumes and viscosities for the binary mixtures of n-Octane, n-Decane, n-Dodecane, and n-Tetradecane with Octan-2-ol at 298.15 K. *J. Thermodyn.* **2013**, *2013*, 1–11. [CrossRef]

31. Idris, Z.; Kummamuru, N.B.; Eimer, D.A. Viscosity measurement and correlation of unloaded and CO2 loaded 3-Amino-1-propanol solution. *J. Chem. Eng. Data* **2018**, *63*, 1454–1459. [CrossRef]

32. Stec, M.; Spietz, T.; Wieclaw-Solny, L.; Tatarczuk, A.; Wilk, A.; Sobolewski, A. Density of unloaded and CO2-loaded aqueous solutions of piperazine and 2-amino-2-methyl-1-propanol and their mixtures from 293.15 to 333.15 K. *Phys. Chem. Liq.* **2015**, *54*, 475–486. [CrossRef]

33. Matin, N.S.; Remias, J.E.; Liu, K. Application of electrolyte-NRTL model for prediction of the viscosity of carbon dioxide loaded aqueous amine solutions Ind. *Eng. Chem. Res* **2013**, *52*, 16979–16984. [CrossRef]

34. Perticaroli, S.; Mostofian, B.; Ehlers, G.; Neuefeind, J.C.; Diallo, S.O.; Stanley, C.B.; Daemen, L.; Egami, T.; Katsaras, J.; Cheng, X.; et al. Structural relaxation, viscosity, and network connectivity in a hydrogen bonding liquid. *Phys. Chem. Chem. Phys.* **2017**, *19*, 25859–25869. [CrossRef]

Article B

Density, viscosity and free energy of activation for viscous flow of CO_2 loaded AMP, MEA and H_2O mixtures

Sumudu S. Karunarathne*, Dag A. Eimer, Lars E. Øi

Faculty of Technology, Natural Sciences and Maritime Sciences, University of South-Eastern Norway. Kjølnes Ring 56, Porsgrunn 3918, Norway.

Abstract

This work presents an experimental study of densities and viscosities of aqueous and CO_2 loaded AMP (2-amino-2-methyl-1-propanol) + MEA (monoethanol amine) + H_2O solutions. Amine concentrations were at AMP to MEA mass % ratios of 21/9, 24/6, 27/3 by maintaining 70 mass % of H_2O. Density measurements were performed in a temperature range from 293.15 K to 343.15 K and viscosity was measured at temperatures from 293.15 K to 363.15 K. The excess molar volume was determined from experimental density data and a Redlich-Kister type polynomial of excess volume was adopted to represent the density of aqueous mixtures. For CO_2 loaded solutions, Setschenow-type correlations and modified Weiland's density and viscosity correlations were used to fit density and viscosity data. Eyring's viscosity model was used to evaluate free energy of activation for viscous flow of mixtures through measured density and viscosity data. The volumetric and viscometric properties of aqueous mixtures were analyzed through the molecular structure and interactions. A correlation was proposed for the free energy of activation of viscous flow to represent viscosity of CO_2 loaded solutions. The results reveal that proposed correlations for the density and viscosity of mixtures are in good agreement with measured data.

Key words: Density, Viscosity, 2-amino-2-methyl-1-propanol (AMP), monoethanol amine (MEA), Excess property.

1. Introduction

The amine-based post combustion CO_2 capture (PCC) is regarded as the most reliable and economical technology [1, 2]. An absorbent having characteristics of higher capacity, faster absorption rates, lower heat of absorption and minimum hazardousness to the environment enables PCC more feasible for the industry [3]. Aqueous alkanolamines of monoethanol amine (MEA), methyldiethanolamine (MDEA) and diethanol amine (DEA) has been used in acid gas removal for decades. Conventional absorbents exhibit several disadvantages such as high regeneration energy, poor absorption capacity and amine degradation. As a result, the interest towards amine blends as an absorbent in CO_2 absorption has increased to optimize the energy demand and operational cost. The applicability of different amine blends have been tested to study mass transfer, reaction kinetics, solubility and absorption capacity [4-8] and pilot plant operations have been performed [9, 10].

2-amino-2-methyl-1-propanol (AMP) is a sterically hindered primary amine and also known as the hinder form of MEA [8]. The attached two methyl group to the tertiary carbon atom in AMP hindered the formation of stable carbamate during the reaction with CO_2 [11]. Nwaoha, et al. [12] pointed that this increase the theoretical CO_2 absorption capacity up to 1 mol CO_2 / mol amine. The molecular structure of AMP is illustrated in Figure 1. MEA is the benchmark absorbent in amine-based PCC to compare the other absorbent for the characteristics of absorption rate, absorption capacity and degradation. Although MEA has a high absorption

rate, it has limited thermodynamic capacity to absorb CO_2 [11]. An aqueous blend of AMP and MEA could overcome the drawbacks of individual aqueous solutions. Mandal and Bandyopadhyay [13] emphasized that increase of MEA in an aqueous AMP solution increased the enhancement factor and rate of absorption over single amine aqueous MEA and AMP mixtures. Another study performed by Sakwattanapong, et al. [5] revealed an increase of overall rate constant in AMP + MEA + H_2O mixtures with MEA concentration. These observations conclude that the mixture of AMP + MEA + H_2O is a potential alternative for CO_2 absorption.
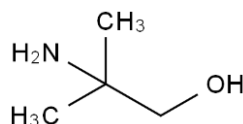
IUPAC name: 2-amino-2-methyl-propan-1-ol

Figure 1: Molecular structure of AMP.

In order to investigate the performance of these blends in pilot or large scale, further studies are required in the form of mathematical modelling and simulations of the absorption and desorption process. In that, available data of measured physical properties like density and viscosity in both CO_2 loaded and unloaded aqueous amine blend is a key factor to perform accurate simulations and engineering design calculations. Measured data of density and viscosity of AMP + MEA + H_2O mixtures are reported in the literature [14, 15].

In this study, the focus was given to measure density and viscosity of both aqueous and CO_2 loaded mixtures of AMP + MEA + H_2O under different amine mass ratios, CO_2 loadings and temperatures at a pressure of 4 bar (N_2 gas). The excess molar volumes were determined for the AMP + MEA + H_2O liquid mixtures and correlated by a Redlich-Kister [16] type polynomial. Same correlation was used to correlate the density of aqueous mixtures and was compared with measured data. For the mixtures of AMP + MEA + H_2O + CO_2, a Setschenow-type correlation and a modified Weiland's density correlation [17] were considered to correlate the densities. For the viscosities, a Setschenow-type correlation and a modified Weiland's viscosity correlation were adopted for the data fit.

The reported density and viscosity of aqueous solutions from Mandal, et al. [14] were considered to find the excess free energy of activation for viscous flow ΔG^{E*} according to the absolute rate theory approach of Eyring [18] on dynamic viscosity of a Newtonian fluid. A correlation based on a Redlich-Kister polynomial was suggested to correlate ΔG^{E*} and examine the possibilities to represent the unloaded solution viscosities. The excess viscosities η^E were determined to examine the types of interaction between component molecules in the mixtures. The free energy of activation for viscous flow ΔG^* was determined by adopting Eyring's dynamic viscosity model. The difference of ΔG^* between CO_2 loaded and aqueous AMP + MEA + H_2O mixtures was considered to correlate ΔG^* of CO_2 loaded solutions. Finally, the proposed correlation was examined for the representation of measured viscosity of CO_2 loaded solutions.

2 Experiments

A description of materials that are used for the all experiments are listed in Table 1. Deionized water (Milli-Q water / resistivity 18.2 MΩ·cm) and chemicals were degassed by using a rotary evaporator (BUCHI, Rotavapor R-210) before the solution preparation. Aqueous solutions of AMP + MEA were prepared on the mass basis (analytical balance Mettler Toledo XS-403S with an accuracy of $\pm\, 1 \times 10^{-7}$kg).

Carbon dioxide was added to the aqueous amine blend by bubbling it through the mixture until the solution was saturated. The solution pH was measured during the CO_2 loading and CO_2 supply was stopped when the pH became steady. Diluted CO_2 loaded amine mixtures were prepared by mixing it with CO_2 unloaded amine mixtures to acquire different CO_2 loadings in the final mixtures.

The CO_2 concentration in solutions was determined by a method based on precipitation of $BaCO_3$ and titration [19, 20]. A sample of (0.25-0.3) g was mixed with 50 mL of 0.1 mol·L^{-1} NaOH and 0.3M $BaCl_2$. Then the mixture was boiled for 10 minutes (approximately) in order to complete the precipitation reaction and was cooled in a water bath. The precipitate was filtered through a hydrophilic polypropylene membrane filter (45 μm). The filter cake was transferred into 100 mL of deionized water and was titrated with 0.1 mol·L^{-1} HCl until the solution pH reached a value 2. Then the excess HCl was determined by titrating back with 0.1 mol·L^{-1} NaOH solution. Finally, the amine concentration was analyzed through a separate titration in which a sample of 1g was transferred into 100 mL of deionized water and titrated with 1 mol·L^{-1} HCl.

Table 1: Materials used in this study.

Chemical name	CAS No.	Source	Purity
AMP	124-68-5	Sigma-Aldrich	BioUltra, ≥99.0% (GC)[a]
MEA	141-43-5	Sigma-Aldrich	≥99.5% (GC)[a]
CO_2	124-38-9	AGA Norge AS	≥99.9%

[a]Gas chromatography

Density measurement

Density measurements were performed using an Anton Paar DMA 4500 density meter. A sample of 3-5 mL volume (typically holds about 0.7 mL of sample) was introduced into the oscillating U tube that is oscillated at its fundamental frequency. The instrument is capable of measuring density with $\pm$ 0.05kg·m^{3} accuracy and can be operated in a temperature range of 273.15 K to 363.15 K ($\pm$ 0.03 K) under atmospheric condition. A density check was performed to check the validity of the factory adjustment. A standard density reference S3S from Paragon Scientific Ltd was used to record any possible deviations in the measurements. Density measurements of both aqueous amine blends and CO_2 loaded aqueous amine blends were done under atmospheric condition for the temperature range of 293.15 K-343.15 K. In order to minimize the error due to evaporation of amines and CO_2, a new sample was fed into the density meter at each temperature level.

Viscosity measurements

The dynamic viscosity of all solutions were measured using a Physica MCR 101 rheometer with a double-gap pressure cell XL from Anton Paar. A sample of 7 mL was placed using a

clean syringe into the volume occupied between two cylinders. The temperatures greater than 303.15 K was controlled by an internal temperature controlling system with a temperature accuracy of ± 0.03 K while an external cooling system of Anton Paar Viscotherm VT2 with temperature accuracy of ± 0.02 K was adopted to control temperatures below 303.15 K. Calibration of the instrument was done using a viscosity reference standard S3S from Paragon Scientific Ltd. The viscosity deviations were recorded by comparing measured viscosity of a standard solution with the reference viscosities at temperatures specified by the supplier. Accordingly, experimental observations have been corrected for those deviations. An expected deviation was considered by interpolation at the temperatures where the standard reference viscosities have not been provided by the manufacturer. As a preventive measure for the possible degassing of CO_2 from mixtures at higher temperatures, the viscosity measurements were performed at 4 bar nitrogen atmosphere in the temperature range of 293.15 K-343.15 K. As per our knowledge, the composition variation of mixtures before and after the experiments is minimum [21] and the effect of pressure on viscosity was in the order of 0.01%.

3 Experimental Uncertainty

The combined standard uncertainty of density and viscosity measurements of aqueous amine mixtures was determined by considering several uncertainty sources of material purity $u(p)$, temperature measurement $u(T)$, weight measurement $u(w)$, CO_2 loading $u(\alpha)$ and repeatability $u(rep)$.

In the uncertainty of density measurement, considered standard uncertainties were $u(p) = \pm 0.006$, $u(T) = \pm 0.012$ K, $u(w) = \pm 2 \times 10^{-4}$ kg, $u(\alpha) = \pm 0.005$ mol CO_2 / mol amine and $u(rep) = \pm 0.13$ kg·m^{-3}. The maximum gradient of density against temperature, $\partial\rho/\partial T$, was found as 0.9 kg·m^{-3}·K^{-1} and the corresponding uncertainty in ρ, $(\partial\rho/\partial T)\cdot u(T)$ was calculated as ± 0.0108 kg·m^{-3}. The gradient of density against CO_2 loading, $\partial\rho/\partial\alpha$, was found as 236 kg·m^{-3} and the corresponding uncertainty in ρ, $(\partial\rho/\partial\alpha)\cdot u(\alpha)$ was determined as ± 1.18 kg·m^{-3}. The Guide to the Expression of Uncertainty in Measurement [22, 23] was followed to evaluate combined standard uncertainty for the density measurement by considering all mentioned uncertainty sources as $u(\rho) = \pm 6.63$ kg·m^{-3}. Then the combined expanded uncertainty of the density measurement $U(\rho)$ was found as $= \pm 13.26$ kg·m^{-3} (level of confidence $= 0.95$).

In the uncertainty of viscosity measurement, considered standard uncertainties for the uncertainty sources are $u(p) = \pm 0.006$, $u(T) = \pm 0.012$ K, $u(w) = \pm 2 \times 10^{-4}$ kg, $u(\alpha) = \pm 0.005$ mol CO_2 / mol amine and $u(rep) = \pm 0.008$ mPa·s. The combined standard uncertainty for the viscosity measurement was calculated as $u(\eta) = \pm 0.018$ mPa·s. Then the combined expanded uncertainty of the viscosity measurement $U(\eta)$ was found as $= \pm 0.036$ mPa·s (level of confidence $= 0.95$).

4 Results and discussion

This section is mainly divided into two sections to discuss the measured densities and viscosities of the AMP + MEA + H$_2$O + CO$_2$ mixtures. The proposed density and viscosity correlations to represent the data are discussed in relevant sections. The performance of the correlations are evaluated using two deviation factors of absolute average relative deviation (AARD%) and absolute maximum deviation (AMD) as given in Eq (1) and (2),

Average Absolute Relative Deviation:

$$AARD\ (\%) = \frac{100\%}{N} \sum_{i=1}^{N} \frac{|Y_i^E - Y_i^C|}{Y_i^E} \tag{1}$$

Maximum Absolute Deviation:

$$AMD = MAX|Y_i^E - Y_i^C| \tag{2}$$

where N, Y_i^E, and Y_i^C are referred to the number of data, the measured property and calculated property respectively.

4.1 Density (ρ) and excess molar volume (V^E) of the AMP (1) + MEA (2) + H$_2$O (3) + CO$_2$ (4) mixtures

The density of pure AMP are available in literature [24-27]. Table 2 provides an overview of density of pure AMP measured in this study with the literature. The measured density in this study is in good accuracy with literature as the AARD showed less than 0.5% and AMD was 4.3 kg·m^{-3}. The deviations may arise due to the impurity of the material, measuring method and uncertainty of the temperature control. The comparison between literature and measured data indicated that the measuring system was calibrated properly for the density measurements. Measured density for AMP + MEA + H$_2$O by Mandal, et al. [14] and Li and Lie [15] are in good agreement with measured densities in this study indicating 2.6 kg·m^{-3} and 1.2 kg·m^{-3} of maximum deviations respectively.

The measured densities of the CO$_2$ unloaded amine mixture under different AMP and MEA mass % over the temperature range from 293.15 K to 343.15 K are listed in Table 3. Density has increased with the increase of MEA mole fraction in the mixture and has decreased with the increase of temperature. The excess molar volume V^E was calculated using measured density data of the aqueous amine mixtures as given in Eq 3. A Redlich and Kister [16] type polynomial was fitted to excess volumes of aqueous mixtures as shown in Eq (4), (5) and (6). Table 4 lists the required parameters of the binary pairs for the correlation. The correlation is in good agreement with measured densities as the AARD for the density of aqueous amine mixtures is 0.02 % and AMD is 0.04 kg·m^{-3} and a comparison between measured densities and correlation is shown in Figure 2.

$$\rho_{unloaded} = \frac{\sum_1^3 x_i M_i}{V^E + \sum_1^3 \frac{x_i M_i}{\rho_i}} \tag{3}$$

where ρ_i, x_i, M_i and V^E represent the density of pure component, mole fraction, molecular weights of AMP $(i = 1)$, MEA $(i = 2)$ and H$_2$O $(i = 3)$ and excess molar volume respectively.

The excess molar volume of AMP + MEA + H$_2$O mixtures of the ternary system is assumed to be

$$V^E = V_{12}^E + V_{23}^E + V_{13}^E \tag{4}$$

$$V_{jk}^E = x_j x_k \sum_{i=0}^{n} A_i (x_j - x_k)^i \tag{5}$$

$$A_i = a + b(T) + c(T)^2 \tag{6}$$

where A_i are pair parameters and are assumed to be temperature dependent.

For the considered mole fractions and temperatures, V^E is negative. The V^E can be negative for two reasons, stronger intermolecular interactions like H-bond between unlike molecules and geometrical fitting due to the structural differences of the molecules giving negative contribution for V^E [28-30]. The variation of V^E with solution temperature is in such a way that the negative value of V^E decreases with increase of temperature for all considered mole fractions. This can be due to the weakening of molecular interactions at higher temperatures in which increased thermal energy of molecules decrease the interaction strength [31].

Table 2. Experimental data of the density ρ / kg·m^{-3} of pure AMP from this work and literature data at different temperatures.

T / K	ρ / kg·m^{-3}				
		Literature			
	This work	Aguila-Hernández, et al. [24]	Henni, et al. [25]	Xu, et al. [26]	Zhang, et al. [27]
303.15					925.72
308.15	921.4				921.48
313.15	917.3	917.2	919.65	921.1	917.30
318.15	913.3				913.09
323.15	909.1	909.2	911.24	913.4	908.86
328.15	905.0				904.59
333.15	900.4	900.7	902.87	905.5	900.29
338.15	896.0				895.95
343.15	891.6		894.28		891.57
348.15	887.2				887.18
353.15	882.7				882.75
358.15	878.3				
363.15	873.7				

Table 3: Experimental data of the density ρ / kgm^{-3} and excess molar volume $V^E/m^3 \cdot mol^{-1}$ of AMP (1) + MEA (2) + H$_2$O (3) at different amine mass (%) and temperatures.

Mixtures	AMP (mass %) / MEA (mass %)					
	21/9		24/6		27/3	
Temperature (K)	ρ / kg·m^{-3}	$10^6 V^E$	ρ / kg·m^{-3}	$10^6 V^E$	ρ / kg·m^{-3}	$10^6 V^E$
293.15	1003.5	-0.42162	1002.2	-0.45295	1000.8	-0.48355
298.15	1001.1	-0.41928	999.7	-0.45035	998.2	-0.47857
303.15	998.5	-0.41673	997.1	-0.44607	995.6	-0.47434
308.15	995.8	-0.41334	994.3	-0.44166	992.7	-0.46887
313.15	993.0	-0.4097	991.4	-0.43685	989.7	-0.46294
318.15	990.0	-0.40542	988.3	-0.43219	986.7	-0.45741
323.15	986.9	-0.40207	985.3	-0.42881	983.5	-0.45171
328.15	983.7	-0.39852	982.0	-0.42363	980.2	-0.44665
333.15	980.4	-0.39485	978.6	-0.41971	976.8	-0.44172
338.15	976.9	-0.39064	975.1	-0.41461	973.3	-0.43717
343.15	973.4	-0.38759	971.6	-0.41209	969.7	-0.43292
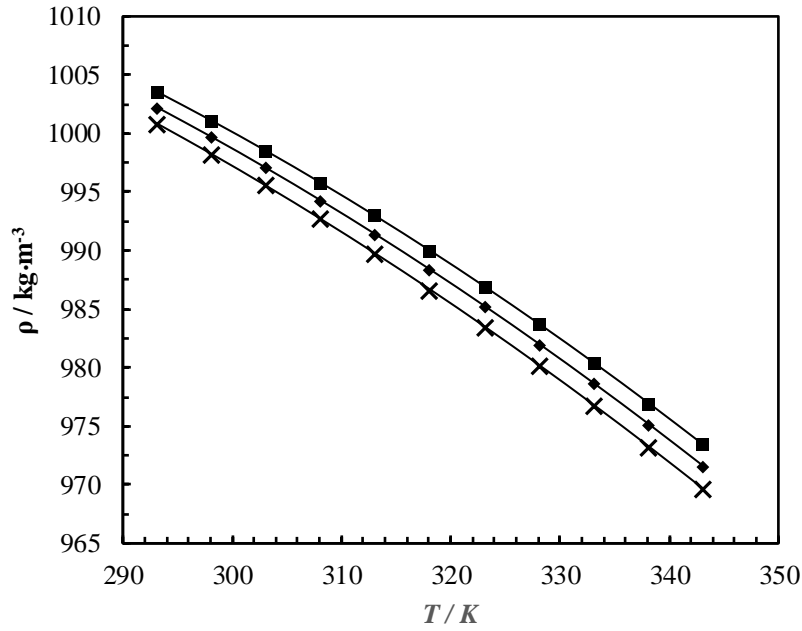
Figure 2: Density of AMP + MEA + H$_2$O mixtures: measured data; 21 mass % AMP + 9 mass % MEA + 70 mass % H$_2$O, '■', 24 mass % AMP + 6 mass % MEA + 70 mass % H$_2$O, '◆', 27 mass % AMP + 3 mass % MEA + 70 mass % H$_2$O, 'x', correlation; '—'.

Table 4: Binary parameters A_0, A_1 and A_2 of the equation $V_{jk}^E = x_j x_k \sum_{i=0}^{n} A_i (x_j - x_k)^i$ for the excess volume for AMP (1) + MEA (2) + H$_2$O (3).

Parameters		Binary pair		
		AMP + MEA	MEA + H$_2$O	AMP + H$_2$O
A_0	a	-694.0568	-264.6428	116.7011
	b	0.8644	0.0465	0.4056
	c	-1.9368	0.0091	0.3441
A_1	a	385918.7826	268.2293	-134.4781
	b	33.9949	0.2138	0.9993
	c	35.7004	0.4921	0.5392
A_2	a	-1.1207×10^7	-267.3226	156.4493
	b	-1132.7308	0.0207	0.6646
	c	-878.1832	0.6274	0.1908

The increase of dissolved CO$_2$ concentration increases the density of AMP + MEA + H$_2$O mixtures. Table 5, 6 and 7 list measured densities of AMP + MEA + H$_2$O + CO$_2$ mixtures with relevant CO$_2$ loadings and temperatures. The mole fraction of CO$_2$ as given by x_4 was calculated from the CO$_2$ loadings. In real mixtures, the dissolved CO$_2$ is in the form of carbamates, bicarbonates and carbonates. This approach is efficient to develop correlations adopted by authors [32, 33].

Table 5: Density ρ / kg·m^{-3} of CO_2 loaded 21 mass % AMP + 9 mass % MEA + 70 mass % H_2O at different temperatures and CO_2 loadings (α / mol CO_2 · mol amine^{-1}).

α/(mol CO_2·mol amine^{-1})	0.107	0.210	0.308	0.400	0.518
x_4	0.0095	0.0185	0.0269	0.0346	0.0444
T / K	ρ / kg·m^{-3}				
293.15	1019.8	1036.4	1053.6	1071.3	1087.2
298.15	1017.4	1034.0	1051.1	1068.7	1084.5
303.15	1014.9	1031.5	1048.6	1066.0	1081.7
308.15	1012.2	1028.9	1045.9	1063.2	1078.9
313.15	1009.4	1026.1	1043.2	1060.3	1075.9
318.15	1006.6	1023.3	1040.3	1057.3	1072.9
323.15	1003.6	1020.3	1037.4	1054.4	1070.0
328.15	1000.5	1017.3	1034.3	1051.3	1066.7
333.15	997.2	1014.2	1031.2	1048.0	1063.4
338.15	993.8	1011.0	1027.9	1044.7	1059.4
343.15	990.4	1007.5	1024.6	1041.3	1054.9

Table 6: Density ρ / kg·m^{-3} of CO_2 loaded 24 mass % AMP + 6 mass % MEA + 70 mass % H_2O at different temperatures and CO_2 loadings (α / mol CO_2 · mol amine^{-1}).

α/(mol CO_2·mol amine^{-1})	0.083	0.165	0.314	0.418	0.508
x_4	0.0071	0.0141	0.0264	0.0349	0.0420
T / K	ρ / kg·m^{-3}				
293.15	1014.8	1029.4	1049.4	1066.4	1081.6
298.15	1012.3	1026.9	1046.8	1063.5	1078.6
303.15	1009.7	1024.3	1044.1	1060.5	1075.5
308.15	1006.9	1021.6	1041.2	1057.4	1072.3
313.15	1004.1	1018.8	1038.2	1054.3	1069.0
318.15	1001.1	1015.8	1035.2	1051.0	1065.7
323.15	998.0	1012.8	1032.0	1047.7	1062.3
328.15	994.8	1009.6	1028.8	1044.3	1058.9
333.15	991.5	1006.4	1025.5	1040.9	1055.4
338.15	988.1	1003.0	1022.1	1037.4	1051.7
343.15	984.1	999.6	1018.6	1033.7	1047.4

Table 7: Density ρ / kg·m^{-3} of CO_2 loaded 27 mass % AMP + 3 mass % MEA + 70 mass % H_2O at different temperatures and CO_2 loadings (α / mol CO_2 · mol amine^{-1}).

α/(mol CO_2·mol amine^{-1})	0.072	0.152	0.246	0.461	0.511
x_4	0.0059	0.0125	0.0200	0.0369	0.0407
T / K	ρ / kg·m^{-3}				
293.15	1013.5	1031.4	1042.2	1066.2	1078.0
298.15	1011.1	1028.7	1039.3	1062.8	1074.5
303.15	1008.4	1025.7	1036.2	1059.3	1071.0
308.15	1005.5	1022.9	1032.9	1055.7	1067.3
313.15	1002.6	1019.8	1029.6	1052.1	1063.7
318.15	999.6	1016.6	1026.3	1048.5	1060.1

323.15	996.3	1013.3	1022.6	1044.8	1056.4
328.15	993.2	1009.9	1019.4	1041.1	1052.7
333.15	989.8	1006.4	1015.9	1037.3	1048.9
338.15	986.2	1002.9	1012.0	1033.3	1045.2
343.15	982.8	999.3	1008.5	1029.7	1041.5

Several empirical correlations have been discussed in the literature for the density of amine + H_2O + CO_2 mixtures and the correlation proposed by Weiland, et al. [17] is highly discussed. The correlation was initially developed for the mixtures with one amine and parameters were found by fitting the density data at 298.15 K. Han, et al. [19] modified the original Weiland's correlation in order to fit the measured density data at different temperatures. Hartono, et al. [32] also proposed a correlation for density of MEA + H_2O + CO_2 mixtures that is capable to fit data at different temperatures. Shokouhi, et al. [34] adopted a modified Setschenow-type correlation [35, 36] to fit the measured physical properties of CO_2 loaded aqueous amine mixtures including more than one amine in the mixture. In this study, a modified Setschenow-type correlation and a modified Weiland's correlation is used to represent the measured densities.

Setschenow-type correlation for density:

$$ln\left(\frac{\rho}{\rho_0}\right) = \left(a_{0,0} + a_{0,1}T\right)x_4 + \left(a_{1,0} + a_{1,1}T\right)x_4{}^2 \tag{7}$$

where ρ/ρ_0 represent the ratio between density of CO_2 loaded and unloaded mixtures at equivalent temperatures. Parameters $a_{i,j}$, x_4 and T indicate temperature dependent parameters, CO_2 mole fraction and temperature in the liquid mixture. The parameters $a_{i,j}$ were found by fitting measured densities to the correlation and values are listed in Table 8 with the relevant amine concentrations in the aqueous mixtures.

Table 8: Parameters of the Setschenow-type correlation (Eq (7)) for the density of AMP + MEA + H_2O + CO_2 mixtures with relevant AARD (%) and AMD.

CO_2 loaded - 21% AMP 9 % MEA 70 % H_2O		AARD (%)	AMD (kg·m⁻³)
$a_{0,0} = 0.6433$	$a_{1,0} = 23.41$	0.09	2.8
$a_{0,1} = 0.003812$	$a_{1,1} = $ -0.07478		
CO_2 loaded - 24% AMP 6 % MEA 70 % H_2O		AARD (%)	AMD (kg·m⁻³)
$a_{0,0} = 0.8895$	$a_{1,0} = 24.47$	0.08	2.11
$a_{0,1} = 0.003001$	$a_{1,1} = $ -0.08178		
CO_2 loaded - 27% AMP 3 % MEA 70 % H_2O		AARD (%)	AMD (kg·m⁻³)
$a_{0,0} = 2.376$	$a_{1,0} = $ -3.719	0.19	4.2
$a_{0,1} = $ -6.204e-05	$a_{1,1} = $ -0.03917		

Modified Weiland's density correlation:

$$\rho = \frac{\sum_{i=1}^{4} x_i M_i}{V} \tag{8}$$

$$V = \sum_{i=1}^{3} x_i V_i + (x_4 V_4 + x_1 x_2 x_3 V^* + x_1 x_2 x_4 V^{**}) \cdot 10^{-6} \tag{9}$$

$$V^{**} = c + dx_1 + ex_2 \tag{10}$$

where V_i, V, ρ, M_i and x_i are molar volumes of pure amine, molar volume of mixture, density of CO_2 loaded mixture, molecular weight of components and mole fraction of components in the mixture. The subscription $i = 1, 2, 3$ and 4 refer to AMP, MEA, H_2O and CO_2 respectively. The molar volumes of pure AMP at different temperatures were determined by the measured density data listed in Table 2. For pure MEA, the data reported by Han, et al. [19] and for pure H_2O data from IAPWS [37] were adopted to obtain molar volumes. The missing density data at low temperatures of AMP and MEA were found by fitting a second order polynomial to available measured densities. $V_4, V^*, c, d,$ and e are fitting parameters including temperature as an independent variable to correlate the dependency of density on temperature.

$$V_4 = a_0 + a_1(T/K - 273.15) + a_2(T/K - 273.15)^2 + a_3(T/K - 273.15)^3 \tag{11}$$

$$V^* = b_0 + b_1(T/K - 273.15) + b_2(T/K - 273.15)^2 + b_3(T/K - 273.15)^3 \tag{12}$$

$$c = c_0 + c_1(T/K) + c_2(T/K)^2 + c_3(T/K)^3 \tag{13}$$

$$d = d_0 + d_1(T/K) + d_2(T/K)^2 + d_3(T/K)^3 \tag{14}$$

$$e = e_0 + e_1(T/K) + e_2(T/K)^2 + e_3(T/K)^3 \tag{15}$$

The values of the fitted parameters from Eq (9) to Eq (15) are presented in Table 9.

Table 9: Correlation parameters of the modified Weiland's density correlation

Parameters		values
V_4	a_0	-20.9140
	a_1	0.2539
	a_2	-0.0011
	a_3	-5.3400×10^{-06}
V^*	b_0	-325.6473
	b_1	-0.8920
	b_2	0.0315
	b_3	-0.0002
c	c_0	3875872.2912
	c_1	-32342.5695
	c_2	87.2773
	c_3	-0.0735
d	d_0	-48039690.4969
	d_1	406197.1671
	d_2	-1107.2697
	d_3	0.9415
e	e_0	-54813637.0204
	e_1	481977.0117
	e_2	-1388.6472
	e_3	1.2924
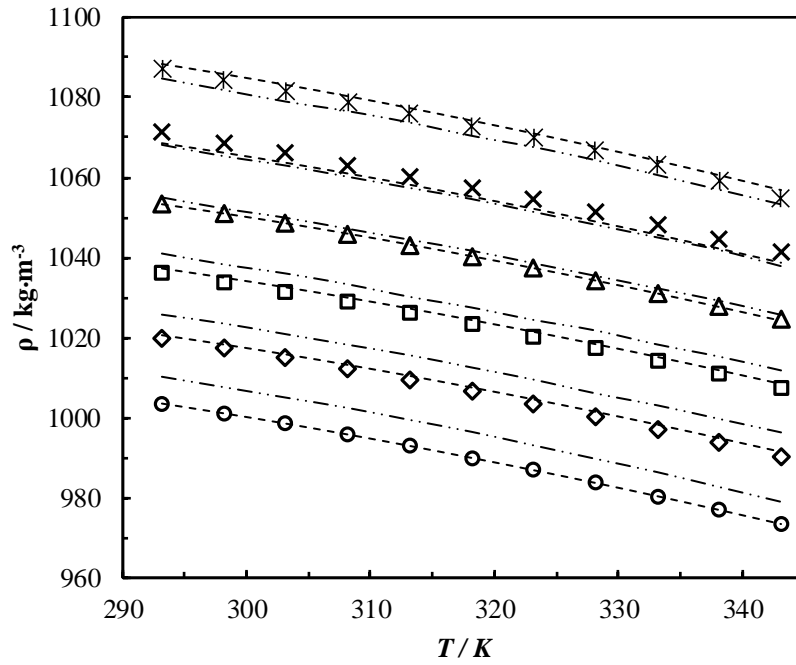
Figure 3: Density of CO_2 loaded 21 mass % AMP + 9 mass % MEA + 70 mass % H_2O at different temperatures and CO_2 loadings (α / mol $CO_2 \cdot$ mol amine^{-1}): 0.000, 'o'; 0.107, '◇'; 0.210, '□'; 0.308, '△'; 0.400, 'x'; 0.518, 'ж'. Correlations: Setschenow-type, '- - -'; Modified Weiland's, '– ·· –'.
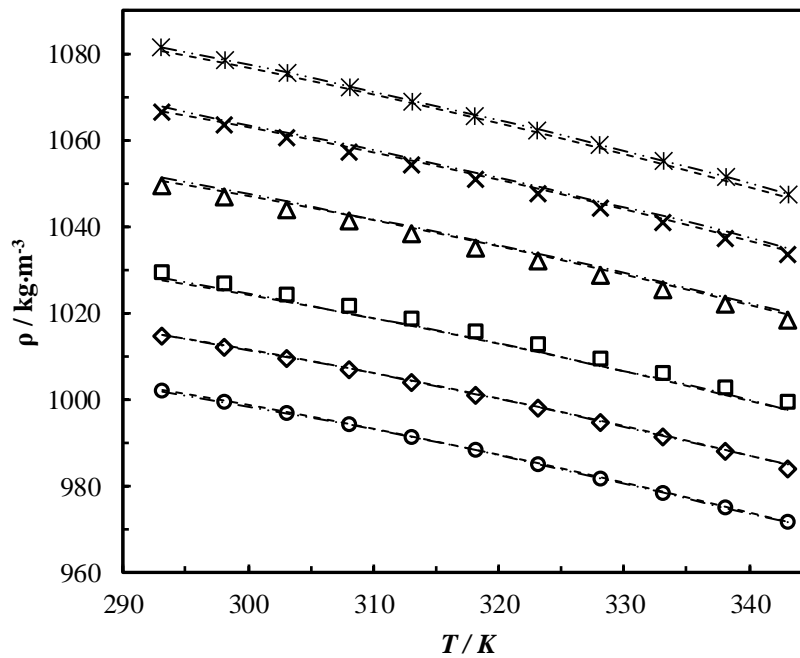
Figure 4: Density of CO_2 loaded 24 mass % AMP + 6 mass % MEA + 70 mass % H_2O at different temperatures and CO_2 loadings (α / mol $CO_2 \cdot$ mol amine^{-1}): 0.000, 'o'; 0.083, '◇'; 0.165, '□'; 0.314, '△'; 0.418, 'x'; 0.508, 'ж'. Correlations: Setschenow-type, '- - -'; Modified Weiland's, '– ·· –'.
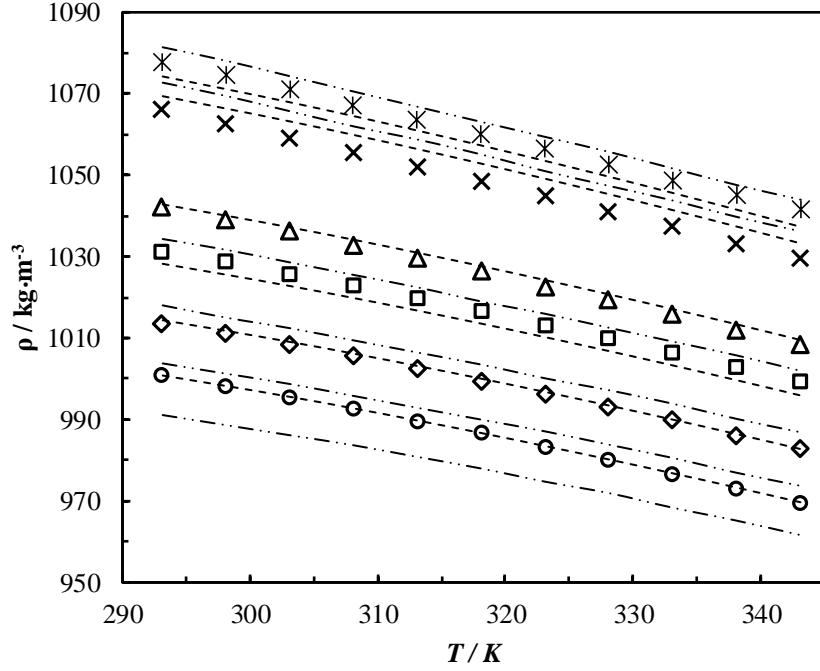
Figure 5: Density of CO_2 loaded 27 mass % AMP + 3 mass % MEA + 70 mass % H_2O at different temperatures and CO_2 loadings (α / mol $CO_2 \cdot$ mol amine^{-1}): 0.000, 'o'; 0.072, '◇'; 0.152, '□'; 0.246, '△'; 0.461, 'x'; 0.511, 'ж'. Correlations: Setschenow-type, '- - -'; Modified Weiland's, '- ·· -'.

The measured densities compared with the Setschenow-type correlation and the modified Weiland correlation are shown in Figure 3, 4 and 5. The correlations are fitted with satisfactory accuracies and Table 8 provides calculated AARD and AMD for the Setschenow-type correlation. The advantage of the modified Weiland's density correlation is that a single correlation is applicable to the entire range of AMP, MEA, H_2O and CO_2 considered in the study with AARD and AMD with 0.42 % and 13.7 kg·m^{-3} respectively. The Setschenow-type correlation show better agreement with measured densities; nevertheless, both correlations are acceptable to use in engineering calculations.

4.2: Viscosity and free energy of activation for viscus flow of AMP (1) + MEA (2) + H_2O (3) + CO_2 (4) mixtures

The viscosity of pure AMP was measured and compared in Table 10 with available data in literature. From Figure 6, it can be seen that measured viscosities for pure AMP and MEA are in good agreement with literature [15, 21, 25, 38]. The data were correlated according to the modified Andrade viscosity model [39] by Vogel [40] as shown in Eq (16). The correlation was able to fit the measured viscosities with acceptable accuracies and calculated parameters are shown in Table 11. Measured viscosity for AMP + MEA + H_2O by Mandal, et al. [14] and Li and Lie [15] are in good agreement with measured viscosities in this study indicating 0.32 mPa·s and 0.02 of maximum deviations respectively. Viscosities measured by Mandal, et al. [14] showed a small discrepancy compared to this study at low temperatures around 293.15 K.

$$ln(\eta) = a + \frac{b}{T+c} \qquad (16)$$

Table 10: Experimental data of the viscosity η / mPa·s of pure AMP from this work and literature at different temperatures.

T / K	η / mPa·s		
		Literature	
	This work	Henni, et al. [25]	Li and Lie [15]
303.15			99.4748
313.15	48.477	47.80	46.9258
318.15	35.161		
323.15	26.001	25.10	24.2108
328.15	19.524		
333.15	15.004	14.40	13.9977
338.15	11.705		
343.15	9.269	8.91	8.6418
348.15	7.482		
353.15	6.109		5.6485
358.15	5.055		
363.15	4.227		

Table 11: Regression parameters, AARD (%) and AMD for correlation given in Eq (16).

Parameter	Value	AARD (%)	AMD (mPa·s)
a	-4.791		
b	1105	0.23	0.23
c	-185.8		
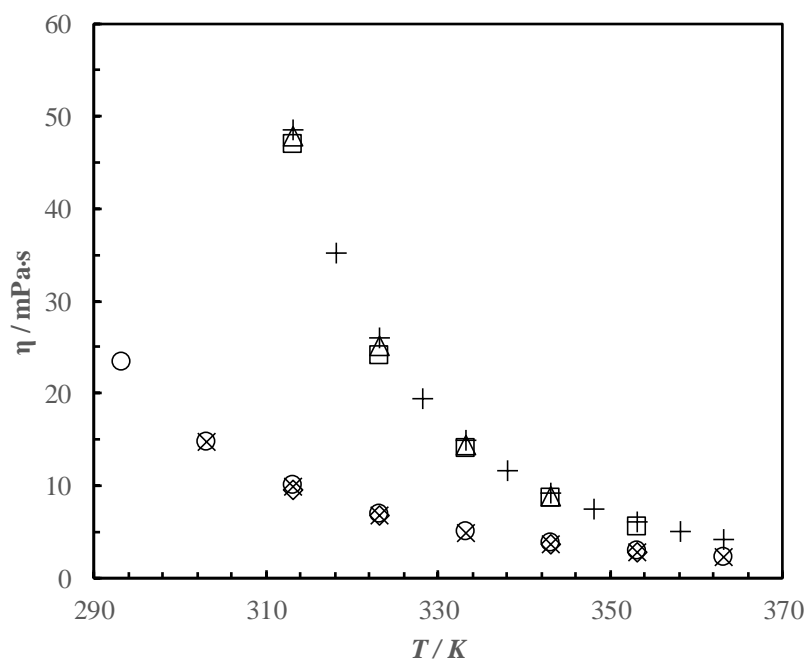
Figure 6: Viscosity of pure amines. Pure AMP: this study, '+'; Henni, et al. [25], '△'; Li and Lie [15], '□'. Pure MEA: this study, '○'; Idris, et al. [21], '✕'; Amundsen, et al. [38], '◇'.

The measured viscosities of AMP + MEA + H_2O + CO_2 mixtures are listed in Table 12, 13 and 14. Viscosity increased with the increase of dissolved CO_2 in the solution and this was observed

in all the different amine mixtures considered in this study. Viscosity decreases with increasing temperature in all mixtures with different amine and CO_2 concentrations. The presence of CO_2 in the mixtures forms ionic products of carbamates and bicarbonate that increases the intermolecular interactions, which results in higher viscosities than aqueous amine mixtures without CO_2. Fu, et al. [41] presented viscosity data for AMP + MEA + H_2O + CO_2 mixtures at different amines concentrations compared to this work.

Table 12. Viscosity of CO_2 loaded 21 mass % AMP + 9 mass % MEA + 70 mass % H_2O at different temperatures and CO_2 loadings (α / mol CO_2 · mol amine^{-1}).

α/(mol CO_2·mol amine^{-1})	0.000	0.107	0.210	0.308	0.400	0.518
x_4	0.0000	0.0095	0.0185	0.0269	0.0346	0.0444
T / K	η / mPa·s					
293.15	3.949	4.419	4.822	5.458	6.012	6.577
303.15	2.744	3.078	3.336	3.771	4.109	4.506
313.15	2.002	2.262	2.443	2.757	2.992	3.275
323.15	1.527	1.725	1.857	2.091	2.267	2.472
333.15	1.209	1.363	1.472	1.651	1.778	1.953
343.15	0.982	1.110	1.200	1.343	1.445	1.576
353.15	0.812	0.924	0.987	1.120	1.197	1.298
363.15	0.693	0.784	0.831	0.947	1.022	1.097

Table 13. Viscosity of CO_2 loaded 24 mass % AMP + 6 mass % MEA + 70 mass % H_2O at different temperatures and CO_2 loadings (α / mol CO_2 · mol amine^{-1}).

α/(mol CO_2·mol amine^{-1})	0.000	0.083	0.165	0.314	0.418	0.508
x_4	0.0000	0.0071	0.0141	0.0264	0.0349	0.0420
T / K	η / mPa·s					
293.15	4.130	4.435	4.941	5.666	6.448	7.096
303.15	2.845	3.048	3.399	3.872	4.358	4.770
313.15	2.061	2.203	2.461	2.788	3.106	3.392
323.15	1.565	1.663	1.857	2.094	2.313	2.523
333.15	1.231	1.302	1.452	1.632	1.789	1.952
343.15	0.995	1.052	1.171	1.318	1.431	1.566
353.15	0.819	0.868	0.968	1.089	1.176	1.305
363.15	0.690	0.729	0.813	0.918	0.992	1.088

Table 14. Viscosity of CO_2 loaded 27 mass % AMP + 3 mass % MEA + 70 mass % H_2O at different temperatures and CO_2 loadings (α / mol CO_2 · mol amine^{-1}).

α/(mol CO_2·mol amine^{-1})	0.000	0.072	0.152	0.246	0.461	0.511
x_4	0.0000	0.0059	0.0125	0.0200	0.0369	0.0407
T / K	η / mPa·s					
293.15	4.288	4.695	5.308	5.908	6.883	7.515
303.15	2.913	3.183	3.591	3.928	4.556	4.943
313.15	2.086	2.295	2.571	2.797	3.194	3.459
323.15	1.566	1.734	1.931	2.090	2.366	2.553

333.15	1.220	1.361	1.513	1.620	1.837	1.973
343.15	0.978	1.099	1.219	1.291	1.477	1.578
353.15	0.803	0.910	1.006	1.058	1.197	1.303
363.15	0.670	0.767	0.849	0.888	1.008	1.099

The measured viscosity and density of aqueous amine solutions were considered to calculate free energy of activation for viscous flow as described by Eyring [18]. For Newtonian fluids, Eyring's viscosity model relates viscosity and molar volume with free energy of activation of viscous flow as shown in Eq (17). Viscosity measurements under different shear rates confirms the Newtonian behavior of solutions. Eyring [18] explains that the fluid at rest continuously undergoes rearrangements. The term ΔG^*in Eq (17) refer the free energy of activation for viscous flow to jump a molecule from its cage into an adjacent hole by overcoming the potential barrier [42].

$$\eta = \frac{hN_A}{V} exp\left(\frac{\Delta G^*}{RT}\right) \tag{17}$$

where $\Delta G^*, \eta, V, h, N_A, R$ and T refer to the free energy of activation for viscous flow (J·mol^{-1}), viscosity (Pa·s), molar volume (m^3·mol^{-1}), Planck's constant (m^2·kg·s^{-1}), Avogadro number (mol^{-1}), gas constant (J·mol^{-1}·K^{-1}) and temperature (K). Considering the Eyring's viscosity model for both real and ideal mixtures following Eq (18) and Eq (19) are derived and excess free energy of activation ΔG^{E*} is introduced. The sign of ΔG^{E*} alone with V^E carries valuable information about viscosity and intermolecular attractions among the components of mixture compared to an ideal mixture

$$ln(\eta V) = ln(\eta V)_{ideal} + \frac{\Delta G^{E*}}{RT} \tag{18}$$

$$ln(\eta V) = \sum_i x_i ln(\eta_i V_i^0) + + \frac{\Delta G^{E*}}{RT} \tag{19}$$

The calculated ΔG^{E*} gives positive values for density and viscosity data presented by Mandal, et al. [14]. This reveals the presence of strong molecular interactions like H-bonds among the unlike molecules [43-46].The calculated viscosity deviation η^E as shown in Eq (20) gives negative values over the amine concentration and temperature range. The negative sign for η^E indicates weak molecular interactions compared to the pure liquids. The molecular interaction is not the only factor that causes viscosity deviation of liquid mixtures [46]. In the analysis of liquid mixtures, aspects of molecular size and shape of the components, size of the intermolecular complexes and dispersion forces are also equally significant [43, 44, 46-48].

$$\eta^E = \eta - \sum_{i=1}^n x_i \eta_i \tag{20}$$

The calculated excess free energy of activation for viscous flow for unloaded aqueous amine mixtures are correlated using a Redlich-Kister polynomial with temperature dependency.

The excess free energy of activation for viscous flow of AMP + MEA + H$_2$O mixtures of the ternary system is assumed to be

$$\Delta G^{E*} = \Delta G_{12}^{E*} + \Delta G_{23}^{E*} + \Delta G_{13}^{E*} \tag{21}$$

$$\Delta G_{jk}^{E*} = x_j x_k \sum_{i=0}^n A_i (x_j - x_k)^i \tag{22}$$

$$A_i = a + b(T) + c(T)^2 \tag{23}$$

The proposed correlation was able to represent measured viscosities by Mandal, et al. [14] with less than 2% AARD of accuracy using Eq (19) and correlation parameters are listed in Table 15.

Table 15: Binary parameters A_0, A_1 and A_2 of the equation $\Delta G_{jk}^{E*} = x_j x_k \sum_{i=0}^{n} A_i (x_j - x_k)^i$ for excess free energy of activation for viscous flow for AMP (1) + MEA (2) + H_2O (3).

Parameters		Binary pair		
		AMP + MEA	MEA + H_2O	AMP + H_2O
A_0	a	-1.7080×10^9	-4.6458×10^8	-1.7924×10^8
	b	-1137.2311	1.2000×10^6	1.3983×10^6
	c	-6691.7632	-2173.76089	-4941.7818
A_1	a	-5.3426×10^9	9.2293×10^7	-2.4931×10^8
	b	2.5976×10^7	487665.0859	5.3142×10^6
	c	-42007.2139	-79.0338	-4631.5400
A_2	a	1.9502×10^{10}	8.4767×10^8	-4.2934×10^7
	b	-1.2101×10^8	-1.1001×10^6	4.3441×10^6
	c	186719.34086	3106.0685	1481.7857

The approaches based on a Setschenow-type correlation, a Weiland's viscosity correlation and Eyring's viscosity model were adopted to fit the viscosities of AMP + MEA + H_2O + CO_2 mixtures. Three Setschenow-type correlations were proposed as given in Eq (24) for each mixture with different amine concentrations. As illustrated in Eq (25), the original Weiland's viscosity correlation was modified to fit viscosity data for mixtures with more than one amine. The free energy of activation for viscous flow in Eyring's viscosity model was calculated from the measured viscosity and density data and was correlated with the proposed expression as shown in Eq (26) and Eq (27).

Setschenow-type correlation for viscosity:

The viscosity of AMP + MEA + H_2O + CO_2 mixtures were correlated according to the Setschenow-type correlation as shown in Eq (24).

$$ln\left(\frac{\eta}{\eta_0}\right) = \left(a_{0,0} + a_{0,1}T\right)x_4 + \left(a_{1,0} + a_{1,1}T\right)x_4{}^2 + \left(a_{2,0} + a_{2,2}T\right)x_4{}^3 \tag{24}$$

where η/η_0 represent the ratio between viscosity of CO_2 loaded and unloaded mixtures at equivalent temperatures. Parameters $a_{i,j}$, x_4 and T indicate temperature dependent parameters, CO_2 mole fraction and temperature in the liquid mixture.

Table 16: Parameters of the Setschenow-type correlation (Eq (24)) for the viscosity of AMP + MEA + H_2O + CO_2 mixtures with relevant AARD (%) and AMD.

CO_2 loaded - 21% AMP 9 % MEA 70 % H_2O			AARD (%)	AMD (mPa·s)
$a_{0,0} = 3.575$	$a_{1,0} = 563.8$	$a_{2,0} = -6516$	0.75	0.07
$a_{0,1} = 0.02196$	$a_{1,1} = -1.516$	$a_{2,2} = 15.49$		
CO_2 loaded - 24% AMP 6 % MEA 70 % H_2O			AARD (%)	AMD (mPa·s)

$a_{0,0} = 13.7$	$a_{1,0} = 299.2$	$a_{2,0} = -2727$	0.99	0.1
$a_{0,1} = -0.008313$	$a_{1,1} = -0.8945$	$a_{2,2} = 8.753$		
CO_2 loaded - 27% AMP 3 % MEA 70 % H_2O			AARD (%)	AMD (mPa·s)
$a_{0,0} = -22.45$	$a_{1,0} = 3157$	$a_{2,0} = -5.298e+04$	0.94	0.31
$a_{0,1} = 0.1433$	$a_{1,1} = -11.86$	$a_{2,2} = 193.5$		
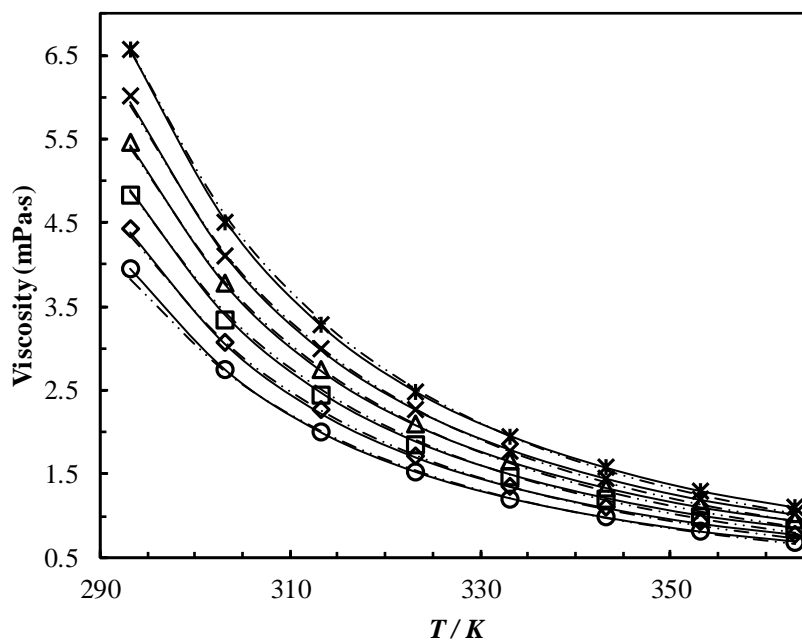
Figure 5: Viscosity of CO_2 loaded 21 mass % AMP + 9 mass % MEA + 70 mass % H_2O at different temperatures and CO_2 loadings (α / mol CO_2 · mol amine^{-1}): 0.000, '○'; 0.107, '◇'; 0.210, '□'; 0.308, '△'; 0.400, 'x'; 0.518, 'ж'. Correlations: Setschenow-type, '——'; Modified Weiland's, '– ·· –'.
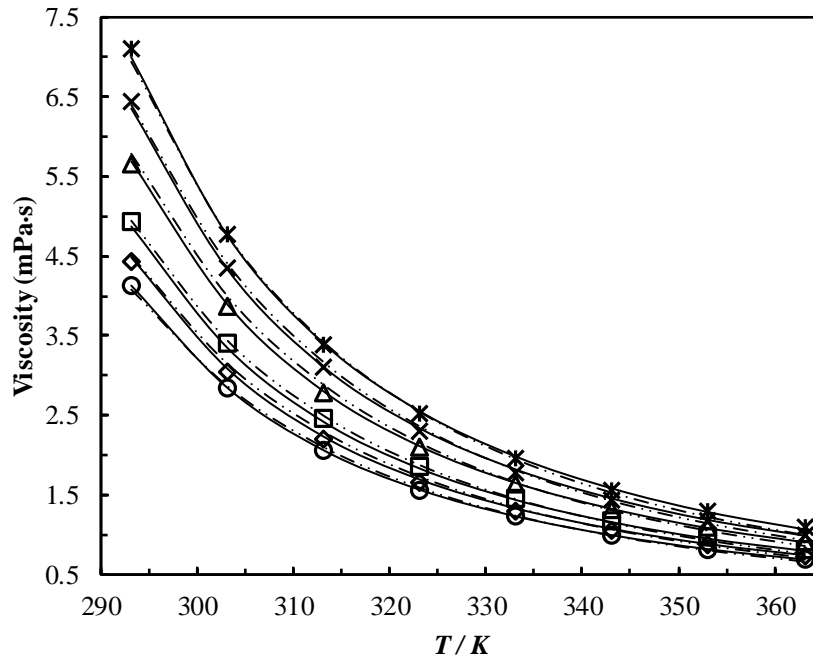
Figure 6: Viscosity of CO_2 loaded 24 mass % AMP + 6 mass % MEA + 70 mass % H_2O at different temperatures and CO_2 loadings (α / mol $CO_2 \cdot$ mol amine^{-1}): 0.000, 'o'; 0.083, '◇'; 0.165, '□'; 0.314, '△'; 0.418, 'x'; 0.508, 'ж'. Correlations: Setschenow-type, '—'; Modified Weiland's, '– ·· –'.
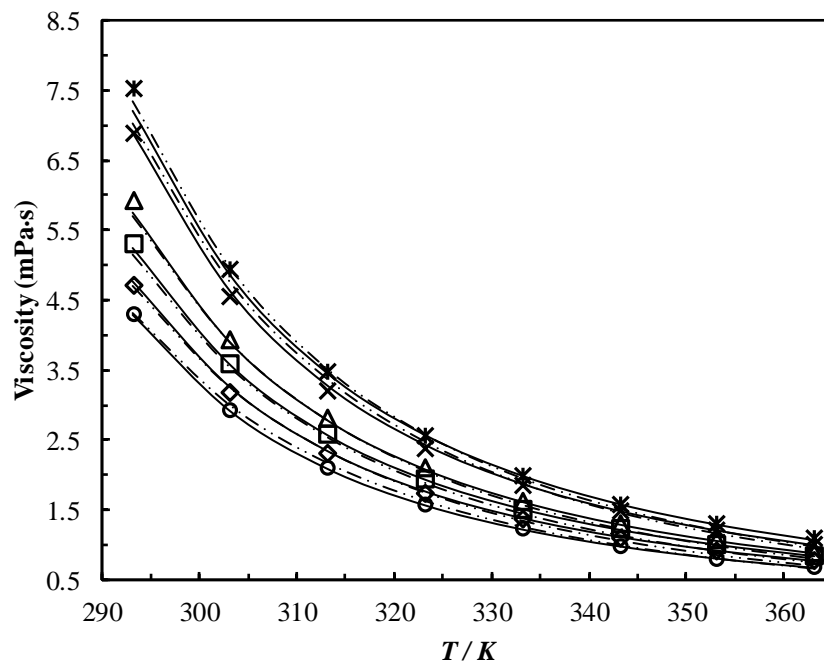
Figure 7: Viscosity of CO_2 loaded 27 mass % AMP + 3 mass % MEA + 70 mass % H_2O at different temperatures and CO_2 loadings (α / mol $CO_2 \cdot$ mol amine^{-1}): 0.000, 'o'; 0.072, '◇'; 0.152, '□'; 0.246, '△'; 0.461, 'x'; 0.511, 'ж'. Correlations: Setschenow-type, '—'; Modified Weiland's, '– ·· –'.

Table 16 lists the calculated parameters, AARD and AMD for Setschenow-type correlation for different mixtures. It reveals that the correlation is capable of fitting viscosities with acceptable accuracy. Viscosity deviation is high at low temperatures and a maximum deviation was observed at 293.15 K.

Modified Weiland's viscosity correlation:

The original Weiland's viscosity correlation [17] was made for the mixtures of amine + H_2O + CO_2 with single amine in which the CO_2 loading was considered as an independent variable. A new fitting parameter with amine mole fractions was considered to fit the viscosities and CO_2 mole fraction in the mixtures were considered instead of CO_2 loading as shown in Eq (25).

$$\frac{\eta}{\eta_{H_2O}} = exp\left[\frac{[(ax_1+bx_2+c)T+(dx_1+ex_2+f)][x_4(gx_1+hx_2+iT+j)+10^3](x_1+x_2)}{T^2}\right] \quad (25)$$

where η, η_{H_2O}, x_4 and T are viscosity of CO_2 loaded mixture, viscosity of H_2O, mole fraction of CO_2 and temperature of the liquid mixture.

Table 17: Parameters for modified Weiland's viscosity correlation

Parameters	value
a	-935.0476
b	-572.0175
c	68.8463
d	244060.7427
e	136455.0491
f	-16162.2200
g	385102.6797
h	257300.7928
i	-26.6921
j	-13288.1829
AARD (%)	2.7
AMD (mPa·s)	0.2

The parameters shown in Eq (25) are given in Table 17. The Weiland's viscosity correlation can be written in a form of $\eta_{Co_2 loaded}/\eta_{H_2O} = exp(f(w)g(\alpha)/T)$ where the function $f(w)$ was determined from CO_2 unloaded solution data. Here, instead of using data from CO_2 unloaded solutions, the information related to CO_2 loaded solutions was adopted for the data fit. The calculated AARD and AMD as given in the Table 17 indicate that correlated viscosities are in good agreement with the measured viscosities and useful in engineering calculations.

Correlation based on Eyring's viscosity model

The calculated free energy of activation for viscous flow ΔG^* from measured densities and viscosities for AMP + MEA + H_2O + CO_2 mixtures was correlated as given in Eq (26) and Eq (27). The ΔG^* increases with the increase of CO_2 loading and decreases with increasing temperature. Matin, et al. [49], described the variations in viscosity with CO_2 loading relating to the solution ionic strength and pH. Increase of CO_2 loading reduce the pH while increasing the ionic strength. The measured pH versus CO_2 loading is presented in Figure S1. The presence of CO_2 in an amine + H_2O mixture creates a pool of cations and anions including carbamate

$(RNHCO_2^-)$, protonated amine (RNH_3^+), bicarbonate (HCO_3^-), carbonate (CO_3^{2-}), OH^- and H^+ ions increase the ionic strength and intermolecular interactions that leads to high viscosity.

$$ln(\eta V)_{CO_2\,loaded} = ln(\eta V)_{unloaded} + f(x_1, x_2, x_4, T) \tag{26}$$

$$f(x_1, x_2, x_4, T) = x_4(k_1 + k_2 T + k_3 x_4)(k_4 x_1 + k_5 x_2 + k_6) \tag{27}$$

where x_i and T are mole fraction and temperature. The subscript $i = 1, 2,$ and 4 refer to AMP, MEA and CO_2 respectively. The function f determines the property of $\left(\Delta G^*_{CO_2\,loaded} - \Delta G^*_{unloaded}\right)/RT$ where $\Delta G^*_{CO_2\,loaded}$ and $\Delta G^*_{unloaded}$ refer to free energy of activation for viscous flow for CO_2 loaded and unloaded solutions respectively.
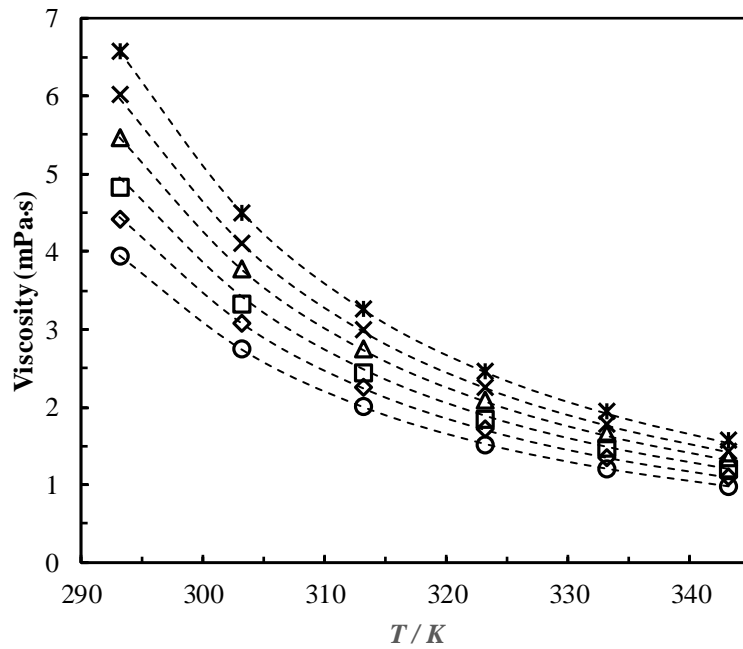
Figure 8: Viscosity of CO_2 loaded 21 mass % AMP + 9 mass % MEA + 70 mass % H_2O at different temperatures and CO_2 loadings (α / mol $CO_2 \cdot$ mol amine^{-1}): 0.000, '○'; 0.107, '◇'; 0.210, '□'; 0.308, '△'; 0.400, '×'; 0.518, 'ж'. Correlation: '- - -'.
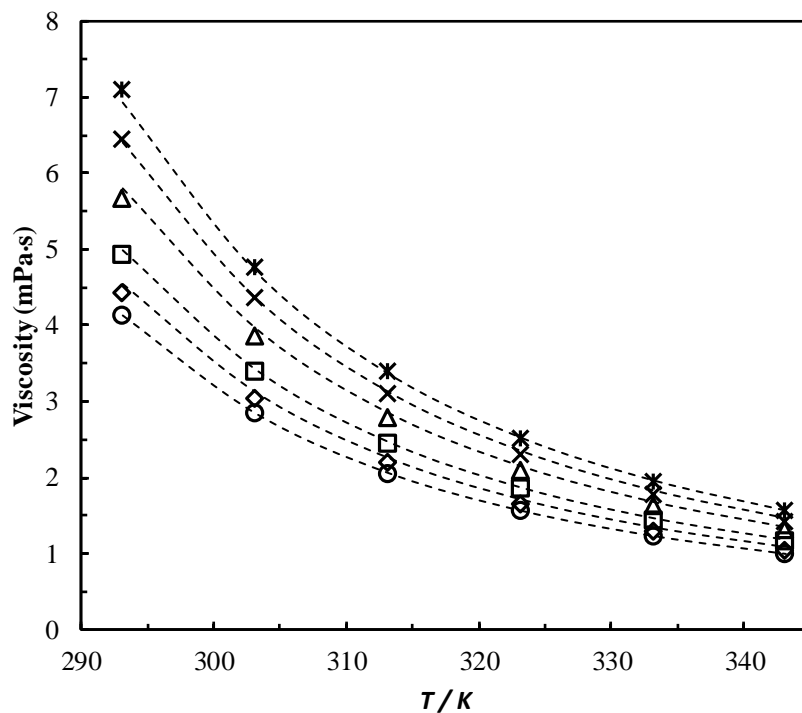
Figure 9: Viscosity of CO_2 loaded 24 mass % AMP + 6 mass % MEA + 70 mass % H_2O at different temperatures and CO_2 loadings (α / mol $CO_2 \cdot$ mol amine^{-1}): 0.000, '○'; 0.083, '◇'; 0.165, '□'; 0.314, '△'; 0.418, 'x'; 0.508, 'ж'. Correlation: '- - -'.
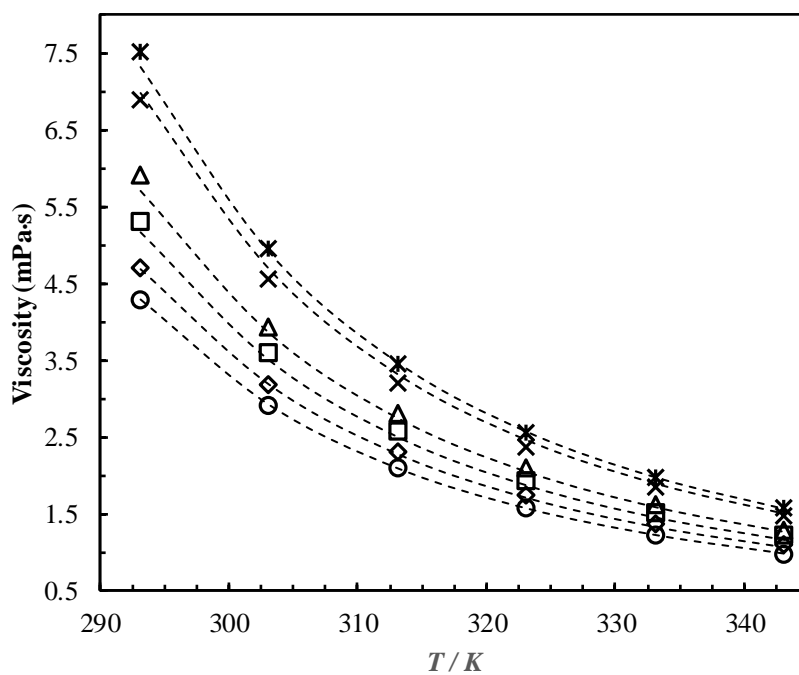
Figure 10: Viscosity of CO_2 loaded 27 mass % AMP + 3 mass % MEA + 70 mass % H_2O at different temperatures and CO_2 loadings (α / mol $CO_2 \cdot$ mol amine^{-1}): 0.000, '○'; 0.072, '◇'; 0.152, '□'; 0.246, '△'; 0.461, 'x'; 0.511, 'ж'. Correlation: '- - -'.

The calculated parameters for the correlation based on Eyring's viscosity model is given in Table 18 with calculated AARD and AMD. The data fit is limited to 343.15 K temperature due to the availability of densities of the mixtures. The correlation is recommended for use in engineering calculation as the AARD is acceptable. The main drawback of this approach is that it requires density data for the viscosity calculations.

Table 18: Parameters for correlation based on Eyring's viscosity model

Parameters	value
k_1	682.5281
k_2	-0.8631
k_3	-2443.1371
k_4	-1.4674
k_5	-1.2432
k_6	0.1512
AARD (%)	1.4
AMD (mPa·s)	0.2

The enthalpy of activation for viscous flow ΔH^* and entropy activation for viscous flow ΔS^* were determined using rearranged Eyring's viscosity model as given in Eq (28). The slope and the intercept of the linear relationship of $Rln(\eta V/hN_A)$ vs $1/T$ provide information about ΔH^* and ΔS^*. Table 19 and 20 list the calculated ΔG^*, ΔH^* and ΔS^* of the mixtures at different CO_2 loadings and temperatures.

$$Rln\left(\frac{\eta V}{hN_A}\right) = \frac{\Delta H^*}{T} - \Delta S^* \tag{28}$$

$$\Delta G^* = \Delta H^* - T\Delta S^* \tag{29}$$

The results reveal that ΔG^* ΔH^* and ΔS^* are positive for all considered mixtures while ΔH^* is greater than $T\Delta S^*$. This indicates that the contribution of enthalpy of activation to the free energy of activation is greater than entropy of activation for viscous flow. For the aqueous mixtures, ΔG^* increases with the increase of AMP concentration indicating that AMP has a higher effect on molecular interactions than MEA. For CO_2 loaded solutions, the mixture becomes an electrolyte with strong molecular interactions compared to an aqueous mixture, which is reflected by high ΔG^*.

Table 19. Free energy of activation for viscous flow $\Delta G^* / kJ \cdot mol^{-1}$ for AMP (1) + MEA (2) + H_2O (3) + CO_2 (4) mixtures.

AMP/MEA mass %	α / mol $CO_2 \cdot$ mol amine^{-1}	x_1	x_2	x_4	$\Delta G^*/ kJ \cdot mol^{-1}$					
					293.15 K	303.15 K	313.15 K	323.15 K	333.15 K	343.15 K
21/9	0.000	0.0552	0.0345	0.0000	13.265	12.813	12.429	12.115	11.861	11.644
	0.107	0.0547	0.0342	0.0095	13.520	13.082	12.726	12.419	12.169	11.967
	0.210	0.0542	0.0339	0.0185	13.713	13.263	12.904	12.593	12.357	12.163
	0.308	0.0537	0.0336	0.0269	13.992	13.549	13.195	12.888	12.649	12.458
	0.400	0.0533	0.0333	0.0346	14.203	13.741	13.382	13.079	12.827	12.638
	0.518	0.0527	0.0330	0.0444	14.406	13.957	13.601	13.295	13.070	12.874
24/6	0.000	0.0633	0.0231	0.0000	13.386	12.916	12.518	12.194	11.925	11.696
	0.083	0.0629	0.0229	0.0071	13.544	13.074	12.674	12.339	12.062	11.836
	0.165	0.0624	0.0228	0.0141	13.787	13.327	12.940	12.612	12.339	12.114
	0.314	0.0616	0.0225	0.0264	14.100	13.634	13.243	12.914	12.640	12.428
	0.418	0.0611	0.0223	0.0349	14.393	13.911	13.503	13.159	12.873	12.641
	0.508	0.0606	0.0221	0.0420	14.607	14.118	13.712	13.371	13.093	12.878
27/3	0.000	0.0715	0.0116	0.0000	13.490	12.989	12.564	12.211	11.916	11.664
	0.072	0.0711	0.0115	0.0059	13.693	13.193	12.791	12.464	12.197	11.972
	0.152	0.0706	0.0114	0.0125	13.962	13.468	13.057	12.723	12.460	12.237
	0.246	0.0700	0.0114	0.0200	14.214	13.685	13.269	12.928	12.641	12.392
	0.461	0.0688	0.0112	0.0369	14.565	14.039	13.594	13.242	12.970	12.758
	0.511	0.0686	0.0111	0.0407	14.761	14.225	13.781	13.425	13.146	12.924

Table 20: Enthalpy of activation for viscous flow ΔH^*/ kJ·mol^{-1} and entropy activation for viscous flow ΔS^*/ J·(mol·K)$^{-1}$.

AMP/MEA mass %	x_4	ΔH^*/ kJ·mol^{-1}	ΔS^*/ J·(mol·K)$^{-1}$
21/9	0.0000	22.733	32.622
	0.0095	22.598	31.278
	0.0185	22.764	31.219
	0.0269	22.958	30.918
	0.0346	23.328	31.484
	0.0444	23.331	30.796
24/9	0.0000	23.250	33.979
	0.0071	23.547	34.446
	0.0141	23.573	33.693
	0.0264	23.898	33.757
	0.0349	24.652	35.323
	0.0420	24.735	34.904
27/3	0.0000	24.152	36.711
	0.0059	23.699	34.513
	0.0125	24.030	34.717
	0.0200	24.772	36.412
	0.0369	25.152	36.537
	0.0407	25.492	37.032

Conclusion

This study discusses the densities and viscosities of unloaded and CO_2 loaded AMP + MEA + H_2O mixtures at different amine concentrations, CO_2 loadings and temperatures. The amine mass % of AMP and MEA were 21/9, 24/6 and 27/3 by maintaining 70 mass % of H_2O in the aqueous solutions. The CO_2 loadings of mixtures were maintained at different levels in which maximum is less than 0.6 (mol CO_2·mol amine $^{-1}$).

The densities of mixtures were measured in the temperature range from 293.15 K to 343.15 K. Density increases with the increase of CO_2 loading and decreases with temperature. The measured density data were fit into a Setschenow-type correlation with 0.09 %, 0.08 % and 0.19 % AARD and 2.8 kg·m^{-3}, 2.21 kg·m^{-3} and 4.2 kg·m^{-3} AMD for mixtures of 21/9, 24/6 and 27/3 of AMP mass % / MEA mass % respectively. The Weiland's density correlation was modified to fit density data of CO_2 loaded aqueous mixtures with more than one amine for the range of amine concentrations and temperatures. The correlation was capable to represent density data at 0.42% AARD and 13.7 kg·m^{-3} AMD. The accuracies of density data fit to the Setschenow-type correlation and modified Weiland's density correlation are regarded as satisfactory for correlations in engineering calculations.

The viscosities of mixtures were measured in the temperature range from 293.15 K to 363.15 K. Viscosity increases with increase of CO_2 loading and decreases with temperature. A Setschenow-type correlation was proposed to fit the measured viscosities and the accuracy of the data fit was calculated to 0.75 %, 0.99 % and 0.94 % AARD and 0.07 mPa·s , 0.1 mPa·s and 0.31 mPa·s AMD for mixtures of 21/9, 24/6 and 27/3 of AMP mass % / MEA mass % respectively. A modified Weiland's viscosity correlation for CO_2 loaded aqueous mixtures with

more than one amine was proposed to represent viscosity data. The accuracy of data fit was calculated to 2.7 % AARD and 0.2 mPa·s AMD for the considered amine concentration and temperature range.

The free energy of activation for viscous flow ΔG^* from Eyring's viscosity model showed that ΔG^* increases with the increase of CO_2 loading and decreases with the increase of temperature. The calculated properties of ΔG^*, ΔH^* and ΔS^* increase with the increase of AMP concentration in the aqueous mixtures. The correlation developed based on Eyring's viscosity model was in good agreement with measured viscosity data showing an accuracy of the regression of 1.4 % AARD and 0.2 mPa·s AMD.

Acknowledgement

References

[1]   P. Singh, D. W. F. Brilman, and M. J. Groeneveld, "Solubility of CO_2 in aqueous solution of newly developed absorbents " *Energy Procedia,* vol. 1, pp. 1257-1264, 2009, doi: 10.1016/j.egypro.2009.01.165.

[2]   S. K. Wai, C. Nwaoha, C. Saiwan, R. Idem, and T. Supap, "Absorption heat, solubility, absorption and desorption rates, cyclic capacity, heat duty, and absorption kinetic modeling of AMP - DETA blend for post - combustion CO_2 capture," *Separation and Purification Technology* vol. 194, pp. 89-95, 2018, doi: 10.1016/j.seppur.2017.11.024.

[3]   A. Hartono and H. F. Svendsen, "Density, viscosity, and excess properties of aqueous solution of diethylenetriamine (DETA)," *J. Chem. Thermodynamics,* vol. 41, pp. 973-979, 2009, doi: 10.1016/j.jct.2008.11.012.

[4]   A. Dey and A. Aroonwilas, "CO_2 absorption into MEA-AMP blend: mass transfer and absorber height index," *Energy Procedia,* vol. 1, pp. 211-215, 2009.

[5]   R. Sakwattanapong, A. Aroonwilas, and A. Veawab, "Reaction rate of CO_2 in aqueous MEA-AMP solution: Experiment and modeling " *Energy Procedia,* vol. 1, pp. 217-224, 2009, doi: 10.1016/j.egypro.2009.01.031.

[6]   M. Usman, "Kinetics study of CO_2 absorption in AMP and Piperazine solutions," MSc, Department of Chemical Engineering, Norwegian University of Science and Technology, 2012.

[7]   M. H. Li and B. C. Chang, "Solubility of mixtures of Carbon Dioxide and Hydrogen Sulfide in Water + Monoethanolamine + 2-Amino-2-methul-1-propanol," *J. Chem. Eng. Data,* vol. 40, pp. 328-331, 1995.

[8]   M. H. Li and M. D. Lai, "Solubility and Diffusivity of N_2O and CO_2 in (Monoethanolamine + N-Methyldiethanolamine + water) and in (Monoethanolamine + 2-Amino-2-methyl-1-propanol+water)," *J. Chem. Eng. Data,* vol. 40, pp. 486-492, 1995.

[9]   D. Śpiewak *et al.*, "PDU1-SCALE EXPERIMENTAL RESULTS OF CO_2 REMOVAL WITH AMP/PZ SOLVENT," *Chemical and Process Engineering: DE GRUYTER OPEN,* vol. 36, no. 39-48, 2015.

[10]   A. Aroonwilas and A. Veawab, "Integration of CO_2 capture unit using blended MEA-AMP solution into coal-fired power plants," *Energy Procedia,* vol. 1, pp. 4315-4321, 2009.

[11] G. Sartori and D. W. Savage, "Sterically Hindered Amines for CO_2 Removal from Gases," *American Chemical Society,* 1983.

[12] C. Nwaoha *et al.*, "Carbon dioxide (CO_2) capture performance of aqueoustri-solvent blends containing 2-amino-2-methyl-1-propanol (AMP) and methyldiethanolamine (MDEA) promoted by diethylenetriamine (DETA)," *International Journal of Greenhouse Gas Control,* vol. 53, pp. 292-304, 2016, doi: 10.1016/j.ijggc.2016.08.012.

[13] B. P. Mandal and S. S. Bandyopadhyay, "Absorption of carbon dioxide into aqueous blends of 2-amino-2-methyl-1-propanol and monoethanolamine " *Chemical Engineering Science* vol. 61, pp. 5440-5447, 2006, doi: 10.1016/j.ces.2006.04.002.

[14] B. P. Mandal, M. Kundu, and S. S. Bandyopadhyay, "Density and viscosity of aqueous solution of (N-Methyldiethanolamine + Monoethanolamine), (N-Methyldiethanolamine + Diethanolamine), (2-Amino-2-methyl-1-propanol + Monoethanolamine), and (2-Amino-2-methyl-1-propanol + Diethanolamine)," *J. Chem. Eng. Data,* vol. 48, pp. 703-707, 2003.

[15] M.-H. Li and Y.-C. Lie, "Densities and viscosities of solutions of Monoethanolamine + N-Methyldiethanolamine + water and Monoethanolamine + 2-Amino-2-methyl-1-propanol + water," *J. Chem. Eng. Data,* vol. 39, pp. 444-447, 1994.

[16] O. Redlich and A. T. Kister, "Algebraic representation of thermodynamic properties and the classification of solutions," *Ind. Eng. Chem.,* vol. 40, no. 2, pp. 345-348, 1948.

[17] R. H. Weiland, J. C. Dingman, D. B. Cronin, and G. J. Browning, "Density and viscosity of some partially carbonated aqueous alkanolamine solutions and their blends," *J. Chem. Eng. Data,* vol. 43, pp. 378-382, 1998.

[18] H. Eyring, "Viscosity, Plasticity, and Diffusion as example of absolute reaction rates," *Journal of chemical physics,* vol. 4, pp. 283-291, 1936.

[19] J. Han, J. Jin, D. A. Eimer, and M. C. Melaaen, "Density of water (1) + Monoethanolamine (2) + CO_2 (3) from (298.15 to 413.15) K and surface tension of water (1) + Monoethanolamine (2) from (303.15 to 333.15) K," *J. Chem. Eng. Data,* vol. 57, pp. 1095-1103, 2012.

[20] S. Jayarathna, A. Weerasooriya, S. Dayarathna, D. A. Eimer, and M. C. Melaaen, "Densities and surface tensions of CO_2 loaded aqueous monoethanolamine solution with r=(0.2 to 0.7) at T=(303.15 to 333.15)K," *J. Chem. Eng. Data,* vol. 58, pp. 986-992, 2013.

[21] Z. Idris, N. B. Kummamuru, and D. A. Eimer, "Viscosity measurement of unloaded and CO_2-loaded aqueous monoethanolamine at higher concentrations," *Journal of Molecular Liquids,* vol. 243, pp. 638-645, 2017.

[22] JCGM, *Evaluation of measurement data — Supplement 1 to the "Guide to the expression of uncertainty in measurement" — Propagation of distributions using a Monte Carlo method*, 2008.

[23] S. L. R. Ellison and A. Williams, *Quantifying uncertainty in analytical measurement* 2012.

[24] J. Aguila-Hernández, R. Gómez-Quintana, F. Murrieta-Guevara, A. Romero-Martínez, and A. Trejo, "Liquid Density of Aqueous Blended Alkanolamines and N-Methylpyrrolidone as a Function of Concentration and Temperature," *Journal of Chemical & Engineering Data,* vol. 46, no. 4, pp. 861-867, 2001, doi: 10.1021/je0002944.

[25] A. Henni, J. J. Hromek, P. Tontiwachwuthikul, and A. Chakma, "Volumetric properties and viscosities for aqueous AMP solutions from 25 °C to 70 °C," *Journal of Chemical & Engineering Data,* vol. 48, no. 3, pp. 551-556, 2003, doi: 10.1021/je0201119.

[26] S. Xu, F. D. Otto, and A. E. Mather, "Physical properties of aqueous AMP solutions," *Journal of Chemical & Engineering Data,* vol. 36, no. 1, pp. 71-75, 1991, doi: 10.1021/je00001a021.

[27] K. Zhang, B. Hawrylak, R. Palepu, and P. R. Tremaine, "Thermodynamics of aqueous amines: excess molar heat capacities, volumes, and expansibilities of {water+ methyldiethanolamine (MDEA)} and {water + 2-amino-2-methyl-1-propanol (AMP)}," *The Journal of Chemical Thermodynamics,* vol. 34, no. 5, pp. 679-710, 2002, doi: 10.1006/jcht.2002.0937.

[28] A. J. Treszczanowicz and G. C. Benson, "Excess volumes for n-alkanols + n-alkanes II. Binary mixtures of n-pentanol, n-hexanol, n-octanol, and n-decanol + n-heptane," *The Journal of Chemical Thermodynamics,* vol. 10, no. 10, pp. 967-974, 1978, doi: 10.1016/0021-9614(78)90058-7.

[29] H. Iloukhani, M. Rezaei-Sameti, and J. Basiri-Parsa, "Excess molar volumes and dynamic viscosities for binary mixtures of toluene+n-alkanes (C5–C10) at T=298.15K – Comparison with Prigogine–Flory–Patterson theory," *The Journal of Chemical Thermodynamics,* vol. 38, no. 8, pp. 975-982, 2006, doi: 10.1016/j.jct.2005.10.011.

[30] A. A. Rostami, M. J. Chaichi, and M. Sharifi, "Densities, Viscosities, and Excess Gibbs Energy of Activation for Viscous Flow, for Binary Mixtures of Dimethyl Phthalate (DMP) with 1-Pentanol, 1-Butanol, and 1-Propanol at Two Temperatures," *Monatshefte für Chemie - Chemical Monthly,* vol. 138, no. 10, pp. 967-971, 2007, doi: 10.1007/s00706-007-0691-5.

[31] S. C. Bhatia, R. Bhatia, and G. P. Dubey, "Studies on transport and thermodynamic properties of binary mixtures of octan-1-ol with chloroform, 1,2-dichloroethane and 1,1,2,2-tetrachloroethane at 298.15 and 308.15 K," *Journal of Molecular Liquids,* vol. 144, no. 3, pp. 163-171, 2009, doi: 10.1016/j.molliq.2008.11.003.

[32] A. Hartono, E. O. Mba, and H. F. Svendsen, "Physical properties of partially CO_2 loaded aqueous monoethanolamine (MEA)," *J. Chem. Eng. Data* vol. 59, pp. 1808-1816, 2014.

[33] S. A. Jayarathna, C. K. Jayarathna, D. A. Kottage, S. Dayarathna, D. A. Eimer, and M. C. Melaaen, "Density and surface tension measurement of partially carbonated aqueous monoethanolamine solutions " *J. Chem. Eng. Data,* vol. 58, pp. 343-348, 2013.

[34] M. Shokouhi, A. H. Jalili, F. Samani, and M. Hosseini-Jenab, "Experimental investigation of the density and viscosity of CO_2-loaded aqueous alkanolamine solutions," *Fluid Phase Equilibria,* vol. 404, pp. 96-108, 2015, doi: 10.1016/j.fluid.2015.06.034.

[35] J. Setschenow, "Über die Konstitution der Salzlösungen auf Grund ihres Verhaltens zu Kohlensäure," in *Zeitschrift für Physikalische Chemie* vol. 4U, ed, 1889, p. 117.

[36] J. M. Prausnitz, R. N. Lichtenthaler, and E. G. d. Azevedo, *Molecular thermodynamics of fluid-phase equilibria.* Prentice Hall PTR, 1999.

[37] A. H. Harvey, *Thermodynamic properties of water.* Boulder, Colorado: NIST, 1998.

[38] T. G. Amundsen, L. E. Øi, and D. A. Eimer, "Density and viscosity of monoethanolamine + water + carbon dioxide from (25 to 80) ºC," *J. Chem. Eng. Data,* vol. 54, pp. 3096-3100, 2009.

[39] E. N. d. C. Andrade, "LVIII. A theory of the viscosity of liquids. Part II, Philosophical Magazine Series 7," vol. 17, no. 113, pp. 698-732, 1934.

[40] D. H. Vogel, "Das Temperaturabhaengigkeitsgesetz der Viskositaet von Fluessigkeiten," *Physikalische Zeitschrift,* vol. 22, pp. 645-646, 1921.

[41] D. Fu, H. Hao, and F. Liu, "Experiment and model for the viscosity of carbonated 2-amino-2-methyl-1-propanol-monoethanolamine and 2-amino-2-methyl-1-propanol-

diethanolamine aqueous solution," *Journal of Molecular Liquids,* vol. 188, pp. 37-41, 2013, doi: 10.1016/j.molliq.2013.09.014.

[42]   R. B. Bird, W. E. Stewart, and E. N. Lightfoot, *Transport Phenomena*, second edition ed. USA: John Wiley & Sons, Inc., 2002.

[43]   R. Meyer, M. Meyer, J. Metzger, and A. Peneloux, "Thermodynamic and physicochemical properties of binary solvent " *Journal de Chimie Physique et de Physico-Chimie Biologique,* vol. 68, pp. 406-412, 1971.

[44]   C. M. Kinart, W. J. Kinart, and A. Ćwiklińska, "2-Methoxyethanol–Tetrahydrofuran– binary liquid system. Viscosities, densities, excess molar volumes and excess Gibbs activation energies of viscous flow at various temperatures," *Journal of Thermal Analysis and Calorimetry,* vol. 68, no. 1, pp. 307-317, 2002, doi: 10.1023/A:1014981921097.

[45]   S. Oswal and M. V. Rathnam, "Viscosity data of binary mixtures: ethyl acetate + cyclohexane, + benzene, + toluene, + ethylbenzene + carbon tetrachloride, and + chloroform at 303.15 K," *Canadian Journal of Chemistry,* vol. 62, no. 12, pp. 2851- 2853, 1984, doi: 10.1139/v84-482.

[46]   A. Ćwiklińska and C. M. Kinart, "Thermodynamic and physicochemical properties of binary mixtures of nitromethane with {2-methoxyethanol+2-butoxyethanol} systems at T=(293.15, 298.15, 303.15, 308.15, and 313.15)K," *The Journal of Chemical Thermodynamics,* vol. 43, no. 3, pp. 420-429, 2011, doi: 10.1016/j.jct.2010.10.016.

[47]   T. M. Aminabhavi, M. I. Aralaguppi, G. Bindu, and R. S. Khinnavar, "Densities, shear viscosities, refractive indices, and speeds of sound of Bis(2-methoxyethyl) Ether with Hexane, Heptane, Octane, and 2,2,4-Trimethylpentane in the temperature interval 298.15-318.15 K," *Journal of Chemical & Engineering Data,* vol. 39, no. 3, pp. 522- 528, 1994, doi: 10.1021/je00015a028.

[48]   K. Ohnishi, I. Fujihara, and S. Murakami, "Thermodynamic properties of decalins mixed with hexane isomers at 298.15 K. II. Excess volumes and isentropic compressibilities," *Fluid Phase Equilibria,* vol. 46, no. 1, pp. 73-84, 1989, doi: 10.1016/0378-3812(89)80276-6.

[49]   N. S. Matin, J. E. Remias, and K. Liu, "Application of electrolyte-NRTL model for prediction of the viscosity of carbon dioxide loaded aqueous amine solutions " *Ind. Eng. Chem. Res,* vol. 52, pp. 16979-16984, 2013.
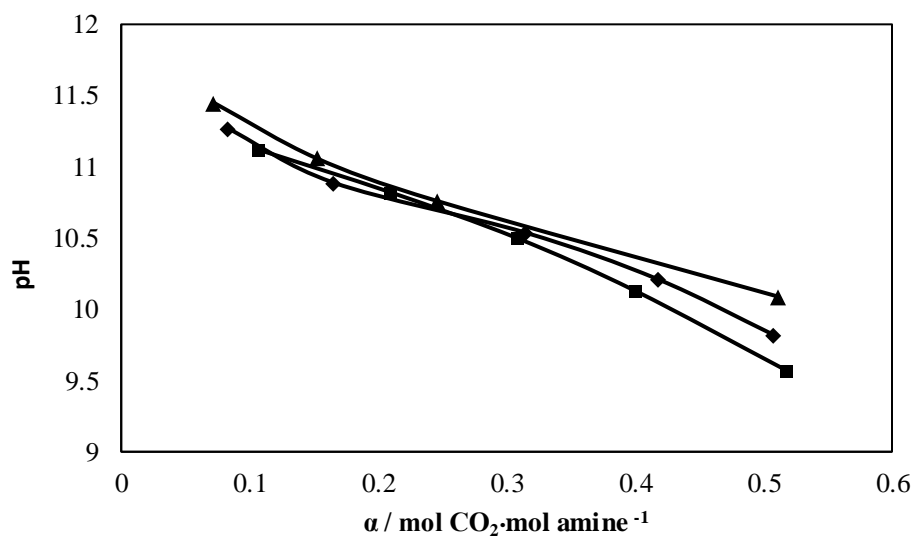
Figure S1 : Variation of pH with CO_2 loading (α); CO_2 loaded 21 mass % AMP + 9 mass % MEA + 70 mass % H_2O, '■'; CO_2 loaded 24 mass % AMP + 6 mass % MEA + 70 mass % H_2O, '◆'; CO_2 loaded 27 mass % AMP + 3 mass % MEA + 70 mass % H_2O, '▲'.

Article C

Density, viscosity and excess properties of ternary aqueous mixtures of MDEA + MEA, DMEA + MEA and DEEA + MEA.

Density, Viscosity, and Excess Properties of Ternary Aqueous Mixtures of MDEA + MEA, DMEA + MEA, and DEEA + MEA

Sumudu S. Karunarathne, Dag A. Eimer, Klaus J. Jens and Lars E. Øi *

Faculty of Technology, Natural Sciences and Maritime Studies, University of South-Eastern Norway, Kjølnes Ring 56, 3901 Porsgrunn, Norway; sumuduunimrt@gmail.com (S.S.K.); Dag.A.Eimer@usn.no (D.A.E.); Klaus.J.Jens@usn.no (K.J.J.)

* Correspondence: lars.oi@usn.no; Tel.: +47-35-575-141

Abstract: This study presents the measured densities and viscosities of three ternary aqueous mixtures of tertiary and primary amines. The tertiary amines of N-methyldiethanolamine (MDEA), dimethylethanolamine (DMEA), diethylethanolamine (DEEA), and the primary amine monoethanolamine (MEA) at different concentrations (mass%) were mixed to prepare the liquid mixtures. The excess molar volume V^E of the mixtures was analyzed using measured densities to acquire a better understanding of the molecular packing and intermolecular interactions in the mixtures. The excess free energy of activation ΔG^{E*} and excess entropy of activation ΔS^{E*} for viscous flow were determined from the measured viscosities by implementing the theory of rate processes of Eyring. Correlations based on the Redlich–Kister type polynomial were adopted to correlate the excess properties V^E and ΔG^{E*} as a function of the amine mole fraction and temperature. The results showed that the correlations were able to represent the measured data with satisfactory accuracies for engineering calculations.

Keywords: density; viscosity; MDEA; DMEA; DEEA; excess property; Redlich–Kister

1. Introduction

The chemical absorption of CO_2 into aqueous alkanolamines is a mature technology that has been used for decades in the natural gas industry. The solvent-based commercial scale post-combustion CO_2 capture plants are generally operated with 15–20 mass% aqueous monoethanolamine (MEA), 30 mass% aqueous MEA, KS-1 based on sterically hindered amines, and DC-103 from Shell Cansolv (50 mass% amine and 50 mass% H_2O) [1–3]. Bernhardsen and Knuutila [4] reviewed the potential amine solvents for CO_2 absorption process by considering the absorption capacity, cyclic capacity, and pKa. The studies performed on 3-amino-1-propanol (3A1P) [5,6] and diethylenetriamine (DETA) [7,8] stated the possibilities of using them as solvents in post-combustion CO_2 capture. The applicability of this technology to post-combustion CO_2 capture is challenging owing to the economic feasibility of the process due to the high-energy penalty in the CO_2 stripping. MEA is a primary amine that shows a high CO_2 absorption rate, which is promising for the process. The main disadvantage of MEA is that it requires a high amount of energy to release CO_2 during the stripping. Tertiary amines like N-methyldiethanolamine (MDEA), dimethylethanolamine (DMEA), and diethylethanolamine (DEEA) have a low heat of reaction, which lowers the energy requirement in the stripping process [9–11]. MDEA is traditionally used for CO_2 removal at high pressures. It is normally not used for CO_2 removal at atmospheric pressure [12]. The MDEA solutions are used for the selective removal of H_2S from gas streams like natural gases, synthesis gases from the gasification

of coal and heavy oils, and tail gases from sulphur plants that contain both CO_2 and H_2S [13,14]. In addition to the selective removal of H_2S, several advantages of MDEA over primary and secondary amines were reported, such as low vapor pressure, high CO_2 absorption capacity, high resistance to degradation, and fewer corrosion problems [15,16]. The low CO_2 absorption rate of tertiary amines makes it inefficient to use them alone with H_2O as a solvent in the absorption–desorption process to deal with gas streams with low CO_2 concentrations. The work performed by Kim and Savage [17] on reaction kinetics of CO_2 absorption in aqueous DEEA claimed that DEEA has a higher reaction rate than MDEA. Alongside the results found by Henni et al. [18] on kinetics of DMEA, it was observed that DMEA and DEEA have a higher absorption performance compared to MDEA [9]. Chakravarty et al. [19] demonstrated that CO_2 absorption can be enhanced by adding a primary or secondary amine to the tertiary amine without changing the stripping characteristics. Studies have been performed to investigate the performance of aqueous blends of tertiary and primary amines in CO_2 absorption [9,20–22]. Conway et al. [21] showed improvements in the cyclic capacity of DMEA + MEA + H_2O and DEEA + MEA + H_2O mixtures compared to aqueous MEA mixtures.

Physical properties, such as the density and viscosity of solvents, are essential for engineering calculations when performing mathematical modelling and simulations for the sizing of process equipment. The density and viscosity are required in many mass and heat transfer correlations that are used in the designing of absorbers, strippers, and heat exchangers in the process. Further properties are useful in flow calculations to select material transfer equipment like pumps and valves. The density and viscosity data of some MDEA + MEA + H_2O mixtures have been reported in literature sources [23–25]. For the mixtures of DMEA + MEA + H_2O and DEEA + MEA + H_2O, literature for measured properties are scarce [21].

In this study, the measurements of density and viscosity of three different aqueous tertiary and primary amines mixtures of MDEA (1) + MEA (2) + H_2O (3), DMEA (1) + MEA (2) + H_2O (3), and DEEA (1) + MEA (2) + H_2O (3) at different amine concentrations and temperatures were performed. The excess properties of molar volume, viscosity, and free energy of activation and entropy for viscous flow were determined to examine the molecular structure and interactions in the mixtures. Finally, the data were fitted to the density and viscosity correlations available in the literature and parameters were determined via regression. The accuracy of the data fitting was examined through average absolute relative deviation (*AARD* (%)) and absolute maximum deviation (*AMD*).

2. Materials and Methods

2.1. Material Description

Table 1 lists the materials that were used in this study. Liquid mixtures of aqueous tertiary and primary amines of MDEA + MEA + H_2O, DMEA + MEA + H_2O, and DEEA + MEA + H_2O were prepared on the mass basis using a balance, model: XS-403S from Mettler Toledo (Greifensee, Switzerland) with a resolution of 1 mg. Amines were used without further purification and dissolved with deionized (resistivity: 18.2 MΩ cm) and degassed water from a rotary evaporator (Rotavapor R-210, Buchi, Flawil, Switzerland).

Table 1. Materials used in this study.

Chemical Name	CAS No.	Source	Purity
MDEA	105-59-9	Merck Schuchardt OHG, Hohenbrunn, Germany	≥98%
DMEA	108-01-0	Alfa Aesar, Kandel, Germany	≥99
DEEA	100-37-8	Sigma-Aldrich, Darmstadt, Germany	≥99.5%
MEA	141-43-5	Sigma-Aldrich, Darmstadt, Germany	≥99.5% (GC) [a]

[a] GC: Gas chromatography.

2.2. Density Measurement

Density of the mixtures was measured using a density meter of DMA 4500 from Anton Paar (Graz, Austria) under atmospheric conditions. DMA 4500 has a temperature controller with an accuracy of ±0.03 K and the accuracy of the density measurement is ±0.05 kg m^{-3}. A liquid sample with a volume of approximately 5 mL was used to take the density reading and a new sample was fed into the U-tube for density measurements at each temperature and composition. In order to check the reliability of the instrument, a density check was performed frequently at 293.15 K using degassed deionized water. As suggested by the manufacturer, the density check is accepted when the deviations between the experimental and stored reference density data is smaller than 0.1 kg m^{-3}. For deviations greater than 0.1 kg m^{-3}, a calibration was performed using both air and degassed deionized water at 293.15 K as per the instruction given by the manufacturer. The density of water was measured at different temperatures and compared with the literature data from the International Association for the Properties of Water and Steam (IAPWS) [26]. The comparison showed that the deviation of the measured density of water was less than 0.01%, which was acceptable.

2.3. Viscosity Measurement

A double-gap rheometer (pressure cell XL, Anton Paar, Graz, Austria) Physica MCR 101 was used for the dynamic viscosity measurements of the aqueous amine mixtures. A liquid sample of 7 mL in volume was transferred using a syringe in the space occupied between the rotating and fixed cylinders in the pressure cell. For the viscosity measurements at temperatures higher than 303.15 K, the internal temperature controller with an accuracy of ±0.03 K was used to maintain different temperatures up to 363.15 K. An external cooling system Viscotherm VT 2 (Anton Paar, Graz, Austria) with an accuracy of ±0.02 K was adopted to acquire precise measurements for the temperature range from 293.15 K to 303.15 K. Following the instructions provided by Anton Paar, an air check and motor adjustment were performed prior to the experiments. The accuracy of the torque measurement is given by the manufacturer as max (0.2 μNm; 0.5%) and the repeatability of the viscosity measurements is ±0.008 mPa s. Further, a standard viscosity solution S3S from Paragon Scientific Ltd. (Prenton, United Kingdom) was used to calibrate the measuring system. The viscosity of the standard viscosity fluid was measured at specific temperatures suggested by the supplier and was compared with the reference data to record deviations. The measured viscosities were corrected for these deviations obtained during the calibration. The experiments were conducted at atmospheric pressure (1 atm).

2.4. Experimental Uncertainty

Several uncertainty sources of material purity $u(p)$, temperature measurement $u(T)$, weight measurement $u(w)$, and repeatability $u(rep)$ were taken into account to determine the combined standard uncertainty of density and viscosity measurements of aqueous amine mixtures.

For the uncertainty of density measurement, the specified standard uncertainties were $u(p)$ = ±0.003, $u(T)$ = ±0.012 K, $u(w)$ = ±2 × 10^{-4} kg, and $u(rep)$ = ±0.13 kg m^{-3}. The maximum gradient of density against temperature, $\partial\rho/\partial T$, was found to be 0.88 kg m^{-3} K^{-1} and the corresponding uncertainty in ρ, $(\partial\rho/\partial T)\cdot u(T)$, was determined to be ±0.0106 kg m^{-3}. The combined standard uncertainty for the density measurement was calculated as described in the Guide to the Expression of Uncertainty in Measurement [27,28] by considering all mentioned uncertainty sources to be $u(\rho)$ = ±2.97 kg m^{-3}. Then, the combined expanded uncertainty of the density measurement $U(\rho)$ was found to be ±5.94 kg m^{-3} (level of confidence = 0.95).

In the uncertainty of viscosity measurement, specified standard uncertainties for the uncertainty sources were $u(p)$ = ±0.003, $u(T)$ = ±0.012 K, $u(w)$ = ±2 × 10^{-4} kg, and $u(rep)$ = ±0.008 mPa s. The combined standard uncertainty for the viscosity measurement was calculated to be $u(\eta)$ = ±0.008 mPa s. Then, the combined expanded uncertainty of the viscosity measurement $U(\eta)$ was found to be ±0.016 mPa s (level of confidence = 0.95).

3. Results

3.1. Density and Excess Molar Volume

The density of pure MDEA, DEEA, DMEA, and MEA are available in the literature. The measured densities of pure amines over a temperature range from 293.15 K to 343.15 K are listed in Table 2 with the relevant literature data and references. The measured density in this work is in good agreement with values reported in literature, which indicates the density meter was properly calibrated during the experiments.

Table 2. Densities ρ/kg m^{-3} of pure amines MDEA, DMEA and DEEA.

Amine	T (K)	This Work	Literature		
			Pinto et al. [29]	Hawrylak et al. [30]	Maham et al. [31]
MDEA	293.15	1040.6	1040.12		
	298.15	1036.8		1036.88	1035.9
	303.15	1033.2			1032.0
	308.15	1029.4		1029.01	
	313.15	1025.6	1024.74		1024.45
	318.15	1021.8		1022.64	
	323.15	1018.0	1017.27		1016.66
	328.15	1014.1			
	333.15	1010.3	1009.56		1009.00
	338.15	1006.4			
	343.15	1002.5			1001.24
	T/(K)	This Work	Literature		
			Maham et al. [32]	Hawrylak et al. [30]	Bernal-García et al. [33]
DMEA	293.15	887.3			887.816
	298.15	883.0	882.57	883.34	883.578
	303.15	878.8	878.35		879.315
	308.15	874.5		875.46	875.017
	313.15	870.1	869.86		870.686
	318.15	865.8		867.28	866.316
	323.15	861.4			861.902
	328.15	856.9			857.460
	333.15	852.5	851.89		852.965
	338.15	847.9			848.423
	343.15	843.3			843.844
	T/(K)	This Work	Literature		
			Zhang et al. [34]	Hawrylak et al. [30]	Pinto et al. [29]
DEEA	293.15	884.3	884.20		
	298.15	879.7	879.54	879.52	879.47
	303.15	875.1	874.82		
	308.15	870.4		871.40	
	313.15	865.8	865.56		865.54
	318.15	861.1		861.82	
	323.15	856.3			856.12
	328.15	851.5			
	333.15	846.7			846.61
	338.15	841.9			
	343.15	837.1			837.03

The measured densities of MDEA + MEA + H$_2$O, DMEA + MEA + H$_2$O, and DEEA + MEA + H$_2$O mixtures over different amine concentrations (mass% of amine) and temperatures from 293.15 K to 343.15 K are listed in Tables 3–5, respectively. For the density of MDEA + MEA + H$_2$O mixtures, the density increased with the increase of the MDEA concentration in the mixture. Moreover, for the

DMEA + MEA + H_2O and DEEA + MEA + H_2O mixtures, the density increased with the decrease of the DMEA and DEEA concentration in the mixtures.

Table 3. Densities ρ (kg m^{-3}) and excess molar volume V^E (m^3 mol^{-1}) of MDEA (1) + MEA (2) + H_2O (3) mixtures.

Mixtures	MDEA/MEA							
(Mass%/Mass%)	15/15		20/10		25/5		30/0	
[a]x_1/x_2	0.0296/0.0577		0.0398/0.0388		0.0502/0.0196		0.0609/0.0000	
T (K)	ρ	V^E ($\times10^6$)	ρ	V^E ($\times10^6$)	ρ	V^E ($\times10^6$)	ρ	V^E ($\times10^6$)
293.15	1019.7	−0.292	1022.1	−0.321	1024.5	−0.351	1026.9	−0.382
298.15	1017.6	−0.288	1019.9	−0.317	1022.3	−0.347	1024.7	−0.377
303.15	1015.3	−0.284	1017.6	−0.313	1020.05	−0.342	1022.4	−0.371
308.15	1012.8	−0.282	1015.2	−0.310	1017.6	−0.339	1019.9	−0.367
313.15	1010.3	−0.281	1012.6	−0.308	1015.0	−0.336	1017.3	−0.364
318.15	1007.6	−0.280	1009.9	−0.306	1012.2	−0.332	1014.6	−0.361
323.15	1004.8	−0.278	1007.1	−0.304	1009.3	−0.329	1011.7	−0.357
328.15	1001.9	−0.277	1004.1	−0.302	1006.3	−0.324	1008.7	−0.354
333.15	998.8	−0.276	1000.9	−0.297	1003.2	−0.323	1005.6	−0.350
338.15	995.6	−0.273	997.5	−0.288	999.7	−0.312	1002.3	−0.346
343.15	991.7	−0.257	993.1	−0.261	995.4	−0.287	998.7	−0.336

[a]x = mole fraction.

Table 4. Densities ρ (kg m^{-3}) and excess molar volume V^E (m^3 mol^{-1}) of DMEA (1) + MEA (2) + H_2O (3) mixtures.

Mixtures	DMEA/MEA							
(Mass%/Mass%)	15/15		20/10		25/5		30/0	
[a]x_1/x_2	0.0391/0.0571		0.0525/0.0383		0.0660/0.0193		0.0797/0.0000	
T (K)	ρ	V^E ($\times10^6$)	ρ	V^E ($\times10^6$)	ρ	V^E ($\times10^6$)	ρ	V^E ($\times10^6$)
293.15	1001.9	−0.463	998.4	−0.550	994.4	−0.626	990.9	−0.715
298.15	999.6	−0.460	995.9	−0.545	991.8	−0.620	988.1	−0.707
303.15	996.7	−0.448	993.2	−0.539	989.0	−0.613	985.2	−0.698
308.15	994.4	−0.453	990.5	−0.536	986.1	−0.608	982.3	−0.693
313.15	991.6	−0.452	987.6	−0.533	983.1	−0.603	979.2	−0.687
318.15	988.7	−0.450	984.6	−0.531	980.0	−0.600	975.9	−0.682
323.15	985.5	−0.444	981.4	−0.528	976.8	−0.596	972.6	−0.678
328.15	982.5	−0.447	978.0	−0.523	973.4	−0.594	969.2	−0.674
333.15	979.3	−0.448	974.6	−0.520	970.0	−0.591	965.7	−0.671
338.15	975.7	−0.442	971.1	−0.517	966.4	−0.589	962.0	−0.668
343.15	972.4	−0.445	967.4	−0.511	962.8	−0.589	958.4	−0.669

[a]x = mole fraction.

Table 5. Densities ρ (kg m^{-3}) and excess molar volume V^E (m^3 mol^{-1}) of DEEA (1) + MEA (2) + H_2O (3) mixtures.

Mixtures	DEEA/MEA							
(Mass%/Mass%)	15/15		20/10		25/5		30/0	
[a]x_1/x_2	0.0301/0.0577		0.0404/0.0388		0.0510/0.0196		0.0618/0.0000	
T (K)	ρ	V^E ($\times10^6$)	ρ	V^E ($\times10^6$)	ρ	V^E ($\times10^6$)	ρ	V^E ($\times10^6$)
293.15	1002.3	−0.489	998.4	−0.575	994.2	−0.654	989.6	−0.724
298.15	999.8	−0.484	995.7	−0.568	991.4	−0.645	986.5	−0.711
303.15	997.1	−0.479	992.9	−0.561	988.4	−0.636	983.4	−0.702
308.15	994.3	−0.476	990.0	−0.556	985.3	−0.629	980.2	−0.693
313.15	991.4	−0.473	986.9	−0.551	982.1	−0.623	976.9	−0.684
318.15	988.5	−0.471	983.7	−0.547	978.8	−0.617	973.4	−0.677

323.15	985.1	−0.464	980.5	−0.544	975.3	−0.611	969.8	−0.669
328.15	981.8	−0.462	977.1	−0.541	971.8	−0.606	966.2	−0.663
333.15	978.5	−0.459	973.6	−0.538	968.2	−0.602	962.4	−0.657
338.15	974.4	−0.443	970.0	−0.535	964.3	−0.595	958.5	−0.651
343.15	971.1	−0.448	966.2	−0.529	960.4	−0.589	954.6	−0.645

$^a x$ = mole fraction.

The excess molar volume V^E of the mixtures were determined using the molar volume of the mixture and pure components as follows:

$$V^E = V - \sum_{i=1}^{n} x_i V_i^0, \tag{1}$$

where V, V_i^0, V^E, and x_i refer to the molar volume of the mixture, molar volume of the pure component, excess molar volume of the mixture, and mole fraction, respectively. Here, $n = 3$ to represent the ternary mixture and subscripts are as follows: $i = 1$ for the tertiary amine, $i = 2$ for the primary amine (MEA), and $i = 3$ for H_2O.

The calculated V^E from Equation (1) for MDEA + MEA + H_2O, DMEA + MEA + H_2O, and DEEA + MEA + H_2O mixtures are given in Tables 3–5, respectively. The following correlation was adopted to correlate the density data at different amine concentrations and temperatures. Redlich–Kister [35] polynomials are one of the most common approaches toward correlating the excess properties of binary mixtures because polynomial expressions are simple and easy to understand. Here, it was assumed that excess molar volume of a ternary mixture as a sum of excess molar volumes from different binary pairs, as given in Equation (3). The binary mixture polynomial shown in Equation (4) was extended by adding ternary coefficients for the ternary mixture with a temperature dependency, as described in Equation (5). Finally, the density was determined as follows:

$$\rho = \frac{\sum_{i=1}^{n} x_i M_i}{V^E + \sum_{i=1}^{n} \frac{x_i M_i}{\rho_i}}, \tag{2}$$

where ρ, ρ_i, V^E, x_i, and M_i are the density of the mixture, density of the pure amine, excess molar volume of the mixture, mole fraction, and molecular weight of the pure component, respectively. The subscripts are as follows: $i = 1$ for tertiary amine, $i = 2$ for primary amine (MEA), and $i = 3$ for H_2O.

$$V^E = V_{12}^E + V_{23}^E + V_{13}^E, \tag{3}$$

$$V_{jk}^E = x_j x_k \sum_{i=0}^{n} A_i \left(x_j - x_k\right)^i, \tag{4}$$

$$A_i = a + b(T) + c(T)^2, \tag{5}$$

where A_i are pair parameters and are assumed to be temperature dependent.

Other correlations have been suggested for the excess molar volume of ternary mixtures were reported by Domínguez et al. [36] and Samanta and Bandyopadhyay [37]. References [38–40] suggested correlations for CO_2-loaded solutions, but in this work, emphasis is on non-loaded aqueous amine mixtures.

The accuracy of the proposed correlation for the fitting of measured densities was examined through the average absolute relative deviation (*AARD* (%)) and the absolute maximum deviation (*AMD*) as defined in Equations (6) and (7), respectively.

Average absolute relative deviation:

$$AARD\ (\%) = \frac{100\%}{N} \sum_{i=1}^{N} \left| \frac{Y_i^E - Y_i^C}{Y_i^E} \right|, \tag{6}$$

and the absolute maximum deviation:

$$AMD = MAX\left|Y_i^E - Y_i^C\right| \tag{7}$$

where N, Y_i^E, and Y_i^C indicate the number of data points, the measured property, and the calculated property, respectively.

　　Figure 1 shows a comparison between the measured versus correlated density data for aqueous amine mixtures. The study reveals that the proposed correlation fits the density data with an acceptable accuracy. The calculated parameters for the excess volume V^E correlation are given in Tables 6–8. The reported *AARD* and *AMD* for the density correlation of MDEA + MEA + H₂O, DMEA + MEA + H₂O, and DEEA + MEA + H₂O are listed in Table 9. The regression performed with a linear temperature dependency in Equation (5) revealed a 13% increase of *AARD* for MDEA + MEA + H₂O mixtures, as given in Table 9. This indicated that the proposed correlation gave a better fit for the density data.
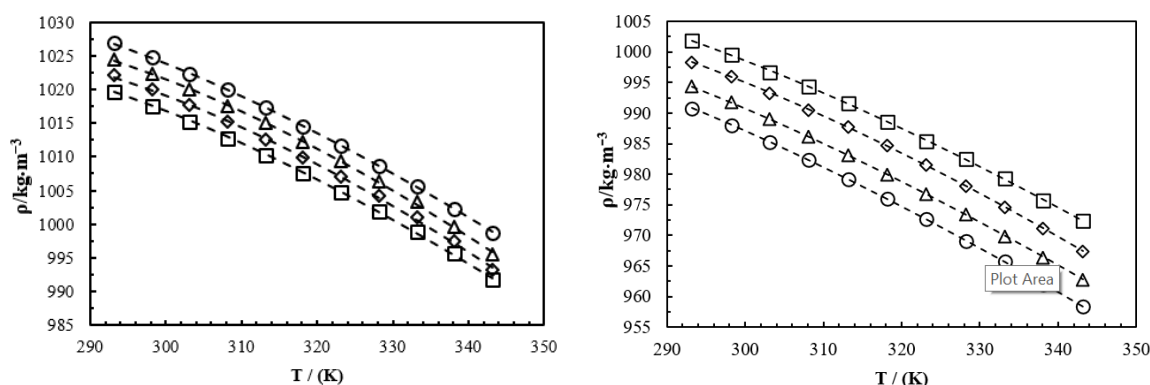
(**a**) Experiment; "□" 15%, "△" 20%, "◇" 25%, "○" 30% (mass% MDEA), correlation; "– – –".

(**b**) Experiment; "□" 15%, "△" 20%, "◇" 25%, "○" 30% (mass% DMEA), correlation; "– – –".
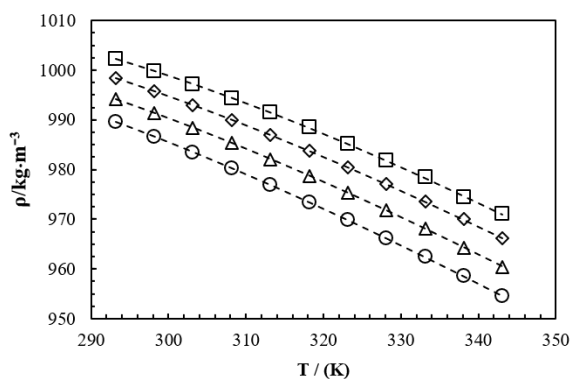
(**c**) Experiment; "□" 15%, "△" 20%, "◇" 25%, "○" 30% (mass% DEEA), correlation; "– – –".

Figure 1. Density of: (**a**) MDEA + MEA + H₂O, (**b**) DMEA + MEA + H₂O, and (**c**) DEEA + MEA + H₂O mixtures in the temperature range 293.15 K–343.15 K.

Table 6. Binary parameters A_0, A_1, and A_2 of the equation $V_{jk}^E = x_j x_k \sum_{i=0}^{n} A_i (x_j - x_k)^i$ for the excess molar volume of MDEA (1) + MEA (2) + H₂O (3).

Parameters		Binary Pair		
		MDEA + MEA	MEA + H₂O	MDEA + H₂O
A_0	a	−5740.7862	110.3506	0.7103
	b	−9.4267	0.5623	0.0984
	c	−6.0994	0.7119	0.6020
A_1	a	47,728.6381	−91.5628	0.5925

	b	82.8194	0.5242	0.3620
	c	70.3044	0.4374	0.6230
A_2	a	−41,5410.0557	70.3808	−0.2463
	b	−724.8059	0.3897	0.2846
	c	−601.8188	−0.0807	−0.0710

Table 7. Binary parameters A_0, A_1, and A_2 of the equation $V_{jk}^E = x_j x_k \sum_{i=0}^{n} A_i (x_j − x_k)^i$ for the excess molar volume of DMEA (1) + MEA (2) + H₂O (3).

Parameters		Binary Pair		
		DMEA + MEA	MEA + H₂O	DMEA + H₂O
A_0	a	1236.6194	−29.4723	−0.2082
	b	1.2313	0.1074	0.3237
	c	−4.8869	0.1673	0.3986
A_1	a	−10,260.3999	24.7205	0.3942
	b	−18.2970	0.9283	0.5201
	c	36.5240	0.3256	0.7509
A_2	a	66,361.3723	−16.8614	0.7635
	b	110.1435	0.8558	0.1605
	c	−240.1085	0.4951	0.3292

Table 8. Binary parameters A_0, A_1, and A_2 of the equation $V_{jk}^E = x_j x_k \sum_{i=0}^{n} A_i (x_j − x_k)^i$ for the excess molar volume of DEEA (1) + MEA (2) + H₂O (3).

Parameters		Binary Pair		
		DEEA + MEA	MEA + H₂O	DEEA + H₂O
A_0	a	1499.9879	−31.3131	−0.3593
	b	−7.4459	0.5442	0.2384
	c	1.3969	0.0633	0.3485
A_1	a	−12,608.1516	24.6564	−0.4664
	b	68.6619	0.4921	0.7533
	c	−19.8546	0.5935	0.6335
A_2	a	107,748.3754	−15.3309	−0.0644
	b	−588.5102	0.2714	0.5491
	c	156.7816	0.5154	0.2691

Table 9. Average absolute relative (*AARD*) and absolute maximum (*AMD*) deviations calculated based on the correlation proposed from Equations (2)–(5).

Mixture	*AARD* (%)	*AMD* (kg m⁻³)
MDEA + MEA + H₂O	0.013	0.4
DMEA + MEA + H₂O	0.004	0.3
DEEA + MEA + H₂O	0.005	0.3

The supplementary materials provide the information of the used MATLAB program for the calculation of parameters involve in density correlation.

The excess molar volume V^E of the ternary mixtures showed a negative sign for the considered amine concentrations and temperatures. The negative sign of V^E can be explained by the intermolecular packing effect and strong intermolecular interactions, such as H-bonding between unlike molecules. The relatively small structures of MEA and H₂O compared to MDEA, DMEA, and DEEA could help to pack molecules efficiently, which resulted in the decrease of the mixture volume. In addition, the formation of H-bonds among the tertiary amines, MEA, and H₂O could also lead the volume of tertiary mixtures to show a negative deviation of V^E. The highest negative values were reported in the mixtures with a 0 mass% MEA concentration. The V^E increased with the increasing

of MEA concentration in the mixtures. Further, V^E increased with the increase of temperature. At high temperatures, the increase of the energy of molecular motion weakens the interaction strength of H-bonds and inhibits the packing effect by leading to an increase of volume [41,42].

3.2. Viscosity and Excess Free Energy of Activation for Viscous Flow

Table 10 provides an overview of the measured viscosities of pure MDEA, DMEA, and DEEA from this study and literature at different temperatures from 293.15 K to 363.15 K. As shown in Figure 2, the measured viscosities in this work were in good agreement with data in the literature. It indicated that the measuring system was properly calibrated during the viscosity measurements. The measured viscosities for MDEA + MEA + H₂O, DMEA + MEA + H₂O, and DEEA + MEA + H₂O mixtures are listed in Tables 11–13, respectively, with the relevant concentrations and temperatures. For the mixtures, the viscosity increased with the increase of the tertiary amine concentration and the viscosity decreased with the increase of temperature.
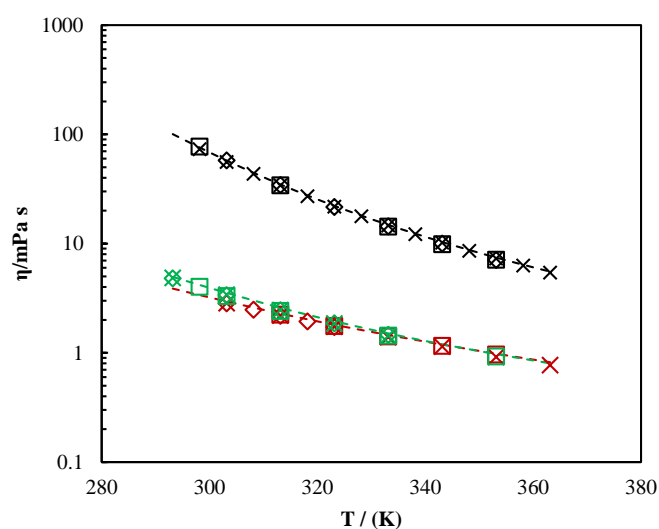
Figure 2. Viscosity of MDEA: "– – –"—this work; "□"—Teng et al. [43]; "◇"—Li and Lie [24]; "x"— Kummamuru et al. [44]. Viscosity of DMEA: "– – –"—this work; "□"—Bernal-García et al. [33]; "◇"— Chowdhury et al. [45]; "x"—DiGuilio et al. [46]. Viscosity of DEEA: "– – –"—this work; "□"—Maham et al. [32]; "◇"—Chen et al. [47]; "x"—Ma et al. [48].

Table 10. Viscosities η (mPa s) of pure amines MDEA, DMEA, and DEEA.

Amine	T (K)	This Work	Literature		
			Teng et al. [43]	Li and Lie [24]	Kummamuru et al. [44]
	293.15	100.630			
	298.15	75.775	77.19		73.10
	303.15	57.658		57.860	55.89
	308.15	44.483			43.45
	313.15	34.786	34.11	34.309	34.15
MDEA	318.15	27.575			27.l5
	323.15	22.145		21.672	21.82
	328.15	18.024			17.79
	333.15	14.820	14.30	14.386	14.63
	338.15	12.319			12.20
	343.15	10.325	9.849	9.979	10.21

	T (K)	This Work	Literature		
	348.15	8.735			8.60
	353.15	7.444	7.115	7.086	7.31
	358.15	6.395			6.29
	363.15	5.535			5.43

	T (K)	This Work	Literature		
			Bernal-García et al. [33]	Chowdhury et al. [45]	DiGuilio et al. [46]
	293.15	3.879			
	298.15	3.381			
	303.15	2.959		2.835	2.849
	308.15	2.595		2.485	
	313.15	2.288	2.238	2.186	2.194
	318.15	2.028		1.938	
	323.15	1.807	1.756	1.723	1.734
DMEA	328.15	1.618			
	333.15	1.455	1.413		1.394
	338.15	1.315			
	343.15	1.190	1.156		1.140
	348.15	1.078			
	353.15	0.981	0.963		0.916
	358.15	0.896			
	363.15	0.820			0.773

	T/(K)	This Work	Literature		
			Maham et al. [32]	Chen et al. [47]	Ma et al. [48]
	293.15	4.950		4.81	4.848
	298.15	4.174	4.022		
	303.15	3.536	3.308	3.37	3.410
	308.15	3.010			
	313.15	2.579	2.414	2.46	2.466
	318.15	2.230			
	323.15	1.943		1.86	1.855
DEEA	328.15	1.704			
	333.15	1.503	1.435	1.46	1.431
	338.15	1.337			
	343.15	1.196			
	348.15	1.076			
	353.15	0.971	0.925		
	358.15	0.881			
	363.15	0.800			

Table 11. Viscosities η (mPa s) and viscosity deviation η^E (mPa s) of MDEA (1) + MEA (2) + H₂O (3) mixtures.

Mixtures	MDEA/MEA							
(Mass%/Mass%)	15/15		20/10		25/5		30/0	
[a]x_1/x_2	0.0296/0.0577		0.0398/0.0388		0.0502/0.0196		0.0609/0.0000	
T/(K)	η	η^E	η	η^E	η	η^E	η	η^E
293.15	3.263	−1.976	3.436	−2.400	3.581	−2.863	3.712	−3.352

298.15	2.780	−1.337	2.917	−1.635	3.034	−1.961	3.136	−2.311
303.15	2.385	−0.900	2.496	−1.107	2.593	−1.334	2.673	−1.584
308.15	2.065	−0.599	2.156	−0.744	2.235	−0.904	2.301	−1.082
313.15	1.803	−0.390	1.879	−0.489	1.946	−0.601	1.995	−0.735
318.15	1.588	−0.243	1.654	−0.311	1.709	−0.391	1.748	−0.490
323.15	1.410	−0.141	1.467	−0.185	1.512	−0.244	1.544	−0.318
328.15	1.264	−0.065	1.314	−0.095	1.350	−0.138	1.376	−0.194
333.15	1.140	−0.012	1.184	−0.029	1.215	−0.061	1.236	−0.104
338.15	1.036	0.030	1.075	0.020	1.099	−0.007	1.117	−0.039
343.15	0.947	0.058	0.979	0.051	0.998	0.030	1.017	0.010
348.15	0.867	0.077	0.896	0.075	0.913	0.060	0.930	0.044
353.15	0.797	0.090	0.824	0.092	0.841	0.082	0.853	0.068
358.15	0.741	0.103	0.763	0.104	0.777	0.097	0.790	0.089
363.15	0.712	0.133	0.722	0.126	0.738	0.125	0.747	0.116

[a]x = mole fraction.

Table 12. Viscosities η (mPa s) and viscosity deviation η^E (mPa s) of DMEA (1) + MEA (2) + H$_2$O (3) mixtures.

Mixtures	DMEA/MEA							
(Mass%/Mass%)	15/15		20/10		25/5		30/0	
[a]x_1/x_2	0.0391/0.0571		0.0525/0.0383		0.0660/0.0193		0.0797/0.0000	
T/(K)	η	η^E	η	η^E	η	η^E	η	η^E
293.15	3.523	1.130	3.744	1.734	4.079	2.456	4.245	3.013
298.15	2.969	0.978	3.130	1.437	3.389	1.996	3.487	2.398
303.15	2.512	0.832	2.644	1.197	2.848	1.639	2.898	1.928
308.15	2.155	0.718	2.256	1.006	2.410	1.349	2.440	1.571
313.15	1.866	0.624	1.943	0.852	2.064	1.126	2.079	1.296
318.15	1.632	0.547	1.691	0.729	1.790	0.953	1.791	1.081
323.15	1.439	0.482	1.485	0.629	1.565	0.813	1.557	0.909
328.15	1.282	0.430	1.319	0.552	1.386	0.706	1.369	0.776
333.15	1.149	0.386	1.180	0.489	1.235	0.616	1.212	0.666
338.15	1.038	0.351	1.063	0.436	1.111	0.545	1.082	0.578
343.15	0.942	0.318	0.962	0.390	1.001	0.481	0.973	0.507
348.15	0.859	0.291	0.874	0.350	0.906	0.427	0.882	0.448
353.15	0.788	0.267	0.800	0.318	0.827	0.384	0.805	0.401
358.15	0.728	0.248	0.735	0.288	0.761	0.349	0.737	0.360
363.15	0.701	0.257	0.703	0.289	0.711	0.328	0.686	0.333

[a]x = mole fraction.

Table 13. Viscosities η (mPa s) and viscosity deviation η^E (mPa s) of DEEA (1) + MEA (2) + H$_2$O (3) mixtures.

Mixtures	DEEA/MEA							
(Mass%/Mass%)	15/15		20/10		25/5		30/0	
[a]x_1/x_2	0.0301/0.0577		0.0404/0.0388		0.0510/0.0196		0.0618/0.0000	
T/(K)	η	η^E	η	η^E	η	η^E	η	η^E
293.15	3.691	1.280	3.963	1.933	4.217	2.575	4.536	3.290
298.15	3.086	1.085	3.281	1.577	3.464	2.063	3.689	2.595
303.15	2.604	0.919	2.746	1.296	2.886	1.675	3.048	2.081
308.15	2.220	0.781	2.325	1.075	2.435	1.378	2.552	1.691
313.15	1.910	0.669	1.991	0.904	2.078	1.147	2.165	1.393
318.15	1.662	0.580	1.726	0.769	1.795	0.967	1.860	1.163

323.15	1.460	0.506	1.507	0.658	1.565	0.823	1.617	0.984
328.15	1.296	0.449	1.330	0.571	1.380	0.710	1.419	0.840
333.15	1.159	0.401	1.182	0.498	1.229	0.621	1.259	0.728
338.15	1.041	0.359	1.057	0.438	1.101	0.547	1.126	0.637
343.15	0.942	0.323	0.953	0.388	0.993	0.484	1.016	0.563
348.15	0.858	0.294	0.874	0.357	0.900	0.431	0.920	0.499
353.15	0.782	0.266	0.797	0.321	0.822	0.388	0.842	0.450
358.15	0.719	0.243	0.730	0.289	0.752	0.349	0.771	0.405
363.15	0.686	0.246	0.691	0.283	0.696	0.320	0.708	0.365

[a] x = mole fraction.

The viscosity deviation of the mixtures was calculated as follows:

$$\eta^E = \eta - \sum_{i=1}^{n} x_i \eta_i^0, \tag{8}$$

where η, η_i^0, η^E, and x_i refer to the viscosity of the mixture, viscosity of the pure component, viscosity deviation of the mixture, and mole fraction, respectively. Here, $n = 3$ represents the ternary mixture and the subscripts are as follows: $i = 1$ for the tertiary amine, $i = 2$ for the primary amine (MEA), and $i = 3$ for H_2O.

The viscosity deviation η^E is a property that provides a qualitative measure of intermolecular interactions between component molecules in a liquid mixture. A negative deviation ($\eta^E < 0$) indicates weak intermolecular interactions, while a positive deviation points out strong intermolecular interactions like H-bonding among unlike molecules in the mixture [42,49]. This method is widely used to analyze binary mixtures and the same analogy is adopted to study ternary mixtures [42]. The MDEA + MEA + H_2O mixtures showed a negative deviation for η^E at temperatures <343.15 K, and η^E gradually increased with increasing temperature. As described by Domínguez et al. [50], the η^E can become negative when intermolecular interactions between the molecules are stronger for the pure compounds than for their mixtures. The gradual increase of η^E with increasing temperature implies that the strength of the interactions between the component molecules in mixtures decreases, which may be attributed to the breaking of the cohesive force in like molecules [51]. The mixtures of DMEA + MEA + H_2O and DEEA + MEA + H_2O showed a positive deviation for η^E for the considered concentrations and temperatures. This revealed the association of strong intermolecular interactions of H-bonds in the mixtures. The increase of temperature resulted in a decrease of η^E owing to weakening of intermolecular interaction between unlike molecules.

Eyring [52] explained that in a liquid at rest, the molecules are constantly undergoing rearrangements. This was elaborated by Bird et al. [53] in terms of one molecule at a time escaping from its cage into an adjacent hole. A cage is an available space for a molecule to vibrate due to the surrounding closely packed neighboring molecules. An energy barrier of height $\Delta G^*/N_A$ represents the cage in which ΔG^* and N_A are the free energy of activation for viscous flow and Avogadro's number, respectively.

The dynamic viscosity model for liquids found by Eyring [52] is given as follows:

$$\eta = \frac{hN_A}{V} exp\left(\frac{\Delta G^*}{RT}\right), \tag{9}$$

where η, V, h, N_A, R, T, and ΔG^* refer to the viscosity, molar volume, Planck's constant, Avogadro's number, gas constant, temperature, and free energy of activation for viscous flow, respectively.

Equations (10) and (11) enable the determination of the excess free energy of activation for viscous flow ΔG^{E*} in terms of the viscosity and molar volume of the pure components:

$$ln(\eta V) = ln(\eta V)_{ideal} + \frac{\Delta G^{E*}}{RT}, \tag{10}$$

$$ln(\eta V) = \sum_{i=1}^{n} x_i ln(\eta_i V_i^0) + \frac{\Delta G^{E*}}{RT}, \tag{11}$$

where η, η_i, V, V_i^0, x_i, R, T, and ΔG^{E*} refer to the viscosity of the mixture, viscosity of pure component, molar volume of the mixture, molar volume of the pure component, mole fraction, gas constant, temperature, and excess free energy of activation for viscous flow, respectively. The subscripts are as follows: $i = 1$ for the tertiary amine, $i = 2$ for the primary amine (MEA), and $i = 3$ for H_2O.

A Redlich–Kister-type [35] polynomial, as given by Equations (12)–(14), was proposed to fit the calculated ΔG^{E*} for the considered amine mixtures:

$$\Delta G^{E*} = \Delta G_{12}^{E*} + \Delta G_{23}^{E*} + \Delta G_{13}^{E*}, \tag{12}$$

$$\Delta G_{jk}^{E*} = x_j x_k \sum_{i=0}^{n} A_i (x_j - x_k)^i, \tag{13}$$

$$A_i = a + b(T) + c(T)^2. \tag{14}$$

The correlation proposed for ΔG^{E*} was adopted to represent the measured viscosities, as illustrated in Figure 3. Due to the non-availability of measured density data beyond 343.15 K, the correlation represents viscosities only in the temperature region of 293.15 K–343.15 K. The calculated parameters of correlation for ΔG^{E*} are given in Tables 14–16. The reported *AARD* and *AMD* for the correlated viscosities of MDEA + MEA + H_2O, DMEA + MEA + H_2O, and DEEA + MEA + H_2O mixtures are listed in Table 17 and show that the proposed correlations fit viscosity data with acceptable accuracy.
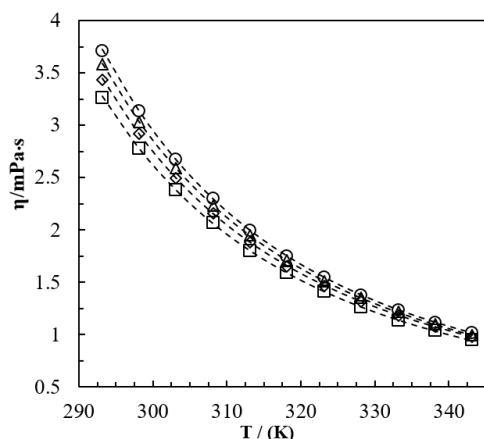
(**a**) Experiment; "□" 15%, "△" 20%, "◇" 25%, "○" 30% (mass% MDEA), correlation; "− − −".
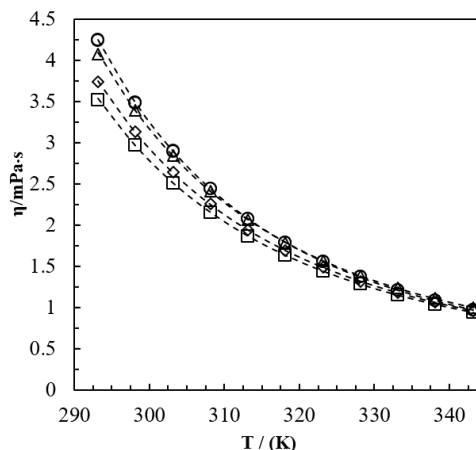
(**b**) Experiment; "□" 15%, "△" 20%, "◇" 25%, "○" 30% (mass% DMEA), correlation; "− − −".
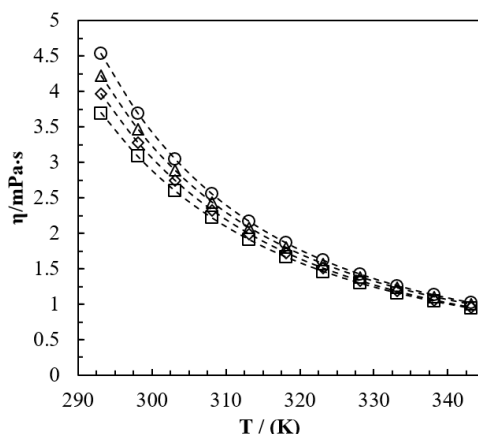
(**c**) Experiment; "□" 15%, "△" 20%, "◇" 25%, "○" 30% (mass% DEEA), correlation; "– – –".

Figure 3. Viscosity of: (**a**) MDEA + MEA + H₂O, (**b**) DMEA + MEA + H₂O, and (**c**) DEEA + MEA + H₂O mixtures in the temperature range 293.15 K–343.15 K.

Table 14. Binary parameters A_0, A_1, and A_2 of the equation $\Delta G_{jk}^{E*} = x_j x_k \sum_{i=0}^{n} A_i (x_j - x_k)^i$ for the excess free energy of activation for the viscous flow of MDEA (1) + MEA (2) + H₂O (3).

Parameters		Binary Pair		
		MDEA + MEA	**MEA + H₂O**	**MDEA + H₂O**
A_0	a	793,598.3561	29,742.8180	88,484.8967
	b	−4103.0875	−151.4883	−415.9737
	c	0.0695	0.9416	1.1885
A_1	a	−24,596,691.6004	−34,368.3693	−100,459.5203
	b	144054.1895	176.3634	472.7640
	c	−147.3226	0.1721	−0.0422
A_2	a	−992,156,463.1846	39,623.1737	114,056.3754
	b	6,459,639.6117	−202.4417	−536.0680
	c	−11,029.3913	0.2259	0.6852

Table 15. Binary parameters A_0, A_1, and A_2 of the equation $\Delta G_{jk}^{E*} = x_j x_k \sum_{i=0}^{n} A_i (x_j - x_k)^i$ for the excess free energy of activation for the viscous flow of DMEA (1) + MEA (2) + H₂O (3).

Parameters		Binary Pair		
		DMEA + MEA	**MEA + H₂O**	**DMEA + H₂O**
A_0	a	408,836.2339	23,045.8957	121,961.3271
	b	−2025.9328	−111.1510	−594.2230
	c	−1.7551	0.3358	1.2015
A_1	a	−7,605,815.8343	−26,647.3964	−142,650.2697
	b	30,647.5124	129.8558	695.9285
	c	7.3689	0.1302	−0.18829
A_2	a	200,073,604.4909	30,794.61597	166,795.8337
	b	−1,158,470.4621	−148.3353	−812.9574
	c	1738.2732	0.7219	1.4276

Table 16. Binary parameters A_0, A_1, and A_2 of the equation $\Delta G_{jk}^{E*} = x_j x_k \sum_{i=0}^{n} A_i (x_j - x_k)^i$ for the excess free energy of activation for the viscous flow of DEEA (1) + MEA (2) + H₂O (3).

Parameters	Binary Pair		
	DEEA + MEA	**MEA + H₂O**	**DEEA + H₂O**

A_0	a	25,126.2870	6568.5853	187,358.9813
	b	1235.2155	6.8875	−956.1233
	c	−1.4932	0.0215	1.6908
A_1	a	−29,279,977.3999	−6903.8084	−212,891.0602
	b	170,793.9954	−12.0764	1087.3001
	c	−281.5476	0.6502	−0.8913
A_2	a	1,130,127,942.1759	7134.8943	241,892.0192
	b	−7,848,704.4368	20.9358	−1233.8639
	c	13,825.2946	0.4399	2.0013

Table 17. Average absolute relative (*AARD*) and absolute maximum (*AMD*) deviations calculated based on correlations proposed using Equations (12)–(14).

Mixture	*AARD* (%)	*AMD* (mPa s)
MDEA + MEA + H_2O	0.14	0.013
DMEA + MEA + H_2O	0.10	0.013
DEEA + MEA + H_2O	0.07	0.010

The supplementary materials provide the information of the used MATLAB program for the calculation of parameters involve in viscosity correlation.

According to Meyer et al. [54], molecular interactions in liquid mixtures can be studied by adopting ΔG^{E*}, similar to the η^E. Studies performed in References [41,55–57] suggested that a positive deviation of ΔG^{E*} indicates strong intermolecular interactions, such as H-bonds among unlike molecules, while a negative deviation of ΔG^{E*} signifies weak molecular interactions, such as dispersive forces.

The mixtures examined in this study demonstrated positive deviations for ΔG^{E*} for the considered amine concentrations and temperatures, indicating the presence of strong intermolecular interactions like H-bonds between the molecules in the mixtures. The presence of (–OH) and (–NH$_2$) groups in amines contributes to the formation of H-bonds between unlike molecules. For the MDEA + MEA + H_2O mixtures, the highest ΔG^{E*} was reported for the mixture of 30 mass% MDEA + 0 mass% MEA + 70 mass% H_2O. The highest ΔG^{E*} for DEEA + MEA + H_2O was reported for the mixture of 30 mass% DEEA + 0 mass% MEA + 70 mass% H_2O, while for DMEA + MEA + H_2O, the highest ΔG^{E*} was reported for the mixture of 30 mass% DMEA + 0 mass% MEA + 70 mass% H_2O. The increases of MEA concentration gradually decreased the ΔG^{E*} for all mixtures, as shown in the Figure 4.
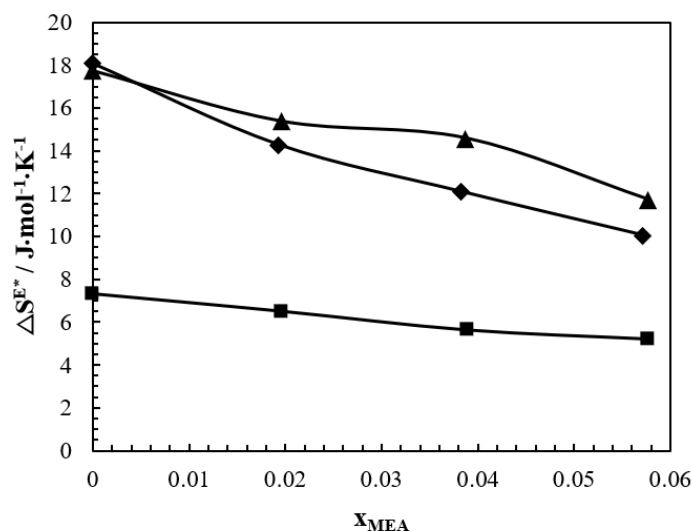
Figure 4. Excess free energy ΔG^{E*} of activation for the viscous flow of "■"—MDEA + MEA + H_2O, "◆"—DMEA + MEA + H_2O, and "▲"—DEEA + MEA + H_2O at 293.15 K.

The slope of the excess free energy of activation ΔG^{E*} against temperature T at certain mole fractions gives the excess entropy of activation ΔS^{E*} for the viscous flow:

$$\Delta S^{E*} = -\left[\frac{\partial \Delta G^{E*}}{\partial T}\right]. \qquad (15)$$

Figure 5 shows the excess entropy of activation ΔS^{E*} for the viscous flow of MDEA + MEA + H_2O, DMEA + MEA + H_2O, and DEEA + MEA + H_2O in the temperature range of 293.15 K–343.15 K over the whole range of concentrations. The values for ΔS^{E*} were determined using Equation (15). Figure 5 reveals that the excess entropy ΔS^{E*} followed the same trend as ΔG^{E*}, that is, ΔS^{E*} decreased with the increase of MEA concentration in the mixture. A maximum value for ΔS^{E*} was observed at solutions with 0 mass% MEA.
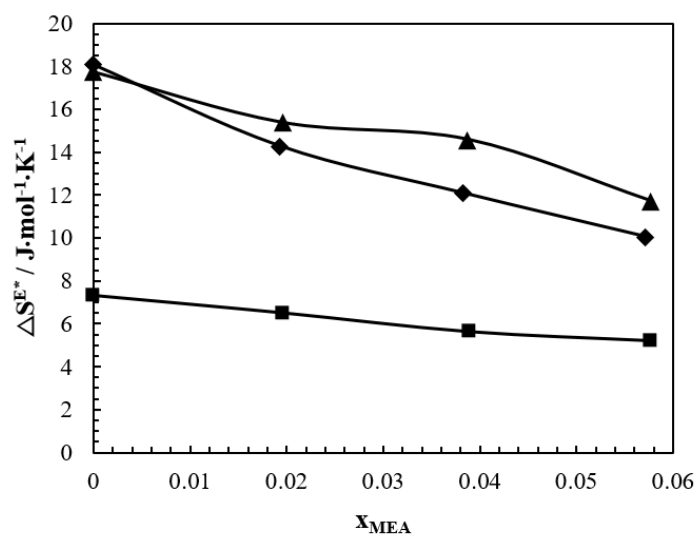
Figure 5. Excess entropy of activation ΔS^{E*} for the viscous flow of "■"—MDEA + MEA + H_2O, "◆"—DMEA + MEA + H_2O, and "▲"—DEEA + MEA + H_2O for a range of MEA mole fractions.

4. Conclusions

This paper discusses the densities and viscosities of MDEA + MEA + H_2O, DMEA + MEA + H_2O, and DEEA + MEA + H_2O mixtures at different concentrations of 15/15, 20/10, 25/5, and 30/0 for mass% (tertiary amine; MDEA, DMEA and DEEA)/mass% (primary amine; MEA) and temperatures.

The density of the mixtures was measured in the temperature range from 293.15 K to 343.15 K. The density of the mixtures increased with the increase of MDEA concentration and the density decreased with the increase of temperature for MDEA + MEA + H_2O mixtures. For the mixtures of DMEA + MEA + H_2O and DEEA + MEA + H_2O, the density decreased with the increase of DMEA and DEEA concentrations and the density decreased with the increase of temperature. The excess volume V^E of the mixtures was determined and were correlated according to a Redlich–Kister-type polynomial to represent the measured densities. A negative sign of the excess volume V^E indicates effective packing of the molecules and the presence of H-bonding among the unlike molecules. The proposed correlation was able to fit the density data with the acceptable accuracies of 0.013%, 0.004%, and 0.005% for *AARD* and 0.4 kg m^{-3}, 0.3 kg·m^{-3}, and 0.3 kg m^{-3} for *AMD* for the MDEA + MEA + H_2O, DMEA + MEA + H_2O, and DEEA + MEA + H_2O mixtures, respectively.

The viscosity of the mixtures was measured in the temperature range from 293.15 K to 363.15 K. The viscosity of the mixture increased with the increase of MDEA, DMEA, and DEEA concentration in the mixtures and the viscosity decreased with the increase of temperature. The viscosity deviation η^E was negative for the MDEA + MEA + H_2O at low temperatures, indicating weak intermolecular interactions in the mixture compared to the pure liquids. A positive η^E was reported for the DMEA + MEA + H_2O and DEEA + MEA + H_2O mixtures for the considered temperature range, signifying the presence of strong intermolecular interactions, such as H-bonds, in the mixtures. The excess free

energy of activation ΔG^{E*} for viscous flow, as described by Eyring, showed positive values for all mixtures for the temperature range. This highlights the existence of strong intermolecular interactions, such as H-bonds, between the molecules in the mixtures. The correlation proposed for the calculated ΔG^{E*} from measured densities and viscosities was able to fit the ΔG^{E*} with 0.15%, 0.09%, and 0.07% for *AARD* for the MDEA + MEA + H₂O, DMEA + MEA + H₂O, and DEEA + MEA + H₂O mixtures, respectively.

Supplementary Materials: The supplementary materials are available online at www.mdpi.com/2311-5521/5/1/27/s1.

Author Contributions: Supervision, L.E.Ø., K.J.J. and D.A.E.; Writing—original draft, S.S.K.

Conflicts of Interest: The authors declare no conflict of interest.

References

1. Metz, B.; Davidson, O.; Coninck, H.D.; Loos, M.; Meyer, L. *IPCC Special Report on Carbon Dioxide Capture and Storage*; Cambridge University Press: New York, NY, USA, 2005.

2. Idem, R.; Supap, T.; Shi, H.; Gelowitz, D.; Ball, M.; Campbell, C.; Tontiwachwuthikul, P. Practical experience in post-combustion CO₂ capture using reactive solvents in large pilot and demonstration plants. *Int. J. Greenh. Gas Control* **2015**, *40*, 6–25, doi:10.1016/j.ijggc.2015.06.005.

3. Singh, A.; Stéphenne, K. Shell Cansolv CO₂ capture technology: Achievement from First Commercial Plant. *Energy Procedia* **2014**, *63*, 1678–1685, doi:10.1016/j.egypro.2014.11.177.

4. Bernhardsen, I.M.; Knuutila, H.K. A review of potential amine solvents for CO₂ absorption process: Absorption capacity, cyclic capacity and pKa. *Int. J. Greenh. Gas Control* **2017**, *61*, 27–48, doi:10.1016/j.ijggc.2017.03.021.

5. da Silva, E.F.; Svendsen, H.F. Computational chemistry study of reactions, equilibrium and kinetics of chemical CO₂ absorption. *Int. J. Greenh. Gas Control* **2007**, *1*, 151–157, doi:10.1016/S1750-5836(07)00022-9.

6. Idris, Z.; Eimer, D.A. Density measurements of unloaded and CO₂ loaded 3 - Amino -1- propanol solutions at temperatures (293.15 to 353.15) K. *J. Chem. Eng. Data* **2016**, *61*, 173–181.

7. Hartono, A.; da Silva, E.F.; Grasdalen, H.; Svendsen, H.F. Qualitative Determination of Species in DETA−H₂O−CO₂ System Using 13C NMR Spectra. *Ind. Eng. Chem. Res.* **2007**, *46*, 249–254, doi:10.1021/ie0603868.

8. Hartono, A.; Svendsen, H.F. Density, viscosity, and excess properties of aqueous solution of diethylenetriamine (DETA). *J. Chem. Thermodyn.* **2009**, *41*, 973–979, doi:10.1016/j.jct.2008.11.012.

9. Jiang, W.; Luo, X.; Gao, H.; Liang, Z.; Liu, B.; Tontiwachwuthikul, P.; Hu, X. A comparative kinetics study of CO₂ absorption into aqueous DEEA/MEA and DMEA/MEA blended solutions *Aiche J.* **2017**, *64*, 1350–1358, doi:10.1002/aic.16024.

10. Kim, I.; Svendsen, H.F. Comparative study of the heats of absorption of post-combustion CO₂ absorbents. *Int. J. Greenh. Gas Control* **2011**, *5*, 390–395, doi:10.1016/j.ijggc.2010.05.003.

11. Zhang, J.; Fennell, P.S.; Trusler, J.P.M. Density and Viscosity of Partially Carbonated Aqueous Tertiary Alkanolamine Solutions at Temperatures between (298.15 and 353.15) K. *J. Chem. Eng. Data* **2015**, *60*, 2392–2399, doi:10.1021/acs.jced.5b00282.

12. Kidnay, A.J.; Parrish, W.R. *Fundamentals of Natural Gas Processing*; Taylor & Francis Group: Boca Raton, FL, USA, 2006.

13. Jou, F.-Y.; Carroll, J.J.; Mather, A.E.; Otto, F.D. The solubility of carbon dioxide and hydrogen sulfide in a 35 wt% aqueous solution of methyldiethanolamine. *Can. J. Chem. Eng.* **1993**, *71*, 264–268, doi:10.1002/cjce.5450710213.

14. Rinker, E.B.; Sami, S.A.; Sandall, O.C. Kinetics and modelling of carbon dioxide absorption into aqueous solutions of N-methyldiethanolamine. *Chem. Eng. Sci.* **1995**, *50*, 755–768, doi:10.1016/0009-2509(94)00444-V.

15. Daviet, G.R.; Sundermann, R.; Donnelly, S.T.; Bullin, J.A. Dome's North Caroline Plant Successful Conversion to MDEA. In Proceedings of the Sixty-Third GPA Annual Convention. Available online: https://www.bre.com/PDF/Dome's-North-Caroline-Plant-Successful-Conversion-to-MDEA.pdf (accessed on 3 January 2020).

16. Blanc, C.; Grall, M.; Demarais, G. Part played by degradation products in the corrosion of gas sweetening plants using DEA and MDEA. In Proceedings of the Annual Oklahoma University gas conditioning conference, Norman, OK, USA, 8 March 1982.

17. Kim, C.J.; Savage, D.W. Kinetics of carbon dioxide reaction with diethylaminoethanol in aqueous solutions. *Chem. Eng. Sci.* **1987**, *42*, 1481–1487, doi:10.1016/0009-2509(87)85020-0.

18. Henni, A.; Li, J.; Tontiwachwuthikul, P. Reaction kinetics of CO_2 in Aqueous 1-Amino-2-Propanol, 3-Amino-1-Propanol, and Dimethylmonoethanolamine solutions in the temperature range of 298−313 K using the stopped-flow technique. *Ind. Eng. Chem. Res.* **2008**, *47*, 2213–2220, doi:10.1021/ie070587r.

19. Chakravarty, T.; Phukan, U.K.; Weilund, R.H. Reaction of Acid gases with mixtures of amines. *Chem. Eng. Prog.* **1985**, *40*, 32–36.

20. Ramachandran, N.; Aboudheir, A.; Idem, R.; Tontiwachwuthikul, P. Kinetics of the Absorption of CO_2 into Mixed Aqueous Loaded Solutions of Monoethanolamine and Methyldiethanolamine. *Ind. Eng. Chem. Res.* **2006**, *45*, 2608–2616, doi:10.1021/ie0505716.

21. Conway, W.; Bruggink, S.; Beyad, Y.; Luo, W.; Melián-Cabrera, I.; Puxty, G.; Feron, P. CO_2 absorption into aqueous amine blended solutions containing monoethanolamine (MEA), N,N-dimethylethanolamine (DMEA), N,N-diethylethanolamine (DEEA) and 2-amino-2-methyl-1-propanol (AMP) for post-combustion capture processes. *Chem. Eng. Sci.* **2015**, *126*, 446–454, doi:10.1016/j.ces.2014.12.053.

22. Glasscock, D.A.; Critchfield, J.E.; Rochelle, G.T. CO_2 absorption/desorption in mixtures of methyldiethanolamine with monoethanolamine or diethanolamine. *Chem. Eng. Sci.* **1991**, *46*, 2829–2845, doi:10.1016/0009-2509(91)85152-N.

23. Li, M.H.; Shen, K.P. Densities and solubilities of solutions of Carbon Dioxide in water+Monoethanolamine+N-Methyldiethanolamine. *J. Chem. Eng. Data* **1992**, *37*, 288–290.

24. Li, M.-H.; Lie, Y.-C. Densities and viscosities of solutions of Monoethanolamine + N-Methyldiethanolamine + water and Monoethanolamine + 2-Amino-2-methyl-1-propanol + water. *J. Chem. Eng. Data* **1994**, *39*, 444–447.

25. Hagewiesche, D.P.; Ashour, S.S.; Sandall, O.C. Solubility and Diffusivity of Nitrous Oxide in Ternary Mixtures of Water, Monoethanolamine and N-Methyldiethanolamine and Solution Densities and Viscosities. *J. Chem. Eng. Data* **1995**, *40*, 627–629, doi:10.1021/je00019a020.

26. Harvey, A.H. *Thermodynamic Properties of Water*; NIST: Boulder, CO, USA, 1998.

27. JCGM. Evaluation of measurement data—Supplement 1 to the "Guide to the expression of uncertainty in measurement"—Propagation of distributions using a Monte Carlo method. Available online: https://www.bipm.org/utils/common/documents/jcgm/JCGM_101_2008_E.pdf (accessed on 3 January 2020).

28. Ellison, S.L.R.; Williams, A. *Quantifying Uncertainty in Analytical Measurement.* Available online: https://www.eurachem.org/images/stories/Guides/pdf/QUAM2012_P1.pdf (accessed on 3 January 2020).

29. Pinto, D.D.D.; Monteiro, J.G.M.S.; Johnsen, B.; Svendsen, H.F.; Knuutila, H. Density measurements and modelling of loaded and unloaded aqueous solutions of MDEA (N-methyldiethanolamine), DMEA (N,N-dimethylethanolamine), DEEA (diethylethanolamine) and MAPA (N-methyl-1,3-diaminopropane). *Int. J. Greenh. Gas Control* **2014**, *25*, 173–185, doi:10.1016/j.ijggc.2014.04.017.

30. Hawrylak, B.; Bruke, S.E.; Palepu, R. Partial molar and excess volumes and adiabatic compressibilities of binary mixtures of ethanolamines with water. *J. Solut. Chem.* **2000**, *29*, 575–593.

31. Maham, Y.; Teng, T.T.; Mather, A.E.; Hepler, L.G. Volumetric properties of (water + diethanolamine) systems. *Can. J. Chem* **1995**, *73*, 1514–1519.

32. Maham, Y.; Lebrette, L.; Mather, A.E. Viscosities and Excess Properties of Aqueous Solutions of Mono- and Diethylethanolamines at Temperatures between 298.15 and 353.15 K. *J. Chem. Eng. Data* **2002**, *47*, 550–553, doi:10.1021/je015528d.

33. Bernal-García, J.M.; Hall, K.R.; Estrada-Baltazar, A.; Iglesias-Silva, G.A. Density and viscosity of aqueous solutions of N,N-dimethylethanolamine at p=0.1 MPa from T=(293.15 to 363.15) K. *J. Chem. Thermodyn.* **2005**, *37*, 762–767, doi:10.1016/j.jct.2004.11.016.

34. Zhang, F.-Q.; Li, H.-P.; Dai, M.; Zhao, J.-P.; Chao, J.P. Volumetric properties of binary mixtures of water with ethanolamine alkyl derivatives. *Thermochim. Acta* **1995**, *254*, 347–357, doi:10.1016/0040-6031(94)02127-A.

35. Redlich, O.; Kister, A.T. Algebraic representation of thermodynamic properties and the classification of solutions. *Ind. Eng. Chem.* **1948**, *40*, 345–348.

36. Domínguez, M.; Rodríguez, S.; López, M.C.; Royo, F.M.; Urieta, J.S. Densities and Viscosities of the Ternary Mixtures 1-Butanol + 1-Chlorobutane + 1-Butylamine and 2-Methyl-1-propanol + 1-Chlorobutane + 1-Butylamine at 298.15 K. *J. Chem. Eng. Data* **1996**, *41*, 37–42, doi:10.1021/je950113b.

37. Samanta, A.; Bandyopadhyay, S.S. Density and Viscosity of Aqueous Solutions of Piperazine and (2-Amino-2-methyl-1-propanol + Piperazine) from 298 to 333 K. *J. Chem. Eng. Data* **2006**, *51*, 467–470, doi:10.1021/je050378i.

38. Hartono, A.; Mba, E.O.; Svendsen, H.F. Physical properties of partially CO_2 loaded aqueous monoethanolamine (MEA). *J. Chem. Eng. Data* **2014**, *59*, 1808–1816.

39. Weiland, R.H.; Dingman, J.C.; Cronin, D.B.; Browning, G.J. Density and viscosity of some partially carbonated aqueous alkanolamine solutions and their blends. *J. Chem. Eng. Data* **1998**, *43*, 378–382.

40. Moioli, S.; Pellegrini, L.A. Physical properties of PZ solution used as a solvent for CO_2 removal. *Chem. Eng. Res. Des.* **2015**, *93*, 720–726, doi:10.1016/j.cherd.2014.06.016.

41. Bhatia, S.C.; Bhatia, R.; Dubey, G.P. Studies on transport and thermodynamic properties of binary mixtures of octan-1-ol with chloroform, 1,2-dichloroethane and 1,1,2,2-tetrachloroethane at 298.15 and 308.15 K. *J. Mol. Liq.* **2009**, *144*, 163–171, doi:10.1016/j.molliq.2008.11.003.

42. Ma, D.; Liu, Q.; Zhu, C.; Feng, H.; Ma, Y. Volumetric and viscometric properties of ternary solution of (N-methyldiethanolamine + monoethanolamine + ethanol). *J. Chem. Thermodyn.* **2019**, *134*, 5–19, doi:10.1016/j.jct.2019.02.019.

43. Teng, T.T.; Maham, Y.; Hepler, L.G.; Mather, A.E. Viscosity of aqueous solutions of N-Methyldiethanolamine and of Diethanolamine. *J. Chem. Eng. Data* **1994**, *39*, 290–293.

44. Kummamuru, N.B.; Idris, Z.; Eimer, D.A. Viscosity Measurement and Correlation of Unloaded and CO_2-Loaded Aqueous Solutions of N-Methyldiethanolamine-Piperazine. *J. Chem. Eng. Data* **2019**, doi:10.1021/acs.jced.9b00021.

45. Chowdhury, F.I.; Akhtar, S.; Saleh, M.A.; Khandaker, M.U.; Amin, Y.M.; Arof, A.K. Volumetric and viscometric properties of aqueous solutions of some monoalkanolamines. *J. Mol. Liq.* **2016**, *223*, 299–314, doi:10.1016/j.molliq.2016.08.033.

46. DiGuilio, R.M.; Lee, R.J.; Schaeffer, S.T.; Brasher, L.L.; Teja, A.S. Densities and viscosity of the ethanolamines *J. Chem. Eng.* **1992**, *37*, 239–242.

47. Chen, S.; Zhang, L.; Zhang, Y.; Chen, S.; Chen, J. Density and viscosity of monoethylethanolamine+H_2O and monoethylethanolamine+diethylethanolamine solutions for CO_2 capture. *Thermochim. Acta* **2016**, *642*, 52–58, doi:10.1016/j.tca.2016.08.021.

48. Ma, D.; Zhu, C.; Fu, T.; Yuan, X.; Ma, Y. Volumetric and viscometric properties of binary and ternary mixtures of monoethanolamine, 2-(diethylamino) ethanol and water from (293.15 to 333.15) K. *J. Chem. Thermodyn.* **2019**, *138*, 350–365, doi:10.1016/j.jct.2019.06.032.

49. Fort, R.J.; Moore, W.R. Viscosities of binary liquid mixtures. *Trans. Faraday Soc.* **1966**, *62*, 1112–1119.

50. Domínguez, M.; Camacho, A.; López, M.C.; Royo, F.M.; Urieta, J.S. Excess molar volumes and excess viscosities of ternary mixtures (2-butanol + 1-chlorobutane + 1-butylamine) and (2-methyl-2-propanol + 1-chlorobutane + 1-butylamine) at 298. 15 K. *Can. J. Chem.* **1995**, *73*, 896–901, doi:10.1139/v95-112.

51. Rafiee, H.R.; Ranjbar, S.; Poursalman, F. Densities and viscosities of binary and ternary mixtures of cyclohexanone, 1,4-dioxane and isooctane from T=(288.15 to 313.15)K. *J. Chem. Thermodyn.* **2012**, *54*, 266–271, doi:10.1016/j.jct.2012.05.005.

52. Eyring, H. Viscosity, Plasticity, and Diffusion as example of absolute reaction rates. *J. Chem. Phys.* **1936**, *4*, 283–291.

53. Bird, R.B.; Stewart, W.E.; Lightfoot, E.N. *Transport PHENOMENA*, 2nd ed.; John Wiley & Sons, Inc.: Hoboken, NJ, USA, 2002.

54. Meyer, R.; Meyer, M.; Metzger, J.; Peneloux, A. Thermodynamic and physicochemical properties of binary solvent. *J. Chim. Phys. Phys. Chim. Biol.* **1971**, *68*, 406–412.

55. Domínguez, M.; Pardo, J.I.; Gascón, I.; Royo, F.M.; Urieta, J.S. Viscosities of the ternary mixture (2-butanol+n-hexane+1-butylamine) at 298.15 and 313.15 K. *Fluid Phase Equilibria* **2000**, *169*, 277–292, doi:10.1016/S0378-3812(00)00332-0.

56. Kinart, C.M.; Kinart, W.J.; Ćwiklińska, A. 2-Methoxyethanol–Tetrahydrofuran–Binary Liquid System. Viscosities, densities, excess molar volumes and excess Gibbs activation energies of viscous flow at various temperatures. *J. Therm. Anal. Calorim.* **2002**, *68*, 307–317, doi:10.1023/A:1014981921097.

57. Ćwiklińska, A.; Kinart, C.M. Thermodynamic and physicochemical properties of binary mixtures of nitromethane with {2-methoxyethanol+2-butoxyethanol} systems at T=(293.15, 298.15, 303.15, 308.15, and 313.15)K. *J. Chem. Thermodyn.* **2011**, *43*, 420–429, doi:10.1016/j.jct.2010.10.016.

Supporting Document

MATLAB code for data fitting into the density correlation

```
load('VE.mat');
load('x.mat');

model=@(p,x)x(:,1).*x(:,2).*(p(1)+p(2).*x(:,4)+p(3).*(x(:,4).^2)+(x(:,1)-
x(:,2)).*(p(4)+p(5).*x(:,4)+p(6).*(x(:,4).^2))+((x(:,1)-
x(:,2)).^2).*(p(7)+p(8).*x(:,4)+p(9).*(x(:,4).^2)))+x(:,2).*x(:,3).*(p(10)+
p(11).*x(:,4)+p(12).*(x(:,4).^2)+(x(:,2)-
x(:,3)).*(p(13)+p(14).*x(:,4)+p(15).*(x(:,4).^2))+((x(:,2)-
x(:,3)).^2).*(p(16)+p(17).*x(:,4)+p(18).*(x(:,4).^2)))+x(:,1).*x(:,3).*(p(1
9)+p(20).*x(:,4)+p(21).*(x(:,4).^2)+(x(:,1)-
x(:,3)).*(p(22)+p(23).*x(:,4)+p(24).*(x(:,4).^2))+((x(:,1)-
x(:,3)).^2).*(p(25)+p(26).*x(:,4)+p(27).*(x(:,4).^2)))

% x=(Xamine1,Xamine2,XH2O,Temperature)

pinitial = rand(1,27);

[beta,R,J,CovB,MSE]=nlinfit(x,VE,model,pinitial);

y=x(:,1).*x(:,2).*(beta(1)+beta(2).*x(:,4)+beta(3).*x(:,4).^2+(x(:,1)-
x(:,2)).*(beta(4)+beta(5).*x(:,4)+beta(6).*x(:,4).^2)+((x(:,1)-
x(:,2)).^2).*(beta(7)+beta(8).*x(:,4)+beta(9).*x(:,4).^2))+x(:,2).*x(:,3).*
(beta(10)+beta(11).*x(:,4)+beta(12).*x(:,4).^2+(x(:,2)-
x(:,3)).*(beta(13)+beta(14).*x(:,4)+beta(15).*x(:,4).^2)+((x(:,2)-
x(:,3)).^2).*(beta(16)+beta(17).*x(:,4)+beta(18).*x(:,4).^2))+x(:,1).*x(:,3
).*(beta(19)+beta(20).*x(:,4)+beta(21).*x(:,4).^2+(x(:,1)-
x(:,3)).*(beta(22)+beta(23).*x(:,4)+beta(24).*x(:,4).^2)+((x(:,1)-
x(:,3)).^2).*(beta(25)+beta(26).*x(:,4)+beta(27).*x(:,4).^2));

plot(x(:,4),VE,x(:,4),y)
```

MATLAB code for data fitting into the viscosity correlation

```
load('GE.mat');
load('x.mat');

model=@(p,x)x(:,1).*x(:,2).*(p(1)+p(2).*x(:,4)+p(3).*x(:,4).^2+(x(:,1)-
x(:,2)).*(p(4)+p(5).*x(:,4)+p(6).*x(:,4).^2)+((x(:,1)-
x(:,2)).^2).*(p(7)+p(8).*x(:,4)+p(9).*x(:,4).^2))+x(:,2).*x(:,3).*(p(10)+p(
11).*x(:,4)+p(12).*x(:,4).^2+(x(:,2)-
x(:,3)).*(p(13)+p(14).*x(:,4)+p(15).*x(:,4).^2)+((x(:,2)-
x(:,3)).^2).*(p(16)+p(17).*x(:,4)+p(18).*x(:,4).^2))+x(:,1).*x(:,3).*(p(19)
+p(20).*x(:,4)+p(21).*x(:,4).^2+(x(:,1)-
x(:,3)).*(p(22)+p(23).*x(:,4)+p(24).*x(:,4).^2)+((x(:,1)-
x(:,3)).^2).*(p(25)+p(26).*x(:,4)+p(27).*x(:,4).^2))

% x=(Xamine1,Xamine2,XH2O,Temperature)

pinitial = rand(1,27);

[beta,R,J,CovB,MSE]=nlinfit(x,GE,model,pinitial);
```

```
y=x(:,1).*x(:,2).*(beta(1)+beta(2).*x(:,4)+beta(3).*x(:,4).^2+(x(:,1)-
x(:,2)).*(beta(4)+beta(5).*x(:,4)+beta(6).*x(:,4).^2)+((x(:,1)-
x(:,2)).^2).*(beta(7)+beta(8).*x(:,4)+beta(9).*x(:,4).^2))+x(:,2).*x(:,3).*
 (beta(10)+beta(11).*x(:,4)+beta(12).*x(:,4).^2+(x(:,2)-
x(:,3)).*(beta(13)+beta(14).*x(:,4)+beta(15).*x(:,4).^2)+((x(:,2)-
x(:,3)).^2).*(beta(16)+beta(17).*x(:,4)+beta(18).*x(:,4).^2))+x(:,1).*x(:,3
).*(beta(19)+beta(20).*x(:,4)+beta(21).*x(:,4).^2+(x(:,1)-
x(:,3)).*(beta(22)+beta(23).*x(:,4)+beta(24).*x(:,4).^2)+((x(:,1)-
x(:,3)).^2).*(beta(25)+beta(26).*x(:,4)+beta(27).*x(:,4).^2));

plot(x(:,4),GE,x(:,4),y)
```

Article D

Density, viscosity and excess properties of binary aqueous mixtures of MDEA + H_2O, DMEA + H_2O and DEEA + H_2O.

Karunarathne, S.S.; Eimer, D.A.; Øi, L.E. Paper submitted in journal of **Applied Science** and is under review. The initial manuscript submitted to the journal is attached in this thesis.

1 *Type of the Paper (Article)*

2 Density, Viscosity and Excess Properties of MDEA +
3 H2O, DMEA + H2O and DEEA + H2O mixtures.

4 **Sumudu S. Karunarathne, Dag A. Eimer and Lars E. Øi***

5 Faculty of Technology, Natural Sciences and Maritime Studies, University of South-Eastern Norway, Kjølnes
6 Ring 56, 3901 Porsgrunn, Norway; sumuduunimrt@gmail.com (S.S.K.); Dag.A.Eimer@usn.no (D.A.E.)
7 * Correspondence: lars.oi@usn.no; Tel.: +47-35-575-141

9 **Abstract:** This study presents measured density and viscosity of MDEA (N-methyldiethanolamine)
10 + H2O, DMEA (Dimethylethanolamine) + H2O and DEEA (Diethylethanolamine) + H2O mixtures.
11 The density was measured at amine mass fraction w_1 from 0.3 to 1 for the temperature range 293.15
12 K-353.15 K. The excess molar volumes V^E were determined from density data. Redlich-Kister type
13 polynomials were proposed to fit V^E and density deviation $ln(\rho_\gamma)$ to represent measured
14 densities. The viscosity was measured at amine mass fraction w_1 from 0.3 to 1 for the temperature
15 range 293.15 K-363.15 K. The viscosity deviation η^E and excess free energy of activation for viscous
16 flow ΔG^{E*} were determined from measured viscosities and examined for intermolecular
17 interactions among mixture molecules. Correlations were proposed to fit viscosity data with
18 acceptable accuracies. The McAllister's three-body model was adopted to fit kinematic viscosities
19 determined from density and dynamic viscosity data. The results showed the importance of
20 examining intermolecular interactions that are discussed in McAllister's four-body model to
21 improve the accuracies of data fits.

22 **Keywords:** density; viscosity; MDEA; DMEA; DEEA; McAllister

23
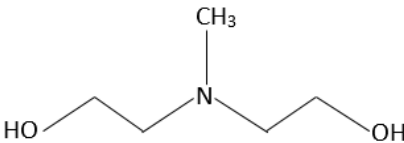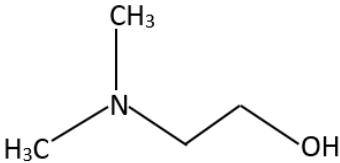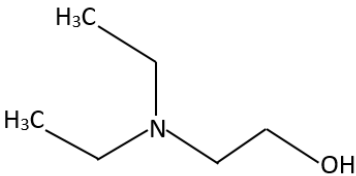
24 1. Introduction

25   Amine based post-combustion CO2 capture (PCC) is a widely discussed emission control
26 approach in which CO2 in flue gas is captured though chemical absorption. The technology has
27 proven the capability of over 90% of CO2 removal efficiency and making amine based PCC as a
28 reliable and economical technology [1,2]. Primary amines are highly reactive compared to secondary
29 and tertiary amines and monoethanol amine (MEA) is the most basic of the amines in acid gas
30 treating. The PCC with MEA is regarded as the benchmark process to compare and evaluate
31 performance of processes with different amines for the CO2 capture performance, energy utilization
32 and amine degradation. Tertiary amines exhibit a low absorption rate, nevertheless fast desorption
33 rate and high absorption capacity compared to primary amines like MEA are advantages. The
34 reaction between CO2 and MEA forms stable carbamate that limits a theoretical absorption capacity
35 at 0.5 mol CO2 / mol amine [3].
36   Tertiary aqueous amines like MDEA (N-methyldiethanolamine), DMEA
37 (Dimethylethanolamine) and DEEA (Diethylethanolamine) have been studied for performance in
38 CO2 removal [4-7]. The low reaction heat of tertiary amines with CO2 reduce the energy penalty due
39 to the CO2 stripping, which make the technology more feasible to use [6]. Tertiary amines do not
40 generate carbamate during the reaction with CO2 and bicarbonate is formed as the only CO2 carrying
41 specie. This leads to increase the theoretical CO2 absorption capacity up to 1 mol CO2 / mol amine [3].
42 The characteristics shown by DMEA and DEEA in CO2 absorption indicate them as alternative
43 solvents for the CO2 caption processes [6,8].

44

45 **Table 1.** Molecular structures and IUPAC names of MDEA, DMEA and DEEA

N-methyldiethanolamine (MDEA)

2-(2-Hydroxyethyl-methyl-amino)ethanol

Dimethylethanolamine (DMEA)

2-(dimethylamino)ethanol

Diethylethanolamine (DEEA)

2-(diethylamino)ethanol

46
47   Physical properties of amine solvents are useful in various aspects in process design, equipment
48 sizing, mathematical modeling and simulations. Density data are useful to evaluate physical
49 solubility of CO_2 in solvent, mass transfer and solvent kinetics. Viscosity data are important to
50 estimate diffusivity using modified Stoke-Einstein equation [9] that is required perform calculation
51 of mass transfer and kinetics properties [10]. This study provides measured density and viscosity
52 data of aqueous MDEA, DMEA and DEEA mixtures at different concentrations and temperatures.
53 The excess properties evaluated from measured data were compared by discussing the molecular
54 structure and intermolecular interactions of the different tertiary amines. Density and viscosity
55 correlations were fitted to the measured data and accuracy of the data fit were analyzed through
56 average absolute relative deviation (AARD %) and absolute maximum deviation (AMD).

57 **2. Materials and Methods**

58 *2.1. Sample preparation*

59   A description of the materials used in this work is listed in Table 2. A series of aqueous amine
60 mixtures were prepared by mixing amines and water with different mass fractions. The deionized
61 water (resistivity: 18.2 MΩ·cm) was degassed using a rotary evaporator (R-210, Buchi, Flawil,
62 Switzerland) and used for the sample preparations. For the weight measurements, an electronic
63 balance model: XS-403S from Mettler Toledo (Greifensee, Switzerland) with a resolution of 1 mg was
64 used to make a sample with 150 mL at each different amine concentrations.

65 **Table 2.** Material description

Chemical Name	CAS no	Source	Mole fraction Purity	Purification
MDEA	105-59-9	Merck KGaA	≥0.98	no
DEEA	100-37-8	Sigma-Aldrich	≥0.995	no
DMEA	108-01-0	Alfa Aesar	≥0.99	no

66

67

68   *2.2. Density measurements*

69   The density measurements of aqueous amine mixtures were performed using a DMA 4500
70   density meter from Anton Paar operating at atmospheric pressure. The DMA 4500 is an oscillating
71   U-tube density meter with an accuracy of ±0.05 kg·m⁻³. The calibration of density meter was carried
72   out using air and H_2O at 293.15 K and a density check was performed with H_2O at 293.15 K frequently
73   to observe the validity of previous calibration. Additionally, the density of a density reference
74   standard S3S from Paragon Scientific Ltd was measured and was compared with reference values to
75   examine any possible deviations. A sample with approximately 5 mL was introduced to the
76   borosilicate glass U-tube (~ 0.7 mL) using a syringe and allowed to reach the desired temperature
77   before the density was measured. The cell was cleaned with water followed by ethanol and dried
78   with air before the next density measurement. A new sample was fed into the cell during the
79   experiments at each different temperature levels. Final density was reported as an average of three
80   replicates.

81   *2.3. Viscosity measurements*

82   A double-gap pressure cell XL in Physica MCR 101 rheometer from Anton Paar was adopted to
83   perform dynamic viscosity measurements in aqueous amine mixtures. The solution temperature (>
84   303.15 K) was controlled by an internal temperature controlling system with standard temperature
85   uncertainty 0.03 K. For the temperatures below 303.15 K, an external Anton Paar Viscotherm VT2
86   cooling system with standard temperature uncertainty 0.02 K was used to acquire precise
87   temperature control [11]. In the experiments, a liquid sample with a volume of 7mL was transferred
88   into the pressure cell using a syringe. An adequate time was given to the sample to reach the desired
89   temperature before taking the viscosity measurements. The experiments were repeated for three
90   times and the final viscosity was reported as the average of 120 different readings at each temperature
91   levels. An air check and motor adjustment were carried out prior to the experiments as suggested by
92   Anton Paar to examine the performance of the bearing in the rotating parts. A generally used
93   viscosity reference standard S3S from Paragon Scientific Ltd was used to calibrate the measuring
94   system at different temperatures. The possible viscosity deviations were recorded by comparing
95   measured viscosity of standard oil with reference values at corresponding temperatures provided by
96   the supplier and corrections for the measured viscosity were made accordingly. For the temperature
97   levels not defined by the supplier, viscosity deviations were found by interpolation.

98   *2.4. Measurement uncertainty*

99   Following uncertainty sources of material purity $u(p)$, temperature measurement $u(T)$, weight
100   measurement $u(w)$, and repeatability $u(rep)$ were considered to evaluate combined standard
101   uncertainty of density and viscosity measurements of aqueous amine mixtures.

102   The specified standard uncertainties for the uncertainty of density measurement were $u(p)$ =
103   ±0.006, $u(T)$ = ±0.012 K, $u(w)$ = ±2 × 10⁻⁴ kg, and $u(rep)$ = ±0.13 kg·m⁻³. The maximum gradient of
104   density against temperature, $\partial\rho/\partial T$, was found to be 1.22 kg·m⁻³·K⁻¹ and the corresponding
105   uncertainty in ρ, $(\partial\rho/\partial T)\cdot u(T)$, was determined to be ±0.015 kg·m⁻³. The combined standard
106   uncertainty for the density measurement was calculated as described in the Guide to the Expression
107   of Uncertainty in Measurement [27,28] by considering all mentioned uncertainty sources to be $u(\rho)$
108   = ±5.95 kg·m⁻³. Then, the combined expanded uncertainty of the density measurement $U(\rho)$ was
109   found to be ±11.9 kg·m⁻³ (level of confidence = 0.95).

110   For the uncertainty of viscosity measurement, specified standard uncertainties for the
111   uncertainty sources were $u(p)$ = ±0.012, $u(T)$ = ±0.012 K, $u(w)$ = ±2 × 10⁻⁴ kg, and $u(rep)$ = ±0.008
112   mPa·s. Then the combined standard uncertainty for the viscosity measurement was calculated to be
113    $u(\eta)$ = ±0.008 mPa·s. The combined expanded uncertainty of the viscosity measurement $U(\eta)$ was
114   found to be ±0.016 mPa·s (level of confidence = 0.95).

115

116 **3. Results and discussion**

117 *3.1. Density and excess molar volume of the binary mixtures*

118   The measured densities of pure MDEA, DMEA and DEEA in the temperature range from 293.15
119 K to 353.15 K under atmospheric pressure are listed in Table 3. A comparison of measured densities
120 of pure amines in this study with available literature data indicates that the instrument was calibrated
121 properly prior to all experiments. Density of aqueous amine mixtures were measured in the
122 temperature range from 293.15 K to 343.15 K under atmospheric pressure. The measured densities
123 are presented in Table 4, Table 5 and Table 6 under different mass fractions, mole fractions and
124 temperatures.

125

126   **Table 3.** Measured density (ρ / kg·m^{-3}) of pure amines MDEA, DMEA and DEEA.

T / K	MDEA		DMEA		DEEA	
	This work	Literature	This work	Literature	This work	Literature
293.15	1040.6		887.9	887.5[d]	884.3	884.2[d]
298.15	1036.8	1036.8[a],	883.7	883.3[a]	879.7	879.5[a]
		1035.9[b]		882.6[c]		879.5[d]
				883.1[d]		879.3[e]
303.15	1033.1	1032.0[b]	879.4	878.4[c]	875.1	874.8[d]
				878.9[d]		874.6[e]
308.15	1029.3	1029.0[a]	875.1	875.5[a]	870.4	871.4[a]
313.15	1025.5	1024.5[b]	870.8	869.9[c]	865.8	865.6[d]
				870.3[d]		865.0[e]
318.15	1021.7	1022.6[a]	866.4	867.3[a]	861.1	861.8[a]
323.15	1017.9	1016.7[b]	862.0		856.3	
328.15	1014.0		857.6		851.6	
333.15	1010.2	1009.0[b]	853.1	851.9[c]	846.8	846.5[e]
338.15	1006.3		848.6		841.9	
343.15	1002.4	1001.2[b]	843.8		837.1	
348.15	998.5		839.6		832.3	
353.15	994.6	993.7[b]	834.7	833.8[c]	827.4	827.2[e]

127 Literature references: [a] Hawrylak, *et al.* [12], [b] Maham, *et al.* [13], [c] Maham, *et al.* [14], [d] Zhang, *et al.* [15], [e]
128 Lebrette, *et al.* [16]

129

Table 4. Measured density (ρ / kg·m^{-3}) and deduced excess molar volume (V^E/ m^3·mol^{-1}) of MDEA (1) + H$_2$O (2) mixtures.

T / K	[a]w_1 0.30		0.40		0.50		0.60		0.70		0.80		0.90		0.94		0.97	
	[b]x_1 0.0609		0.0916		0.1313		0.1849		0.2608		0.3768		0.5764		0.7031		0.8302	
	ρ	$V^E \times 10^6$	ρ	$V^E \times 10^6$	ρ	$V^E \times 10^6$	ρ	$V^E \times 10^6$	ρ	$V^E \times 10^6$	ρ	$V^E \times 10^6$	ρ	$V^E \times 10^6$	ρ	$V^E \times 10^6$	ρ	$V^E \times 10^6$
293.15	1026.9	-0.381	1036.8	-0.572	1045.6	-0.784	1052.5	-0.998	1056.5	-1.185	1056.0	-1.245	1050.7	-1.018	1046.8	-0.730	1043.7	-0.422
298.15	1024.7	-0.376	1034.2	-0.563	1042.6	-0.770	1049.2	-0.981	1052.9	-1.167	1052.4	-1.231	1047.0	-1.011	1043.2	-0.727	1040.1	-0.423
303.15	1022.4	-0.372	1031.5	-0.554	1039.5	-0.757	1045.7	-0.964	1049.3	-1.149	1048.6	-1.214	1043.3	-0.999	1039.4	-0.721	1036.3	-0.419
308.15	1019.9	-0.368	1028.6	-0.546	1036.3	-0.744	1042.2	-0.947	1045.6	-1.130	1044.9	-1.198	1039.5	-0.989	1035.7	-0.714	1032.6	-0.415
313.15	1017.3	-0.364	1025.6	-0.539	1033.0	-0.733	1038.6	-0.932	1041.8	-1.114	1041.0	-1.182	1035.7	-0.980	1031.8	-0.709	1028.8	-0.415
318.15	1014.5	-0.360	1022.5	-0.532	1029.6	-0.722	1035.0	-0.918	1038.0	-1.098	1037.1	-1.166	1031.8	-0.969	1028.0	-0.702	1024.9	-0.411
323.15	1011.7	-0.357	1019.4	-0.525	1026.1	-0.711	1031.2	-0.903	1034.1	-1.080	1033.2	-1.150	1027.9	-0.958	1024.1	-0.695	1021.1	-0.404
328.15	1008.7	-0.354	1016.1	-0.519	1022.5	-0.701	1027.4	-0.889	1030.2	-1.064	1029.2	-1.133	1024.0	-0.946	1020.2	-0.686	1017.2	-0.400
333.15	1005.5	-0.349	1012.7	-0.512	1018.9	-0.691	1023.6	-0.875	1026.2	-1.047	1025.1	-1.116	1020.0	-0.934	1016.3	-0.679	1013.3	-0.396
338.15	1002.2	-0.345	1009.2	-0.505	1015.1	-0.680	1019.6	-0.861	1022.1	-1.030	1021.0	-1.098	1015.8	-0.912	1012.3	-0.668	1009.4	-0.393
343.15	998.6	-0.335	1005.4	-0.492	1011.3	-0.670	1015.6	-0.847	1018.0	-1.013	1016.9	-1.080	1011.9	-0.909	1008.3	-0.659	1005.5	-0.388
348.15			1001.5	-0.481	1007.4	-0.659	1011.5	-0.832	1013.8	-0.995	1012.7	-1.062	1007.8	-0.895	1004.3	-0.649	1001.5	-0.383
353.15			996.9	-0.450	1003.4	-0.646	1007.3	-0.813	1009.5	-0.977	1008.4	-1.042	1003.7	-0.879	1000.3	-0.636	997.5	-0.375

[a] mass fraction, [b] mole fraction of MDEA

Table 5. Measured density (ρ / kg·m^{-3}) and deduced excess molar volume (V^E/ m^3·mol^{-1}) of DMEA (1) + H$_2$O (2) mixtures.

T / K	[a]w_1 0.30		0.40		0.50		0.60		0.70		0.80		0.90		0.94		0.97	
	[b]x_1 0.0797		0.1187		0.1681		0.2326		0.3204		0.4470		0.6452		0.7600		0.8673	
	ρ	$V^E \times 10^6$	ρ	$V^E \times 10^6$	ρ	$V^E \times 10^6$	ρ	$V^E \times 10^6$	ρ	$V^E \times 10^6$	ρ	$V^E \times 10^6$	ρ	$V^E \times 10^6$	ρ	$V^E \times 10^6$	ρ	$V^E \times 10^6$
293.15	991.0	-0.712	987.1	-1.020	979.9	-1.305	969.3	-1.550	954.9	-1.704	936.6	-1.678	914.2	-1.274	904.2	-0.931	896.5	-0.567
298.15	988.2	-0.704	983.8	-1.004	976.2	-1.286	965.4	-1.534	950.9	-1.692	932.6	-1.675	910.1	-1.279	900.2	-0.941	892.4	-0.579
303.15	985.4	-0.696	980.3	-0.990	972.3	-1.268	961.4	-1.518	946.8	-1.680	928.4	-1.668	906.0	-1.284	896.0	-0.947	888.3	-0.589
308.15	982.4	-0.689	976.8	-0.977	968.4	-1.253	957.3	-1.502	942.7	-1.669	924.3	-1.666	901.8	-1.287	891.8	-0.956	884.0	-0.591
313.15	979.2	-0.683	973.1	-0.965	964.5	-1.239	953.2	-1.488	938.4	-1.659	920.0	-1.661	897.5	-1.291	887.6	-0.960	879.7	-0.596
318.15	976.0	-0.679	969.5	-0.957	960.5	-1.226	949.0	-1.476	934.1	-1.649	915.7	-1.657	893.3	-1.295	883.3	-0.964	875.4	-0.601
323.15	972.7	-0.674	965.7	-0.948	956.4	-1.215	944.7	-1.464	929.8	-1.640	911.3	-1.653	888.9	-1.298	878.9	-0.968	871.0	-0.603

328.15	969.3	-0.670	961.9	-0.941	952.3	-1.205	940.4	-1.454	925.4	-1.632	906.9	-1.649	884.5	-1.301	874.5	-0.973	866.6	-0.605
333.15	965.8	-0.668	958.0	-0.934	948.1	-1.195	936.0	-1.444	920.9	-1.624	902.4	-1.645	880.0	-1.301	870.0	-0.973	862.2	-0.611
338.15	962.1	-0.665	954.0	-0.928	943.8	-1.187	931.5	-1.435	916.4	-1.616	897.9	-1.643	875.5	-1.304	865.6	-0.980	857.6	-0.613
343.15	958.3	-0.663	950.0	-0.928	939.5	-1.184	927.0	-1.433	911.8	-1.617	893.2	-1.650	870.9	-1.322	861.0	-1.007	853.1	-0.642
348.15	954.3	-0.652	945.7	-0.914	935.1	-1.170	922.4	-1.414	907.1	-1.596	888.6	-1.625	866.3	-1.292	856.4	-0.973	848.5	-0.604
353.15	950.4	-0.653	941.5	-0.912	930.7	-1.172	917.8	-1.413	902.3	-1.596	882.5	-1.546	861.6	-1.306	851.7	-0.989	843.9	-0.633

[a] mass fraction, [b] mole fraction of DMEA

Table 6. Measured density (ρ / kg·m^{-3}) and deduced excess molar volume (V^E/ m^3·mol^{-1}) of DEEA (1) + H$_2$O (2) mixtures.

T / K	[a]w_1	0.30		0.40		0.50		0.60		0.70		0.80		0.90		0.94		0.97	
	[b]x_1	0.0618		0.0930		0.1332		0.1874		0.2640		0.3808		0.5805		0.7066		0.8325	
		ρ	$V^E \times 10^6$	ρ	$V^E \times 10^6$	ρ	$V^E \times 10^6$	ρ	$V^E \times 10^6$	ρ	$V^E \times 10^6$	ρ	$V^E \times 10^6$	ρ	$V^E \times 10^6$	ρ	$V^E \times 10^6$	ρ	$V^E \times 10^6$
293.15		989.6	-0.724	983.2	-0.990	974.6	-1.258	963.9	-1.531	950.8	-1.786	934.4	-1.941	912.9	-1.706	902.4	-1.313	893.6	-0.788
298.15		986.6	-0.712	979.7	-0.973	970.7	-1.240	959.8	-1.513	946.5	-1.771	930.0	-1.932	908.5	-1.707	897.9	-1.319	889.1	-0.800
303.15		983.4	-0.701	976.0	-0.957	966.7	-1.222	955.6	-1.497	942.0	-1.755	925.4	-1.922	903.9	-1.705	893.3	-1.321	884.5	-0.802
308.15		980.2	-0.692	972.3	-0.944	962.6	-1.206	951.2	-1.481	937.6	-1.742	920.8	-1.913	899.2	-1.695	888.7	-1.327	879.9	-0.808
313.15		976.8	-0.684	968.5	-0.931	958.5	-1.191	946.8	-1.465	933.0	-1.727	916.1	-1.898	894.6	-1.699	884.0	-1.324	875.2	-0.809
318.15		973.4	-0.676	964.6	-0.920	954.3	-1.177	942.4	-1.450	928.4	-1.712	911.4	-1.888	889.8	-1.693	879.3	-1.324	870.5	-0.812
323.15		969.8	-0.669	960.6	-0.909	950.0	-1.164	937.8	-1.436	923.6	-1.698	906.6	-1.875	884.9	-1.677	874.5	-1.322	865.7	-0.809
328.15		966.2	-0.663	956.5	-0.900	945.6	-1.152	933.2	-1.422	918.8	-1.683	901.7	-1.861	880.2	-1.679	869.7	-1.316	861.0	-0.807
333.15		962.4	-0.657	952.4	-0.890	941.1	-1.140	928.5	-1.407	914.0	-1.666	896.8	-1.850	875.3	-1.668	864.8	-1.308	856.1	-0.804
338.15		958.5	-0.651	948.2	-0.881	936.6	-1.127	923.8	-1.393	909.1	-1.650	891.7	-1.822	870.3	-1.655	859.9	-1.294	851.3	-0.804
343.15		954.6	-0.645	943.8	-0.872	932.0	-1.115	919.0	-1.379	904.1	-1.633	886.6	-1.806	865.3	-1.639	854.9	-1.282	846.4	-0.799
348.15		950.5	-0.641	939.5	-0.863	927.3	-1.102	914.1	-1.363	899.1	-1.617	881.5	-1.786	860.2	-1.621	849.9	-1.270	841.4	-0.788
353.15		946.3	-0.632	935.0	-0.853	922.6	-1.091	909.1	-1.346	893.8	-1.592	876.3	-1.763	855.0	-1.599	844.8	-1.252	836.4	-0.776

[a] mass fraction, [b] mole fraction of DEEA

Table 8. Partial molar volume $\overline{V_1^\infty}$ / m³·mol⁻¹ of MDEA, DMEA and DEEA at infinite dilution in H₂O and molar volume of pure species V_1^0 / m³·mol⁻¹ at various temperatures.

T / K	MDEA (1) at infinite dilution in H₂O (2)			DMEA (1) at infinite dilution in H₂O (2)			DEEA (1) at infinite dilution in H₂O (2)		
	$\overline{V_1^\infty} \times 10^6$	$\overline{V_1^\infty} \times 10^6$ Literature	$V_1^0 \times 10^6$	$\overline{V_1^\infty} \times 10^6$	$\overline{V_1^\infty} \times 10^6$ Literature	$V_1^0 \times 10^6$	$\overline{V_1^\infty} \times 10^6$	$\overline{V_1^\infty} \times 10^6$ Literature	$V_1^0 \times 10^6$
293.15	108.7		114.5	92.0	93.6[c,d]	100.4	118.9	122.1[d,e]	132.5
298.15	109.1	109.5[a], 108.9[b]	114.9	92.4	93.7[b], 94.1[c], 93.9[c,d]	100.9	119.6	117.6[b], 122.6[e], 122.7[d,e]	133.2
303.15	109.6	110.7[a]	115.3	92.8	94.3[c], 94.2[c,d]	101.4	120.4	123.0[e], 122.7[d,e]	133.9
308.15	110.0	110.0[b]	115.8	93.3	95.7[b]	101.9	121.2	118.0[b]	134.6
313.15	110.5	110.7[a]	116.2	93.7	94.8[c], 94.9[c,d]	102.4	122.0	123.7[e], 123.6[d,e]	135.4
318.15	110.9	110.7[b]	116.6	94.2	97.2[b]	102.9	122.8	118.3[b]	136.1
323.15	111.4	111.4[a]	117.1	94.6		103.4	123.6		136.9
328.15	111.8		117.5	95.1		103.9	124.4		137.6
333.15	112.3	112.5[a]	118.0	95.6	96.3[c]	104.5	125.2	125.3[e]	138.4
338.15	112.8		118.4	96.1		105.0	126.1		139.2
343.15	113.3	113.1[a]	118.9	96.6		105.6	126.9		140.0
348.15	113.7		119.3	97.1		106.2	127.8		140.8
353.15	114.2	113.8[a]	119.8	97.6	98.1[c]	106.8	128.7	128.0[e]	141.6

Literature references: [a]Maham, *et al.*[13], [b]Hawrylak, *et al.*[12], [c]Maham, *et al.*[14], [d]Zhang, *et al.*[15], [e]Lebrette, *et al.*[16]

Table 11. Measured viscosity (η / mPa·s) and deduced viscosity deviation (η^E/ mPa·s) of MDEA (1) + H₂O (2) mixtures.

T / K	[a]w_1 0.30 [b]x_1 0.0609		0.40 0.0916		0.50 0.1313		0.60 0.1849		0.70 0.2608		0.80 0.3768		0.90 0.5764		0.94 0.7031		0.97 0.8302	
	η	η^E	η	η^E	η	η^E	η	η^E	η	η^E	η	η^E	η	η^E	η	η^E	η	η^E
293.15	3.712	-3.358	6.410	-3.723	11.633	-2.465	21.915	2.480	42.784	15.778	76.266	37.686	107.892	49.414	111.511	40.394	108.675	24.890
298.15	3.136	-2.319	5.290	-2.468	9.323	-1.418	16.721	1.965	32.161	11.711	56.123	26.967	79.249	35.126	82.357	28.727	80.921	17.762
303.15	2.673	-1.594	4.410	-1.609	7.561	-0.725	13.075	1.737	24.522	8.854	41.834	19.548	58.937	25.273	61.546	20.654	60.950	12.815
308.15	2.301	-1.090	3.721	-1.018	6.200	-0.285	10.404	1.570	18.988	6.821	31.721	14.458	44.492	18.469	46.689	15.102	46.555	9.390
313.15	1.995	-0.742	3.170	-0.618	5.152	0.002	8.418	1.435	14.936	5.354	24.435	10.879	34.108	13.719	35.949	11.220	36.084	7.005
318.15	1.748	-0.496	2.732	-0.343	4.335	0.183	6.916	1.315	11.930	4.273	19.137	8.338	26.566	10.363	28.108	8.473	28.378	5.304
323.15	1.544	-0.322	2.376	-0.155	3.683	0.289	5.759	1.205	9.659	3.460	15.206	6.490	20.977	7.936	22.277	6.489	22.607	4.065

T/K	η	η^E	η	η^E	η	η^E	η	η^E	η	η^E	η	η^E	η	η^E	η	η^E	η	η^E
328.15	1.376	-0.199	2.088	-0.027	3.168	0.353	4.863	1.106	7.938	2.846	12.272	5.138	16.823	6.179	17.927	5.053	18.264	3.155
333.15	1.236	-0.109	1.849	0.062	2.749	0.389	4.147	1.014	6.600	2.372	10.019	4.117	13.644	4.865	14.580	3.973	14.924	2.485
338.15	1.117	-0.043	1.649	0.121	2.408	0.406	3.572	0.930	5.554	2.005	8.281	3.346	11.201	3.882	11.996	3.163	12.326	1.975
343.15	1.017	0.006	1.478	0.161	2.128	0.414	3.104	0.856	4.722	1.716	6.923	2.760	9.291	3.136	9.962	2.543	10.278	1.591
348.15	0.930	0.041	1.335	0.188	1.894	0.413	2.723	0.792	4.055	1.486	5.844	2.300	7.788	2.567	8.353	2.067	8.642	1.289
353.15	0.853	0.066	1.213	0.206	1.698	0.408	2.407	0.736	3.513	1.301	4.984	1.943	6.587	2.124	7.065	1.698	7.337	1.064
358.15	0.790	0.086	1.108	0.218	1.528	0.394	2.144	0.685	3.072	1.149	4.290	1.659	5.619	1.772	6.026	1.406	6.268	0.873
363.15	0.747	0.114	1.018	0.224	1.377	0.374	1.925	0.641	2.710	1.028	3.725	1.434	4.834	1.494	5.181	1.1761	5.395	0.723

145   [a] mass fraction, [b] mole fraction of MDEA

146   **Table 12.** Measured viscosity (η / mPa·s) and deduced viscosity deviation (η^E/ mPa·s) of DMEA (1) + H$_2$O (2) mixtures.

T / K	[a]w_1	0.30		0.40		0.50		0.60		0.70		0.80		0.90		0.94		0.97	
	[b]x_1	0.0797		0.1187		0.1681		0.2326		0.3204		0.4470		0.6452		0.7600		0.8673	
		η	η^E	η	η^E	η	η^E	η	η^E	η	η^E	η	η^E	η	η^E	η	η^E	η	η^E
293.15		4.214	2.981	6.814	5.469	10.169	8.681	14.010	12.335	16.750	14.822	15.539	13.245	9.712	6.845	7.129	3.931	5.383	1.875
298.15		3.457	2.367	5.464	4.278	8.011	6.701	10.886	9.416	12.989	11.299	12.214	10.208	7.955	5.454	5.976	3.189	4.591	1.537
303.15		2.869	1.900	4.446	3.392	6.398	5.237	8.571	7.271	10.197	8.707	9.704	7.941	6.565	4.374	5.031	2.593	3.937	1.267
308.15		2.413	1.545	3.664	2.723	5.189	4.155	6.848	5.694	8.120	6.802	7.796	6.241	5.458	3.533	4.264	2.124	3.391	1.052
313.15		2.055	1.272	3.060	2.215	4.262	3.336	5.548	4.517	6.540	5.366	6.340	4.961	4.577	2.877	3.637	1.750	2.937	0.876
318.15		1.768	1.059	2.590	1.825	3.552	2.718	4.562	3.636	5.362	4.312	5.220	3.990	3.877	2.367	3.131	1.459	2.564	0.740
323.15		1.536	0.890	2.216	1.521	2.999	2.244	3.794	2.958	4.442	3.497	4.340	3.239	3.307	1.959	2.708	1.218	2.249	0.625
328.15		1.349	0.757	1.918	1.284	2.564	1.876	3.199	2.441	3.723	2.868	3.652	2.659	2.845	1.635	2.363	1.028	1.987	0.535
333.15		1.193	0.649	1.676	1.094	2.215	1.586	2.725	2.034	3.151	2.375	3.099	2.200	2.462	1.371	2.071	0.870	1.765	0.460
338.15		1.064	0.562	1.478	0.943	1.934	1.356	2.346	1.712	2.703	1.994	2.653	1.835	2.146	1.158	1.828	0.741	1.575	0.397
343.15		0.955	0.490	1.315	0.821	1.701	1.169	2.038	1.457	2.324	1.676	2.289	1.544	1.882	0.985	1.621	0.637	1.413	0.347
348.15		0.865	0.434	1.179	0.721	1.505	1.014	1.786	1.251	2.022	1.428	1.988	1.308	1.658	0.844	1.444	0.552	1.274	0.309
353.15		0.790	0.388	1.064	0.638	1.341	0.886	1.572	1.078	1.770	1.223	1.739	1.115	1.468	0.725	1.291	0.478	1.151	0.274
358.15		0.722	0.347	0.968	0.571	1.203	0.780	1.401	0.943	1.560	1.055	1.532	0.958	1.308	0.626	1.159	0.416	1.045	0.244
363.15		0.674	0.323	0.884	0.514	1.080	0.686	1.251	0.826	1.385	0.917	1.358	0.829	1.170	0.544	1.046	0.365	0.954	0.221

147   [a] mass fraction, [b] mole fraction of DMEA

148

149

150 **Table 13.** Measured viscosity (η / mPa·s) and deduced viscosity deviation (η^E/ mPa·s) of DEEA (1) + H₂O (2) mixtures.

| T / K | $^a w_1$ 0.30 | | 0.40 | | 0.50 | | 0.60 | | 0.70 | | 0.80 | | 0.90 | | 0.94 | | 0.97 | |
| | $^b x_1$ 0.0618 | | 0.0930 | | 0.1332 | | 0.1874 | | 0.2640 | | 0.3808 | | 0.5805 | | 0.7066 | | 0.8325 | |
	η	η^E	η	η^E	η	η^E	η	η^E	η	η^E	η	η^E	η	η^E	η	η^E	η	η^E
293.15	4.511	3.266	7.057	5.688	10.454	8.927	14.648	12.907	18.849	16.806	20.569	18.064	15.023	11.730	10.786	6.996	7.593	3.305
298.15	3.666	2.573	5.616	4.421	8.157	6.829	11.239	9.734	14.255	12.499	15.446		11.561	8.767	8.548	5.340	6.191	2.570
303.15	3.025	2.059	4.536	3.484	6.477	5.315	8.731	7.420	10.922	9.401	11.757	13.307	9.009	6.623	6.905	4.173	5.092	2.016
308.15	2.529	1.668	3.713	2.781	5.222	4.197	6.903	5.755	8.510	7.185	9.104	9.917	7.122	5.072	5.607	3.268	4.223	1.595
313.15	2.143	1.371	3.090	2.257	4.223	3.312	5.546	4.531	6.740	5.577	7.161	7.512	5.711	3.938	4.609	2.592	3.536	1.276
318.15	1.839	1.141	2.607	1.858	3.517	2.702	4.533	3.629	5.425	4.396	5.729	5.774	4.649	3.101	3.810	2.055	2.999	1.038
323.15	1.597	0.964	2.226	1.549	2.964	2.230	3.750	2.940	4.432	3.514	4.650	4.509	3.822	2.461	3.184	1.646	2.560	0.845
328.15	1.397	0.819	1.926	1.309	2.535	1.869	3.151	2.420	3.676	2.852	3.832	3.569	3.187	1.981	2.704	1.346	2.205	0.695
333.15	1.238	0.707	1.678	1.115	2.189	1.583	2.675	2.013	3.086	2.343	3.196	2.867	2.697	1.624	2.302	1.097	1.919	0.582
338.15	1.105	0.616	1.480	0.962	1.911	1.356	2.311	1.707	2.619	1.944	2.703	2.332	2.282	1.319	1.981	0.902	1.678	0.485
343.15	0.998	0.545	1.314	0.836	1.682	1.171	2.010	1.456	2.265	1.649	2.304	1.922	1.967	1.097	1.717	0.746	1.477	0.405
348.15	0.905	0.484	1.180	0.736	1.491	1.018	1.756	1.245	1.943	1.378	1.983	1.594	1.681	0.891	1.513	0.633	1.310	0.341
353.15	0.834	0.441	1.076	0.663	1.330	0.892	1.545	1.073	1.697	1.177	1.717	1.335	1.471	0.751	1.342	0.542	1.172	0.293
358.15	0.765	0.398	0.984	0.599	1.194	0.786	1.372	0.934	1.493	1.012	1.497	1.123	1.299	0.640	1.183	0.452	1.059	0.257
363.15	0.703	0.359	0.906	0.546	1.077	0.697	1.221	0.814	1.316	0.871	1.321	0.950	1.154	0.549	1.052	0.384	0.961	0.230

151 ^{a} mass fraction, ^{b} mole fraction of DEEA

152
153
154

155   Density of pure and aqueous amine mixtures decreases with increasing temperature. For the
156 MDEA + H$_2$O mixtures, the density starts to increase with MDEA concentration from $x_1 = 0$ and
157 reach a maximum value and then decreases. A shift of maximum from $x_1 = 0.3$ at 293.15 K to $x_1 =$
158 0.28 at 353.15 K was observed due to the influence from temperature. The density of DMEA + H$_2$O
159 and DEEA + H$_2$O mixtures continues to decrease from $x_1 = 0$ and a minimum was observed at $x_1 =$
160 1.

161   The excess molar volume V^E of a binary mixture is given by Equation (1) and Equation (2) and
162 is a property that can be used to fit density data of a binary mixture. The sign of V^E carries
163 information of intermolecular interactions and molecular structure of the molecules in a mixture. The
164 excess molar volume V^E becomes negative when the intermolecular interaction between unlike
165 molecules are stronger than in like molecules [17,18]. Further, V^E is negative when the molecules are
166 efficiently packed in the solution [19]. For the mixtures having weak intermolecular interactions such
167 as dispersion forces have positive deviation for V^E [20].

168

$$V^E = V - (x_1 V_1^0 + x_2 V_2^0) \tag{1}$$

169

$$V^E = \left[\frac{x_1 M_1 + x_2 M_2}{\rho}\right] - \frac{x_1 M_1}{\rho_1} - \frac{x_2 M_2}{\rho_2} \tag{2}$$

170

171   The calculated V^E for MDEA + H$_2$O, DMEA + H$_2$O and DEEA + H$_2$O are shown in Table 4, Table
172 5 and Table 6 respectively. A negative deviation for V^E was observed for the whole range of amine
173 concentration with a minimum in H$_2$O-rich region at x_1 of 0.36, 0.38 and 0.38 for MDEA, DMEA and
174 DEEA respectively. This indicates the existence of strong intermolecular interactions like H-bonds
175 among unlike molecules and efficient packing of molecules in the mixtures. Figure 1 (a) and (b)
176 compares the variation of V^E between three different mixtures at 293.15 K and 353.15 K.
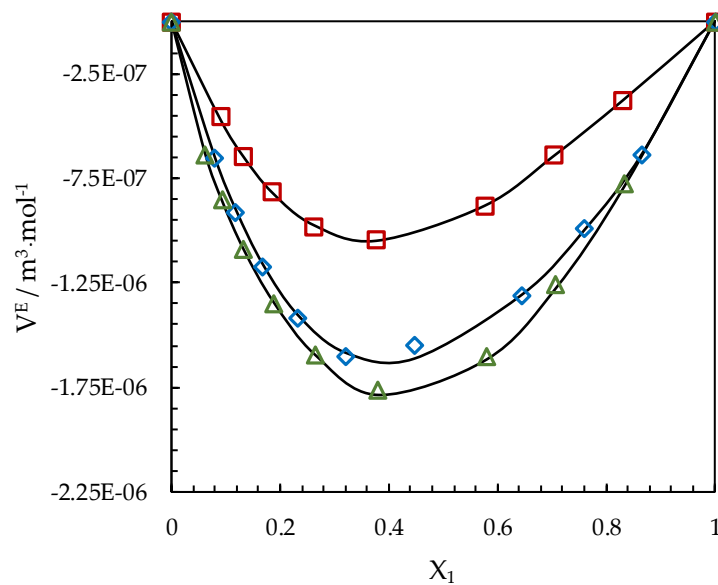
177
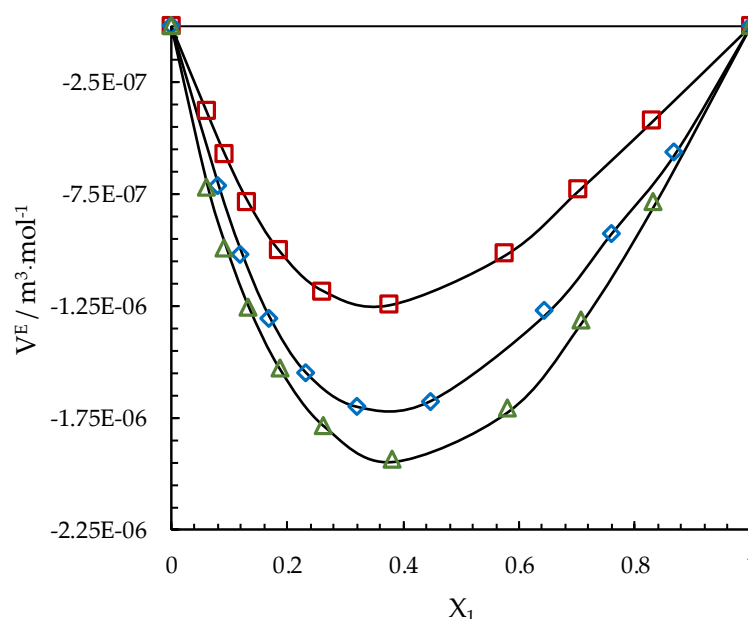
178

179 **Figure 1(a).** Excess molar volumes V^E of MDEA (1) + H$_2$O (2), '□'; DMEA (1) + H$_2$O (2), '◊' and DEEA
180 (1) + H$_2$O (2), '△' at 293.15 K, Correlation; "—".

181

182

183

184 **Figure 1(b).** Excess molar volumes V^E of MDEA (1) + H₂O (2), '□'; DMEA (1) + H₂O (2), '◊' and DEEA
185 (1) + H₂O (2), '△' at 353.15 K, Correlation; "—".

186   A negative V^E or a volume contraction in the systems further reveals that considered tertiary
187 amines and H₂O are completely miscible (polar organic solvent + H₂O) systems [21]. The calculated
188 V^E for MDEA + H₂O mixtures showed the lowest deviation for the range of amine concentrations
189 compared to DMEA + H₂O and DEEA + H₂O mixtures. The largest deviation for V^E was observed in
190 DEEA + H₂O mixtures indicating the existence of strong intermolecular interactions and efficient
191 molecular packing in the mixtures. Compared to V^E of MDEA, a significant deviation was reported
192 with DMEA ($\approx$ 1.4 times) and DEEA ($\approx$ 1.6 times) at the minimum point of 293.15 K. The
193 substitution of one methyl (-CH₃) group for one ethanol (–CH₂CH₂OH) group in MDEA might results
194 an increase of intermolecular interactions especially the H-bonding between N and OH in amine and
195 H₂O or increase of packing efficiency. Two ethyl groups (-CH₂CH₃) in DEEA compared to two methyl
196 (-CH₃) groups in DMEA has further negatively contributed to V^E. The introduction of methyl (-CH₃)
197 or ethyl (-CH₂CH₃) groups increases the hydrophobicity of amine [15]. As explained by Begum, *et*
198 *al.*[18], the H₂O molecules restructure around the hydrophobic part of the organic solute forming a
199 cage-like structure. Accordingly, more structured H₂O molecules around the hydrophobic groups (-
200 CH₃) and (-CH₂CH₃) in DMEA and DEEA respectively might explain the reported volume
201 contraction in the mixtures.
202   A Redlich-Kister [22] type polynomial as given in the Equation (3) was proposed to fit calculated
203 V^E for all aqueous mixtures. The measured densities at low amine concentrations (< 30% mass)
204 presented in literature for MDEA + H₂O mixtures from Maham, Teng, Mather and Hepler [13], DMEA
205 + H₂O mixtures from Maham, *et al.*[14] and DEEA + H₂O mixtures from Lebrette, *et al.*[16] were
206 adopted for this work to improve the accuracy of data fitting into the proposed correlation. A
207 temperature dependency for the Redlich-Kister coefficients (A_i) was suggested as given in Equation
208 (4) to determine optimum values for (A_i) at each temperature. Table 7 lists the parameters for
209 temperature dependency of the Redlich-Kister coefficients (A_i) for V^E of different mixtures.
210

$$Y^E = x_1 x_2 \sum_{i=0}^{i=n} A_i (1 - 2x_2)^i \tag{3}$$

211

$$A_i = \sum_{i=0}^{i=n} a_i T^i \tag{4}$$

212
213 The partial molar volume of each component $\overline{V_i}$ is defined as shown in Equation (5)
214

$$\overline{V_i} = \left(\frac{\partial V}{\partial n_i}\right)_{T,P,n_j} \tag{5}$$

215
216 For a binary mixture, partial molar volume $\overline{V_i}$ can be determined by following Equations [23]
217

$$\overline{V_1} = V^E + V_1^0 - x_2 \left(\frac{\partial V^E}{\partial x_2}\right)_{p,T} \tag{6}$$

218

$$\overline{V_2} = V^E + V_2^0 + (1 - x_2) \left(\frac{\partial V^E}{\partial x_2}\right)_{p,T} \tag{7}$$

219
220 Equation (8) and Equation (9) can be derived by differentiating Equation (3) for V^E with respect to
221 x_2 and combining it with Equation (6) and Equation (7).
222

$$\overline{V_1} = V_1^0 + x_2^2 \sum_{i=0}^{i=n} A_i (1 - 2x_2)^i + 2x_2^2 (1 - x_2) \sum_{i=0}^{i=n} A_i (i) (1 - 2x_2)^{i-1} \tag{8}$$

223

$$\overline{V_2} = V_2^0 + (1 - x_2)^2 \sum_{i=0}^{i=n} A_i (1 - 2x_2)^i - 2x_2 (1 - x_2)^2 \sum_{i=0}^{i=n} A_i (i) (1 - 2x_2)^{i-1} \tag{9}$$

224
225   The partial molar volume of amines at infinite dilution in H_2O $\overline{V_1^\infty}$ can be determined by
226 considering the scenario of $x_2 = 1$ as given in the Equation (10) and partial molar volume of H_2O at
227 infinite dilution in amines $\overline{V_2^\infty}$ can be found by considering the scenario of $x_2 = 0$ as shown in
228 Equation (11).
229

$$\overline{V_1^\infty} = V_1^0 + \sum_{i=0}^{i=n} A_i (-1)^i \tag{10}$$

230

$$\overline{V_2^\infty} = V_2^0 + \sum_{i=0}^{i=n} A_i \tag{11}$$

231
232
233
234
235

Table 7. Temperature dependency of the Redlich-Kister coefficients (A_i) for the excess molar volume ($10^6 \cdot V^E/m^3 \cdot mol^{-1}$) of different aqueous amine mixtures.

Parameters	Mixtures					
	MDEA (1) + H$_2$O (2)		DMEA (1) + H$_2$O (2)		DEEA (1) + H$_2$O (2)	
	a_0	a_1	a_0	a_1	a_0	a_1
A_0	-7.847	0.0111	-7.363	0.00313	-10.120	0.00884
A_1	5.378	-0.009324	6.103	-0.01065	5.082	-0.00770
A_2	-2.584	0.00663	-1.532	0.00017	-2.175	0.00491
A_3	8.187	-0.02062	18.490	-0.05285	13.530	-0.04196
A_4	1.599	-0.00537	-0.774	0.00274	-2.203	0.00395
A_5	-15.300	0.03798	-29.660	0.08247	-16.060	0.05570
AARD (%)	0.007		0.015		0.011	
AMD (kg·m^{-3})	0.97		1.04		0.80	
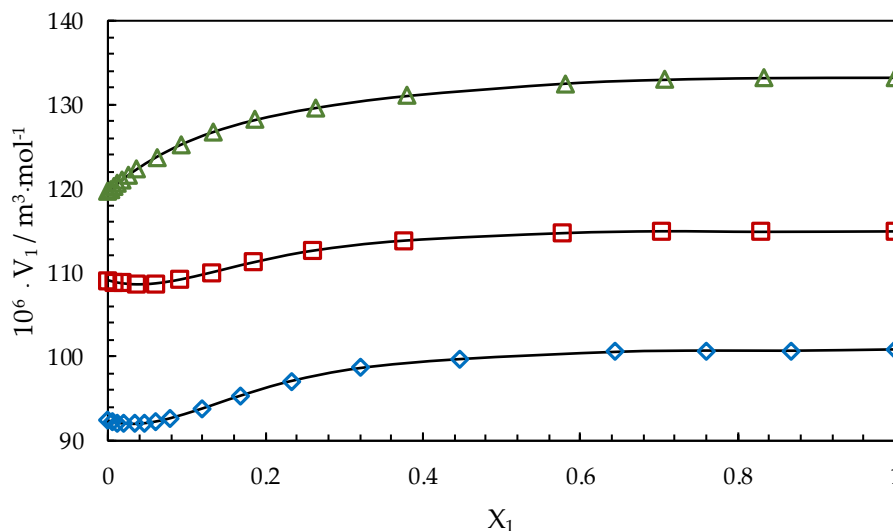
Figure 2(a). Partial molar volumes of MDEA in (MDEA + H$_2$O), '□'; DMEA in (DMEA + H$_2$O), '◇' and DEEA in (DEEA + H$_2$O), '△' at 298.15 K.

Table 8 presents the calculated partial molar volume $\overline{V_1^\infty}$ of amines at infinite dilution in H$_2$O with molar volume V_1^0 of pure amines. The proposed temperature dependency for the Redlich-Kister coefficients (A_i) was able to calculate $\overline{V_1^\infty}$ with a deviation around 1% AARD compared to literature data. The partial molar volume $\overline{V_1^\infty}$ of amines were smaller than the corresponding molar volume V_1^0 of pure amines. This can be explained for MDEA, DMEA and DEEA by the existence of (partially) ice-like structure in pure H$_2$O [24], which is more open than a nearly close packed arrangement, enables to fit (partially) amine molecules into the open or empty spaces in liquid H$_2$O [23]. Hepler [24] explained structure making solute and structure breaking solute based on the sign of $\left(\partial^2 \overline{V_1^\infty}/\partial T^2\right)_P$ in which the positive sign is associated with structure making solute while the negative sign is associated with structure breaking solute. The study shows that for all considered tertiary amines, variation of $\overline{V_1^\infty}$ with temperature is linear ($R^2 > 0.999$) by making the first derivative of $\overline{V_1^\infty}$ with respect to temperature a positive constant. This does not provide any information about second derivation for a positive or a negative sign. Similar observation was reported by Maham, Teng, Hepler and Mather [23] for MDEA. Accordingly, this does not indicate that MDEA, DMEA and DEEA in dilute aqueous mixtures can be considered as either net structure makers or net structure breakers. Figure 2(a) and 2(b) illustrate the composition dependence of the partial molar volume of MDEA in (MDEA + H$_2$O), DMEA in (DMEA + H$_2$O) and DEEA in (DEEA +

259 H₂O) at 298.15 K and 353.15 K respectively. The Figure 2(a) shows a minimum value for $\bar{V}_1$ around
260 $x_1 = 0.04$ for MDEA and DMEA at 298.15 K and it disappears with the increase of temperature as
261 shown in Figure 2(b).
262
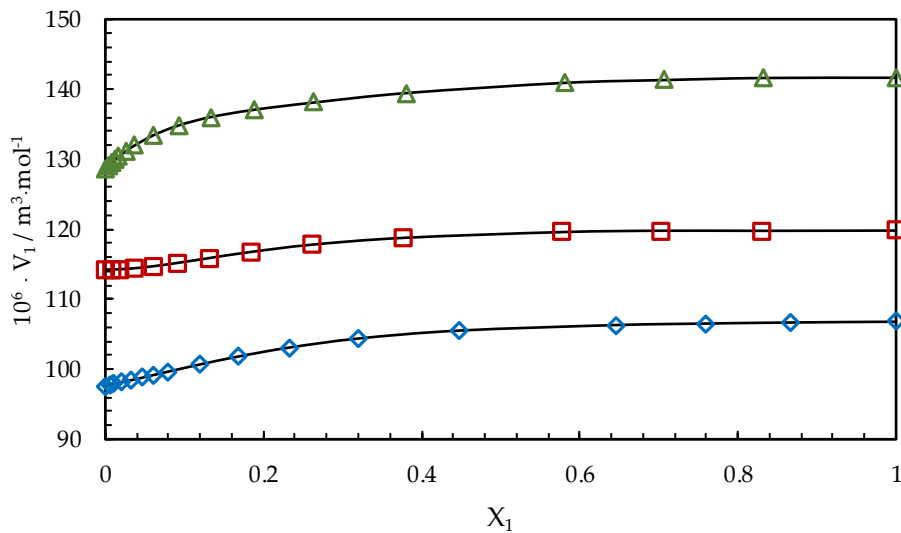
263

264 **Figure 2(b).** Partial molar volumes of MDEA in (MDEA + H₂O), '□'; DMEA in (DMEA + H₂O), '◇' and
265 DEEA in (DEEA + H₂O), '△' at 353.15 K.

266 The accuracy of the data fit was determined by average absolute relative deviation (AARD) and
267 absolute maximum deviation (AMD) as given in Equation (12) and Equation (13). A density
268 correlation based on a Redlich-Kister type polynomial for V^E and density deviation defined as
269 $ln(\rho_\gamma)$ in Equation (15) were examined to fit the measured densities of MDEA + H₂O, DMEA + H₂O
270 and DEEA + H₂O mixtures at different concentrations and temperatures.
271

272 Average absolute relative deviation:
273

$$AARD \ (\%) = \frac{100\%}{N} \sum_{i=1}^{i=N} \left| \frac{Y_i^m - Y_i^c}{Y_i^m} \right| \tag{12}$$

274
275 Absolute maximum deviation:
276

$$AMD = max|Y_i^m - Y_i^c| \tag{13}$$

277

278 For binary mixtures, the use of excess molar volume to correlate mixture density is a widely
279 adopted approach described in Equation (14). The evaluated correlation parameters for different
280 mixtures are listed in Table 9 with relevant AARD and AMD.
281

$$\rho = \frac{\sum_{i=1}^{2} x_i M_i}{V^E + \sum_{i=1}^{2} \frac{x_i M_i}{\rho_i}} \tag{14}$$

282

$$ln(\rho) = ln(\rho_\gamma) + \sum_{i=1}^{i=2} x_i \rho_i \tag{15}$$

$$ln(\rho_\gamma) = x_1 x_2 \sum_{i=0}^{i=n} A_i (1 - 2x_2)^i \qquad (16)$$

Table 9. Temperature dependency of the Redlich-Kister coefficients (A_i) for the density deviation $ln(\rho_\gamma)$ of different aqueous amine mixtures.

Parameters	Mixtures					
	MDEA (1) + H₂O (2)		DMEA (1) + H₂O (2)		DEEA (1)+ H₂O (2)	
	a_0	a_1	a_0	a_1	a_0	a_1
A_0	0.3054	$-6.25 \cdot 10^{-4}$	0.2197	$-9.27 \cdot 10^{-4}$	0.2491	$-11.42 \cdot 10^{-4}$
A_1	-0.4206	$8.48 \cdot 10^{-4}$	-0.3892	$12 \cdot 10^{-4}$	-0.4277	$14.91 \cdot 10^{-4}$
A_2	0.4459	$-9.12 \cdot 10^{-4}$	0.3690	$-10.5 \cdot 10^{-4}$	0.5542	$-17.69 \cdot 10^{-4}$
AARD (%)	0.1		0.03		0.04	
AMD (kg·m⁻³)	3.0		1.5		2.7	

For MDEA + H₂O mixtures, a maximum deviation of measured density from the correlation was found at MDEA mole fraction $x_1 = 0.0916$ and temperature 353.15 K. Similarly, for DMEA + H₂O and DEEA + H₂O mixtures, maximum deviations were reported at $x_1 = 0.447$ and $x_1 = 0.0618$ at temperature 353.15 K and 293.15 K respectively. Table 9 lists the calculated parameters for the correlation based on density deviation with corresponding AARD and AMD for each binary mixture. It was observed that MDEA + H₂O shows a maximum deviation of measured density from the correlation at $x_1 = 0.5764$ at 293.15 K. For the DMEA + H₂O mixtures, a maximum deviation of measured density from the correlation was found at $x_1 = 0.1187$ at 293.15 K while DEEA + H₂O mixtures revealed a maximum deviation at $x_1 = 0.0618$ at 293.15 K. The study showed that the correlation based on V^E for density provided higher accuracies in the data fits. However, the reported accuracies from both considered correlations are acceptable to use them in the engineering calculations.

3.2. Viscosity of the binary mixtures

A comparison of measured viscosity of pure amines in this study with available data in literature is given in Table 10. The study shows that measured viscosities agree with literature data with around 3.5% AARD. The measured viscosities of the binary aqueous mixtures are shown in Table 11, 12 and 13. The mixture viscosity varies with the composition and temperature. For the MDEA + H₂O mixtures at 293.15 K, a maximum viscosity was observed around $x_1 = 0.7$. The study shows that DEEA + H₂O mixtures have a maximum viscosity around $x_1 = 0.36$ at 293.15 K and the DMEA + H₂O mixtures exhibit a maximum viscosity around $x_1 = 0.38$ at 293.15 K. Figure 3 compares viscosity variations of different aqueous amine mixtures at 293.15 K.

**Table 10.** Measured viscosity (η / mPa·s) of pure amines MDEA, DMEA and DEEA.

T / K	MDEA		DMEA		DEEA	
	This work	Literature	This work	Literature	This work	Literature
293.15	100.72		3.89		4.95	
298.15	75.90	77.19[a]	3.39		4.17	4.02[b]
303.15	57.82		2.96		3.54	3.31[b]
308.15	44.62		2.59		3.01	
313.15	34.89	34.11[a]	2.28	2.24[c]	2.58	2.41[b]
318.15	27.67		2.01		2.24	
323.15	22.22		1.79	1.76[c]	1.95	
328.15	18.10		1.60		1.71	
333.15	14.89	14.30[a]	1.43	1.41[c]	1.51	1.44[b]
338.15	12.38		1.29		1.35	

Appl. Sci. **2019**, *9*, x FOR PEER REVIEW

7 of 25

343.15	10.38	9.85[a]	1.17	1.16[c]	1.21	
348.15	8.78		1.05		1.09	
353.15	7.48	7.12[a]	0.96	0.96[c]	0.98	0.93[b]
358.15	6.43		0.87		0.90	
363.15	5.56		0.80		0.82	

Literature references: [a]Teng, *et al.* [25], [b]Maham, *et al.* [26], [c]Garcia, *et al.* [27]
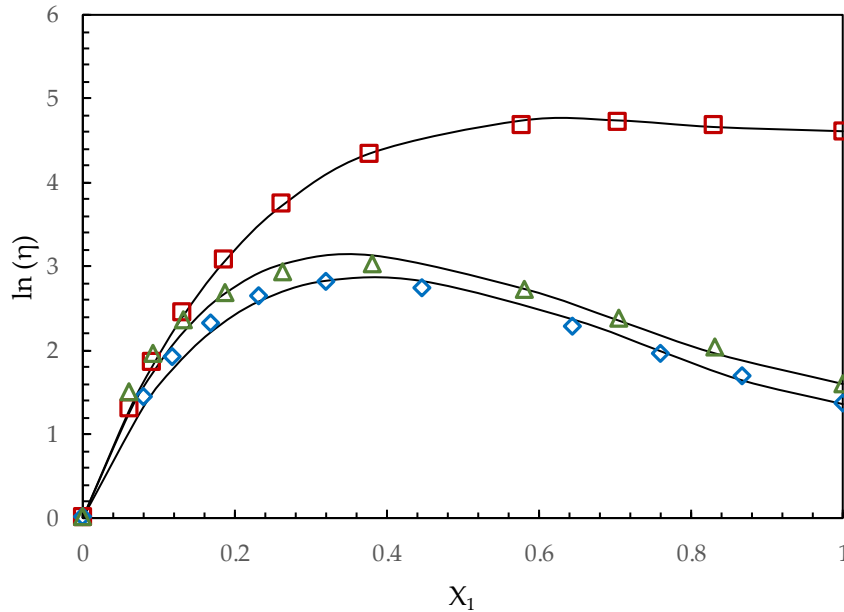
Figure 3. Viscosities of MDEA (1) + H₂O (2), '□'; DMEA (1) + H₂O (2), '◊' and DEEA (1) + H₂O (2), '△' mixtures at 293.15 K, Correlation; "—".

The viscosity deviation η^E or the excess viscosity of the mixtures is calculated as shown in the Equation (17).

$$\eta^E = \eta - \sum_{i=1}^{i=2} x_i \eta_i \tag{17}$$

According to Kauzmann and Eyring [28], the viscosity of a mixture strongly depends on the entropy of the mixture that is related to the structure of the component molecules, bond enthalpy and consequently with the molecular interactions between components in the mixture [29]. Hence, viscosity deviation is attributed to the difference in size and shape of the component molecules and molecular interactions between unlike molecules such as H-bonds (strong interactions) and dispersion forces (weak interactions). The value of η^E becomes positive due to the presence of strong interactions like H-bond formation [30] and η^E is negative where the weak interactions (weak dipole and dispersion forces) are dominant [30,31].

The semiempirical model suggested by Grunberg and Nissan [32] can be adopted to interpret the strength of the molecular interactions between components in a binary mixture [30]. The model is consisting of one adjustable parameter G_{12} that is beneficial to correlate dynamic viscosity of binary mixtures using pure component viscosities. The model for a binary mixture is given as follows.

$$ln(\eta) = \sum_{i=1}^{i=2} x_i ln(\eta_i) + x_1 x_2 G_{12} \tag{18}$$

329   The variation of G_{12} with composition is similar to that of η^E. Accordingly G_{12} is negative for
330   systems in which dispersion forces are dominant and G_{12} become positive as the strength of the
331   interaction increases [30].
332   The dynamic viscosity model proposed by Eyring [33] based on the theory of absolute reaction
333   rate provides another approach to examine the molecular interaction in a binary mixture. For a liquid
334   mixture, the viscosity is represented according to the Eyring's model as follows.
335

$$\eta = \frac{hN_A}{V} exp\left(\frac{\Delta G^*}{RT}\right) \tag{19}$$

336

337   Accordingly, excess free energy of activation for viscous flow ΔG^{E*} is defined as follows using
338   pure component viscosities and molar volumes.
339

$$ln(\eta V) = ln(\eta V)_{ideal} + \frac{\Delta G^{E*}}{RT} \tag{20}$$

340

341

$$ln(\eta V) = \sum_{i=1}^{i=2} x_i ln(\eta_i V_i^0) + \frac{\Delta G^{E*}}{RT} \tag{21}$$

342

343   Meyer, *et al.* [34] discussed the applicability of the sign of ΔG^{E*} as in viscosity deviation η^E to
344   understand the types of intermolecular interactions. It has been reported by authors [34-37] that the
345   positive ΔG^{E*} indicates strong interactions like H-bond and negative ΔG^{E*} signifies weak molecular
346   interactions like dispersion forces. The $ln(\eta_\gamma)$ shown in Equation (22) is similar to the term $x_1 x_2 G_{12}$
347   in the Grunberg and Nissan [32] model. Figure 4 (a), (b) and (c) illustrate the variation of η^E, $ln(\eta_\gamma)$
348   and ΔG^{E*} with amine concentration in different mixtures at 293.15 K.
349

$$ln(\eta) = ln(\eta_\gamma) + \sum_{i=1}^{i=2} x_i ln(\eta_i) \tag{22}$$

(a): η^E (b): $ln(\eta_\gamma)$

(c): ΔG^{E*}
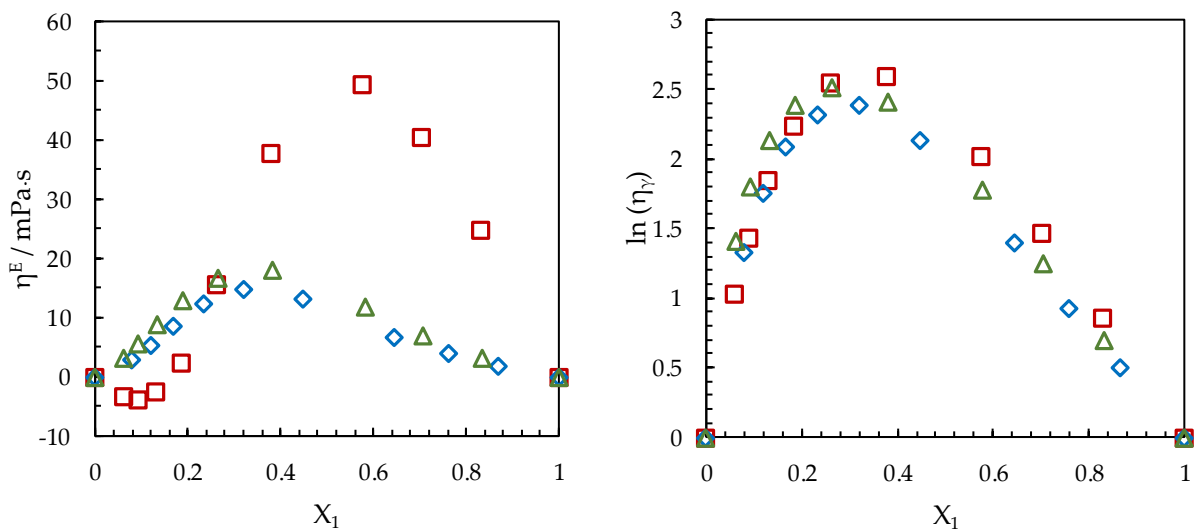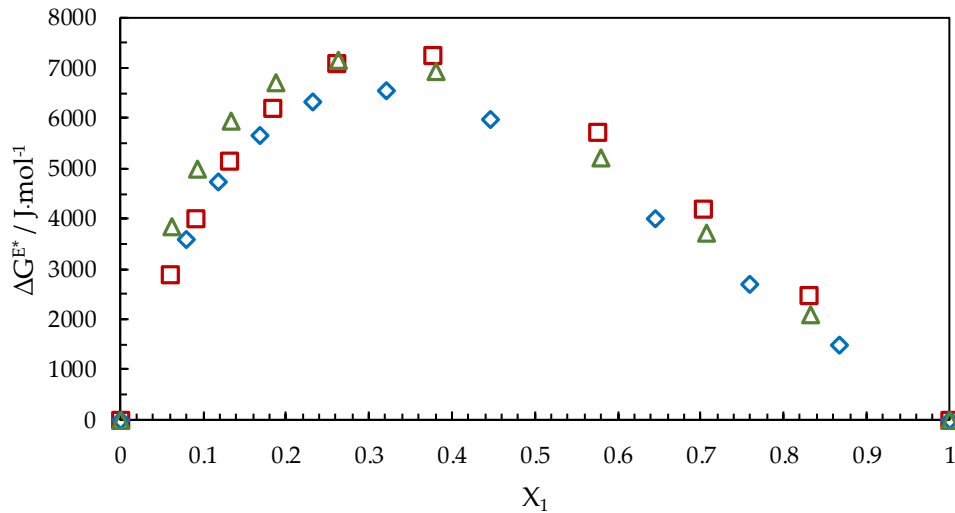
Figure 4. η^E, $ln(\eta_\gamma)$ and ΔG^{E*} of MDEA (1) + H₂O (2), '□'; DMEA (1) + H₂O (2), '◊' and DEEA (1) + H₂O (2), '△' mixtures at 293.15 K.

Figure 4 (a) shows that η^E was negative for low MDEA concentrations indicating the presence of weak intermolecular interactions like weak dipole and dispersion forces. As MDEA concentration increases, η^E increases and becomes positive signifying the existence of strong intermolecular interactions like H-bonds among unlike molecules. The DMEA + H₂O and DEEA + H₂O mixtures showed positive deviation for η^E for the whole amine concentrations revealing that the intermolecular interactions between those amines and H₂O are stronger than interactions between like molecules. The highest positive deviation for η^E was reported by MDEA + H₂O mixtures around $x_1 = 0.6$. The DMEA + H₂O and DEEA + H₂O mixtures reached their highest η^E around $x_1 = 0.35$. The calculated G_{12} and ΔG^{E*} showed positive deviations for all considered aqueous amine mixtures for the whole range of amine concentrations. This shows that the considered aqueous amine mixtures are having strong intermolecular interactions among unlike molecules for the whole range of amine concentrations. The MDEA + H₂O mixtures showed a highest peak round $x_1 = 0.35$ while DMEA + H₂O and DEEA + H₂O mixtures showed peaks around $x_1 = 0.3$ and $x_1 = 0.25$ respectively. Figure 4 (c) illustrates that DEEA + H₂O mixtures have a higher ΔG^{E*} in H₂O rich region than MDEA + H₂O mixtures and ΔG^{E*} of MDEA + H₂O showed higher values than DMEA + H₂O and DEEA + H₂O for the amine rich region.

The slope of the excess free energy of activation for viscous flow ΔG^{E*} against temperature (T) carries the information about the excess entropy of activation for viscous flow ΔS^{E*}. The plot of ΔG^{E*} versus temperature (T) was linear in the temperature range from 293.15 K to 363.15 K at a certain mole fraction for the mixtures studied.

$$\Delta S^{E*} = -\left[\frac{\partial(\Delta G^{E*})}{\partial T}\right] \tag{23}$$

Figure 5 illustrates the excess entropy of activation for viscous flow ΔS^{E*} for MDEA + H₂O, DMEA + H₂O and DEEA + H₂O mixtures over the whole range of concentrations. Equation (21) was adopted to calculate ΔS^{E*} for temperature range 293.15-363.15 K. Similar to the ΔG^{E*} variation with the mole fraction, ΔS^{E*} increases with the increase of mole fraction up to a maximum and then decreases. The peaks were observed around $x_1 = 0.38$ for MDEA + H₂O and DEEA + H₂O mixtures while DMEA + H₂O showed a peak around $x_1 = 0.32$. The ΔS^{E*} of DEEA + H₂O mixtures was higher than that of MDEA + H₂O and DMEA + H₂O mixtures for the whole range of amine concentration.
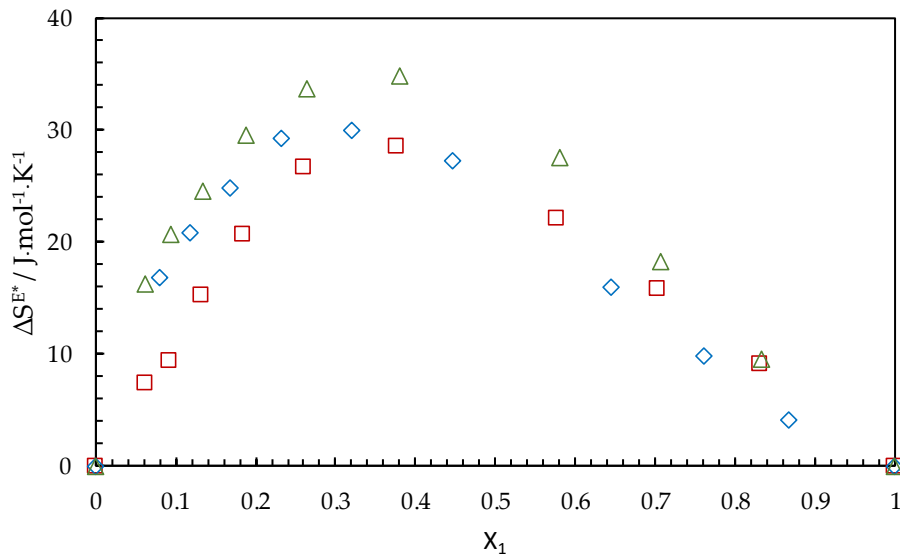
Figure 5. ΔS^{E*} of MDEA (1) + H_2O (2), '□'; DMEA (1) + H_2O (2), '◇' and DEEA (1) + H_2O (2), '△' mixtures as a function of mole fractions.

The measured viscosities from 293.15 K to 363.15 K of the mixtures were fitted to the empirical correlation shown in Equation (22). The Redlich-Kister model [22] is a good candidate to correlate excess properties in a binary mixtures. In order to acquire a good accuracy in data fit, a higher degree polynomial is required with a large number of fitting parameters. A simplified lower degree polynomial was suggested as given in Equation (24). Similar work have been reported by Hartono, *et al.* [38] for the viscosity of MEA + H_2O mixtures.

$$ln(\eta_\gamma) = (A_1 + A_2T + A_3T^2 + A_4x_1 + A_5Tx_1^2 + A_6x_1^3)\cdot x_1x_2 \tag{24}$$

Table 14 lists the calculated parameters of Equation (24) for different mixtures. The correlations provide acceptable accuracies for use in engineering calculations. For MDEA + H_2O mixtures, AMD shows a relatively high deviation as 6.4 mPa·s, but measured viscosity is as high as 114.261 mPa·s.

Table 14. Coefficients (A_i) for the viscosity deviation $ln(\eta_\gamma)$ of different aqueous amine mixtures.

Parameters	Mixtures		
	MDEA(1) + H₂O(2)	DMEA(1) + H₂O(2)	DEEA(1) + H₂O(2)
A_1	98.13	99.61	123.5
A_2	-0.4163	-0.4218	-0.528
A_3	$5.008\cdot10^{-4}$	$5.013\cdot10^{-4}$	$6.291\cdot10^{-4}$
A_4	-29.09	-33.79	-45.8
A_5	0.08377	0.1083	0.1498
A_6	-10.47	-14.69	-18.31
AARD (%)	1.7	2.7	4.7
AMD (mPa·s)	6.4	1.3	2.4

McAllister [39] developed a semiempirical model based on Eyring's theory of absolute reaction rates to represent kinematic viscosities in a binary mixture. The McAllister [39] three-body model considered interactions among three molecules that are all in one plane.

The McAllister's three-body model

$$ln(v) = x_1^3 \cdot ln(v_1) + 3x_1^2 x_2 \cdot ln(v_{12}) + 3x_1 x_2^2 \cdot ln(v_{21}) + x_2^3 \cdot ln(v_2) \tag{25}$$
$$- ln(x_1 + x_2 \cdot [M_2/M_1]) + 3x_1^2 x_2 \cdot ln([2 + M_2/M_1]/3) + 3x_1 x_2^2$$
$$\cdot ln([1 + 2M_2/M_1]/3) + x_2^3 \cdot ln(M_2/M_1)$$

402

403   McAllister's three-body model have two fitting parameters of v_{12} and v_{21}. For each type of ΔG^*
404 considered during the model development, a corresponding kinematic viscosity were assigned as
405 shown in Equations (26)-(30). With the assumption of temperature independent enthalpies and
406 entropies of activation for viscous flow, it provides a kinematic viscosity model with both
407 composition and temperature as independent variables. The unknown enthalpies and entropies can
408 be calculated by fitting kinematic viscosity data at different compositions and temperatures to the
409 model. Our previous work based on kinematic viscosities of MEA (monoethanolamine) + H_2O
410 mixtures provided acceptable accuracies by following this method [40].

411

$$\Delta G^* = \Delta H^* - T\Delta S^* \tag{26}$$

412

$$v_1 = \frac{hN}{M_1} e^{-\Delta s_1^*/R} e^{\Delta H_1^*/RT} \tag{27}$$

413

$$v_{12} = \frac{hN}{M_{12}} e^{-\Delta s_{12}^*/R} e^{\Delta H_{12}^*/RT} \tag{28}$$

414
415

$$v_{21} = \frac{hN}{M_{21}} e^{-\Delta s_{21}^*/R} e^{\Delta H_{21}^*/RT} \tag{29}$$

416
417

$$v_2 = \frac{hN}{M_2} e^{-\Delta s_2^*/R} e^{\Delta H_2^*/RT} \tag{30}$$

418
419   The explained approach was adopted in this study to represent kinematic viscosities that were
420 calculated via measured dynamic viscosities and densities. It was calculated accuracies as 23%, 17%
421 and 15% for MDEA + H_2O, DMEA + H_2O and DEEA + H_2O mixtures. These deviations are relatively
422 high and questioning that adopted method with McAllister's three-body model is viable to use for
423 correlating kinematic viscosities of the considered mixtures. Accordingly, kinematic viscosity data
424 were fitted at different temperatures instead of a temperature range using Equation (25) to see
425 improvements in the accuracies. The reported AARD using Equation (25) are 8.4%, 9.2% and 16% for
426 MDEA + H_2O, DMEA + H_2O and DEEA + H_2O mixtures. It indicates that data fitting at different
427 temperatures improves the accuracies of viscosity representation except for the DEEA + H_2O. Table
428 15 lists the calculated parameters of Equation (25) at different temperatures. McAllister stated the
429 necessity of taking into account other interactions that are involving more than three molecules in a
430 three dimensional space instead of one plane for the scenario of two types of molecules having a size
431 (radius) difference by more than a factor of 1.5 [39]. McAllister's four-body model discusses such
432 interactions however the fitting of kinematic viscosity data into four-body model is not discussed in
433 this work.

434

435   **Table 15.** Calculated parameters of McAllister's three-body model

| T / K | Mixtures | | | | | |
| | MDEA(1) + H₂O(2) | | DMEA(1) + H₂O(2) | | DEEA(1) + H₂O(2) | |
	$v_{12}(\times 10^6)$	$v_{21}(\times 10^6)$	$v_{12}(\times 10^6)$	$v_{21}(\times 10^6)$	$v_{12}(\times 10^6)$	$v_{21}(\times 10^6)$
293.15	44.0582	2089.1458	3.2724	596.7573	2.7885	1646.6703
298.15	33.9711	1340.1148	2.9023	385.8739	2.3762	1001.7568
303.15	26.1935	883.1637	2.6000	255.3182	2.0452	624.2248
308.15	20.3995	597.3544	2.3060	173.9052	1.7780	402.8284
313.15	16.2081	414.6814	2.0658	121.4510	1.5613	266.5363
318.15	13.0073	296.0447	1.8692	87.3140	1.3573	184.4744
323.15	10.4386	216.2663	1.6745	64.2968	1.1800	131.5663
328.15	8.5464	162.4728	1.5001	48.5945	1.0466	96.5934
333.15	7.0675	124.2767	1.3573	37.5439	0.9282	72.6396
338.15	5.8446	97.0776	1.2282	29.5331	0.8151	56.2896
343.15	4.8818	77.1314	1.1113	23.7008	0.7229	44.5010
348.15	4.2867	59.2349	1.0055	19.2115	0.6412	35.7128
353.15	3.6529	48.6431	0.9190	15.7291	0.5801	28.9483
AARD (%)	8.4		9.2		16	

4. Conclusions

Densities of MDEA + H₂O, DMEA + H₂O and DEEA + H₂O mixtures were measured for amine mass fraction range from 0.3 to 1 for the temperature range from 293.15 K to 353.15 K. The measured density of MDEA + H₂O mixtures increases with increase of MDEA concentration until a maximum and then decreases. For the density of DMEA + H₂O and DEEA + H₂O mixtures, a maximum reported at $x_1 = 0$ and density continues to decrease with increase of amine concentration. The excess molar volumes V^E were negative for the all mixtures and temperature dependent. This indicates efficient molecular packing and existence of strong intermolecular interactions such as H-bonds among unlike molecules in the mixtures. The density correlations based on Redlich-Kister type polynomials for excess molar volume V^E and density deviation $ln(\rho_\gamma)$ represented measured densities with good accuracy signifying their applicability to perform engineering calculations. The proposed Redlich-Kister type polynomials with linear temperature dependency were able to calculate partial molar volume $\overline{V_1^\infty}$ of amines at infinite dilution in H₂O with acceptable accuracies compared to values reported in literature.

Viscosities of MDEA + H₂O, DMEA + H₂O and DEEA + H₂O mixtures were measured for amine mass fraction w_1 range from 0.3 to 1 for the temperature range from 293.15 K to 363.15 K. The calculated viscosity deviation η^E and excess free energy of activation for viscous flow ΔG^{E*} could be explained the intermolecular interactions among unlike molecules in the mixtures. The proposed viscosity correlations were able to represent measured data with acceptable accuracies. The McAllister's three-body model was adopted to correlate kinematic viscosities calculated from measured viscosities and densities at different concentrations and temperatures. The accuracies of the data fits into three-body model are relatively low compared to the proposed viscosity correlations in this work and it is recommended to examine McAllister's four-body model for better data representation.

Nomenclature

Latin symbols		Greek symbols	
G_{12}	Characteristic constant	η	Viscosity (dynamic) of the mixture, mPa·s
ΔG^*	Free energy of activation for viscous flow, J·mol⁻¹	η^E	Viscosity deviation in Equation (17), mPa·s
ΔG^{E*}	Excess free energy of activation for viscous flow, J·mol⁻¹	η_i	Viscosity of pure component, mPa·s

h	Planck's constant, J·s	η_γ	Viscosity deviation in Equation (22), mPa·s	
ΔH^*	Enthalpy of activation for viscous flow, J·mol^{-1}	ρ	Density of the mixture, kg·m^{-3}	
M	Molecular weight, kg·mol^{-1}	ρ_i	Density of pure components, kg·m^{-3}	
M_1	Molecular weight of amine, kg·mol^{-1}	ρ_1	Density of pure amine, kg·m^{-3}	
M_2	Molecular weight of H$_2$O, kg·mol^{-1}	ρ_2	Density of pure H$_2$O, kg·m^{-3}	
N	Number of data points	ρ_γ	Density deviation, kg·m^{-3}	
N_A	Avogadro's number, mol^{-1}	ν	Kinematic viscosity, m^2·s^{-1}	
R	Gas constant, J·mol^{-1}·K^{-1}	ν_{12}, ν_{21}	McAllister's model parameters	
ΔS^{E*}	Excess entropy of activation for viscous flow, J·mol^{-1}·K^{-1}			
ΔS^*	Entropy of activation for viscous flow, J·mol^{-1}·K^{-1}			
T	Temperature, K			
V	Molar volume of the mixture, m^3·mol^{-1}			
V^E	Excess molar volume, m^3·mol^{-1}			
V_1^0	Molar volume of pure amine, m^3·mol^{-1}			
V_2^0	Molar volume of pure H$_2$O, m^3·mol^{-1}			
$\overline{V_i}$	Partial molar volume of component in the mixture, m^3·mol^{-1}			
$\overline{V_1}$	Partial molar volume of amine in the mixture, m^3·mol^{-1}			
$\overline{V_2}$	Partial molar volume of H$_2$O in the mixture, m^3·mol^{-1}			
$\overline{V_1^\infty}$	Partial molar volume of amine at infinite dilution in H$_2$O, m^3·mol^{-1}			
$\overline{V_2^\infty}$	Partial molar volume of H$_2$O at infinite dilution in amine, m^3·mol^{-1}			
x_i	Mole fraction of component in the mixture			
x_1	Mole fraction of amine in the mixture			
x_2	Mole fraction of H$_2$O in the mixture			
Y^E	Excess property			
Y_i^m	Measured property			
Y_i^c	Calculated property			

Conflicts of Interest: The authors declare no conflict of interest.

References

1. Metz, B.; Davidson, O.; Coninck, H.D.; Loos, M.; Meyer, L. *IPCC Special Report on Carbon Dioxide Capture and Storage*; United States of America, New York, 2005.

2. Nwaoha, C.; Tontiwachwuthikul, P.; Benamor, A. A comparative study of novel activated AMP using 1,5-diamino-2-methylpentane vs MEA solution for CO$_2$ capture from gas-fired power plant. *Fuel* **2018**, *234*, 1089-1098, doi:10.1016/j.fuel.2018.07.147.

3. Nwaoha, C.; Saiwan, C.; Supap, T.; Idem, R.; Tontiwachwuthikul, P.; Rongwong, W.; Al-Marri, M.J.; Benamor, A. Carbon dioxide (CO_2) capture performance of aqueoustri-solvent blends containing 2-amino-2-methyl-1-propanol (AMP) and methyldiethanolamine (MDEA) promoted by diethylenetriamine (DETA). *International Journal of Greenhouse Gas Control* **2016**, *53*, 292-304, doi:10.1016/j.ijggc.2016.08.012.

4. Kim, C.J.; Savage, D.W. Kinetics of carbon dioxide reaction with diethylaminoethanol in aqueous solutions. *Chemical Engineering Science* **1987**, *42*, 1481-1487, doi:10.1016/0009-2509(87)85020-0.

5. Rinker, E.B.; Sami, S.A.; Sandall, O.C. Kinetics and modelling of carbon dioxide absorption into aqueous solutions of N-methyldiethanolamine. *Chemical Engineering Science* **1995**, *50*, 755-768, doi:10.1016/0009-2509(94)00444-V.

6. Monteiro, J.G.M.S.; Pinto, D.D.D.; Zaidy, S.A.H.; Hartono, A.; Svendsen, H.F. VLE data and modelling of aqueous N,N-diethylethanolamine (DEEA) solutions. *International Journal of Greenhouse Gas Control* **2013**, *19*, 432-440, doi:10.1016/j.ijggc.2013.10.001.

7. Henni, A.; Li, J.; Tontiwachwuthikul, P. Reaction kinetics of CO_2 in Aqueous 1-Amino-2-Propanol, 3-Amino-1-Propanol, and Dimethylmonoethanolamine solutions in the temperature range of 298−313 K using the stopped-flow technique. *Industrial & Engineering Chemistry Research* **2008**, *47*, 2213-2220, doi:10.1021/ie070587r.

8. Zhang, J.; Fennell, P.S.; Trusler, J.P.M. Density and Viscosity of Partially Carbonated Aqueous Tertiary Alkanolamine Solutions at Temperatures between (298.15 and 353.15) K. *Journal of Chemical & Engineering Data* **2015**, *60*, 2392-2399, doi:10.1021/acs.jced.5b00282.

9. Versteeg, G.F.; Van Swaaij, W.P.M. Solubility and diffusivity of acid gases (carbon dioxide, nitrous oxide) in aqueous alkanolamine solutions. *J. Chem. Eng. Data* **1988**, *33*, 29-34, doi:10.1021/je00051a011.

10. Aronu, U.E.; Hartono, A.; Svendsen, H.F. Density, viscosity, and N_2O solubility of aqueous amino acid salt and amine amino acid salt solutions *J. Chem. Thermodynamics* **2012**, *45*, 90-99.

11. Idris, Z.; Kummamuru, N.B.; Eimer, D.A. Viscosity measurement of unloaded and CO_2-loaded aqueous monoethanolamine at higher concentrations. *Journal of Molecular Liquids* **2017**, *243*, 638-645.

12. Hawrylak, B.; Bruke, S.E.; Palepu, R. Partial molar and excess volumes and adiabatic compressibilities of binary mixtures of ethanolamines with water. *Journal of Solution Chemistry* **2000**, *29*, 575-593.

13. Maham, Y.; Teng, T.T.; Mather, A.E.; Hepler, L.G. Volumetric properties of (water + diethanolamine) systems. *Can. J. Chem* **1995**, *73*, 1514-1519.

14. Maham, Y.; Teng, T.T.; Hepler, L.G.; Mather, A.E. Volumetric properties of aqueous solutions of monoethanolamine, mono- and dimethylethanolamines at temperatures from 5 to 80 °C I. *Thermochimica Acta* **2002**, *386*, 111-118, doi:10.1016/S0040-6031(01)00812-7.

15. Zhang, F.-Q.; Li, H.-P.; Dai, M.; Zhao, J.-P.; Chao, J.P. Volumetric properties of binary mixtures of water with ethanolamine alkyl derivatives. *Thermochimica Acta* **1995**, *254*, 347-357, doi:10.1016/0040-6031(94)02127-A.

16. Lebrette, L.; Maham, Y.; Teng, T.T.; Hepler, L.G.; Mather, A.E. Volumetric properties of aqueous solutions of mono, and diethylethanolamines at temperatures from 5 to 80 °C II. *Thermochimica Acta* **2002**, *386*, 119-126, doi:10.1016/S0040-6031(01)00813-9.

17. Ma, D.; Liu, Q.; Zhu, C.; Feng, H.; Ma, Y. Volumetric and viscometric properties of ternary solution of (N-methyldiethanolamine + monoethanolamine + ethanol). *The Journal of Chemical Thermodynamics* **2019**, *134*, 5-19, doi:10.1016/j.jct.2019.02.019.

18. Begum, S.K.; Clarke, R.J.; Ahmed, M.S.; Begum, S.; Saleh, M.A. Volumetric, viscosimetric and surface properties of aqueous solutions of triethylene glycol, tetraethylene glycol, and tetraethylene glycol dimethyl ether. *Journal of Molecular Liquids* **2013**, *177*, 11-18, doi:10.1016/j.molliq.2012.09.015.

19. Rafiee, H.R.; Frouzesh, F. Volumetric properties for binary and ternary mixtures of allyl alcohol, 1,3-dichloro-2-propanol and 1-ethyl-3-methyl imidazolium ethyl sulfate [Emim][EtSO4] from T=298.15 to 318.15K at ambient pressure. *Thermochimica Acta* **2015**, *611*, 36-46, doi:10.1016/j.tca.2015.04.027.

20. Aminabhavi, T.M.; Aralaguppi, M.I.; Bindu, G.; Khinnavar, R.S. Densities, Shear Viscosities, Refractive Indices, and Speeds of Sound of Bis(2-methoxyethyl) Ether with Hexane, Heptane, Octane, and 2,2,4-Trimethylpentane in the Temperature Interval 298.15-318.15 K. *Journal of Chemical & Engineering Data* **1994**, *39*, 522-528, doi:10.1021/je00015a028.

21. Hartono, A.; Svendsen, H.F. Density, viscosity, and excess properties of aqueous solution of diethylenetriamine (DETA). *J. Chem. Thermodynamics* **2009**, *41*, 973-979, doi:10.1016/j.jct.2008.11.012.

22. Redlich, O.; Kister, A.T. Algebraic representation of thermodynamic properties and the classification of solutions. *Ind. Eng. Chem.* **1948**, *40*, 345-348.

23. Maham, Y.; Teng, T.T.; Hepler, L.G.; Mather, A.E. Densities, excess molar volumes, and partial molar volumes for binary mixtures of Water with Monoethanolamine, Diethnolamine, and Triethanolamine from 25 to 80 °C. *Journal of Solution Chemistry* **1994**, *23*, 195-205.

24. Hepler, L.G. Thermal expansion and structure in water and aqueous solutions. *Can. J. Chem* **1969**, *47*, 4613-4617.

25. Teng, T.T.; Maham, Y.; Hepler, L.G.; Mather, A.E. Viscosity of aqueous solutions of N-Methyldiethanolamine and of Diethanolamine. *J. Chem. Eng. Data* **1994**, *39*, 290-293.

26. Maham, Y.; Lebrette, L.; Mather, A.E. Viscosities and Excess Properties of Aqueous Solutions of Mono- and Diethylethanolamines at Temperatures between 298.15 and 353.15 K. *Journal of Chemical & Engineering Data* **2002**, *47*, 550-553, doi:10.1021/je015528d.

27. Bernal-García, J.M.; Hall, K.R.; Estrada-Baltazar, A.; Iglesias-Silva, G.A. Density and viscosity of aqueous solutions of N,N-dimethylethanolamine at p=0.1 MPa from T=(293.15 to 363.15) K. *The Journal of Chemical Thermodynamics* **2005**, *37*, 762-767, doi:10.1016/j.jct.2004.11.016.

28. Kauzmann, W.; Eyring, H. The Viscous Flow of Large Molecules. *Journal of the American Chemical Society* **1940**, *62*, 3113-3125, doi:10.1021/ja01868a059.

29. Oskoei, A.G.; Safaei, N.; Ghasemi, J. Densities and Viscosities for Binary and Ternary Mixtures of 1,4-Dioxane + 1-Hexanol + N,N-Dimethylaniline from T = (283.15 to 343.15) K. *Journal of Chemical & Engineering Data* **2008**, *53*, 343-349, doi:10.1021/je700344f.

30. Fort, R.J.; Moore, W.R. Viscosities of binary liquid mixtures. *Transactions of the faraday society* **1966**, *62*, 1112-1119.

31. Bhatia, S.C.; Bhatia, R.; Dubey, G.P. Studies on transport and thermodynamic properties of binary mixtures of octan-1-ol with chloroform, 1,2-dichloroethane and 1,1,2,2-tetrachloroethane at 298.15 and 308.15 K. *Journal of Molecular Liquids* **2009**, *144*, 163-171, doi:10.1016/j.molliq.2008.11.003.

32. Grunberg, L.; Nissan, A.H. Mixture Law for Viscosity. *Nature* **1949**, *164*, 799-800, doi:10.1038/164799b0.

33. Eyring, H. Viscosity, Plasticity, and Diffusion as example of absolute reaction rates. *Journal of chemical physics* **1936**, *4*, 283-291.

34. Meyer, R.; Meyer, M.; Metzger, J.; Peneloux, A. Thermodynamic and physicochemical properties of binary solvent *Journal de Chimie Physique et de Physico-Chimie Biologique* **1971**, *68*, 406-412.

558   35.   Kinart, C.M.; Kinart, W.J.; Ćwiklińska, A. 2-Methoxyethanol–Tetrahydrofuran–Binary Liquid System.
559   Viscosities, densities, excess molar volumes and excess Gibbs activation energies of viscous flow at
560   various temperatures. *Journal of Thermal Analysis and Calorimetry* **2002**, *68*, 307-317,
561   doi:10.1023/A:1014981921097.

562   36.   Oswal, S.; Rathnam, M.V. Viscosity data of binary mixtures: ethyl acetate + cyclohexane, + benzene, +
563   toluene, + ethylbenzene + carbon tetrachloride, and + chloroform at 303.15 K. *Canadian Journal of*
564   *Chemistry* **1984**, *62*, 2851-2853, doi:10.1139/v84-482.

565   37.   Ćwiklińska, A.; Kinart, C.M. Thermodynamic and physicochemical properties of binary mixtures of
566   nitromethane with {2-methoxyethanol+2-butoxyethanol} systems at T=(293.15, 298.15, 303.15, 308.15,
567   and 313.15)K. *The Journal of Chemical Thermodynamics* **2011**, *43*, 420-429, doi:10.1016/j.jct.2010.10.016.

568   38.   Hartono, A.; Mba, E.O.; Svendsen, H.F. Physical properties of partially CO_2 loaded aqueous
569   monoethanolamine (MEA). *J. Chem. Eng. Data* **2014**, *59*, 1808-1816.

570   39.   McAllister, R.A. The viscosity of liquid mixtures. *A.I.Ch.E. Journal* **1960**, *6*, 427-431.

571   40.   Karunarathne, S.S.; Øi, L.E. Density and viscosity correlations for aqueous 3-amino-1-propanol and
572   monoethanol amine mixtures. In Proceedings of SIMS 60, Västerås, Sweden.

573

574

Article E

Artificial neural networks (ANNs) for density and viscosity predictions of CO_2 loaded alkanolamine + H_2O mixtures.

Karunarathne, S.S.; Chhantyal, K.; Eimer, D.A.; Øi, L.E. Paper submitted in journal of **Chemengineering** and is under review. The initial manuscript submitted to the journal is attached in this thesis.

1   *Type of the Paper (Article)*

Artificial Neural Networks (ANNs) for Density and Viscosity Predictions of CO_2 loaded Alkanolamine + H_2O mixtures.

5   **Sumudu S. Karunarathne [1], Khim Chhantyal [2], Dag A. Eimer [1] and Lars E. Øi [1,*]**

6   [1]   Faculty of Technology, Natural Sciences and Maritime Studies, University of South-Eastern Norway,
7   Kjølnes Ring 56, Porsgrunn 3901, Norway; sumuduunimrt@gmail.com
8   [2]   National Oilwell Varco; khim.chhantyal@nov.com
9   *   Correspondence: lars.oi@usn.no; Tel.: +47-35575141

11 **Abstract:** Physical properties like density and viscosity of alkanolamine + H_2O (water) + CO_2
12 (Carbon dioxide) mixtures take a significant attention as they are essential in equipment sizing,
13 mathematical modelling and simulations of amine-based post-combustion CO_2 capture processes.
14 Non-linear models based on Artificial Neural Networks (ANNs) were trained to correlate measured
15 densities and viscosities of MEA (Monoethanol amine) + H_2O, MEA + H_2O + CO_2, and AMP (2-
16 amino-2-methyl-1-propanol) + MEA + H_2O + CO_2 mixtures are discussed and results are compared
17 with conventional correlations found in literature. For CO_2 loaded aqueous amine mixtures, results
18 from the ANN models are in good agreement with measured properties with less than 1% AARD
19 (average absolute relative deviation). ANN based methodology shows much better agreement
20 between calculated and measured values than conventional correlations.

21 **Keywords:** Density; Viscosity; CO_2 capture; ANN; Alkanolamine

22

1. Introduction

24   Carbon dioxide (CO_2) removal from flue gas using chemical absorption has been studied
25 intensively to find a suitable alkanolamine to make the process feasible. It has been proven that
26 chemical absorption with aqueous alkanolamines is an efficient method for CO_2 capture where the
27 gas streams have low CO_2 concentrations. Alkanolamines exhibit different physicochemical
28 properties depending on the structural characteristics due to the hydroxyl and the amino groups. The
29 amino group in the alkanolamine turns amine into a base, which allows reacting amine with acid
30 gases [1,2]. The presence of a hydroxyl group enhances the water solubility and reduces the volatility.
31 Monoethanol amine (MEA) is a primary amine known as the most basic and reactive amine for acid
32 gas removal [1]. Although MEA provides high reactivity, it has thermodynamic limitations that limit
33 the overall performance of the CO_2 capture [3]. As a result, the interest has shifted towards other
34 amine solvents like sterically hindered amines, which overcome several issues with using MEA. The
35 2-amino-2-methyl-1-propanol (AMP) is a sterically hindered primary amine, which provides high
36 absorption capacity with superior stripping qualities [4,5]. The aqueous blend of AMP with MEA can
37 provide high absorption capacity and reaction rate under low energy demand in favour of process
38 feasibility.

39   Physical properties such as density and viscosity of CO_2 loaded aqueous amine mixtures are
40 used in process equipment design, modelling and simulation of the amine-based post-combustion
41 CO_2 capture processes. Several empirical correlations were developed by Weiland, *et al.* [6], Han, *et*
42 *al.* [7] and Jayarathna, Weerasooriya, Dayarathna, Eimer and Melaaen [2], which are acceptable and
43 can be used in process design and simulations. For the density of aqueous MEA mixtures, the
44 approach of suggesting a Redlich – Kister type polynomial for the excess molar volume is commonly

45   used [8]. Similarly, the viscosity deviation from the ideal mixtures was correlated to fit viscosity data
46   of the aqueous mixtures. Constructing a theoretical model that suits the CO_2 loaded aqueous amine
47   mixtures is a difficult task due to inadequate understanding of the physics and chemistry of the
48   mixtures. The Redlich – Kister model for excess properties of binary mixtures is given as
49

$$Y^E = x_2(1 - x_2) \sum_{i=0}^{i=n} A_i(1 - 2x_2)^i \tag{1}$$

50

51   where Y^E, x_i and A_i are excess property, mole fraction of the components and regression
52   parameters respectively.
53   This model has been applied in several studies to correlate excess volume of the aqueous amine
54   or amine mixtures to correlate density of the solutions [7,9-11]. It requires a higher degree polynomial
55   with a large number of parameters to achieve a good fit for the measured data. Hartono, Mba and
56   Svendsen [11] suggested a lower degree polynomial with less number of parameters for the aqueous
57   monoethanol amine (MEA) mixtures. The Redlich – Kister approach can be extended to ternary
58   mixtures by considering binary parameters as explained in Equation (1) [12,13]. Literature can be
59   found for the application of Redlich – Kister equation to correlate excess viscosity of binary amine
60   mixtures [14], while Hartono, Mba and Svendsen [11] used a lower degree polynomial to achieve an
61   acceptable accuracy of predictions.
62   It is important to correlate the physical properties of CO_2 loaded aqueous amine mixtures as the
63   absorber and desorber operate with solvents with dissolved CO_2. The accuracy of design of such a
64   process highly depends on solution properties. Only a few attempts have been made to develop
65   correlations for CO_2 loaded amine solutions and they are based on statistical regression on measured
66   data. Weiland, Dingman, Cronin and Browning [6] and Hartono, Mba and Svendsen [11] proposed
67   correlations for density and viscosity of CO_2 loaded aqueous MEA mixtures. Zhang, *et al.* [15]
68   discussed the density and viscosity of CO_2 loaded aqueous 2-dimethylaminoethanol (DMAE) and 2-
69   diethylaminoethanol (DEAE) solutions.

70   *1.1. Weiland's density and viscosity correlations*

71   1.1.1. Density correlation

72   Weiland's density correlation [6] is defined by Equation (2) to (5)

$$\rho_{loaded} = \frac{x_1 M_1 + x_2 M_2 + x_3 M_3}{V} \tag{2}$$

$$V = x_1 V_1 + x_2 V_2 + x_3 V_3 + x_1 x_2 V^* + x_1 x_3 V^{**} \tag{3}$$

$$V_1 = \frac{M_1}{aT^2 + bT + c} \tag{4}$$

$$V^{**} = d + ex_1 \tag{5}$$

73   where ρ_{loaded}, V_i, T, x_i and M_i are density of the CO_2 loaded aqueous MEA mixture, molar
74   volume, temperature, mole fraction and molecular weight of the species. Molar volume with no
75   subscription refers the molar volume of the mixture and subscription $i = 1, 2$ and 3 are referred to
76   MEA, H_2O and CO_2 in the mixture. V^* and V^{**} are regression parameters used to fit the density
77   data.

78

79

80   1.1.2. Viscosity correlation

81   Weiland's viscosity correlation [6] is defined by Equation (6)

$$\frac{\eta_{loaded}}{\eta_{H_2O}} = exp\left(\frac{[(a \cdot w_{MEA} + b)T + (c \cdot w_{MEA} + d)][\alpha(e \cdot w_{MEA} + f \cdot T + g) + 1]w_{MEA}}{T^2}\right) \quad (6)$$

where η_{loaded}, η_{H_2O}, T, α and w_{MEA} are viscosity of CO_2 loaded aqueous MEA mixture, viscosity of H_2O, temperature, CO_2 loading and weight percentage of MEA in the aqueous mixture respectively.

82   *1.2. Hartono's density and viscosity correlations*

83   1.2.1. Density correlation

84   Hartono's density correlations [11] are defined by Equation (7) to (11)
85   For non-loaded solutions,

$$V^E = x_1 x_2 \cdot 10^{-6} \cdot (A_0 + A_1 t + A_2 x_1 + A_3 x_1^2) \quad (7)$$

$$\rho_{unloaded} = \frac{\sum_1^2 x_i \cdot M_i}{V^E + \sum_1^2 \frac{x_i \cdot M_i}{\rho_i}} \quad (8)$$

86   where V^E, t, x_i, M_i, $\rho_{unloaded}$ and ρ_i are excess molar volume, temperature, mole fractions,
87   molecular weight, density of the aqueous mixture and density of the pure components respectively.
88
89   For CO_2 loaded solutions,
90

$$\rho_{loaded} = \frac{\rho_{unloaded}}{1 - w_{CO2loaded}(1 - \Phi^3)} \quad (9)$$

$$w_{CO2loaded} = \frac{\alpha x_1 M_3}{x_1 M_1 + (1 - x_1 - \alpha x_1)M_2 + \alpha x_1 M_3} \quad (10)$$

$$\Phi = \frac{a_1 x_1 \alpha + a_2 x_1}{a_3 + x_1} \quad (11)$$

91
92   where ρ_{loaded}, $\rho_{unloaded}$, $w_{CO2loaded}$, x_i, M_i, α and Φ are density of the CO_2 loaded aqueous
93   MEA mixture, density of the aqueous MEA mixture, CO_2 added to the solution on a mass basis, mole
94   fractions and molecular weight, CO_2 loading and volume expansion caused by the CO_2 addition
95   respectively. Here, $i = 1, 2$ and 3 are referred to MEA, H_2O and CO_2.

96   1.2.2. Viscosity correlation

97   Hartono's viscosity correlation [11] are defined by Equation (12) to (15)
98   For non-loaded solutions,

$$ln(\eta_{unloaded}) = ln(\Delta\eta) + \sum_{i=1}^2 x_i ln(\eta_i) \quad (12)$$

$$ln(\Delta\eta) = x_1 x_2 (l_1 + l_2 t + l_3 t^2 + l_4 x_1) \quad (13)$$

99
100   where $\eta_{unloaded}, \Delta\eta, \eta_i$ and x_i are viscosity of the aqueous MEA mixture, viscosity deviation from
101   ideal mixture viscosity, viscosity of pure components and mole fractions respectively.
102

103 For CO_2 loaded solutions,
104

$$ln(\eta_{loaded}) = x_3 ln(\Delta\eta^*) + (1 - x_3)ln(\eta_{unloaded}) \tag{14}$$

$$ln(\Delta\eta^*) = \frac{b_1 \alpha x_1 + b_2 x_1}{b_3 + x_1} \tag{15}$$

105
106 where $\eta_{loaded}, \eta_{unloaded}, \Delta\eta^*, \alpha$ and x_i are viscosity of the CO_2 loaded aqueous MEA mixture,
107 viscosity of the aqueous MEA mixture, viscosity deviation, CO_2 loading and mole fractions
108 respectively. Here, $i = 1, 2$ and 3 are referred to MEA, H_2O and CO_2.
109
110   The approach of constructing an artificial neural network (ANN) to correlate physical properties
111 has been done for various liquid mixtures including different amine blends that can be used in post-
112 combustion CO_2 capture. A properly trained ANN is able to correlate data with high accuracy. Garg,
113 *et al*. [16] reported a study of density prediction using ANNs for aqueous MEA mixtures under
114 different compositions and temperatures. Pouryousefi, *et al*. [17] discussed ANNs for various
115 physical properties including density, viscosity, refractive index, heat capacity, thermal conductivity
116 and thermal diffusivity of CO_2 loaded MEA + DEAB (4-(diethylamino)-2-butanol) + H_2O and MEA+
117 MDEA (methyldiethanol amine) + H_2O mixtures. Haratipour, *et al*. [18] adopted an approach of
118 training ANNs for density and viscosity of various blends of alkanolamine with H_2O. Pierantozzi, *et*
119 *al*. [19] investigated the applicability of ANNs for predicting the thermal conductivity of liquid
120 alcohols for a wide range of temperatures. The approach has been taken into more complex mixtures
121 such as biodiesel that contains various components. Several properties like density, viscosity, cetane
122 number, iodine value and induction period were correlated using ANNs by Rocabruno-Valdés, *et al*.
123 [20] and Barradas Filho, *et al*. [21].
124   In this study, several feedforward backpropagation artificial neural networks are trained to
125 predict density and viscosities of MEA + H_2O + CO_2 and AMP + MEA + H_2O + CO_2 mixtures. The
126 predictions are compared with existing correlations found in the literature.

127 **2. Materials and Methods**

128 *2.1 Material description and sample preparation*

129   Table 1 lists the material used in this study. Deionized water (resistivity 18.2 MΩ·cm) was
130 degassed using a rotary evaporator for the preparation of aqueous amine solutions. The weight of
131 the materials was measured via an electronic balance from METTLER TOLEDO (XS403S) with a
132 resolution of 1 mg. The CO_2 loading of aqueous amine solutions was performed by bubbling CO_2
133 through an aqueous amine mixture until the pH becomes steady. Later, a series of CO_2 loaded
134 solutions were prepared by mixing CO_2 loaded aqueous amine solution and aqueous amine solution
135 with different mass ratios. The CO_2 concentration in the solutions was determined by a titration
136 method as explained by Jayarathna, Weerasooriya, Dayarathna, Eimer and Melaaen [2] and Han, Jin,
137 Eimer and Melaaen [7].

138   **Table 1.** **D**escription of materials used for the experiments.

Material	CAS Reg. No.	Purity[a]	Source	Purification
AMP	124-68-5	BioUltra, ≥0.99 (GC)[b]	Sigma-Aldrich	no
MEA	141-43-5	≥0.995	Sigma-Aldrich	no
CO_2	124-38-9	≥0.9999	AGA Norge AS	no
N_2	7727-37-9	≥0.9999	AGA Norge AS	no

139   [a]As given by the supplier. [b]Gas-liquid Chromatography.
140

141 *2.2. Density Measurements*

142 The density of the mixtures was measured using a density meter DMA 4500 from Anton Paar.
143 The density meter consists of a vibrating U-tube in which the resonance frequency of the U-tube with
144 the sample is measured and used for the density calculations. The accuracy of the measurements
145 highly depends on the calibration of the instrument. Accordingly, the DMA 4500 was calibrated with
146 air and degassed water and the validity of the calibration was examined via density check frequently.
147 During the experiments, the sample (approximately 5 mL) should be carefully injected into the U-
148 tube to avoid any bubble formation that causes errors in the final reading. The density measurements
149 in DMA 4500 were performed at atmospheric pressure and the maximum temperature was limited
150 to 363.15 K. A separate sample was used for each measurement at each temperature and composition.
151 Final density measurements were considered as the average of three replicates.

152 *2.3. Viscosity Measurements*

153 The dynamic viscosity of the mixtures was measured using an Anton Paar Physica MCR 101
154 rheometer with a double-gap measuring system. The calibration of the measuring system was
155 performed by using viscosity reference standard S3S from Paragon Scientific Ltd. The viscosity of the
156 viscosity standard fluid was measured and compared with the values at different temperatures as
157 provided by the supplier. The deviations between measured and reference data were considered and
158 measured viscosities of amine + H_2O + CO_2 mixtures were corrected accordingly. For the viscosity of
159 measured temperatures where reference data are not available, viscosity deviations were determined
160 through linear interpolation. In order to maintain the solution temperature precisely, a temperature
161 controlling system with temperature uncertainty 0.03 K is equipped with the instrument. The
162 measurements below the temperature of 303.15 K were obtained using an external Anton Paar
163 Viscotherm VT 2 cooling system with a standard temperature uncertainty of 0.02 K. A liquid sample
164 of 7 mL was transferred into the pressure cell. The pressure cell XL was pressurized with N_2 gas at 4
165 bar to avoid degassing of CO_2 from the sample. The viscosity data were considered as the average of
166 three replicates.

167 *2.4. Experiments*

168 For MEA + H_2O mixtures (30-100 mass% of MEA), the viscosities were measured under the
169 temperature range of 293.15 K - 353.15 K. The density and viscosity of MEA + H_2O + CO_2 mixtures
170 were measured under different MEA concentrations (30-50 by mass% of aqueous solution), five
171 different CO_2 loadings (< 0.6 mol CO_2/ mol MEA) and the temperatures (293.15 K - 353.15 K).
172 Similarly, the density and viscosity of AMP + MEA + H_2O + CO_2 mixtures were over range of different
173 compositions of AMP, MEA and H_2O, five different CO_2 loadings (< 0.6 mol CO_2/mol amine) and the
174 temperature range of 293.15 K-353.15 K. The concentrations of aqueous MEA + H_2O and AMP + MEA
175 + H_2O mixtures with corresponding CO_2 loadings are given in Table 2.

176 **Table 2.** Characteristics of the amine mixtures.

Mixture	CO_2 loading (mol CO_2/mol amine)
30 mass% MEA + 70 mass% H_2O	0, 0.095, 0.175, 0.328, 0.445, 0.543
40 mass% MEA + 60 mass% H_2O	0, 0.105, 0.215, 0.325, 0.436, 0.548
50 mass% MEA + 50 mass% H_2O	0, 0.092, 0.186, 0.290, 0.395, 0.495
21 mass% AMP + 9 mass% MEA + 70 mass% H_2O	0, 0.107, 0.210, 0.308, 0.400, 0.518
24 mass% AMP + 6 mass% MEA + 70 mass% H_2O	0, 0.083, 0.165, 0.314, 0.418, 0.508
27 mass% AMP + 3 mass% MEA + 70 mass% H_2O	0, 0.072, 0,152, 0.246, 0.461, 0.511

177
178
179
180

181 *2.5. Activation Function of the ANN*

182   Several activation functions are available to use in hidden layer as sigmoid, inverse tangent,
183 hyperbolic tangent and saturated linear function. For the ANN developed in this study, the activation
184 or transfer function in the hidden layer is a hyperbolic tangent (τ) and a linear relation (ψ) is used
185 for the output layer. The output of the network can be described as follows
186

$$\theta_s = IW_{(s,1)}In_1 + IW_{(s,2)}In_2 + \cdots + IW_{(s,k)}In_k + b_s^{(1)} \tag{12}$$

187

188 where θ_s, IW, In and $b^{(1)}$ are the input of the neurons in the hidden layer, the input weights, the
189 inputs and bias of neuron in the hidden layer respectively.
190

191 The hyperbolic tangent (τ) and linear relation (ψ) are given in the Equation (13) and (14).

$$f = \tau(\theta_s) = \frac{2}{1 + exp(-2\theta_s)} - 1 \tag{13}$$

$$g = \psi\big(LW \cdot f + b^{(2)}\big) \tag{14}$$

192 where LW, and $b^{(2)}$ are the input weights and bias in the output layer respectively.

193 *2.6. ANN Training*

194   In the developed ANN models, the mole fractions of components and the temperature are
195 considered as the inputs for the network. One hidden layer with multiple neurons is adopted for the
196 training with learning algorithm of Bayesian Regularization (BR). The optimum number of neurons
197 for the hidden layer was found by analyzing the cost function of Mean Squared Error (MSE) for BR
198 [22] as given in Equation (15) over thirty neurons. All the networks are with a single output for
199 density and viscosity in each amine mixture. The input data sets were divided into 70%, 15% and
200 15% randomly for the training, validation and testing. Data were scaled in the range of (-1,1) before
201 they were used for the training of ANN. Figure 1 illustrates a schematic of neurons in an ANN
202 consisting of one hidden layer with a single output. The measured data by the authors to perform
203 this study can be found in the sources [23] and [24].
204
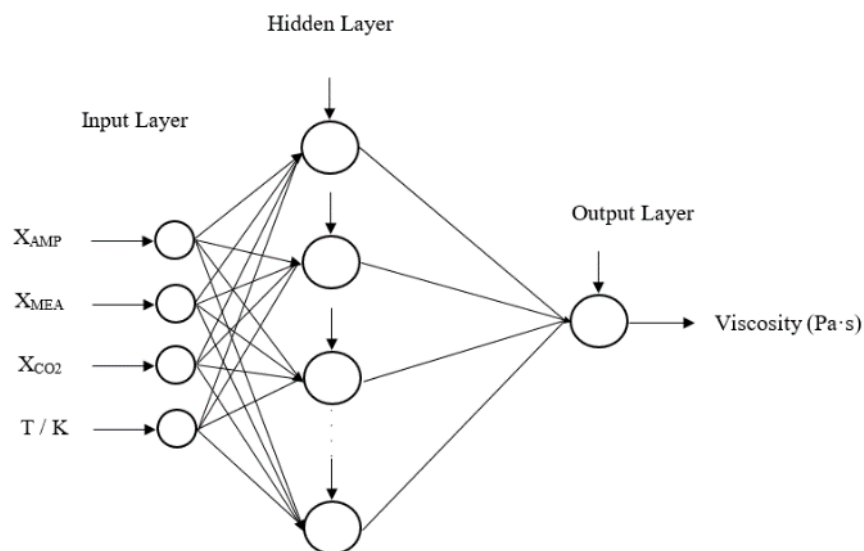
206 **Figure 1.** A schematic of feed forward artificial neural network with one hidden layer.

$$MSE = \frac{1}{2N} \sum_{i=1}^{N} \{(Y_i^E - Y_i^C)^2 + \lambda W^2\} \qquad (15)$$

208 where N, Y_i^E, Y_i^C, λ and W refer the number of data points, the measured property, calculated
209 property, regularization parameter and weight parameter vector respectively.

3. Results and Discussions

211 This section discusses the performance of ANN in density and viscosity predictions of
212 considered CO_2 loaded alkanolamine + H_2O mixtures. The ANN based models were evaluated using
213 average absolute relative deviation (AARD) as given in the Equation (16).

$$AARD \ (\%) = \frac{100\%}{N} \sum_{i=1}^{N} \left| \frac{Y_i^E - Y_i^C}{Y_i^E} \right| \qquad (16)$$

214 where N, Y_i^E and Y_i^C refer to the number of data points, the measured property and calculated
215 property respectively.

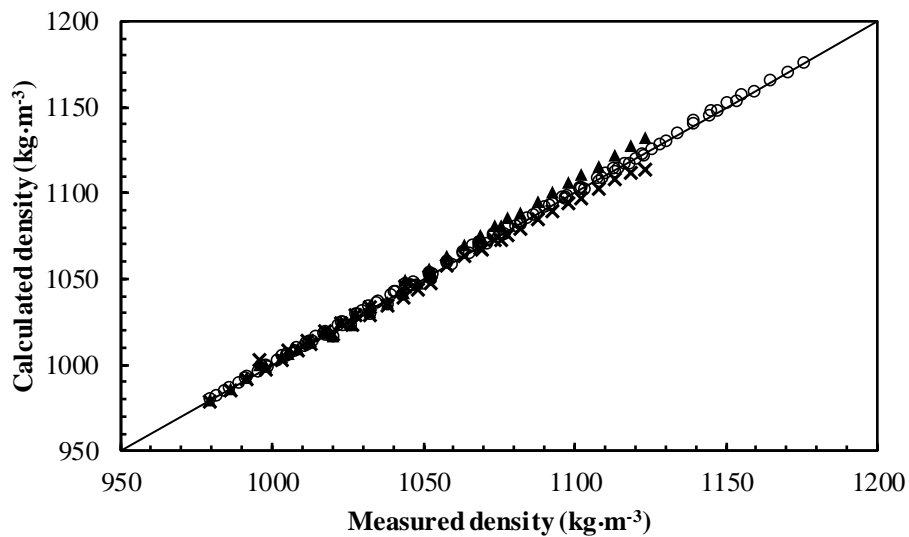*3.1. Density from ANN Based Models and Empirical Correlations*

217 The measured density of MEA + H_2O + CO_2 and AMP + MEA + H_2O + CO_2 mixtures were used
218 to train, validate and test two feed forward back propagation ANNs. The density of the mixtures
219 increases with the increase of dissolved CO_2 and decreases with the increase of temperature. The
220 prediction accuracy was analyzed through calculated AARD between measured data and
221 predictions. Here the measured data were the same data that have been used to train, validate and
222 test the ANNs. Han, Jin, Eimer and Melaaen [7] improved Weiland's correlation to fit data at different
223 temperatures. Accordingly, the improved Weiland's density correlation was adopted to compare
224 with predictions from ANN to study the possible deviations between different approaches. For the
225 density of MEA + H_2O + CO_2 mixtures, mole fractions of MEA, CO_2 and temperature were considered
226 as the inputs. In the CO_2 loaded mixtures, CO_2 reacts with amines to produce carbamate and
227 bicarbonate. The mole fractions of CO_2 in the mixtures were calculated considering it as unreacted
228 with the amine. This method was adopted by several authors [6,11] to develop correlations and the
229 same technique was followed. In AMP + MEA + H_2O + CO_2 mixtures, inputs were considered as mole
230 fractions of AMP, MEA, CO_2 and temperature. Table 3 lists the information related to the trained
231 ANNs for densities.

232 **Table 3.** Performance of trained ANNs for density.

| Property	Liquid mixture	No. of neurons in the hidden layer	AARD %
Density	MEA + H_2O + CO_2	3	0.09
	AMP + MEA + H_2O + CO_2	24	0.004

234 Figure 2 illustrates the comparison of ANN predictions with correlations from Han, Jin, Eimer
235 and Melaaen [7] and Hartono, Mba and Svendsen [11] for MEA + H_2O + CO_2 mixtures. The correlation
236 presented by Han, Jin, Eimer and Melaaen [7] is a modified Weiland's correlation that was fitted for
237 densities of MEA + H_2O + CO_2 mixtures over a range of temperatures. Han's correlation was capable
238 of predicting densities at 0.4 % AARD while Hartono's correlation predicts at a 0.3% AARD.
239 Comparison of these correlations with ANN shows that a properly trained network is capable of
240 predicting density at a high accuracy compared to measured data. A modified Weiland's correlation
241 for amine mixtures with more than one amine is adopted for molar volume of AMP + MEA + H_2O +
242 CO_2 mixtures [24] to fit density and was compared with ANN predictions. The correlation was able
243 to fit density with 0.4% AARD and ANN predictions showed better accuracies compared to the

244 correlation. Figure 3 shows the comparison of correlated densities from ANN and the modified
245 Weiland's correlation.
246

247

248 **Figure 2.** Comparison of correlated density with measured density for MEA + H_2O + CO_2 mixtures.
249 ANN, '○'; Hartono, Mba and Svendsen [11], '▲'; Han, Jin, Eimer and Melaaen [7], '✗'.
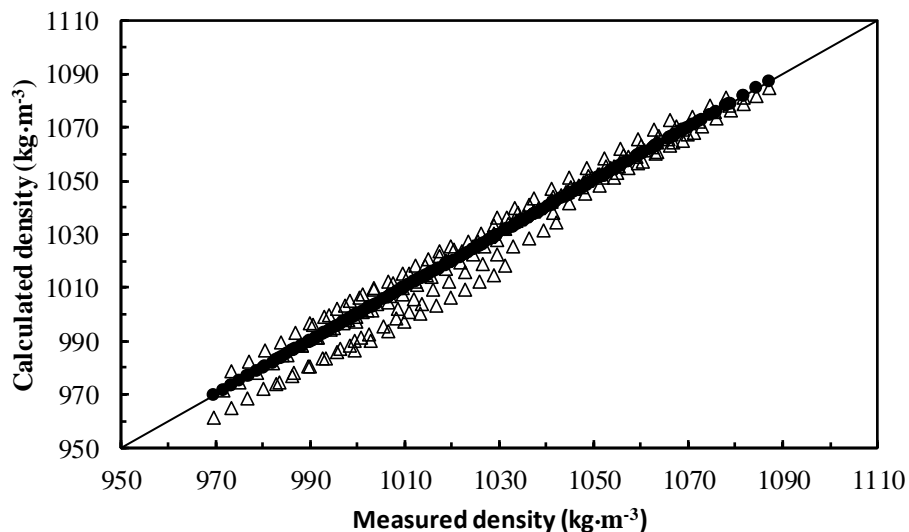
250

251 **Figure 3.** Comparison of correlated density with measured density for AMP + MEA + H_2O + CO_2
252 mixtures. ANN, '●'; Modified Weiland, Dingman, Cronin and Browning [6], '△'.

253 *3.2. Viscosity from ANN based models and emperical correlations*

254 Three feed forward back propagation ANNs were developed for measured viscosities of MEA
255 + H_2O, MEA + H_2O + CO_2 and AMP + MEA + H_2O + CO_2 mixtures. Table 4 summarized the
256 performance (AARD %) of ANN predictions and the number of neurons in each network.
257
258
259
260

261

Table 4. Performance of trained ANNs for viscosity.

| Property	Liquid mixture	No. of neurons in the hidden layer	AARD %
Viscosity	MEA + H_2O	15	0.72
	MEA + H_2O + CO_2	17	0.15
	AMP + MEA + H_2O + CO_2	21	0.16

262

263   The ANN models were developed based on the mixtures with different amine concentrations
264 and CO_2 loadings as given in Table 2. The measured viscosity of MEA + H_2O mixtures were compared
265 with Hartono's correlation and Arachchige's [25] correlation in which the calculated AARD for
266 correlations are 3.14% and 3.5% respectively. This shows that predictions from ANN for MEA + H_2O
267 mixtures have good accuracy compared to the correlations as shown in Figure 4. For the MEA + H_2O
268 + CO_2 mixtures, Hartono's correlation was compared with the ANN model and Figure 5 illustrates
269 the performance of the ANN compared to the correlation. The results revealed that Hartono's
270 correlation was able to predict viscosity at 2.7% AARD for the viscosity of CO_2 loaded 30 mass% MEA
271 mixture and it is higher than the AARD was obtained from trained ANN.

272

273
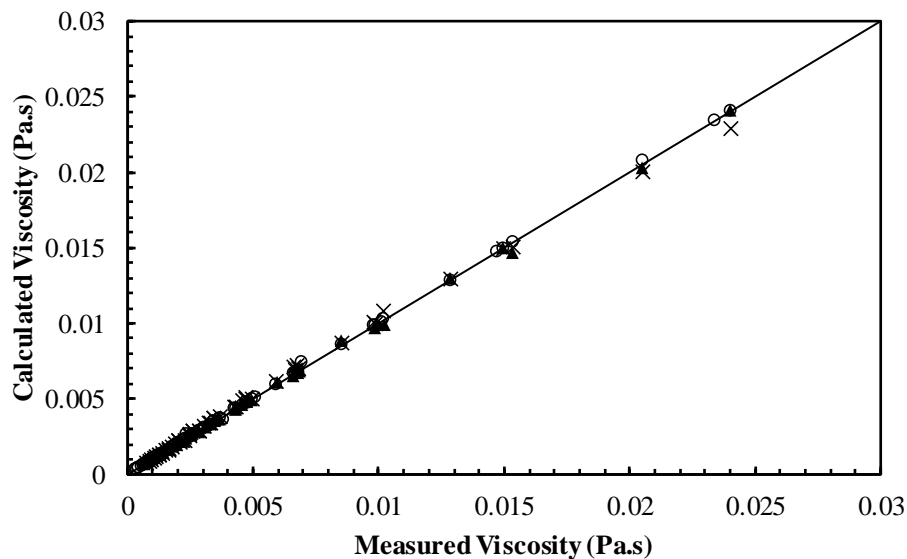
274   **Figure 4.** Comparison of correlated viscosity with measured viscosity for MEA + H_2O mixtures. ANN,
275   '○'; Arachchige, Aryal, Eimer and Melaaen [25], '✗'; Hartono, Mba and Svendsen [11], '▲'.

276   For the viscosities of AMP + MEA + H_2O + CO_2 mixtures, an ANN was trained and validated for
277 the mixtures with different amine concentrations and CO_2 loadings as given in Table 2. The predicted
278 viscosities are in good agreement with measured data with accuracy as mentioned in Table 4. A
279 modified Weiland's viscosity correlation [24] was adopted to compare the performance of ANN as
280 illustrated in Figure 6. The modified Weiland's viscosity correlation was able to fit the measured
281 viscosities with 2.7% AARD. The accuracy of ANN predictions was high in accuracy and the overall
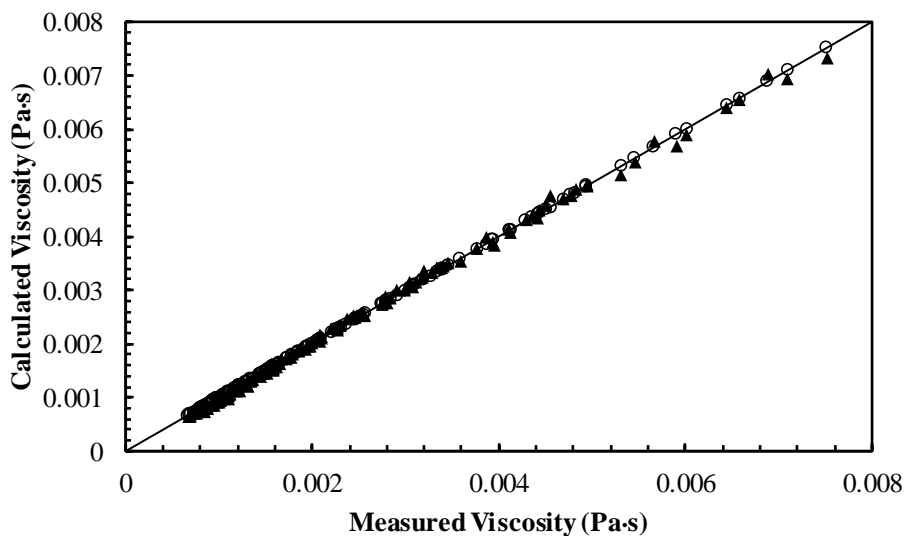282 performance is reported in Table 4.

283

284
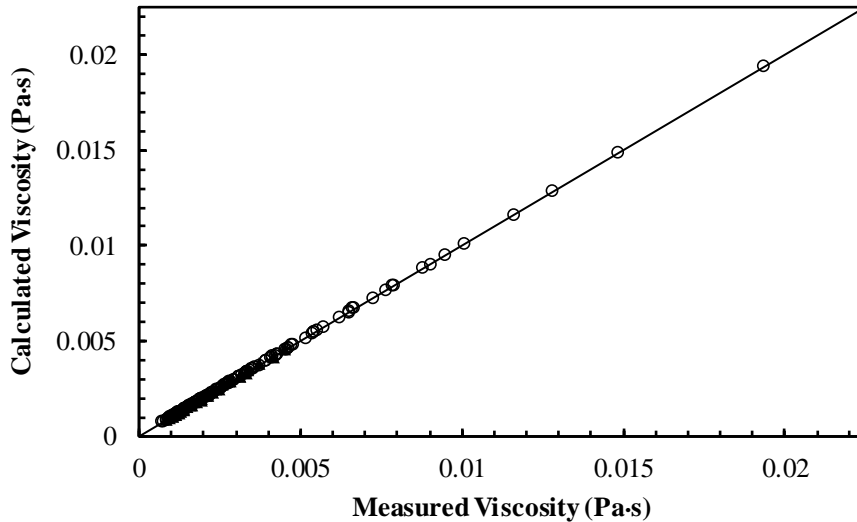
Figure 5. . Comparison of correlated viscosity with measured viscosity for MEA + H_2O + CO_2 mixtures. ANN, '○'; Hartono, Mba and Svendsen [11], '▲'.

287

Figure 6. Comparison of correlated density with measured density for AMP + MEA + H_2O + CO_2 mixtures. ANN, '○'; Modified Weiland, Dingman, Cronin and Browning [6], '▲'.

The study reveals that properly trained feedforward backpropagation ANN models are capable of predicting physical properties of alkanolamine + H_2O + CO_2 mixtures with good accuracy and models are appropriate for engineering applications of designing process equipment and performing mathematical modelling and simulations of absorption and desorption systems.

5. Conclusions

In this work, the use of non-linear models based on feedforward backpropagation ANNs were investigated to predict physical properties of MEA + H_2O, MEA + H_2O + CO_2 and AMP + MEA + H_2O + CO_2 mixtures. ANNs with a single hidden layer and a single output were considered with amine and CO_2 mole fractions and temperature as inputs. Multiple neurons were adopted in the hidden layer to minimize the mean squared error to acquire a good fit with reasonable accuracy. The predictions were compared with conventional physical property correlations proposed by Hartono, Mba and Svendsen [11] and Han, Jin, Eimer and Melaaen [7] for density and Arachchige, Aryal, Eimer

302 and Melaaen [25], Hartono, Mba and Svendsen [11] and modified Weiland, Dingman, Cronin and
303 Browning [6] for viscosity.

304   For the density of MEA + H_2O + CO_2 and AMP + MEA + H_2O + CO_2 mixtures, developed ANN
305 models were able to correlate measured data with an accuracy of 0.09% and 0.004% AARD
306 respectively. Moreover, for the viscosity of MEA + H_2O, MEA + H_2O + CO_2 and AMP + MEA + H_2O +
307 CO_2 mixtures, the accuracies of estimations through developed ANN models were 3.08%, 0.15% and
308 0.16% AARD respectively. Consequently, the estimated properties were found to be in good
309 agreement with measured data. The accuracies of conventional correlations were lower than the
310 accuracies of ANN models indicating that this approach can enhance the reliability of engineering
311 calculations in the equipment sizing, mathematical modelling and simulations of amine-based post-
312 combustion CO_2 capture process.

313

316

317 **Conflicts of Interest:** The authors declare no conflict of interest.

318

319 **References**

320 1.   Kidnay, A.J.; Parrish, W.R. *Fundamentals of Natural Gas Processing*; Taylor & Francis Group: Boca Raton,,
321   2006.

322 2.   Jayarathna, S.; Weerasooriya, A.; Dayarathna, S.; Eimer, D.A.; Melaaen, M.C. Densities and surface
323   tensions of CO_2 loaded aqueous monoethanolamine solution with r=(0.2 to 0.7) at T=(303.15 to 333.15)K.
324   *J. Chem. Eng. Data* **2013**, *58*, 986-992.

325 3.   Sartori, G.; Savage, D.W. Sterically Hindered Amines for CO_2 Removal from Gases. *American Chemical
326   Society* **1983**.

327 4.   Henni, A.; Hromek, J.J.; Tontiwachwuthikul, P.; Chakma, A. Volumetric Properties and Viscosities for
328   Aqueous AMP Solutions from 25 °C to 70 °C. *Journal of Chemical & Engineering Data* **2003**, *48*, 551-556,
329   doi:10.1021/je0201119.

330 5.   Li, M.H.; Lai, M.D. Solubility and Diffusivity of N_2O and CO_2 in (Monoethanolamine + N-
331   Methyldiethanolamine + water) and in (Monoethanolamine + 2-Amino-2-methyl-1-propanol+water). *J.
332   Chem. Eng. Data* **1995**, *40*, 486-492.

333 6.   Weiland, R.H.; Dingman, J.C.; Cronin, D.B.; Browning, G.J. Density and viscosity of some partially
334   carbonated aqueous alkanolamine solutions and their blends. *J. Chem. Eng. Data* **1998**, *43*, 378-382.

335 7.   Han, J.; Jin, J.; Eimer, D.A.; Melaaen, M.C. Density of water (1) + Monoethanolamine (2) + CO_2 (3) from
336   (298.15 to 413.15) K and surface tension of water (1) + Monoethanolamine (2) from (303.15 to 333.15) K.
337   *J. Chem. Eng. Data* **2012**, *57*, 1095-1103.

338 8.   Redlich, O.; Kister, A.T. Algebraic representation of thermodynamic properties and the classification of
339   solutions. *Ind. Eng. Chem.* **1948**, *40*, 345-348.

340 9.   Lee, M.J.; Lin, T.K. Density and viscosity for Monoethanolamine+Water,+Ethanol, and+2-Propanol. *J.
341   Chem. Eng. Data* **1995**, *40*, 336-339.

342 10.   Amundsen, T.G.; Øi, L.E.; Eimer, D.A. Density and viscosity of monoethanolamine+water+carbon
343   dioxide from (25 to 80) °C. *J. Chem. Eng. Data* **2009**, *54*, 3096-3100.

344 11.   Hartono, A.; Mba, E.O.; Svendsen, H.F. Physical properties of partially CO_2 loaded aqueous
345   monoethanolamine (MEA). *J. Chem. Eng. Data* **2014**, *59*, 1808-1816.

346 12.   Hsu, C.H.; Li, M.H. Densities of aqueous blended amines. *J. Chem. Eng. Data* **1997**, *42*, 502-507.

347   13.   Mandal, B.P.; Kundu, M.; Bandyopadhyay, S.S. Density and viscosity of aqueous solution of (N-
348   Methyldiethanolamine + Monoethanolamine), (N-Methyldiethanolamine + Diethanolamine), (2-
349   Amino-2-methyl-1-propanol + Monoethanolamine), and (2-Amino-2-methyl-1-propanol +
350   Diethanolamine). *J. Chem. Eng. Data* **2003**, *48*, 703-707.

351   14.   Islam, M.N.; Islam, M.M.; Yeasmin, M.N. Viscosity of aqueous solution of 2-methoxyethanol, 2-
352   ethoxyethanol, and ethanolamine. *J. Chem. Thermodynamics* **2004**, *36*, 889-893.

353   15.   Zhang, J.; Fennell, P.S.; Trusler, J.P.M. Density and Viscosity of Partially Carbonated Aqueous Tertiary
354   Alkanolamine Solutions at Temperatures between (298.15 and 353.15) K. *Journal of Chemical &*
355   *Engineering Data* **2015**, *60*, 2392-2399, doi:10.1021/acs.jced.5b00282.

356   16.   Garg, S.; Shariff, A.M.; Shaikh, M.S.; Lal, B.; Aftab, A.; Faiqa, N. A neural network approach to predict
357   the density of aqueous MEA solution. *Australian Journal of Basic and Applied Sciences* **2015**, *9*, 415-422.

358   17.   Pouryousefi, F.; Idem, R.; Supap, T.; Tontiwachwuthikul, P. Artificial Neural Networks for Accurate
359   Prediction of Physical Properties of Aqueous Quaternary Systems of Carbon Dioxide (CO2)-Loaded 4-
360   (Diethylamino)-2-butanol and Methyldiethanolamine Blended with Monoethanolamine. *Industrial &*
361   *Engineering Chemistry Research* **2016**, *55*, 11614-11621, doi:10.1021/acs.iecr.6b03018.

362   18.   Haratipour, P.; Baghban, A.; Mohammadi, A.H.; Nazhad, S.H.H.; Bahadori, A. On the estimation of
363   viscosities and densities of CO2-loaded MDEA, MDEA+AMP, MDEA+DIPA, MDEA+MEA, and
364   MDEA+DEA aqueous solutions. *Journal of Molecular Liquids* **2017**, *242*, 146-159,
365   doi:10.1016/j.molliq.2017.06.123.

366   19.   Pierantozzi, M.; Di Nicola, G.; Latini, G.; Coccia, G. Artificial neural network modelling of liquid
367   thermal conductivity for alcohols. *Physics and Chemistry of Liquids* **2018**, *56*, 363-380,
368   doi:10.1080/00319104.2017.1341980.

369   20.   Rocabruno-Valdés, C.I.; Ramírez-Verduzco, L.F.; Hernández, J.A. Artificial neural network models to
370   predict density, dynamic viscosity, and cetane number of biodiesel. *Fuel* **2015**, *147*, 9-17,
371   doi:10.1016/j.fuel.2015.01.024.

372   21.   Barradas Filho, A.O.; Barros, A.K.D.; Labidi, S.; Viegas, I.M.A.; Marques, D.B.; Romariz, A.R.S.; de
373   Sousa, R.M.; Marques, A.L.B.; Marques, E.P. Application of artificial neural networks to predict
374   viscosity, iodine value and induction period of biodiesel focused on the study of oxidative stability.
375   *Fuel* **2015**, *145*, 127-135, doi:10.1016/j.fuel.2014.12.016.

376   22.   Chhantyal, K. Sensor data fusion based modelling of drilling fluid return flow through open channels.
377   University of South-Eastern Norway, 2018.

378   23.   Karunarathne, S.S.; Eimer, D.A.; Øi, L.E. Density, viscosity and free energy of activation for viscous
379   flow of monoethanol amine (1) + H2O (2) + CO2 (3) mixtures. *Fluids* **2019**, *under review*.

380   24.   Karunarathne, S.S.; Eimer, D.A.; Øi, L.E. Density, viscosity and free energy of activation for viscous
381   flow of CO2 loaded AMP, MEA and H2O mixtures. *Journal of Molecular Liquids* **2019**, *under review*.

382   25.   Arachchige, U.S.P.R.; Aryal, N.; Eimer, D.A.; Melaaen, M.C. Viscosities of pure and aqueous solutions
383   of Monoethanolamine (MEA), Diethanolamine (DEA), and N-Methyldiethanolamine (MDEA). In
384   Proceedings of Annual transactions of the nordic rheology society.

385

Supporting Document

Density models:

1. MEA + H$_2$O + CO$_2$ mixtures

ANN with 3 inputs, 3 neurons and one output

Table S1. Weight matrix (hidden layer)

Neurons (hidden layer)	Inputs			Layer bias
	X$_{MEA}$	X$_{CO2}$	T	
1	-0.12091	0.71104	0.00485	-0.60191
2	-0.09968	-0.69287	0.03905	-1.011291
3	-0.11552	-0.18913	-0.41026	0.24566

Table S2. Weight matrix (output layer)

Neurons (output layer)	Neurons (hidden layer)	Outputs	Output bias
1	1	1.12227	
	2	-1.21305	-0.34818
	3	0.42781	

2. AMP + MEA + H$_2$O + CO$_2$ mixtures

ANN with 4 inputs, 24 neurons and one output

Table S3. Weights matrix (hidden layer)

Neurons (hidden layer)	Inputs				Layer bias
	X$_{AMP}$	X$_{MEA}$	X$_{CO2}$	T	
1	-0.05210	0.05901	-0.00451	0.05145	-0.10659
2	-0.90375	0.75732	1.18077	-0.00153	0.94526
3	0.01601	-0.46312	2.13591	-0.01008	-0.55497
4	0.05062	-0.05742	0.00412	-0.04888	0.10261
5	0.02298	-0.02612	-0.00513	-0.01226	0.04441
6	-0.00351	0.17740	-0.75311	0.27562	0.98613
7	-0.29373	0.30125	0.142043	0.07230	-0.39184
8	-0.18744	0.20992	0.55720	0.88477	-0.72515
9	-0.04657	0.04660	-0.03479	0.29373	-0.30196
10	-0.40735	0.51358	-0.19078	-0.40706	-0.51853
11	-0.26779	0.23294	0.11701	-0.77299	0.10123
12	-0.15480	0.02936	0.80148	0.45986	-0.41456
13	0.21811	-0.51763	1.04911	-0.18558	0.54167
14	0.05269	-0.05587	-0.00448	-0.07378	0.12144
15	0.09707	-0.00608	-0.62670	-0.20274	-0.78984

16	0.26487	-0.33695	0.10798	0.59241	-0.34503
17	-1.13753	1.68383	-1.83587	0.00384	0.83268
18	0.16798	-0.47597	1.34563	-0.01885	1.66820
19	0.02119	-0.20040	0.79585	-0.52064	0.17594
20	0.32345	-0.13851	-0.92573	-0.20358	0.42038
21	-0.05810	0.06469	-0.00420	0.066159	-0.12634
22	0.02086	-0.02294	-0.01082	-0.00475	0.03709
23	-0.42892	0.55187	-0.38923	0.15801	-0.56050
24	-0.04502	0.04793	0.00355	0.05999	-0.10062

Table S4. Weight matrix (output layer)

Neurons (output layer)	Neurons (hidden layer)	Outputs	Output bias
1	1	0.01505	-0.37028
	2	0.22070	
	3	-0.21548	
	4	-0.01135	
	5	0.02896	
	6	-0.28852	
	7	-0.00827	
	8	-2.58690	
	9	0.29340	
	10	-0.30324	
	11	0.97090	
	12	-0.56310	
	13	1.06638	
	14	-0,05659	
	15	0.66429	
	16	0.33911	
	17	-0.23316	
	18	0.00108	
	19	0.155119	
	20	-0.63906	
	21	0.03762	
	22	0.03803	
	23	0.32032	
	24	0.04558	

Viscosity models:

1. MEA + H₂O mixtures

ANN with 2 inputs, 15 neurons and one output

Table S5. Weight matrix (hidden layer)

Neurons (hidden layer)	Inputs		Layer bias
	X_{MEA}	T	
1	0.2245	-1.2971	-1.5087
2	0.8637	0.4644	-0.8894
3	-1.3993	1.4101	1.6576
4	1.5413	0.4746	0.5499
5	0.0686	0.6741	-0.2779
6	0.5300	0.9786	-0.2856
7	0.0568	0.6385	-0.3649
8	-1.7444	0.2513	-0.0811
9	-0.2317	-0.1855	-0.1651
10	-0.6630	1.2350	0.5540
11	1.6238	-1.0245	-0.5036
12	-1.0604	-1.0187	-1.0502
13	1.9133	0.2991	1.0949
14	-0.8338	1.9871	1.7637
15	2.6824	0.3432	1.6273

Table S6. Weight matrix (output layer)

Neurons (output layer)	Neurons (hidden layer)	Outputs	Output bias
1	1	2.3324	0.7901
	2	-1.0708	
	3	-1.3661	
	4	-1.1938	
	5	0.6559	
	6	-0.4975	
	7	0.7482	
	8	-0.5149	
	9	-0.4021	
	10	0.8836	
	11	0.4382	
	12	0.5315	
	13	1.9752	
	14	1.1577	
	15	-0.5346	

2. MEA + H2O + CO2 mixtures

ANN with 3 inputs, 17 neurons and one output

Table S7. Weight matrix (hidden layer)

Neurons (hidden layer)	Inputs			Layer bias
	X_{MEA}	X_{CO2}	T	
1	0.4215	1.5806	-1.3023	-3.9205
2	-0.2344	0.5974	-0.6894	-0.8913
3	-0.8085	-0.0628	1.2529	1.3788
4	-0.5030	0.3295	-0.0247	-0.8453
5	0.4080	-0.4435	-0.2740	1.1696
6	0.8007	0.3399	-1.8701	-3.2754
7	-0.7889	0.3388	1.0321	-0.1477
8	-0.9704	1.7818	-0.0356	-1.0910
9	0.1012	0.8761	-0.5348	-0.1678
10	0,1178	-0.24392	0.0089	0.2577
11	-0.1780	-0.3137	0.3835	-0.7124
12	0.9322	-1.4933	0.0055	-0.2371
13	1.0636	-0.7079	-0.1355	-1.0869
14	-1.4288	1.2783	0.2322	-0.3898
15	0.1027	-0.5182	0.0248	-0.0912
16	-0.6402	0.2737	0.8040	-0.0355
17	0.9365	-1.1699	-0.0440	-1.5421

Table S8. Weight matrix (output layer)

Neurons (output layer)	Neurons (hidden layer)	Outputs	Output bias
1	1	1.2099	0.4268
	2	0.0852	
	3	-0.2394	
	4	-0.8036	
	5	0.8988	
	6	0.9236	
	7	0.1669	
	8	0.5541	
	9	-0.1432	
	10	0.4532	
	11	0.4183	
	12	-0.5843	
	13	0.6157	
	14	-0.1240	
	15	0.5650	
	16	-0.4293	

	17	-0.9215	

3. AMP + MEA + H$_2$O + CO$_2$ mixtures

ANN with 4 inputs, 21 neurons and one output

Table S9. Weight matrix (hidden layer)

Neurons (hidden layer)	Inputs				Layer bias
	X$_{AMP}$	X$_{MEA}$	X$_{CO2}$	T	
1	0.2216	-0.6316	1.4361	0.2245	1.676
2	0.4142	-0.5168	0.2170	0.4405	0.0802
3	-0.4101	-0.0097	2.1167	0.3400	0.4680
4	0.5100	-0.3251	-1.0026	0.4519	-0.7992
5	0.0190	-0.2026	0.6807	0.4634	0.7985
6	-0.1046	0.0900	0.1634	-0.0046	-0.1509
7	-0.3881	-0.1690	2.7031	0.2672	0.6816
8	-0.0509	-0.3419	1.5805	0.3919	1.3835
9	0.4085	-0.1697	-1.3428	-0.6928	-0.1062
10	-0.3967	0.3633	0.4395	-0.3609	-0.2131
11	0.0838	-0.0176	0.2786	-2.0380	-3.0030
12	0.0341	-0.0768	-0.0357	1.0345	1.0156
13	-0.5975	0.6170	0.4216	-1.1214	-0.7334
14	-0.0840	0.0706	0.1543	-0.0068	-0.1925
15	-0.4036	0.1014	1.6125	0.5219	0.2234
16	0.0570	-0.1294	0.1683	0.0780	0.6446
17	-0.0842	0.2360	-0.5301	0.0445	-0.6221
18	-0.3362	0.5310	-0.7098	-0.1479	-0.0196
19	-0.0760	0.0631	0.1512	-0.0071	-0.2106
20	0.1815	-0.3076	0.2484	0.7108	1.1051
21	0.2236	-0.1986	-0.5607	0.5194	1.4540

Table S10. Weight matrix (output layer)

Neurons (output layer)	Neurons (hidden layer)	Outputs	Output bias
1	1	-0.6625	1.0660
	2	0.4872	
	3	-1.4390	
	4	-0.1681	
	5	-0.8790	
	6	-0.5065	
	7	0.5558	
	8	0.5777	

	9	0.5998	
	10	0.4333	
	11	1.7062	
	12	-0.9315	
	13	0.0557	
	14	-0.5100	
	15	1.4947	
	16	0.7281	
	17	-0.7252	
	18	0.5711	
	19	-0.5129	
	20	1.1657	
	21	-0.7167	

Article F

Physical properties of MEA + Water + CO₂ mixtures in post-combustion CO₂ capture: A review of correlations and experimental studies.

Review Article

Physical Properties of MEA + Water + CO$_2$ Mixtures in Postcombustion CO$_2$ Capture: A Review of Correlations and Experimental Studies

Sumudu S. Karunarathne [ID]**, Dag A. Eimer, and Lars E. Øi** [ID]

Faculty of Technology, Natural Sciences and Maritime Studies, University of South-Eastern Norway, Kjølnes Ring 56, 3901 Porsgrunn, Norway

Correspondence should be addressed to Lars E. Øi; lars.oi@usn.no

The knowledge of physicochemical properties of a mixture of amine, water, and CO$_2$ is beneficial in evaluating the post-combustion CO$_2$ capture process and process equipment design. This study reviews the literature of density, viscosity, and surface tension measurements with the evaluated measurement uncertainties and proposed correlations for monoethanol amine (MEA), water, and CO$_2$ mixtures. Adequate research has been performed to measure and develop correlations for pure MEA and aqueous MEA mixtures, but further studies are required for CO$_2$-loaded aqueous MEA mixtures. The correlations fit measured properties with an acceptable accuracy, and they are recommended to use in process equipment design, mathematical modelling, and simulations of absorption and desorption.

1. Introduction

Knowledge of physical properties of solvents is important for chemical engineering work like process modelling and simulations, pilot plant operation, and the design of commercial plants [1]. An amine-based CO$_2$ capture process contains equipment like absorption columns, desorption columns, pumps, and heat exchangers. The design of such equipment is depended on physical properties like density, viscosity, and surface tension. As the benchmark solvent, physicochemical properties of MEA (monoethanol amine) in a wide range of concentrations, temperatures, and pressures are essential to examine and compare other potential solvents in postcombustion CO$_2$ capture. The measured physical properties of density, viscosity, surface tension, and thermal expansion coefficient of pure and aqueous MEA mixtures are available in the literature. There is a lack of data on the measured physical properties of CO$_2$-loaded aqueous MEA [2]. Recent studies have extended the range of data available for the CO$_2$-loaded MEA, and correlations have been proposed to fit the data [1, 3, 4].

The main objective of this review is to gather the literature of measured physical properties and semiempirical and empirical correlations of density, viscosity surface tension, and thermal expansion coefficient. The areas with a lack of measured data were identified and challenges were discussed in the experimental studies. The performance of proposed correlations was compared considering the accuracies of the data fit and applicability in the aspects such as mathematical modelling and simulations. The reported measurement uncertainties of pure MEA, aqueous MEA, and CO$_2$-loaded aqueous MEA solutions were tabulated and compared.

2. Density, Viscosity, and Surface Tension Measurements

Density, viscosity, and surface tension are used in the mass transfer and interfacial area correlations that were developed for both random and structured packings. The measured data of MEA + H$_2$O mixtures and MEA + H$_2$O + CO$_2$ mixtures have been published in various sources in which the

measurements were performed under different MEA concentrations, temperatures, and CO_2 loadings. Various advanced instruments have been used to acquire a high accuracy of measurements. In the analysis of CO_2 capture processes, it is essential to measure physical properties that cover all the conditions of the process.

2.1. Density of MEA and H_2O Mixtures.

2.1. Density of MEA and H_2O Mixtures. Table 1 summarizes the performed studies on density measurements of pure MEA under different temperatures in which most of the previous density measurements were limited to the temperature range of 293.15 to 353.15 K [2, 4–24]. DiGuilio et al. [9] studied densities of various ethanolamines and MEA in the temperature range of 294.4 to 431.3 K. There is a lack of information about densities of MEA at high pressures. Sobrino et al. [25] were able to measure densities of aqueous MEA mixtures at both high temperatures and pressures. The study was performed within the temperature range of 293.15 to 393.15 K and the pressure range from 0.1 MPa to 120 MPa. The density of aqueous MEA has been measured extensively under a wide range of MEA concentrations as shown in Table 2. The data are highly valuable because of their usability in the calculation of other important physiochemical parameters in the process. In the process, the absorption column operates with CO_2-loaded aqueous MEA solution. Typical operating conditions for the absorption process with CO_2 loading are from generally 0.2 to 0.5 mol CO_2/mol MEA [30]. The studies performed on density measurement of CO_2-loaded aqueous MEA are listed in Table 3. Several challenges were noticed in density measurement of aqueous MEA and CO_2-loaded aqueous MEA solutions. There is a high probability to evaporate MEA from the mixtures at high temperatures. Further, a desorption of CO_2 is also present in CO_2-loaded aqueous mixtures at high temperatures and high CO_2 loadings. Accordingly, care must be given to minimize occurrence of such phenomena through visual observations to get accurate density measurements. CO_2 or MEA evaporation is observed as bubble formation inside the U-tube in oscillating density meters, which leads to an error in density measurement.

2.2. Viscosity of MEA and Water Mixtures. Viscosity measurements of MEA and water mixtures are equally important as density measurements in the postcombustion absorption process. Viscosity has a high impact on the mass transfer coefficient of gas into a liquid in a packed bed absorber [32]. The viscosity of MEA varies with the amount of water and CO_2 present in the solution and decreases as the solution temperature increases. The available literature for the viscosity measurements of pure MEA is shown in Table 4 [2, 9, 13–17, 19, 23, 24, 28, 33]. Previous studies have attempted to cover the viscosity data in the range of 0–100 mass% MEA [14, 17, 33]. Measurements at a temperature above 373.15 K are reported in [33, 36]. For CO_2-loaded aqueous MEA, most of the reported studies presented the viscosity of 30 mass% MEA solutions within the CO_2-loading range of 0–0.5 mol CO_2/mol MEA. Idris et al. [34] discussed the viscosity measurements at higher (>50 mass%)

MEA concentrations. The study performed by Arachchige et al. [37] presented data at higher temperatures (>373.15 K). Tables 5 and 6 list studies performed on viscosity measurements of aqueous MEA and CO_2-loaded aqueous MEA, respectively. The evaporation and desorption of MEA and CO_2 from aqueous MEA and CO_2-loaded aqueous MEA solutions cause errors in the viscosity measurements. Idris et al. [34] adopted a method to suppress the CO_2-loaded aqueous MEA mixture using N_2 gas with 4 bar pressure to avoid the escape of CO_2 from the system. Further, Idris et al. [34] claim that the applied pressure would not influence the outcome of the experiments.

2.3. Surface Tension of MEA and Water Mixtures. Surface tension has a high influence on the effective interfacial area of the packing material [32] and ultimately influences the overall mass transfer rate. Accurate and reliable surface tension data can enhance the confidence in process simulations, which will reduce the cost and safety margins [40]. The surface tension measurement of MEA solutions also can be performed for pure MEA, aqueous MEA, and CO_2-loaded aqueous MEA. Literature is available for the measured surface tension of MEA for all kinds of solutions. Vazquez et al. [41] measured both pure MEA and aqueous MEA at different temperatures from 298.15 to 333.15 K using a Traube stalagmometer and a Prolabo tensiometer based on the Wilhemy plate method. Idris et al. [40] and Han et al. [4] measured the surface tension of pure MEA and aqueous MEA at different temperatures using Rame-Hart advanced goniometer model 500. For CO_2-loaded aqueous MEA, Jayarathna et al. [31] measured aqueous solutions of 20–70 mass% MEA with CO_2 loading 0–0.5 mol CO_2/mol MEA at temperatures from 303.15 to 333.15 K and also 80 mass% MEA with CO_2 loading 0–0.5 mol CO_2/mole MEA at temperatures from 313.15 to 343.15 K.

2.4. Uncertainty of Density, Viscosity, and Surface Tension Measurements. Analysis of the measurement uncertainty provides a quantitative indication of the quality of the measurement result [42]. Subsequently, it gives information about the confidence in any decision based on its use. Effective identification of uncertainty sources is vital and (combined) standard uncertainty is calculated by combining the respective uncertainty components of all important uncertainty sources. Guide to the Expression of Uncertainty in Measurement (GUM) published by ISO facilitates a guidance to evaluate the uncertainty in the output of a measurement system [43].

The functional relationship between measured quantity $x = \{x_i\}$ (the input) and the measurement result y (the output) is shown as

$$y = f(x), \tag{1}$$

$$u^2(y) = \sum_{i=1}^{n} \left(\frac{\partial f}{\partial x_i}\right)^2 u^2(x_i) + 2\sum_{i=1}^{n-1}\sum_{j=i+1}^{n} \frac{\partial f}{\partial x_i}\frac{\partial f}{\partial x_j} u(x_i, x_j). \tag{2}$$

TABLE 1: Previous measurements of density of pure MEA.

Source	T (K)		No of points	Method
	Low	High		
Touhara et al. [5]	298.15		1	Pycnometer
Yang et al. [6]	293.15	343.15	6	Anton Paar (DMA 5000M)
Li and Shen [7]	303.15	353.15	8	Pycnometer
Wang et al. [8]	293.45	360.65	5	Pycnometer
DiGuilio et al. [9]	294.4	431.3	8	Pycnometer
Page et al. [10]	283.15	313.15	3	Flow densimeter
Maham et al. [11]	298.15	353.15	5	Anton Paar (DMA 45)
Guevara and Rodriguez [12]	298.15	333.15	8	Sodev 03D vibrating densimeter
Li and Lie [13]	303.15	353.15	6	Pycnometer
Lee and Lin [14]	303.15	323.15	3	Pycnometer
Song et al. [15]	303.15	343.15	5	Pycnometer
Kapadi et al. [16]	303.15	318.15	4	Anton Paar (DMA 5000)
Islam et al. [17]	293.15		1	Pycnometer
Valtz et al. [18]	281.15	353.15	37	Anton Paar (DMA 5000)
Geng et al. [19]	288.15	323.15	8	Pycnometer
Pouryousefi and Idem [20]	295.15	333.15	4	Anton Paar (DMA 4500/DMA 5000)
Amundsen et al. [2]	298.15	353.15	5	Anton Paar (DMA 4500)
Taib and Murugesan [21]	303.15	353.15	6	Anton Paar (DMA 5000)
Taib and Murugesan [22]	293.15	353.15	16	Anton Paar (DMA 5000M)
Han et al. [4]	298.15	423.15	20	Anton Paar (DMA 4500/DMA HP)
Abuin et al. [23]	298.15		1	Anton Paar (DSA 5000)
Yang et al. [6]	293.15	343.15	6	Anton Paar (DMA 5000M)
Xu et al. [24]	293.15	333.15	5	Anton Paar (DMA 5000)
Ma et al. [27]	293.15	333.15	5	Anton Paar (DMA 4500M)

TABLE 2: Sources of reported density measurements of aqueous MEA.

Source	Concentration: MEA (x_1)		T (K)		No of points	Method
	Low	High	Low	High		
Weiland et al. [26]	0.0317	0.1643	298.15		4	Hydrometer
Amundsen et al. [2]	0.0687	0.7264	298.15	353.15	30	Anton Paar (DMA 4500)
Han et al. [4]	0.1122	0.7264	298.15	423.15	140	Anton Paar (DMA4500/DMA HP)
Hartono et al. [1]	0.0191	0.1122	293.15	353.15	15	Anton Paar (DMA 4500M)
Page et al. [10]	0.00118	0.99695	283.15	313.15	62	Flow densimeter
Maham et al. [11]	0.0054	0.9660	298.15	353.15	100	Anton Paar (DMA 45)
Lee and Lin [14]	0.1000	0.9000	303.15	323.15	27	Pycnometer
Kapadi et al. [16]	0.1122	0.8486	303.15	383.15	32	Anton Paar (DMA 5000)
Pouryousefi and Idem [20]	0.0155	0.9192	295.15	333.15	80	Anton Paar (DMA 4500/DMA 5000)
Ma et al. [27]	0.1000	0.8995	293.15	333.15	45	Anton Paar (DMA 4500M)
Mandal et al. [28]	0.1122		293.15	323.15	7	Pycnometer
Li and Lie [13]	0.0687		303.15	353.15	6	Pycnometer
Zhang et al. [29]	0.1122		298.15	353.15	9	Anton Paar (DMA 5000M)

TABLE 3: Sources of reported density measurements of CO_2-loaded aqueous MEA.

Source	Concentration: mass% MEA in (MEA + water) solutions		CO_2 loading: α (mol CO_2/ mol MEA)		T (K)	No. of points	Method
	Low	High	Low	High			
Weiland et al. [26]	10	40	0.05	0.5	298.15	40	Hydrometer
Amundsen et al. [2]	20	40	0.1	0.5	298.15–353.15	68	Anton Paar (DMA 4500)
Han et al. [4]	30	60	0.1	0.56	298.15–423.15	240	Anton Paar (DMA 4500/DMA HP)
Jayarathna et al. [31]	20	70	0.1	0.5	303.15–333.15	144	Anton Paar (DMA 4500M)
Jayarathna et al. [3]	80		0.07	0.51	313.15–343.15	64	Anton Paar (DMA 4500M)
Hartono et al. [1]	6.2	30	0.1	0.5	293.15–353.15	68	Anton Paar (DMA 4500M)
Zhang et al. [29]	30		0.14	0.49	298.15–353.15	33	Anton Paar (DMA 5000M)

Table 4: Sources of reported viscosity measurements of pure MEA.

Source	T (K)		No of points	Method
	Low	High		
DiGuilio et al. [9]	303.6	423.7	8	Cannon-Ubbelohde capillary viscometer
Li and Lie [13]	303.15	353.15	6	Cannon-Fenske routine viscometer
Lee and Lin [14]	303.15	323.15	3	Haake falling-ball viscometer
Song et al. [15]	303.15	343.15	5	Ubbelohde viscometer
Kapadi et al. [16]	303.15	318.15	4	Ubbelohde viscometer
Islam et al. [17]	293.15	323.15	6	U-tube Ostwald viscometer
Geng et al. [19]	288.15	323.15	8	Ubbelohde viscometer
Amundsen et al. [2]	298.15	353.15	5	ZIDIN viscometer
Abuin et al. [23]	298.15		1	Ubbelohde viscometer
Arachchige et al. [33]	293.15	423.15	15	Anton Paar MCR 101 with a double gap measuring cell
Xu et al. [24]	293.15	333.15	5	Anton PaarAMVn
Ma et al. [27]	293.15	333.15	5	LUNDA iVisc capillary viscometer
Idris et al. [34]	298.15	373.15	16	Anton Paar MCR 101 with a double gap measuring cell
Maham et al. [35]	298.15	353.15	5	Ubbelohde viscometer/capillary viscometer

Table 5: Sources of reported viscosity measurements of aqueous MEA.

Source	Concentration: (x_1) MEA		T (K)		No of points	Method
	Low	High	Low	High		
Weiland et al. [26]	0.0317	0.1643	298.15		4	Cannon-Fenske viscometer
Amundsen et al. [2]	0.0687	0.7264	298.15	353.15	30	ZIDIN viscometer
Arachchige et al. [33]	0.0317	0.7264	293.15	353.15	72	Anton Paar MCR 101 with a double gap measuring cell
Hartono et al. [1]	0.0191	0.1122	293.15	353.15	26	Anton Paar MCR 100 with a double gap measuring cell
Arachchige et al. [38]	0.0317	0.7264	363.15	423.15	63	Anton Paar MCR 101 with a double gap measuring cell
Idris et al. [34]	0.2278	0.7264	298.15	373.15	128	Anton Paar MCR 101 with a double gap measuring cell
Lee and Lin [14]	0.1000	0.9000	303.15	323.15	27	Haake falling-ball viscometer
Kapadi et al. [16]	0.1122	0.8486	303.15	318.15	32	Ubbelohde viscometer
Islam et al. [17]	0.0322	0.7296	303.15	323.15	45	U-tube Ostwald viscometer
Ma et al. [27]	0.1000	0.8995	293.15	333.15	45	LUNDA iVisc capillary viscometer
Maham et al. [35]	0.0313	0.8446	298.15	353.15	60	Ubbelohde viscometer/capillary viscometer
Li and Lie [13]	0.0687	0.1122	303.15	353.15	6	Cannon-Fenske routine viscometer
Zhang et al. [29]	0.1122		298.15	353.15	7	U-tube capillary viscometer
Mandal et al. [28]	0.1122		298.15	323.15	7	Ostwald viscometer

Table 6: Sources of reported viscosity measurements of CO_2-loaded aqueous MEA.

Source	Concentration: mass% MEA		CO_2 loading: α (mol CO_2/mol MEA)		T (K)		No of points	Method
	Low	High	Low	High	Low	High		
Weiland et al. [26]	10	40	0.05	0.5	298.15		20	Cannon-Fenske viscometer
Amundsen et al. [2]	20	40	0.1	0.5	298.15	353.15	75	ZIDIN viscometer
Fu et al. [39]	20	40	0.1	0.5	298.15		15	NDJ-1 rotational viscometer
Hartono et al. [1]	6.2	30	0.11	0.5	293.15	353.15	100	Anton Paar MCR 100 with a double gap measuring cell
Idris et al. [34]	50	80	0.08	0.52	298.15	373.15	320	Anton Paar MCR 101 with a double gap measuring cell
Arachchige et al. [37]	10	50	0.1	0.5	293.15	423.15	375	Anton Paar MCR 101 with a double gap measuring cell
Zhang et al. [29]	30		0.14	0.49	298.15	353.15	23	U-tube capillary viscometer

Equation (2) describes the propagation of uncertainty based on a first-order Taylor series expansion in which $u^2(y)$, $\partial f / \partial x_i$, $u^2(x_i)$, and $u(x_i, x_j)$ are variance of the measuring result, partial derivative, variance of the input quantity x_i and covariance between x_i and x_j [44].

Literature studies on density measurements of MEA reveal that many studies have given great attention to the uncertainty analysis to calculate the standard uncertainty for the measurements. Several density measurement data rely only on the uncertainty or accuracy of the measuring instrument, and it was not given a significant interest to calculate the combined uncertainty. Many factors contribute to the uncertainty of density measurements. Typical uncertainty sources in density and viscosity measurements are the purity of the material, weight measurements in sample preparation, and temperature variation in the measuring instrument. The calculated $u(y)$ depends on the number of uncertainty sources considered in the evaluation. If the solutions are loaded with CO_2, then the uncertainty of the CO_2 concentration in solution is important and cannot be neglected. Reported uncertainties on previous studies are shown in Table 7.

The uncertainty of CO_2 loading $u(\alpha)$ is challenging to evaluate. Many uncertainty sources are involved, and Jayarathna et al. [45] performed a detailed analysis on $u(\alpha)$ based on the titration method using $BaCl_2$ and $NaOH$. Amundsen et al. [2] has reported $u(\alpha)$ as 2% which is higher than what Jayarathna et al. [45] reported as 1.3%. In density measurements, although the same instrument was used Hartono et al. [1] stated a lower value for $U_c(\rho)$ compared to Jayarathna et al. [3]. For viscosity measurements, the $U_c(\eta)$ reported by Arachchige et al. [33] was higher than what was calculated by Hartono et al. [1]. Calculated $U_c(\eta)$ by Amundsen et al. [2] for CO_2-loaded aqueous MEA is greater than what Hartono et al. [1] described. In surface tension measurements, the effect of $u(\alpha)$ act similarly on $u(\sigma)$ as in density and viscosity measurement uncertainty.

3. Correlations for Density, Viscosity, Surface Tension, and Thermal Expansion Coefficient

It is useful to fit the measured physical property data in semiempirical and empirical correlations in which they can be used in mathematical modelling and simulations of absorption and desorption process. Several statistical parameters were used by different authors to evaluate the accuracy of the data fit into the correlations as given in equations (3)–(5). This section summarizes recent development in the field and correlations derived for different physical properties.

Average Absolute Deviation

$$\text{AAD} = \frac{1}{N} \sum_{i=1}^{N} \left| Y_i^E - Y_i^C \right|. \tag{3}$$

Average Absolute Relative Deviation

$$\text{AARD} = \frac{100\%}{N} \sum_{i=1}^{N} \left| \frac{Y_i^E - Y_i^C}{Y_i^E} \right|. \tag{4}$$

Maximum Deviation

$$\text{MD} = \text{MAX} \left| Y_i^E - Y_i^C \right|. \tag{5}$$

3.1. Density Correlations. This section discusses the empirical correlations developed for different types of MEA solutions. It also highlights the theoretical background of those correlations especially the excess volume of MEA and water mixtures. Table 8 summarizes the various published correlations for the density of pure, aqueous, and CO_2-loaded aqueous MEA mixtures. The density of pure liquids at different temperatures was fitted into a second-order polynomial as shown in equations (6), and coefficients were found through a regression [3, 6, 9, 12, 49]. Table 9 lists the parameters found for the polynomial correlation. Valtz et al. [18] used the correlation presented in Reid et al. [50] as given in equation (7) to predict the density of pure MEA at different temperatures. The parameters are given in Table 10.

In binary mixtures, excess molar volume V^E as given in equations (8) and (9) arises due to the different shape and size of the component molecules, physical interactions, and specific or chemical interactions among the component molecules [51–53]. Mathematically, it is defined as the difference of molar volumes between real and ideal mixtures. The theory of Prigogine–Flory–Patterson [54, 55] discusses V^E as a summation of interactional contribution, a free volume contribution, and a pressure contribution [56].

Redlich and Kister [57] illustrate an algebraic representation to adopt the excess thermodynamic properties of nonelectrolyte solutions. Therefore, the excess molar volume is presented in a power series with temperature-dependent parameters. This approach has been adopted to correlate excess molar volumes of the MEA and water binary mixture. The effect of temperature on excess volume is figured by introducing a second-order polynomial for parameters in the Redlich–Kister type correlation as shown in equations (10) and (11).

Amundsen et al. [2] and Lee and Lin [14] calculated the coefficients (A_i) for different temperatures while Hsu and Li [49] presented (A_i) for the entire temperature range of (303.15–353.15) K. A similar work was performed by Han et al. [4] in which the temperature dependence was correlated as a linear relation with respect to temperature. Hartono et al. [1] and Yang et al. [6] also developed a simplified Redlich–Kister type algebraic representation to fit the measured data as given in equations (12) and (13), respectively. The influence of pressure on the density of

Table 7: Literature of measurement uncertainty.

Property	Source	Instrument	Uncertainty	Comment
Density	Jayarathna et al. [31]	Anton Paar DMA HP	$U_c(\rho) = \pm 4.42 \, \text{kg·m}^{-3}$ Level of confidence = 0.95, where $k = 2$	CO_2-loaded aqueous MEA (20–70 mass%)
	Jayarathna et al. [3]	Anton Paar DMA 4500	$U_c(\rho) = \pm 6.34 \, \text{kg·m}^{-3}$ Level of confidence = 0.95, where $k = 2$	CO_2-loaded aqueous MEA (80 mass%)
	Han et al. [4]	Anton Paar DMA 4500 at $T < 373.15$ K DMA HP at $T \geq 373.15$ K	$U_c(\rho) = \pm 0.68 \, \text{kg·m}^{-3}$ at $T < 373.15$ K Level of confidence = 0.95, where $k = 2$	Aqueous MEA
			$U_c(\rho) = \pm 0.70 \, \text{kg·m}^{-3}$ 2.6 kg·m^{-3} at $T \geq 373.15$ K Level of confidence = 0.95, where $k = 2$	CO_2-loaded aqueous MEA
	Abuin et al. [23]	Anton Paar DSA 5000	$U_c(\rho) = \pm 2 \times 10^{-4} \, \text{g·cm}^{-3}$ Level of confidence = 0.95, where $k = 2$	Pure MEA
	Xu et al. [24]	Anton Paar DSA 5000	$u(\rho) = \pm 0.0001 \, \text{gcm}^{-3}$ Standard uncertainty	Pure MEA
	Yang et al. [6]	Anton Paar DMA 5000 M	$u(\rho) = \pm 5 \times 10^{-6} \, \text{gcm}^{-3}$ Standard uncertainty	Pure MEA
	Amundsen et al. [2]	Anton Paar DMA 4500 M	$u(\rho) = \pm 5 \times 10^{-5} \, \text{gcm}^{-3}$ Standard uncertainty	CO_2-loaded and unloaded aqueous MEA
	Hartono et al. [1]	Anton Paar DMA 4500 M	$U_c(\rho) = \pm 0.02 \, \text{kg·m}^{-3}$ Level of confidence = 0.95, where $k = 2$	CO_2-loaded and unloaded aqueous MEA
Viscosity	Xu et al. [24]	Anton PaarAMVn	$u(\eta) = \pm 2\%$ Standard uncertainty	Pure MEA
	Amundsen et al. [2]	ZIDIN viscometer	$u(\eta) = \pm 0.01 \, \text{MPa·s}$ Standard uncertainty	CO_2-loaded and unloaded aqueous MEA
	Hartono et al. [1]	Anton Paar MCR 100	$U_c(\eta) = \pm 0.007 \, \text{MPa·s}$ Level of confidence = 0.95, where $k = 2$	CO_2-loaded and unloaded aqueous MEA
	Arachchige et al. [33]	Anton Paar MCR 101	$U_c(\eta) = \pm 0.015 \, \text{MPa·s}$ Level of confidence = 0.95, where $k = 2$	Aqueous MEA
Surface tension	Jayarathna et al. [31]	Rame-Hart advanced goniometer model 500	$U_c(\eta) = \pm 0.0004 \, \text{N·m}^{-1}$ Level of confidence = 0.95, where $k = 2$	Aqueous MEA
			$0.0012 \, \text{N·m}^{-1}$ Level of confidence = 0.95, where $k = 2$	CO_2-loaded aqueous MEA (20–70 mass%)
	Jayarathna et al. [3]	Rame-Hart advanced goniometer model 500	$0.0018 \, \text{N·m}^{-1}$ Level of confidence = 0.95, where $k = 2$	CO_2-loaded aqueous MEA (80 mass%)
	Han et al. [4]	Rame-Hart advanced goniometer model 500	$0.0004 \, \text{N·m}^{-1}$ Level of confidence = 0.95, where $k = 2$	Aqueous MEA

aqueous MEA was studied by Sobrino et al. [25]. The measured densities from 0.1 MPa up to 120 MPa under different temperatures (293.15–393.15) K and MEA compositions (10–40 mass%) were fitted to a modified Tammann–Tait equation as given in equation (14). Cheng et al. [47] developed a correlation as illustrated in equation (15) based on densities of pure liquids and mass fraction of MEA in the mixture. The correlation is capable of representing densities at different temperatures.

The construction of a proper correlation to fit the density of CO_2-loaded aqueous MEA solutions is challenging as the CO_2 dissolve and react with MEA forming various ions including carbamate, bicarbonate, and protonated MEA. The solution becomes an electrolyte and molecular interactions are more dominant than a MEA and water mixture without CO_2. Various attempts have been taken to build an effective correlation that can be easily used in process design and simulations. Licht and Weiland [48] proposed a

TABLE 8: Correlations for the density of MEA + H₂O + CO₂ mixtures.

Correlation		T (K)	P (MPa)	Data sources
$\rho = a_1 + a_2 T + a_3 T^2$	(6)	293.15–343.15	0.097	[6]
		294.4–431.3	0.1013	[9]
		303.15–333.15	0.8	[31]
		281.15–317.15	0.1013	[18]
$\rho = (A/(B^{[1+(1-(T/T_C))^C]})) \cdot (M_i/1000)$	(7)			
$V^E = V_m - x_1 V_1^0 - x_2 V_2^0$	(8)			
$V^E = ([x_1 M_1 + x_2 M_2]/\rho) - ((x_1 M_1)/\rho_1) - ((x_2 M_2)/\rho_2)$	(9)	298.15–423.15	0.1 from (298.15–363.15) 0.7 from (363.15–423.15)	[4]
$V^E = x_2(1-x_2)\sum_{i=0}^{i=n} A_i (1-2x_2)^i$	(10)			
$A_i = a + b(T - 273.15)$	(11)			
$V^E = x_1 x_2 \cdot 10^{-6} \cdot (A_0 + A_1 t + A_2 x_1 + A_3 x_1^2)$	(12)	293.15–353.15	0.1013	[46]
$V^E = x_1 x_2 \cdot (A_0 + A_1 T + A_2 x_1)$	(13)	283.15–333.15	0.097	[6]
$\rho(T,p) = (A_0 + A_1 T + A_2 T^2)/(1 - C \ln((B_0 + B_1 T + B_2 T^2 + p)/(B_0 + B_1 T + B_2 T^2 + 0.1\,\text{MPa})))$	(14)	293.15–393.15	0.1–120	[25]
$\rho = (1 - wf_1)\rho_2 + wf_1 \rho_1 + wf_1(1 - wf_1)(a + bt + cwf_1 t^d)$	(15)	283.15–373.15	0.1013	[47]
$1/\rho = u_w V_w^o e^{[\beta_w(T-T_o)]} + u_{A_1} V_{A_1}^o e^{[\beta_{A_1}(T-T_o)]} + u_{A_2} V_{A_2} A_2^o e^{[\beta_{A_2}(T-T_o)]} + w_{CO_2} V_{CO_2}^o e^{[\beta_{CO_2}(T-T_o)]}$	(16)			[48]
$\rho = (x_1 M_1 + x_2 M_2 + x_3 M_3)/V$	(17)			
$V = x_1 V_1 + x_2 V_2 + x_3 V_3 + x_1 x_2 V^* + x_1 x_3 V^{**}$	(18)	298.15	0.1013	[26]
$V_1 = M_1/(aT^2 + bT + c)$	(19)			
$V^{**} = d + e x_1$	(20)			
$\rho_{\text{loaded}} = \rho_{\text{unloaded}}/(1 - w_{CO_2\text{added}}(1 - \Phi^3))$	(21)			
$w_{CO_2,\text{added}} = (\alpha x_1 M_3)/(x_1 M_1 + (1 - x_1 - \alpha x_1)M_2 + \alpha x_1 M_3)$	(22)	293.15–353.15	0.1013	[1]
$\Phi = (a_1 x_1 \alpha + a_2 x_1)/(a_3 + x_1)$	(23)			

Density measurements performed under atmospheric conditions are mentioned with 0.1013 MPa pressure.

TABLE 9: Parameters of density correlation for pure MEA.

Sources	Density parameters		
Density (kg/m³)	$a_1 (kg/m^3)$	$a_2 (kg/m^3 \cdot K)$	$a_3 (kg/m^3 \cdot K^2)$
DiGuillo et al. [9]	1181.9	−0.38724	$−6.1668 \times 10^4$
Jayarathna et al. [3]	1195	−0.4566	$−5.327 \times 10^4$
Density (g/cm³)	$a_1 (g/cm^3)$	$a_2 (g/cm^3 \cdot K)$	$a_3 (g/cm^3 \cdot K^2)$
Hsu and Li [49]	1.190	$−4.29990 \times 10^{-4}$	$−5.66040 \times 10^{-7}$
Yang et al. [6]	1.2213	$−6.1156 \times 10^{-4}$	$−2.9982 \times 10^{-7}$
Guevara and Rodriguez [12]	1.03297	$−8.0498 \times 10^{-4}$	$−3.595 \times 10^{-7}$

TABLE 10: Parameters of Valtz et al. [18] density correlation for pure MEA.

T_c (K)	A (kmol·m⁻³)	B	C
678.20	1.0002	0.2244	0.2238

correlation to predict the density of CO_2-loaded aqueous amines including MEA as described in equation (16). Weiland et al. [26] proposed a new correlation as from equations (17) to (20) for several amines, and it is extensively used in various studies related to MEA. The correlation shown from equations (21) to (23) was developed by Hartono et al. [1] for CO_2-loaded mixtures. The correlation requires the density of unloaded mixtures to represent the density data of CO_2-loaded mixtures. Literature can be found related to the verification and parameter estimation of Weiland's correlation for various MEA concentrations and temperatures. Weiland's correlation was used to fit measured density under different MEA concentrations (10–40 mass%) and CO_2 loading 0.05–0.25 mol CO_2/mol MEA at 298.15 K. Amundsen et al. [2] extended the temperature range of density measurement from 298.15 K to 353.15 K and used the same parameter values as given by Weiland et al. [26] to validate the correlation. The maximum deviation between the measurement and the correlation obtained by Amundsen et al. [2] is 1.6% at 353.15 K. Jayarathna et al. [31] extended the measured MEA concentration up to 70 mass% of aqueous MEA and CO_2 loading 0.1–0.5 mol CO_2/mol MEA in the temperature range of 303.15–333.15 K. The parameters of Weiland's correlation were estimated within that range and accuracy of the data fit was reported as 2.03 kg·m⁻³ of AAD. Han et al. [4] also used Weiland's correlation for the density prediction in an extended temperature range up to 413.15 K of the CO_2-loaded solutions. It introduced a nonlinear temperature dependence for the correlation parameters and gained a deviation between measured and correlated as 3.8 kg·m⁻³ of AAD. The main difference between Hartono's correlation and Weiland's correlation is that Hartono's correlation needs the density of unloaded density to calculate the density of loaded solutions.

A study was performed to investigate the accuracies of correlations proposed for aqueous MEA and CO_2-loaded aqueous MEA mixtures. The calculated AARD and AMD for different density correlations of aqueous MEA are listed in Table 11. Hartono's correlation for density of aqueous MEA used density data from Maham et al. [11] while Han et al.'s correlation used data from their own experiments [4]. The

highest AARD of 0.16% was observed for Han's correlation for the density data published by Amundsen et al. [2] while a maximum deviation of 4.07 kg·m⁻³ at $x_1 = 0.1$ and $T = 293.15$ K for the presented data by Ma et al. [27]. For Hartono's correlation, a maximum AARD of 0.05% and a maximum deviation of 1.79 kg·m⁻³ at $x_1 = 0.1$ and $T = 293.15$ K were found for measured viscosities given by Ma et al. [27].

Table 12 lists the calculated AARD and AMD of correlations proposed for density of CO_2-loaded aqueous MEA mixtures. Therefore, Hartono's correlation and Weiland's correlation, which was modified by Han et al. [4] for CO_2-loaded aqueous MEA, were studied with different literature for density data of 30 mass% CO_2-loaded mixtures. Correlations were able to represent literature data with less than 1% AARD. Weiland's correlation showed a higher deviation for data presented by Amundsen et al. [2] and Zhang et al. [29] compared to Hartono et al. [1] and Han et al. [4]. Hartono's correlation showed a good agreement with data given by Zhang et al. [29]. The maximum deviation is beyond the expanded combined uncertainties reported in data sources, and calculated AARD shows that the agreement between correlated and experimental densities is satisfactory.

3.2. Viscosity Correlations. The nature of the model depends on the solution characteristics. Generally, the liquid viscosity decreases with the increase of temperature, and it increases with the increase of pressure. For pure MEA, an exponential model was frequently used to correlate the temperature dependence of viscosity. Table 13 summarizes the various published correlations for the viscosity of different MEA solutions. The relation between the viscosity of pure MEA with temperature can be represented by the Arrhenius equation shown in equation (30) and Teng et al. [59] calculated the activation energy for viscous flow from the data presented in DiGuilio et al. [9]. DiGuilio et al. [9] used a modified Andrade from (1934) viscosity model [60] by Vogel [61] as shown in equation (31).

Unlike ideal density, several mathematical relations have been proposed to determine ideal viscosity in a liquid mixture in the literature.

Kendall and Monroe [62]:

$$\ln(\eta_{\text{ideal}}) = \sum_i^n x_i \ln(\eta_i). \tag{24}$$

TABLE 11: Comparison of density correlations with different literature data for aqueous MEA mixtures.

Data source	Ma et al. [27]	Amundsen et al. [2]	Maham et al. [11]
T (K)	293.15–333.15	293.15–353.15	298.15–353.15
x_1	0.1000–0.8995	0.0687–0.7264	0.0054–0.9660
Han's correlation			
AARD (%)	0.11	0.16	0.10
MD ($kg \cdot m^{-3}$)	4.07	3.52	3.64
Hartono's correlation			
AARD (%)	0.05	0.03	0.03
MD ($kg \cdot m^{-3}$)	1.79	1.09	1.02

TABLE 12: Comparison of density correlations with different literature data for CO_2-loaded aqueous MEA mixtures.

Data source	Hartono et al. [1]	Amundsen et al. [2]	Zhang et al. [29]	Han et al. [4]
T (K)	293.15–353.15	293.15–353.15	298.15–353.15	298.15–413.15
α (mol CO_2/mol MEA)	0.11–0.5	0.1–0.5	0.14–0.49	0.1–0.56
Weiland's correlation				
AARD (%)	0.25	0.50	0.58	0.26
MD ($kg \cdot m^{-3}$)	6.46	16.08	13.86	10.81
Hartono's correlation				
AARD (%)	0.67	0.37	0.09	0.57
MD ($kg \cdot m^{-3}$)	8.13	7.05	3.54	19.53

Bingham [63]:

$$\frac{1}{\eta_{\text{ideal}}} = \sum_i^n x_i \frac{1}{\eta_i}. \tag{25}$$

Cronauer et al. [64] for ideal kinematic viscosity:

$$\ln(\nu_{\text{ideal}}) = \sum_i^n x_i \ln(\nu_i). \tag{26}$$

And the following expression is frequently used in recent publications [65].

$$\eta_{\text{ideal}} = \sum_i^n x_i \eta_i. \tag{27}$$

The viscosity of aqueous MEA deviates from the ideal mixture viscosity. This deviation of excess viscosity has been studied to make correlations fit the measured viscosity of the mixture. Accordingly, correlations are built to fit the viscosity deviation that is the viscosity difference between a real solution and an ideal solution.

$$\Delta\eta = \eta - \sum_{i=1}^2 x_i \eta_i, \tag{28}$$

$$\ln(\Delta\eta) = \ln(\eta) - \sum_{i=1}^2 x_i \ln(\eta_i). \tag{29}$$

McAllister presented a model to calculate kinematic viscosity in a binary mixture [2, 66, 67]. It is a semiempirical model, which is based on Eyring's absolute rate theory [68]. This model is given in two forms as the McAllister Three-Body Model and Four-Body Model considering different intermolecular interactions with neighbouring molecules.

Lee and Lin [14] and Amundsen et al. [2] adopted the Three-Body model as shown in equation (32) to fit viscosity data of aqueous MEA at different temperatures. Arachchige et al. [33] used a correlation suggested by Teng et al. [59] given in equation (33) to correlate measured viscosity of aqueous MEA at different temperatures. This correlation uses the viscosity of pure water and a polynomial to fit the viscosity of the binary mixture. The polynomial coefficients were found through a regression analysis at different temperatures. A Redlich–Kister type correlation as illustrated in equation (34) was proposed by Islam et al. [17] to determine $\Delta\eta$ (excess viscosity), and the parameters were found for different temperatures through a regression. A similar work was performed by Hartono et al. [1]. Then a Redlich–Kister type model was proposed to fit $\ln(\Delta\eta)$ given in equation (35). The main advantage of Hartono's aqueous MEA viscosity correlation is that it comprises the temperature dependence of viscosity that is not considered in Islam's correlation. Idris et al. [34] discussed the applicability of correlations based on the work by Heric-Brewer [69], Jouyban-Acree [70], Herráez et al. [71], and Redlich-Kister [57] as given in equations (36)–(39) respectively. The fitting parameters are in the form of a second-order polynomial of temperature to correlate temperature dependency of the viscosity as given in equation (40).

Limited attempts have been made to build correlations for the viscosity data of CO_2-loaded aqueous MEA mixtures. Accordingly, more measurements are still required to validate the existing data and correlations. Weiland et al. [26] developed a correlation for CO_2-loaded aqueous MEA for viscosity under different CO_2 loadings, MEA concentrations, and temperatures as described by equation (41). It is applicable for viscosities up to 40 mass% of MEA aqueous solutions at CO_2 loading of 0.6 mol CO_2/mol MEA to a

TABLE 13: Correlations for the Viscosity of MEA + H$_2$O + CO$_2$ mixtures.

Correlation		T (K)	P (MPa)	Data sources
$\eta = Ae^{E/RT}$	(30)	303.6–423.7	0.1013	[9]
$\ln(\eta) = A + (B/(T+C))$	(31)	303.6–423.7	0.1013	[9]
$\ln(v) = x_1^3 \cdot \ln(v_1) + 3x_1^2 x_2 \cdot \ln(v_{12}) + 3x_1 x_2^2 \cdot \ln(v_{21}) + x_2^3 \cdot \ln(v_2) - \ln(x_1 + x_2 \cdot [M_2/M_1]) + 3x_1^2 x_2 \cdot \ln([2 + M_2/M_1]/3) + 3x_1 x_2^2 \cdot \ln([1 + 2M_2/M_1]/3) + x_2^3 \cdot \ln(M_2/M_1)$	(32)	298.15–353.15	0.1013	[2]
$\ln(\eta) = \ln(\eta_0) + \sum_{i=1}^{i=n} a_i x_1^i$	(33)	293.15–353.15	0.1013	[33]
$\Delta\eta = x_1 x_2 \sum_{i=0}^n B_i (2x_1 - 1)^i$	(34)	303.15–323.15	0.1013	[17]
$\ln(\Delta\eta) = x_1 x_2 (b_1 + b_2 t + b_3 t^2 + b_4 x_1)$	(35)	293.15–353.15	0.1013	[1]
$\ln(\eta) = x_1 \ln(\eta_1) + x_2 \ln(\eta_2) + x_1 \ln(M_1) + x_2 \ln(M_2) - \ln(x_1 M_1 + x_2 M_2) + x_1 x_2 \sum_{i=0}^n [A_i (x_1 - x_2)^i]$	(36)			
$\ln(\eta) = x_1 \ln(\eta_1) + x_2 \ln(\eta_2) + x_1 x_2 \sum_{i=0}^n [A_i (x_1 - x_2)^i]$	(37)	298.15–373.15	0.4	[34]
$\eta = \eta_1 + (\eta_2 - \eta_1) x_2^{\sum_{i=0}^n (A_i x_2^i)}$	(38)			
$\eta = x_1 \eta_1 + x_2 \eta_2 + x_1 x_2 \sum_{i=0}^n A_i (x_1 - x_2)^i$	(39)			
$A_{ij} = A_{i0} + A_{i1}T + A_{i2}T^2$	(40)			
$\eta/\eta_{H_2O} = \exp((([(a \cdot w_{MEA} + b)T + (c \cdot w_{MEA} + d)][\alpha(e \cdot w_{MEA} + f \cdot T + g) + 1]w_{MEA})/T^2)$	(41)	298.15	0.1013	[26]
$\ln(\eta_{loaded}) = x_3 \ln(\eta_l^*) + (1 - x_3)\ln(\eta_{unloaded})$	(42)	293.15–353.15	0.1013	[1]
$\ln(\eta_l^*) = (a_1 x_1 + a_2 \alpha x_1)/(a_3 + x_1)$	(43)			
$\ln(\eta_{loaded}/\eta_{unloaded}) = \sum_{i=1}^2 A_i \alpha^i$	(44)	293.15–373.15	0.4	[34]
$A_i = a_{i,0} + a_{i,1}T$	(45)			
$\eta = (hN_A/V)\exp(\Delta F^*/RT)$	(46)	313.15–343.15	0.1013	[58]
$\eta/\eta_{ideal} = (V_{ideal}/V)\exp(\Delta F^{E*}/RT)$	(47)			
$\ln(\eta V) = \ln(\eta V)_{ideal} + (\Delta F^{E*}/RT)$	(48)			
$\ln(\eta V) = \sum_i x_i \cdot \ln(\eta_i V_i^0) + (\Delta F^{E*}/RT)$	(49)			

Viscosity measurements performed under atmospheric conditions are mentioned with 0.1013 MPa pressure.

maximum temperature of 298.15 K. Amundsen et al. [2] adopted Weiland's correlation to fit the measured viscosities at different amine concentrations, CO_2 loadings, and temperatures. Hartono et al. [1] developed a correlation for different CO_2 loadings and temperatures by making a relation between viscosities of CO_2-loaded and unloaded aqueous MEA solutions as given in equation (42). The correlation was fit for CO_2-loaded viscosities of 30 and 40 mass% MEA and claimed 3.9% maximum AARD. Idris et al. [34] adopted a modified Setschenow-type [72] correlation as shown in equations (44) and (45) to fit CO_2-loaded aqueous MEA data at high MEA concentrations. This approach has been tested for the physical properties of amine solutions by Shokouhi et al. [73, 74]. A new approach was taken by Matin et al. [58] using Eyring's absolute rate theory [68] as illustrated in equations (46)–(49). Therefore, assuming the equivalence between the Gibbs free energy of activation for viscous flow and the equilibrium Gibbs free energy of mixing, the concepts of classical thermodynamics can be extended to the viscous flow behaviour of liquid mixtures [65]. The electrolyte-NRTL model is used to calculate the excess Gibbs free energy. Having tested for different terms, Matin et al. [58] revealed that the Gibbs free energy of mixing is the appropriate thermodynamic quantity to substitute for the excess free energy of activation for viscous flow for CO_2-loaded aqueous MEA mixture. The absolute rate theory with a reliable thermodynamic model is applicable for viscosity estimation of strong electrolyte systems, such as CO_2-loaded alkanolamine solutions.

The proposed correlations for viscosity of aqueous MEA were examined for accuracies compared to literature viscosity data. Table 14 lists the calculated AARD and maximum deviation for the McAllister model based on fitted parameters by Amundsen et al. [2] and Hartono's correlation for the considered three data sources. It was observed that the AARD for viscosity correlations are greater than the AARD for density correlations for aqueous MEA. For Amundsen's correlation, the highest AARD of 5.66% was reported for data presented by Ma et al. [27] and a maximum deviation was observed as 0.871 MPa·s at $x_1 = 0.6220$ and $T = 298.15$ K for data given by Maham et al. [35]. Hartono's correlation showed a highest AARD of 4.35% for the viscosity data presented by Ma et al. [27] and a maximum deviation of 0.854 MPa·s for data presented by Maham et al. [35] at $x_1 = 0.8446$ and $T = 303.15$ K.

The accuracies for the correlations proposed for viscosity of CO_2-loaded MEA were in the same order as with viscosity correlations for aqueous MEA. Weiland's correlation and Hartono's correlation were studied for their accuracies of the data predictions compared to the measured viscosities of 30 mass% CO_2-loaded aqueous MEA mixtures at different temperatures, and calculated AARD and maximum deviation are shown in Table 15. Weiland's correlation showed a highest AARD of 4% and a maximum deviation of 0.176 MPa·s at the CO_2 loading of 0.5 mol CO_2/mol MEA and $T = 298.15$ K for viscosities published by Amundsen et al. [2]. This could be due to the uncertainties related to the

TABLE 14: Comparison of viscosity correlations with different literature data for aqueous MEA mixtures.

Data source	Ma et al. [27]	Amundsen et al. [2]	Maham et al. [35]
T (K)	293.15–333.15	293.15–353.15	293.15–353.15
x_1	0.1000–0.8995	0.0687–0.7264	0.0313–0.8446
McAllister model			
AARD (%)	5.66	3.30	2.15
MD (mPa·s)	0.773	0.105	0.871
Hartono's correlation			
AARD (%)	4.35	2.38	2.39
MD (mPa·s)	0.825	0.774	0.854

experiments. Hartono's correlation showed a highest AARD of 3.80% for work done by Amundsen et al. [2] and a maximum deviation of 0.195 MPa·s at the CO_2 loading of 0.38 mol CO_2/mol MEA and $T = 303.15$ K for data presented by Zhang et al. [29].

3.3. Surface Tension Correlations.
Table 16 lists the relevant correlations for the surface tension. The behaviour of surface tension of pure and aqueous MEA is claimed to be linear with the temperature [4, 41], and data were fitted according to the correlation proposed for pure components as given in equation (50) [75]. The nonlinearity of surface tension with MEA concentration at a given temperature was correlated as illustrated in equation (51) [31, 76] by Vazquez et al. [41] and Han et al. [4] over a range of MEA concentrations and temperatures.

Surface tension measurements performed under atmospheric conditions are mentioned with 0.1013 MPa pressure.

For the surface tension of CO_2-loaded aqueous MEA, several attempts have been made by Jayarathna et al. [31] to build an appropriate correlation and a polynomial function was proposed including the CO_2 loading and temperature as independent variables as in equation (52). In this correlation, there is no variable defined to represent MEA concentration in the solution. The parameters of the polynomial were found through a regression analysis using measured surface tension data of 20–70 mass% MEA with CO_2 loading 0–0.5 mol CO_2/mol MEA at temperatures from 303.15 K to 333.15 K. Another correlation was introduced as given in equation (53) for the experiments with 80 mass% MEA with CO_2 loading 0–0.5 mol CO_2/mol MEA at temperatures from 313.15 K to 343.15 K in which the coefficients of the polynomial were found under different temperatures [3]. The applicability of the Connors and Wright model was discussed. The surface tension of liquid CO_2 was considered as a fitting parameter in equation (55) since it does not exist under such conditions [31].

3.4. Thermal Expansion Coefficient Correlations.
The thermal expansion coefficient describes the volume variation

TABLE 15: Comparison of viscosity correlations with different literature data for CO_2-loaded aqueous MEA mixtures.

Data source	Hartono et al. [1]	Amundsen et al. [2]	Zhang et al. [29]
T (K)	293.15–353.15	293.15–353.15	298.15–353.15
α (mol CO_2/mol MEA)	0.11–0.5	0.1–0.5	0.14–0.49
Weiland's correlation			
AARD (%)	1.57	4.00	2.80
MD (mPa·s)	0.077	0.176	0.119
Hartono's correlation			
AARD (%)	3.47	3.80	3.69
MD (mPa·s)	0.154	0.188	0.195

against temperature and is defined as in equation (56) for a liquid:

$$\beta = -\rho^{-1}\left(\frac{\partial \rho}{\partial T}\right). \tag{56}$$

For a mixture, equation (57) can be derived in terms of excess volume of the mixture and thermal expansions of the pure liquids [6]:

$$\beta = V^{-1}\left[\left(\frac{\partial V^E}{\partial T}\right) + \sum_{i}^{n}(x_i \beta_i V_i)\right]. \tag{57}$$

Only a few studies have been performed on MEA solutions and Yang et al. [6] present data of thermal expansion coefficient for pure MEA.

4. Discussion

The correlations found for the density of all types of studied mixtures including pure, aqueous MEA, and CO_2-loaded aqueous MEA were able to fit measured densities with acceptable accuracies to perform engineering calculations. Correlations for the density of aqueous mixtures based on the excess volume of aqueous MEA provide some theoretical insight to analyse the mixtures for molecular size and shape of the components. The need for a higher number of parameters to enhance accuracy is a drawback in this type of correlations. Available correlations are empirical and measured data are required to estimate the correlation parameters. The reported accuracies for density correlations of nonloaded solutions are as expected to be better than for correlations of CO_2-loaded solutions.

The comparison of the correlations with available density data in literature showed that Hartono's density correlation for aqueous MEA gave a minimum AARD of 0.03%. Han's correlation and Hartono's density correlation for CO_2-loaded aqueous MEA showed a minimum AARD of 0.09%.

For engineering purposes, all the density correlations are satisfactory. Most of the used methods are empirical. For scientific evaluations, theoretical models are more attractive to evaluate reasonable dependencies of different parameters. One promising example is to make use of Prigogine–Flory–Patterson's [54, 55] approach for aqueous MEA mixtures and extend to the CO_2-loaded aqueous MEA mixtures.

For the viscosities, correlations are available for viscosities of all types of studied mixtures. The reported

accuracies of data fitting are satisfactory to perform calculations in design, mathematical modelling, and simulation. Correlations reported by Heric-Brewer [69], Jouyban-Acree [70], and McAllister [67] demonstrate a theoretical background in the model structure. Lack of theoretical insight is a drawback in viscosity correlations related to the CO_2-loaded aqueous MEA solutions. The method proposed by Matin et al. [58] to use Gibbs free energy of mixing from the electrolyte-NRTL model for the excess free energy of activation for viscous flow in the Eyring [68] viscosity model to predict viscosities of CO_2-loaded solutions has benefits and drawbacks. The electrolyte-NRTL is a complex model with many parameters involved. Commercial process simulation packages such as ASPEN Plus have the electrolyte-NRTL model with relevant interaction parameters for CO_2-loaded aqueous MEA systems that make it easy to adopt the model to perform viscosity calculations.

The performed correlation comparison for viscosity with available viscosity data in the literature showed that Hartono's correlation for viscosity of aqueous MEA and Weiland's correlation for viscosity of CO_2-loaded aqueous MEA were reasonably good for considered viscosity data. For today's use, the correlations proposed by Weiland et al. [26] and Hartono et al. [1] are attractive in the aspects of accuracy, easy understanding, and implementation. In the future, it is recommended to work towards use of more theoretically based models. One example with potential is Eyring's viscosity model combined with NRTL model for viscosity predictions.

5. Conclusion

This study summarizes measured data and correlations developed for the density, viscosity, surface tension, and thermal expansion coefficient of pure, aqueous MEA, and CO_2-loaded aqueous MEA solutions. For the density, an adequate amount of data is available for pure and aqueous MEA mixtures under different concentrations and temperatures. There is a lack of density data of CO_2-loaded aqueous MEA especially at higher concentrations of MEA. The correlations available in literature for all studied types of solutions are in good agreement with measured densities.

For viscosities, data are available for pure MEA and aqueous MEA to cover mole fractions from 0 to 1 up to temperature 423.15 K. The available data for CO_2-loaded aqueous MEA mixtures are limited to some special MEA concentrations and CO_2 loadings. Recent studies have

TABLE 16: Correlations for the surface tension of MEA + H_2O + CO_2 mixtures.

Correlation		T (K)	P (MPa)	Data sources
$\sigma = K_1 - K_2 t$	(50)	298.15–333.15	0.1013	[4, 41]
$\sigma_{mix} = \sigma_1 + \sum_{i\geq2}(1+(a_i x_i/(1-b_i)(1+\sum_{j\geq2}b_j/(1-b_j)x_j)))x_i(\sigma_i-\sigma_1)$	(51)	303.15–333.15	0.1013	[4]
$\sigma_{mix} = a_1 + a_2\cdot\alpha+a_3\cdot T+a_4\cdot\alpha^2+a_5\cdot\alpha\cdot T+a_6\cdot T^2+a_7\cdot\alpha^3+a_8\cdot\alpha^2\cdot T+a_9\cdot\alpha^4+a_{10}\cdot\alpha^3\cdot T+a_4\cdot\alpha^2\cdot T^2$	(52)	303.15–333.15	0.1013	[31]
$\sigma_{mix} = a\cdot\alpha^2+b\cdot\alpha+c$	(53)	313.15–343.15	0.1013	[3]
$\sigma_{mix} = \sigma_2 + \sum_{i=1,3}(1+(a_i x_i/(1-b_i)(1+\sum_{j=1,3}(b_j/(1-b_j)x_j)))x_i(\sigma_i-\sigma_2)$	(54)	303.15–333.15	0.1013	[31]
$\sigma_{CO_2} = a_1 + a_2 T$	(55)			

measured viscosities of CO_2-loaded mixtures at high MEA concentrations. Further studies are required to fill the gaps and validate the existing data. The correlations and semi-empirical models used for pure and aqueous MEA are capable of fitting data with acceptable accuracy. The developed correlations for CO_2-loaded mixtures need improvements to fit measured data in a wide range of MEA concentrations and temperatures. For engineering purposes, it is recommended to make use of more theoretically based models.

Surface tension data for pure and aqueous MEA mixtures are available in the literature. The data have been correlated to different types of correlations with acceptable accuracy. It is recommended to perform further studies to measure the surface tension of CO_2-loaded aqueous MEA mixtures to fill the gaps and check the validity of the existing data. For the thermal expansion coefficient, studies are needed to determine the thermal expansion coefficient for CO_2-loaded aqueous MEA mixtures.

Nomenclature

E: Activation energy of viscous flow, $J \cdot mol^{-1}$
ΔF^*:   Free energy of activation for viscous flow, $J \cdot mol^{-1}$
ΔF^{E*}:   Excess free energy of activation for viscous flow, $J \cdot mol^{-1}$
h: Planck's constant, $m^2 \cdot kg \cdot s^{-1}$
K: Regression parameter
M_1:   Molecular weight of MEA, $g \cdot mol^{-1}$
M_2:   Molecular weight of water, $g \cdot mol^{-1}$
N: Number of data
N_A: Avogadro number, mol^{-1}
R: Universal gas constant, $J \cdot mol^{-1} \cdot K^{-1}$
t: Temperature, $°C$
T: Temperature, K
T_c: Critical temperature, K
T_0:   Reference temperature 308 K
u: Uncertainty
U: Expanded uncertainty
v: Kinematic viscosity, $m^2 \cdot s^{-1}$
v_{ideal}:   Kinematic viscosity of an ideal mixture, $m^2 \cdot s^{-1}$
V_i^0:   Molar volume of ith pure component, $m^3 \cdot mol^{-1}$
V_1^0:   Molar volume of MEA, $m^3 \cdot mol^{-1}$
V_2^0:   Molar volume of water, $m^3 \cdot mol^{-1}$
V^E: Excess molar volume, $m^3 \cdot mol^{-1}$
V_m: Molar volume of the mixture, $m^3 \cdot mol^{-1}$
w_{MEA}:   Mass percent MEA
x_i: Mole fraction of ith component
x_1:   Mole fraction of MEA
x_2:   Mole fraction of water
Y_i^E: Measured property
Y_i^C: Calculated property
Greek letters
ρ: Density, $kg \cdot m^{-3}$
ρ_1:   Density of pure MEA, $kg \cdot m^{-3}$
ρ_2:   Density of pure water, $kg \cdot m^{-3}$
η: Viscosity, $Pa \cdot s$
$\Delta \eta$:   Viscosity difference, $Pa \cdot s$
η_{ideal}:   Viscosity of an ideal mixture, $Pa \cdot s$
η_{H_2O}:   Viscosity of water, $Pa \cdot s$
η_γ: Viscosity deviation, $Pa \cdot s$
$\eta_{unloaded}$:   Viscosity of unloaded solution, $Pa \cdot s$
σ: Surface tension, $N \cdot m^{-1}$
σ_{mix}:   Surface tension of a mixture, $N \cdot m^{-1}$
β: Bulk thermal expansively, K^{-1}
β: Thermal expansion coefficient, K^{-1}
α: CO_2 loading, mol CO_2/mol MEA.

Conflicts of Interest

The authors declare that they have no conflicts of interest.

Acknowledgments

References

[1] A. Hartono, E. O. Mba, and H. F. Svendsen, "Physical properties of partially CO_2 loaded aqueous monoethanolamine (MEA)," *Journal of Chemical & Engineering Data*, vol. 59, no. 6, pp. 1808–1816, 2014.

[2] T. G. Amundsen, L. E. Øi, and D. A. Eimer, "Density and viscosity of monoethanolamine + water + carbon dioxide from (25 to 80)°C," *Journal of Chemical & Engineering Data*, vol. 54, no. 11, pp. 3096–3100, 2009.

[3] S. A. Jayarathna, C. K. Jayarathna, D. A. Kottage, S. Dayarathna, D. A. Eimer, and M. C. Melaaen, "Density and surface tension measurements of partially carbonated aqueous monoethanolamine solutions," *Journal of Chemical & Engineering Data*, vol. 58, no. 2, pp. 343–348, 2013.

[4] J. Han, J. Jin, D. A. Eimer, and M. C. Melaaen, "Density of water (1) + monoethanolamine (2) + CO_2 (3) from (298.15 to 413.15) K and surface tension of water (1) + monoethanolamine (2) from (303.15 to 333.15) K," *Journal of Chemical & Engineering Data*, vol. 57, no. 4, pp. 1095–1103, 2012.

[5] H. Touhara, S. Okazaki, F. Okino, H. Tanaka, K. Ikari, and K. Nakanishi, "Thermodynamic properties of aqueous mixtures of hydrophilic compounds 2. Aminoethanol and its methyl derivatives," *The Journal of Chemical Thermodynamics*, vol. 14, no. 2, pp. 145–156, 1982.

[6] F. Yang, X. Wang, W. Wang, and Z. Liu, "Densities and excess properties of primary amines in alcoholic solutions," *Journal of Chemical & Engineering Data*, vol. 58, no. 3, pp. 785–791, 2013.

[7] M. H. Li and K. P. Shen, "Densities and solubilities of solutions of carbon dioxide in water + monoethanolamine + N-methyldiethanolamine," *Journal of Chemical & Engineering Data*, vol. 37, no. 3, pp. 288–290, 1992.

[8] Y. W. Wang, S. Xu, F. D. Otto, and A. E. Mather, "Solubility of N_2O in alkanolamines and in mixed solvents," *The Chemical Engineering Journal*, vol. 48, no. 1, pp. 31–40, 1992.

[9] R. M. DiGuilio, R. J. Lee, S. T. Schaeffer, L. L. Brasher, and A. S. Teja, "Densities and viscosities of the ethanolamines," *Journal of Chemical & Engineering Data*, vol. 37, no. 2, pp. 239–242, 1992.

[10] M. Pagé, J.-Y. Huot, and C. Jolicoeur, "A comprehensive thermodynamic investigation of water-ethanolamine mixtures at 10, 25, and 40°C," *Canadian Journal of Chemistry*, vol. 71, no. 7, pp. 1064–1072, 1993.

[11] Y. Maham, T. T. Teng, L. G. Hepler, and A. E. Mather, "Densities, excess molar volumes, and partial molar volumes for binary mixtures of water with monoethanolamine, diethanolamine, and triethanolamine from 25 to 80°C," *Journal of Solution Chemistry*, vol. 23, no. 2, pp. 195–205, 1994.

[12] F. M. Guevara and A. T. Rodriguez, "Liquid density as a function of temperature of five organic solvents," *Journal of Chemical & Engineering Data*, vol. 29, pp. 204–206, 1984.

[13] M.-H. Li and Y.-C. Lie, "Densities and viscosities of solutions of monoethanolamine + N-methyldiethanolamine + water and monoethanolamine + 2-amino-2-methyl-1-propanol + water," *Journal of Chemical & Engineering Data*, vol. 39, no. 3, pp. 444–447, 1994.

[14] M.-J. Lee and T.-K. Lin, "Density and viscosity for monoethanolamine + water + ethanol, and +2-propanol," *Journal of Chemical & Engineering Data*, vol. 40, no. 1, pp. 336–339, 1995.

[15] J.-H. Song, S.-B. Park, J.-H. Yoon, H. Lee, and K.-H. Lee, "Densities and viscosities of monoethanolamine + ethylene glycol + water," *Journal of Chemical & Engineering Data*, vol. 41, no. 5, pp. 1152–1154, 1996.

[16] U. R. Kapadi, D. G. Hundiwale, N. B. Patil, and M. K. Lande, "Viscosities, excess molar volume of binary mixtures of ethanolamine with water at 303.15, 308.15, 313.15 and 318.15 K," *Fluid Phase Equilibria*, vol. 201, no. 2, pp. 335–341, 2002.

[17] M. N. Islam, M. M. Islam, and M. N. Yeasmin, "Viscosity of aqueous solution of 2-methoxyethanol, 2-ethoxyethanol, and ethanolamine," *The Journal of Chemical Thermodynamics*, vol. 36, pp. 889–893, 2004.

[18] A. Valtz, C. Coquelet, and D. Richon, "Volumetric properties of the monoethanolamine-methanol mixture at atmospheric pressure from 283.15 to 353.15 K," *Thermochimica Acta*, vol. 428, no. 1-2, pp. 185–191, 2005.

[19] Y. Geng, S. Chen, T. Wang et al., "Density, viscosity and electrical conductivity of 1-butyl-3-methylimidazolium hexafluorophosphate + monoethanolamine and +N, N-dimethylethanolamine," *Journal of Molecular Liquids*, vol. 143, no. 2-3, pp. 100–108, 2008.

[20] F. Pouryousefi and R. O. Idem, "New analytical technique for carbon dioxide absorption solvents," *Industrial & Engineering Chemistry Research*, vol. 47, no. 4, pp. 1268–1276, 2008.

[21] M. M. Taib and T. Murugesan, "Densities and excess molar volumes of binary mixtures of bis(2-hydroxyethyl) ammonium acetate + water and monoethanolamine + bis(2-hydroxyethyl)ammonium acetate at temperatures from (303.15 to 353.15) K," *Journal of Chemical & Engineering Data*, vol. 55, no. 12, pp. 5910–5913, 2010.

[22] M. M. Taib and T. Murugesan, "Density, refractive index, and excess properties of 1-butyl-3-methylimidazolium tetrafluoroborate with water and monoethanolamine," *Journal of Chemical & Engineering Data*, vol. 57, no. 1, pp. 120–126, 2012.

[23] A. G. Abuin, D. G. Diaz, and J. M. Navaza, "Density, speed of sound, and viscosity of Monoethanolamine + Water + N-Ethyl-2-pyrrolidone from T = (293.15 to 323.15) K," *Journal of Chemical & Engineering Data*, vol. 58, pp. 3387–3391, 2013.

[24] F. Xu, H. Gao, H. Dong et al., "Solubility of CO_2 in aqueous mixtures of monoethanolamine and dicyanamide-based ionic liquids," *Fluid Phase Equilibria*, vol. 365, pp. 80–87, 2014.

[25] M. Sobrino, E. I. Concepción, Á. Gómez-Hernández, M. C. Martín, and J. J. Segovia, "Viscosity and density measurements of aqueous amines at high pressures: MDEA-water and MEA-water mixtures for CO_2 capture," *The Journal of Chemical Thermodynamics*, vol. 98, pp. 231–241, 2016.

[26] R. H. Weiland, J. C. Dingman, D. B. Cronin, and G. J. Browning, "Density and viscosity of some partially carbonated aqueous alkanolamine solutions and their blends," *Journal of Chemical & Engineering Data*, vol. 43, no. 3, pp. 378–382, 1998.

[27] D. Ma, C. Zhu, T. Fu, X. Yuan, and Y. Ma, "Volumetric and viscometric properties of binary and ternary mixtures of monoethanolamine, 2-(diethylamino) ethanol and water from (293.15 to 333.15) K," *The Journal of Chemical Thermodynamics*, vol. 138, pp. 350–365, 2019.

[28] B. P. Mandal, M. Kundu, and S. S. Bandyopadhyay, "Density and viscosity of aqueous solutions of (N-methyldiethanolamine + monoethanolamine), (N-methyldiethanolamine + diethanolamine), (2-amino-2-methyl-1-propanol + monoethanolamine), and (2-amino-2-methyl-1-propanol + diethanolamine)," *Journal of Chemical & Engineering Data*, vol. 48, no. 3, pp. 703–707, 2003.

[29] J. Zhang, P. S. Fennell, and J. P. M. Trusler, "Density and viscosity of partially carbonated aqueous tertiary alkanolamine solutions at temperatures between (298.15 and 353.15) K," *Journal of Chemical & Engineering Data*, vol. 60, no. 8, pp. 2392–2399, 2015.

[30] L. E. Øi, P. M. Hansen, and M. Henriksen, "CO_2 absorption efficiency and heat consumption measured at high gas to liquid ratios in laboratory rig," *Energy Procedia*, vol. 114, pp. 1273–1281, 2017.

[31] S. A. Jayarathna, A. Weerasooriya, S. Dayarathna, D. A. Eimer, and M. C. Melaaen, "Densities and surface tensions of CO_2 loaded aqueous monoethanolamine solutions with $r = (0.2$ to $0.7)$ at $T = (303.15$ to $333.15)$ K," *Journal of Chemical & Engineering Data*, vol. 58, no. 4, pp. 986–992, 2013.

[32] S. S. Karunarathne, D. A. Eimer, and L. E. Øi, "Model uncertainty of interfacial area and mass transfer coefficients in absorption column packings," in *Proceedings of the 58th SIMS*, pp. 144–150, Reykjavik, Iceland, September 2017.

[33] U. S. P. R. Arachchige, N. Aryal, D. A. Eimer, and M. C. Melaaen, "Viscosities of pure and aqueous solutions of Monoethanolamine (MEA), Diethanolamine (DEA), and N-Methyldiethanolamine (MDEA)," in *Annual Transactions of the Nordic Rheology Society*, Vol. 21, ACS, Washington, DC, USA, 2013.

[34] Z. Idris, N. B. Kummamuru, and D. A. Eimer, "Viscosity measurement of unloaded and CO2-loaded aqueous monoethanolamine at higher concentrations," *Journal of Molecular Liquids*, vol. 243, pp. 638–645, 2017.

[35] Y. Maham, C.-N. Liew, and A. E. Mather, "Viscosities and excess properties of aqueous solutions of ethanolamines from 25 to 80°C," *Journal of Solution Chemistry*, vol. 31, no. 9, pp. 743–756, 2002.

[36] S. S. Karunarathne and L. E. Øi, "Evaluation of systematic error and uncertainty of viscosity measurements of mixtures of monoethanol amine and water in coaxial cylinder rheometers," *International Journal of Modeling and Optimization*, vol. 8, no. 5, pp. 260–265, 2018.

[37] U. S. P. R. Arachchige, B. Singh, K. Prajapati, and M. C. Melaaen, "Dynamic viscosity of partially carbonated aqueous monoethanolamine (MEA) from (20 to 150)°C," *Applied Chemical Engineering*, vol. 1, pp. 1–10, 2018.

[38] U. S. P. R. Arachchige, B. Singh, K. Prajapati, and M. C. Melaaen, "Viscosities of aqueous solutions of Monoethanolamine (MEA), Diethanolamine (DEA) and

N-Methyldiethanolamine (MDEA) at T = (90–150)°C," in *Annual Transactions of the Nordic Rheology Society*, Vol. 22, ACS, Washington, DC, USA, 2014.

[39] D. Fu, L. Chen, and L. Qin, "Experiment and model for the viscosity of carbonated MDEA-MEA aqueous solutions," *Fluid Phase Equilibria*, vol. 319, pp. 42–47, 2012.

[40] Z. Idris, J. Han, S. Jayarathna, and D. A. Eimer, "Surface tension of alkanolamine solutions: an experimentally based review," *Energy Procedia*, vol. 114, pp. 1828–1833, 2017.

[41] G. Vázquez, E. Alvarez, J. M. Navaza, R. Rendo, and E. Romero, "Surface tension of binary mixtures of water-+ monoethanolamine and water + 2-amino-2-methyl-1-propanol and tertiary mixtures of these amines with water from 25°C to 50°C," *Journal of Chemical & Engineering Data*, vol. 42, no. 1, pp. 57–59, 1997.

[42] P. R. G. Couto, J. C. Damasceno, and S. P. D. Oliveira, "Monte carlo simulation applied to uncertainty in measurement," *Theory and Applications of Monte Carlo Simulation*, INTECH, Open Science, Open Minds, London, UK, 2013.

[43] M. Cox and P. Harris, Up a GUM tree? Try the full Monte.

[44] M. Désenfant and M. Priel, "Road map for measurement uncertainty evaluation," *Measurement*, vol. 39, no. 9, pp. 841–848, 2006.

[45] C. K. Jayarathna, A. B. Elverhøy, Y. Jiru, and D. Eimer, "Experimentally based evaluation of accuracy of absorption equilibrium measurements," *Energy Procedia*, vol. 37, pp. 834–843, 2013.

[46] A. Hartono, E. O. Mba, and H. F. Svendsen, "Prediction of N_2O solubility in alkanolamine solutions from the excess volume property," *Energy Procedia*, vol. 37, pp. 1744–1750, 2013.

[47] S. Cheng, A. Meisen, and A. Chakma, "Predict amine solution properties accurately," *Hydrocarbon Processing*, vol. 75, no. 2, pp. 81–86, 1996.

[48] D. A. Glasscock, *Modelling and experimental study of carbondioxide absorption into aqueous alkanolamines*, Ph.D. thesis, University of Texas at Austin, Austin, TX, USA, 1990.

[49] C.-H. Hsu and M.-H. Li, "Densities of aqueous blended amines," *Journal of Chemical & Engineering Data*, vol. 42, no. 3, pp. 502–507, 1997.

[50] R. C. Reid, J. M. Prausnitz, and B. E. Poling, *The Properties of Gas and Liquids*, McGraw-Hill, New York, NY, USA, 1987.

[51] A. J. Treszczanowicz and G. C. Benson, "Excess volumes for n-alkanols + n-alkanes II. Binary mixtures of *n*-pentanol, *n*-hexanol, *n*-octanol, and *n*-decanol + *n*-heptane," *The Journal of Chemical Thermodynamics*, vol. 10, no. 10, pp. 967–974, 1978.

[52] H. Iloukhani, M. Rezaei-Sameti, and J. Basiri-Parsa, "Excess molar volumes and dynamic viscosities for binary mixtures of toluene + *n*-alkanes (C5–C10) at T = 298.15 K-comparison with Prigogine-Flory-Patterson theory," *The Journal of Chemical Thermodynamics*, vol. 38, no. 8, pp. 975–982, 2006.

[53] A. A. Rostami, M. J. Chaichi, and M. Sharifi, "Densities, viscosities, and excess Gibbs energy of activation for viscous flow, for binary mixtures of dimethyl phthalate (DMP) with 1-pentanol, 1-butanol, and 1-propanol at two temperatures," *Monatshefte für Chemie-Chemical Monthly*, vol. 138, no. 10, pp. 967–971, 2007.

[54] P. J. Flory, "Statistical thermodynamics of liquid mixtures," *Journal of the American Chemical Society*, vol. 87, no. 9, pp. 1833–1838, 1965.

[55] D. Patterson and G. Delmas, "Corresponding states theories and liquid models," *Discussions of the Faraday Society*, vol. 49, pp. 98–105, 1970.

[56] F. Qi and H. Wang, "Application of Prigogine-Flory-Patterson theory to excess molar volume of mixtures of 1-butyl-3-methylimidazolium ionic liquids with *N*-methyl-2-pyrrolidinone," *The Journal of Chemical Thermodynamics*, vol. 41, no. 2, pp. 265–272, 2009.

[57] O. Redlich and A. T. Kister, "Algebraic representation of thermodynamic properties and the classification of solutions," *Industrial & Engineering Chemistry*, vol. 40, no. 2, pp. 345–348, 1948.

[58] N. S. Matin, J. E. Remias, and K. Liu, "Application of electrolyte-NRTL model for prediction of the viscosity of carbon dioxide loaded aqueous amine solutions," *Industrial & Engineering Chemistry Research*, vol. 52, no. 47, pp. 16979–16984, 2013.

[59] T. T. Teng, Y. Maham, L. G. Hepler, and A. E. Mather, "Viscosity of aqueous solutions of N-methyldiethanolamine and of diethanolamine," *Journal of Chemical & Engineering Data*, vol. 39, no. 2, pp. 290–293, 1994.

[60] E. N. d. C. Andrade, "LVIII. A theory of the viscosity of liquids. Part II," *The London, Edinburgh, and Dublin Philosophical Magazine and Journal of Science*, vol. 17, no. 113, pp. 698–732, 1934.

[61] D. H. Vogel, "Das temperaturabhaengigkeitsgesetz der Viskositaet von Fluessigkeiten," *Physikalische Zeitschrift*, vol. 22, pp. 645-646, 1921.

[62] J. Kendall and K. P. Monroe, "The viscosity of liquids. II. The viscosity-composition curve for ideal liquid mixtures," *Journal of the American Chemical Society*, vol. 39, no. 9, pp. 1787–1802, 1917.

[63] E. C. Bingham, *Fluidity and Plasticity*, McGraw-Hill, New York, NY, USA, 1922.

[64] D. C. Cronauer, R. R. Rothfus, and R. I. Kermode, "Viscosity and density of the ternary liquid system acetone-benzene-ethylene dichloride," *Journal of Chemical & Engineering Data*, vol. 10, no. 2, pp. 131–133, 1965.

[65] R. J. Martins, M. J. E. d. M. Cardoso, and O. E. Barcia, "Excess gibbs free energy model for calculating the viscosity of binary liquid mixtures," *Industrial & Engineering Chemistry Research*, vol. 39, no. 3, pp. 849–854, 2000.

[66] A. H. Nhaesi and A.-F. A. Asfour, "Prediction of the McAllister model parameters from pure component properties of regular binary liquid mixtures," *Industrial & Engineering Chemistry Research*, vol. 37, no. 12, pp. 4893–4897, 1998.

[67] R. A. McAllister, "The viscosity of liquid mixtures," *AIChE Journal*, vol. 6, no. 3, pp. 427–431, 1960.

[68] H. Eyring, "Viscosity, plasticity, and diffusion as examples of absolute reaction rates," *The Journal of Chemical Physics*, vol. 4, no. 4, pp. 283–291, 1936.

[69] E. L. Heric and J. G. Brewer, "Viscosity of some binary liquid nonelectrolyte mixtures," *Journal of Chemical & Engineering Data*, vol. 12, no. 4, pp. 574–583, 1967.

[70] A. Jouyban, M. Khoubnasabjafari, Z. Vaez-Gharamaleki, Z. Fekari, and W. E. Acree Jr., "Calculation of the viscosity of binary liquids at various temperatures using Jouyban-Acree model," *Chemical & Pharmaceutical Bulletin*, vol. 53, no. 5, pp. 519–523, 2005.

[71] J. V. Herráez, R. Belda, O. Díez, and M. Herráez, "An equation for the correlation of viscosities of binary mixtures," *Journal of Solution Chemistry*, vol. 37, no. 2, pp. 233–248, 2008.

[72] J. Setschenow, "Über die konstitution der salzlösungen auf grund ihres verhaltens zu kohlensäure," *Zeitschrift für Physikalische Chemie*, vol. 4U, no. 1, 1889.

[73] M. Shokouhi, A. H. Jalili, F. Samani, and M. Hosseini-Jenab, "Experimental investigation of the density and viscosity of CO_2-loaded aqueous alkanolamine solutions," *Fluid Phase Equilibria*, vol. 404, pp. 96–108, 2015.

[74] M. Shokouhi, A. H. Jalili, M. Hosseini-Jenab, and M. Vahidi, "Thermo-physical properties of aqueous solutions of N,N-dimethylformamide," *Journal of Molecular Liquids*, vol. 186, pp. 142–146, 2013.

[75] J. J. Jasper, "The surface tension of pure liquid compounds," *Journal of Physical and Chemical Reference Data*, vol. 1, no. 4, pp. 841–1010, 1972.

[76] K. A. Connors and J. L. Wright, "Dependence of surface tension on composition of binary aqueous-organic solutions," *Analytical Chemistry*, vol. 61, no. 3, pp. 194–198, 1989.

Article G

The effect of CO$_2$ loading on the flow behaviour of amine and water mixtures.

The effect of CO_2 loading on the flow behaviour of amine and water mixtures

Sumudu S. Karunarathne[1], Dag A. Eimer[1], and Lars E. Øi[1]

[1]University of South-Eastern Norway, Norway

ABSTRACT

The understanding of flow behaviour of liquid is essential in chemical engineering applications in many aspects such as equipment design, process modelling and simulations. This study examines the effect of the presence of CO_2 in amine + H_2O mixtures of monoethanol amine (MEA) + H_2O and 2-amino-2-methyl-1-propanol (AMP) + MEA + H_2O. The relationship between shear stress and shear rate was investigated under different shear rates for both aqueous amine and CO_2 loaded aqueous amine mixtures. The study reveals that considered mixtures behave according to the Newtonian fluids indicating that the presence of CO_2 has a minimum effect on CO_2 loaded aqueous amine mixtures.

INTRODUCTION

The viscosity of liquid mixtures is important in chemical engineering applications as they are used in heat and mass transfer correlations in industrial processes[1]. In post-combustion CO_2 capture, viscosity data are involved in process simulations and design of the absorber-desorber system. The correlations are required to use the measured viscosities to perform engineering calculations for the design and mathematical modelling of the absorber column.

Understanding of the flow behaviour of amine + H_2O + CO_2 mixtures leads to the development of theoretical viscosity models with high accuracy. Semi-theoretical models

like Eyring's viscosity model[2] based on absolute rate theory provide a theoretical basis for the viscosity with a parameter to correlate with measured viscosities.

Eyring pointed out that the individual molecules in a liquid at rest undergo rearrangements through molecular movements. These motions lay the foundation of the viscosity model by introducing the term of free energy of activation for viscous flow. This parameter is useful to extract the thermodynamic and structural information of pure and liquid mixtures. The proportionality between shear stress and shear rate was assumed in the model derivation[3].

The increase of CO_2 concentration in aqueous amine mixtures increases the viscosity. The studies performed by Weiland et al.[4] and Hartono et al.[5] show the viscosity variations with amine concentration, CO_2 loading and temperature in different amine + H_2O + CO_2 mixtures.

Amine + H_2O + CO_2 solution is a mixture of various ions with carbamates, bicarbonates and protonated amines. The ionic strength of the mixture increases with the increase of dissolved CO_2 and at the same time solution pH decreases. Matin et al.[6] explained how the increase of CO_2 loading could affect the viscosity in the solution. At higher CO_2 loadings, the ionic strength is high and the solution has a greater polarity. This could lead to cluster formation, higher viscosity and even phase separation.

The motivation for this study is to examine the effect of CO_2 loading on fluid behaviour of CO_2 loaded aqueous amine solutions. Both aqueous amine mixtures and CO_2 loaded aqueous amine mixtures were studied investigating the relationship between shear stress vs shear rate.

METHODOLOGY

This section discusses the experimental method for the sample preparation, CO_2 loading analysis and viscosity measurements.

Sample preparation

Table 1 lists a description of the materials used in this study. The aqueous solutions were prepared by mixing amines with degassed deionized water using a rotary evaporator. The weights of the materials were measured by using an electronic balance from METTLER TOLEDO (XS403S) having a resolution of 1 mg. Series of aqueous amine + H_2O mixtures were prepared and used to make CO_2 loaded solution by bubbling CO_2 through the solution.

Table 1. Materials used in this study.

Material	Purity [a]	source
MEA	≥ 0.995	Sigma-Aldrich
AMP	≥ 0.99	Sigma-Aldrich
CO_2	0.9999	AGA Norge AS

[a] mole fraction as given by the supplier.

CO_2 loading analysis

A titration method was adopted to determine the amount of CO_2 present in the amine + H_2O mixtures. 50 ml of each from 0.1M NaOH and 0.3M $BaCl_2$ solutions were added to a 0.1-0.2g of CO_2 loaded aqueous amine solution and boiled for approximately 10 min to fix dissolved CO_2 as $BaCO_3$. Then precipitated $BaCO_3$ was filtered and transferred into 100 ml of distilled water and titrated with 0.1M HCl until the solution pH reaches a value of 2. Subsequently, the solution was boiled and cooled again and titrated with 0.1M NaOH. Another titration

was performed between 1g of CO_2 loaded solution dissolved in 100 ml of distilled water with 1M of HCl to determine the amine concentration.

Viscosity measurements

Viscosity measurements were performed using a Physica MCR 101 double-gap rheometer from Anton Paar. A liquid sample with 7ml was poured into the pressure cell. 4 bar of pressure was applied using N_2 gas to avoid amine escape due to evaporation. Variable shear rates of 200, 400, 600, 800 and 1000 1/s were maintained at the temperature of 303.15 K during the study and viscosity was measured via measured torque and shear stress by the instrument. Viscosities of both CO_2 unloaded and CO_2 loaded aqueous amine mixtures were analysed to examine the possible deviations from Newtonian behaviour.

RESULTS AND DISCUSSION

The study was performed for two types of amine + H_2O + CO_2 mixtures. Table 2 gives the details of the mixtures used in this study with relevant amine concentrations and CO_2 loadings.

Table 2. Mixtures considered in this study.

Mixtures	
MEA+H_2O+CO_2 MEA wt%	CO_2 loading (mol CO_2 / mol amine)
30	0
	0.543
40	0
	0.548
50	0
	0.495
AMP+MEA+H_2O+CO_2 (AMP / MEA) wt%	CO_2 loading (mol CO_2 / mol amine)
21/9	0
	0.518
24/6	0
	0.508
27/3	0
	0.511

MEA + H_2O + CO_2 mixtures contain monoethanol amine with the concentrations of 30, 40 and 50 wt% in aqueous solutions. The corresponding CO_2 loaded MEA solutions have 0.543, 0.548 and 0.495 mol CO_2/mol MEA respectively.

Fig. 1 illustrates the relation between shear stress and shear rate for CO_2 unloaded aqueous mixtures. The increase of MEA percentage in the mixtures increases the viscosity. Considered unloaded solutions exhibit the proportionality between shear stress and shear rate indicating that aqueous MEA solutions behave as a Newtonian fluid.
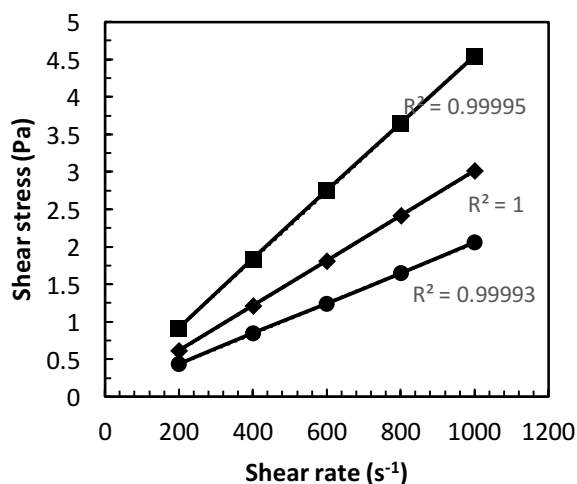
Figure 1. Shear stress vs shear rate of MEA + H_2O mixtures at 303.15 K: 30 wt% '●', 40 wt% '◆', 50 wt% '■'.

A similar study that was performed for the CO_2 loaded aqueous MEA solutions is shown in Fig. 2. The presence of CO_2 in aqueous MEA solution increases the viscosity. Fig. 2 illustrates that MEA + H_2O + CO_2 mixtures behave as Newtonian fluids as the shear stress is directly proportional to the shear rate. The formation of different ions has not affected much to change the nature of the fluid.
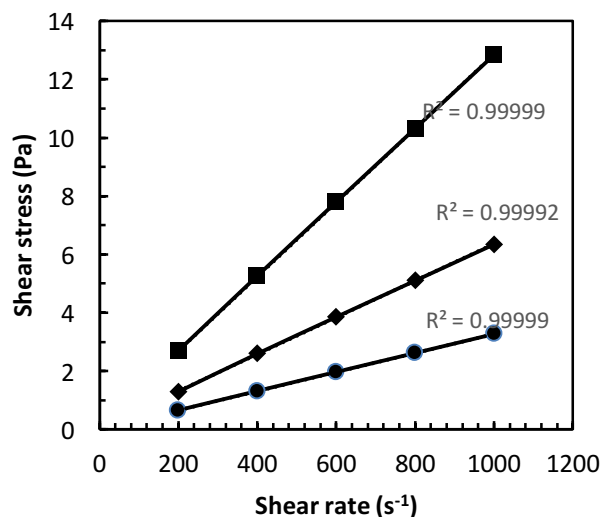
Figure 2. Shear stress vs shear rate of MEA + H_2O + CO_2 mixtures at 303.15 K: 30 wt% '●', 40 wt% '◆', 50 wt% '■'.

AMP is a sterically hindered amine and it does not form stable carbamate by reacting with CO_2. The CO_2 is converted into the form of carbonate and bicarbonate and increase the ion concentration in the mixture. The mixtures of AMP + MEA + H_2O and AMP + MEA + H_2O + CO_2 were examined for deviations from the Newtonian behaviour. AMP + MEA + H_2O + CO_2 mixtures contain 2-amino-2-methyl-1-propanol and monoethanol amine with different amine concentrations. The total amine weight percentage of all mixtures is 30 wt% and the remaining 70 wt% is H_2O. Corresponding CO_2 loadings of the solutions are given in Table 2.

Fig. 3 to 5. illustrate the comparison of relation between shear stress and shear rate of AMP + MEA + H_2O and AMP + MEA + H_2O + CO_2 mixtures. The variation in the amine concentrations caused the changes in viscosities in the mixtures. The excess properties such as excess volume, excess viscosity and excess free energy of activation for viscous flow indicates what type of intermolecular interactions are present indicating whether they are dispersion forces,

weak interaction or strong interactions like H-bonds in AMP + MEA + H_2O mixtures. Both CO_2 loaded and unloaded solutions show a linear relationship ($R^2 > 0.99$) between shear stress and shear rate. Accordingly, this reveals that solutions exhibit a Newtonian behaviour and formation of ionic species due to that the reaction between CO_2 and amines has not changed its flow characteristics compared to AMP + MEA + H_2O mixtures under considered different amine concentrations.

viscosity and a non-linear stress-strain behaviour in the correlation development.
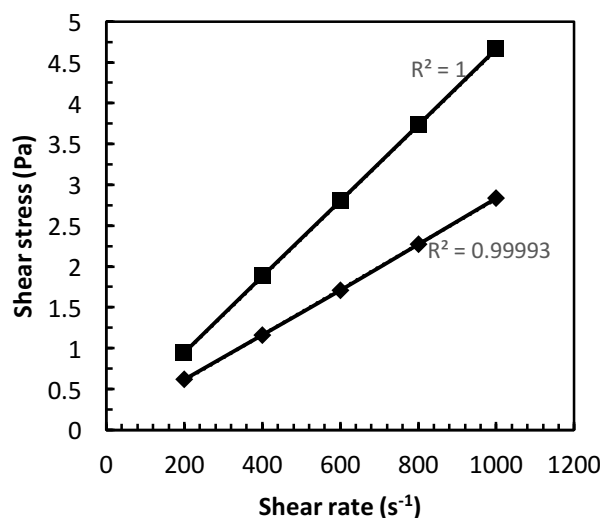
Figure 4. Shear stress vs shear rate of 24 wt % AMP + 6 wt% MEA + 70 wt% H_2O mixtures at 303.15 K: aqueous solution '◆, CO_2 loaded aqueous solution '■'.

Figure 3. Shear stress vs shear rate of 21 wt % AMP + 9 wt% MEA + 70 wt% H_2O mixtures at 303.15 K: aqueous solution '◆, CO_2 loaded aqueous solution '■'.

The CO_2 loadings considered in this study for all CO_2 loaded mixtures are relatively high compared to the CO_2 loading in rich amine stream in an absorber column. Here it is assumed that the flow behaviour at less loading values exhibit the same as the results obtained.

The study shows that increase of ionic strength due to the presence of CO_2 in all considered amine + H_2O + CO_2 mixtures have minimum effect on variations in the flow behaviour even though CO_2 increases the viscosity considerably. This enables to omit the count for time-dependent change in

Figure 5. Shear stress vs shear rate of 27 wt % AMP + 3 wt% MEA + 70 wt% H_2O mixtures at 303.15 K: aqueous solution '◆, CO_2 loaded aqueous solution '■'.

The Eyring's viscosity representation for Newtonian fluids can be adopted to fit viscosity data to obtain a correlation with

composition and temperature as independent variables.

CONCLUSION

This study examined the fluid behaviour of different amine + H_2O and amine + H_2O + CO_2 mixtures to investigate any deviations due to the presence of CO_2 in the amine + H_2O mixtures.

First, MEA + H_2O and AMP + MEA + H_2O mixtures were studied in which the shear stress was measured under different shear rates. The observations reveal a linear relationship between shear stress and shear rate ($R^2 > 0.99$) indicating that both MEA + H_2O and AMP + MEA + H_2O mixtures behave as Newtonian fluids under different amines concentrations.

Subsequently, the same mixtures under the presence of dissolved CO_2 were examined to observe their variation of shear stress with different shear rates. Generally, the addition of CO_2 increases the viscosity. The shear stress vs shear rate relationship was linear ($R^2 > 0.99$) indicating that considered amine + H_2O + CO_2 mixtures well behave as Newtonian fluids. The formation of ionic species due to the reaction between amine with CO_2 has a negligible effect on flow behaviour. Accordingly, the viscosity models developed based on the fundamentals of Newtonian fluids can be adopted to correlate measured viscosity data.

REFERENCES

1. L. E. Øi, "Removal of CO2 from exhaust gas," PhD, Faculty of Technology, Telemark University College, Porsgrunn, Norway, 2012.

2. H. Eyring, "Viscosity, Plasticity, and Diffusion as example of absolute reaction rates," *Journal of chemical physics,* vol. 4, pp. 283-291, 1936.

3. R. B. Bird, W. E. Stewart, and E. N. Lightfoot, *Transport Phenomena*, second edition ed. USA: John Wiley & Sons, Inc., 2002.

4. R. H. Weiland, J. C. Dingman, D. B. Cronin, and G. J. Browning, "Density and viscosity of some partially carbonated aqueous alkanolamine solutions and their blends," *J. Chem. Eng. Data,* vol. 43, pp. 378-382, 1998.

5. A. Hartono, E. O. Mba, and H. F. Svendsen, "Physical properties of partially CO_2 loaded aqueous monoethanolamine (MEA)," *J. Chem. Eng. Data* vol. 59, pp. 1808-1816, 2014.

6. N. S. Matin, J. E. Remias, and K. Liu, "Application of electrolyte-NRTL model for prediction of the viscosity of carbon dioxide loaded aqueous amine solutions " *Ind. Eng. Chem. Res,* vol. 52, pp. 16979-16984, 2013.

Article H

Free energies of activation for viscous flow of different amine mixtures in post combustion CO_2 capture.

Karunarathne, S.S.; Eimer, D.A.; Øi, L.E. TCCS -10, Trondheim, Norway, pp. 77-82, 2019.

FREE ENERGIES OF ACTIVATION FOR VISCOUS FLOW OF DIFFERENT AMINE MIXTURES IN POST COMBUSTION CO2 CAPTURE

S.S. Karunarathne, D.A. Eimer, L.E. Øi*

Faculty of Natural Sciences and Maritime Sciences - University of South-Eastern Norway, Norway

* Corresponding author e-mail: lars.oi@usn.no

Abstract

The viscosity of ternary mixtures of N-methyldiethanol amine (MDEA) + monoethanol amine (MEA) + H_2O, N-methyldiethanol amine (MDEA) + diethanol amine (DEA) + H_2O and 2-amino-2-methyl-1-propanol (AMP) + diethanol amine (DEA) + H_2O were correlated using Eyring's viscosity model based on absolute rate theory. The correlations were capable of representing viscosity data within AARD 1.9%, 1.4% and 2.1% for the mixtures MDEA + MEA + H_2O, MDEA + DEA + H_2O and AMP + DEA + H_2O respectively. These accuracies are acceptable in engineering calculations. The excess properties of volume V^E, viscosity η^E and free energy of activation for viscous flow ΔG^{E*} were studied to understand the intermolecular interactions in the mixtures. The study shows that all mixtures have a negative sign for V^E, η^E and a positive sign for ΔG^{E*}. This indicates weak intermolecular interactions in mixtures compared to the pure liquids and strong molecular attractions like H-bonds in the mixtures.

Keywords: Viscosity, Excess free activation energy, Eyring's viscosity model, Amines

1. Introduction

The applicability of different amine mixtures to capture CO_2 in a post-combustion absorption and desorption process has gained interest during past years. The combined effect of higher equilibrium capacities of tertiary and sterically hindered amines with the fast reaction rates of primary and secondary amines make this technology more feasible for large scale implementations. MEA (monoethanol amine) is regarded as the benchmark solvent in Post Combustion Capture (PCC) as it shows high CO_2 absorption rate, is relatively cheap and is less harmful to the environment compared to other commercial amines in PCC [1]. The main disadvantage of MEA is the high energy demand for regeneration and that limits the use of MEA + H_2O mixture as a solvent. DEA (diethanol amine) is a secondary amine that exhibits high absorption rate [2]. The irreversible side reactions and the formation of corrosive products are the disadvantages of using DEA. A tertiary amine like MDEA (N-methyldiethanol amine) has a relatively low absorption rate and high absorption capacity compared to MEA. The reaction between MDEA and CO_2 has a low heat of reaction and reduces the energy penalty of the amine regeneration. AMP (2-amino-2-methyl-1-propanol) is a sterically hindered primary amine that has both acceptable absorption capacity, absorption rate and regeneration energy demand, which is suitable for PCC.

Some studies of blends of aqueous alkanolamines as solvents in acid gas treating have been reported in the literature. As the studies reveal, those blends can enhance the physicochemical properties compared to amine and water mixtures with one amine [3,4]. There, the primary or secondary amine is mixed with a tertiary amine and water. Primary and secondary amines enhance the absorption rate while tertiary amines increase the absorption capacity and reduce the regeneration energy.

Densities and viscosities are important for the design of process equipment due to the influence on flow behavior, typically in pumps and pipes. Densities and viscosities are also influencing the heat and mass transfer performance in heat exchangers, absorbers and stripper units. Especially the density and viscosity appear in correlations for estimating heat and mass transfer coefficients and interfacial areas in random and structured packings. Reduction of the uncertainty in estimation methods for the density and viscosity in mixtures will improve design methods considerably. Several studies have been reported in the literature regarding density and viscosity measurements for the mixtures of (MEA + MDEA + H_2O), (DEA + MDEA + H_2O) and (DEA + AMP + H_2O) under different amine concentrations and temperatures [5].

In this study, the Eyring's [6] absolute rate theory approach on dynamic viscosity of Newtonian fluids was considered to evaluate the free energy of activation for viscous flow of different amine solutions based on available density and viscosity data that have been published by Mandal *et al.* [5]. The excess volume and the excess viscosity were determined to analyze the intermolecular attractions of the mixtures.

2. Methodology

The excess free energies of activation were calculated and correlated according to a Redlich-Kister [7] type polynomial. Eyring's viscosity model for Newtonian fluids is given in Eq (1).

$$\eta = \frac{hN}{V} exp\left(\frac{\Delta G^*}{RT}\right) \tag{1}$$

Where, $\eta, V, \Delta G^*, h, \ N, \ R$ and T are dynamic viscosity, molar volume, free energy of activation for viscous flow, Planck's constant, Avogadro's number, gas constant and temperature respectively. In order to compare with ideal solutions and calculate the excess activation energy properties following Eq (2) and (3) are obtained by using Eq (1).

$$ln(\eta V) = ln(\eta V)_{ideal} + \frac{\Delta G^{E*}}{RT} \tag{2}$$

$$ln(\eta V) = \sum_i x_i ln(\eta_i V_i^o) + \frac{\Delta G^{E*}}{RT} \tag{3}$$

The excess free energy of activation for viscous flow ΔG^{E*} was determined from the density and viscosity data reported by Mandal *et al.* [5] as shown in Eq (3). A Redlich-Kister type polynomial with temperature dependency as given in Eq (5) and Eq (6) is proposed to correlate ΔG^{E*} of the amine mixtures according to the Eq (4). Here η_i and V_i^o are viscosity and molar volume of the pure liquids.

$$\frac{\Delta G^{E*}}{RT} = \Delta G_{12}^{E*} + \Delta G_{13}^{E*} + \Delta G_{23}^{E*} \tag{4}$$

$$\Delta G_{jk}^{E*} = x_j x_k \sum_{i=0}^{n} A_i \left(x_j - x_k\right)^i \tag{5}$$

$$A_i = a + b(T) + c(T)^2 \tag{6}$$

There are several ways to determine ideal viscosity contribution in a mixture [8-10]. The excess viscosity η^E as given in Eq (7) provides a quantitative approach to determine the deviation of the viscosity of a real mixture from its ideal conditions. The sign of η^E signifies the molecular interactions between unlike molecules in the mixture [11]. The molecular interaction between molecules in the mixture has a significant effect on viscosity. Heric and Brewer [12] explained, $\Delta G^{E*} > 0$ for a mixture that exhibits higher viscosities in the real mixtures than that of the ideal mixture.

$$\eta^E = \eta - \sum_{i=1}^{n} x_i \eta_i \tag{7}$$

A positive sign of η^E indicates that the mixture exhibits strong intermolecular interaction and negative sign specify weak interaction among the unlike molecules [13]. Intermolecular interaction is not the only aspect that influences the viscosity deviation of liquid mixtures [14, 15]. The excess molar volume of mixtures also can reveal intermolecular attractions in a liquid mixture [16]. The excess molar volume V^E represent the molar volume variation of a real mixture compared to its ideal condition. Three characteristics have been discussed in the literature that contribute to determining the sign of V^E. The mixtures having specific or chemical interactions including charge transfer, forming of H-bonds and other complex forming interactions provide a negative contribution for V^E. The molecules with different shape and size can rearrange within vacant spaces by giving a negative contribution to V^E [17].

$$V^E = V - \sum_{i=1}^{n} x_i V_i \tag{8}$$

The V^E gets a positive contribution where the mixtures have interactions owing to the dispersion forces or weak dipole-dipole interaction.

The Eyring's viscosity model enables to analyze viscosity data from a thermodynamic point of view to extract further information about liquid mixtures. Meyer *et al.* [18] reported the possibilities of using ΔG^{E*} to examine molecular interactions as the viscosity deviation. A positive deviation ΔG^{E*} signifies strong specific interactions between unlike molecules and classifiable as dispersion forces show negative deviation as suggested by authors in the references [18, 19]. All these parameters of ΔG^{E*}, η^E and V^E help to understand the nature of molecular interactions, size and shape of the molecules. Further, they are useful to correlate measured density and viscosity data of liquid mixtures.

3. Results and Discussion

The proposed correlation able to predict excess free energy of activation for viscous flow of the amine mixture with below 2% average absolute relative deviation (AARD %) for all mixtures. Table 1-3 give the calculated parameters of the correlation given in Eq 4-6 for the mixtures. Viscosity predictions were compared with measured data. Figure 1 shows the comparison between measured and correlated data for MDEA + MEA + H_2O mixtures. The correlation was able to fit the data within AARD 1.9% and maximum deviation (AMD) of 0.1 mPa·s.
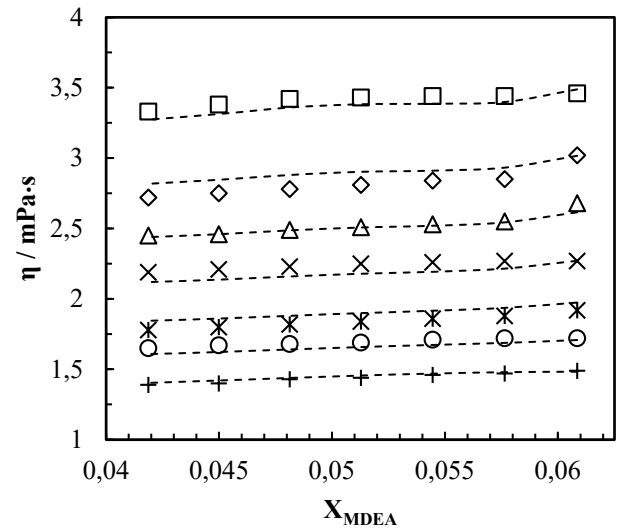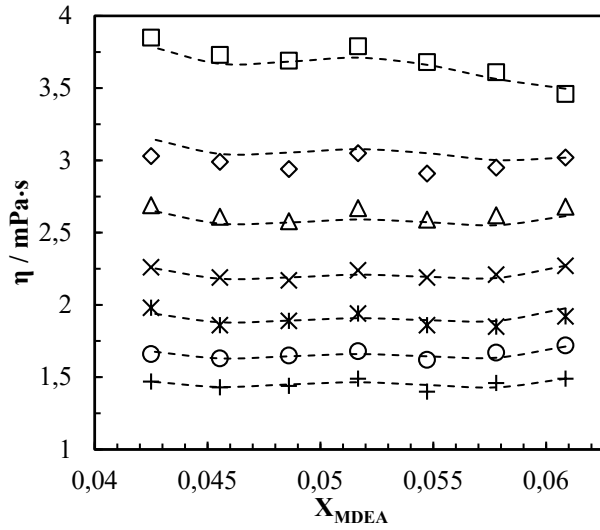

Figure 1: Viscosity variation of MDEA + MEA + H_2O mixtures with MDEA mole fraction and temperature: Experimental data from ref [5]; 293.15 K, '□'; 298.15 K, '◇'; 303.15 K, '△'; 308.15 K, 'x'; 313.15 K, 'ж'; 318.15 K, '○'; 323.15 K, '+'. The dotted lines represent the correlation in this work.

A comparison between measured and correlated viscosities was performed for the MDEA + DEA + H_2O mixtures as shown in Figure 2. It was found that the AARD and AMD for this mixture were 1.4% and 0.14 mPa·s respectively. Figure 3 illustrates the measured data with correlation for AMP + DEA + H_2O mixtures in which AARD and AMD were determined as 2.1% and 0.15 mPa·s respectively. The parameters of the correlation for the mixtures are given in Table 1 and the

accuracies of the data fit are acceptable for engineering calculations.

A qualitative analysis was performed to investigate the intermolecular attractions in the mixtures. The summary of the excess properties of the amine mixtures is given in Table 4. The η^E was calculated as shown in the Eq (7). The calculated η^E is negative for all mixtures at considered concentrations and temperatures. It emphasizes weak intermolecular interactions between the unlike molecules compared to pure liquids. The pure MDEA, DEA and AMP are able to form strong H-bonds due to the presence of O-H in the molecule [20]. MDEA and DEA have two O-H groups while AMP has only one to contribute for H-bonds. During the mixing of amines with water, the breaking of H-bonds may result in a negative sign in η^E. The temperature has an effect of η^E in such a way that η^E becomes less negative with the increase of temperature. The strength of molecular interactions may get weaker due to the increase of thermal energy of the molecules.

Table 1: Binary parameters A_o, A_1 and A_2 of the equation $\Delta G_{jk}^{E*} = x_j x_k \sum_{i=0}^{n} A_i (x_j - x_k)^i$ for the excess free energy of activation for viscous flow for MDEA + MEA + H_2O

Parameter		Binary pair		
		MDEA + MEA	MEA + H_2O	MDEA + H_2O
A_0	a	5.3631×10^4	1.7589×10^4	-7.2961×10^3
	b	-1.6978×10^2	1.0270×10^1	9.8700
	c	2.1304×10^{-1}	1.5794×10^{-1}	3.4820×10^{-1}
A_1	a	1.1958×10^5	2.5656×10^4	-3.979×10^3
	b	8.4487×10^2	-1.4979×10^1	1.9979×10^1
	c	-4.6806	5.9708×10^{-1}	6.3296×10^{-1}
A_2	a	1.3708×10^6	3.4239×10^3	4.6638×10^3
	b	-1.8188×10^4	-2.0450×10^1	1.1958×10^1
	c	4.2780×10^1	4.6224×10^{-1}	2.6581×10^{-1}

Table 2: Binary parameters A_o, A_1 and A_2 of the equation $\Delta G_{jk}^{E*} = x_j x_k \sum_{i=0}^{n} A_i (x_j - x_k)^i$ for the excess free energy of activation for viscous flow for MDEA + DEA + H_2O

Parameter		Binary pair		
		MDEA + DEA	DEA + H_2O	MDEA + H_2O
A_0	a	1.0027×10^8	4.1277×10^7	-5.0908×10^6
	b	3.1414×10^5	1.1918×10^5	-1.7794×10^4
	c	9.5620×10^2	3.7002×10^2	-6.3678×10^1
A_1	a	4.3279×10^7	4.5805×10^6	-2.5435×10^5
	b	1.3742×10^5	-1.1254×10^4	5.5912×10^2
	c	4.7546×10^2	-3.3341×10^1	-3.5906×10^{-3}
A_2	a	1.4787×10^7	-5.0089×10^7	6.3095×10^6
	b	-4.8893×10^4	-1.7303×10^5	2.3706×10^4
	c	4.8911×10^1	-5.3515×10^2	8.2541×10^1

Table 3: Binary parameters A_o, A_1 and A_2 of the equation $\Delta G_{jk}^{E*} = x_j x_k \sum_{i=0}^{n} A_i (x_j - x_k)^i$ for the excess free energy of activation for viscous flow for AMP + DEA + H_2O

| Parameter		Binary pair		
		AMP + DEA	DEA + H_2O	AMP + H_2O
A_0	a	1.1157×10^4	2.7551×10^3	1.5131×10^3
	b	8.4643×10^1	2.0589×10^1	2.3656
	c	-9.8481×10^{-1}	5.2882×10^{-1}	-1.0803×10^{-1}
A_1	a	-3.0081×10^5	7.6788×10^3	4.2936×10^2
	b	1.0653×10^3	-1.7424×10^1	5.1912
	c	2.0884×10^{-1}	1.1355	3.6564×10^{-1}
A_2	a	4.4827×10^6	4.7115×10^3	-1.5476×10^3
	b	-2.5146×10^4	-4.9228×10^1	2.6677
	c	3.3641×10^1	6.1636×10^{-1}	5.8774×10^{-1}

Figure 2. Viscosity variation of MDEA + DEA + H_2O mixtures with MDEA mole fraction and temperature: Experimental data from ref [5]; 293.15 K, '□'; 298.15 K, '◇'; 303.15 K, '△'; 308.15 K, 'x'; 313.15 K, 'ж'; 318.15 K, '○'; 323.15 K, '+'. The dotted lines represent the correlation in this work.

As shown by Kauzmann and Eyring [21], the viscosity of a mixture highly depends on the entropy of the mixture that is related to the molecular structure, interaction between molecules and enthalpy of the mixture [22, 23]. The negative deviation of V^E for all mixtures in their different compositions and temperatures indicates strong intermolecular interactions among the unlike molecules. Further, V^E gets a negative contribution by arranging molecules within vacant spaces in each other's structure due to the different size and shape of the molecules. This also affects the viscosity of a mixture as intermolecular interactions.

As shown in Figure 4, the calculated ΔG^{E*} from Eyring's viscosity representation is positive for the considered mixture compositions and temperatures indicating that the mixtures have strong intermolecular interactions. This is supported by excess volume property giving a negative sign for V^E. The formation of new H-bond between unlike molecules can result in a positive deviation in ΔG^{E*}. MEA has the potential to form H-bonds with other amines and H_2O due to the presence of hydroxyl and amino functional groups. For (MDEA + MEA + H_2O) mixtures at 293.15 K, highest excess activation energy is shown at the mixture composition of 30 mass% MDEA + 0 mass% MEA + 70 mass% H_2O mixture and it gradually decreased with the decrease of MDEA and increase of MEA concentrations under constant weight percent of H_2O. The decrease of ΔG^{E*} with the increase of MEA mole fraction shows that intermolecular attractions have been weakened by MEA.

Table 4: Excess properties of ΔG^{E*}, η^E and V^E of the amine mixtures.

Mixture	ΔG^{E*}	η^E	V^E
MDEA + MEA + H_2O	> 0	< 0	< 0
MDEA + DEA + H_2O	> 0	< 0	< 0
AMP + DEA + H_2O	> 0	< 0	< 0
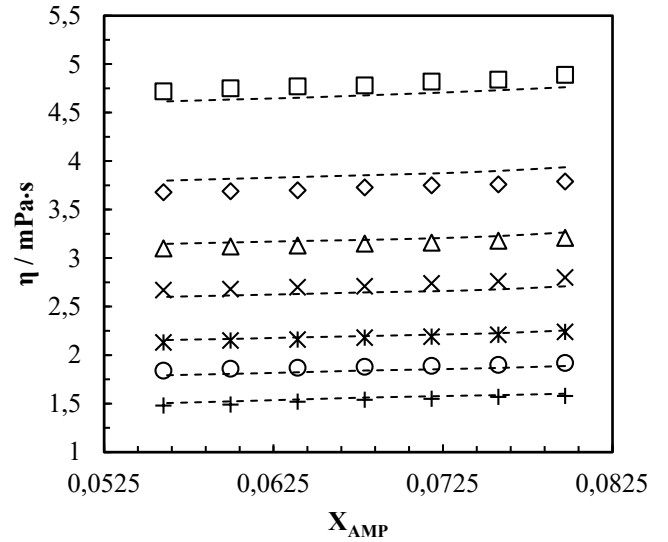
Figure 3. Viscosity variation of AMP + DEA + H_2O mixtures with AMP mole fraction and temperature: Experimental data from ref [5]; 293.15 K, '□'; 298.15 K, '◇'; 303.15 K, '△'; 308.15 K, 'x'; 313.15 K, 'ж'; 318.15 K, '○'; 323.15 K, '+'. The dotted lines represent the correlation in this work.

For the AMP + DEA + H_2O mixtures at 293.15 K, highest excess free activation energy is observed at the mixture composition of 30 mass% AMP + 0 mass% DEA + 70 mass% H_2O mixture. The increase of DEA mole fraction decreases the ΔG^{E*} indicating weak intermolecular interactions compared to the mixture of 30 mass% AMP + 0 mass% DEA + 70 mass% H_2O.

The excess free energy of activation for viscous flow of MDEA + DEA + H_2O mixtures shows a peak at the mixture composition of 25.5 mass% MDEA + 4.5 mass% DEA + 70 mass% H_2O at 293.15 K. This indicates that the intermolecular interactions are stronger at that particular composition than the other amine composition at 293.15 K.

The free energy of activation for viscous flow was determined by using Eq (1). Figure 5 illustrates the variation of ΔG^* with amine mole fraction of the mixtures at 293.15 K. The AMP + DEA + H_2O mixtures show the highest free energy among the considered mixtures while MDEA + MEA + H_2O has the lowest free energy.

The increase in temperature decreases both ΔG^{E*} and ΔG^*. Figure 6 shows the influence of temperature on ΔG^* for the mixtures with 24 mass% AMINE (1) + 6 mass% AMINE (2) + 70 mass% H_2O. The increase in molecular energy has weakened the strength of H-bonds and has enhanced the movements of the molecules. The decrease in ΔG^{E*} indicates that solution characteristics change toward the ideal conditions with the increase of temperature.
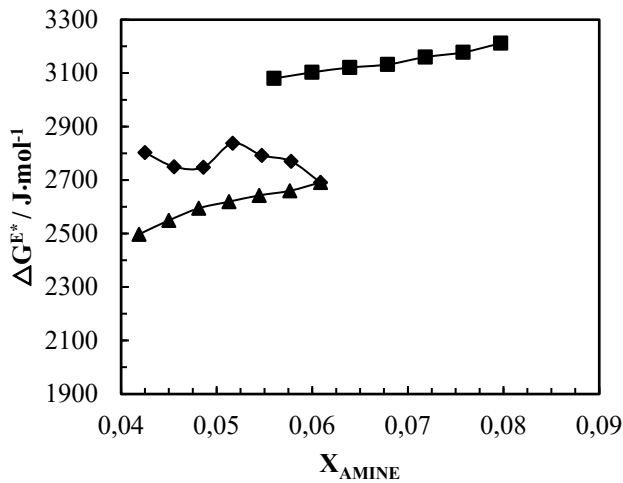
Figure 4. Variation of ΔG^{E*} with amine mole fractions at temperature of 293.15 K. X_{AMP} in AMP + DEA + H₂O '■'; X_{MDEA} in MDEA + DEA + H₂O '◆'; X_{MDEA} in MDEA + MEA + H₂O '▲'.
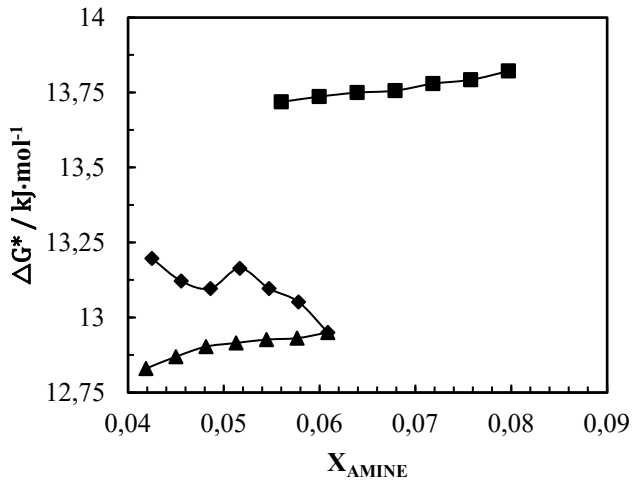
Figure 5. Variation of ΔG^* with amine mole fractions at temperature of 293.15 K. X_{AMP} in AMP + DEA + H₂O '■'; X_{MDEA} in MDEA + DEA + H₂O '◆'; X_{MDEA} in MDEA + MEA + H₂O '▲'.
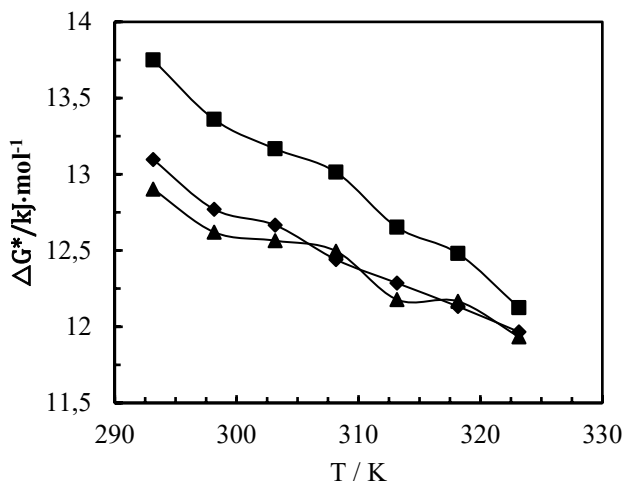
Figure 6. Variation of ΔG^* with temperature. AMP + DEA + H₂O '■'; MDEA + DEA + H₂O '◆'; MDEA + MEA + H₂O '▲'.

This study analyzed the density and viscosity of amine and water ternary mixtures to understand the molecular interactions. The correlation represents the viscosity data of ternary amines and water mixtures with acceptable accuracy to use them in engineering calculations. Further, the correlations can be improved to fit viscosities of CO₂ loaded amine and water mixtures as they are important in post-combustion amine based CO₂ capture.

4. Conclusions

Three aqueous amine mixtures of MDEA + MEA + H₂O, MDEA + DEA + H₂O and AMP + DEA + H₂O were analyzed based on viscosity and density data in the literature for their free energy of activation for viscous flow. The excess free energy was evaluated and correlated by a Redlich-Kister polynomial to fit the viscosity data. The proposed correlations were able to correlate the ΔG^{E*} within 2% AARD.

The same correlation was able to represent viscosities of MDEA + MEA + H₂O mixtures within AARD 1.9% and AMD of 0.1 mPa·s. For the MDEA + DEA + H₂O mixtures the viscosity data were fitted within AARD 1.4% and AMD 0.14 mPa·s. And for the AMP + DEA + H₂O mixtures that are of AARD 2.1% and 0.15 mPa·s. These accuracies are acceptable in engineering calculations.

The excess properties of molar volume, viscosity and free energy of activation for viscous flow show the presence of strong intermolecular interactions in all mixtures. The negative and positive signs for excess volume and excess free energy of activation for viscous flow indicate the presence of H-bonds between unlike molecules while negative signs of excess viscosity predict weak intermolecular interactions compared to the ideal mixture condition. This may occur due to the breaking of H-bond during the mixing. The mixtures exhibit $\Delta G^{E*}_{AMP+DEA+H_2O}$ > $\Delta G^{E*}_{MDEA+DEA+H_2O}$ > $\Delta G^{E*}_{MDEA+MEA+H_2O}$ for the considered amine concentrations. Accordingly, AMP + DEA + H₂O mixtures possess the highest intermolecular interactions among the unlike molecules and MDEA + MEA + H₂O mixtures indicate the lowest.

References

[1] Øi, L.E. Removal of CO₂ from exhaust gas, in Faculty of Technology. 2012, Telemark University College: Porsgrunn, Norway.

[2] Dawodu, O.F., & Meisen, A. Solubility of carbon dioxide in aqueous mixtures of alkanolamines. J. Chem. Eng. Data, 1994. 39: p. 548-552.

[3] Li, M. H., & Lai, M. D. Solubility and Diffusivity of N₂O and CO₂ in (Monoethanolamine + N-Methyldiethanolamine + water) and in (Monoethanolamine + 2-Amino-2-methyl-1-propanol+water), J. Chem. Eng. Data, 1995. 40: pp. 486-492.

[4] Glasscock, D. A., Critchfield, J.E., & Rochelle, G. T. CO₂ absorption/desorption in mixtures of methyldiethanolamine with monoethanolamine or diethanolamine. Chemical Engineering Science, 1991. 56: pp. 2829-2845.

[5] Mandal, B.P., Kundu, M., & Bandyopadhyay, S.S. Density and viscosity of aqueous solution of (N-Methyldiethanolamine + Monoethanolamine), (N-Methyldiethanolamine + Diethanolamine), (2-Amino-2-methyl-1-propanol + Monoethanolamine), and (2-Amino-

2-methyl-1-propanol + Diethanolamine). J. Chem. Eng. Data, 2003. 48: p. 703-707.

[6] Eyring, H. Viscosity, Plasticity, and Diffusion as example of absolute reaction rates. Journal of chemical physics, 1936. 4: p. 283-291.

[7] Redlich, O., & Kister, A.T. Algebraic representation of thermodynamic properties and the classification of solutions. Ind. Eng. Chem., 1948. 40(2): p. 345-348.

[8] Kendall, J., & Monroe, P. The viscosity of liquids. II. The viscosity-composition curve for ideal liquid mixtures. J. Am. Chem. Soc, 1917. 39: p. 1787-1802.

[9] Bingham, E.C. Fluidity and plasticity 1922, New York: McGraw-Hill.

[10] Cronauer, D.C., Rothfus, R.R., & Kernmore, R.I. Viscosity and density of the ternary liquid system acetone-benzene-ethylene dichloride J. Chem. Eng. Data, 1965. 10: p. 131-133.

[11] Fort, R.J., & Moore, W.R. Viscosities of binary liquid mixtures. Transactions of the faraday society, 1966. 62: p. 1112-1119.

[12] Heric, E.L., & Brewer, J.G. Viscosity of some binary liquid nonelectrolyte mixtures. J. Chem. Eng. Data, 1967. 12(04): p. 574-583.

[13] Bhatia, S.C., Bhatia, R., & Dubey, G.P. Studies on transport and thermodynamic properties of binary mixtures of octan-1-ol with chloroform, 1,2-dichloroethane and 1,1,2,2-tetrachloroethane at 298.15 and 308.15 K. Journal of Molecular Liquids, 2009. 144(3): p. 163-171.

[14] Ćwiklińska, A., & Kinart, C.M. Thermodynamic and physicochemical properties of binary mixtures of nitromethane with {2-methoxyethanol+2-butoxyethanol} systems at T=(293.15, 298.15, 303.15, 308.15, and 313.15)K. The Journal of Chemical Thermodynamics, 2011. 43(3): p. 420-429.

[15] Iloukhani, H., & Mohammadlou, Z.B. Densities, viscosities, and refractive indices for binary and ternary mixtures of formamide (1)+N,N-dimethylacetamide (2)+2-methyl-1-butanol (3) at 298.15K for the liquid region and at ambient pressure. Arabian Journal of Chemistry, 2016.

[16] Aminabhavi, T.M., Aralaguppi, M.I., Gopalakrishna, B., & Khinnavar, R.S. Densities, Shear Viscosities, Refractive Indices, and Speeds of Sound of Bis(2-methoxyethyl) Ether with Hexane, Heptane, Octane, and 2,2,4-Trimethylpentane in the Temperature Interval 298.15-318.15 K. Journal of Chemical & Engineering Data, 1994. 39(3): p. 522-528.

[17] Mahajan, A.R., & Mirgane, S.R. Excess molar volumes and viscosities for the binary mixtures of n-Octane, n-Decane, n-Dodecane, and n-Tetradecane with Octan-2-ol at 298.15 K. Journal of Thermodynamics, 2013: p. 1-11.

[18] Meyer, R., Meyer, M., Metzger, J., & Peneloux, A. Thermodynamic and physicochemical properties of binary solvent Journal de Chimie Physique et de Physico-Chimie Biologique, 1971. 68: p. 406-412.

[19] Oswal, S. & Rathnam, M.V. Viscosity data of binary mixtures: ethyl acetate + cyclohexane, + benzene, + toluene, + ethylbenzene + carbon tetrachloride, and + chloroform at 303.15 K. Canadian Journal of Chemistry, 1984. 62(12): p. 2851-2853.

[20] Abdollahi, F., Razmkhah, M., & Moosavi, F. The role of hydrogen bond interaction on molecular orientation of alkanolamines through temperature and pressure variation: A mixed molecular dynamics and quantum mechanics study. Computational Materials Science, 2017. 131: p. 239-249.

[21] Kauzmann, W., & Eyring, H. The Viscous Flow of Large Molecules. Journal of the American Chemical Society, 1940. 62(11): p. 3113-3125.

[22] Rafiee, H.R., Ranjbar, S., & Poursalman, F. Densities and viscosities of binary and ternary mixtures of cyclohexanone, 1,4-dioxane and isooctane from T=(288.15 to 313.15)K. The Journal of Chemical Thermodynamics, 2012. 54: p. 266-271.

[23] Ma, D., Liu, Q., Zhu, C., Feng, H., & Ma, Y. Volumetric and viscometric properties of ternary solution of (N-methyldiethanolamine + monoethanolamine + ethanol). The Journal of Chemical Thermodynamics, 2019. 134: p. 5-19.

Article I

Applicability of NRTL model for prediction of the viscosity of alkanolamine + water mixtures.

Applicability of NRTL Model for Prediction of the Viscosity of Alkanolamine + Water Mixtures

Sumudu S. Karunarathne   Lars E. Øi

Faculty of Technology, Natural Sciences and Maritime Sciences, University of South-Eastern Norway, Norway,
{Sumudu.karunarathne,lars.oi}@usn.no

Abstract

This study discusses the applicability of the non-random two-liquid (NRTL) model to represent viscosity for MEA (monoethanol amine) + H_2O and AMP (2-amino-2-methyl-1-propanol) + MEA (monoethanol amine) + H_2O mixtures under different amine concentrations at temperature ranges of 293.15 K– 363.15 K and 293.15 K – 343.15 K respectively. The NRTL model is adopted to determine excess Gibbs free energy of mixing ΔG^{E*} and the Eyring's viscosity model based on absolute rate theory is used to obtain excess free energy of activation for viscous flow ΔF^{E*}. The correlations are proposed for ΔF^{E*} as a function of concentration of the components, temperature and ΔG^{E*}. Correlations are capable of representing measured viscosities at 1.3 % and 0.3 % of absolute average relative deviation (AARD %) for MEA + H_2O and AMP + MEA + H_2O mixtures respectively. These deviations are acceptable for engineering calculations and correlations can be used in process design and simulations like Aspen HYSYS and ASPEN Plus.

Keywords: NRTL model, Eyring's viscosity model, MEA, AMP

1   Introduction

In the design of units involving liquid flow like gas/liquid separators and heat exchangers, it is important to predict reasonably accurate physical properties like viscosity. Correlations depending on parameters from experiments are available for some systems. Estimation methods without the need for fitted parameters is a possibility. A possibility to use parameters from e.g. vapor/liquid equilibrium models to predict viscosity.

In post combustion CO_2 capture, the physical properties of aqueous alkanolamine solutions is a key factor in various aspects such as equipment design, modeling and simulations of absorber and desorber columns. Physical properties are present in various mass and heat transfer correlations and interfacial area correlations that are necessary to evaluate in engineering applications. Accordingly, the viscosity data of aqueous alkanolamine mixtures are highly relevant to build correlations to predict viscosities for unmeasured conditions. Further correlations developed for the viscosity of aqueous alkanolamines can be used to develop correlations for the viscosity of CO_2 loaded alkanolamine mixtures.

Correlations based on statistical regression for the viscosity data have high uncertainties beyond the experimental range. The approach of Redlich-Kister (Redlich and Kister, 1948) type polynomial to fit physical properties is widely used and Islam *et al.*, (2004) and Hartono *et al.*, (2014) have taken this approach for viscosity data of aqueous MEA solutions. The Grunberg and Nissan model was used by Mandal *et al.*, (2003) to correlate different aqueous tertiary mixtures. The McAllister model (McAllister, 1960) based on Eyring's absolute rate theory for dynamic viscosity (Eyring, 1936) is used by Amundsen *et al.*, (2009) and Lee and Lin, (1995) for aqueous MEA solutions and found the parameters to fit measured viscosities. These models are capable of predicting viscosities at acceptable accuracies within the experimental range and can be used in engineering designs.

The thermodynamic information like vapor-liquid equilibrium (VLE) of liquid mixtures can be combined with a viscosity model and such models may be stated as thermodynamics-viscosity models (Cao *et al.*, 1993). The VLE data delivers information about molecular interaction, which can be used in local composition models like nonrandom two-liquid (NRTL) and UNIQUAC. This approach has been applied several times for various multicomponent liquid mixtures. Martins *et al.*, (2000) discussed the applicability of the UNIQUAC model for the viscosity predictions of binary and ternary systems. Novak *et al.*, (2004) discussed segment based Eyring-NRTL viscosity model, which was concerned about the similarities between intermolecular friction and viscosity with a local composition model like NRTL to model excess properties as both are affected by nearest neighbor molecules. The viscosity of electrolyte solutions using Eyrings's absolute rate theory has been discussed to replace excess free energy of activation for viscous flow with Gibbs free energy of mixing (Hu, 2004). For electrolyte solutions of MEA (monoethanol amine) + H_2O + CO_2, the excess free energy of activation for viscous flow was replaced by the Gibbs free energy of mixing that was calculated using the electrolyte-NRTL model (Matin *et al.*, 2013).

This study investigates the possibility to relate excess Gibbs free energy of mixing with the excess free energy of activation for viscous flow from Eyring's absolute rate theory to predict viscosities at different compositions and temperatures of MEA + H₂O and AMP (2-amino-2-methyl-1-propanol) + MEA + H₂O mixtures. Measured density and viscosity data were used to calculate the excess free energy of activation for viscous flow. The NRTL model was adopted for calculating excess Gibbs free energy of mixing and compared with the excess free energy of activation for viscous flow for the considered mixtures. Finally, viscosity predictions were compared with measured data and the accuracy was determined by calculating average absolute relative deviation (AARD %).

2 Methodology

2.1 Dynamic Viscosity Based on Eyring's Absolute Rate Theory

A universal model to predict the viscosity of any solution is challenging as solutions exhibit different characteristics that are difficult to discuss in one model. Most of the amine solutions and their blends that are discussed in amine-based CO₂ capture shows Newtonian behavior as the molecular weights are less than 5000 g·mol⁻¹ (Bird *et al.*, 2002). Introducing a qualitative picture of the mechanism of momentum transport of liquids, Eyring and coworkers developed a model to predict the viscosity of liquids from other physical properties (Eyring, 1936; Bird *et al.*, 2002). Eyring's viscosity model for Newtonian fluids is given in (1) and is valid for both pure liquids and liquid mixtures (Martins *et al.*, 2000).

$$\eta = \frac{hN}{V} exp\left(\frac{\Delta F^*}{RT}\right) \tag{1}$$

Where, $\eta, V, \Delta F^*, T, h, N$ and R are dynamic viscosity, molar volume, free energy of activation for viscous flow, temperature, Planck's constant, Avogadro's number and the gas constant respectively.

In order to compare with ideal solutions and to calculate the excess free energy of activation properties ΔF^{E*}, following (2) and (3) are obtained by using (1).

$$ln(\eta V) = ln(\eta V)_{ideal} + \frac{\Delta F^{E*}}{RT} \tag{2}$$

$$ln(\eta V) = \sum_i x_i ln(\eta_i V_i^o) + \frac{\Delta F^{E*}}{RT} \tag{3}$$

Where, x_i, η_i, V_i^o and ΔF^{E*} are mole fraction, viscosity of pure liquids, molar volume of pure liquids and excess free energy of activation for viscous flow respectively.

In this approach, the combination of terms of an ideal mixture and excess energy leads to an expression of viscosity in a real mixture. The ideal term of the (2) is calculated using the properties of pure liquids as given in the (3). The term $\Delta F^{E*}/RT$ describes the non-ideality of the solution viscosity (Matin *et al.*, 2013) and an appropriate model can enhance the prediction of the viscosity. Here, the possibility of using Gibbs free energy of mixing is discussed as it has been related in various ways to ΔF^{E*} in the literature. Generally, it is related as Gibbs free energy, excess Gibbs energy through proportionality factor, Gibbs free energy of mixing and Gibbs free energy of mixing multiplied by a general constant (Matin *et al.*, 2013). This study investigates the excess Gibbs free energy of mixing for MEA + H₂O and AMP + MEA + H₂O mixtures and compares it with ΔF^{E*} calculated from the measured density and viscosity data. The NRTL model was adopted to calculate Gibbs free energy of mixing for different compositions and temperatures of the mixtures.

2.2 NRTL Model

The local composition theory explains the deviation of local compositions from the bulk composition due to different strength of attractions among the molecules in the mixture. The non-random two liquid model (NRTL) is based on the local composition theory as Wilson's model (Wilson, 1964), which explains the composition variations. For a solution of m components, the excess Gibbs free energy of mixing is given as (Prausnitz *et al.*, 1999)

$$\frac{\Delta G^{E*}}{RT} = \sum_{i=1}^{m} x_i \frac{\sum_{j=1}^{m} \tau_{ji} G_{ji} x_j}{\sum_{l=1}^{m} G_{li} x_l} \tag{4}$$

$$\tau_{ji} = \frac{g_{ji} - g_{ii}}{RT} \tag{5}$$

$$G_{ji} = exp(-\alpha_{ji}\tau_{ji}) \quad (\alpha_{ji} = \alpha_{ij}) \tag{6}$$

Where, g_{ji} and g_{ii} are energy parameters to characterize i-j and i-i interactions respectively. α_{ji} is a non-randomness parameter.

Then the ΔG^*_{mix} is calculated as a sum of both ideal mixing and an excess term due to the non-ideal behavior of the solutions.

A study performed by Schmidt *et al.*, (2007) on VLE and NRTL model for various aqueous amine solutions provide binary interaction parameters for MEA + H₂O mixtures. A similar work done by Hartono *et al.*, (2013) found relevant parameters for AMP + H₂O mixtures. There is a lack of information about interaction parameters between AMP and MEA. Hence, for the tertiary AMP + MEA + H₂O system, parameters from two binary solutions were used for the calculations. It is also possible to use the commercial process simulation program Aspen Plus to perform all the

Table 1. Summary of the Compositions and Temperatures Considered for the Density and Viscosity Measurements of Aqueous Amine Mixtures.

Solution	Composition / wt % (by weight)		Temperature / K
MEA + H₂O	0 – 100 (MEA)		293.15 – 363.15
AMP + MEA + H₂O	21/9/70	(AMP/MEA/H₂O)	293.15 – 343.15
	24/6/70		
	27/3/70		

excess free energy of mixing calculations as it has binary interaction parameters for many components in the data banks. For the missing binary interactions parameters of NRTL model, the UNIFAC model can be used to make estimations.

The density and viscosity of mixtures were measured using a DMA 4500 vibrational density meter and Physica MCR 101 rheometer with a double-gap pressure cell XL from Anton Paar. The properties were measured at different compositions and temperatures as given in Table 1.

3   Results and Discussion

The spontaneous mixing of MEA and H₂O gives negative values for Gibbs free energy of mixing. The excess Gibbs free energy ΔG^{E*} of mixing was analyzed for the compositions of x_{MEA} from 0 to 1 of MEA + H₂O mixtures. Figure 1 illustrates the calculated ΔG^{E*} from the NRTL model under different MEA concentrations and temperatures. The calculated ΔF^{E*} from measured density and viscosity is positive while the excess viscosity η^E calculated from (7) gives negative values for the low MEA concentration region indicating weak intermolecular attractions and gives positive values for high MEA concentration region signifying strong interactions.

$$\eta^E = \eta - \sum_{i=1}^{n} x_i \eta_i \qquad (7)$$

(n=2 for MEA + H₂O mixtures and n=3 for AMP + MEA + H₂O mixtures)

The ratio of $\Delta G^{E*}/\Delta F^{E*}$ was determined and following correlations is proposed with $R^2 = 0.99$.

$$-\Delta G^{E*}/\Delta F^{E*} = f(x_{MEA}, T) \qquad (8)$$

$$f(x_{MEA}, T) = a + b x_{MEA} T + c T^2 \qquad (9)$$

The suggested correlation was used to replace ΔF^{E*} in (3) and the viscosities were obtained accordingly. Figure 2 illustrates the comparison between measured viscosity and the correlation fit for aqueous MEA. The fit was in good agreement with measured data with AARD of 1.3% and AMD (maximum deviation) of 1.0 mPa·s as given in Table 4. This deviation is acceptable for engineering calculations and can be used to develop

correlations for the CO₂ loaded solutions. The estimated parameters for the correlation shown in (9) are given in Table 2.
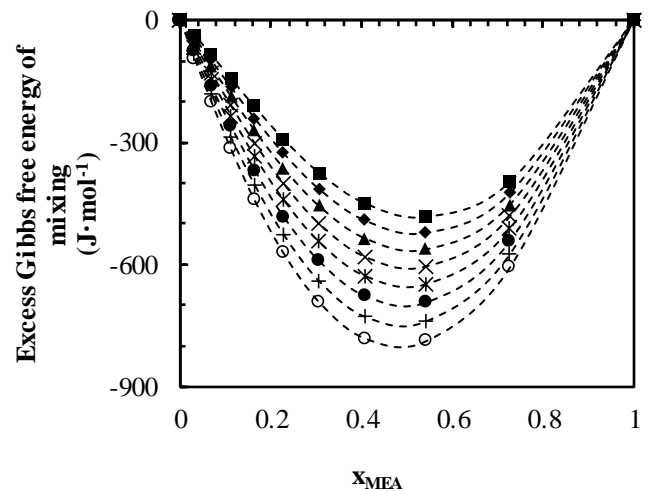
Figure 1. The variation of excess Gibbs free energy vs MEA mole fraction and temperatures: 293.15 K, '○'; 303.15 K, '+'; 313.15 K, '●'; 323.15 K, 'ж'; 333.15 K, 'x'; 343.15 K, '▲'; 353.15 K, '◆'; 363.15 K, '■'.
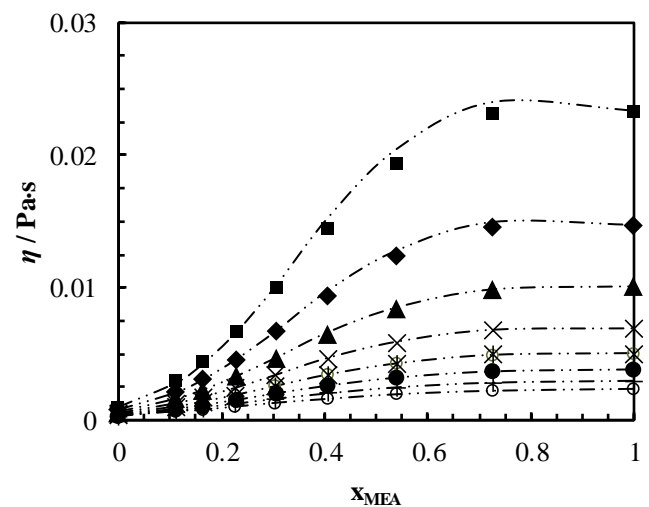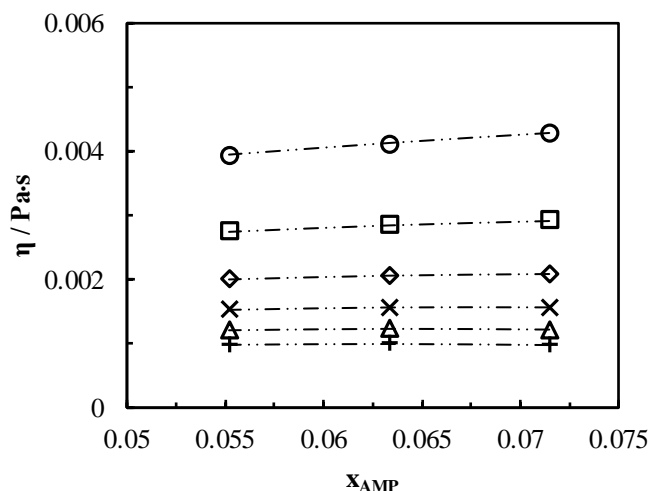

Figure 2. Comparison of measured viscosity of MEA + H₂O mixtures with correlation at temperatures: 293.15 K, '■'; 303.15 K, '◆'; 313.15 K, '▲'; 323.15 K, 'x'; 333.15 K, 'ж'; 343.15 K, '●'; 353.15 K, '+'; 363.15 K, '○'. The dash — dotted lines represent the correlation.

Table 2. Estimated Parameters for Correlation of Viscosity of Aqueous MEA.

MEA (wt%)	Temperature (K)	No. points	Parameters
0 – 100	293.15 – 363.15	72	$a = 0.2801 \pm 0.008$ $b = (5.557 \pm 0.0164) \times 10^{-04}$ $c = (-1.623 \pm 0.0735) \times 10^{-06}$

Table 3. The Estimated Binary Parameters for the Correlation Shown in (10-13).

Parameter		AMP + MEA	MEA + H₂O	AMP + H₂O
A_0	a_{00}	-1.724×10^4	141.854	-117.059
	a_{01}	-9.370	0.562	0.296
	a_{02}	-2.516	0.598	0.623
A_1	a_{10}	-1.870×10^5	-143.070	141.824
	a_{11}	-97.727	-0.992	-0.040
	a_{12}	101.381	0.540	0.609
A_2	a_{20}	5.812×10^6	111.435	-119.768
	a_{21}	5.348×10^3	0.473	0.558
	a_{22}	-2.233×10^3	-0.168	-0.067

The ΔG^{E*} for AMP + MEA + H₂O mixtures were examined using the NRTL model. Figure 3 shows the calculated ΔG^{E*} for the mixtures considered in this work. The ΔG^{E*} is negative for the considered AMP concentrations and temperatures. Further, negative η^E implies weak intermolecular interactions for the range of AMP concentrations and temperatures. As discussed in the MEA + H₂O mixtures, the ratio (r) of $-\Delta G^{E*}/\Delta F^{E*}$ was determined and a correlation was proposed as given in (10-13) to find the best fit for AMP + MEA + H₂O mixtures.

$$-\Delta G^{E*}/\Delta F^{E*} = f\left(x_{AMP}, x_{MEA}, x_{H_2O}, T\right) \quad (10)$$

The ratio $-\Delta G^{E*}/\Delta F^{E*} = r_{12} + r_{23} + r_{13}$ (11)

$$r_{jk} = x_j x_k \sum_{i=0}^{n} A_i \left(x_j - x_k\right)^i \quad (12)$$

$$A_i = a_{io} + a_{i1}(T) + a_{i2}(T)^2 \quad (13)$$

The proposed correlation was able to represent measured viscosities with acceptable accuracy as illustrated by AARD and AMD in Table 4. Figure 4 shows the comparison of the correlation with measured data in which maximum deviations were observed at low temperatures. These deviations are smaller compared to the MEA + H₂O mixtures since only three different compositions were considered for the study.

Table 4. Calculated AARD% and AMD (mPa·s) for Comparison of Correlation with Measured Data.

Mixture	AARD (%)	AMD (mPa·s)
MEA + H₂O	1.3	1.0
AMP + MEA + H₂O	0.3	0.02
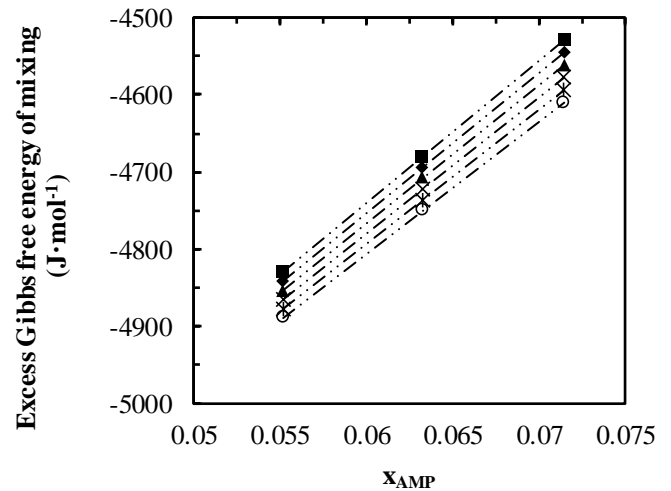
Figure 3. The variation of excess Gibbs free energy vs AMP mole fractions and temperatures: 293.15 K, '○'; 303.15 K, 'ж'; 313.15 K, 'х'; 323.15 K, '▲'; 333.15 K, '◆'; 343.15 K, '■'.

The viscosity of CO₂ loaded AMP + MEA + H₂O mixtures are highly important in the design and mathematical modelling and simulations of CO₂ capture process based on absorption. The correlation discussed in this study for AMP + MEA + H₂O mixtures can be adopted to developed viscosity correlations for CO₂ loaded solutions using measured data. For use in e.g. a process simulation program like Aspen HYSYS or Aspen Plus, It is shown that the viscosities can be estimated by Hartono's correlation (Hartono *et al.*, 2014) with fitted parameters for MEA + H₂O mixtures with AARD 4.2 % and the semiempirical model discussed in this work can estimate viscosity with 1.3% AARD. Mandal *et al.*, (2003) used the Grunberg and

Nissan correlation (Li and Lie, 1994) to fit the viscosity data with 3.08% AARD and it is higher than that from this study for AMP + MEA + H_2O mixtures.

Figure 4. Comparison of measured viscosity of AMP + MEA + H_2O mixtures with correlation at temperatures: 293.15 K, '○'; 303.15 K, '□'; 313.15 K, '◇'; 323.15 K, 'x'; 333.15 K, '△'; 343.15 K, '+'. The dash — dotted lines represent the correlation.

4   Conclusion

This work presents the applicability of the NRTL model to represent viscosities of MEA + H_2O and AMP + MEA + H_2O mixtures. The Eyring's viscosity model was adopted to determine excess free energy of activation for viscous flow. Correlations based on the regression for the ratio between excess Gibbs free energy of mixing from NRTL model and excess free energy of activation for viscous flow was proposed to represent measured viscosities. The accuracy of the correlation predictions are acceptable as the AARD (%) is 1.3 and 0.3 for MEA + H_2O and AMP + MEA + H_2O mixtures respectively. The NRTL model is available in the Aspen Plus commercial software to determine vapor – liquid equilibrium. In this paper, it is shown that these types of correlations can be integrated to determine viscosity in aqueous alkanolamines.

References

T. G. Amundsen, L. E. Øi, and D. A. Eimer. Density and viscosity of monoethanolamine+water+carbon dioxide from (25 to 80) °C. *J. Chem. Eng. Data,* 54: 3096-3100, 2009.

R. B. Bird, W. E. Stewart, and E. N. Lightfoot. *Transport Phenomena (second edition).* USA: John Wiley & Sons Inc., 2002.

W. Cao, K. Knudsen, A. Fredenslund, and P. Rasmussen. Group-contribution viscosity predictions of liquid mixtures using UNIFAC-VLE parameters. *Ind. Eng. Chem. Res,* 32: 2088-2092, 1993.

H. Eyring. Viscosity, Plasticity, and Diffusion as example of absolute reaction rates. *Journal of chemical physics,* 4: 283-291, 1936.

A. Hartono, M. O. Mba, and H. F. Svendsen. Physical properties of partially CO_2 loaded aqueous monoethanolamine (MEA). *J. Chem. Eng. Data,* 59: 1808-1816, 2014.

A. Hartono, M. Saeed, A. F. Ciftja, and H. F. Svendsen. Modeling of binary and ternary VLE of the AMP/Pz/H_2O system. *Energy Procedia,* 37: 1736-1743, 2013.

Y.-F. Hu. Prediction of viscosity of mixing electrolyte solutions based on the Eyring's absolute rate theory and the equations of Patwardhan and Kumar. *Chemical Engineering Science,* 59: 2457-2464, 2004.

M. N. Islam, M. M. Islam, and M. N. Yeasmin. Viscosity of aqueous solution of 2-methoxyethanol, 2-ethoxyethanol, and ethanolamine. *J. Chem. Thermodynamics,* 36: 889-893, 2004.

M. J. Lee and T. K. Lin. Density and viscosity for Monoethanolamine+Water,+Ethanol, and + 2-Propanol. *J. Chem. Eng. Data,* 40: 336-339, 1995.

M.-H. Li and Y.-C. Lie. Densities and viscosities of solutions of Monoethanolamine + N-Methyldiethanolamine + water and Monoethanolamine + 2-Amino-2-methyl-1-propanol + water. *J. Chem. Eng. Data,* 39: 444-447, 1994.

B. P. Mandal, M. Kundu, and S. S. Bandyopadhyay. Density and viscosity of aqueous solution of (N-Methyldiethanolamine + Monoethanolamine), (N-Methyldiethanolamine + Diethanolamine), (2-Amino-2-methyl-1-propanol + Monoethanolamine), and (2-Amino-2-methyl-1-propanol + Diethanolamine). *J. Chem. Eng. Data,* 48: 703-707, 2003.

R. J. Martins, M. J. D. M. Cardoso, and O. E. Barcia. Excess Gibbs free energy model for calculating the viscosity of binary liquid mixtures. *Ind. Eng. Chem. Res,* 39: 849-854, 2000.

N. S. Matin, J. E. Remias, and K. Liu. Application of electrolyte-NRTL model for prediction of the viscosity of carbon dioxide loaded aqueous amine solutions. *Ind. Eng. Chem. Res,* 52: 16979-16984, 2013.

R. A. McAllister. The viscosity of liquid mixtures. *A.I.Ch.E. Journal,* 6: 427-431, 1960.

L. T. Novak, C.-C. Chen, and Y. Song. Segment-Based Eyring-NRTL viscosity model for mixtures containing polymers. *Ind. Eng. Chem. Res,* 43: 6231-6237, 2004.

J. M. Prausnitz, R. N. Lichtenthaler, and E. G. d. Azevedo. *Molecular thermodynamics of fluid-phase equilibria (Third Edition).* Prentice Hall PTR, 1999.

O. Redlich and A. T. Kister. Algebraic representation of thermodynamic properties and the classification of solutions. *Ind. Eng. Chem.,* 40(2): 345-348, 1948.

K. A. G. Schmidt, Y. Maham, and A. E. Mather. Use of the NRTL equation for simultaneous correlation of vapour-liquid equilibria and excess enthalpy. *Journal of Thermal Analysis and Calorimetry,* 89: 61-72, 2007.

G. M. Wilson. Vapor–Liquid Equilibrium. XI. A New Expression for the Excess Free Energy of Mixing. *J. Am. Chem. Soc,* 86: 127-130, 1964.

Article J

Density and Viscosity Correlations for Aqueous 3-Amino-1-propanol and Monoethanol Amine Mixtures

Sumudu S. Karunarathne   Lars E. Øi

Faculty of Technology, Natural Sciences and Maritime Sciences, University of South-Eastern Norway, Norway,
{Sumudu.karunarathne,lars.oi}@usn.no

Abstract

Density and viscosity data and relevant correlations are essentially needed to perform mathematical modelling and simulations for the design of process equipment. Correlations that are developed to cover a range of concentrations and temperatures help to use them in mathematical modelling and simulations of absorption - desorption processes. In this study, a density correlation was proposed for 3A1P (3-Amino-1-propanol) + H₂O mixtures. The McAllister three body model was adopted to correlate kinematic viscosity data of MEA (monoethanol amine) + H₂O mixtures and kinematic viscosity data for 3A1P + H₂O mixtures. The Eyring's viscosity model based on absolute rate theory was used to correlate dynamic viscosity data. A Redlich – Kister type polynomial was proposed to fit the excess free energy of activation for viscous flow for 3A1P + H₂O mixtures. The developed correlations were able to represent density and viscosity data with accepted accuracy and can be used to perform engineering calculations.

Keywords: density, viscosity, MEA, 3A1P, McAllister model

1 Introduction

Acid gas removal using aqueous alkanolamines through chemical absorption has been in practice for decades to remove CO_2 from natural gas (Eimer, 2014; Rochelle, 2009). The integration of this technology to a commercial level in Post-Combustion CO_2 Capture is halted by economic feasibility due to the energy demand of the process. High reaction rate with CO_2 and low regeneration energy in stripping are ideal characteristics for an absorbent to reduce the cost of operation.

Physical properties like density, viscosity and surface tension are essential in various aspects such as designing/sizing of process equipment and process simulations. They appear in many mass and heat transfer correlations that are essential in the mathematical modelling transport process and design of the absorption column. Empirical correlations of such properties can provide the required data within a considered concentration and temperature range. Abundant resources are available for the density and viscosity of aqueous MEA (monoethanol amine) in the literature with suggested correlations, while reported studies are limited for 3A1P (3-Amino-1-propanol) (Idris and Eimer, 2016; Idris *et al.*, 2018).

2 Density and Viscosity Correlations for Binary Mixtures

Correlations based on excess volume V^E are commonly adopted to fit density data of liquid mixtures and the Redlich-Kister (Redlich and Kister, 1948) type polynomial is suggested to correlate V^E. This approach requires a higher number of parameters to correlate V^E to acquire high accuracy of data fit (Aronu *et al.*, 2012). Such studies are reported for densities of aqueous MEA and 3A1P solutions under different compositions and temperatures in the literature (Han *et al.*, 2012; Idris and Eimer, 2016).

$$V^E = V - \sum_{i=1}^{n} x_i V_i^o \qquad (1)$$

$$\rho = \frac{\sum_{i=1}^{n} x_i \cdot M_i}{V^E + \sum_{i=1}^{n} \frac{x_i \cdot M_i}{\rho_i}} \qquad (2)$$

McAllister, (1960) viscosity model presents a theoretical approach based on molecular attractions arises from different molecular arrangements to predict kinematic viscosities in binary mixtures. McAllister derived model with two forms for the kinematic viscosity of binary liquid mixtures based on absolute rates theory approach of Eyring's viscosity (Eyring, 1936). The McAllister three-body model is shown in (3-7).

$$
\begin{aligned}
ln(v) = {}& x_1^3 \cdot ln(v_1) + 3x_1^2 x_2 \cdot ln(v_{12}) + 3x_1 x_2^2 \\
& \cdot ln(v_{21}) + x_2^3 \cdot ln(v_2) \\
& - ln(x_1 + x_2 \cdot [M_2/M_1]) + 3x_1^2 x_2 \\
& \cdot ln([2 + M_2/M_1]/3) + 3x_1 x_2^2 \\
& \cdot ln([1 + 2M_2/M_1]/3) + x_2^3 \\
& \cdot ln(M_2/M_1)
\end{aligned}
\qquad (3)
$$

$$v_1 = \frac{hN}{M_1} e^{-\Delta S_1^*/R} e^{\Delta H_1^*/RT} \qquad (4)$$

$$v_{12} = \frac{hN}{M_{12}} e^{-\Delta S_{12}^*/R} e^{\Delta H_{12}^*/RT} \qquad (5)$$

$$v_{21} = \frac{hN}{M_{21}} e^{-\Delta s_{21}^*/R} e^{\Delta H_{21}^*/RT} \qquad (6)$$

$$v_2 = \frac{hN}{M_2} e^{-\Delta s_2^*/R} e^{\Delta H_2^*/RT} \qquad (7)$$

Eyring's viscosity model for Newtonian fluids is given in (8) (Eyring, 1936).

$$\eta = \frac{hN}{V} exp\left(\frac{\Delta F^*}{RT}\right) \qquad (8)$$

The following (9) and (10) represent the relationship between real and ideal solutions. The excess property ΔF^{E*} is called the excess free energy of activation for viscous flow.

$$ln(\eta V) = ln(\eta V)_{ideal} + \frac{\Delta F^{E*}}{RT} \qquad (9)$$

$$ln(\eta V) = \sum_{i=1}^{n} x_i ln(\eta_i V_i^o) + \frac{\Delta F^{E*}}{RT} \qquad (10)$$

$$ln(\eta V) = \sum_{i=1}^{n} x_i ln(\eta_i V_i^o) + \frac{x_1 x_2 W}{RT} \qquad (11)$$

A positive ΔF^{E*} reveals that the real mixture has a greater viscosity than that of an ideal mixture (Heric and Brewer, 1967). Stronger interaction between unlike molecules gives positive values to ΔF^{E*} and excess viscosity η^E. Further, Meyer $et\ al.$, (1971) discussed that $\Delta F^{E*} < 0$ for the solutions with solute-solute associations. According to Fort and Moore (1966), the G_{12} from Grunberg and Nissan (1949) as shown in (13) provides a better measure for the strength of interactions between components. The interchange energy or the interaction parameter W/RT from the Eyring's viscosity model is proportional to G_{12} and shows the same trend as that of G_{12} (Mukesh $et\ al.$, 2015).

The ideal viscosity of a liquid mixture is defined in several ways in the literature (Kendall and Monroe, 1917; Bingham, 1922; Cronauer $et\ al.$, 1965; Martins $et\ al.$, 2000). Correlations based on Redlich-Kister polynomials to fit the data of η^E were reported for aqueous MEA solutions (Islam $et\ al.$, 2004). Nigam and Mahl, (1971) illustrated that the sign of G_{12} along with η^E from (12) reveals what type of interaction such as strong, weak or dispersion is dominant in the solution.

$$\eta^E = \eta - (x_1\eta_1 + x_2\eta_2) \qquad (12)$$

$$ln(\eta_{12}) = x_1 ln(\eta_1) + x_2 ln(\eta_2) + x_1 x_2 G_{12} \qquad (13)$$

3 Methodology

This study focuses on density and viscosity correlations for aqueous MEA and 3A1P mixtures. The study is based on measured density and viscosity data of this and previous works performed in University of South-Eastern Norway (USN) (Idris and Eimer, 2016; Idris $et\ al.$, 2018). Idris and Eimer, (2016) and Idris $et\ al.$, (2018) discussed the density and viscosity of aqueous 3A1P solutions under the range of mass fractions w_1 (i=1 and 2 refer amine and water respectively) within 0-1 and temperatures 293.15-353.15K and 298.15-373.15K respectively. The correlation suggested by Aronu $et\ al.$, (2012) as given in (14) was adopted to correlate aqueous 3A1P density data.

$$\rho = \left(k_1 + \frac{k_2 x_2}{T}\right) exp\left(\frac{k_3}{(T)^2} + \frac{k_4 x_1}{T} + k_5\left(\frac{x_1}{T}\right)^2\right) \qquad (14)$$

The McAllister three-body model is adopted to predict kinematic viscosities of MEA + H_2O and 3A1P + H_2O mixtures. The parameters related to the enthalpy and the entropy for viscous flow shown in the (3) to (7) are estimated via regression. The ΔF^{E*} for 3A1P + H_2O mixtures is calculated using Eying's viscosity model and a Redlich-Kister type polynomial is fitted to represent the viscosity data.

3.1 Density and Viscosity Measurements

Densities of aqueous amine solutions were measured using a DMA 4500 density meter from Anton Paar. The measurements of dynamic viscosity performed using a Physica MCR 101 rheometer from Anton Paar. A detailed description of the density meter and rheometer is given in publications based on previous at USN (Han $et\ al.$, 2012; Idris $et\ al.$, 2017).

4 Results and Discussion

In this section, the accuracy of the data fit of the density and viscosity correlations are determined using Average Absolute Relative Deviation (AARD) and Absolute Maximum Deviation (AMD) as given in (15) and (16).

$$AARD(\%) = \frac{100\%}{N} \sum_{i=1}^{N} \left|\frac{Y_i^E - Y_i^C}{Y_i^E}\right| \qquad (15)$$

$$AMD = MAX\left|Y_i^E - Y_i^C\right| \qquad (16)$$

4.1 Density Correlation of 3A1P + H₂O Mixtures

The density data of 3A1P + H_2O mixtures were fitted to the correlation described in (14) with $R^2 = 0.97$. The comparison of measured data with the correlation reveals that the deviation of correlated properties from measured is high at lower temperatures for the different 3A1P concentrations. Nevertheless, the correlation was able to represent data at AARD of 0.2 % and AMD of 6.7 kg·m⁻³. The estimated parameters are given in Table 1. Idris and Eimer, (2016) reported several density

correlation studies based on a Redlich-Kister type polynomial on excess volume, Jouyban-Acree (Jouyban *et al.*, 2005) and Gonzalez-Olmos and Iglesias (Gonzalez-Olmos and Iglesias, 2008). Table 2 summarize absolute average deviations of different correlations fitted for the aqueous 3A1P solutions.

Table 1. Parameters for the Density Correlation for 3A1P + H$_2$O Mixtures

Parameter	Value
k_1	706
k_2	1.155 x10^5
k_3	-7633
k_4	112.1
k_5	3602

Table 2. Absolute Average Deviation Measured and Correlated Densities for 3A1P + H$_2$O Mixtures

Correlation	Absolute average deviation ($kg \cdot m^{-3}$)
Aronu (this work)	1.9
Redlich-Kister	0.5
Jouyban-Acree	2
Gonzalez-Olmos and Iglesias	0.7

The correlation for excess volume was based on a Redlich-Kister polynomial with 39 parameters for the considered temperature range. Three parameters were estimated at each temperature level by fitting the correlation into the calculated excess volume using measured densities. The Jouyban-Acree correlation used only three parameters and absolute average deviation is similar to this study. A semiempirical model proposed by Gonzalez-Olmos and Iglesias with 12 parameters was used to correlate densities over the range of 3A1P mole fractions and temperatures.

The considered correlations in this study and the literature for the density of 3A1P have acceptable accuracy. The advantage of correlations proposed by Aronu, Jouyban-Acree and Gonzalez-Olmos and Iglesias is that they can be easily used in the mathematical modelling and simulations of a pilot or large-scale absorption processes. The models including parameters can be implemented in simulation programs like Aspen Plus or in programming tool like MATLAB.

4.2 Viscosity Correlation of MEA + H$_2$O and 3A1P + H$_2$O Mixtures

The calculated kinematic viscosity of MEA + H$_2$O and 3A1P + H$_2$O mixtures from dynamic viscosity and density were correlated using McAllister three-body model. The estimated parameters that are related to the activation energies of the mixtures are given in Table 3. These parameters were assumed constant over the considered temperature range.

Table 3. Parameter in McAllister Three-Body Model

Mixture	$\Delta H^* / kJ \cdot mol^{-1}$	$\Delta S^* / J \cdot mol^{-1} K^{-1}$
MEA + H$_2$O	$\Delta H_1^* = 28.068$	$\Delta S_1^* = 28.39$
	$\Delta H_{12}^* = 31.668$	$\Delta S_{12}^* = 15.32$
	$\Delta H_{21}^* = 30.271$	$\Delta S_{21}^* = 42.45$
	$\Delta H_2^* = 13.677$	$\Delta S_2^* = 36.45$
3A1P + H$_2$O	$\Delta H_1^* = 33.073$	$\Delta S_1^* = 39.03$
	$\Delta H_{12}^* = 31.410$	$\Delta S_{12}^* = 11.27$
	$\Delta H_{21}^* = 43.316$	$\Delta S_{21}^* = 40.30$
	$\Delta H_2^* = 12.429$	$\Delta S_2^* = 67.08$
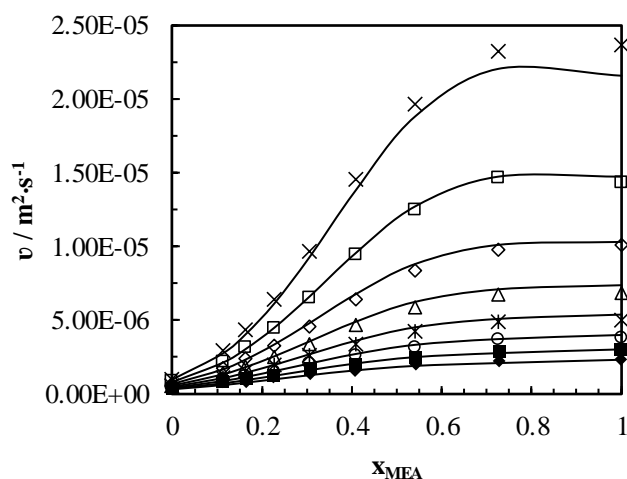
Figure 1. Kinematic viscosity of MEA + H$_2$O mixtures at temperatures: 293.15 K, 'x'; 303.15 K, '□'; 313.15 K, '◇'; 323.15 K, '△'; 333.15 K, 'ж'; 343.15 K, '○'; 353.15 K, '■'; 363.15 K, '◆'. The solid lines represent the McAllister model.
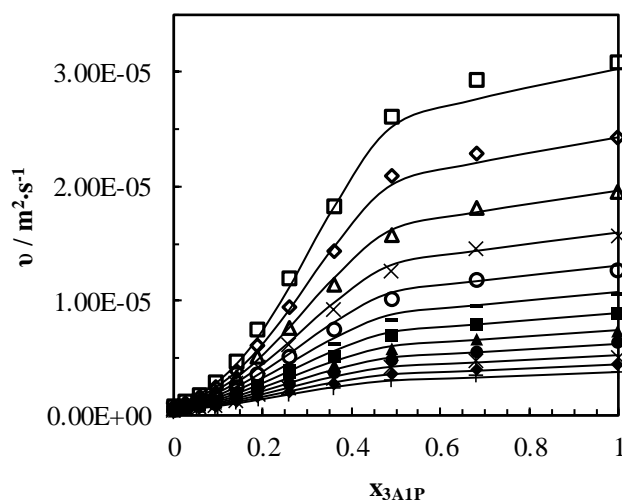
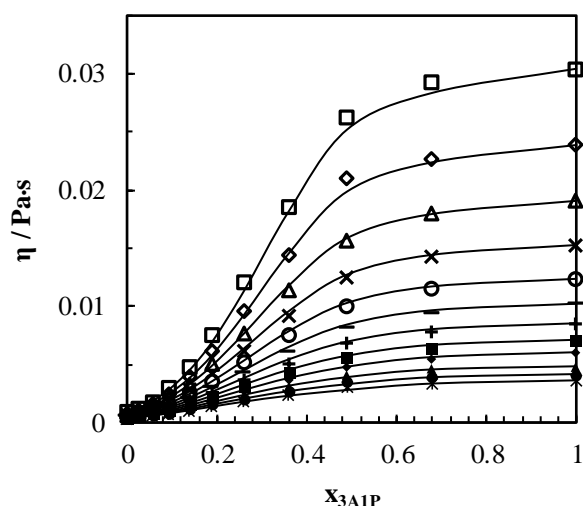**Figure 2**. Kinematic viscosity of 3A1P + H$_2$O mixtures at temperatures: : 298.15 K, '□'; 303.15 K, '◇'; 308.15 K, '△'; 313.15 K, 'x'; 318.15 K, '○'; 323.15 K, '-'; 328.15 K, '■'; 333.15 K, '▲'; 338.15 K, '●'; 343.15 K, 'ж'; 348.15 K, '◆'; 353.15 K, '+'. The solid lines represent the McAllister model.

The McAllister three-body model was able to represent the kinematic viscosity of MEA + H$_2$O and 3A1P + H$_2$O with acceptable accuracy. Table 2 provides an overview of the accuracy based on AARD and AMD of the mixtures. For MEA + H$_2$O, model deviates from the data at high MEA concentrations and low temperatures as shown in Figure 1. The highest deviations were observed at X$_{MEA}$ = 0.726 (w_1 = 0.9) and X$_{MEA}$ = 1 (w_1 = 1) at 293.15 K. The average absolute deviation of the correlated data is 1.68 x10^{-7} m^2·s^{-1}. For 3A1P + H$_2$O mixtures, the deviation is high at higher temperatures for the mixtures up to X$_{3A1P}$ ≤ 0.057 and it becomes high at lower temperatures for the mixtures with X$_{3A1P}$ > 0.057 as illustrated in Figure 2. The average absolute deviation of the correlated data is 1.62 x10^{-7} m^2·s^{-1}.

Table 4. Calculated AARD and AMD of the McAllister Three-Body Model for the MEA + H$_2$O and 3A1P + H$_2$O

Mixture	AARD %	AMD m^2·s^{-1}
MEA + H$_2$O	3.17	1.42x10^{-6}
3A1P + H$_2$O	3.66	1.71 x10^{-6}

The ΔF^{E*} was determined using measured density and viscosity for aqueous 3A1P mixtures at different temperatures. A Redlich-Kister type polynomial was fitted for the ΔF^{E*} and viscosity of aqueous 3A1P mixtures were obtained accordingly. This correlation used molar volumes of mixtures to determine the viscosity. For this study, the calculated molar volumes from density data were used and it is possible to use the density correlation that was discussed in this study or correlations in the literature to acquire molar volumes for the situations when measured data are not available. The correlation was able to fit the viscosity data with AARD of 2.7% and AMD of 1.1 mPa·s at w_1 = 0.8 and temperature of 303.15 K. These deviations are acceptable for engineering calculations.

Figure 3 shows the comparison between measured and correlated viscosities for 3A1P + H$_2$O mixtures. The ΔF^{E*} is positive for the considered range of 3A1P concentrations and temperatures. According to Heric and Brewer, (1967), if $\Delta F^{E*} > 0$, the viscosity of a real mixture is greater than that of an ideal mixture. This emphasizes strong intermolecular attractions in the solution. As reported by Idris *et al.*, (2018), $\eta^E < 0$ for the water rich region indicates weak intermolecular attractions. The presence of strong intermolecular attractions is determined as $\eta^E > 0$ for amine rich region. The interaction parameter G_{12} proposed by Grunberg and Nissan, (1949) for binary mixtures behaves similar to ΔF^{E*}, that is positive for considered 3A1P concentrations. Nigam and Mahl, (1971) show that for the weak intermolecular attractions $G_{12} > 0$ and $\eta^E < 0$.

Figure 3. Dynamic viscosity of 3A1P + H$_2$O mixtures at temperatures: 298.15 K, '□'; 303.15 K, '◇'; 308.15 K, '△'; 313.15 K, 'x'; 318.15 K, '○'; 323.15 K, '-'; 328.15 K, '+'; 333.15 K, '■'; 338.15 K, '◆'; 343.15 K, '▲'; 348.15 K, '●'; 353.15 K, 'ж'. The solid lines represent the correlation.

4.3 Recommended Correlations for Simulations

Mathematical modelling of the absorption process is based on material and energy balance of the gas/liquid interface. The composition and the temperature of the solvent vary continuously through the column for both steady state and dynamic conditions. Physical property correlations as a continuous function of composition and temperature can be easily implemented in a programming tool like MATLAB for both steady state and dynamic simulations.

In this study, the parameters of the Aronu's density correlation were evaluated in such a way that concentration and temperatures can be considered as continuous independent variables. The other advantages of this correlation are it is simple and accuracy is acceptable. The McAllister three-body model for kinematic viscosity can be easily converted into code with all the parameters as discussed in this study. The proposed Redlich-Kister polynomial for the Eyring's viscosity model is a continuous function of concentration and temperature. Accordingly, viscosity variations related to the changes in compositions and temperatures in the column can be observed and correlation can be used in other mass and heat transfer correlations.

5 Conclusion

This study discusses the density and viscosity correlations for the mixtures of MEA + H$_2$O and 3A1P + H$_2$O. The considered correlations can be used in mathematical models such as continuity, momentum

and energy equations to perform simulations in e.g. amine based absorption and desorption processes.

The correlations for measured density and viscosity data of aqueous mixtures of MEA and 3A1P were discussed. Density data of aqueous 3A1P was correlated by the empirical correlation proposed by Aronu and was able to represent density data with AARD of 0.2% that is satisfactory in engineering calculations.

The McAllister three-body model was adopted to fit kinematic viscosity data for aqueous MEA and aqueous 3A1P mixtures. The energy parameters in the model were evaluated through a regression. The three-body model can correlate kinematic viscosities for considered mixtures with acceptable accuracy having AARD of 3% and 4% for aqueous MEA and aqueous 3A1P mixtures respectively.

The viscosity correlation based on a Redlich – Kister type polynomial for the excess free energy of activation for viscous flow using the Eyring's viscosity model was developed to correlate viscosity data of 3A1P + H_2O mixtures. The viscosity data were in good agreement with correlated viscosities with AARD of 2.7%.

Nomenclature

ΔF^*	Free energy of activation for viscous flow (J·mol^{-1})
ΔF^{E*}	Excess free energy of activation for viscous flow (J·mol^{-1})
G_{12}	Characteristic constant
h	Planck's constant (J·s)
ΔH^*	Enthalpy of activation for viscous flow (J·mol^{-1})
k	Parameters of Eq (14)
M	Molecular weight (kg·mol^{-1})
N	Avogadro's number
R	Gas constant (J·mol^{-1}·K^{-1})
ΔS^*	Entropy of activation for viscous flow (J·mol^{-1}·K^{-1})
T	Temperature (K)
V	Molar volume of mixture (m^3·mol^{-1})
V^E	Excess molar volume (m^3·mol^{-1})
V_i^o	Molar volume of pure liquids (m^3·mol^{-1})
W	Interchange energy (J·mol^{-1})
x	Mole fraction
Y_i^E	Measured property
Y_i^C	Calculated property

Greek letters

η	Dynamic viscosity (Pa·s)
ν	Kinematic viscosity (m^2·s^{-1})
ρ	Density (kg·m^{-3})

References

T. G. Amundsen, L. E. Øi, and D. A. Eimer. Density and viscosity of monoethanolamine + water + carbon dioxide from (25 to 80) ºC. *J. Chem. Eng. Data,* 54: 3096-3100, 2009.

U. E. Aronu, A. Hartono, and H. F. Svendsen. Density, viscosity, and N_2O solubility of aqueous amino acid salt and amine amino acid salt solutions. *J. Chem. Thermodynamics,* 45: 90-99, 2012.

E. C. Bingham. *Fluidity and plasticity.* McGraw-Hill, New York, 1922.

D. C. Cronauer, R. R. Rothfus, and R. I. Kernmore. Viscosity and density of the ternary liquid system acetone-benzene-ethylene dichloride. *J. Chem. Eng. Data,* 10: 131-133, 1965.

D. A. Eimer. *Gas Treating: Absorption Theory and Practice.* John Wiley & Sons Ltd, 2014.

H. Eyring. Viscosity, Plasticity, and Diffusion as example of absolute reaction rates. *Journal of chemical physics,* 4: 283-291, 1936.

R. J. Fort and W. R. Moore. Viscosities of binary liquid mixtures. *Transactions of the faraday society,* 62: 1112-1119, 1966.

R. Gonzalez-Olmos and M. Iglesias. Influence of temperature on thermodynamics of ethers + xylenes. *Fluid Phase Equilibria,* 267(2):133-139, 2008. doi:10.1016/j.fluid.2008. 03.004.

L. Grunberg and A. H. Nissan. Mixture Law for Viscosity. *Nature,* 164(4175): 799-800, 1949. doi:10.1038/164799b0.

J. Han, J. Jin, D. A. Eimer, and M. C. Melaaen. Density of water (1) + Monoethanolamine (2) + CO_2 (3) from (298.15 to 413.15) K and surface tension of water (1) + Monoethanolamine (2) from (303.15 to 333.15) K. *J. Chem. Eng. Data,* 57: 1095-1103, 2012.

A. Hartono, M. O. Mba, and H. F. Svendsen. Physical properties of partially CO_2 loaded aqueous monoethanolamine (MEA). *J. Chem. Eng. Data,* 59: 1808-1816, 2014.

E. L. Heric and J. G. Brewer. Viscosity of some binary liquid nonelectrolyte mixtures. *J. Chem. Eng. Data,* 12(04): 574-583, 1967.

Z. Idris and D. A. Eimer. Density measurements of unloaded and CO_2 loaded 3-Amino-1-propanol solutions at temperatures (293.15 to 353.15) K. *J. Chem. Eng. Data,* 61(1): 173-181, 2016.

Z. Idris, N. B. Kummamuru, and D. A. Eimer. Viscosity measurement of unloaded and CO_2-loaded aqueous monoethanolamine at higher concentrations. *Journal of Molecular Liquids,* 243: 638-645, 2017.

Z. Idris, N. B. Kummamuru, and D. A. Eimer. Viscosity measurement and correlation of unloaded and CO_2 loaded 3-Amino-1-propanol solution. *J. Chem. Eng. Data,* 63: 1454-1459, 2018.

M. N. Islam, M. M. Islam, and M. N. Yeasmin. Viscosity of aqueous solution of 2-methoxyethanol, 2-ethoxyethanol, and ethanolamine. *J. Chem. Thermodynamics,* 36: 889-893, 2004.

A. Jouyban, A. Fathi-Azarbayjani, M. Khoubnasabjafari, and W. E. Acree. Mathematical representation of the density of

liquid mixtures at various temperatures using Jouyban-Acree model. *Indian Journal of Chemistry,* 44A: 1553-1560, 2005.

J. Kendall and P. Monroe. The viscosity of liquids. II. The viscosity-composition curve for ideal liquid mixtures. *J. Am. Chem. Soc,* 39: 1787-1802, 1917.

R. J. Martins, M. J. D. M. Cardoso, and O. E. Barcia. Excess Gibbs free energy model for calculating the viscosity of binary liquid mixtures. *Ind. Eng. Chem. Res,* 39: 849-854, 2000.

R. A. McAllister. The viscosity of liquid mixtures. *A.I.Ch.E. Journal,* 6: 427-431, 1960.

R. Meyer, M. Meyer, J. Metzger, and A. Peneloux. Thermodynamic and physicochemical properties of binary solvent. *Journal de Chimie Physique et de Physico-Chimie Biologique,* 68: 406-412, 1971.

B. Mukesh, M. G. Sankar, M. C. Shekar, and T. Srikanth. Effect of placement of hydroxyl groups in isomeric butanol on the behavior of thermophysical and spectroscopic properties of 2-Methoxyaniline. *Journal of Solution Chemistry,* 44(12): 2267-2296, 2015. doi:10.1007/s10953-015-0406-1.

R. K. Nigam and B. S. Mahl. Molecular interaction in binary liquid mixtures of dimethylsulfoxide with chlroethanes & chlroethenes. *Indian Journal of Chemistry,* 9:1255-1258, 1971.

O. Redlich and A. T. Kister. Algebraic representation of thermodynamic properties and the classification of solutions. *Industrial and engineering chemistry,* 40(2): 345-348, 1948.

G. T. Rochelle. Amine Scrubbing for CO_2 Capture. *Science,* 325(5948): 1652-1654, 2009.

Article K

Aspen HYSYS and Aspen Plus simulations for amine based absorption process compared to results from experiments in CO_2-rig.

ASPEN HYSYS AND ASPEN PLUS SIMULATIONS FOR AMINE BASED ABSORPTION PROCESS COMPARED TO RESULTS FROM EXPERIMENTS IN CO$_2$-RIG

S.S. Karunarathne, L.E. Øi*

Faculty of Natural Sciences and Maritime Sciences - University of South-Eastern Norway, Norway

* Corresponding author e-mail: lars.oi@usn.no

Abstract

In this study, equilibrium-based and rate-based simulations in Aspen HYSYS and Aspen Plus were performed to compare the removal efficiency and physical properties of density and viscosity in a CO$_2$ absorption column. The experimental results from our previous study were used for comparison. In the equilibrium-based simulations, removal efficiency at 40 kg/hr of solvent flow rate was fitted with simulation by adjusting the Murphree efficiency of 12% in all stages. Accordingly, the equilibrium-based performed for other considered flow rates by keeping adjusted constant Murphree efficiency for all the stages in the absorber column. The variations of physical properties like density and viscosity were simulated and compared with measured properties under three different liquid to gas (L/G) ratios. Performed rate-based simulations with default molar volume/density and viscosity models of Clarke model and Jones-Dole model respectively were able to predict the properties with acceptable accuracy, but a deviation of 25% between measured and simulated viscosities for the lean MEA mixture was observed.

Keywords: Equilibrium-based, Rate-based, CO$_2$ capture, MEA

1. Introduction

Process simulation provides the ability to understand the process behavior under various process conditions and help to identify optimum conditions. The process of post-combustion carbon dioxide (CO$_2$) capture through amine based absorption process has been evaluated in various ways through mathematical modelling and simulations to identify the key factors in order to optimize the configuration and efficiency of the process [1-4].

Aspen HYSYS and Aspen Plus are two process simulation packages that are widely used in the industry for steady state process simulations and calculations of equilibrium data for various gas liquid mixtures. Two approaches of equilibrium-based and rate-based modelling are facilitated for simulation of the amine-based post-combustion CO$_2$ capture process. For equilibrium-based modelling, an amine package with Kent-Eisenberg [5] and Li-Mather [6] equilibrium models is available in Aspen HYSYS. The equilibrium-based column model can be refined using a Murphree efficiency on each stage. For rate-based modelling, the Electrolyte-NRTL equilibrium that is based on Austgen *et al.* [7] model is adopted to model the vapour-liquid equilibrium of the reacting system in Aspen Plus. The column can be modelled based on both equilibrium stages with Murphree efficiencies and rate-based approaches.

In literature, studies related to process simulations using Aspen HYSYS and Aspen Plus are widely available for amine based post-combustion CO$_2$ capture. An Aspen Plus model was developed by Lim et al. [8] and performed a validation against a pilot plant operated at Boryeong, South Korea. There was a good agreement for the estimation of CO$_2$ loading, heat duty and temperature in the stripper between developed model and pilot plant

results. Plaza et al. [9] worked with absorber and stripper models in Aspen Plus in which a thermodynamic model proposed by Hilliard [10] was used for modeling CO$_2$ removal from aqueous MEA (monoethanol amine). Zhang and Chen [11] also performed validation of a rate-based MEA model in Aspen Plus with a pilot plant. The study extended from simulation model for CO$_2$ absorption with MEA to both absorption and desorption process and was validated against recently published pilot plant data. For Aspen HYSYS simulation, different absorption and desorption configurations were investigated using an equilibrium-stage model in Aspen HYSYS for natural gas based pilot plants [12]. A comparison between equilibrium-based model in Aspen HYSYS and rate-based model in Aspen Plus was performed by Øi [1] for the CO$_2$ absorption into MEA from atmospheric gas. Results show that it is difficult to conclude which model gives more accurate predictions. According to Zhang and Chen [11], a rate-based model is capable of predicting the overall performance of the CO$_2$ capture system excellently.

In this work, CO$_2$ absorption into MEA was studied using the two simulation packages Aspen HYSYS (equilibrium-based model) and Aspen Plus (equilibrium and rate-based models). Series of laboratory experiments have been performed in an experimental CO$_2$-rig located at the University of South-Eastern Norway [13]. The experiments were done to investigate the CO$_2$ removal efficiency under different inlet CO$_2$ concentrations and solvent flow rates. The measured physical properties of density and viscosity at the absorber top for lean MEA and the bottom for rich MEA were compared with rate-based simulations from Aspen Plus.

2. Murphree efficiency based and rate – based simulation

2.1 Murphree efficiency

In distillation and absorption, the tray efficiency is described in several ways [14]. The point efficiency is defined as the ratio of change of composition at a point to the change of composition that would occur on a theoretical stage. Instead of a single point, Murphree efficiency is defined for the entire tray as given in Eq (1).

$$E_M = \frac{(y_n - y_{n-1})}{(y_n^* - y_{n-1})} \tag{1}$$

Where, y_n^* is the composition of vapour in equilibrium with the liquid leaving the tray, y_n is the actual composition of vapour leaving the tray.

The overall column efficiency E_o is given as

$$E_o = \frac{number\ of\ ideal\ stages}{number\ of\ real\ stages} \tag{2}$$

And these two efficiencies can be related as

$$E_o = \frac{ln\left[1 + E_M\left(\frac{mV}{L} - 1\right)\right]}{ln\left(\frac{mV}{L}\right)} \tag{3}$$

Where, m is the slope of the equilibrium line, V and L are molar flow rates of the vapour and liquid respectively.

For a packed column, Murphree efficiency of a tray is applicable for a packing section with a certain height.

2.2 Rate-based model

The rate-based approach considers the mass and heat transfer and chemical kinetics as the governing phenomena in the separation process. The driving force for the mass transfer is directly proportional to the deviation from the equilibrium between gas and liquid and is proportional to the contact area between the two phases [15]. The reaction model for MEA + CO$_2$ + H$_2$O is given in reactions R1 to R5 as described by the Austgen *et al.* [7] for primary and secondary amines.

Ionization of water

$$2H_2O \leftrightarrow H_3O^+ + OH^- \tag{R1}$$

Dissociation of carbon dioxide

$$2H_2O + CO_2 \leftrightarrow H_3O^+ + HCO_3^- \tag{R2}$$

Dissociation of bicarbonate

$$H_2O + HCO_3^- \leftrightarrow H_3O^+ + CO_3^{2-} \tag{R3}$$

Dissociation of protonated MEA

$$H_2O + MEAH^+ \leftrightarrow H_3O^+ + MEA \tag{R4}$$
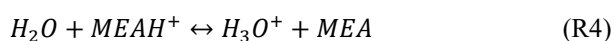
Carbamate reversion to bicarbonate

$$MEACOO^- + H_2O \leftrightarrow MEA + HCO_3^- \tag{R5}$$
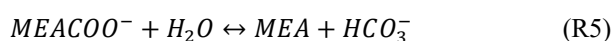
3. Methodology

3.1 Pilot plant and process description

An amine-based laboratory CO$_2$-rig located at the University of South-Eastern Norway is shown in Figure 1. The process is consisting of absorption and desorption columns for chemical absorption and stripping of CO$_2$. Feed with air and CO$_2$ pass through the absorber countercurrently with aqueous MEA and the structured packing enhances the mass transfer between CO$_2$ and absorbent. The absorber column is filled with Sulzer 250Y packing to build a packing section with 1500 mm height. Detailed information about the laboratory CO$_2$-rig can be found in a previous publication with a piping and instrumentation diagram (P&ID) [13].

Figure 1: Amine based CO$_2$ capture pilot plant at USN

3.2 Experiments

3.2.1 CO$_2$ rig experiments

A controlled flow of CO$_2$ with purity 99.5% from AGA Norge AS was mixed with constant air supply to achieve 5% and 10% CO$_2$ concentration (mol%) in the gas feed. The solvent flow rate was adjusted from 10 kg/hr to 100 kg/hr with 10 kg/hr increments. Finally, the CO$_2$ concentration of the treated gas was measured to determine the CO$_2$ removal efficiency. All the gas analysis were performed by an NDIR (Non-Dispersive InfraRed) instrument from ADC.

For the study of physical property variations of the absorber column, experiments that were performed in our previous work [16] were used for the simulations. There, three different liquid flows were considered. Samples were taken from liquid streams at the top and the bottom of the absorber and the temperatures were recorded in each case. Density and viscosity of collected samples were measured in the laboratory.

3.2.2 Density measurements

Density measurements of the liquid MEA + H$_2$O + CO$_2$ mixtures were performed using a DMA 4500 density meter from Anton Paar. A liquid volume of 5 ml approximately was injected into the U-tube of the density meter using a syringe. The temperature was set as it was recorded at the sampling point. The measurements were

repeated three times to verify the repeatability of the measurements and the average was taken as the final reading. A density check was performed with degassed water frequently to verify the validity of the previous calibration at 293.15 K.

3.2.3 Viscosity measurements

Viscosity measurements of the MEA + H_2O + CO_2 mixtures were carried out using a Physica MCR 101 rheometer from Anton Paar. A double-gap measuring system was adopted, as it was suitable for low viscous fluids. The calibration of the rheometer was performed using a standard calibration fluid S3S from Paragon Scientific Ltd. The viscosities of the calibration fluid measured were compared with the standard given by the supplier. The deviations of the measurements were noted at different temperatures and viscosities of the MEA + H_2O + CO_2 mixtures and corrected accordingly.

3.3 Simulations

The equilibrium-based simulations were carried out in Aspen HYSYS V10 environment. The amine package with Kent-Eisenberg [5] model was used to perform relevant calculations in the vapour and liquid phases. An absorber with four stages with defined Murphree efficiencies in each stage simulated the CO_2 removal efficiencies under different flow conditions.

In Aspen Plus rate-based simulations, an absorber column developed from RadFrac absorber model was used for the simulations. The property method of Electrolyte-non-random two-liquid (ELECNRTL) was selected as the mixture behaves as an electrolyte. All the simulations were performed under open-loop conditions.

For the physical properties, it is possible to regress experimental density and viscosity results of MEA + H_2O + CO_2 from Weiland *et al.* [17] or Hartono *et al.* [18] to estimate relevant model parameters in Aspen Plus. The Clarke model, called VAQCLK in Aspen Plus for liquid molar volume is available with regressed model parameters. The model calculates liquid molar volume of aqueous electrolytes solutions using Amagat's law as given in Eq (4) and the relationship between partial molar volume of an electrolyte and its mole fraction in the solvent as given in Eq (5) [19].

$$V_m^l = \sum_i x_i V_i \qquad (4)$$

Where, V_m^l, x_i and V_i are molar volume of the mixture, mole fraction and the molar volume of component respectively.

$$V_{ca} = V_{ca}^\infty + A_{ca} \frac{\sqrt{x_{ca}}}{1+\sqrt{x_{ca}}} \qquad (5)$$

Where, V_{ca} is the partial molar volume of electrolytes, x_{ca} is the apparent electrolyte mole fraction and V_{ca}^∞, A_{ca} are regression parameters.

The option code 1 represents the quadratic mixing rule for solvent in which the interaction parameter VLQKIJ for MEA and H_2O can be regressed against MEA + H_2O density data from Kapadi *et al.* [20] and Han *et al.* [21]. The Clarke model parameters V_{ca}^∞ named as VLCLK/1 can also be regressed for the main electrolyte (MEAH⁺,

HCO₃⁻), (MEAH⁺, MEACOO⁻) and (MEAH⁺, CO₃²⁻) against experimental MEA + H_2O + CO_2 density data. The Jones-Dole electrolyte correction model, referred as MUL2JONS in Aspen Plus can be adopted to model the liquid viscosities in a MEA + H_2O + CO_2 mixture. Due to the presence electrolytes, model calculates the correction to the liquid mixture viscosity of a solvent mixture. The Jones-Dole electrolyte correction model is given as follows [19],

$$\eta = \eta_{solv}(1 + \sum_{ca} \Delta\eta_{ca}) \qquad (6)$$

Where, η, η_{solv} and $\Delta\eta_{ca}$ are viscosity of the liquid mixture, viscosity of the liquid mixture calculated by the Andrade/DIPPR model and contribution to the viscosity correction due to apparent electrolyte *ca* from cation *c* and anion *a* respectively.

The interaction parameters between MEA and H_2O in the Aspen liquid mixture model, MUKIJ and MULIJ, can be regressed against experimental MEA + H_2O viscosity data. Further, the Jones-Dole model parameters in $\Delta\eta_{ca}$, IONMUB, for MEAH⁺ and MEACOO⁻ are possible to regress against MEA + H_2O + CO_2 viscosity data [22]. The data regression to estimate parameters is beyond the scope of this study, and density and viscosity predictions were obtained using default parameter values in Aspen Plus.

The experimental input data for the physical property simulations are given in Table 1 and Table 2. The Aspen Plus simulations were performed in the Aspen Plus V10 environment.

Table 1: Scenarios considered in CO₂-rig experiments

Case no	Air flow rate (Nm³/hr)	Liquid flow rate (kg/hr)	CO₂ in feed (%)	T_Absorber,in (ºC)
Case 1	15	47.92	10.2	19.5
Case 2	15	106.56	9.9	25.7
Case 3	15	151.17	9.9	30.1

Table 2: Lean amine loading with corresponding (L/G) in mass basis

Case no	Liquid flow rate (kg/hr)	(L/G)	Lean MEA loading (mol CO₂ / mol MEA)
Case 1	47.92	2.3	0.213
Case 2	106.56	5.4	0.280
Case 3	151.17	7.8	0.279

4 Results

4.1 CO₂ removal efficiency

For the investigation of CO_2 removal efficiency, two case studies were performed by keeping inlet gas CO_2 concentration at 5% and 10% (mole basis) of total gas flow. Figure 2 illustrates the variation of CO_2 removal efficiency under different liquid flow rates from 10 kg/hr to 100 kg/hr, which is equivalent to a range of liquid to gas (L/G) ratio from 0.3 to 3 on a mass basis approximately.

As shown in Figure 2 the CO_2 removal efficiency increases with the increase of liquid flow rate. Under low flow rates, the driving force for the mass transfer is reduced as the aqueous amine solution reaches high CO_2 loadings rapidly. This is reversed under high flow rates as more liquid with high driving force increase the CO_2 removal efficiency. Further, the increase of amine flow enhances the gas/liquid interfacial area while passing through the structured packing. This effect also increases the mass transfer through the gas/liquid interface.

In the equilibrium-based model, the Murphree efficiency on each of four plates were fitted to 12% for 40 kg/hr to get equal CO_2 removal efficiency in simulation and experiment. At other liquid flows the Murphree efficiency were kept constant at 12%. The rate-based simulations in Aspen Plus were performed by adjusting the interfacial area factor (IAF) to 1.98 to achieve a similar removal efficiency at 40 kg/hr compared to experiment. The results for other flow rates were taken at the adjusted IAF of 1.98.

This high interface area factor indicates that the rate-based model does not describe the absorption mechanisms accurately. Because the IAF is expected to increase with increasing liquid flow, the liquid flow influence on removal efficiency with a constant IAF in Figure 2 is opposite of what was expected. In Table 3 the IAF shows a more reasonable dependence of increasing liquid flow. A possible factor that may also influence on the CO_2 removal efficiency is the temperature, which may vary in the measured data in Figure 2.

Table 3. IAF and CO_2 out (%) in treated gas

Case no	IAF	CO_2 out (%) in treated gas
Case 1	1.04	5.8
Case 2	1.37	4.8
Case 3	1.43	4.1

As shown in Figure 2, the equilibrium-based model with constant Murphree efficiency predicted removal efficiency closer to the experiments at low flow rates below 50 kg/hr. The deviation between measured and simulation increases at higher flow rates. For the rate-based model, predictions are closer to the experiment at higher flow rates and the deviations are greater at low flow rates.

Neither the equilibrium based nor the rate-based model give a good qualitative description of the CO_2 removal as a function of liquid flow. This was also the conclusion in comparisons of equilibrium-based and rate-based models with performance data at TCM Mongstad [4]. The accuracy in simulated CO_2 removal efficiencies shown in Figure 2 are however reasonable for both models.

In Aspen HYSYS simulations, the removal efficiency increased with liquid flow rate, until it reached 30 kg/hr. Subsequently, the removal efficiency became a steady value after 30 kg/hr of liquid flow rate. Similar behavior was observed for 10% inlet CO_2 concentration in which a steady removal efficiency of 33% after 60 kg/hr of liquid flow in the HYSYS simulation.

In case of using a rate-based model in Aspen Plus, the absorption efficiency will vary slightly with the liquid

flow and the removal efficiency as a function of liquid flow will be expected to be simulated more accurately.
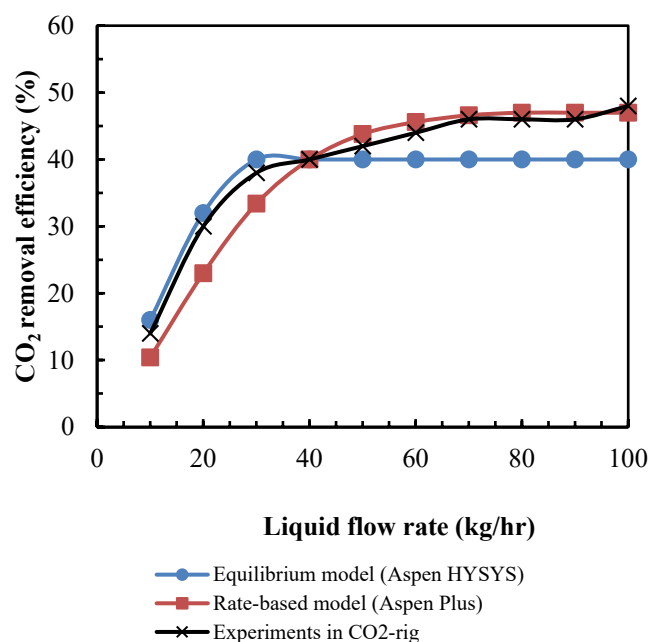
Figure 2: Comparison of CO_2 removal efficiency from experiments, equilibrium-based model and rate-based model

4.2 Physical property analysis

Density and viscosity of the lean and rich MEA solvent have been measured at three different liquid flow rates as shown in Table 1 [16] were used for the rate-based simulations in Aspen Plus. For each case, the interfacial area factor was adjusted to achieve the removal efficiency observed during the experiments. IAF was adjusted by trial and error until the relative deviation between measured and simulated CO_2 concentrations at the treated gas becomes < 1%. The simulated CO_2 concentration of the treated gas at absorber out and corresponding IAFs are given in Table 3.

Accordingly, the corresponding density and viscosity of the lean and rich amine stream were evaluated. Figure 3 compares the experimental results with the simulation of the density variations in the liquid stream at the top and bottom of the absorber. Absorption of CO_2 increases the CO_2 loading in the solvent. The experiments revealed that the density of the MEA + H_2O + CO_2 increased at the absorber bottom compared to the absorber top even though the temperature increases due to the exothermal reaction between MEA and CO_2. The simulations were able to predict this trend as shown in Figure 3. The maximum relative deviation of measured density from the simulation is 6%. The model called VAQCLK with option code 1 in the property set was adopted to simulate the measured densities.

Rate-based simulations for the density of liquid streams were able to predict the trend of density variation with the increase of liquid flow in the absorber. Further simulations follow the trend of increase of density in the rich amine solution compared to that of lean amine. The temperature obtained through the simulations for rich amine mixture deviates around 5% from the measured.
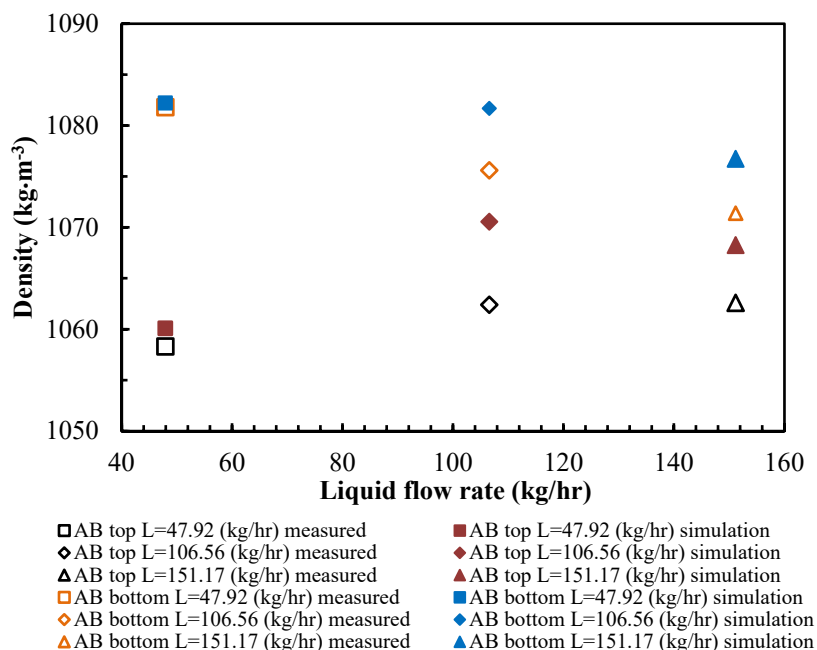
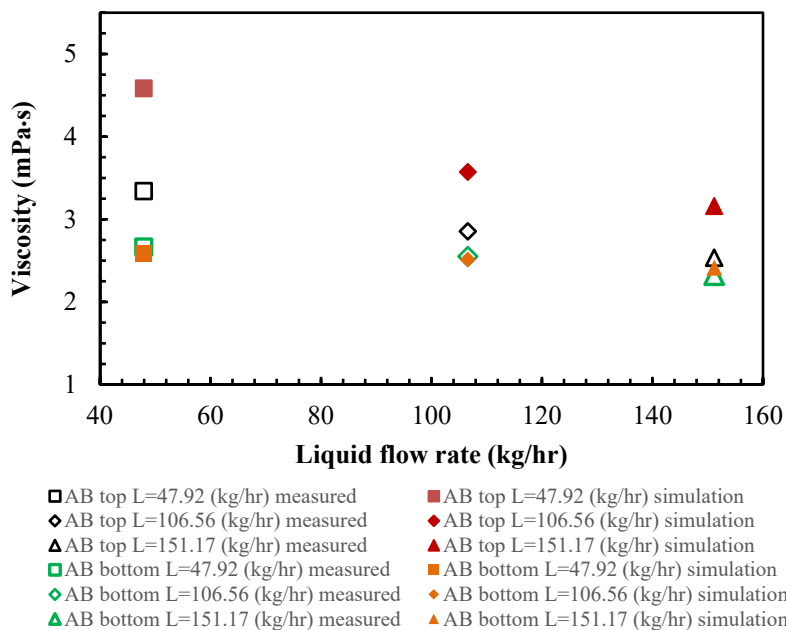Figure 3: Comparison of the measured densities with the simulation

Figure 4: Comparison of the measured viscosities with the simulation

For the viscosity predictions based on rate-based simulations in Aspen Plus, Figure 4 illustrate the comparison between simulated viscosities and measured data at both lean and rich amine solutions. As shown by the experiments, viscosity at the lean MEA solution is higher than that of rich MEA. Generally, the increase of CO_2 in MEA + H_2O + CO_2 mixture increase the viscosity [17, 23], but the increase of temperature dominate to reduce the viscosity at rich MEA mixture.

Rate-based simulations were able to predict the trend of viscosity variation in the absorber column under different liquid flow rates. As described in Figure 4, simulated viscosities showed large deviations around 25% compared to that of measured at the lean MEA mixture. Lower deviations were reported for the viscosity of rich MEA mixture and it was around 4%. The measured

viscosities agree with the viscosity data published for MEA + CO_2 + H_2O mixtures under different CO_2 loadings and temperatures [18]. A possible cause for such deviations can be that the property model parameters were not regressed against the actual measured data. The causes can be found by performing simulations after estimating the required parameters through a regression.

Several other viscosity models such as Andrade model (MUL2ANDR), TRAPP model (MUL2TRAP) and Eyring-NRTL model (EYRING) for liquid mixture viscosity were also examined and compared with measured viscosities. The predictions deviate highly compared to the Jones-Dole electrolyte viscosity model with a factor around 2. This indicates that the selection of property models needs to be selected carefully to acquire the best results.

4.3 Uncertainty of experiments and simulations

The experiments in the CO_2-rig involve different types of uncertainties. These uncertainties are related to inaccuracies of the measuring instruments and the process samplings. The extracted samples for the density and viscosity measurements should be representative of the system. The CO_2-rig in USN has performed several modifications in order to achieve theories of process sampling to improve the accuracy of the measurements. In earlier work [13], uncertainties have been evaluated. It has been problems with the consistency in the amount of absorbed CO_2 calculated from the gas and liquid side. The absorbed CO_2 amount calculated from the liquid side has been assumed to have the highest uncertainty due to the uncertainty in measured difference of CO_2 concentration between lean and rich amine. In this work, the CO_2 removal efficiency is calculated based on CO_2 concentrations in the gas in and out which are assumed to have reasonable accuracy.

In the simulations, equilibrium and physical property models have uncertainties due to the assumptions considered during the model developments. Our recent publication on uncertainty analysis of interfacial area and mass transfer coefficient models [24] revealed the propagation of uncertainty of physical properties through such models. Those uncertainties in physical properties can appear from the sampling to measuring device. Uncertainties in viscosity are expected to give more impact on design than uncertainties in density.

5 Conclusion

Simulations based on an equilibrium-based model in Aspen HYSYS and a rate-based model in Aspen Plus were performed and compared with CO_2 removal efficiencies obtained via experimental study performed with the CO_2-rig located at USN, Norway.

In the equilibrium-based model, for the study of 5% CO_2 feed gas concentration, the Murphree efficiency was adjusted to 12% to fit the removal efficiency at 40 kg/hr of liquid flow rate. The assumption of a constant Murphree efficiency is doubtful when variables like gas or liquid flow are varied. But performance data can be fitted by adjusting the Murphree efficiency as a function of gas- or liquid flow.

In case of using a rate-based model, the IAF can be adjusted. So far, neither fitting the Murphree efficiency in an equilibrium model or fitting the IAF in a rate-based model give qualitatively reasonable results. The calculated CO_2 removal as a function of liquid flow are however reasonably accurate for both models.

For the physical properties based on rate-based simulations, the default Jones-Dole model (MUL2JONS) was able to predict the measured viscosities with measurable deviation and may be improved by estimating model parameters through a regression using available measured viscosity data in the literature. Other considered models the Andrade model (MUL2ANDR), TRAPP model (MUL2TRAP) and Eyring-NRTL model (EYRING) for liquid mixture viscosity deviated largely from measured data. Accordingly, they are not adopted in this application. The default molar volume and density model VAQCLK was able to predict densities in the $MEA + H_2O + CO_2$ with acceptable accuracy.

References

[1] Øi, L.E. Comparison of Aspen HYSYS and Aspen Plus simulation of CO_2 absorption into MEA from atmospheric gas. Energy Procedia, 2012. 23: p. 360-369.

[2] Kvamsdal, H.M., Chikukwa, A., Hillestad, M., Zakeri, A., & Einbu, A. A comparison of different parameter correlation models and the validation of an MEA-based absorber model. Energy Procedia, 2011. 4: p. 1526-1533.

[3] Kvamsdal, H.M., & Hillestad, M. Selection of model parameter correlations in a rate-based CO_2 absorber model aimed for process simulation. International Journal of Greenhouse Gas Control, 2012. 11: p. 11-20.

[4] Øi, L.E., Sætre, K.A., and Hamborg, E.S. Comparison of simulation tools to fit and predict performance data of CO_2 absorption into monoethanol amine at CO_2 technology centre mongstad (TCM), in Proceedings of the 59th conference on simulation and modelling (SIMS 59), 26-28 September 2018. 2018: Oslo Metropolitan University Norway. p. 230-235.

[5] Kent, R.L., & Eisenberg, B. Better data for amine treating Hydrocarbon Processing, 1976. 55(2): p. 87-90.

[6] Li, Y., & Mather, A.E. Correlation and prediction of the solubility of carbon dioxide in a mixed alkanol solution Ind. Eng. Chem. Res, 1994. 33: p. 2006-2015.

[7] Austgen, D.M., Rochelle, G.T., Peng, X., & Chen, C.C. Model of vapor-liquid equilibria for aqueous acid gas-alkanolamine systems using the electrolyte-NRTL equation. Industrial & Engineering Chemistry Research, 1989. 28(7): p. 1060-1073.

[8] Lim, Y., Kim, J., Jung, J., Lee, C.S., & Han, C. Modeling and Simulation of CO_2 Capture Process for Coal- based Power Plant Using Amine Solvent in South Korea. Energy Procedia, 2013. 37: p. 1855-1862.

[9] Plaza, J.M., Van Wagener, D., & Rochelle, G.T. Modeling CO_2 capture with aqueous monoethanolamine. International Journal of Greenhouse Gas Control, 2010. 4(2): p. 161-166.

[10] Hilliard, M.D. A predictive thermodynamic model for an aqueous blend of potassium carbonate, piperazine, and monoethanolamine for carbon dioxide capture from flue gas, in Chemical Engineering. 2008, The University of Texas at Austin.

[11] Zhang, Y., & Chen, C.C. Modeling CO_2 absorption and desorption by aqueous monoethanolamine solution with Aspen rate-based model. Energy Procedia, 2013. 37: p. 1584-1596.

[12] Øi, L.E., Bråthen, T., Berg, C., Brekne, S.K., Flatin, M., Johnsen, R., Moen, I.G., & Thomassen, E. Optimization of Configurations for Amine based CO_2 Absorption Using Aspen HYSYS. Energy Procedia, 2014. 51: p. 224-233.

[13] Øi, L.E., Hansen, P.M., & Henriksen, M. CO_2 absorption efficiency and heat consumption measured at high gas to liquid ratios in laboratory rig Energy Procedia, 2017. 114: p. 1273-1281.

[14] Kister, H.Z. Distillation Design 1992, USA: McGraw-Hill, Inc.

[15] Eimer, D.A. Gas Treating: Absorption Theory and Practice. 2014: John Wiley & Sons. Ltd

[16] Karunarathne, S.S., Eimer, D.A., & Øi, L.E. Density and viscosity variations in an amine based absorption column,

in 14th Greenhouse Gas Control Technologies Conference (GHGT-14). 2018: Melbourne

[17] Weiland, R.H., Dingman, J.C., Cronin, D.B., Browning, G.J. Density and viscosity of some partially carbonated aqueous alkanolamine solutions and their blends. J. Chem. Eng. Data, 1998. 43: p. 378-382.

[18] Hartono, A., Mba, E.O., & Svendsen, H.F. Physical properties of partially CO_2 loaded aqueous monoethanolamine (MEA). J. Chem. Eng. Data 2014. 59: p. 1808-1816.

[19] Aspen physical property system: Physical property methods and models 11.1, USA: Aspen Technology, Inc., 2001.

[20] Kapadi, U.R., Hundiwale, D.G., Patil, N.B., & Lande, M.K. Viscosity, excess molar volume of binary mixtures of ethanolamine with water at 303.15, 303.15, 313.15 and 318.15K. Fluid Phase Equilibria, 2002. 201: p. 335-341.

[21] Han, J., Jin, J., Eimer, D.A., & Melaaen, M.C. Density of water (1) + Monoethanolamine (2) + CO_2 (3) from (298.15 to 413.15) K and surface tension of water (1) + Monoethanolamine (2) from (303.15 to 333.15) K. J. Chem. Eng. Data, 2012. 57: p. 1095-1103.

[22] Rate-Based model of the CO_2 capture process by MEA using Aspen Plus. Aspen Technology, Inc, 2008.

[23] Amundsen, T.G., Øi, L.E., & Eimer, D.A. Density and viscosity of monoethanolamine+water+carbon dioxide from (25 to 80) ℃. J. Chem. Eng. Data, 2009. 54: p. 3096-3100.

[24] Karunarathne, S.S., Eimer, D.A., & Øi, L.E. Model uncertainty of interfacial area and mass transfer coefficients in absorption column packings. in Proceedings of the 58th SIMS. 2017. Reykjavik, Iceland.

Article L

Density and viscosity variations in an amine based absorption column.

Karunarathne, S.S.; Eimer, D.A.; Øi, L.E. In Proceedings of 14th Greenhouse Gas Control Technologies Conference (GHGT-14), Melbourne.

Density and viscosity variations in an amine based absorption column

Sumudu S. Karunarathne[a*], Dag A. Eimer[b], Lars E. Øi[a]

^{a}University of South-Eastern Norway, Kjølnes ring 56, Porsgrunn 3901, Norway
^{b}Tel-Tek, Porsgrunn, Kjølnes ring 30, Porsgrunn 3918, Norway

Abstract

In this study, the variations of physicochemical properties like density and viscosity in CO_2 loaded aqueous monoethanol amine were studied in a laboratory rig. Liquid samples were collected from the top and the bottom of the absorber column and temperature and liquid flow rate were recorded for further analysis. CO_2 concentration in the solution was determined by using a precipitation and titration method. Density and viscosity were measured from the collected samples under the recorded column temperatures. The measured physicochemical properties were compared with correlations given by Weiland and Hartono. The study showed that both correlations could predict density and viscosity with acceptable deviations. Further, these correlations can be used in equipment design and process simulations. pH of the liquid was also measured to relate it with the CO_2 concentration in the top and bottom of the absorber column. The variation of the measured pH is a possible measure of the variations of CO_2 concentration.

Keywords: density; viscosity; laboratory rig; MEA

1. Introduction

Carbon capture and storage (CCS) is a method to avoid excess CO_2 emissions. Post-combustion CO_2 capture (PCC) with amine-based absorption and desorption has been widely investigated for many years for various aspects such as removal efficiency, different types of amines, energy demand and different process configurations. CO_2 absorption with monoethanol amine (MEA) is considered as a benchmark process to evaluate PCC. Physical properties like density and viscosity of MEA change through the process due to changes in process conditions, especially temperature and CO_2 loading. In the design of process equipment, it is important to know how these properties vary in operation in order to optimize the design.

In this study, the main interest is given to analyze the variations in density and viscosity of MEA in the CO_2 absorption and compare them with predictions obtained through literature correlations. The laboratory rig located at the University of South-Eastern Norway was used for all experiments. The experiments were done at different gas to liquid ratios and samples were taken at top and bottom of the column. For each point, temperature, CO_2 loadings, viscosity and density of MEA were measured. The temperatures were measured by Pt-1000 temperature sensors, CO_2 loading was analyzed by titration, density was measured by an Anton Paar 4500 density meter and viscosity was measured by an Anton Paar Physica 101 rheometer. The measured density and viscosity were compared with correlations given by Weiland and Hartono for the CO_2 loaded MEA.

* Corresponding author. Tel.: +4745115191.
 E-mail address: sumudu.karunarathne@usn.no

Fig. 1. Amine based post combustion CO_2 capture pilot plat at University of Southeast Norway [1]

Nomenclature

t	temperature [°C]
T	temperature [K]
w_{MEA}	weight percentage of MEA
x_{MEA}	mole faction of MEA
x_{H2O}	mole fraction of H_2O
x_{CO2}	mole fraction of CO_2
α	CO_2 loading [mol CO_2 / mol MEA]
η	viscosity [Pa·s]
η_{MEA}	viscosity of MEA [Pa·s]
η_{H2O}	viscosity of water [Pa·s]
$\Delta\eta$	viscosity deviation [Pa·s]
η_{loaded}	viscosity of CO_2 loaded solutions [Pa·s]
$\eta_{unloaded}$	viscosity of CO_2 unloaded solutions [Pa·s]

A photograph of the rig is shown in Fig.1. The absorber column is shown on the left. The design, control and operation is described in [1].

2. Method

2.1. Pilot plant experiments

A pilot plant with an absorption and desorption process at the University of South-Eastern Norway was used for all experiments. The absorber in the pilot plant is with 100mm of diameter and 2500mm of height. It is filled with stainless steel Sulzer Mellapak 250Y structured packing up to 1500mm. The desorption column is with 265mm of diameter and 3000mm of height. The column is consisting of Sulzer P-rings up to 1000mm and steam is given to heat the reboiler and column is operated under pressure of 0.8 bar (Gauge pressure).

The experiments were done under both cold and hot conditions (Table 1). In cold conditions, the steam is not sent into the stripper and CO_2 absorption take place in the absorber and desorption does not take place in the stripper. There, the CO_2 concentration of solvent continues to rise until it is saturated. During the hot conditions, steam is sent to the stripper and desorption from MEA take place in the desorber. Lean and rich CO_2 concentrations in the solvent can be maintained at the top and the bottom of the absorber and continuous CO_2 removal from the feed gas can be achieved.

Table 1. Scenarios that were performed during the experiments.

Condition	Case no	Air flow rate (Nm^3/h)	Liquid flow rate (kg/hr)	CO_2 in feed (%)	$T_{Absorber,in}$ (°C)	$T_{Absorber,out}$ (°C)
Cold condition	Case 01	15	49	10.2	15.8	24.6
Hot condition	Case 02	15	47.92	10.2	19.5	31.5
	Case 03	15	106.56	9.9	25.7	32.4
	Case 04	15	151.17	9.9	30.1	35

In the feed, the constant air supply is mixed with CO_2 (purity: 99.5%) to achieve the desired CO_2 concentration at the absorber inlet. The amount of CO_2 present in the inlet and the outlet of the absorber column was measured by an NDIR (Non-Dispersive InfraRed) instrument from ADC.

2.2. Density measurements

The density of partially carbonated aqueous MEA solution extracted at both absorber top and bottom were measured by using an Anton Paar density meter (DMA 4500) under measured temperatures. The density meter is consisting of a U-tube that is oscillated at its fundamental frequency and the oscillation frequency is a function of sample density [2]. The sample was introduced to the instrument using a 5 ml syringe and waited until the cell becomes to the desired temperature. All the densities were measured under atmospheric pressure and calibration and density check was performed prior to the density measurements.

2.3. Viscosity measurements

The dynamic viscosity was measured for the samples taken at both absorber top and bottom. A rheometer from Anton Paar (Physica MCR 101) was used for dynamic viscosity measurements at temperatures where the samples were extracted. All the viscosity measurements were obtained under 1000 s^{-1} of shear rate under the pressure of 4 bar to avoid the escape of MEA and CO_2 from the mixture during the test. Air measurement and motor adjustment were performed prior to viscosity measurements to check the quality of the motor adjustment and the conditions of the bearings [3].

2.4. CO₂ analysis and pH measurements

    The concentration of CO_2 in the aqueous MEA solution was determined by using a titration method. A sample with 0.1-0.3g of CO_2 loaded solution mixed together with 50 ml of 0.3M $BaCl_2$ and 50 ml of 0.1M NaOH solutions. The mixture was boiled for approximately 10 min to complete the $BaCO_3$ formation and it was cooled in a water bath. Then the mixture was filtered through a membrane filter (0.45μm) and the filter cake was added to 100ml of distilled water. During the first titration, 0.1M HCl was added until the precipitate dissolve completely and pH reaches two. Here it was assumed that $BaCO_3$ reacts completely with HCl and the mixture was boiled again to release all dissolved CO_2 from the mixture. In the second titration, 0.1M NaOH was added to the mixture to react with excess HCl and the consumed NaOH volume was recorded at the pH 5.27 [4]. Another titration was performed to determine the concentration of MEA in the mixture. Here, 1M of HCl was reacted with a 1g of CO_2 loaded solution and the consumed HCl volume was recorded. Since the reaction was a strong acid and a weak base, the equivalence point can be observed below pH 7.

    pH of the all extracted solutions was measured using Beckman Φ 390 pH meter to observe the variation of pH under different operating conditions of the pilot plant.

2.5. Density and viscosity correlations

    Density and viscosity correlations developed by Weiland et al. from 2014 [5] and Hartono et al. from 2012 [6] were used to compare the density and viscosity predictions with measured data. Correlations are used to predict viscosity at unmeasured conditions in process design and mathematical modeling and simulations. The Weiland's viscosity correlation is capable of predicting viscosity of MEA, MDEA, and DEA solutions up to amine concentration of 40 wt% , 60 wt% and 77.2 wt% respectively, with CO_2 loading up to 0.6 mole CO_2/ mole amine for MEA and 0.5 mole CO_2/ mole amine for MDEA and DEA at a maximum temperature of 398 K. Following equations (1) and (2) illustrate the Weiland's viscosity correlation

$$(\eta/\eta_{H2O}) = exp\{f(w)g(\alpha)/T\} \tag{1}$$

$$(\eta/\eta_{H2O}) = exp\{[(a \cdot w_{MEA} + b)T + (c \cdot w_{MEA} + d)][\alpha(e \cdot w_{MEA} + f \cdot T + g) + 1]w_{MEA}/T\} \tag{2}$$

    Hartono et al. [6] has developed two correlations to predict the dynamic viscosity of aqueous MEA with and without CO_2. For the viscosity of CO_2 unloaded aqueous MEA, the excess viscosities were calculated and a regression model was proposed as shown in Eq (4).

$$ln(\Delta\eta) = ln(\eta_{unloaded}) - (x_{MEA}ln(\eta_{MEA}) + x_{H2O}ln(\eta_{H2O})) \tag{3}$$

$$ln(\Delta\eta) = x_{MEA}x_{H2O}(b_1 + b_2t + b_3t^2 + b_4x_{MEA}) \tag{4}$$

Viscosity of CO_2 loaded aqueous MEA was correlated as a function of the viscosity of unloaded viscosity and CO_2 mole fraction. Eq (5) and (6) show the relevant correlations

$$ln(\eta_{loaded}) = x_{CO2}ln(\eta^*) + (1 - x_{CO2})ln(\eta_{unloaded}) \tag{5}$$

$$ln(\eta^*) = (a_1x_{MEA} + a_2\alpha x_{MEA})/(a_3 + x_{MEA}) \tag{6}$$

3. Results

    The temperature at the absorber bottom compared to the absorber top is higher due to the exothermic reaction between CO_2 and MEA. CO_2 absorbed into the aqueous MEA results in a higher CO_2 loading at the bottom of the absorber compared to the top. A higher density was observed at the absorber bottom. The measured density and viscosity were compared with density and viscosity correlations proposed by Weiland and Hartono. Table 2 lists the

measured density and viscosity under cold and hot conditions of the column operation.

Table 2. Measured density and viscosity in the absorption column

Absorber characteristics Operation / Liquid flow rate (kg/hr)	CO_2 loading (mol CO_2/ mol MEA)	Temperature (ºC)	Density (kg/m^3)	Viscosity (mPa·s)
49 CC : Absorber top	0.334	15.8	1075.8	3.9844
49 CC : Absorber bottom	0.425	24.6	1094.6	3.3279
47.92 HC : Absorber top	0.213	19.5	1058.3	3.3406
47.92 HC : Absorber bottom	0.369	31.5	1081.8	2.6647
106.56 HC : Absorber top	0.280	25.7	1062.4	2.8553
106.56 HC : Absorber bottom	0.358	32.4	1075.6	2.5521
151.17 HC : Absorber top	0.279	30.1	1062.6	2.5351
151.17 HC: Absorber bottom	0.336	35	1071.4	2.3247

CC: Cold condition, HC: Hot condition

Table 3 compares the measured density and viscosity with predictions according to the correlations proposed by Weiland and Hartono. The CO_2 mole fractions and loadings in liquid at absorber top and bottom were calculated through the titrations and were used in the density and viscosity calculations.

Table 3. Comparison of measured density and viscosity with correlation predictions

Condition	Property		Measured	Weiland	Hartono
CC 49 kg/hr	Density (kg/m^3)	Top	1075.8	1082.0	1085.6
		Bottom	1094.6	1098.8	1104.6
	Viscosity (mPa·s)	Top	3.9844	4.3328	4.2289
		Bottom	3.3279	3.5380	3.5441
HC 47.92 kg/hr	Density (kg/m^3)	Top	1058.3	1055.3	1058.0
		Bottom	1081.8	1085.0	1085.0
	Viscosity (mPa·s)	Top	3.3406	3.4569	3.4584
		Bottom	2.6647	2.7990	2.8000
HC 106.56 kg/hr	Density (kg/m^3)	Top	1062.4	1067.7	1069.1
		Bottom	1075.6	1082.5	1082.3
	Viscosity (mPa·s)	Top	2.8553	3.0402	3.0407
		Bottom	2.5521	2.7086	2.7113
HC 151.17 kg/hr	Density (kg/m^3)	Top	1062.6	1066.5	1066.8
		Bottom	1071.4	1077.0	1076.0
	Viscosity (mPa·s)	Top	2.5351	2.6904	2.6932
		Bottom	2.3247	2.4868	2.4872

CC: Cold condition, HC: Hot condition

For the density measurements, both correlations were able to predict similar results and those are in good agreement with the measured density data of the absorber column. It is difficult to say about what is the best correlation to predict density in the column since both predictions are acceptable (maximum deviation from measurements is <

1%). Weiland's density correlation has been used in many publications and Hartono's density correlation is relatively new. The correlations of viscosity also predict viscosity of CO_2 loaded aqueous MEA with a good agreement. The maximum deviation for measured viscosity and prediction is less than 10%.

Under hot conditions, the measured CO_2 concentration in gas at the absorber out shows that the increase of liquid flowrate enhances the CO_2 removal efficiency. Due to the high flow rates, the liquid retention time decreases. Therefore, the CO_2 loading difference between absorber top and the bottom decreases with the increase of liquid flow.

CO_2 absorption makes changes in physicochemical properties of the aqueous MEA solution. The literature reveals that absorption of CO_2 into aqueous MEA causes to increase both the density and viscosity of the mixture [5-7]. Martin et al. (2013) [8] examined the relationship between viscosity and CO_2 loading. Higher CO_2 loading leads to increase the ionic strength and decrease the solution pH. At a higher ionic strength, a solution has a greater polarity that causes higher viscosity due to cluster formation.

In the absorber column, the temperature of the liquid at the absorber bottom is always higher than the temperature at the absorber top due to the exothermic reaction between MEA and CO_2 [9]. Accordingly, the viscosity of the MEA solution decreased and higher viscosity appears at the absorber top than the absorber bottom under considered liquid flowrates. Fig. 2 illustrates the variation of viscosities with temperature under different flow conditions in the column. The liquid density variation shows the similar behavior as viscosity. The increase of liquid temperature resulted in the decrease of density as shown in Fig. 3.
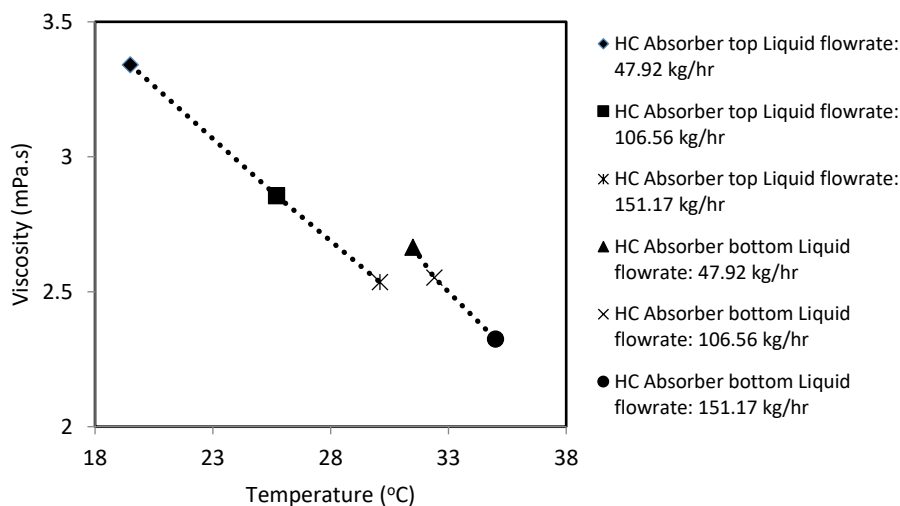
Fig. 2 Viscosity variation at different temperatures under different liquid flow rates at Absorber top and bottom. HC: Hot Condition

The pH of the CO_2 loaded aqueous MEA was measured at both the absorber top and the bottom. The [H$^+$] concentration increases with the amount of CO_2 absorbed into the solution. Consequently, pH will be lower at higher CO_2 loadings and pH variation under different liquid flow rates is plotted in Fig. 4. There, the measured pH at the absorber top is higher than measured pH at the absorber bottom due to the CO_2 absorption through the column.
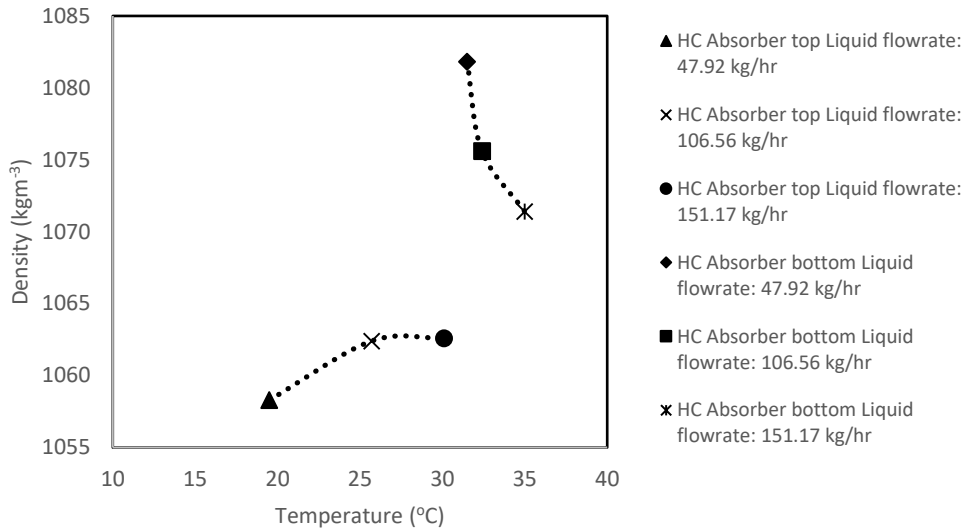
Fig. 3 Density variation at different temperatures under different liquid flow rates at Absorber top and bottom. HC: Hot Condition
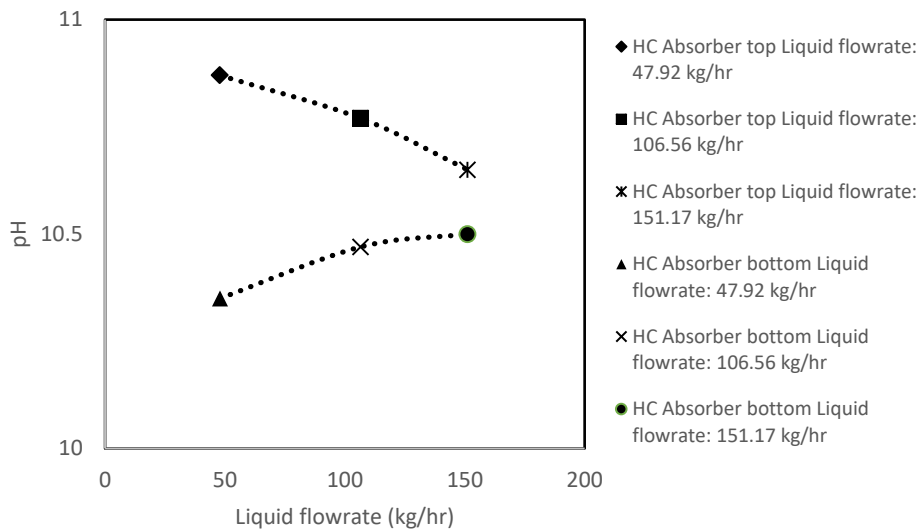
Fig. 4 pH at different temperatures under different liquid flow rates at Absorber top and bottom. HC: Hot Condition

4. Conclusion

The density and viscosity increased with the increase of CO_2 loading of the aqueous MEA. This confirms the variation discussed in the literature. Both correlations were able to predict density and viscosity in the absorber column and both have acceptable accuracy through a comparison with measured data. Correlations can be used in the design of process equipment and mathematical modeling and simulations of the absorption process. There is a possibility to build a regression model to predict density and viscosity using CO_2 loading, liquid flow rate and temperature. More measurements are required for such a study to improve the accuracy of the model.

References

[1] Øi LE, Lundberg J, Pedersen M, Hansen PM, Melaaen MC. Laboratory rig for atmospheric CO2 absorption and desorption under pressure. Energy Procedia. 2013;37:1933-40.

[2] Fitzgerald D. Technical assessment of the anton paar DMA 5000 density meter 2000.

[3] Intelligence in rheometry Tips and tricks from joe flow, calibration and adjusting rheometer systems: keep your rheometer fit [Internet].

[4] Han J, Jin J, Eimer DA, Melaaen MC. Density of water(1)+Monoethanolamine(2)+CO2(3) from (298.15 to 413.15)K and surface tension of water(1)+monoethanolamine(2) from (303.15 to 333.15)K. J Chem Eng Data. 2012;57:1095-103.

[5] Weiland RH, Dingman JC, Benjamin D, Browning GJ. Density and viscosity of some partially carbonated aqueous alkanolamine solutions and their blends. J Chem Eng Data. 1998;43:378-82.

[6] Hartono A, Mba EO, Svendsen HF. Physical properties of partially CO2 loaded aqueous monoethanolamine (MEA). J Chem Eng Data. 2014;59:1808-16.

[7] Amundsen TG, Øi LE, Eimer DA. Density and viscosity of monoethanolamine+water+carbon dioxide from (25 to 80)C. J Chem Eng Data. 2009;54:3096-100.

[8] Matin NS, Remias JE, Liu K. Application of electrolyte-NRTL model for prediction of the viscosity of carbon dioxide loaded aqueous amine solutions Ind Eng Chem Res. 2013;52:16979-84.

[9] Lv B, Guo B, Zhou Z, Jing G. Mechanism of CO2 capture into monoethanolamine solution with different CO2 loading during absorption/desorption processes. Environ Sci Technol. 2015;49:10728-35.

Article M

Model Uncertainty of interfacial area and mass transfer coefficients in absorption column packings.

Model Uncertainty of Interfacial Area and Mass Transfer Coefficients in Absorption Column Packings

Sumudu S. Karunarathne [1]   Dag A. Eimer [2]   Lars Erik Øi [1]

[1]Department of Process, Energy and Environmental Technology, University College of Southeast Norway,
{Sumudu.Karunarathne,Lars.Oi}@usn.no
[2]Tel-Tek, Norway, dag.a.eimer@tel-tek.no

Abstract

Uncertainty in model input parameters propagates through the model to make model output imprecision. Here, mathematical models used to calculate interfacial area and mass transfer coefficient for both random and structured packing in a packed bed absorption column was studied to investigate the propagation of model input parameters of viscosity, density and surface tension through the models. Monte Carlo simulation was used to examine the uncertainty propagation, and expectation $E(Y)$ and standard deviation σ for the model output values were determined. This study reveals $\pm5\%$ model output uncertainty for mass transfer coefficient and $\pm3.7\%$ uncertainty for interfacial area for the Onda, Bravo and Fair models used in random packings. Further, the analysis predicts $\pm1.3\%$ of uncertainty for interfacial area and $\pm0.8\%$ of uncertainty for mass transfer coefficient for the Rocha's correlations used in structured packings.

Keywords: uncertainty, absorption, mass transfer, interfacial area

1   Introduction

A mathematical model is a simplified version of a complex phenomenon in which assumptions are made during the model derivation to formulate the relations between parameters through mathematical equations. When input data are not precise, this leads to imprecise output results from the model. It is vital to quantify the uncertainty in model output to acquire an understanding about how accurate the estimated values through models. Generally, uncertainties are described by a probability distribution (Loucks *et al*, 2005).

Uncertainty of a model output is a result of both uncertain model structure and parameter values (Loucks *et al*, 2005). In model structure uncertainty, the errors in the model structure compared to the real system, assumptions and numerical approximations in simulation caused to create uncertainty in model output. The uncertain estimates of model parameters also make the model output uncertain. It is difficult to estimate the model structure uncertainty compared to model uncertainty caused by the parameter value. Increase of precision in model parameters can reduce the parameter uncertainty but it does not mean that predictions are accurate.

The analysis of model uncertainty is useful in many scientific applications. Krewski *et al,* (1995) performed an uncertainty analysis on physiological models using Monte Carlo Simulation. In this study, most of the model parameters were assumed to have a nature of the doubly truncated normal distribution. Spek *et al,* (2016) discussed improving uncertainty evaluation of process models in CO_2 capture by using pedigree analysis. A study on investigating the effect of process uncertainty on the optimal design of a CO_2 capture plant was done by Bahakim and Ricardez-Sandoval, (2014). The intention was to find the most economically feasible design for process equipment and acquire optimal operating conditions under uncertain conditions. Mathias and Gilmartin, (2014) evaluated the effect of uncertainty in property models on the simulated performance of solvent-based CO_2 capture process.

Gas absorption is a frequently used unit operation in gas treating processes. Packed bed absorption columns are made of either random or structured packing materials. The mass transfer coefficient and the interfacial area are the most important parameters involved with efficiency of packing materials. There have been many attempts to make mathematical models to evaluate both mass transfer coefficient and interfacial area for the both packing materials. Physical properties of viscosity, density and surface tension have an influence on the mass transfer coefficient. Uncertainties of those physical properties propagate through the mass transfer and interfacial area models to make the uncertain model output.

In this study, model uncertainty $U(Y/X)$ analysis was performed to investigate the input uncertainty propagation of a selected amine through the mass transfer and interfacial area models of the packed bed. The mass transfer coefficient and interfacial area of random packings are calculated by Onda, Bravo and Fair's models (Onda *et al*, 1967, Bravo and Fair, 1982). Rocha's correlations are used to calculate the mass transfer coefficient of structured packings including sheet metal packing (Rocha *et al*, 1996). The uncertainties related to measurements and predictions of physical properties were considered as the input uncertainties in Gaussian probability distributions.

2 Theory

In the field of gas treating, various mathematical models are available to calculate desired physical properties in the absorption process. Calculation of gas and liquid side mass transfer coefficients and interfacial area of packed beds have been highly concerned in many research works. Several mathematical models were built to approximate those properties using physical properties of an absorbent such as density, viscosity and surface tension. Most of the available models are based on either two-film theory or penetration theory with some reasonable assumptions (Wang *et al*, 2005).

The model developed by Onda, Bravo and Fair (Onda *et al*, 1967, Wang *et al*, 2005) is widely used to determine the gas and liquid side mass transfer coefficients of random packings. The model is given as,

For the gas side mass transfer coefficient,

$$k_G = c \left(\frac{D_G}{a_p d_p^2} \right) \left(\frac{\rho_G u_G}{a_p \mu_G} \right)^{0.7} Sc_G^{\frac{1}{3}} \tag{1}$$

For the liquid side,

$$k_L = \frac{0.0051}{\left(a_p d_p\right)^{-0.4}} \left(\frac{\mu_L g}{\rho_L} \right)^{\frac{1}{3}} \left(\frac{\rho_L u_L}{a_e \mu_L} \right)^{\frac{2}{3}} Sc_L^{-0.5} \tag{2}$$

The interfacial area can be determined by,

$$\frac{a_e}{a_p} = 1 - \exp\left[-1.45 \left(\frac{\sigma_c}{\sigma_L} \right)^{0.75} Re_L^{0.1} Fr_L^{-0.05} We_L^{0.2} \right] \tag{3}$$

For this study, Rocha's correlations were considered for structured packing (Rocha *et al*, 1996).

$$k_G = 0.054 \frac{D_G}{s} \left[\frac{\rho_G s (u_{Le} + u_{Ge})}{\mu_G} \right]^{0.8} Sc_G^{0.33} \tag{4}$$

$$k_L = 2 \sqrt{\frac{0.9 D_L u_{Le}}{\pi s}} \tag{5}$$

Where $u_{Ge} = \dfrac{u_G}{\varepsilon (1 - h_L) \sin \alpha}$ (6)

And $u_{Le} = \dfrac{u_L}{\varepsilon h_L \sin \alpha}$ (7)

The interfacial area is determined by

$$\frac{a_e}{a_p} = F_{SE} \frac{29.12 (We_L Fr_L)^{0.15} S^{0.359}}{Re_L^{0.2} \varepsilon^{0.6} (1 - 0.93 \cos(\theta))(\sin(\alpha))^{0.3}} \tag{8}$$

For the models mentioned, physical properties of density, viscosity and surface tension in amines were considered as input parameters and the uncertainty associated with these parameters were taken into account for the examination of model uncertainty. This analysis mainly focuses on the evaluation of parameter uncertainty of the models and uncertainty due to models structure will not be discussed here.

Physical properties can be determined by laboratory experiments. In addition to that, it can be determined by models, created using experimental data. Both approaches deal with some level of uncertainty. Eventually, the physical properties are needed to be presented with an uncertainty to get an idea about the level of accuracy. Table 1 lists some measurement uncertainty of viscosity, density and surface tension of different amines.

Guide to the expression of uncertainty in measurement (GUM) (JCGM, 2011) discussed the way of distributions propagate in mutually independent inputs through a model. *Figure* 1 illustrates the concept of propagation of distribution through a model. The assigned probability distribution function (PDF) for the inputs are represented as $g_{X_i}(\xi_i)$ and model output Y is characterized by joint PDF $g_Y(\eta)$.

During the model validation, the physical properties predictions are compared with the measured values to observe the model predictability. It gives information about deviation between model predictions and actual values. This also can be considered as a model uncertainty and it contains many uncertainty sources. Onda's correlations for liquid-phase mass transfer fulfill $\pm 20\%$ of agreement with the large amount of data on organic liquids and water (Potnis and Lenz, 1996).

Table 1. Measurement Uncertainty of physical properties

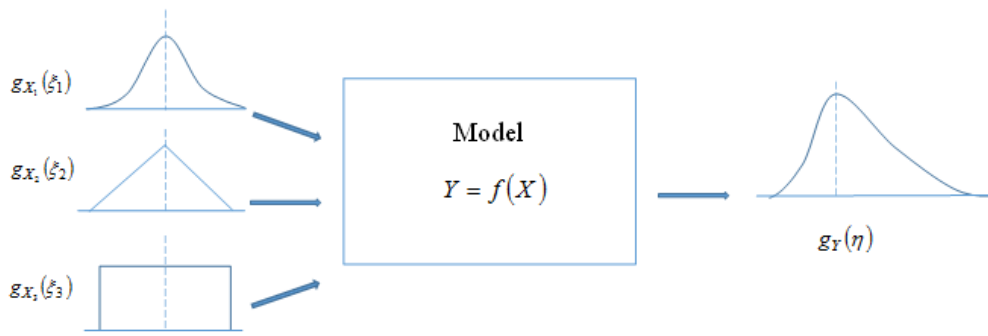| *Property*	*Uncertainty*
Viscosity	$\pm$ 0.015 mPa·s (95% confident level, k=2) (Arachchige *et al*, 2013)
	$\pm$ 0.12 mPa·s (95% confident level, k=2) (Sobrino *et al*, 2016)
Density	$\pm$ 4.42 kg/m^3 (95% confident level, k=2)(CO$_2$ loaded solution) (Jayarathna *et al*, 2013)
	$\pm$0.05 kg/m^3 (Standard uncertainty) (CO$_2$ loaded solution) (Amundsen *et al*, 2009)
Surface tension	$\pm$ 0.02 mN/m (accuracy) (Vazquez *et al*, 1997)
	$\pm$ 1.2 mN/m (95% confident level, k=2) (Jayarathna *et al*, 2013)

Figure 1. Illustration of the propagation of distribution (JCGM, 2011)

Nookuea *et al*, (2016) summarized possible uncertainty ranges for different properties of gas and liquid CO_2 mixtures and a sensitivity analysis was done considering ±20% deviation of physical properties to investigate their impact on the design of an absorber.

The standard uncertainty in Y due to uncertainty in X

$$U(Y) = \sqrt{Var(Y)} \qquad (9)$$

$$RU(Y) = \frac{\sqrt{Var(Y)}}{E(Y)} \times 100\% \qquad (10)$$

The standard uncertainty in Y due to uncertainty in X_j is $U(Y \setminus X_j)$

Then the relative uncertainty is defined as

$$RU(Y \setminus X_j) = \frac{U(Y \setminus X_j)}{E(Y)} \times 100\% \qquad (11)$$

3 Methodology

In this study, CO_2 absorption into 30% (by weight) monoethanol amine was considered as the physical process. It was assumed that the uncertainty of the physical properties has a Gaussian distribution. Experimentally measured values of viscosity, density and surface tension of monoethanol amine with standard uncertainty ±5 % at 313.15 K were considered as model input parameters and Monte Carlo techniques were used to estimate uncertainty for the liquid side mass transfer coefficient and interfacial area of the packing materials. Simulations were performed in MATLAB environment and a built-in random number generator was used to generate values from Gaussian distribution for the input properties within the considered uncertainty levels. Table 2 shows the values for the considered inputs with uncertainties.

For the random packings, Ceramic Raschig Rings (25mm) and for the structured packings, Sulzer BX

(Gauze) packing were selected for this study. The diffusion coefficients of CO_2 (m^2/s) in gas and liquid are 1.70×10^{-5} and 2.82×10^{-9} respectively (Eimer, 2014). The gas and liquid flow rates were assumed as 1.7 $kg/m^2 \cdot s$ and 1.85 $kg/m^2 \cdot s$.

Table 2. Input parameter values and uncertainties

Parameter	Value	Uncertainty
Viscosity	1.628 mPa· s	± 0.0814 mPa· s
Density	1003.3 kg/m³	± 50.165 kg/m³
Surface tension	0.0624 N/m	± 0.00312 N/m

4 Results

Initially, all the input parameters were considered together to evaluate uncertainty propagation through the model. The model of interfacial area (Eq (3)) for random packing was considered first and the model output was described using a histogram. Subsequently, the uncertainty predicted for interfacial area was used for the uncertainty evaluation of liquid side mass transfer coefficient from Eq (2). *Figure* 2 illustrates a histogram of values obtained for the interfacial area of random packing.
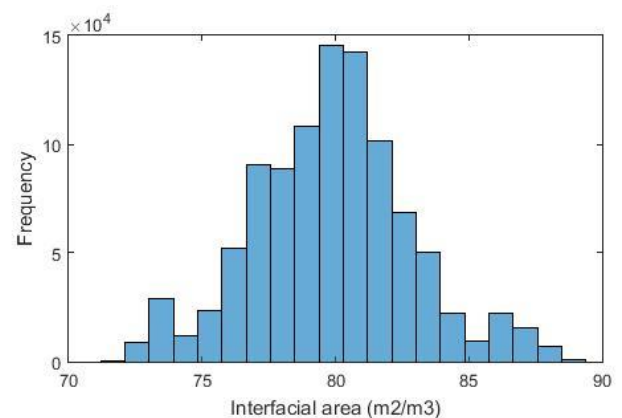
Figure 2. Histogram of interfacial area of random packing

Figure 3 shows the variation occurred for the liquid side mass transfer coefficient under considered input

uncertainty. Table 3 summarized the calculated expectation and standard deviation for both interfacial area and mass transfer coefficient of Onda, Bravo and Fair's correlations.
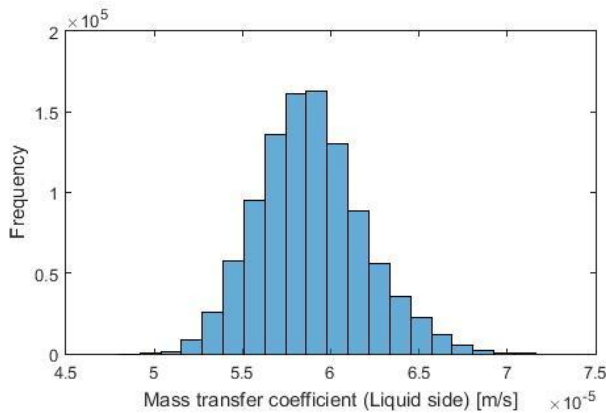

Figure 3. Histogram of mass transfer coefficient (liquid side) of random packing

Table 3. Estimated expectation and standard deviation for the random packings

Model	Expectation $E(x)$	Standard deviation (σ)
Interfacial area	79.88 m^2/m^3	2.97 m^2/m^3
Mass transfer coefficient	5.9x10^{-5} m/s	2.97x10^{-06} m/s

Similarly, for the structured packing, *Figure* 4 shows a histogram created from the values obtained for the interfacial area of structured packing.
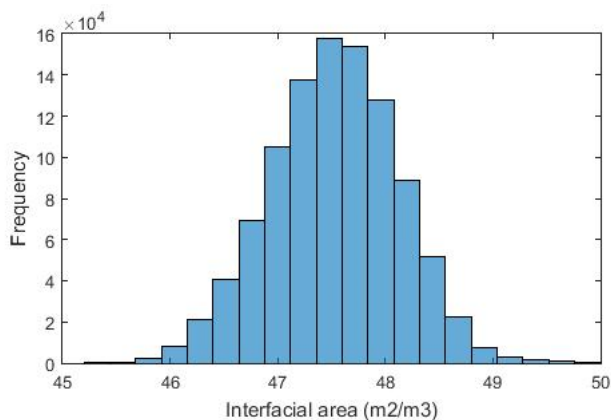
Figure 4. Histogram of interfacial area of structured packing
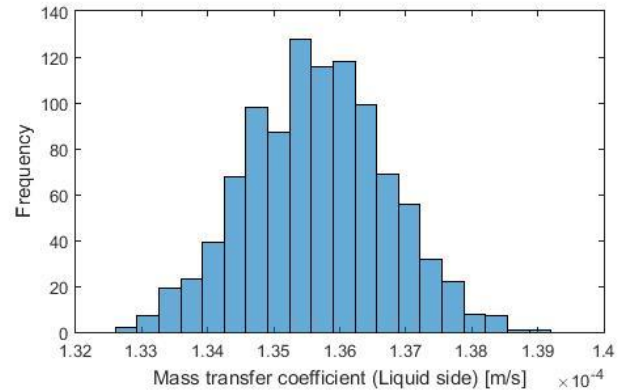
Figure 5. Histogram of mass transfer coefficient (liquid side) of structured packing

Simulation results on mass transfer coefficient (liquid side) of structured packing are shown in *Figure* 5. Calculated expectation and standard deviation for the interfacial area and mass transfer coefficient of Rocha's correlations under Sulzer BX (Gauze) packing is listed in Table 4.

Table 4. Estimated expectation and standard deviation for the structured packings

Model	Expectation $E(x)$	Standard deviation (σ)
Interfacial area	47.5 m^2/m^3	0.6 m^2/m^3
Mass transfer coefficient	1.36x10^{-04} m/s	1.04x10^{-06} m/s

Results reveal the propagation of uncertainty in model parameters through the mathematical model. This method only addresses the parameter uncertainty and uncertainty due to the model structure is not discussed here.

The relative uncertainty of the parameters uncertainty was evaluated according to the Eq (10). It shows ±3.7% of uncertainty for interfacial area and ±5% of uncertainty for mass transfer coefficient for the random packing. Similarly for the structured packings, ±1.3% of uncertainty for interfacial area and ±0.8% of uncertainty for mass transfer coefficient.

One advantage of performing this analysis is being able to estimate the relative impacts of input parameter uncertainties. This relative effect of uncertain parameters (viscosity, density and surface tension) were considered individually in uncertainty analysis. Estimated expectations and standard deviations due to the relative parameters in Onda, Bravo and Fair's correlation for random packings are shown in Table 5.
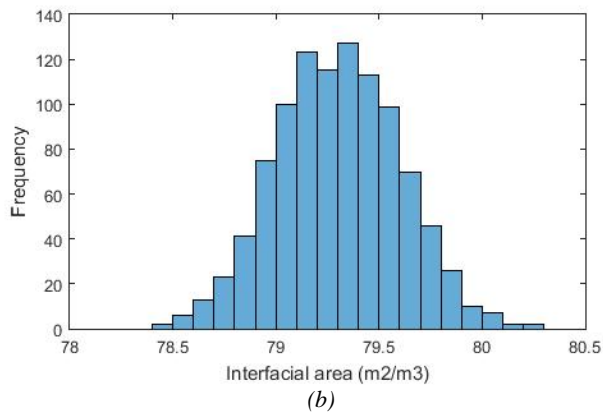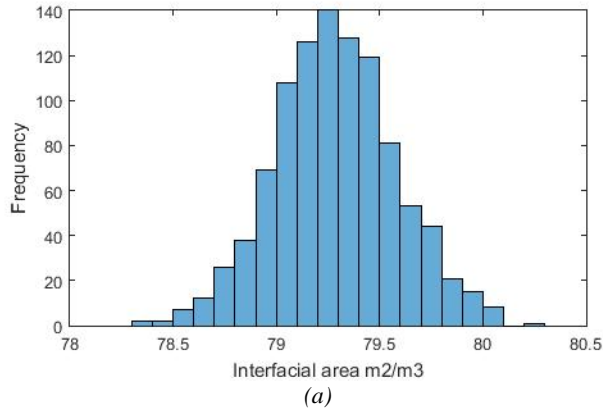
(a)

(b)

(c)
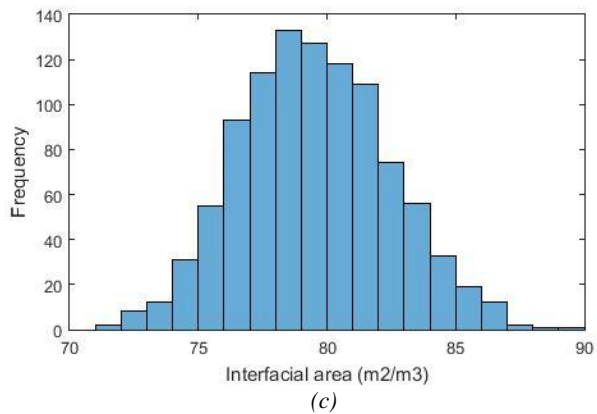
Figure 6. Histogram of the interfacial area under relative parameter uncertainty. (*a,b,c* for interfacial area due to viscosity, density and surface tension respectively)

Table 5. Estimated expectations and standard deviations due to the relative parameters. a_e (m²/m³), k_L (m/s)

		Viscosity	Density	Surface tension
a_e	E(Y/X$_j$)	79.3	79.3	79.5
	σ(Y/X$_j$)	0.3	0.3	2.9
k_L	E(Y/X$_j$)	5.9x10⁻⁵	5.9x10⁻⁵	5.9 x10⁻⁵
	σ(Y/X$_j$)	2.42x10⁻⁶	0.5x10⁻⁶	1.36x10⁻⁶

The relative uncertainty $RU(Y\backslash X_j)$ of the effect created by individual model parameters are shown in Table 6. Uncertainties were estimated for random packings under same input parameter uncertainties as shown in Table 2. The histogram created from model outputs

within the study of the effect of individual parameter uncertainty are shown in *figure* 6 and 7.

Table 6. The relative uncertainty $RU(Y\backslash X_j)$ of the effect created by individual model parameters

Parameter	Model	
	Mass transfer coefficient k_L	*Interfacial area* a_e
Viscosity	± 4.1%	± 0.38%
Density	± 0.85%	± 0.38%
Surface tension	± 2.3%	± 3.65%

(a)

(b)

(c)
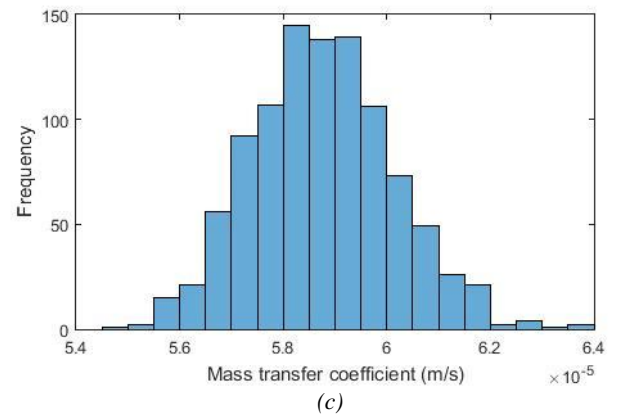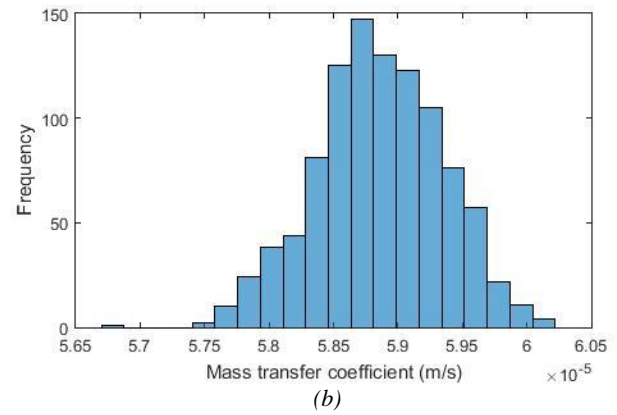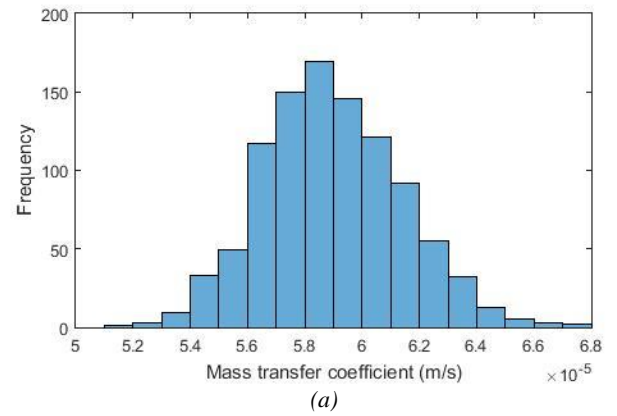
Figure 7. Histogram of the mass transfer coefficient under relative parameter uncertainty. (*a,b,c* for mass transfer coefficient due to viscosity, density and surface tension respectively)

The effect of individual parameters on parameter uncertainty of the model was compared. Uncertainty of surface tension has a major impact on interfacial area as shown in the results. Viscosity and density have a minor effect in interfacial area. For the mass transfer coefficient, viscosity shows a significant influence in model uncertainty. There, density and surface tension has minor effects.

5   Conclusion

Monte Carlo simulation was used to examine uncertainty propagation of model input parameters of viscosity, density and surface tension on the interfacial area and mass transfer coefficients in random and structured packings.

Overall uncertainty of model output gives information about how the model behaves under random behavior of all the input parameters. This study reveals ±5% model output uncertainty for mass transfer coefficient and ±3.7% uncertainty for interfacial area for the Onda, Bravo and Fair models used in random packings. Further, the analysis predicts ±1.3% of uncertainty for interfacial area and ±0.8% of uncertainty for mass transfer coefficient for the Rocha's correlations used in structured packings.

The relative impact of individual parameters predicts the model sensitivity and individual uncertainty contribution. Uncertainty in surface tension has a significant effect on the uncertainty of interfacial area in random packings that is ±3.65%. According to the considered correlations on random packing, the uncertainty of interfacial area can be reduced by reducing the imprecision of surface tension. Mass transfer coefficient gets a greater influence from viscosity with ±4.1%. Precise input parameter values on viscosity enhance the precision of the mass transfer coefficient.

Nomenclature

a_e	Effective specific interfacial area, (m^2/m^3)
a_p	Packing specific surface area, (m^2/m^3)
c	Packing-specific constant
D	Diffusion constant, m^2/s
d_p	Particle diameter, m
F_{SE}	Packing surface enhancement factor
Fr	Froude number
g	Gravitational acceleration, m/s^2
h_L	Liquid holdup m^3/m^3
k	Mass transfer coefficient, m/s
s	Corrugation side length, m
Sc	Schmidt number
u	Superficial velocity, m/s
We	Weber number

Greek letters

α	Corrugation inclination angle, deg
ε	Void fraction of packing
θ	Contact angle between liquid and surface
μ	Viscosity, Pa· s
ρ	Density, kg/m^3
σ	Surface tension, N/m

Subscripts

G	Gas
L	Liquid
e	Effective
c	Critical

References

D. Krewski, Y. Wang, S. Bartlett and K. Krishnan. Uncertainty, variability, and sensitivity analysis in physiological pharmacokinetic models. *Journal of Biopharmaceutical Statistics,* 5**:** 245-271, 1995.

D. P. Loucks, E. V. Beek, J. R. Stedinger, J. P. M. Dijkman and M. T. Villars. Water resources systems planning and management: An introduction to methods, models and applications. *UNESCO*, 2005.

D. Eimer. *Gas Treating* John Wiley & Sons, Ltd, 2014.

G. Vazquez, E. Alvarez, J. Navaza, R. Rendo and E. Romero. Surface tension of binary mixtures of water + monoethanolamine and water + 2-amino-2-methyl-1-propanol and tertiary mixtures of these amines with water from 25 °c to 50 °c. *Journal of Chemical & Engineering Data,* 42**:** 57-59, 1997.

G. Wang, X. Yuan and K. Yu. Review of mass-transfer correlation for packed column. *Ind.Eng.Chem.Res,* 44**:** 8715-8729, 2005.

J. A. Rocha, J. Bravo and J. Fair. Distillation Columns Containing Structured Packings: A comprehensive model for their performance. 2. mass-transfer model. *Americal Chemical Society*, 1660-1667, 1996.

JCGM. Evaluation of measurement data – supplement 2 to the "guide to the expression of uncertainty in measurement" – extension to any number of output quantities. *JCGM 102:2011.*

J. L. Bravo and J. R. Fair. Generalized correlation for mass transfer in packed distillation columns. *Ind. Eng. Chem. Process Des. Dev,* 21: 162-170, 1982.

K. Onda, E. Sada and H. Takeuchi. Gas absorption with chemical reaction in packed columns. *Journal of Chemical Engineering of Japan***,** 62-66, 1967.

M. Spek, A. Ramirez and A. Faaij. Improving uncertainty evaluation of process models by using pedigree analysis. a

case study on co$_2$ capture with monoethanolamine. *Computers and Chemical Engineering,* 85**:** 1-15, 2016.

M. Sobrino, E. Concepcion, A. Hernandez and M. Martin. Viscosity and density measurements of aqueous amines at high pressures: mdea-water and mea-water mixtures for co$_2$ capture. *J.Chem.Thermodynamics,* 98**,** 231-241, 2016.

P. Mathias and J. Gilmartin. Quantitative evaluation of the effect of uncertainty in property models on the simulated performance of solvent-based co$_2$ capture. *Energy Procedia : GHGT-12,* 63**:** 1171-1185, 2014.

S. Bahakim and L. Ricardez-Sandoval. Optimul steady-state design of a post-combustion co$_2$ capture plant under uncertainty. *Energy Procedia,* 63**:** 1608-1616, 2014.

S. Jayarathna, A. Weerasooriya, S. Dayarathna, D. Eimer and M. Melaaen. Densities and surface tensions of co$_2$ loaded aqueous monoethanolamine solutions with r = (0.2 to 0.7) at t = (303.15 to 333.15) k. *Journal of Chemical & Engineering Data,* 58**:** 986-992, 2013.

S. Potnis and T. lenz. Dimensionless mass-transfer correlations for packed-bed liquid desiccant contactors. *Americal Chemical Society***,** 4185-4193, 1996.

T. Amundsen, L. Øi and D. Eimer. Density and viscosity of monoethanolamine+water+carbon dioxide from (25 to 80) ^{0}c. *Journal of Chemical & Engineering Data,* 54**:** 3096-3100, 2009.

U. Arachchige, N. Aryal, D. Eimer and M. Melaaen. Viscosities of pure and aqueous solutions of monoethanolamine (mea), diethanolamine (dea) and n-methyldiethanolamine (mdea). *Annual Transaction of the Nordic Rheology Society,* 21**:** 299-306, 2013.

W. Nookuea, Y. Tan, H. Li, E. Thorin and J. Yan. Impact of thermo-physical properties of gas and liquid phases on design of absorber for CO$_2$ capture using monoethanolamine. *International Journal of Greenhouse Gas Control,* 52**:** 190-200, 2016.

Article N

Evaluation of systematic error and uncertainty of viscosity measurements of mixtures of monoethanol amine and water in coaxial cylinder rheometers

Evaluation of Systematic Error and Uncertainty of Viscosity Measurements of Mixtures of Monoethanol Amine and Water in Coaxial Cylinder Rheometers

Sumudu S. Karunarathne, Dag A. Eimer, and Lars E. Øi

Abstract—In this study, the use of coaxial cylinder viscometer in viscosity measurements of monoethanol amine and water mixture is discussed. Random and systematic effects engage with the rheometer lead to deviate the measured quantity from its actual value. Compensation for the systematic effect is called as the bias and this compensation can not be done perfectly. The measurement uncertainty arises due to the lack of exact knowledge on what is being measured. Identification of uncertainty sources is vital in uncertainty analysis to evaluate the total uncertainty of a measuring technique. The calculated expanded (k=2) uncertainty of viscosity measurement of an alkanol amine and water mixture using a coaxial cylinder viscometer in this work is 0.0162 mPa s. Further, the viscosities of mixtures of monoethanol amine and water mixtures under temperature 20-130 °C are measured. This is the normal temperature range for a traditional amine based CO_2 capture process. Viscosity deviations are modeled according to Redlich-Kister type correlation and parameters are found through a regression analysis.

Index Terms — Viscosity, systematic error, uncertainty, MEA.

I. INTRODUCTION

Accurate measurement of viscosity in amine solutions is necessary for various aspects of gas treatment. Measurement of liquid viscosity is useful to determine flow behaviors and gas-liquid mass and heat transfer coefficients. Various viscometers are available to measure fluid viscosity with different measuring techniques. Capillary and coaxial cylinder type viscometers are widely used to measure fluid viscosity and coaxial cylinder viscometers are available in several geometries.

The uncertainty associated with viscosity measurements depends on many factors, which are engaged with the method that is used. Rheometer calibration provides valuable information about the systematic error of the instrument. The viscosity of a standard oil is measured and checked with the standard viscosities provided by the rheometer manufacturer to check for any kind of deviation between measured and standard viscosity. This difference is simply known as the error of the instrument and it can be further specified as a combination of both random and systematic errors in the instrument. Random errors are caused by unpredictable and unknown changes in the experiment. Changes can happen in

the measuring instrument or environment conditions. Gaussian distribution is often used to describe the nature of the random error. Systematic errors generally appear from the measuring instruments. In the instrument, systematic errors are present due to several reasons as poor calibration of the instrument, observational factors, environmental factors and use of simplified models and approximations. This error can be identified and reduced through careful analysis of the possible sources of systematic error.

Laun *et al.* [1] provided guidelines for checking performance and verifying the accuracy of rotational rheometers. Functional relations of viscosity with torque and angular speed for several types of rotational rheometers are also listed. Marvin [2] performed a study to investigate the systematic error of capillary type rheometer that was used for the viscosity measurement of water. Bringas *et al.* [3] discuss a calibration method for a new type of rheometer having a shaft with an uneven geometry. For the measurement uncertainty, Arachchige *et al.* [4] have calculated the combined uncertainty for the MCR 101 Anton Paar double-gap rheometer as 0.015 mPa s for the monoethanol amine (MEA) solutions. Hartono et al. [5] reported a value for the combined uncertainty for both CO_2 loaded and unloaded MEA solutions as 0.007 mPa s for the Anton Paar MCR 100 rheometer. Amundsen *et al.* [6] estimated the measurement uncertainty of 0.01 mPa s for all viscosity measurements of MEA solutions.

In this study, a coaxial cylinder type rheometer placed in the CO_2 laboratory in University college of Southeast Norway was examined to analyze the measurement errors during the viscosity measurements of mixtures of MEA and water. Experiments were performed to measure the viscosity of MEA, water mixture under MEA concentration from 20 % to 50 % by weight for the temperature range of 20 °C to 130 °C. The uncertainty of the viscosity measurement was determined according to the guidelines provided by GUM (Guide to the expression of uncertainty in measurement) [7].

II. METHOD

A. Random, Systematic Error of the Instrument

Random and systematic errors of the instrument were examined through several viscosity measurements on a standard fluid. The viscosities of a standard fluid (calibration viscosities) were compared with measured viscosities of the same fluid through the rheometer under different temperatures as provided by the manufacturer. The viscosity of the standard fluid was measured several times to observe the consistency of the error. Further, measurement errors were predicted for the other temperatures through a regression

analysis. The temperature range between 20 °C and 130 °C is the normal temperature range for a traditional amine based CO_2 capture process. Predicted values were used to correct the viscosity measurements of MEA and water mixtures without CO_2.

B. Uncertainty of Viscosity Measurement

The uncertainty of viscosity measurements signifies the quality of the measurement. It indirectly evaluates the measuring technique and is useful to improve the measurements. QUAM (Quantifying Uncertainty in Analytical Measurement) suggested some typical uncertainty sources that can be involved in a measuring process [8]. A cause and effect diagram is a graphical interpretation of uncertainty sources and it shows how individual uncertainties direct into a combined uncertainty. GUM provides guidance to evaluate the uncertainty of a measuring system [7].

The functional relationship between a measured quantity $x = \{x_i\}$ (the input) and the measurement result y (the output) can be shown as [7].

$$y = f(x) \tag{1}$$

$$u^2(y) = \sum_{i=1}^{n} \sum_{j=1}^{n} \frac{\partial f}{\partial x_i} \frac{\partial f}{\partial x_j} u(x_i, x_j) \tag{2}$$

where, $\partial f / \partial x_i$ and $u(x_i, x_j)$ are the sensitivity coefficient and the covariance of x_i and x_j respectively. There, $u(x_i, x_i) = u^2(x_i)$ is the variance of x_i.

C. Model for a Coaxial Cylinder Rheometer

A mathematical model is useful to understand the parameter that involves calculating the viscosity of the liquid in a coaxial cylinder rheometer. It is also helpful to identify the uncertainty sources in the uncertainty analysis. In the rheometer, there are two fluid compartments and the central cup rotates with a certain angular velocity. Fig. 1 shows the velocity profile of the liquids near the fixed and rotating boundaries.

Fluid behaviour can be illustrated by three differential equations in cylindrical coordinates [9].

$$-\frac{\rho v_\vartheta^2}{r} = -\frac{\partial p}{\partial r} \tag{3}$$

$$-\frac{1}{r^2} \frac{\partial}{\partial r} \left[r^2 \tau_{r\vartheta} \right] = 0 \tag{4}$$

$$-\frac{\partial p}{\partial z} = \rho g \tag{5}$$

where ρ is density, τ is shear stress, v is velocity and r is radius. Consider $r = kR$

R is the radius of inner fixed cylinder

$$k_1 = \frac{R_1}{R}, \ k_2 = \frac{R_2}{R} \text{ and } k_3 = \frac{R_3}{R}$$

Boundary conditions of the fluid flow in coaxial cylinder rheometer is summarized in Table I.

T ABLE I: BOUNDARY CONDITION

Inner region : $1 < k < k_1$		Outer region : $k_2 < k < k_3$	
Boundary condition	Velocity	Boundary condition	Velocity
$r = R$	$v_\vartheta = 0$	$r = k_2 R$	$v_\vartheta = \omega k_2 R$
$r = k_1 R$	$v_\vartheta = \omega k_1 R$	$r = k_3 R$	$v_\vartheta = 0$

Then, torque provided by the motor can be found as

$$T = 4\pi \mu L \varpi R^2 \left(\frac{k_1^2}{k_1^2 - 1} + \frac{k_2^2 k_3^2}{k_3^2 - k_2^2} \right) \tag{6}$$

Here, T is torque, μ is viscosity, L is the liquid height and ω is angular velocity
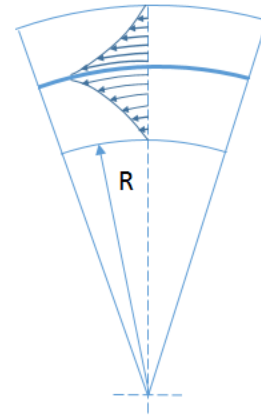

Fig. 1. Velocity profile of fluid in the coaxial cylinder.

Then the viscosity can be determined as shown in (7) and later it is used for the evaluation of measurement uncertainty of viscosity.

$$\mu = \frac{T}{4\pi L \varpi R^2 \left(\frac{k_1^2}{k_1^2 - 1} + \frac{k_2^2 k_3^2}{k_3^2 - k_2^2} \right)} \tag{7}$$

D. Viscosity of MEA, Water Mixtures

A series of experiments was performed to determine the viscosity of MEA and water mixtures at a temperature range of 20 °C to 130 °C. The MEA content of the mixture varied from 20% to 50% (wt%). The calculated instrument error and uncertainty were used to present the measured data to enhance the accuracy of the measurements.

In experiments, the viscosity was measured using Physica MCR 101 rheometer supplied by Anton Paar. MEA with assay $\geq 99.5\%$ provided by the ALDRICH was used for the sample preparation. Both MEA and water were degassed using Buchi R-210 Rotavapor, evaporator to remove dissolved gases in the liquids. Liquids were weighed using an analytical balance, model XS403S from Mettler Toledo. A sample of 7 ml MEA / water mixture was measured and transferred into the rheometer for measurements. The numbers in Table AI are average values of three original measurements.

III. RESULTS

A. Systematic Error

The calibration fluid from Paragon scientific has been used to examine the measurement error of the instrument. Three calibration tests were performed at the beginning, middle and end of viscosity measurements of monoethanol amine and water mixtures. The results of the calibration test were compared with standard viscosities of calibration fluid to calculate instrument error at different temperatures. These experiments showed that the instrument error is not constant and it was concluded to perform several calibration tests to determine instrument error during the viscosity measurements of monoethanol amines. Fig. 2 shows the average values of the instrument error considering three different calibration tests.

In order to present the measured viscosities, a single value for the instrument error is needed to be calculated. The effective way to do it is to get the average value of instrument error for the measured temperature range. It also leads to eliminate the random error and systematic error will remain unchanged. Then, polynomial regression was performed on averaged errors to find a better relation to predicting instrument error for unknown temperatures. Fig. 2 shows the 4th order polynomial fit for the instrument errors obtained through calibration tests.
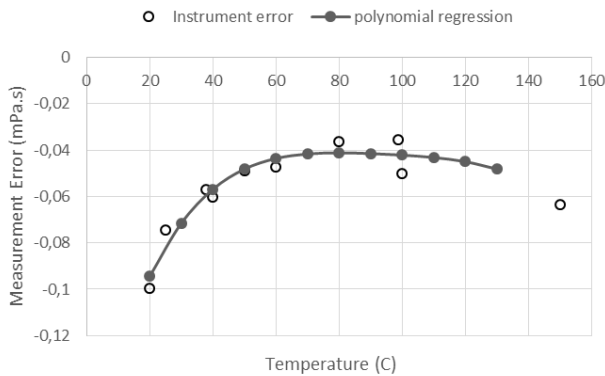
Fig. 2. Error in viscosity measurement of standard liquid.

Consequently, the measured viscosities of MEA and water mixtures were adjusted according to the evaluated instrument error.

Parameters of the mathematical model (8) for the calibration viscosities were obtained through a regression analysis to compare with the measured viscosities of standard fluid with predicted measurement errors for the temperature range of 20-130 °C. The estimated values of the coefficients of (8) are shown in Table II.

$$ln(\mu) = a + \frac{b}{T-c} \qquad (8)$$

where, μ is viscosity (mPa s), T is temperature (K) and a, b and c are coefficients [4].

TABLE II: ESTIMATED PARAMETERS OF THE EQUATION

Parameter	Values
a	-3.298
b	834.1
c	112

B. Uncertainty

The mathematical relation shown in (7) provides the relation between liquid viscosity with torque, angular speed, level of liquid fill and radius. In the experiments, a certain measured volume (7ml) of liquid is filled into the coaxial cylinder of the rheometer. The instrument provides the required torque to rotate the cup to maintain the shear rate at a desired level and the motor torque is measured. There are many uncertainty sources involved in viscosity measurements of amine solutions. A cause and effect diagram shown in Fig. 3 summarizes most of the uncertainty sources engaged in the experiment.
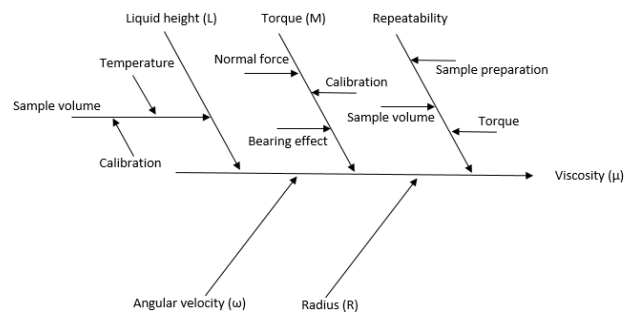

Fig. 3. Cause and effect diagram for uncertainties in viscosity measurements of a MEA / water mixture

The derived mathematical expression was used to identify the list of uncertainty sources. In addition to the parameters in the expression, there are some other parameters, which affect the measurement result but do not explicitly appear in the expression [8]. Those parameters are introduced as correction factors to the measurand. The following parameters have been identified as potential uncertainty sources but they are not included in the mathematical expression.

f_p: Purity of MEA
f_t: Temperature
f_w: Weight measurement
f_{rep}: Repeatability

Then the expanded equation for viscosity measurement of the coaxial cylinder rheometer with considered correction factors can be shown as

$$\mu = \frac{T}{4\pi L \varpi R^2 \left(\frac{k_1^2}{k_1^2 - 1} + \frac{k_2^2 k_3^2}{k_3^2 - k_2^2} \right)} f_p f_t f_w f_{rep} \qquad (9)$$

Combined uncertainty of the viscosity measurement was determined considering (9) as it covers most of the uncertainty sources in measuring. Kragten's approach [10] was used to estimate the sensitivity coefficient of combined uncertainty expression of (10).

$$u_c(\mu) = \sqrt{\left[\frac{\partial\mu}{\partial T}u(T)\right]^2 + \left[\frac{\partial\mu}{\partial\omega}u(\omega)\right]^2 + \left[\frac{\partial\mu}{\partial L}u(L)\right]^2 + \left[\frac{\partial\mu}{\partial R}u(R)\right]^2 + \left[\frac{\partial\mu}{\partial f_p}u(f_p)\right]^2 + \left[\frac{\partial\mu}{\partial f_t}u(f_t)\right]^2 + \left[\frac{\partial\mu}{\partial f_w}u(f_w)\right]^2 + \left[\frac{\partial\mu}{\partial f_{rep}}u(f_{rep})\right]^2} \quad (10)$$
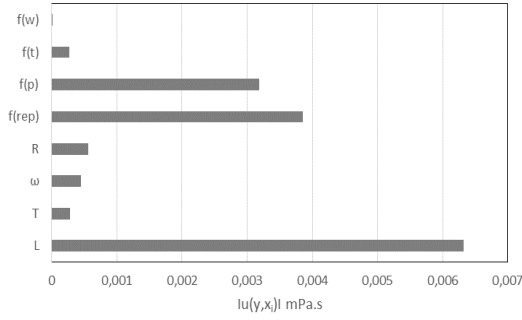

Fig. 4. Uncertainty contribution in viscosity measurements.

Fig. 4 shows the values obtained for the uncertainty sources. Thus, the calculated standard uncertainty of viscosity measurements in a coaxial cylinder rheometer is ± 0.0081 mPa s.

C. Viscosity of MEA (1) + Water (2) Mixtures

The corrected measured viscosities of aqueous MEA solutions from 20% to 50% of MEA in the temperature range of 20-130 °C are shown in Fig. 5 and the values are listed in Table AI. The measured viscosities through rheometer were corrected according to the instrument error that was found in section III *A*. The calibration test results are shown in Table AII.
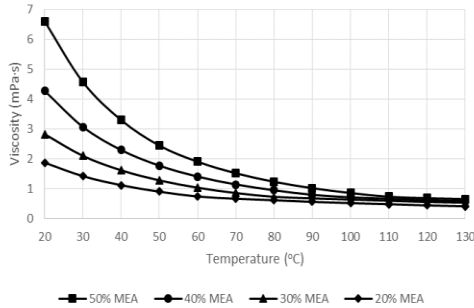

Fig. 5. Corrected viscosity vs Temperature in MEA and water mixtures.

The unloaded viscosity ($\mu_{unloaded}$) can be presented as the sum of "ideal" viscosity based on the weighted sum of solution component's pure viscosities and a viscosity deviation (μ_γ).

$$ln(\mu_{unloaded}) = ln(\mu_\gamma) + \sum_1^2 x_i ln\mu_i \quad (11)$$

Hartono *et al*. [5] suggested a simplified Redlich-Kister [11] type correlation to model the viscosity deviation as a function of temperature and concentration.

$$ln(\mu_\gamma) = (a_1 + a_2 T + a_3 T^2 + a_4 x_1)x_1 x_2 \quad (12)$$

where, (μ_i) represents viscosity of the pure liquid, x_i represents mole fraction and T (°C) represents the temperature. The

coefficients a_1, a_2, a_3 and a_4 are determined by a regression analysis on calculated viscosity deviation. The viscosities of pure solutions of MEA and water were obtained from Joseph *et al*. [12] and Udara *et al*. [4] respectively.

The calculated parameters for viscosity deviation are shown in Table III. The absolute average relative deviation (AARD) was calculated to examine the competence of model prediction and it was 6.2%. The parameters found in this study are in the same order of magnitude compared to the Hartono *et al*. [5].

TABLE III: PARAMETERS FOR THE VISCOSITY DEVIATION

MEA (mass %)	Temperature (°C)	Parameters (with 95% confidence)
20 to 50	20 to 130	a_1 [-]= 10.23 ±1.075
		a_2 [(°C)$^{-1}$]= -0.07747 ±0.02614
		a_3 [(°C)$^{-2}$]= (4.351 ±1.708) .10^{-4}
		a_4 [-]= -11.53 ±3.471

IV. DISCUSSION

The analysis of instrument error in the rheometer enhance the accuracy of the final viscosity measurements. The method discussed in section III *A* gives simple guidance to evaluate the random and systematic errors of rheometer in viscosity measurement of MEA solutions.

The AARD for the modeled and measured viscosities of the standard fluid was calculated to 0.7 % for the measured temperature range of 20-130 °C under 10 °C degrees increment. The final viscosity values of MEA solutions obtained through this work were compared with data available in the literature. The viscosities obtained in this study showed a good agreement (difference < 2%) with viscosity data presented by Hartono et al. [5] for low temperatures around 20 °C. The measured viscosities by Hartono et al. [5], Arachchige et al. [4] and Amundsen et al. [6] were compared using the correlation developed in section III *C*. Table IV summarizes the AARD of the model for different sources.

TABLE IV: AVERAGE ABSOLUTE RELATIVE DEVIATION OF THE MODEL FOR MEA SOLUTIONS

[MEA] (mass%)	Temperature (°C)	Source	AARD (%)
30	20-80	Hartono et al. (2014) [5]	4.2
20-50	20-80	Arachchige et al. (2013) [4]	5
20-50	25-80	Amundsen et al. (2009) [6]	4.2
20-50	20-130	This work	6.2

The AARD was found to be 4.2% for the viscosity predictions using this correlation and measured viscosity by Hartono et al. [5]. It is similar to the AARD of literature data and predictions from the original correlation proposed by Hartono et al. [5]. The AARD found in this study for the temperature range of (20-130 °C) is higher (6.2%). This is probably due to the higher temperature levels that the

viscosities were measured. Amundsen et al. [6] have stated that the higher temperatures increase the uncertainty.

The reported uncertainties for the viscosity measurement were compared with the uncertainty obtained through this study. The uncertainty calculated in this work showed a higher value compared to the reported measurement uncertainties in section I. The method discussed in section III *B* considered most of the possible uncertainty sources involved in the measurement method, which resulted in a higher value of combined uncertainty.

Currently, various researches have given attention to measuring physicochemical properties of different amine solutions. As a continuation of this study, the viscosity of CO_2 loaded MEA and other different amines will be measured and correlated to extend the range of measurement. The uncertainty of viscosity measurements in CO_2 loaded aqueous amine solutions also will be determined and validated using Monte Carlo simulation (MCS) method.

V. CONCLUSION

Both random and systematic errors have influenced on final viscosity measurements of MEA and water mixtures in the rheometer. Viscosity measurements on calibration fluid can be used to estimate the systematic error of the instrument. Random effects of the measurement error are reduced by taking multiple viscosity measurements on the calibration fluid.

A mathematical expression was obtained relating parameters involved in the viscosity measurements in the coaxial cylinder rheometer. It is useful to identify the uncertainty sources involved in the measurement method. The calculated expanded uncertainty (k=2) for the coaxial cylinder rheometer is 0.0162 mPa s.

The viscosity of MEA and water mixtures increases with the rise of MEA content in the mixture. In addition to that, the viscosity of MEA and water mixtures gradually decreased when the temperature of the mixture increased. The developed model for viscosity deviation was able to predict measured data with an AARD within 6.2%.

APPENDIX A

TABLE AI: CORRECTED VISCOSITY MEASUREMENTS OF MEA AND WATER MIXTURES

Temperature (^{o}C)	Viscosity (mPa s) at different MEA wt%			
	20 %	30 %	40 %	50 %
20	1.8819	2.8359	4.2851	6.6100
30	1.4308	2.1094	3.0801	4.5803
40	1.1286	1.6279	2.3052	3.3093
50	0.9122	1.2897	1.7821	2.4543
60	0.7503	1.0456	1.4168	1.9145
70	0.6749	0.8660	1.1541	1.5280
80	0.6252	0.7398	0.9604	1.2430
90	0.5697	0.6872	0.8077	1.0291
100	0.5294	0.6481	0.7232	0.8676
110	0.4919	0.6088	0.6742	0.7408
120	0.4521	0.5693	0.6285	0.6943
130	0.4226	0.5423	0.5991	0.6624

Uncertainty: $U(\mu) = \pm 0.0162$ mPa s (Level of confidence =0.95 where k=2)

TABLE AII: VISCOSITY OF THE STANDARD FLUID

Temperature (^{o}C)	Viscosity of Standard fluid (mPa s)	Measured Viscosity of Standard fluid (mPa s)
20	3.714	3.614247
25	3.267	3.192492
37.78	2.439	2.382142
40	2.327	2.266567
50	1.913	1.864058
60	1.603	1.555717
80	1.177	1.140617
98.89	0.918	0.882373
100	0.9065	0.856242
150	0.5365	0.472868

REFERENCES

[1] M. Laun *et al.*, "Guidelines for checking performance and verifying accuracy of rotational rheometers: Viscosity measurements in steady and oscillatory shear (IUPAC Technical Report)," *Pure Appl. Chem.*, vol. 86, no. 12, pp. 1945-1968, 2014.

[2] R. S. Marvin, "The accuracy of measurements of viscosity of liquids," *Journal Of Research at the National Bureau of Standards,* vol. 75A, no. 6, pp. 535-540, 1971.

[3] C. S. Bringas, W. K. Jeksrud, O. I. Lekang, and R. B. Schuller, "A calibration method for a new type of rheometer," *Annual Transactions of the Nordic Rheology Society,* vol. 14, 2006.

[4] U. S. P. R. Arachchige, N. Aryal, D. A. Eimer, and M. C. Melaaen, "Viscosities of pure and aqueous solutions of monoethanolamine (MEA), diethanolamine (DEA) and N-Methyldiethanolamine (MDEA)," *Annual Transactions of the Nordic Rheology Society* vol. 21, 2013.

[5] A. Hartono, E. O. Mba, and H. Svendsen, "Physical properties of partially CO2 loaded aqueous monoethanolamine (MEA)," *J. Chem. Eng,* vol. 59, pp. 1808-1816, 2014.

[6] T. G. Amundsen, L. E. Øi, and D. A. Eimer, "Density and viscosity of monoethanolamine + water + carbon dioxide from (25 to 80) C," *J.Chem.Eng.Data,* vol. 54, pp. 3096-3100, 2009.

[7] " Evaluation of measurement data — Guide to the expression of uncertainty in measurement," 2008.

[8] S. L. R. Ellison and A. Williams, "Quantifying uncertainty in analytical measurement," 2012.

[9] R. B. Bird, W. E. Stewart, and E. N. Lightfoot, *Transport Phenomena*, John Wiley & Sons, Inc, 2002.

[10] I. Leito, L. Jalukse, and I. Helm, "Estimation of measurement uncertainty in chemical analysis (analytical chemistry) course."

[11] O. Redlich and A. T. Kister, "Algebraic representation of thermodynamic properties and the classification of solutions," *Industrial and Engineering Chemistry*, vol. 40, no. 2, pp. 345-348, 1948.

[12] J. Kestin, M. Sokolov, and W. A. Wakeham, "Viscosity of liquid water in the range -8 C to 150 C," *J. Phys. Chem. Ref. Data,* vol. 7, no. 3, pp. 941-948, 1978.

Sumudu S. Karunarathne received his second MSc degree in process technology (University of Southeast Norway (USN), Porsgrunn, Norway, 2016) and first MSc degree in sustainable process development (University of Moratuwa (UOM), Moratuwa, Sri Lanka, 2012) after a BSc in chemical and process engineering (UOM, 2008).

He is a PhD student at USN since 2016, where his

topic is related to measurement of physicochemical data for amine based CO_2 capture process. He has worked as a lecturer in Institute of Technology, University of Moratuwa (ITUM) (2011-2016), and as a chemical engineer in Aqua Technologies (Pvt) Ltd, Sri Lanka.

Sumudu's research interests are post combustion CO_2 capture, modelling and simulation, powder technology and water and wastewater treatment.

Dag Eimer has a PhD in chemical engineering from NTNU, Trondheim, Norway (1994), and a B.Sc. in chemical enigeering from University of Strathclyde, Glasgow, Scotland (1970). He is a professor of chemical engineering in the University of South-Eastern Norway since 2008 where he is engaged in CO_2 capture research. He was previously at Norsk Hydro Research Centre, and later Norsk Hydro Oil & Energy for 37 years, and is the author on the book Gas Treating – Absorption theory and practice, published by Wiley in 2014.

Lars Erik Øi is a professor in process technology at University of Southeast Norway. He received his master in chemical engineering from NTH in Trondheim in 1983 and his PhD in process, energy and automation engineering from Telemark University College in 2012.

He has worked 8 years as a researcher for the company Norsk Hydro and 23 years as an associate professor and full professor at University College of Southeast Norway (earlier Telemark University College). He is lecturing courses in Thermodynamics and Gas purification and energy optimization. His research fields are process technology and separation technology in general, and glycol dehydration and CO_2 capture in special.

Article O

Uncertainty comparison of viscosity measurements of CO_2 loaded MEA and water mixtures in a coaxial rheometer using Monte Carlo simulation and GUM method.

Uncertainty comparison of viscosity measurements of CO₂ loaded MEA and water mixtures in a coaxial rheometer using Monte Carlo simulation and GUM method

Sumudu S. Karunarathne, Dag A. Eimer, Lars E. Øi

University of South-Eastern Norway, Kjølnes ring 56, Porsgrunn 3901, Norway.

Abstract
Evaluation of measurement uncertainty is vital in the measurement of physicochemical properties. The uncertainty of viscosity measurement of a mixture of monoethanol amine (MEA), water and CO_2 is evaluated according to the Guide to the expression of Uncertainty in Measurement (GUM) and validated using Monte Carlo Simulation (MCS) method. This helps to estimate the truncation error due to the first order approximation of Taylor series on nonlinear models in GUM. In literature, only one method is normally used. Calculated uncertainty according to GUM for CO_2 loaded aqueous MEA is 0.035 mPa·s. For the uncertainty of viscosity in unloaded aqueous MEA solutions, the confidence interval calculated by GUM deviates from calculated confidence interval according to MCS. This deviation is beyond the numerical tolerance defined for the comparison. The probability distributions of the uncertainty sources influence the distribution of the model output in the MCS method. For the uncertainty of viscosity in CO_2 loaded aqueous MEA solutions, the confidence interval calculated by GUM is within the defined numerical tolerance and closer to the calculated confidence interval according to MCS. Combining GUM and MCS will improve confidence in the uncertainty evaluation.

Keywords: Viscosity; Uncertainty; monoethanol amine; GUM; MCS.

1. Introduction
Viscosity measurements of alkanolamines are intensively carried out in the field of amine based post combustion CO_2 capture. Various alkanolamines are tested for their performance to capture CO_2 in the form of rate of mass transfer and absorption capacity. Viscosity data in both CO_2 loaded and unloaded alkanolamines are also significant since it is needed in designing process equipment like absorption and desorption columns, heat exchangers, pumps and useful for correlating mass transfer.
The accuracy of viscosity measurements depends on many factors starting from sample preparation to the measuring instrument. Many mathematical models that have been developed to determine mass transfer coefficients and interfacial area use viscosity data in their correlations. Thus, the accuracy of the design parameters such as packed bed height and pressure drop depends on the accuracy of viscosity measurements. The information about measurement uncertainty of physical properties influences the safety margins in such a system [1].

The uncertainty of viscosity measurement characterizes a range that the measured viscosity could occupy in a considered measuring technique. Currently, different types of rheometers are available to measure liquid viscosities; the uncertainty of each method should be evaluated separately. Evaluating measurement uncertainty is considered a difficult task [2]. Defining uncertainty for the viscosity measurements allows making various decisions in different phases such as plant design and mathematical modelling and simulations. Consequently, it is vital to evaluate measurement uncertainty precisely to evaluate possible fluctuations in the results [3, 4]. For analytical chemistry, a separate document was published called QUAM (Quantifying uncertainty in analytical measurement) [5] following the principles given from GUM (Guide to the expression of uncertainty in measurement). In the GUM uncertainty framework, propagation of uncertainty is concerned with [6] and output is characterized by a Gaussian distribution or scaled and shifted t-distribution to define an appropriate coverage interval. Monte Carlo simulation (MCS) is an alternative approach for the uncertainty evaluation in which the propagation of distributions is estimated by performing random sampling from probability distributions [7].

MCS is a useful technique to validate the results obtained through the GUM. There are circumstances that GUM is not applicable where the linearized model does not give sufficient information and the probability density function (PDF) of the output quantity deviate from a Gaussian distribution or a scaled and shifted t-distribution. Several attempts have been made to compare the output of both the GUM and MCS methods to evaluate measurement uncertainty of various physical parameters. Jalid et al [8] compared both the GUM and the MCS method to estimate measurement uncertainty associated with the flatness error. A study on measurement uncertainty of indirect measurements was done by Sediva and Havlikova [9]; uncertainty was compared according to both GUM and MCS. Uncertainty evaluation and comparison on perspiration measurement system were done by Andrew and Chiachung [10]. Evaluated uncertainty by GUM is smaller than MCS and no significant difference observed considering the precision at two decimal points.

Sumudu et al. [11] discussed a detailed measurement uncertainty analysis of viscosity for unloaded aqueous MEA solutions using the GUM framework. This study extended the uncertainty analysis for the CO_2 loaded aqueous MEA mixtures. There, sources that contribute to the measurement uncertainty in a mixture of monoethanol amine, water (both unloaded and loaded with CO_2) using a coaxial cylinder type rheometer is discussed. Further, a comparison of both GUM and MCS methods on viscosity evaluation was studied for the best estimate. All the simulations were performed in the MATLAB R2017a environment and inbuilt random number generators were used for the sampling from PDF.

2. Methods of uncertainty evaluation

2.1 Uncertainty evaluation in GUM

The International Organization for Standardization (ISO) made the first publication of GUM in 1993. The Joint Committee for Guides in Metrology (JCGM) republished the GUM in 2008 with several additional documents including supplements related to measurement uncertainty [3]. GUM describes two types (Type A and Type B) of uncertainty evaluations. In type A, uncertainty is evaluated from the statistical distribution obtained through results of series of measurements while type B evaluate uncertainty through probability density functions (PDF) based on experience or other information [7].

The propagation of uncertainty based on the first order Taylor series approximation is the main aspect in GUM uncertainty evaluation. In a measuring system, inputs and outputs are combined through a functional relationship.

$$y = f(x_1, x_2, \ldots, x_N)$$
(1)

Where y is the measurand and $x_1, x_2, \ldots, x_N$ are input quantities. The propagation of uncertainty according to the Taylor series expansion of y,

$$u^2(y) = \sum_{i=1}^{N} \left(\frac{\partial f}{\partial x_i}\right)^2 u^2(x_i) + 2 \sum_{i=1}^{N-1} \sum_{j=i+1}^{N} \frac{\partial f}{\partial x_i} \frac{\partial f}{\partial x_j} u(x_i, x_j)$$
(2)

In Eq (2), $\left(\frac{\partial f}{\partial x_i}\right)$ gives the partial derivatives (sensitivity coefficients) [12, 13], $u^2(y)$ is the variance of the measuring result, the variance of the input quantity x_i is given by $u^2(x_i)$ and the covariance between x_i and x_j is given by $u(x_i, x_j)$ [13].

The functional relation (*f*) represent the uncertainty sources involved with the measuring system. It defines both physical laws and the measurement process in which it provides correlations for both systematic effects and other variable sources like instruments, laboratories, samples, different observers and times that the observations are made [12].

Measurement uncertainty is presented as a confidence interval, which explains what percentage (%) of measured data lies within the considered range. The relation of expanded and standard uncertainties are correlated by a factor *k* in such a way that

$$U(y) = ku(y) \tag{3}$$

k is known as the coverage factor; *k*=1.96 for 95% confidence level for normally distributed measurements [4, 14].

2.2 Uncertainty evaluation in MCS
MCS is a numerical approach with a random sampling technique and is applied in many scientific and engineering applications. Sampling is done from the PDFs for inputs (x_i) to evaluate the output (y) quantity. MCS discuss the propagation of distribution in which probability distributions of input quantities propagate through a model to provide the distribution of the output [6]. Figure 1 illustrates the propagation of density functions $g_{x_i}(\xi_i)$, *i*=1,…,*N*, of inputs through a model to provide the propagation of density function $g(\eta)$ for the output quantity.
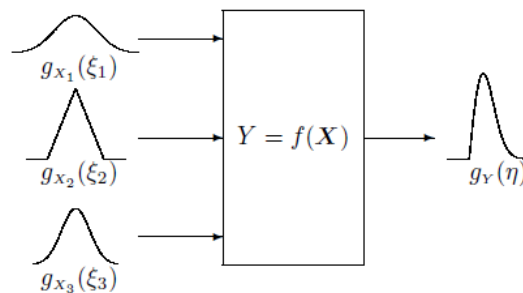

Figure 1. Propagation of distribution for three independent input variables [7].

2.3 Comparison of GUM and MCS methods in measurement uncertainty estimation
The evaluation of partial derivation in the GUM method of a complex model can be a difficult task. The truncation error due to the first order approximation of Taylor series on nonlinear models is a major limitation in this framework. The GUM approach assumes that the probability distribution of the output quantity is approximately a normal distribution and can be characterized by a t-distribution. The use of Welch-Satterthwaite formula to determine the effective degree of freedom, which is necessary to calculate expanded uncertainty is an unsolved problem [6]. The MCS method is capable of giving the probability distribution of the output [15], which is not given in the GUM method. In some scenarios, it is useful to have knowledge about probability distributions to understand the characteristics of the output. MCS can deal with both small and large uncertainties in the input quantities and there is no need for performing partial differentiation to evaluate sensitivity coefficients [12]. Even though it is difficult, the sensitivity coefficient derived in GUM framework conveys valuable facts to enhance the measurement performance [10]. Consequently, MCS is a good validation approach to compare the results obtained through the propagation of uncertainty through GUM.

3. Viscosity measurements of MEA and water mixtures with uncertainty evaluation
3.1 Viscosity measurement in a coaxial cylindrical rheometer
The viscosity measurements of MEA and water mixtures were carried in a coaxial cylindrical rheometer manufactured by Anton Paar. It has a double gap geometry that provide two fluid compartments with a rotating cup. It is good for the measurement of low viscous fluid with high accuracy since the probe provided high surface area between fluid and probe [16]. Figure 2 shows a schematic of double gap geometry of a coaxial cylindrical rheometer.
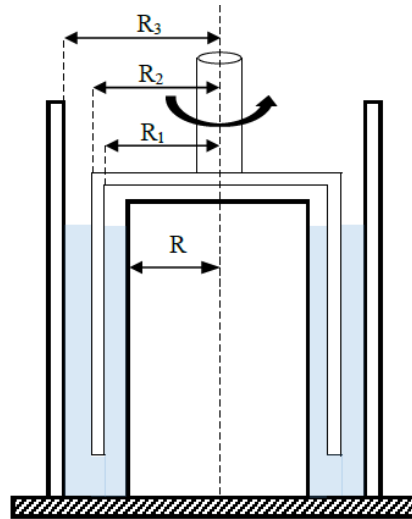
Figure 2. Schematic of double gap geometry of a coaxial cylindrical rheometer.

3.2 Measurement model

A mathematical relation was derived to correlate the parameters involved in the measuring system, which is also useful in the identification of uncertainty sources in viscosity measurements. Considering the conservation of momentum under cylindrical coordinates, the following expression can be obtained for the dynamic viscosity for the rheometer arrangement shown in Figure 2.

$$\mu = \frac{T}{4\pi L \omega R^2 \left(\frac{k_1^2}{k_1^2 - 1} + \frac{k_2^2 k_3^2}{k_3^2 - k_2^2} \right)} \tag{4}$$

Here, T is torque, μ is dynamic viscosity, L is the liquid height, R is the radius of the inner fixed cylinder, ω is angular velocity, $R_1 = K_1 R$, $R_2 = K_2 R$ and $R_3 = K_3 R$.

The schematic of the velocity profile in the liquid compartment is shown in Figure 3.
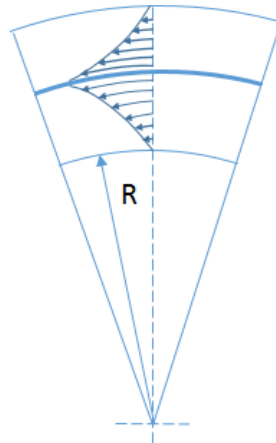

Figure 3. Velocity profile of fluid in the coaxial cylinder [11].

3.3 Cause and effect analysis

A cause and effect diagram is a graphical method to represent uncertainty sources in a measuring system. It describes how the uncertainty of individual sources is connected to propagate into a final measurement uncertainty. The cause and effect analysis performed for the viscosity measurement of aqueous MEA solutions was published elsewhere [11]. Figure 4 shows the cause and effect analysis performed for the viscosity measurements of aqueous MEA solutions.
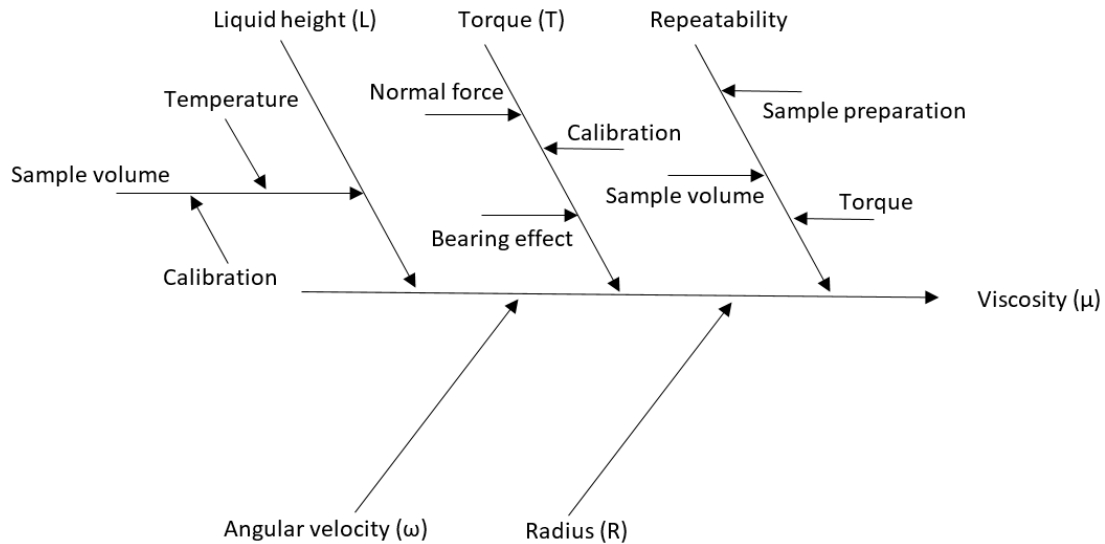
Figure 4. Cause and effect diagram for uncertainties in viscosity measurements of a MEA / water mixture [11].

3.4 Uncertainty calculation using GUM
The combined uncertainty of viscosity of aqueous MEA solutions was calculated according to the proposed mathematical model using GUM. The calculated expanded uncertainty for aqueous MEA solutions is 0.0162 mPa·s at k=2 [11]. The modified Eq (1) for the uncertainty analysis of viscosity measurement in aqueous MEA according to QUAM is shown as

$$\mu = \frac{T}{4\pi L\omega R^2 \left(\frac{k_1^2}{k_1^2-1}+\frac{k_2^2 k_3^2}{k_3^2-k_2^2}\right)} f_p f_t f_w f_{rep} \tag{5}$$

Where the f_p is purity of MEA, f_t is temperature, f_w is weight measurement and f_{rep} is repeatability. Those factors are added to the original viscosity expression to consider uncertainty sources, which are not shown in Eq (1).
For the viscosity of CO_2 loaded solutions, another factor of f_{CO_2} is introduced into Eq (5) to account for the effect of CO_2 loading in the solution. There are various uncertainty sources involved in CO_2 loading in which a detailed analysis can be found in Jayarathna et al [17]. Finally, the GUM guidelines were followed to evaluate the uncertainty as described in section 2.1.

3.5 Uncertainty calculation using MCS method
The numerical values for the uncertainty sources and factors in the model shown in Eq (5) are considered as the random output of a PDF $gX_i(\xi_i)$. It is assumed that the input quantities are uncorrelated for both viscosity measurement of CO_2 loaded and unloaded scenarios. Many sources are available in literature that explains the necessary steps to follow in order to perform MCS. The Adaptive Monte Carlo Method (AMCM) describes that the number of Monte Carlo trials M needs to be selected as $M = max(J, 10^4)$ where J is the smallest integer greater than or equal to $100/(1 - p)$ and p is a coverage probability and M is the selected adaptively until the various results of interest have established in a statistical sense [18]. There, the numerical tolerance was set in such a way that $\delta = (1/2) \cdot 10^l$. The MCS method discussed here was performed considering the non-adaptive approach as described in JCGM 101:2008 [7].
The validation of the GUM uncertainty framework using MCS was performed to verify that both methods provide results to agree within a stipulated numerical tolerance. The comparison of coverage intervals obtained by both methods is performed as shown in Eq (6).

$$d_{low} = [y - U_p - y_{low}]$$
$$d_{high} = [y + U_p - y_{high}] \tag{6}$$

When both absolute differences d_{low} and d_{high} no greater than δ, the comparison is considered to be favorable and the GUM uncertainty framework is validated in this instance [7].

4. Results and discussion

The uncertainty evaluation of viscosity for unloaded aqueous MEA solutions was presented in a previous study [11]. It was found that 0.0159 mPa·s under $k =1.96$ for combined expanded uncertainty, as it is the most appropriate coverage factor for the 95% confidence interval. A similar methodology was applied for the CO_2 loaded aqueous MEA solutions in which Eq (7) was used for the uncertainty analysis in GUM.

$$\mu = \frac{T}{4\pi L\omega R^2\left(\frac{k_1^2}{k_1^2-1}+\frac{k_2^2 k_3^2}{k_3^2-k_2^2}\right)} f_p f_t f_w f_{rep} f_{CO_2} \tag{7}$$

The combined standard uncertainty can now be found through the Tayler expansion as shown in section 2.1. The partial derivatives $\partial\mu/\partial x_i$ were obtained and listed as follows. Based on this the combined standard uncertainty of viscosity for the CO_2 loaded aqueous MEA solutions was calculated using the expression shown in Eq (17).

For better overview $k = \frac{k_1^2}{k_1^2-1} + \frac{k_2^2 k_3^2}{k_3^2-k_2^2}$

$$\frac{\partial\mu}{\partial T} = \frac{1}{4\pi L\omega R^2 k} f_p f_t f_w f_{rep} f_{CO_2} \tag{8}$$

$$\frac{\partial\mu}{\partial L} = \frac{T}{4\pi\omega R^2 k} f_p f_t f_w f_{rep} f_{CO_2}\left(\frac{-1}{L^2}\right) \tag{9}$$

$$\frac{\partial\mu}{\partial\omega} = \frac{T}{4\pi LR^2 k} f_p f_t f_w f_{rep} f_{CO_2}\left(\frac{-1}{\omega^2}\right) \tag{10}$$

$$\frac{\partial\mu}{\partial R} = \frac{T}{4\pi L\omega k} f_p f_t f_w f_{rep} f_{CO_2}\left(\frac{-2}{R^3}\right) \tag{11}$$

$$\frac{\partial\mu}{\partial f_p} = \frac{T}{4\pi L\omega R^2 k} f_t f_w f_{rep} f_{CO_2} \tag{12}$$

$$\frac{\partial\mu}{\partial f_t} = \frac{T}{4\pi L\omega R^2 k} f_p f_w f_{rep} f_{CO_2} \tag{13}$$

$$\frac{\partial\mu}{\partial f_w} = \frac{T}{4\pi L\omega R^2 k} f_p f_t f_{rep} f_{CO_2} \tag{14}$$

$$\frac{\partial\mu}{\partial f_{rep}} = \frac{T}{4\pi L\omega R^2 k} f_p f_t f_w f_{CO_2} \tag{15}$$

$$\frac{\partial\mu}{\partial f_{CO_2}} = \frac{T}{4\pi L\omega R^2 k} f_p f_t f_w f_{rep} \tag{16}$$

$$u_c(\mu)_{CO_2\ loaded} = \sqrt{\begin{array}{l}\left[\frac{\partial\mu}{\partial T}u(T)\right]^2 + \left[\frac{\partial\mu}{\partial\omega}u(\omega)\right]^2 + \left[\frac{\partial\mu}{\partial L}u(L)\right]^2 + \left[\frac{\partial\mu}{\partial R}u(R)\right]^2 + \left[\frac{\partial\mu}{\partial f_p}u(f_p)\right]^2 \\ + \left[\frac{\partial\mu}{\partial f_t}u(f_t)\right]^2 + \left[\frac{\partial\mu}{\partial f_w}u(f_w)\right]^2 + \left[\frac{\partial\mu}{\partial f_{rep}}u(f_{rep})\right]^2 + \left[\frac{\partial\mu}{\partial f_{CO_2}}u(f_{CO_2})\right]^2\end{array}} \tag{17}$$

The calculated uncertainty sources and probability distributions are summarized in Table 1. Most of the distributions are selected according to the guidelines provided in QUAM. The uncertainty of CO_2 loading was considered as 1.3% according to the study carried by Jayarathna et al. [17]. The cause and effect diagram shown in Figure 4 illustrates how the uncertainty sources contribute to the combined uncertainty. For CO_2 loaded MEA solutions, the uncertainty of CO_2 concentration measurements conveys a significant impact on the uncertainty of viscosity compared to unloaded solutions.

Table 1. Uncertainty sources and probability distributions.

Input quantity X_i	Probability Distribution	Uncertainty $U(x_i)$
Torque (T)	Triangular	$0.082\ \mu Nm$
Level (L)	Gaussian	$0.45\ mm$
Angular velocity (ω)	Triangular	$0.01\ rad \cdot s^{-1}$
Radius (R)	Triangular	$4.1\ \mu m$
Purity	Rectangular	2.886×10^{-3}
Temperature	Triangular	2.45×10^{-4}
Weight measurement	Rectangular	8×10^{-6}
CO_2 loading	Gaussian	0.013
Repeatability	Gaussian	0.00348

The Kragten's approach [5] described a way to perform uncertainty calculations according to the GUM uncertainty framework without evaluating partial derivatives. The expression to estimate standard uncertainty according to GUM is shown in Eq (17). Calculated expanded uncertainty for a CO_2 loaded viscosity measurement, $U(\mu)_{CO_2\ loaded}$ at $k = 1.96$ is 0.0346 mPa·s.

In the MCS method, the uncertainty of a viscosity measurement in CO_2 unloaded aqueous MEA solutions was evaluated according to the method illustrated in section 3.5. There, n_{dig}=2 and $u_c(\mu)$ can be expressed as 81×10^{-7}, and so $c = 81$ and $l = -7$. In the application of the MCS method, a coverage probability p is set to 0.95. It is often considered a value of $M = 10^6$ for providing a confidence interval of 95% and M at least 10^4 times greater than $1/(1 - p)$ [7, 19]. The estimated y values were sorted in non-descending order to determine the boundaries of the confidence intervals. A Gaussian distribution was assumed for the GUM uncertainty evaluation and the PDF from both the GUM and MCS method were compared in Figure 5. The dashed and vertical full line illustrates the 95% coverage intervals determined by MCS and GUM respectively.
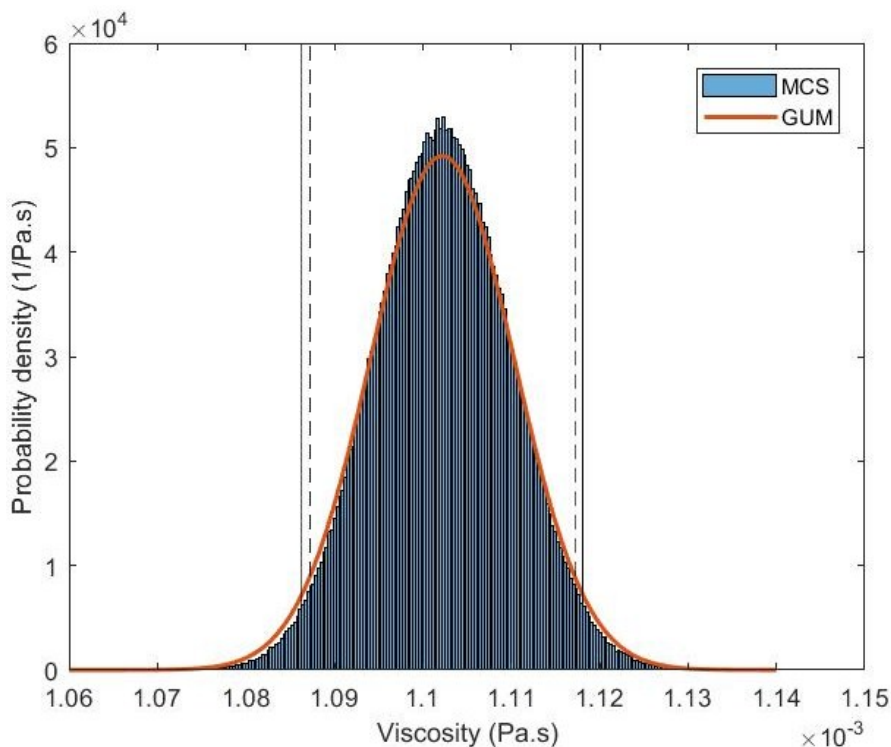

Figure 5. Probability density distribution of unloaded aqueous MEA viscosity from GUM and MCS method, ' __ ' GUM, '---' MCS.

d_{low} and d_{high} were determined to validate the GUM according to the expression shown in Eq (6). The calculated y_{low} and y_{high} from cumulated probability distribution is shown in Table 2. In this scenario,

GUM is not validated since both endpoints of the coverage interval does not satisfy the condition with numerical tolerance δ.

Table 2. Uncertainty evaluation results for unloaded solutions.

Method	M	$\mu_{unloaded}$ (mPa·s)	$U(\mu)_{unloaded}$ (mPa·s)	Probabilistically symmetric 95% coverage interval	d_{low}	d_{high}
GUM		1.1022	0.0081 (0.0159)	(0.0010863, 0.0011181)	-	-
MCS	10^6	1.1022	0.0077 (0.0150)	(0.0010872, 0.0011173)	9.89×10^{-07}	7.16×10^{-07}

The MCS method for CO_2 loaded aqueous MEA solutions considered the uncertainty of CO_2 loadings as proposed by Jayarathna et al. [17]. In the simulation, $u(f_{CO_2}) = 0.013$ considered with Gaussian distribution and all other uncertainty sources were considered to be the same as in the previous scenario. The relevant parameters considered in the simulation are listed in Table 3.

Table 3. Numerical parameters in MCS for CO_2 loaded solutions.

Parameter	Value
n_{dig}	2
c	-6
l	17
M	10^6

In order to validate GUM, d_{low} and d_{high} were determined as shown in Eq (6) and PDF from both GUM and MCS method were compared in Figure 6. A Gaussian distribution was assumed for the GUM uncertainty evaluation as considered in the previous scenario. All the required parameters for the validation of GUM for the uncertainty of viscosity measurement of CO_2 loaded MEA solutions are listed in Table 4.

Table 4. Uncertainty evaluation results for CO_2 loaded solutions.

Method	M	$\mu_{CO_2\ loaded}$ (mPa·s)	$U(\mu)_{CO_2\ loaded}$ (mPa·s)	Probabilistically symmetric 95% coverage interval	d_{low}	d_{high}
GUM		1.1814	0.0176 (0.0345)	(0.0011468, 0.0012160)	-	-
MCS	10^6	1.1813	0.0174 (0.0341)	(0.0011472, 0.0012155)	4.75×10^{-07}	2.79×10^{-07}

As in the previous scenario, the validation was done by analyzing d_{low} and d_{high} for the uncertainty of CO_2 loaded solution. The calculated y_{low} and y_{high} from cumulated probability distribution is shown in Table 4. The calculated numerical tolerance δ for this scenario satisfies the condition shown in Eq (6) for both endpoints of the confidence intervals. Consequently, GUM is validated for the uncertainty of viscosity measurement of CO_2 loaded solutions.
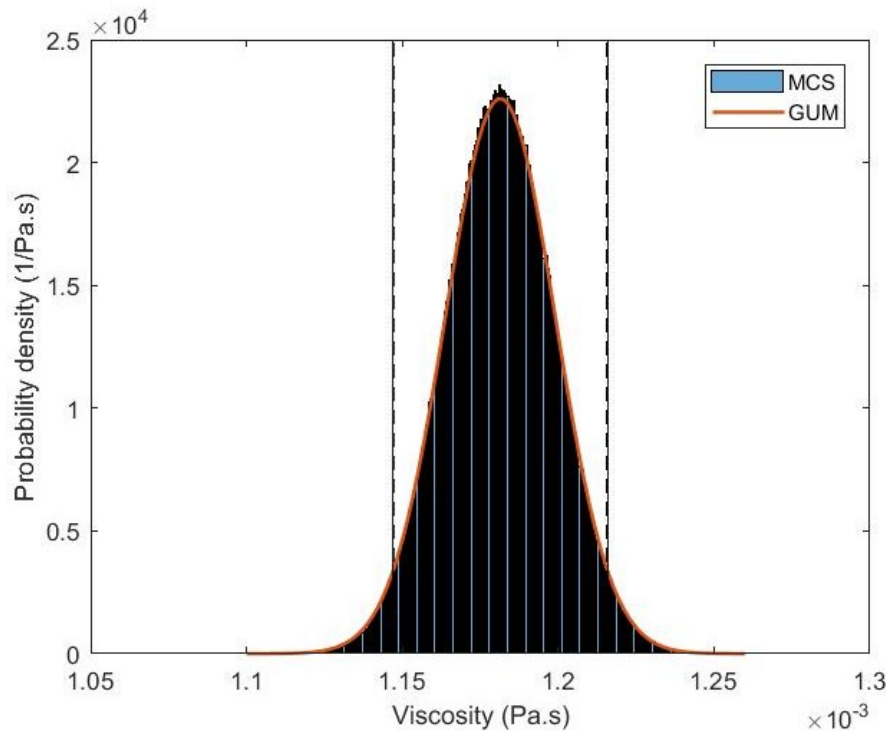
Figure 6. Probability density distribution of CO_2 loaded aqueous MEA viscosity from GUM and MCS method, ' __ ' GUM, '---' MCS.

5. Conclusion

This study performs an uncertainty evaluation of viscosity measurement in a coaxial rheometer of CO_2 loaded MEA solutions according to GUM. The uncertainty of a viscosity measurement performed for unloaded solutions has been discussed in a previous study was used by modifying the model equation according to QUAM guidelines for the new scenario. The calculated uncertainty for CO_2 loaded MEA solutions is in good agreement with uncertainties reported in the literature.

For the CO_2 unloaded solutions, the comparison of GUM by the MCS method reveals that endpoints of the two coverage intervals do not satisfy the condition with numerical tolerance δ. As a result, the GUM is not validated for this scenario. This can be due to various reasons including model nonlinearity, covariation of parameters involved in the model and nature of selected uncertainty distributions for the uncertainty sources. For the CO_2 loaded solutions, the numerical tolerance satisfied the conditions for the GUM validation. The numerical tolerance fulfilled the condition defined in the JCGM 101:2008.

References

[1]   L. Kirkup and R. B. Frenkel, "An introduction to uncertainty in measurement using the GUM (Guide to the expression of uncertainty in measurement)," The importance of uncertainty in science and technology

[2]   M. Desenfant and M. Priel, "Road map for measurement uncertainty evaluated" Measurement, vol. 39, pp. 841-848, 2006.

[3]   L. T. Stant, P. H. Aaen, and N. M. Ridler, "Comparing methods for evaluating measurement uncertainty given in the JCGM 'Evaluation of measurement data' document " Measurement vol. 94, pp. 847-851, 2016.

[4]   V. R. Meyer, "Measurement uncertainty," Journal of Chromatography, vol. 1158, pp. 15-24, 2007.

[5]   I. Leito, L. Jalukse, and I. Helm, "Estimation of measurement uncertainty in chemical analysis (analytical chemistry) course," Available: https://sisu.ut.ee/measurement.

[6]   P. R. G. Couto, J. C. Damasceno, and S. P. D. Oliveira, "Monte carlo simulation applied to uncertaninty in measurement ", Theory and applications of monte carlo simulation: INTECH, open science, open minds, 2013. [Online]. Available.

[7]   JCGM, "Evaluation of measurement data — Supplement 1 to the "Guide to the expression of uncertainty in measurement" — Propagation of distributions using a Monte Carlo method," JCGM 101:2008,

[8]   A. Jalid, S. Hariri, A. E. Gharad, and J. P. Senelaer, "Comparison of the GUM and Monte Carlo methods on the flatness uncertainty estimation in coordinate measuring machine " Int.J.Metrol.Qual.Eng, vol. 7, no. 302, 2016.

[9]   S. Sediva and M. Havlikova, "Comparison of GUM and Monte Carlo method for evaluation measurement uncertainty of indirect measurement " in Proceedings of the 14th International Carpathian Control Conference (ICCC), Rytro, Poland, 2013: IEEE.

[10]   A. Chen and C. Chen, "Comparison of GUM and Monte Carlo methods for evaluationg measurement uncertainty of perspiration measurement " Measurement, vol. 87, pp. 27-37, 2016.

[11]   S. S. Karunarathne, D. A. Eimer, and L. E. Øi, "Evaluation of systematic error and uncertainty of viscosity measurements of mixtures of monoethanol amine and water in coaxial cylinder rheometers," International Journal of Modeling and Optimization, vol. 8, no. 5, pp. 260-265, 2018.

[12]   C. E. Papadopoulos and H. Yeung, "Uncertainty estimation and Monte Carlo simulation method," Flow Measurement and Instrumentation vol. 12, pp. 291-298, 2001.

[13]   M. Desenfant and M. Priel, "Road map for measurement uncertainty evaluation" Measurement, vol. 39, pp. 841-848, 2006.

[14]   W. F. C. Rocha and R. Nogueira, "Monte Carlo simulation for the evaluation of measurement uncertainty of pharmaceutical certified reference materials," J. Braz. Chem. Soc, vol. 23, no. 3, pp. 385-391, 2012.

[15]   M. A. Herrador and A. G. Gonzalez, "Evaluation of measurement uncertainty in analytical assays by means of Monte-Carlo simulation " Talanta vol. 64, pp. 415-422, 2004.

[16]   Food Network Solution Complete Food Network Information Center. Available: http://www.foodnetworksolution.com/wiki/word/6044/concentric-cylinder-viscometer

[17]   C. K. Jayarathna, A. B. Elverhøy, Y. Jiru, and D. Eimer, "Experimentally based evaluation of accuracy of absorption equilibrium measurements," Energy Procedia, vol. 37, pp. 834-843, 2013.

[18]   X.-l. Wen, Y.-b. Zhao, D.-x. Wang, and J. Pan, "Adaptive Monte Carlo and GUM methods for the evaluation of measurement uncertainty of cylindricity error," Precision Engineering, vol. 37, pp. 856-864, 2013.

[19]   H. B. Motra, J. Hildebrand, and F. Wettke, "The Monte Carlo method for evaluating measurement uncertainty: Application for determining the properties of materials " Probabilistic Engineering Mechanics, vol. 45, pp. 220-228, 2016.

—

usn.no